

GEOHERMAL EXPLORATION OF NEWBERRY VOLCANO, OREGON

SUMMARY REPORT

By

Albert F. Waibel¹

Zachary S. Frone²

David D. Blackwell²

December 2014

Final Report for the DOE Innovative Exploration Technology (IET) Grant 109 program supporting geothermal exploration of Newberry Volcano, Oregon.

ABSTRACT

Davenport Newberry (Davenport) has completed 8 years of exploration for geothermal energy on Newberry Volcano in central Oregon. Two deep exploration test wells were drilled by Davenport on the west flank of the volcano, one intersected a hydrothermal system; the other intersected isolated fractures with no hydrothermal interconnection. Both holes have bottom-hole temperatures near or above 315°C (600°F). Subsequent to deep test drilling an expanded exploration and evaluation program was initiated. These efforts have included reprocessing existing data, executing multiple geological, geophysical, geochemical programs, deep exploration test well drilling and shallow well drilling. The efforts over the last three years have been made possible through a DOE Innovative Exploration Technology (IET) Grant 109, designed to facilitate innovative geothermal exploration techniques. The combined results of the last 8 years have led to a better understanding of the history and complexity of Newberry Volcano and improved the design and interpretation of geophysical exploration techniques with regard to blind geothermal resources in volcanic terrain.

¹ Columbia Geoscience

² Southern Methodist University

DEDICATION

This publication is dedicated to Hiram A. (Tony) Bingham. His dedication to the geothermal industry and his vision for the geothermal resource potential of Newberry Volcano was the driving force behind Davenport's efforts. Without his insight and enthusiasm for geothermal energy, the discovery well NWG 46-16 and the EGS well NWG 55-29 would never have been drilled.

TABLE OF CONTENTS

ABSTRACT	i
DEDICATION	ii
TABLE OF CONTENTS	iii
LIST OF FIGURES	vi
LIST OF TABLES	x
INTRODUCTION	1
PREVIOUS EXPLORATION	3
DOE INNOVATIVE EXPLORATION TECHNOLOGY (IET) Grant 109	5
GEOLOGY	7
DEEP EXPLORATION WELLS	9
Well NWG 46-16 Discussion.....	17
WELL DATA CORRELATIONS, GEOCHEMISTRY and PETROLOGY	19
Geochemistry	19
Cutting Samples	20
Core Samples.....	22
Surface Samples	25
Correlations	25
Wells 55-29, N-2, and NC-01	26
Wells 55-29 and 46-16 Correlation.....	28
Within Well NWG 55-29	30
Well Data and Regional Correlations.....	31
GROUNDWATER HYDROLOGY	33
Groundwater Hydrology Interpretation.....	37
GEOPHYSICS	38
Temperature Gradient	38
Gravity.....	42
Gravity Interpretation.....	46
Magnetotellurics (MT)	48
MT Discussion.....	52
Aeromagmetics.....	56
LIDAR	57

DISCUSSION	64
The Western Flank Thermal Anomaly: Temperature at Depth.....	64
MICROSCEISMIC MONITORING	73
Low Amplitude Seismic Emission Analysis (LASEA)	73
Methodology	74
Recording and Analysis	77
Northern Array Results	80
EVALUATION OF EXPLORATION METHODS FOR BLIND GOETHERMAL RESOURCES IN VOLCANIC TERRAIN	97
CONCLUSIONS AND RECOMMENDATIONS	99
ACKNOWLEDGEMENTS	100
BIBLIOGRAPHY	101
APPENDIX A: TEMPERATURE DATA FOR WELLS 55-29 and 46-16	1
Temperature and Heat Flow Data	1
Data for Well 55-29	1
Data for Well 46-16	2
Temperature Interpretation for Well 46-16	3
Appendix A - References	9
APPENDIX B: Geochemistry Data Analysis	1
‘Cuttings’ geochemical data collected	Appendix B, Page 2
‘Core’ XRF data collected	Appendix B, Page 38
APPENDIX C: Geologica Reports to Davenport Power	1
APPENDIX D: Well 44-16 Notes and Information	1
Well 46-16 Time Sequence Flowing of Well, 8, 9, 10 September 2013	1
Additional Notes on Sequence of Flow, September 8-10, 2013	2
Initial Rough Calculations:	3
Well 46-16 Status & History as Regarding Flow Tests of September 2013	4
Excerpt of 46-16 Well Summary Report	7
46-16 Well SURVEY INFORMATION	9
APPENDIX E: USGS Well Gas Chemistry Data, September 25, 2013	1
APPENDIX F: Map of CO ₂ in Soil Gas for Newberry Volcano	1
APPENDIX G: APEX HIPOINT SIGMA ³ REPORTS TO DAVENPORT/NEWBERRY	1
Letter authorizing release of information, 11/18/2014, 1 pp	Appendix G, page 2
Proposal of Work and Strategy, 5/13/2011, 13 pp	Appendix G, page 3

Interim Report Data Processing Results, 3/27/2012, 50 pp	Appendix G, page 16
Final Report Passive Seismic Monitoring Project, 12/13/2012, 46 pp	Appendix G, page 66
Interim Report 2013 Low-amplitude Passive Seismic Monitoring Project, 1/2/2014, 25 pp	Appendix G, page 112
Quick View of Current Status, 3/13/2014, 3 pp	Appendix G, page 137
Draft Version (Rev. 4) Final Project Report, 4/27/2014, 47 pp	Appendix G, page 140
Final Version (Rev. 6) of Final Project Report, 9/10/2014, 63 pp	Appendix G, page 187

LIST OF FIGURES

FIGURE 1: LOCATION OF NEWBERRY VOLCANO, OREGON (FROM JENSEN, 2006).	2
FIGURE 2: GEOLOGIC SETTING OF NEWBERRY VOLCANO (FROM JENSEN, 2006).....	3
FIGURE 3: GEOLOGIC MAP OF THE WESTERN FLANK OF NEWBERRY VOLCANO, OREGON (AFTER MACLEOD ET AL., 1995). RING FRACTURES OF VOLCANIC VENTS SHOWN AS EAST-WEST TRENDING RED CURVED LINES JUST NORTHWEST OF PAULINA LAKE.	8
FIGURE 4: WELL LOCATION MAP: RED TRIANGLES ARE DEEP EXPLORATION TEST WELLS. BLUE DOTS ARE TEMPERATURE GRADIENT AND SHALLOW TEST WELLS. RED X ARE INCOMPLETE DAVENPORT TEMPERATURE GRADIENT WELLS, CASED TO ACCOMMODATE MICROSEISMIC MONITORING. THESE WELLS HAVE NOT BEEN DRILLED TO PERMITTED DEPTH, AND ARE NOT DEEP ENOUGH TO PROVIDE TEMPERATURE GRADIENT DATA.	10
FIGURE 5: DENSITY AND NATURAL GAMMA RAY LOGS OF NWG WELLS 46-16 AND 55-29.....	11
FIGURE 6: NATURAL GAMMA RAY LOGS OF SIX WELLS ON THE WEST SIDE OF NEWBERRY VOLCANO. NWG 46-16 AND 55-29 ARE DAVENPORT WELLS. CE WELLS 86-21 AND 23-22 ARE CALIFORNIA ENERGY CO. WELLS. N-2 AND N-5 ARE GEOTHERMAL RESOURCES INTERNATIONAL (GRI) TEMPERATURE GRADIENT WELLS.....	12
FIGURE 7: TEMPERATURE GRADIENT PROFILES OF THE FOUR DEEP EXPLORATION WELLS, NWG 46-16, NWG 55-29, CE 23-22 AND CE 86-21. THE EQUILIBRIUM TEMPERATURE PROFILE FOR WELL 55-29 (GREEN) SHOWS A GOOD STRAIGHT CONDUCTIVE GRADIENT WITHOUT FORMATION FLUID FLOW. THIS MATCHES WELL-SITE DATA OBSERVED WHILE THE DRILL HOLE WAS BEING DRILLED. THE PROFILES FOR WELL NWG 46-16 (RED AND BLUE LINES) SHOW SIGNIFICANT PERTURBATION INDICATIVE OF FORMATION FLUID FLOW AFFECTING THE TEMPERATURE PROFILE OF THE WELL. THE PROFILE FOR WELL 86-21 SHOWS A DOMINANT CONDUCTIVE GRADIENT. THE PROFILE FOR WELL 23-22 SHOWS A GENERAL CONDUCTIVE GRADIENT WITH APPARENT CONVECTIVE INFLUENCE BETWEEN 1400 AND 1900 M. IT IS NOT CLEAR, HOWEVER, IF THE MEASUREMENT WAS TAKEN UNDER THERMAL EQUILIBRIUM CONDITIONS .THE RED ARROWS ARE LOCATIONS WHERE D.D. BLACKWELL OBSERVED EVIDENCE IN THE TEMPERATURE PROFILES OF FORMATION FLUID FLOW.....	13
FIGURE 8: A GRAPH SHOWING CO ₂ VALUES MEASURED BY EPOCH MUD LOGGING DURING DRILLING OF WELL NWG 46-16 (EPOCH, 2008). TO THE RIGHT ARE NOTED THE DEPTH OF THE CASING SHOE AND THE LOCATION OF HYDROTHERMALLY PRECIPITATED DRUSE QUARTZ AND EPIDOTE OBSERVED IN THE DRILL CUTTINGS. THE SHALLOWER OCCURRENCES OF CO ₂ ARE ATTRIBUTED TO BIOGENIC GAS FROM ORGANIC MATTER WITHIN CLASTIC LAYERS.	15
FIGURE 9: INITIAL GAS FLOW FROM WELL NWG 46-16. NOTE THE ENDOTHERMIC REACTION OF GAS DECOMPRESSING, RESULTING IN FROST FORMING ON THE FLOW LINE WHEN THE VALVE IS FIRST OPENED (8 SEPTEMBER 2013).	18
FIGURE 10: DRILLING FLUID FLOWING FROM THE WELL NWG 46-16, APPROXIMATELY 45 MINUTES AFTER THE LIQUID FLOW COMMENCED. (8 SEPTEMBER 2013).....	19
FIGURE 11: DEVIATION CORRECTED GAMMA RAY LOGS FROM CE 23-22, NWG 46-16, AND NWG 55-29 PLOTTED VS ELEVATION. COLORED BANDS SHOW INTER-WELL CORRELATIONS, WITH SOLID COLORS BEING SILICIC UNITS AND HATCHED/CROSS-HATCHED BEING MAFIC UNITS. YELLOW SYMBOLS SHOW LOCATION OF GEOCHEMICAL SAMPLES. ARROWS INDICATE THE BASE OF NEWBERRY VOLCANICS, BASED ON CORRELATION WITH DATED FLOWS FROM GEO N-1. DARK STIPPLED AREAS BETWEEN PLOTS INDICATE INFERRED DESCHUTES FORMATION LITHOLOGIES. SOLID BLACK LINE AT THE TOP OF EACH PLOT SHOWS THE WELLHEAD ELEVATION.	21
FIGURE 12: GAMMA RAY AND/OR MUD LOGS FOR TWO WEST FLANK CORE WELLS, GEO N-2 AND SF NC-01. YELLOW, BLUE AND GREEN POINTS SHOW GEOCHEMICAL SAMPLE LOCATIONS: YELLOW POINTS ANALYZED BY XRF, BLUE POINTS ANALYZED BY ICP/ICP-MS, AND GREEN POINTS ARE DATA FROM GRI. THE ANALYTICAL TECHNIQUE USED FOR THE GRI DATA IS UNKNOWN. DATA FOR NC-01 ARE FROM ARESTAD AND POTTER (1988) AND DATA FOR GEO N-2 ARE FROM WELL REPORTS AVAILABLE FROM THE DOGAMI WEBSITE. 'CORR.' SHOWS INTER WELLBORE CORRELATIONS OF DIFFERENT GEOLOGIC UNITS.....	23
FIGURE 13: GAMMA RAY AND/OR MUD LOGS FOR TWO WEST FLANK CORE WELLS, GEO N-5 AND NC 72-3. YELLOW AND BLUE POINTS SHOW GEOCHEMICAL SAMPLE LOCATIONS: YELLOW POINTS ANALYZED BY XRF AND BLUE POINTS ANALYZED BY ICP/ICP-MS. 'LITH.' IS A SIMPLIFIED LITHOLOGIC LOG FOR EACH WELL. DATA FOR GEO N-2 ARE FROM WELL REPORTS AVAILABLE FROM THE DOGAMI WEBSITE DATA AND DATA FOR NC 72-3 ARE	

FROM ARESTAD AND POTTER (1988). 'CORR.' SHOWS INTER WELLBORE CORRELATIONS OF DIFFERENT GEOLOGIC UNITS.....24

FIGURE 14: WELL TRACES COLORED BY GAMMA RAY (GR) LOG VALUES FOR NWG 55-29 AND N-2; NC-01 DOES NOT HAVE AN AVAILABLE GR LOG. SYMBOLS SHOW LOCATION AND DEPTH OF GEOCHEMICAL SAMPLES; LABEL VALUES REFER TO MEASURED DEPTH IN FEET. COLORED BOXES REPRESENT CORRELATED LITHOLOGIES, CROSS HATCHED LITHOLOGIES ARE MAFIC, AND SOLID BOXES ARE SILICIC. COLORS IN BOXES ARE THE SAME AS FIGURES 12 AND 13. THE SOLID BLACK LINE AT THE TOP IS THE TOPOGRAPHIC SURFACE AND THE SOLID RED LINES SHOW THE UPPER AND LOWER SURFACES OF THE 10 OHM-M CONDUCTOR FROM THE MT SURVEY. X-AXIS UNITS ARE UTM LOCATION ALONG CROSS SECTION, X AND Y AXES ARE 1:1. INSET MAP SHOWS THE LOCATION OF THE CROSS SECTION IN RELATION TO OTHER WEST FLANK WELLS.....28

FIGURE 15 A AND B (TOP AND BOTTOM): GEOCHEMICAL DATA CORRELATIONS FOR NWG 46-16 AND CE 23-22. A (TOP) DISPLAYS GEOCHEMICAL DATA FOR BASALTS IN WELL NWG 46-16 AND CE 23-22. B (BOTTOM) DISPLAYS TUFF CORRELATED WITH GEOCHEMICAL DATA FROM NWG 46-16 AND CE 23-22. OXIDES ARE PLOTTED IN WT% WHILE TRACE ELEMENTS ARE NORMALIZED TO PRIMITIVE MANTLE.30

FIGURE 16: TEMPERATURE - DEPTH PLOTS OF TWO WELLS INSIDE THE CALDERA LOGGED BY THE SMU GEOTHERMAL LABORATORY.....35

FIGURE 17: MAP OF GENERALIZED HYDROLOGIC HEAD AND GROUND-WATER FLOW DIRECTIONS FOR THE AREA AROUND NEWBERRY VOLCANO (ADAPTED FROM GANNETT, LITE, MORGAN AND COLLINS, 2001, FIGURE 28, P. 60).37

FIGURE 18: TEMPERATURE-DEPTH PLOTS FOR THE SIX SHALLOW TEMPERATURE GRADIENT WELLS ON NEWBERRY VOLCANO THAT WERE ALSO USED FOR PASSIVE LOW ENERGY SEISMIC SIGNAL MONITORING (SEE SEISMIC SECTION BELOW).39

FIGURE 19: TEMPERATURE-DEPTH PLOTS FOR THE TEMPERATURE GRADIENT WELLS ON NEWBERRY VOLCANO. RDO-1 AND USGS NB2 ARE LOCATED WITHIN THE CALDERA.40

FIGURE 20: TEMPERATURE-DEPTH PLOTS FOR THE DEEP EXPLORATION WELLS DRILLED ON THE WEST SIDE OF NEWBERRY VOLCANO. THE RED ARROWS ON RUN 1 OF 46-16 INDICATE POSSIBLE FLUID LOSS ZONES.41

FIGURE 21: TOPOGRAPHIC MAP OF THE CENTRAL AND WESTERN FLANK PORTION OF NEWBERRY VOLCANO. THE BLACK DOTS IDENTIFY THE LOCATIONS OF GRAVITY STATIONS.43

FIGURE 22: COMPLETE BOUGUER ANOMALY WITH A REDUCTION DENSITY VALUE OF 2.50 GM/CC. EAST LAKE, PAULINA LAKE AND PAULINA CREEK ARE SHOWN WITH BLUE OUTLINES. THE MONUMENT BOUNDARY IS OUTLINED IN BLACK.45

FIGURE 23: COMPLETE BOUGUER ANOMALY WITH A REDUCTION DENSITY VALUE OF 2.60 GM/CC. EAST LAKE, PAULINA LAKE AND PAULINA CREEK ARE SHOWN WITH BLUE OUTLINES. THE MONUMENT BOUNDARY IS OUTLINED IN BLACK.46

FIGURE 24: REGIONAL GRAVITY MAP OF SOUTHEASTERN OREGON, ROBERTS ET AL., 2008. THE BLACK OUTLINE SHOWS THE MAXIMUM EXTENT OF LAVA FLOWS FROM NEWBERRY VOLCANO. THE LOCATION OF THE CALDERA IS MARKED BY A GREEN TRIANGLE. THE SHIELD PHYSIOGRAPHIC FORM OF THE VOLCANO IS LOCALIZED AROUND THE CALDERA.47

FIGURE 25: MT STATION LOCATIONS, DAVENPORT SURVEYS, ON NEWBERRY VOLCANO. GEOSYSTEMS 2006 STATIONS ARE IN RED AND ZONGE INTERNATIONAL 2011 STATIONS ARE IN BLACK (WAIBEL ET AL., 2013)..49

FIGURE 26: E-W 05 CROSS SECTION SHOWING THE RESULTS OF THE 2008 PROCESSING OF THE 2006 DATA. THE LOCATIONS OF DAVENPORT DEEP EXPLORATION WELL NWG 55-29 AND SANTA FE TEMPERATURE GRADIENT WELL NC-01 ARE IDENTIFIED. THE SMALL ARROWS IDENTIFY THE LOCATION OF MT STATIONS (WAIBEL ET AL., 2013).50

FIGURE 27: E-W 05 CROSS SECTION SHOWING THE RESULTS OF 2012 PROCESSING. THE LOCATIONS OF DAVENPORT DEEP EXPLORATION WELL NWG 55-29 AND SANTA FE TEMPERATURE GRADIENT WELL NC-01 ARE IDENTIFIED. THE SMALL ARROWS IDENTIFY THE LOCATION OF MT STATIONS. OTHER GEOGRAPHIC POINTS ARE ALSO IDENTIFIED (WAIBEL ET AL., 2013).51

FIGURE 28: MAP OF NEWBERRY VOLCANO SHOWING MT STATION LOCATIONS. THE RED LINES SHOW THE LOCATION OF FOUR MT SLICES OF LINES 05, D, E, AND F. THE BLUE DOTS IDENTIFY MT STATION LOCATIONS FROM THE 2006 SURVEY. THE RED CIRCLES IDENTIFY MT STATION LOCATIONS FROM THE 2011 SURVEY (WAIBEL ET AL., 2013).52

FIGURE 29: 2-D MT SLICE LINE D. THE TWO DIGIT NUMBERS ACROSS THE TOP IDENTIFY MT STATIONS. THIS FIGURE IS COMPRESSED HORIZONTALLY (WAIBEL ET AL., 2013).54

FIGURE 30: 2-D MT SLICE LINE E. THE ONE, TWO AND THREE DIGIT NUMBERS ACROSS THE TOP IDENTIFY MT STATIONS.55

FIGURE 31: 2-D MT SLICE LINE F. THE TWO AND THREE DIGIT NUMBERS ACROSS THE TOP IDENTIFY MT STATIONS.55

FIGURE 32: MAP OF TOTAL AEROMAGNETIC FIELD REDUCED TO POLE AND MEAN REMOVED. FROM USGS SURVEY 1975. THE BLACK LINE OUTLINES THE NEWBERRY NATIONAL VOLCANIC MONUMENT BOUNDARY.57

FIGURE 33: LIDAR IMAGE OF NEWBERRY VOLCANO WITH THE ILLUMINATION AT 80 DEGREES.59

FIGURE 34: SILICIC OUTCROPS ON THE FLANK OF NEWBERRY VOLCANO. LIDAR IMAGE WITH THE ILLUMINATION AT 320 DEGREES. THE RED AREAS DENOTE THE LOCATION OF QUATERNARY RHYOLITE AND DACITE OUTCROPS ON THE FLANK OF THE VOLCANO (QER AND QED OF MACLEOD ET AL., 1995). THE YELLOW DOTS IDENTIFY THE TWO DAVENPORT WELL SITES. THE HOLOCENE SILICIC VOLCANIC OUTCROPS WITHIN THE CALDERA ARE NOT NOTED.60

FIGURE 35: VIEW OF LIDAR IMAGE OF THE UPPER WESTERN FLANK OF NEWBERRY VOLCANO WITH THE HIGH DENSITY GRAVITY ANOMALY OVERLAIN. THE BLACK LINE BOUNDARY ENCLOSING A SHADED AREA IDENTIFIES THE LOCATION OF THE NEWBERRY NATIONAL VOLCANIC MONUMENT.62

FIGURE 36: LIDAR IMAGE OF THE WEST FLANK OF NEWBERRY VOLCANO. THE YELLOW DOTS MARK DAVENPORT DEEP EXPLORATION WELLS NWG 46-16 (NORTH) AND NWG 55-29 (SOUTH). THE BLUE DOTS MARK DEEP EXPLORATION WELLS CE 23-22 (NORTH) AND CE 86-21 (SOUTH). THE YELLOW ASTERISKS MARKS THE LOCATIONS OF RECENTLY RECORDED SMALL EARTHQUAKES. THE PURPLE LINE MARKS THE ARCUATE BOUNDARY BETWEEN PREDOMINANTLY UNBROKEN SURFACE AREA TO THE EAST AND THE MORE BROKEN SURFACE AREAS TO THE WEST AND NORTH. THE GREEN LINE IDENTIFIES THE LOCATION OF MT LINE F (FIGURE 31). THE RED LINES IDENTIFY A FEW OF THE LINEAR PATTERNS, SOME OF WHICH MAY REFLECT SURFACE BREAKAGE ASSOCIATED WITH DEEPER STRAIN.63

FIGURE 37: COMPARISON OF THE DEPTH TO THE 200°F, 300 °F. 400°F (93°C, 150°C, 204°C) ISOTHERMS AND THE TOP OF THE CONDUCTOR LAYER (TOP) AND BOTTOM OF THE CONDUCTOR LAYER (BOTTOM) FROM THE 3-D MT INTERPRETATION.65

FIGURE 38: MAP SHOWING THE DEPTH TO THE BASE OF THE SHALLOW CONDUCTIVE LAYER. MT STATION LOCATIONS ARE MARKED WITH BLACK TRIANGLES AND WITH STATION NUMBERS SHOWN.66

FIGURE 39: TEMPERATURE GRADIENTS OF TG AND DEEP WELLS (SHOWN AS CURRENT SITES ON FIGURE 40).68

FIGURE 40: ISOTHERM MAP, DEPTH TO 200°F (93°C) ISOTHERM FROM AVAILABLE WELL DATA. NOTE THAT THE "TG" WELLS MARKED ON THE MAP ARE NOT DATA POINTS, RATHER PERMITTED BUT NEVER COMPLETED TO FULL DEPTH. SIX OF THESE WELLS WERE DRILLED TO ABOUT 213 M (700 FT) AND CASED FOR SEISMIC MONITORING PURPOSES. THE TEMPERATURE GRADIENTS OF THESE WELLS ARE SHOWN IN FIGURE 19.69

FIGURE 41: DEPTH TO 400°F (204°C) ISOTHERM FROM WELL DATA. NOTE THAT THE "TG" WELLS MARKED ON THE MAP ARE NOT TEMPERATURE DATA POINTS. THEY WERE PERMITTED BUT NEVER COMPLETED.70

FIGURE 42: INTERPRETED TEMPERATURE AT A DEPTH OF 3 KM (10,000 FT) BELOW THE SURFACE. INTERPRETATION METHOD EXPLAINED IN TEXT. THE RED LINE IDENTIFIES THE BOUNDARIES OF THE DAVENPORT LEASES AND THE ROYAL BLUE LINE INDICATES THE MONUMENT BOUNDARY. NOTE THE CONTOURS IN THE UPPER AND LOWER LEFT CORNERS ARE COMPUTER-GENERATED ARTIFACTS NOT BASED ON TEMPERATURE GRADIENT WELL (FIGURE 4) OR MT STATION MEASUREMENTS (FIGURE 25).71

FIGURE 43: ZUCCA AND EVANS INFERRED TWO-PHASE HYDROTHERMAL LOCATION UNDER THE CALDERA AND THE WEST FLANK OF NEWBERRY VOLCANO, ILLUSTRATED IN THIS WEST-EAST CROSS-SECTION (FIGURE FROM ZUCCA AND EVANS, 1992).74

FIGURE 44: MAP OF THE UPPER WESTERN FLANK OF NEWBERRY VOLCANO, WITH SEISMIC MONITORING HOLES AND DEEP EXPLORATION HOLES IDENTIFIED. PAULINA LAKE AND THE BIG OBSIDIAN FLOW IN THE UPPER RIGHT ARE WITHIN THE CALDERA.76

FIGURE 45: ONE OF THE HIGH-GRADE DIGITAL GEOPHONES, MANUFACTURED BY GEOSPACE OF HOUSTON, TEXAS, DEPLOYED BY THE APEX HIPOINT/ SIGMA3 FIELD TEAM IN THE MONITORING WELLS.77

FIGURE 46: THE FOUR HIGHEST-AMPLITUDE ENERGY CLUSTERS ARE OUTLINED HERE DURING THE SOUTHERN ARRAY DEPLOYMENT WITH START AND END TIMES OF 0900 TO 1600. GIVEN THE REGULARITY OF THE START AND END TIMES OF THESE PERIODS, THEY ARE ALMOST CERTAINLY MAN-MADE CULTURAL NOISE RELATED TO

DAILY BUSINESS OPERATING HEAVY EQUIPMENT SOMEWHERE IN THE AREA (SLIDE 7, APEX HIPOINT/ SIGMA³ SOUTHERN ARRAY FINAL REPORT TO DAVENPORT).....78

FIGURE 47: SOUTHERN ARRAY SHOWS A DOMINANT TREND OF EPISODIC MICROSEISMIC SIGNALS OBSERVED IN THE PROCESSED DATA. THE FOUR LARGER BLUE DOTS IDENTIFY THE FOUR MONITORING HOLE LOCATIONS. THE SMALLER DOTS REPRESENT RESOLVED SIGNALS. THE GRID SPACING IS 100 M (SLIDE 27, APEX HIPOINT/ SIGMA³ SOUTHERN ARRAY FINAL REPORT TO DAVENPORT).....79

FIGURE 48: 9 SEPTEMBER 2013 16:40 GMT, 09:40:11 AM PDT SIGMA³ IMAGE IDENTIFIED AS A VIEW OF ENERGY MEASURED 16 HOURS PRIOR TO OPENING 46-16 WELLHEAD. THE BAR TOWARD THE BOTTOM OF THE IMAGE SHOWS A DARK LINE LABELED "9/9/2013 4:40:11 PM" WITH IMAGE IN GMT. THIS GMT WOULD EQUATE TO 09:40:11 AM PDT ON 9 SEPTEMBER 2013, AT WHICH TIME WELL 46-16 WAS FLOWING GAS PHASE (TABLE 2, THIS SECTION). NO DEPTH RANGE FOR SIGNAL PROCESSING IS PROVIDED. NO DEPTH RANGE FOR EARTHQUAKE (RED DOTS) OR MICROSEISMS ARE PROVIDED (SIGMA³ IMAGE, APPENDIX G: APEX HIPOINT SIGMA³ REPORTS TO DAVENPORT/NEWBERRY, MARCH 13, 2014 QUICK VIEW OF CURRENT STATUS).....81

FIGURE 49: SIGMA³ IMAGE IDENTIFIED AS A VIEW OF ENERGY MEASURED 2 HOURS IMMEDIATELY AFTER OPENING 46-16 WELLHEAD. THE BAR TOWARD THE BOTTOM OF THE IMAGE SHOWS A DARK LINE LABELED "9/9/2013 7:38:18 PM" WITH IMAGE TIME IN GMT. THIS GMT WOULD EQUATE TO 12:38:18 PM PDT ON 9 SEPTEMBER 2013, AT WHICH TIME WELL 46-16 WAS FLOWING LIQUID PHASE (TABLE 2, THIS SECTION). NO DEPTH RANGE FOR SIGNAL PROCESSING IS PROVIDED. NO DEPTH RANGE FOR EARTHQUAKE (RED DOTS) OR MICROSEISMS ARE PROVIDED. (SIGMA³ IMAGE, APPENDIX G: APEX HIPOINT SIGMA³ REPORTS TO DAVENPORT/NEWBERRY, MARCH 13, 2014 QUICK VIEW OF CURRENT STATUS).82

FIGURE 50: LARGE AMPLITUDE SIGNALS DETECTED BY THE NORTHERN ARRAY FOR A 20 HOUR PERIOD PRIOR TO, DURING AND AFTER THE FIRST FLOWING OF WELL NWG 46-16, 8 SEPTEMBER 2013. (SIGMA³, 2014 NEWBERRY FINAL REPORT, FIGURE 30).83

FIGURE 51: LARGE AMPLITUDE SIGNALS IN THE NORTHERN ARRAY FOR A 21 HOUR SPAN ON 9 SEPTEMBER 2013, INCLUDING PRIOR TO, DURING, AND AFTER FLOWING OF WELL NWG 46-16 (SIGMA³, 2014 NEWBERRY FINAL REPORT, FIGURE 31).....84

FIGURE 52: LARGE AMPLITUDE SIGNALS DETECTED BY THE NORTHERN ARRAY ONE DAY AFTER THE LAST FLOW TEST OF WELL NWG 46-16 FLOW TESTS, 11 SEPTEMBER 2013. (SIGMA³, 2014 NEWBERRY FINAL REPORT, FIGURE 32).85

FIGURE 53: LOWEST LEVEL OF SEISMIC AMPLITUDE ACTIVITY DETECTED IN THE NORTHERN ARRAY PRIOR TO OPENING WELL NWG 46-16, 8 SEPTEMBER 2014 (SIGMA³, 2014 NEWBERRY FINAL REPORT, FIGURE 37).86

FIGURE 54: LOWEST LEVEL OF SEISMIC AMPLITUDE ACTIVITY DETECTED IN THE NORTHERN ARRAY DURING AND SUBSEQUENT TO FLOWING OF WELL NWG 46-16 ON 8 SEPTEMBER 2014 (SIGMA³, 2014 NEWBERRY REPORT, FIGURE 38).87

FIGURE 55: LOWEST LEVEL OF SEISMIC AMPLITUDE ACTIVITY DETECTED IN THE NORTHERN ARRAY FOR A 24 HOUR PERIOD, PRIOR TO, DURING AND AFTER DURING FLOWING OF WELL NWG 46-16 ON 9 SEPTEMBER 2014 (SIGMA³, 2014, NEWBERRY REPORT, FIGURE 39).....88

FIGURE 56: LOWEST LEVEL OF SEISMIC AMPLITUDE ACTIVITY DETECTED IN THE NORTHERN ARRAY FOR A 24 HOUR PERIOD, PRIOR TO, DURING AND AFTER DURING FLOWING OF WELL NWG 46-16 ON 10 SEPTEMBER 2014 (SIGMA³, 2014 NEWBERRY REPORT, FIGURE 40).89

FIGURE 57: LOWEST LEVEL OF SEISMIC AMPLITUDE ACTIVITY DETECTED IN THE NORTHERN ARRAY FOR A 24 HOUR PERIOD, PRIOR TO, DURING AND AFTER DURING FLOWING OF WELL NWG 46-16 ON 12 SEPTEMBER 2014 (SIGMA³, 2014 NEWBERRY REPORT, FIGURE 42).90

FIGURE 58: 11:53 PDT 8 SEPTEMBER 2013, PRIOR TO FLOWING NWG 46-16. (SIGMA³, 2014 NEWBERRY REPORT).92

FIGURE 59: 14:53 PDT 8 SEPTEMBER 2013, WELL FLOWING "FIGURE 9 - 14:53 LOCAL TIME. PERSPECTIVE IS NORTH UP. SAME AS FIGURE 13, HOWEVER ONLY THE TOP 50% OF ENERGY IS IMAGED. THIS CORRESPONDS TO TIME 43 MINUTES AFTER OPENING OF THE VALVES. ONE NOTES FROM THIS PERSPECTIVE THAT THERE IS A CONSISTENT LASEA RESPONSE. WE SEE ACTIVITY AT FRACTURE ZONES A, B & C." (FROM SIGMA³ NEWBERRY REPORT)92

FIGURE 60: 14:53 PDT 8 SEPTEMBER 2013, WELL FLOWING. "FIGURE 10 - 14:53 LOCAL TIME. PERSPECTIVE IS NORTH UP. SAME PERSPECTIVE AS FIGURE 14, HOWEVER VISUALIZED USING CONVENTIONAL SPHERES WITH GRIDDED AMPLITUDES COLORED BY RELATIVE INTENSITY OF COHERENT AMPLITUDES. THIS CORRESPONDS TO TIME 43

MINUTES AFTER OPENING OF THE VALVES. ONE NOTES FROM THIS PERSPECTIVE THAT THERE IS A CONSISTENT LASEA RESPONSE. WE SEE ACTIVITY AT FRACTURE ZONES A, B & C." (SIGMA³, 2014 NEWBERRY FINAL REPORT)93

FIGURE 61: 14:53 PDT 8 SEPTEMBER 2013, WELL FLOWING, FIGURE 8 - 14:53 – LOCAL TIME. PERSPECTIVE IS NORTH UP. VISUALIZED USING HOTSPOT TECHNOLOGY. THIS CORRESPONDS TO TIME 43 MINUTES AFTER OPENING OF THE VALVES. ONE NOTES FROM THIS PERSPECTIVE THAT THERE IS A SIGNIFICANT RISE IS LASEA RESPONSE. WE SEE ACTIVITY AT FRACTURE ZONES A, B & C." (SIGMA³, 2014 NEWBERRY FINAL REPORT).93

FIGURE 62: 22:24 PDT 8 SEPTEMBER 2013, WELL SHUT IN AT 18:35 PDT, FIGURE 16 - 22:24 LOCAL TIME. PERSPECTIVE IS WEST UP. VISUALIZED USING CONVENTIONAL TECHNOLOGY. THIS CORRESPONDS TO THE LASEA RESPONSE FOUR (4) HOURS AFTER OF SHUT-IN (18:35) LOCAL. ONE CLEARLY SEES THE HIGHEST INTENSITY RESPONSE AT FRACTURE ZONES B & C, WITH SOME CONNECTIVITY TO ZONE A." (SIGMA³, 2014 NEWBERRY REPORT) COMPARISON OF THIS FIGURE WITH FIGURE 60 SHOWS THE LEFT PANEL IS ROTATED TO WEST RATHER THAN NORTH BEING UP, AND IS NOTED. THE LOWER RIGHT PANEL IS SUPPOSED TO BE PROVIDING A VIEW TO THE NORTH. THE DIRECTIONAL TRACE OF THE WELL IS TO THE SOUTH AND WEST. THE LOWER RIGHT PANEL MAY ACTUALLY BE PRESENTING A VIEW TO THE SOUTH, WITH WEST TO THE RIGHT, RATHER THAN A VIEW TO THE NORTH.....94

FIGURE 63: 14:34 PDT 10 SEPTEMBER 2013, WELL FLOWING "FIGURE 21 - 14:34. SHUT WELL IN AT 14:14 TO ATTACH GAS SAMPLE BOTTLE. NORTH UP. TOP 50% ENERGY" (SIGMA³, 2014 NEWBERRY REPORT).95

APPENDIX A, FIGURE 1: HISTOGRAM OF THE MONTE CARLO METHOD CALCULATED HORNER TEMPERATURES FOR R² VALUES BETWEEN 0.9 AND 1.0. LEFT AXIS IS THE NUMBER OF OCCURRENCES.4

APPENDIX A, FIGURE 2: FROM BIRCH AND CLARK, 1940, FIGURE 4. THE TEMPERATURE DEPENDENT THERMAL CONDUCTIVITY OF VARIOUS ROCK TYPES IS SHOWN. NOTE UNITS ON THIS FIGURE ARE IN CAL/CM*SEC*DEG AND APPENDIX A TABLES 1-3 ARE IN W/M*K.....5

APPENDIX A, FIGURE 3: EXAMPLE OF HORNER TEMPERATURE CORRECTIONS. THE Y-INTERCEPT OF 311.75 REPRESENTS THE CORRECTED TEMPERATURE.6

APPENDIX A, FIGURE 4: TEMPERATURE DEPTH DATA FROM 46-16 IN FEET AND °F. THE BLACK DASHED LINE IS FROM METHOD 1 (CONSTANT GRADIENT EXTRAPOLATION), THE BLACK DOT IS FROM METHOD 2 (HORNER CORRECTION), PURPLE CURVE IS FROM METHOD 3 (THERMAL CONDUCTIVITY CALCULATED GRADIENTS). THE EQUILIBRIUM TEMPERATURE DATA FROM 55-29 IS PLOTTED FOR REFERENCE.7

APPENDIX A, FIGURE 5: TEMPERATURE DEPTH DATA FROM 46-16 IN METERS AND °C. THE BLACK DASHED LINE IS FROM METHOD 1 (CONSTANT GRADIENT EXTRAPOLATION), THE BLACK DOT IS FROM METHOD 2 (HORNER CORRECTION), PURPLE CURVE IS FROM METHOD 3 (THERMAL CONDUCTIVITY CALCULATED GRADIENTS). THE EQUILIBRIUM TEMPERATURE DATA FROM 55-29 IS PLOTTED FOR REFERENCE.8

LIST OF TABLES

TABLE 1: ESTIMATED EGS POTENTIAL FOR DAVENPORT LEASE AREA ON WEST SIDE OF NEWBERRY VOLCANO AT 10,000 FEET AND 12,000 FEET DEPTHS.....72

TABLE 2: 46-16 FLOW CYCLE TIMING80

APPENDIX A, TABLE 1: HEAT FLOW FOR WELL 55-29.1

APPENDIX A, TABLE 2: THERMAL CONDUCTIVITY, EQUILIBRIUM TEMPERATURE MEASUREMENTS, AND HEAT FLOW FOR WELL 46-162

APPENDIX A, TABLE 3: THERMAL CONDUCTIVITY RESULTS AND CALCULATED HEAT FLOW FOR 46-16. CALCULATED INTERVAL GRADIENTS ASSUME CONSTANT HEAT FLOW WITH DEPTH (NOTE THE HEAT FLOW VALUE OF 180.9 USED TO CALCULATE THE GRADIENT IS FROM TABLE 2 ABOVE).2

INTRODUCTION

Newberry Volcano (Figure 1 and Figure 2) has been the focus for geothermal exploration for more than thirty-five years. The main attraction for geothermal explorers has been the size of the volcano, the long history of volcanic eruptions, and the silicic character of the caldera-centered Holocene lavas. Perceived conflicting cultural use of the volcano by various interests was resolved in 1990 with the passage of the Newberry National Volcanic Monument (NNVM) legislation, which set aside the central part of the volcano, including the caldera and related young volcanic vent areas to the north, as a national monument, to be administered by the U.S. Forest Service. The legislation specifically designated the area outside the monument as open for timber harvest and for geothermal exploration.

Newberry Volcano (Figure 1 and Figure 2) is a Pleistocene to Holocene large bimodal volcano with a central nested caldera structure. It is located in central Oregon near the juncture of three geologic provinces, the Cascade Range, the High Lava Plains portion of the Basin and Range, and the Blue Mountains (Jensen, 2006; MacLeod et al., 1995). The most recent eruption occurred within the caldera 1,350 years ago. Holocene silicic and basaltic volcanism attracted geothermal interest to the volcano by the early 1970s. High temperature gradients were observed in temperature gradient holes drilled on the upper west flank of the volcano (Oregon Department of Geology and Mineral Industries). This west flank thermal anomaly has no expression at the surface, either active or fossil. It is a true "blind" prospect. Exploration for geothermal drilling targets in a true "blind" geothermal area has its challenges. These high temperature gradients, however, led to four deep exploration wells being drilled, all on the upper northwestern flank of the volcano. Three of the deep wells encountered high temperatures (California Energy Co. well CE 23-22, 550°F; California Energy Co. well CE 86-21, 600°F; and Davenport well NWG 55-29, 625°F) though little or no flow. The fourth well (Davenport 46-16) intersected fractures hosting a flow of hydrothermal fluids, has a projected bottom-hole temperature of between 600 and 635°F, and has a shut-in well-head pressure of 575 to 600 psi (Waibel et al., 2012).

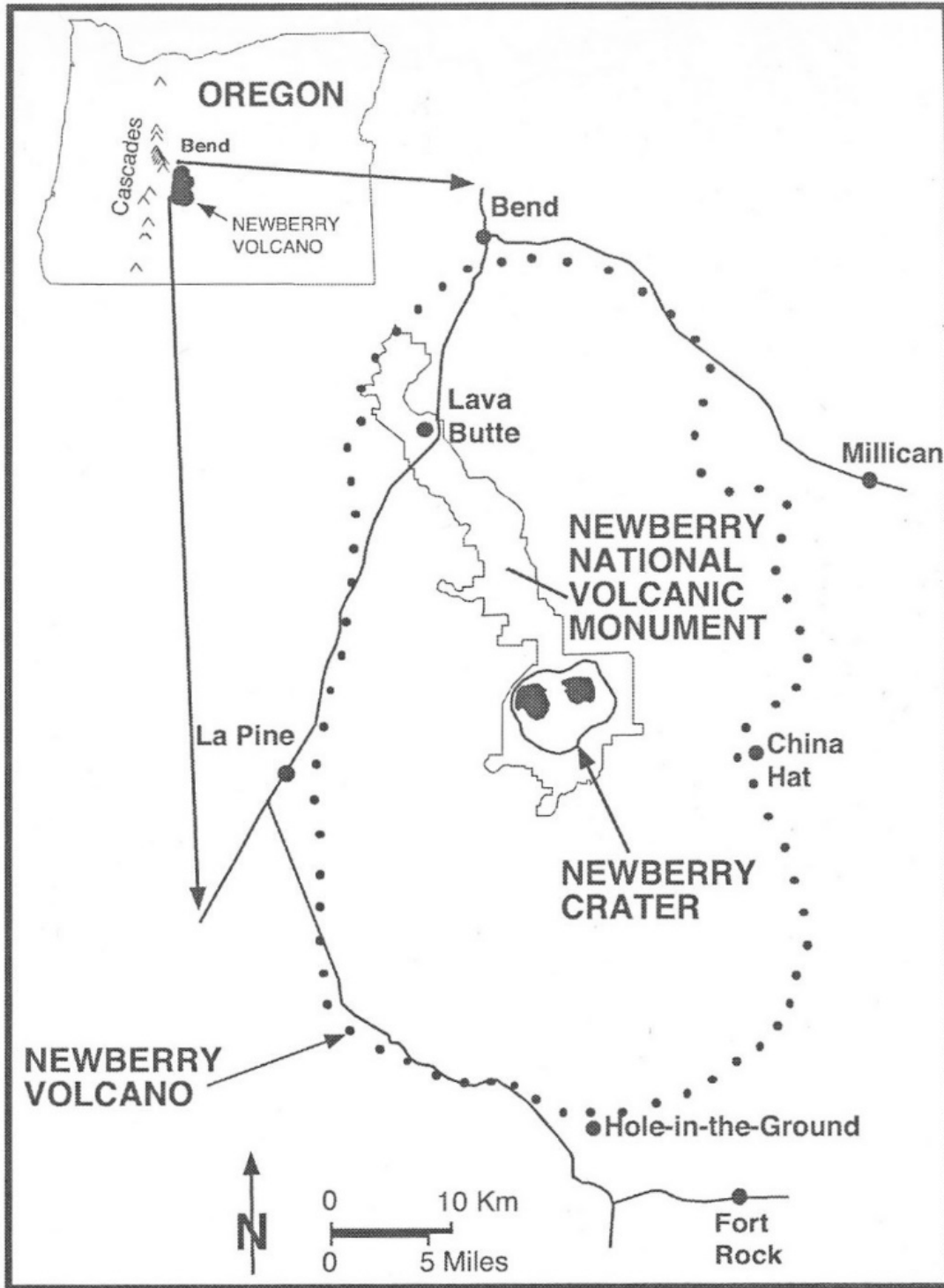


Figure 1: Location of Newberry Volcano, Oregon (from Jensen, 2006).

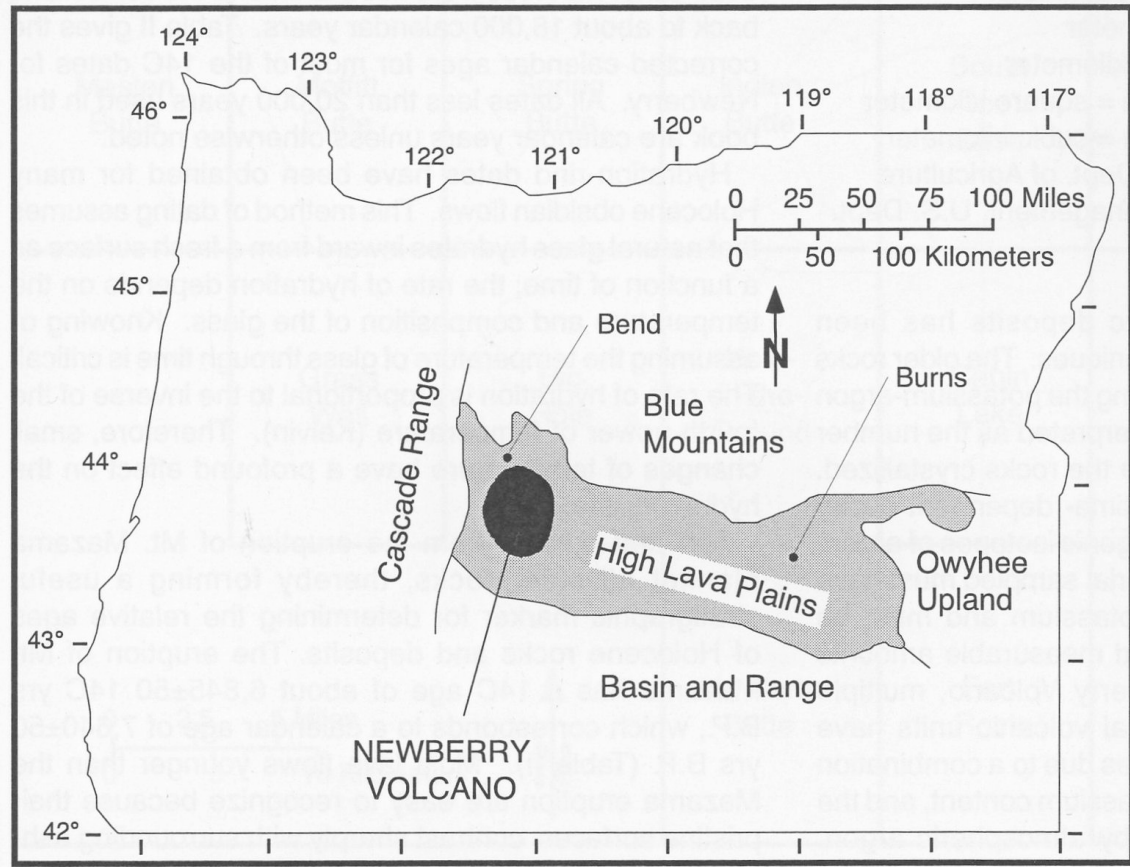


Figure 2: Geologic Setting of Newberry Volcano (from Jensen, 2006).

PREVIOUS EXPLORATION

The first documentation of Europeans to visit the caldera of Newberry Volcano is in the Journals of Peter Skene Ogden (Davies and Johnson, 1961). It is noted in his journals that on the 16th of November 1826 his trapping party entered the caldera from the east (Davies, 1961, p. 26). The earliest geologic reports addressing the geology of Newberry Volcano were Russell (1905) and Williams (1935, 1957). Russell described the volcano and named it after John Newberry, a scientist with the Williamson portion of the Pacific Railroad Survey whose work included the central Oregon area. Howell Williams conducted more detailed geologic and petrologic work on the lavas of Newberry Volcano (1935) and published a broader geologic map of the central Oregon area, including the volcano (1957). Multiple investigations related to the geology, geochemistry and petrology were conducted in the 1960s and 1970s, including Beyer (1973) and Higgins (1973). The most extensive of these published works is a detailed geologic map of Newberry Volcano (MacLeod et al., 1982 & 1995) (Figure 3). The MacLeod work on Newberry Volcano included drilling two stratigraphic test wells in 1981, Newberry 1 at Red Hill on the eastern upper flank of the volcano, and Newberry 2 near the center of the caldera (Keith and Bargar, 1988; J.C. Eichelberger, unpublished notes). A section of a Journal of Geophysical Research was dedicated to publishing results of various research on Newberry Volcano by the USGS, universities and technical groups (JGR Vol. 93, No. B9, 1988). Currently Donnelly-Nolan (USGS) and Jensen

(USFS ret.) are completing a detailed geological mapping, petrological and geochemical study of the entirety of Newberry Volcano. More recently Zachary Frone has completed his PhD studies of the petrology and geochemistry of core and cuttings recovered from drill holes on the volcano (Frone et al., 2014; Frone, 2014).

Geothermal evaluation of Newberry Volcano began in the late 1970s with Occidental Petroleum's geothermal group (later Santa Fe), Phillips Petroleum, Sunedco, GRI (GEO Newberry), California Energy Co. and Union. Efforts by these groups ranged from geologic mapping, geochemical evaluations and geophysical surveys. Temperature gradient holes drilled to 2,000 ft or greater were completed by Occidental, GRI, California Energy Co., and Union in the 1980's. Data from these wells identified a large area underlying the upper west flank of the volcano with high thermal gradients. Figure 3 shows the locations of the wells drilled on the central and western portions of Newberry Volcano.

In 1976 both the Newberry Known Geothermal Resource Area (KGRA) and the Newberry Crater National Natural Landmark were created. These designations formalized conflicting use agendas of the Newberry Volcano area. Data from stratigraphic test and temperature gradient holes completed in the 1980s documented a large high-temperature exploration target on Newberry Volcano. This brought overlapping and potentially conflicting land use issues by conservation groups, recreational industry, timber industry and geothermal industry to the forefront.

The central caldera part of Newberry Volcano was considered for National Monument status in 1989, and a Monument Committee was formed. The Monument Committee was made up of representatives of all interested groups, including the geothermal, timber and recreational industries and the local area environmental groups. In 1990 the central caldera and a narrow band of land running north from the volcano to Lava Butte was designated Newberry National Volcanic Monument. Through a geothermal lease swap, geothermal exploration and development was removed from all Forest Service land within the newly created Newberry National Volcanic Monument. The agreement reached and the enforcing legislation identified the land outside the monument as appropriate for geothermal exploration and development (Newberry National Volcanic Monument legislation, section 8). The legislation also designated the U.S. Forest Service as manager of the monument.

Northwest Geothermal Company, operated by Davenport Power, LLC (now Davenport Holdings), began a systematic exploration program in 2006. The first phase consisted of integrating all available data. Based on the results of these data, gravity and MT surveys were conducted, centered on the western flank of the volcano. In 2008 two deep exploration wells were drilled. The first, well NWG 55-29, encountered high temperatures, but had no sustained fluid flow. The second, NWG 46-16, encountered both high temperatures and substantive evidence of fractures hosting hydrothermal fluid flow. However, a bridge in the well formed during the rig well test, halting the test before a full flow test was completed.

Davenport applied for and was awarded a DOE grant to test innovative geothermal exploration procedures (Grant 109 Project) in 2010. Moneys were released in the latter part of 2010, and a limited amount of work began before winter weather closed access for the season. In 2011 and 2012 several drilling activities were initiated, including: gravity, MT and shallow sections of seven Temperature Gradient (TG) holes were drilled and cased, to accommodate microseismic

monitoring. The first of two arrays for microseismic monitoring was conducted in late 2012. The second of the arrays was carried out in September of 2013, completing the DOE-coupled geothermal program on Newberry Volcano.

DOE INNOVATIVE EXPLORATION TECHNOLOGY (IET) Grant 109

Davenport was awarded a DOE grant 109 in 2010 to conduct a combination of traditional and innovative geothermal exploration tools on Newberry Volcano. The project objectives were:

"Applicant seeks to develop an innovative exploration strategy that would lead to the commercial development of geothermal energy in the Cascade Range of the Pacific Northwest, where shallow meteoric water movement effectively hides underlying hot plutons and their associated geothermal systems. A combination of cutting-edge traditional, adapted and established exploration techniques will be applied to delineate a hot shallow pluton on the flank of Newberry Volcano and identify which portions of the pluton host convection of geothermal fluid. The immediate benefits of this program will be to locate "blind" (no surface indications) geothermal systems for commercial power production at Newberry Volcano. The long-term benefits of this program will be to provide a combination of exploration tools that can be applied throughout the Cascade Range and elsewhere to locate and develop "blind" geothermal resources."

(Davenport proposal submitted to the DOE)

The proposed approach:

"The Cascade Range of the Pacific Northwest is rife with young volcanism and high heat flow. Yet, to date, sporadic exploration has not led to commercial geothermal development. One of the significant impediments to exploration in this area is the deep downward percolation of cold meteoric water, effectively masking deeper geothermal systems. Overcoming this exploration barrier requires reassessment of traditional exploration tools and some newly developed and newly adapted exploration techniques. On the western flank of Newberry Volcano, temperature gradient holes have identified a large thermal anomaly with no surface indications of the underlying heat. Subsequent deep exploration drilling encountered a hot shallow pluton. A total of four deep exploration holes have been drilled on the northeastern portion of this large thermal anomaly. The problem is how to effectively explore for geothermal systems associated with hot shallow plutons that have no surface leakage. The flank of Newberry Volcano provides an ideal setting to test a combination of exploration techniques.

An innovative exploration strategy, applying a combination of cutting-edge and traditional technology, has been designed to overcome the past exploration impediments encountered in this geologic setting. Modeling of data from U.S.G.S. and industry sources has been used to identify a key combination of information required to target and drill these blind geothermal resources.

Applicant is proposing a five-step combination that we believe has not been used before:

- (1) identify the geometry of the pluton;
- (2) identify the electrical resistivity associated with the pluton;
- (3) locate areas of fluid movement in and around the pluton using three-dimensional tools;
- (4) measure the heat associated with various parts of the pluton; and

- (5) look for geochemical indications for degassing of circulating geothermal fluid.

The first two steps apply traditional gravity and MT surveys, though at much higher density than typical. The third step employs patent pending, 3-D seismic measurement tools that have been successful in detecting oil and gas movement through fractures in hydrocarbon exploration. Newberry believes that this pioneering use of geothermal seismic monitoring tools can detect geothermal resources in a way that would significantly decrease drilling risk across the industry. The fourth step uses strategies for detecting deep degassing of geothermal fluid. Special flux measurement equipment will be used at the temperature gradient well sites to sample for CO₂ degassing from depth while the deeper portions of the wells are drilled. Secondary mineral samples collected from the temperature gradient well core will be analyzed for stable carbon, oxygen and sulfur isotopes, looking for isotope fractionation during geothermal fluid degassing. X-R diffraction analyses will be used to characterize the thermal history of the cored rock. The fifth step will use temperature gradient data to map out the thermal characteristics across the pluton. The resulting model will be used to identify hot areas associated with the pluton that has fluid moving through fractures and is discharging gasses. One additional innovation designed into this program is multiple-use of temperature gradient drilling. The upper portion of the wells will be used for the 3-D seismic array. CO₂ flux measurements will be employed during drilling of these holes, and the completed wells will provide the very valuable temperature profiles. This strategy will reduce both the cost and the time required for the exploration program."

(Davenport proposal submitted to the DOE)

LIDAR coverage for the western portion of Newberry Volcano became available during the initial year of the program. This unanticipated dataset proved a valuable integrated component of the program.

Two events have adversely affected the ability of Davenport to fully complete the Newberry Volcano geothermal program. The first, timing of the release of funding, disrupted the scheduling in the signed contract with the drilling company. The second, a marked drop in the price of natural gas, changed the economic viability of geothermal development projects for financial investment firms that are the backers of geothermal development. The first event would only have resulted in a delayed program except for the subsequent sharp change in economic projections of the cost of electricity. The financial investment partners in the Davenport Newberry Volcano project made the strategic decision to curtail funding for the program. This decision has resulted in the Davenport Newberry Volcano geothermal program being closed with only partial completion of the original goals. The program, however, has resulted in some important strategic re-evaluations of the methodologies for geothermal exploration in volcanic terrain, both for resources with no surface expressions (blind) and for resources with surface expressions. The incomplete portion of the program entails deepening the seven temperature gradient holes to their final completion depths, the geochemical studies associated with coring the deeper portions of the temperature gradient wells, and the identification of a deep exploration drilling target. The seven temperature gradient wells with the shallow cased section completed will not be deepened to the originally proposed depths at this time.

The results from the exploration work completed with this grant are integrated within the relevant sections throughout this report. An evaluation of each exploration technique applied is described

in the section titled "Evaluation of Exploration Methods for Blind Geothermal Resources in Volcanic Terrain, Grant 109".

GEOLOGY

Newberry Volcano in Deschutes County, Oregon, is a large bi-modal Quaternary volcano with a central caldera approximately 6.5 by 8 km (4 by 5 miles) across (Figure 1). The volcano is situated near the junction of three geologic provinces and is bounded along the north by the Brothers Fault Zone. Newberry Volcano has been active for approximately the last 600,000 years.

The volcano is located in an area that has been volcanically active since late Eocene time with lithologies dominated by bimodal volcanism depositing lavas, pyroclastic layers, tephra layers and volcanoclastic sediments. The volcanic rocks of the John Day formation extend through into the Newberry Volcano area, with major calderas in the Powell Butte and Prineville areas. Sherrod et al. (2004) describe up to 4,300 meters of rhyolite, basalt, andesite tuffs and related pyroclastic and sedimentary deposits of John Day material in the Bend quadrangle, just to the north of Newberry Volcano. Unconformably overlying the John Day Formation are basalt flows and silicic volcanic products of the Miocene Mescall Formation. Above the Mescall Formation lie the mafic and silicic volcanic rocks of the Pliocene Deschutes Formation, followed by Pliocene to Recent post-Deschutes lavas, pyroclastic deposits and volcanic sedimentary deposits. Portions of the above formations had been projected and reasonably anticipated to underlie the flanks of Newberry Volcano.

The expansive moderately sloping north and south flanks of the volcano are composed predominantly of basalt and basaltic andesite lava flows, pyroclastic deposits and cinder cones. The east and west slopes are made up of silicic tuffs and lahars, in addition to basaltic lava and minor cinder cones. The central highlands are constructed largely of silicic lavas and pyroclastic deposits, with lesser amounts of basaltic lava and cinder. The floor of the caldera is dominated by silicic lava and pumice, and basaltic maars. Silicic lavas on the western flank of the volcano (i.e. McKay Butte Domes, West Flank Dome, Southwest Flank Dome) date from 400,000 years before present (Qer and Qrd, Figure 3). The most recent major caldera-related eruptions resulting in significant ash and pyroclastic deposits occurred approximately 300,000 and 80,000 years ago. A large-volume basaltic eruption occurred about 78,000 years ago, resulting in the extensive Bend Lavas which covered an area some 20 miles to the north of the central caldera. About 6,000 years ago, numerous basaltic eruptions occurred along the northwest fracture zone. The most recent eruption, a silicic obsidian flow and associated pumice fall vented from within the caldera, has been dated at 1,350 ybp (Jensen, 2006; MacLeod et al., 1995).

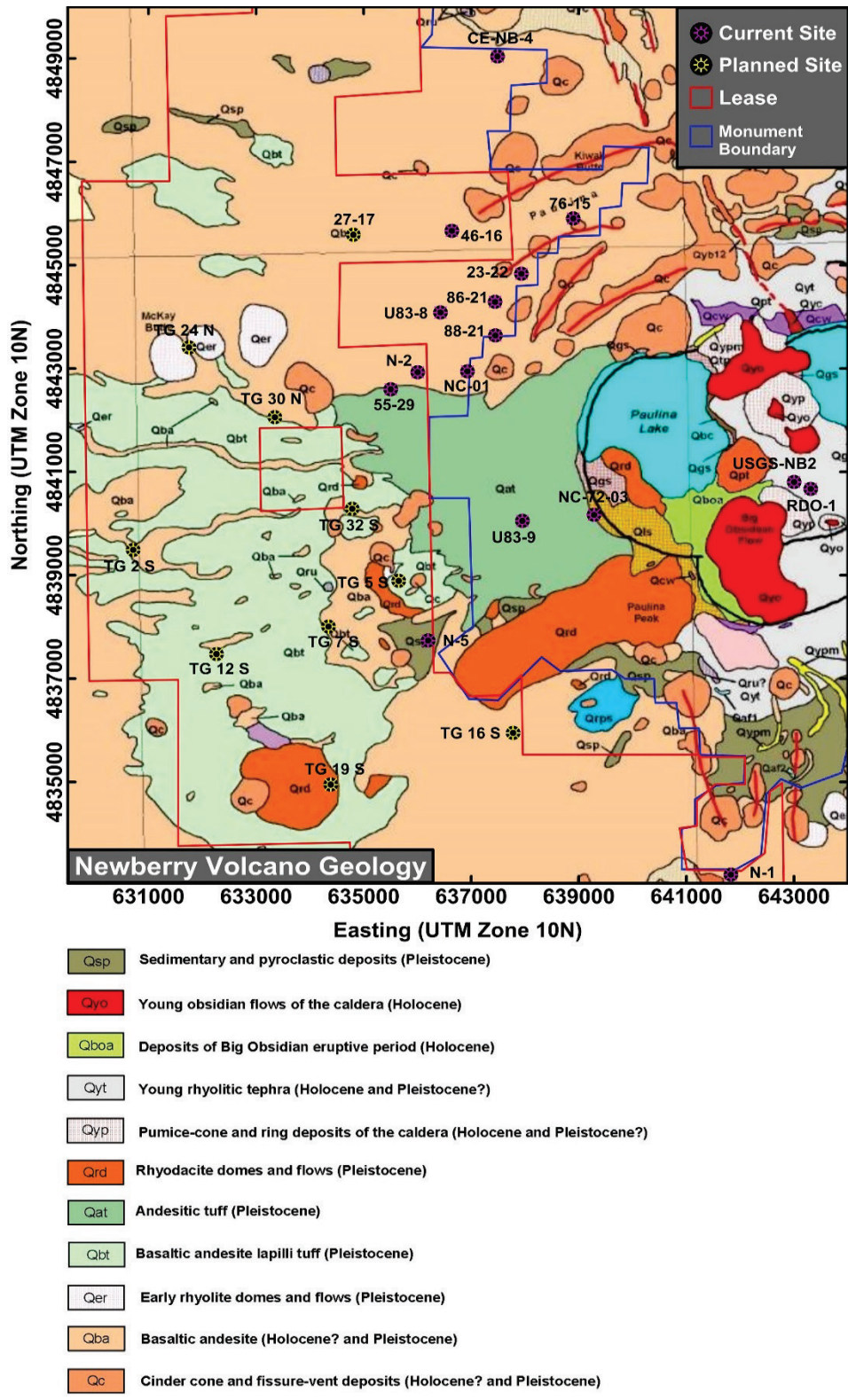


Figure 3: Geologic Map of the western flank of Newberry Volcano, Oregon (after MacLeod et al., 1995). Ring fractures of volcanic vents shown as east-west trending red curved lines just northwest of Paulina Lake.

Two geologic structural patterns dominate the area of Newberry Volcano. First is the volcanic and caldera-related structure of Newberry Volcano itself. Second is the roughly northwest and northeast trending fault pattern of the Basin-and-Range. The west-northwest trending Brothers Fault Zone structure does not appear to extend southward through the volcano. Arcuate vent crater and ring-fracture patterns are the most dominant structural features of the upper central portion of the volcano. The caldera is a nested caldera, a composite of a number of overlapping smaller explosive volcanic eruption craters. Arcuate vent patterns on the upper northwestern flank have been interpreted as ring faults associated with the caldera development. These are identified more by arcuate vent patterns rather than by identifiable fracture or fault traces, and show no surface evidence of off-set. The deep California Energy Company test wells were designed to intersect these "ring faults" at depth. The well data provided no clear evidence of ring fault intersects. Lahar deposits from the volcano and a thick mantle of ash from the eruption of Mt. Mazama (Crater Lake) about 6,000 years ago tend to hide or obscure most structural features on the flanks of the volcano.

Extensional fault patterns of the Basin-and-Range province dominate the surface morphology south and east of Newberry Volcano. This pattern extends through the volcano and becomes obscure as it intersects the Cascade Range. The trend of this extensional faulting is generally northwest and northeast in the vicinity of Newberry Volcano. Vents for the series of basaltic andesite eruptions that occurred about 7,000 years ago are aligned to the Basin-and-Range fault pattern. The vents reach from Lava Butte, along Highway 97 well off the northwest flank of Newberry Volcano, to vents and fissures across the upper north flank and into the caldera, to vents on the southern flank of the volcano. The vent patterns of these eruptions suggest that the Basin-and-Range structure may survive as an active tectonic feature, with the volcano overlaid.

DEEP EXPLORATION WELLS

Four deep exploration test wells have been completed on the upper northwestern flank of Newberry Volcano: two drilled by California Energy Company (CE 23-22 and CE 86-21) and two drilled by Davenport (NWG 46-16 and NWG 55-29) (Figure 4). The California Energy Company wells were drilled in the mid-1990s. Davenport drilled their wells in 2008. All four wells exhibited high bottom-hole temperatures, ranging from 288 to 330°C (550 to 625°F). Progressive changes in the rock mechanics are observed in each of the wells. Lithification due to increasing lithostatic load with depth and metamorphism due to increased temperatures with depth progressively changes the mechanical character of the rock. The potential to sustain open fractures in areas of local or tectonic strain increases with these changes associated with increased temperature and pressure.

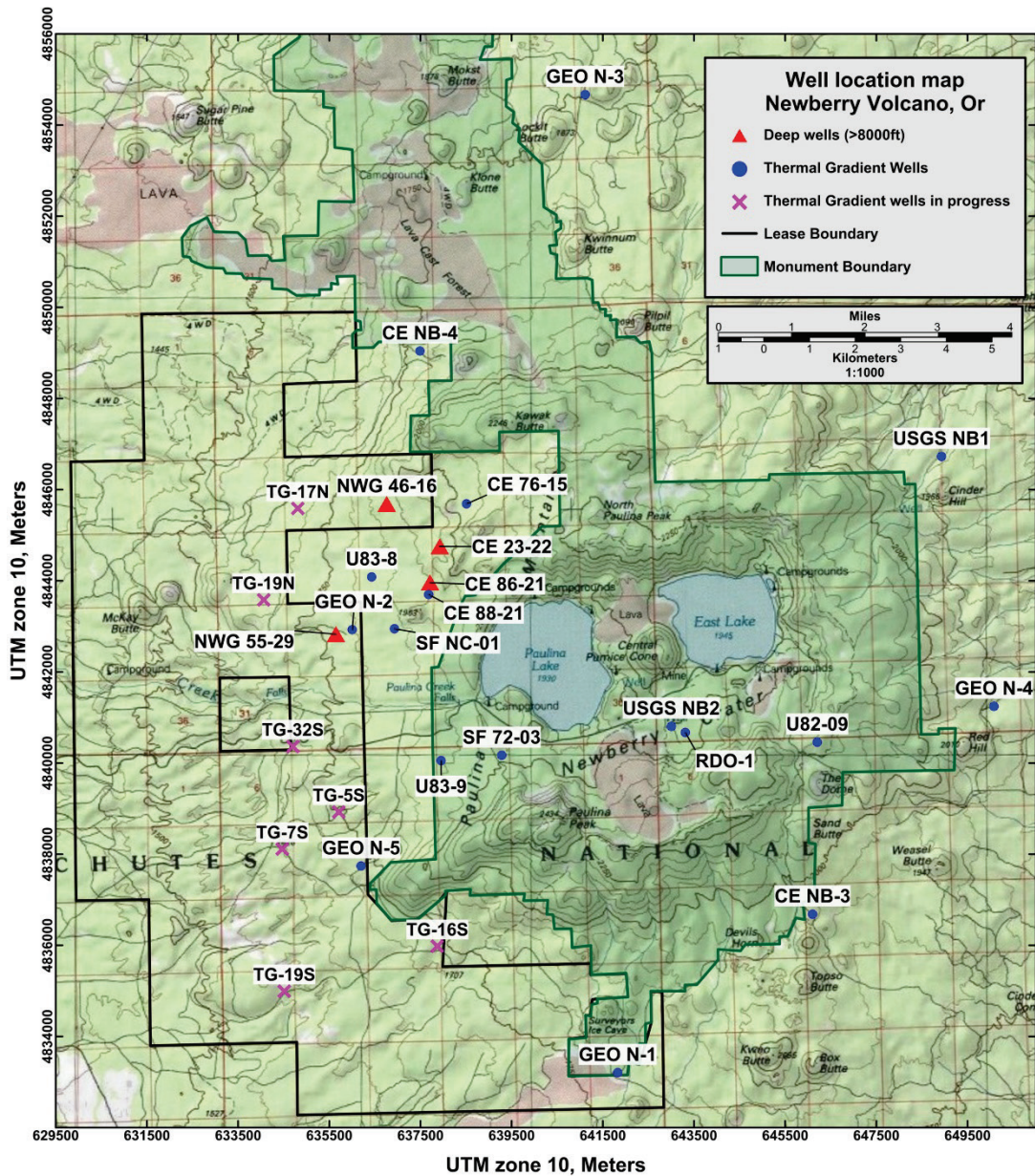


Figure 4: Well location map: Red triangles are deep exploration test wells. Blue dots are temperature gradient and shallow test wells. Red x are incomplete Davenport temperature gradient wells, cased to accommodate microseismic monitoring. These wells have not been drilled to permitted depth, and are not deep enough to provide temperature gradient data.

The lithologies of the wells show wells CE 23-22 and CE 86-21 penetrated Newberry Volcano-related granodiorite (tentatively dated at 300,000 ybp, Donnelly-Nolan, personal communication). Well NWG 55-29 penetrated thermally metamorphosed volcanic rock and subvolcanic dikes associated with Newberry Volcano plutons. Well NWG 46-16 was drilled entirely in volcanic and volcanoclastic rock (Davenport data base). Available geophysical logs show the lower sections of all four wells are characterized by high gamma radiation and high density. Figure 5 shows gamma

and density logs comparisons between the two Davenport deep exploration wells. Figure 6 shows the gamma logs for six key wells located in the upper northeast portion of the west flank (see Figure 4 for locations). Natural gamma radiation from the rock is emitted from unstable nuclides of uranium, thorium and potassium. High gamma radiation implies silicic igneous rocks and high density implies dense crystalline rock. Both of the geophysical parameters agree with lithologic descriptions of the rock from all four wells. Gamma logs from proximal wells in many geologic settings are used to identify specific formations from well to well, the basis for a 3-D view of the subsurface geology. This formation boundary identification does not work as well in volcanic terrain with multiple volcanic centers over millions of years. This is particularly true for the west flank of Newberry Volcano where underlying plutons suggest deeper stratigraphic turmoil underlying overlapping eruption craters. On the west flank, older eruptive craters have been filled in and obscured by subsequent phreatic eruptions.

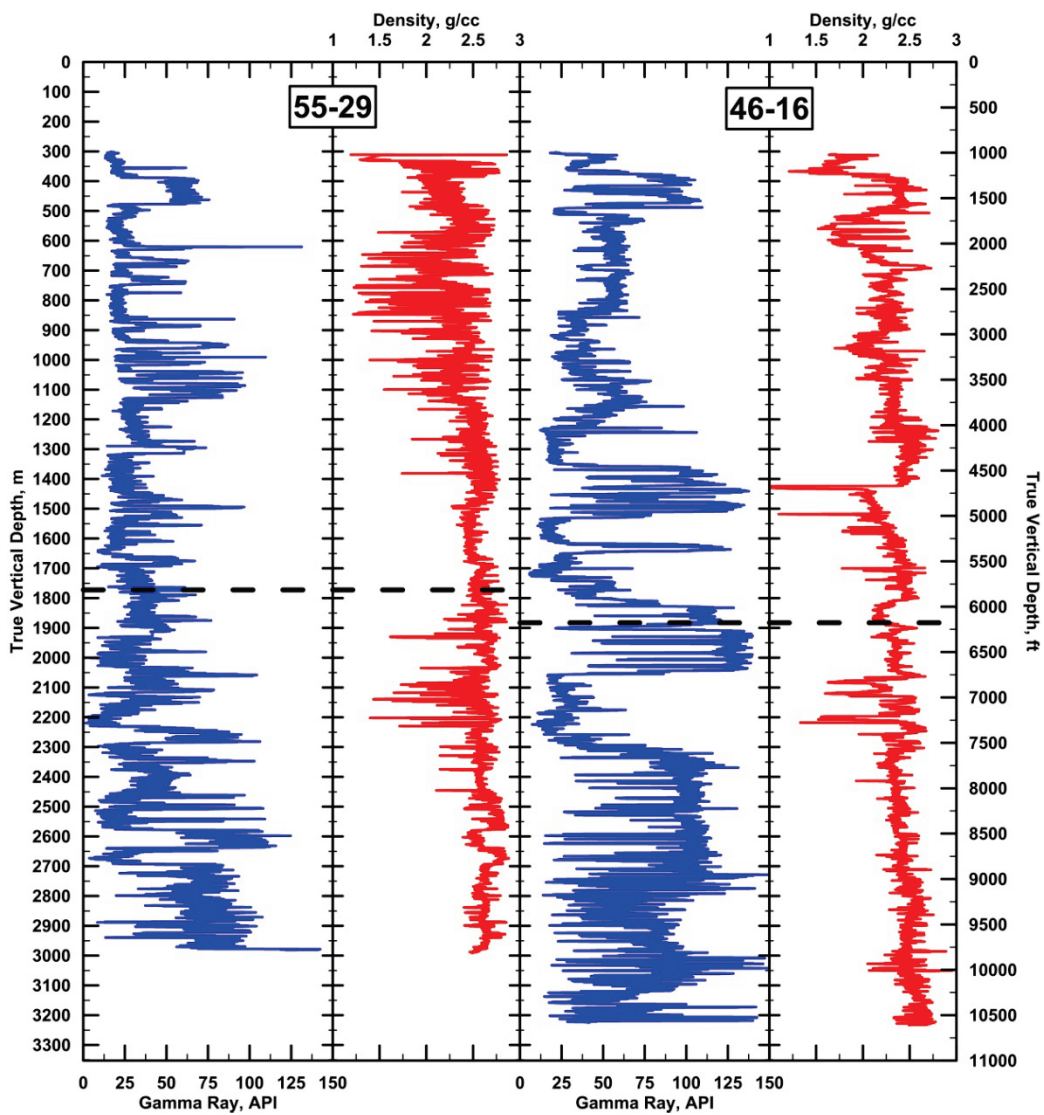


Figure 5: Density and Natural Gamma Ray logs of NWG wells 46-16 and 55-29.

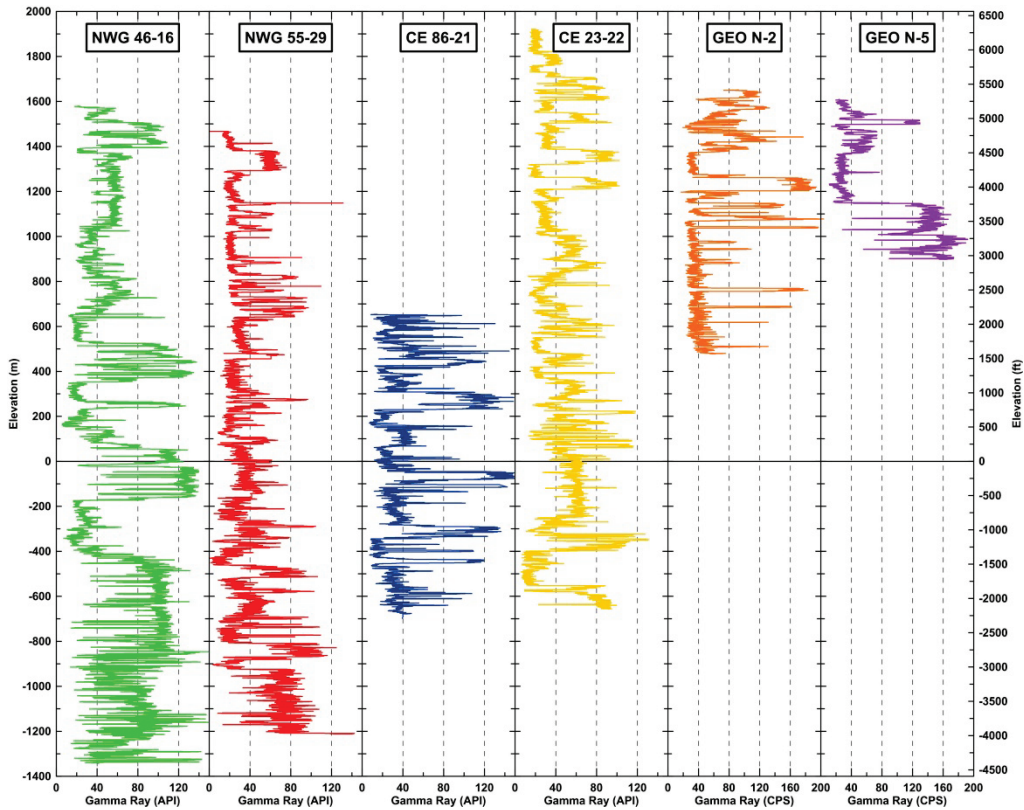


Figure 6: Natural Gamma Ray logs of six wells on the west side of Newberry Volcano. NWG 46-16 and 55-29 are Davenport wells. CE wells 86-21 and 23-22 are California Energy Co. wells. N-2 and N-5 are Geothermal Resources International (GRI) temperature gradient wells.

Mud logs show well CE 23-22 intersecting a granodiorite intrusion at 8,780 ft, and continued in the granodiorite to a depth of 9,602 ft (DOGAMI on-line data). The well had a reported bottom-hole temperature of 288°C (550°F), and had no indications of large-scale fracture permeability. The granodiorite is a holocrystalline intrusive rock, brittle and capable of sustaining fractures when stressed. Well CE 86-21 intersected a section of intrusive dikes and contact metamorphosed volcanic rock at a depth of 8,200 feet, and into granodiorite at a depth of 8,700 feet. The well had a reported bottom-hole temperature of 316°C (600°F). Figure 7 shows the thermal profiles for these two wells and the two Davenport wells. The thermally metamorphosed volcanic rock, the intrusive dikes and the granodiorite are all brittle and capable of sustaining fractures when stressed. The age of the granodiorite is tentatively placed at 300,000 ybp, old enough for the magmatic heat of the body to have significantly dissipated. The temperature in the granodiorite, therefore, likely is augmented by a younger hotter pluton of close proximity.

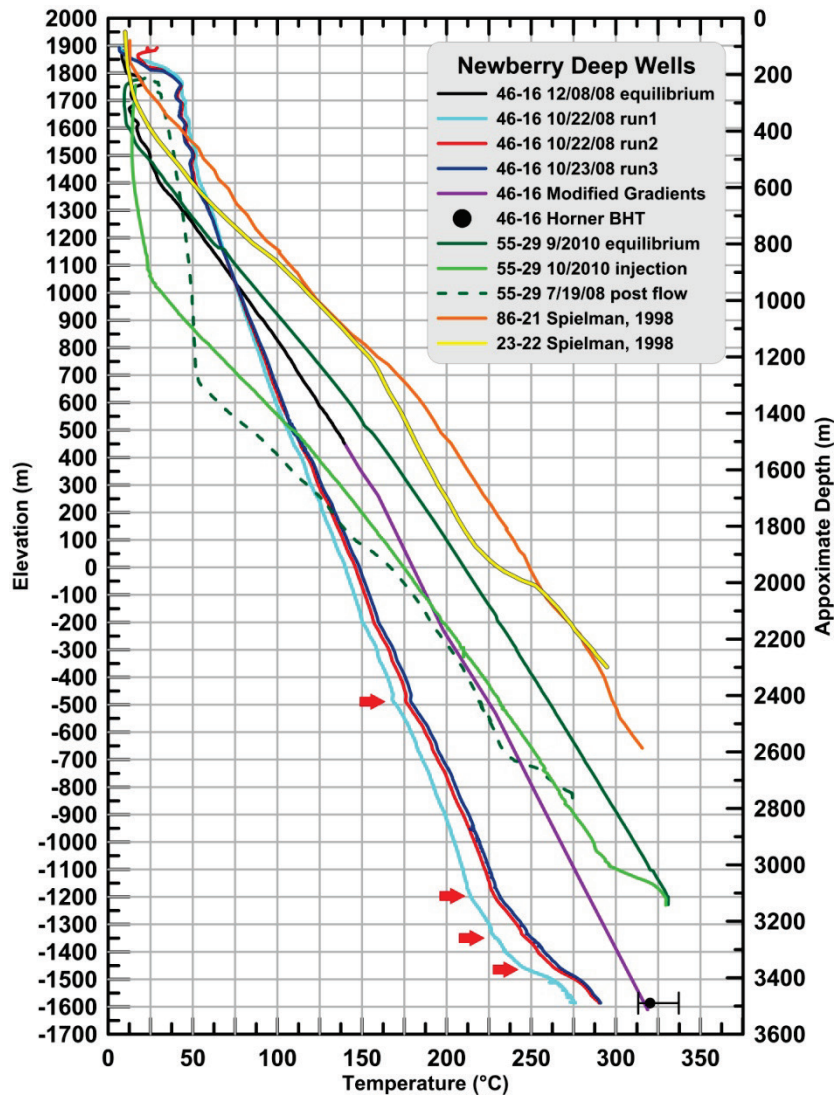


Figure 7: Temperature gradient profiles of the four deep exploration wells, NWG 46-16, NWG 55-29, CE 23-22 and CE 86-21. The equilibrium temperature profile for well 55-29 (green) shows a good straight conductive gradient without formation fluid flow. This matches well-site data observed while the drill hole was being drilled. The profiles for well NWG 46-16 (red and blue lines) show significant perturbation indicative of formation fluid flow affecting the temperature profile of the well. The profile for well 86-21 shows a dominant conductive gradient. The profile for well 23-22 shows a general conductive gradient with apparent convective influence between 1400 and 1900 m. It is not clear, however, if the measurement was taken under thermal equilibrium conditions. The red arrows are locations where D.D. Blackwell observed evidence in the temperature profiles of formation fluid flow.

Well NWG 55-29 encountered greenschist epidote facies thermally metamorphosed volcanic rock by a depth of 6,400 feet. Below 7,500 feet both silicic and basaltic subvolcanic dikes were encountered. The well has a measured bottom-hole temperature of more than 316°C (600°F). Small pulses of non-condensable gas (predominantly CO₂) were observed intermittently during drilling, and were more common below 9,200 ft. Drilling perturbations associated with the gas pulses were

observed by the driller. These data are interpreted to indicate fracture intersects. No evidence of hydrothermal fluid, fossil or current, were observed in the drill cuttings, and flow testing of the well eventually depleted fluid in the well. This indicates that open fractures were encountered in these wells, though they were isolated with no extended connectivity with larger fluid-bearing fracture systems.

Well NWG 46-16, the geothermal discovery well, is the only deep exploration well to have intersected hydrothermal fluid bearing fractures. It was drilled approximately 2 km WNW of well CE 23-22, and encountered epidote facies thermally metamorphosed volcanic rock at a depth of 7,200 ft. The well was drilled to a measured depth of 11,600 ft, and had an estimated bottom-hole temperature in excess of 316°C (600°F). The well was located to explore a westerly-striking linear gravity boundary. This well is located within two miles of the caldera boundary, further outward of this boundary than the two California Energy Company deep exploration wells. This is the only deep exploration well to have encountered a hydrothermal system. Druze epidote and epidote-quartz crystal clusters were observed in the cuttings at 7,330 ft., 7,360-70 ft, 9,280 ft, 9,350 ft, and ,9400 ft. Significant increases in gasses were observed in these zones, particularly pronounced in the 9,000-9,500 ft range (Figure 8). Non-thermally degradable lost circulation material (LCM) was intermittently added to the drilling fluid below a 120 bbl mud loss between 8,100 and 8,200 ft. The reason for adding LCM to the drilling fluid was to protect smaller fractures from being sealed with drilling mud. After logging of the hole the well could be tested and the LCM would be released from the fracture faces, allowing possible formation fluid to enter the well bore.

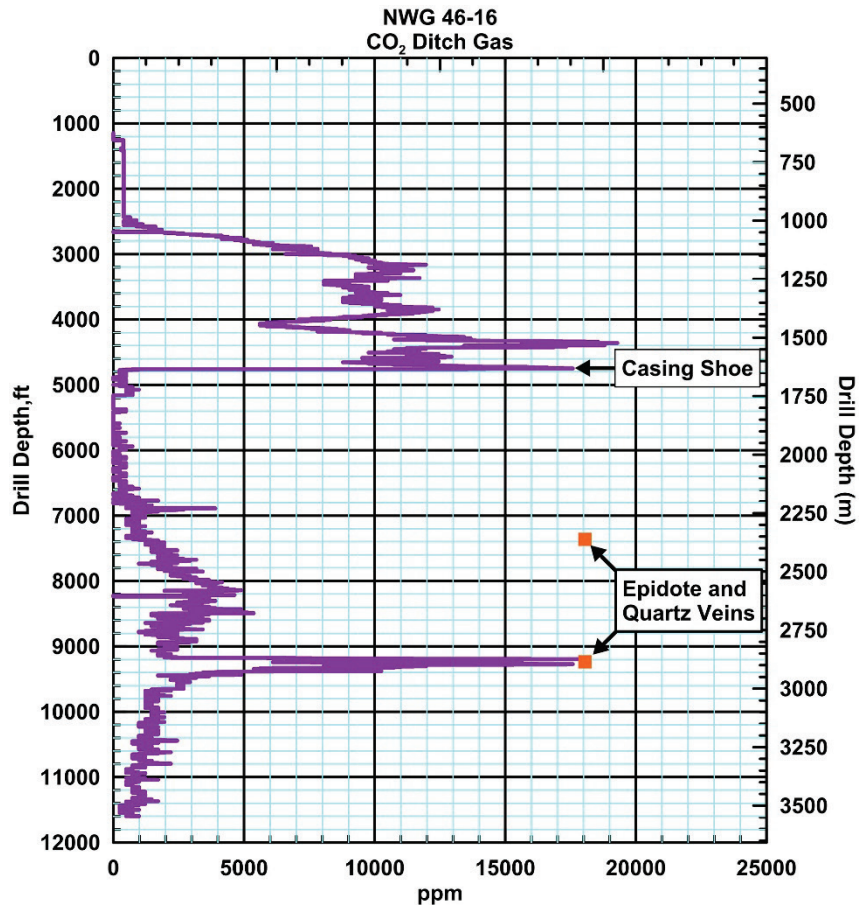


Figure 8: A graph showing CO₂ values measured by Epoch Mud logging during drilling of well NWG 46-16 (Epoch, 2008). To the right are noted the depth of the casing shoe and the location of hydrothermally precipitated druse quartz and epidote observed in the drill cuttings. The shallower occurrences of CO₂ are attributed to biogenic gas from organic matter within clastic layers.

A rig flow test was attempted upon reaching TD. The well was progressively unloaded using air from compressors. Fluid temperature increased with each step. Well stability problems were encountered during this flow test. Light gray to gray-green cemented crystal tuff encountered near 5000 ft began to fail and come into the hole when well bore fluid was markedly decreased. The tuff had been lithified from compaction. With a formation temperature of about 150°C (300°F), recrystallization is limited predominantly to phyllosilicates. Evidence of plastic shearing in the tuff was found in recovered rock fragments from the bridge, though no evidence of shear-related permeability is indicated. This cemented tuff does appear to have micro-porosity, with extremely limited permeability. This section of hole showed good stability during drilling, with high bore hole fluid pressure. Problems occurred when the bore hole fluid pressure dropped during the flow test. The most likely cause of formation failure/hole instability appears to be from pore-fluid pressure exceeding the formation strength when the fluid pressure in the well bore was reduced.

Formation fluid flow from hydrothermal fractures intersected by well NWG 46-16 has shown remarkable resilience in spite of well condition problems. Currently there are four mechanical conditions in the well that have the potential to restrict hydrothermal fluid flow. The bridge in well 46-16 creates a major constriction in the well bore. The bentonite component of the drilling mud entering formation fractures would be irreversibly thermally metamorphosed to illite, a non-swelling phyllosilicate. This transition is an effective method for constricting fracture permeability. LCM was added to the drilling fluid during drilling. There is no way of reliably estimating where the LCM is and how it may affect fracture permeability in the well at this time. Another unknown is the amount of lithic debris that has accumulated in the lower portion of the well, possibly restricting or blocking flow from any fractures in the bottom 1,000 ft of the well.

Approximately one year after the well was shut in it was discovered that the well was producing a steady flow of non-condensable gasses, and that the water level in the well had dropped to approximately 2070 ft below surface level with a well-head pressure of about 500 psi, measured while logging the well in 2009. After logging the well, the wellhead valve was opened for short periods of time to release the built-up pressure. The wellhead valve was closed, and the pressure built back up to near 600 psi within 3 to 4 hours. Shut-in wellhead pressure in well 55-29 was also measured at near 600 psi prior to EGS injection tests. Well 55-29 was shut in during May of 2013. As of the second week in August of 2013 the well-head pressure has built back up to 12 psi. Later monitoring showed a slow build-up of wellhead pressure, eventually returning to near 600 psi. This slow build-up of pressure can be accounted for by natural micro-fracture permeability in plutons and subvolcanic rock, augmented by hydrofracturing which occurred as part of an EGS experiment in well 55-29.

Well NWG 46-16 was opened again on the 8th, 9th and 10th of September, 2013, as part of the Sigma³ microseismic monitoring program. The program called for the well to be opened to bleed off the pressure for about four hours, then shut in to re-build well-head pressure. The goal of this exercise was to stimulate fluid flow within the hydrothermal fractures (see Low Amplitude Seismic Emission Analysis (LASEA) , below). The flow line was a four inch pipe with a 90 degree elbow at the end to direct the flow upward (Figure 9 and Figure 10). The well-head valve was opened and a strong flow of gas, reflective of the 600 psi, began. Gas flowed for almost 2 hours, at which time the pressure gage showed a reading of 300 psi. After almost two hours the flow changed abruptly from gas to light brown water, drilling fluid that had been left in the hole. The temperature of the liquid started out as slightly warm, increasing over time to quite warm, though not really hot. The flow of drilling mud lasted for about one and a quarter hours, then changing to gas with short bursts of very thick drilling mud. Variations on this pattern occurred each of the three daily flowing cycles. Total flow volume for the three days is estimated to be about 10,000 gal., about 1500 ft of volume in the 13 3/8 inch casing. This would equal about one half of that volume of water in the well between the pressurized water level (2070 ft below ground elevation) and the bridge below the casing shoe (5000 ft below ground elevation). Fluid flowed from the well from below the bridge would have passed through the bridge and past up through a substantial column of thermally equilibrated water/drilling mud (150°C (300°F)), at the bridge depth of 5000 ft, Figure 8). The limited flow volume for the three days was far too small to heat up the well bore enough to produce fluid with temperatures reflecting formation fracture fluid from the deeper part of the well.

Well NWG 46-16 Discussion

A few deductions can be made from the well-flowing episodes. Non-constable gas accumulating within the well bore reached a pressure of 600 psi because it was acting as a piston within the confines of the casing, pushing downward the liquid level within the well, pushing water back into formation fractures. A well-head pressure of 600 psi would indicate a depression of the water column of about 1000 ft. The very aggressive gas discharge through the 4-inch flow line is effected by the formation water pressure acting as the piston, pushing the gas out of the well. This action requires liquid flow upward through the bridge, which in turn would require water flow from the formation fractures into the well bore. The flow rate was too low through the bridge and four-inch flow line, and the upper well bore too cool, for steam "flashing" within the well bore to have contributed to the discharge. However, degassing of CO₂ within the liquid ascending within the well likely occurred. The combination of liquid flow from the formation into the well bore and exsolution of CO₂ within the water column appears to have been enough for the well to flow on each of the three days that the well was unloaded in September of 2013.

At this time there is little insight as to the condition of the bridge, other than it is permeable to both gas and liquid phase fluids. If any of the rock within the bridge were jostled during the flowing of the well, the noise should have been detected by the Sigma³ array. Both liquid and gas phases would have had to past through the bridge for the well to have flowed. This would require fluid to flow from formation fractures into the well bore during each flow event, and for gas to accumulate in the well between flow events.

The one-well intersect of hydrothermal fracture provides scant data regarding the geometry of the structure hosting the geothermal cell. Data from mining of fossil geothermal cells in similar volcanic settings do provide a generalized model of what one might anticipate.



Figure 9: Initial gas flow from well NWG 46-16. Note the endothermic reaction of gas decompressing, resulting in frost forming on the flow line when the valve is first opened (8 September 2013).



Figure 10: Drilling fluid flowing from the well NWG 46-16, approximately 45 minutes after the liquid flow commenced. (8 September 2013).

WELL DATA CORRELATIONS, GEOCHEMISTRY and PETROLOGY

Geochemistry

Rock chip samples from three exploration wells (NWG 55-29, NWG 46-16, and CE 23-22) and core samples from seven temperature gradient holes (N-1, N-2, N-3, N-4, N-5, NC-01 and NC-72-3) were analyzed in an attempt to identify and correlate lithologic units between the drill holes (Figure 4). For samples from the deeper portions of the wells, we analyzed for correlation with Oligocene to Pliocene formations cropping out in areas off the edge of the volcano, primarily to the North and Northeast. Sherrod et al. (2004) indicates that north of Newberry (Bend quadrangle) there is up to a 4.3 km thick section of the John Day formation, consisting of sandstones, shales, ash-flow and fall tuffs, lava flows, and rhyolite domes. The geologic map by MacLeod et al. (1995) suggests that these units extend beneath Newberry Volcano. Correlated and non-correlated

stratigraphy in the upper portions of the wells give insights into the eruptive history, depositional setting, and structure of the volcanic edifice. Correlations from deeper in the wells provide data on regional stratigraphy and the intrusive history of the volcano. In the following sections the locations of wellbore correlations are shown as elevation in meters with respect to sea level.

Cutting Samples

Rock samples from Northwest Geothermal wells NWG 55-29 and 46-16 were collected from well cuttings housed in the NWG office in Bend, Oregon. Cuttings were collected every 6.1 m (20 ft) in the shallow portions (above ~2,000 ft) of both wells. Below this depth cutting samples were collected every 3.05 m (10 ft). Each sample represents an averaged lithology for the interval. Cuttings samples from well CE 23-22 were analyzed by Julie Donnell-Nolan (USGS, unpublished). Additionally, samples from intervals between 2,313 to 2,920 m (7,590-9,580 ft) were provided by Alex Schriener, Jr. of CalEnergy for this study to compare with USGS values. Cutting samples for chemical analysis were chosen using the gamma ray and mud logs to identify zones with a relatively consistent lithology. For this study a total of 145 samples were collected: 85, 53, and 7 samples from wells NWG 55-29, NWG 46-16, and CE 23-22, respectively from 365 m (1,200 ft) to total depth. An additional 58 sample analyses for well 23-22 were contributed by the USGS, for a total of 203 samples. Samples were identified by well number followed by driller's (measured) depth. For example, the sample from well NWG 55-29 collected from 5,000 to 5,010 ft was coded 5529-5000.

Due to the mixed nature of the drill cuttings, each sample was viewed under a binocular microscope in order to identify the dominant rock type and sorted using two primary methods. The first method was grain picking with tweezers; generally larger grains (>~3 mm) were picked with this method. The second method involved sieving and sorting smaller grains using a magnetic separator. The magnetic separator separates grains primarily based on their iron content. In general, tuffs and silicic lithologies could be separated from mafic lithologies. However, some more intermediate lithologies were difficult to separate from mafic or silicic end members. In these cases, samples were sorted using the magnetic separator and were then picked with tweezers to remove selected grains. Sorted samples of between 7 and 15 g were sent to Acme Labs for analysis by Inductively Coupled Plasma Emission Spectrometer (ICP-ES) and Inductively Coupled Plasma Mass Spectrometer (ICP-MS). A total of 59 elements and loss on ignition (LOI) were analyzed. Raw data is presented in APPENDIX B.

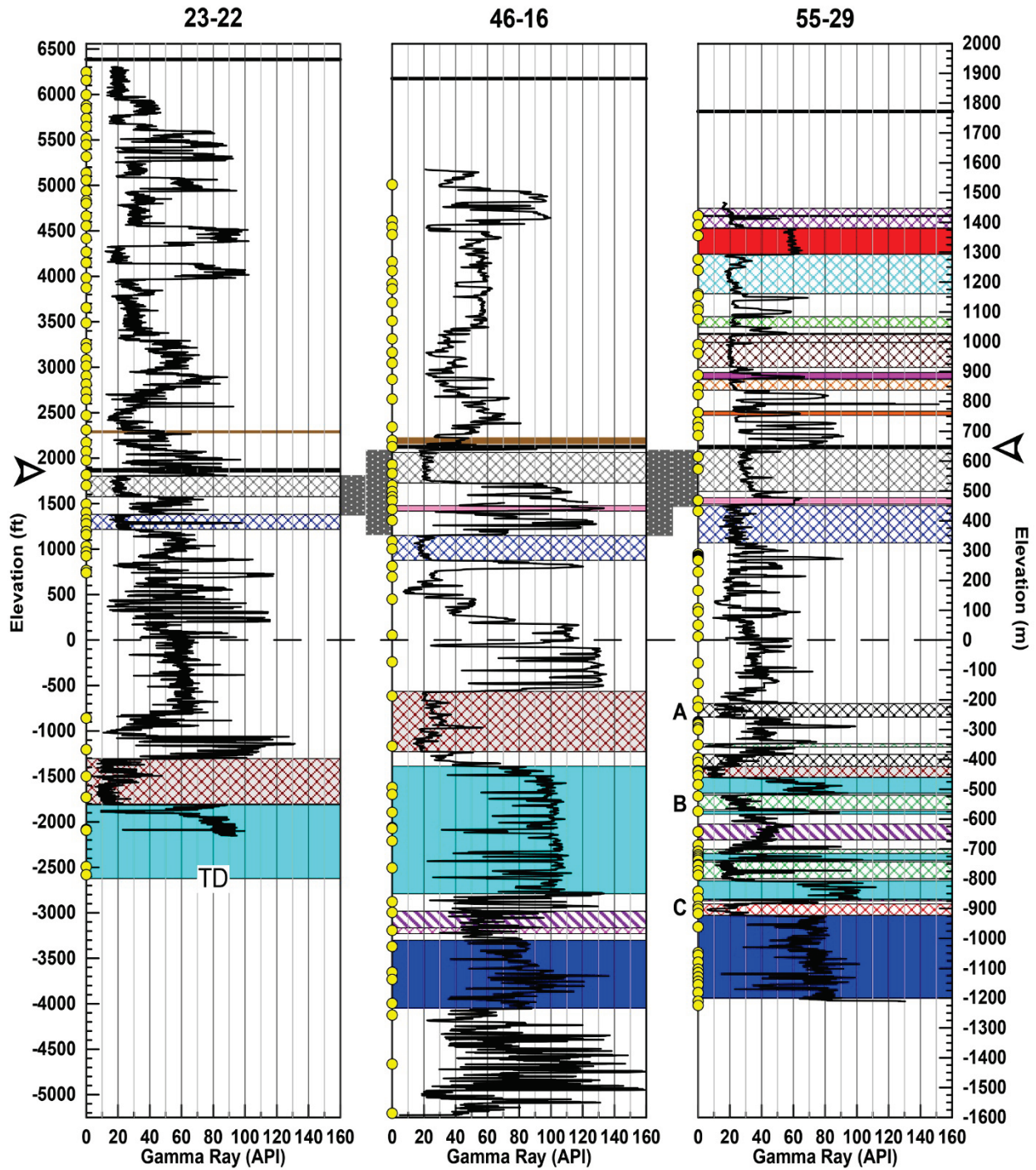


Figure 11: Deviation corrected gamma ray logs from CE 23-22, NWG 46-16, and NWG 55-29 plotted vs elevation. Colored bands show inter-well correlations, with solid colors being silicic units and hatched/cross-hatched being mafic units. Yellow symbols show location of geochemical samples. Arrows indicate the base of Newberry volcanics, based on correlation with dated flows from GEO N-1. Dark stippled areas between plots indicate inferred Deschutes formation lithologies. Solid black line at the top of each plot shows the wellhead elevation.

Core Samples

Core samples from seven thermal gradient wells GEO N-1, GEO N-2, GEO N-3, GEO N-4, GEO N-5, NC-01, and NC-72-3 were analyzed using a Bruker Tracer III-V hand-held XRF (X-Ray fluorescence) spectrometer to determine the chemical composition. A total of 54 cores from GEO N-2, GEO N-5, and NC-01 were analyzed on-site at the University of Utah Energy and Geoscience Institute (EGI) core warehouse in Salt Lake City, Utah. Core samples were targeted on zones with a high gamma ray response or high silica content.

Newberry cores, originally collected in the past for thermal conductivity measurements, were also stored at Southern Methodist University (SMU) from all seven wells. In general, the SMU core samples span the sections of each well with conductive temperature gradients. An additional 150 core samples were analyzed at SMU using the XRF spectrometer. The XRF allowed for the analysis of 29 elements on all 150 cores. Raw data from the handheld XRF were reported as element percent and converted to weight percent oxides. Figure 12 and Figure 13 show the gamma logs, lithologic logs, and SiO₂ concentration with the locations of the core samples for the wells on the west flank of Newberry (GEO N-2, GEO N-5, NC-01, and NC-72-3). As seen in Figure 12 and Figure 13 for wells GEO N-5 and GEO N-2, the SiO₂ concentrations can be a proxy for a gamma ray log in wells without geophysical logs.

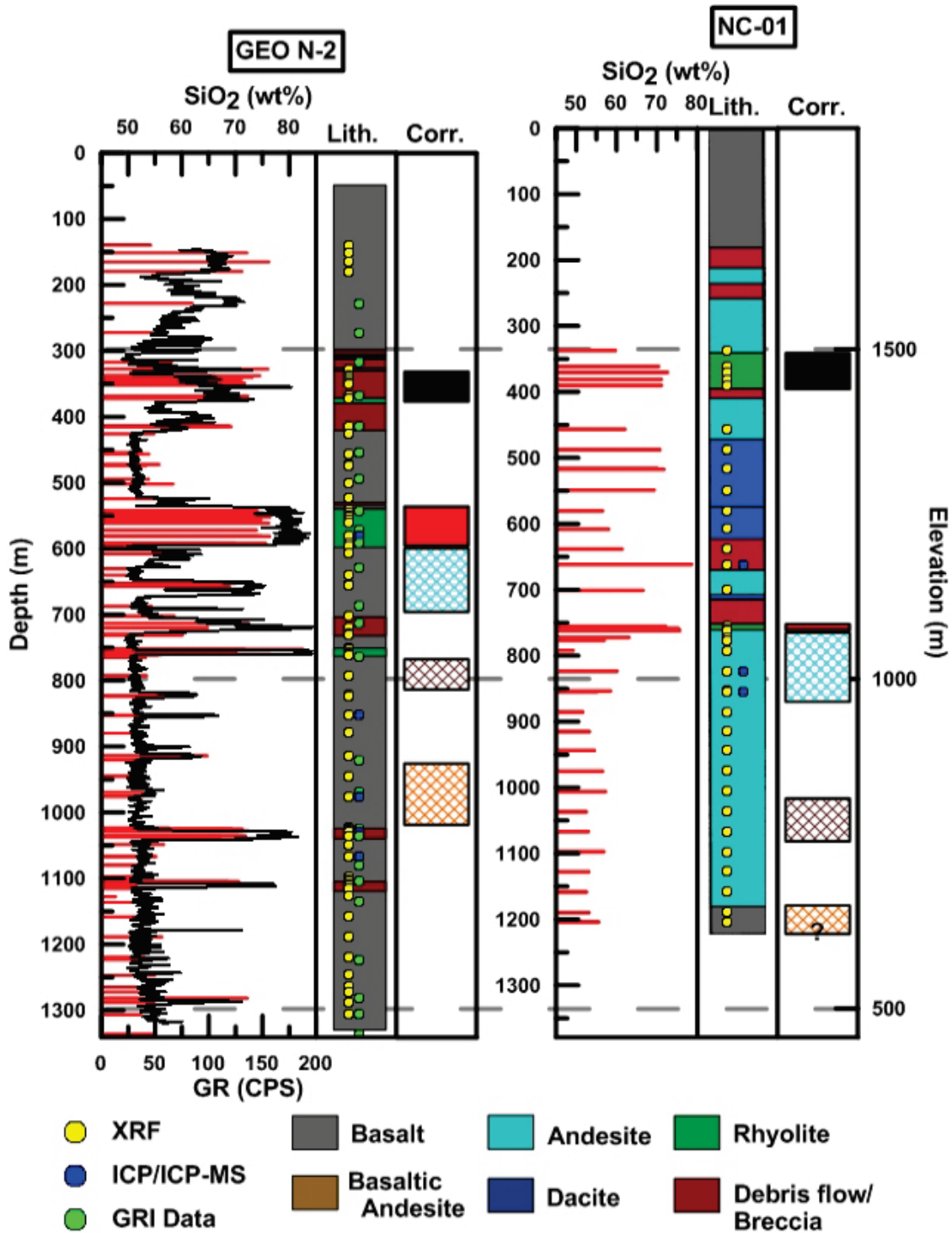


Figure 12: Gamma ray and/or mud logs for two west flank core wells, GEO N-2 and SF NC-01. Yellow, Blue and Green points show geochemical sample locations: yellow points analyzed by XRF, blue points analyzed by ICP/ICP-MS, and green points are data from GRI. The analytical technique used for the GRI data is unknown. Data for NC-01 are from Arestad and Potter (1988) and data for GEO N-2 are from well reports available from the DOGAMI website. 'Corr.' shows inter wellbore correlations of different geologic units.

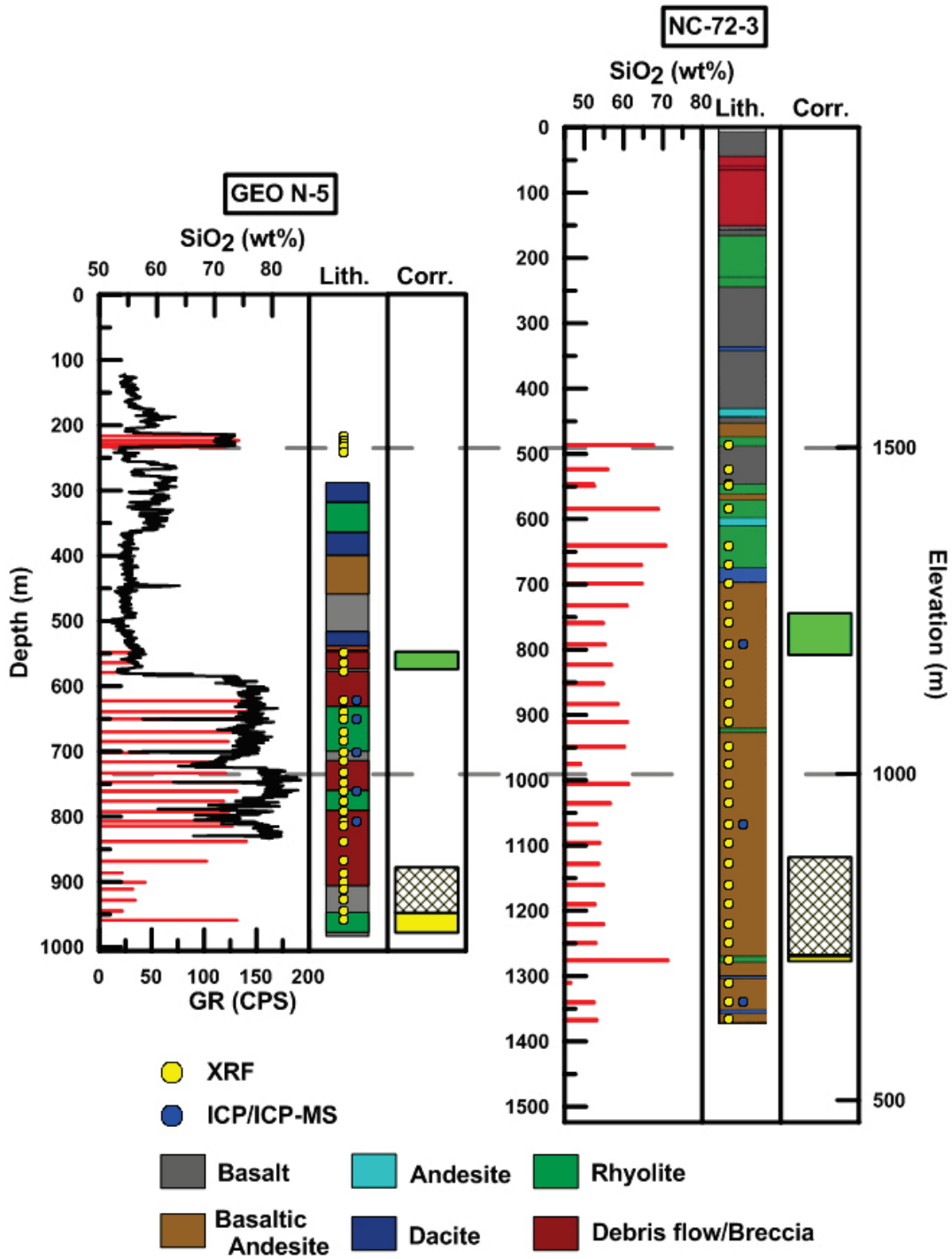


Figure 13: Gamma ray and/or mud logs for two west flank core wells, GEO N-5 and NC 72-3. Yellow and Blue points show geochemical sample locations: yellow points analyzed by XRF and blue points analyzed by ICP/ICP-MS. 'Lith.' is a simplified lithologic log for each well. Data for GEO N-2 are from well reports available from the DOGAMI website Data and data for NC 72-3 are from Arestad and Potter (1988). 'Corr.' shows inter wellbore correlations of different geologic units.

With the Bruker Tracer III-V XRF the light major elements (Na, Mg, Al, Si, P, K, Ca, and Ti) and heavy elements (Fe+) were run with two separate settings. Due to the inhomogeneity of most cores, each core was analyzed three times (for both settings) using different locations on the core sample in order to get an averaged composition for the core. The resulting data were averaged for the final composition of the core. Results of Na₂O, MgO, Al₂O₃, and SiO₂ show significant variation from data collected by ICP-ES. This is due to the attenuation of the lower energy x-rays associated with these elements, as well as overlaying peaks in the raw XRF data (Kaiser, personal communication). A correction was applied to the XRF data based on samples and standards analyzed using multiple sample techniques. The correction methodology used data on an element (X₁) and a neighboring element (X₂) to adjust the raw values of X₁. The difference between the accepted value and the raw value from the XRF for X₁ (ΔX_1) was plotted against the accepted value for X₂. The slope and intercept of a best fit line to this plot was then used to determine the amount to be added to the raw XRF value for X₁. The remaining samples in the dataset were corrected for X₁ using a fit to the correction amount to the raw XRF value for X₁. This correction was applied to the major elements and Barium (Ba) due to the interaction between Ti K-alpha and Ba L-alpha lines. The final results for the XRF samples are shown in APPENDIX B along with the standard deviation for each sample.

Surface Samples

To compare geochemical data in this study to regional geologic formations, previously collected and published geochemical data from surface samples (Bargar and Keith, 1999; Cannon, 1984; Higgins, 1973; Jensen et al., 2009; Kuehn, 2002; Linneman, 1990; Lite and Gannett, 2002; MacLeod et al., 1995; McDannel, 1989; McKay et al., 2009; Patridge, 2010; Smith, 1986; and Streck, 1994) were reviewed. These data include samples from Newberry as well as other regional formations. Sixteen (16) surface samples from outcrops were also collected and analyzed for this study, including five from Newberry Volcano outcrops.

For all geochemical data, major element oxide data was normalized to 100%. FeO was calculated from Fe₂O₃ assuming a Fe₂O₃/FeO ratio of 0.1 (Donnelly-Nolan, personal communication). Trace elements were normalized to primitive mantle using values from Sun and McDonough (1989). Analytical errors for ICP-ES/ICP-MS samples were determined from Acme Lab's repeated samples and standards.

Correlations

A correlation matrix was used in order to compare the geochemical results of the subsurface and surface rocks. Analytic results for the samples, and a compositional range for each oxide and element, were put into the matrix in order to determine how well each sample correlated with every other sample. The compositional range used was the larger of either the analytical error or the error associated with a mix of bimodal lithic fragments. An estimate of the potential compositional error associated with sampling errors (mixing of different lithologies) was made using two end-member mixing. Mafic and silicic end-members were calculated from samples with SiO₂wt% >55 and <70 respectively. A calculated mixture of the two end members was made for various percentages and the % error from each end-member was calculated. Samples with at least 50% correlation were selected and plotted to determine the nature of the correlation. The gamma ray response, cutting notes, and general stratigraphic relations were used in addition to the chemical composition to aid in determining whether two or more samples could be correlated.

To determine how well a set of samples correlated, a *similarity coefficient* (SC) was used (Knott et al., 2007). The similarity coefficient is an average of elemental concentration ratios in two different samples (Sarna-Wojcicki et al., 1984). This method has primarily been used in the correlation of glass and tephra beds for tephrochronology studies (Lowe, 2011). In the case of Newberry, the similarity coefficient is being applied to a wide range of whole rock data. In past studies (Knott et al., 2007) a subset of elements were used to calculate this value. In this study all available elements were used due to the incomplete analyses of some of the samples incorporated into the final dataset. Four SC values were calculated for each potential correlation group, one for the major element compounds (SiO₂, Al₂O₃, FeO, MgO, CaO, Na₂O, K₂O, TiO₂, P₂O₅, and MnO), trace elements (Cs, Rb, Ba, Th, U, Nb, K, La, Ce, Pb, Pr, Sr, P, Nd, Zr, Sm, Eu, Ti, Dy, Y, Yb, and Lu), rare earth elements (REE) (La, Ce, Pr, Nd, Sm, Eu, Gd, Tb, Dy, Ho, Er, Tm, Yb, and Lu), and finally a combined value for all elements was calculated. The trace element group follows the primitive mantle abundance pattern from Sun and McDonough (1989). The similarity coefficient equation used (after Knott et al., 2007) is:

Equation 1

$$d_{(A,B)} = \frac{\sum_{i=1}^n R_i}{n}$$

where $d_{(A,B)}=d_{(B,A)}$ is the similarity coefficient between samples A and B, i is the element number, n is the number of elements, $R_i = X_{i,A}/X_{i,B}$ if $X_{i,B} \geq X_{i,A}$ otherwise $X_{i,B}/X_{i,A}$, and X_i is the concentration of element i in sample A or B. This equation results in a value between 0 and 1 with one being a perfect correlation. In tephra studies, focused on detailed analysis of individual glasses, there have been various cut-off values used to determine correlation, ranging from 0.92 to 0.96 (Lowe, 2011). From lab standards and sample duplicates, the best similarity coefficient that can be expected for this data is 0.98 for major element test and 0.96 for the remaining tests. Due to the use of mixed cuttings in this study, a value of 0.90 was considered indicative of correlation between two samples. Additionally, based on a visual inspection of the data plots, values between 0.85 and 0.90 are considered possible correlations.

Wells 55-29, N-2, and NC-01

The two datasets with the highest correlation were the cuttings of well NWG 55-29 and the core from temperature gradient hole N-2. The wellhead locations for these wells are 370 m apart on the western flank of Newberry and due to the inclination of 55-29 towards the east, the wellbores are only ~200 m apart at ~1,300 m depth. Superficially, the gamma logs from these two wells do not seem to correlate, with N-2 encountering a higher proportion of mafic rock than NWG 55-29 (Figure 6). Based on the chemical data, however, there are more correlations between these wells than the gamma logs indicate. There does not appear to be a consistent dip or thickness of the chemically correlated units between the two wells. This demonstrates the non-uniform deposition that can occur on the flanks of volcanoes. Well N-2 contains a greater proportion of basaltic lava flows and distinct interbedded silicic units. Well NWG 55-29 contains less defined lava flows and more interbedded debris flows between thinner basalt flows. This could be explained by N-2 having been located in a topographic low compared to NWG 55-29 prior to the basalt flow eruptions.

Two rhyolite flows encountered in the upper portion of N-2 are also seen in NC-01, located ~925

m to the east. The first of these formations is roughly flat lying and thicker in NC-01, suggesting that the flow originated from east of the wells. Data from this formation is not available from 55-29 because it should occur shallower than the surface casing at depths where no cuttings were collected. The second rhyolite flow is seen in NWG 55-29, N-2, and NC-01. In the gamma ray logs from NWG 55-29 and N-2 it has a prominent high gamma signature (Figure 12 left side red box and Figure 14, red filled section). This flow is thickest in NWG 55-29 (~90 m) and thins to the east (~60 m in N-2 and 10 m in NC-01). An apparent dip of 10-15 degrees to the east suggests that the flow originated from the west, potentially from near McKay Buttes. Below the second rhyolite flow there are three correlated basalt flows. The first has a vertical offset of 125 m while the other two have an offset of between 210 and 225 m. All three offsets are down to the east. The change in apparent dip of these formations between NWG 55-29 and N-2 and N-2 and NC-01, suggests that there has been up to 225 m of down to the east offset between N-2 and NC-01. This offset likely occurred in at least two stages because of the smaller offset observed in the younger (shallower) flow. In NC-01 between the two rhyolites there are two intervals of tuffs potentially from caldera eruptions. No ages are available for these flows to further aid in determining the timing and source of eruptions.

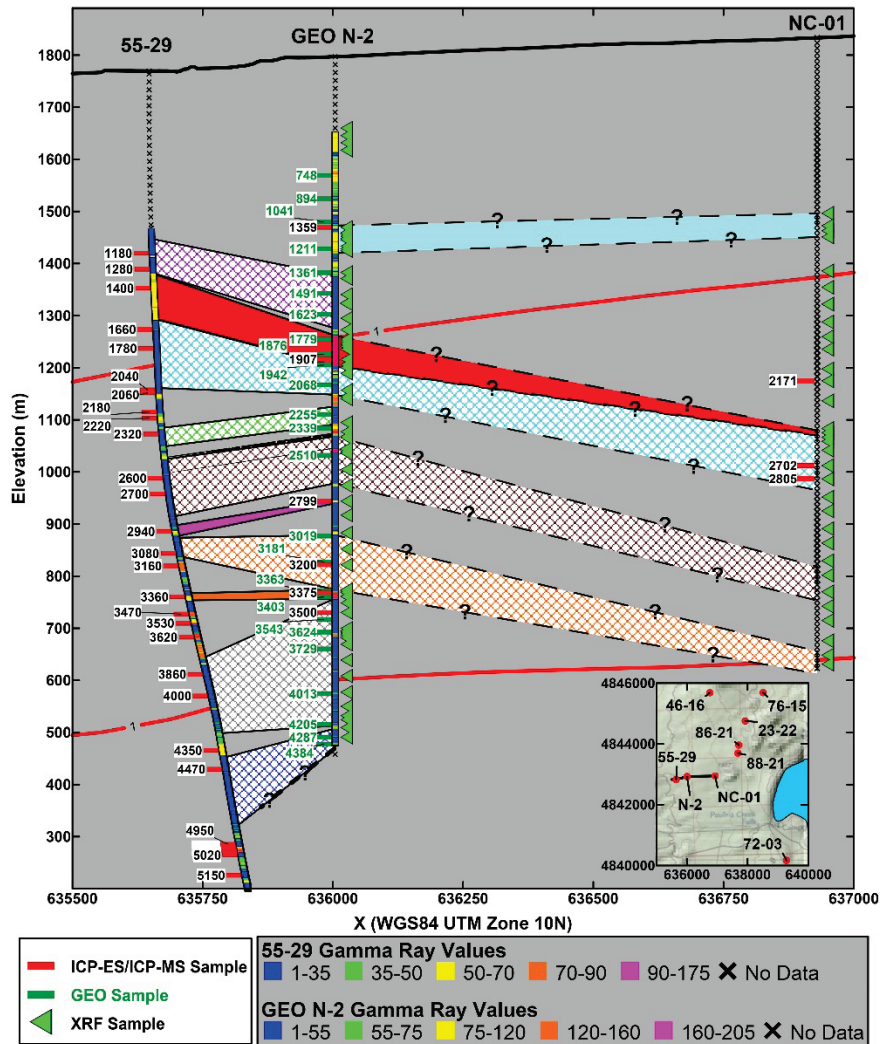


Figure 14: Well traces colored by gamma ray (GR) log values for NWG 55-29 and N-2; NC-01 does not have an available GR log. Symbols show location and depth of geochemical samples; label values refer to measured depth in feet. Colored boxes represent correlated lithologies, cross hatched lithologies are mafic, and solid boxes are silicic. Colors in boxes are the same as Figures 12 and 13. The solid black line at the top is the topographic surface and the solid red lines show the upper and lower surfaces of the 10 ohm-m conductor from the MT survey. X-axis units are UTM location along cross section, x and y axes are 1:1. Inset map shows the location of the cross section in relation to other west flank wells.

Wells 55-29 and 46-16 Correlation

There is limited correlation between wells NWG 55-29 and NWG 46-16 as seen in the gamma ray logs in Figure 11. Chemical data from the two wells shows similarity between a thick silicic ($\text{SiO}_2 \sim 73\text{wt}\%$) zone in well NWG 46-16 between -450 m and -875 m (7,800-9,200 ft TVD) and distinct silicic zones in well NWG 55-29 around -475 m, -725 m, and -800 m (Figure 11, light aqua-blue boxes). This zone appears to be a metamorphosed tuff unit with chlorite and trace euhedral pyrite as an alteration mineral within the tuff. This interval also correlated with samples from -635 m in well CE 23-22 (Figure 15, B (bottom)). Basalts encountered just above this formation in both well NWG 46-16 and CE 23-22 also have similar chemistry (Figure 15, A (top)). In well CE 23-22, the top of the correlated silicic formation is at -565 m. This implies a down-to-the-east offset of

around 125 m, between CE 23-22 and NWG 46-16. A less silicic (SiO_2 67 wt%) zone between -1,000 m and -1,240 m (9,500-10,400 ft TVD) in well NWG 46-16 and -925 m and -1,200 m (8,900-9,800 ft TVD) in well NWG 55-29 are also correlated based on chemical data. Between these two correlated units there is a thin (<10 m) andesite unit. Above these zones is another basaltic andesite that is correlated between the two wells. An intrusive micro-granodiorite intersected in the final 15 m of well NWG 55-29 is potentially correlated with zones in well NWG 46-16 at -1,325 m, -1,450 m, and -1,500 m. This correlation is based solely on the gamma logs where the logs show values of 120 API or more in NWG 46-16. The deep micro-granodiorite sampled in well NWG 55-29 is chemically similar to a glass and a rhyolite flow in samples from 1,390 m and 1,355 m (1,290 ft and 1,400 ft TVD) in well NWG 55-29 and may represent the intrusive equivalent of an erupted rhyolite flow.

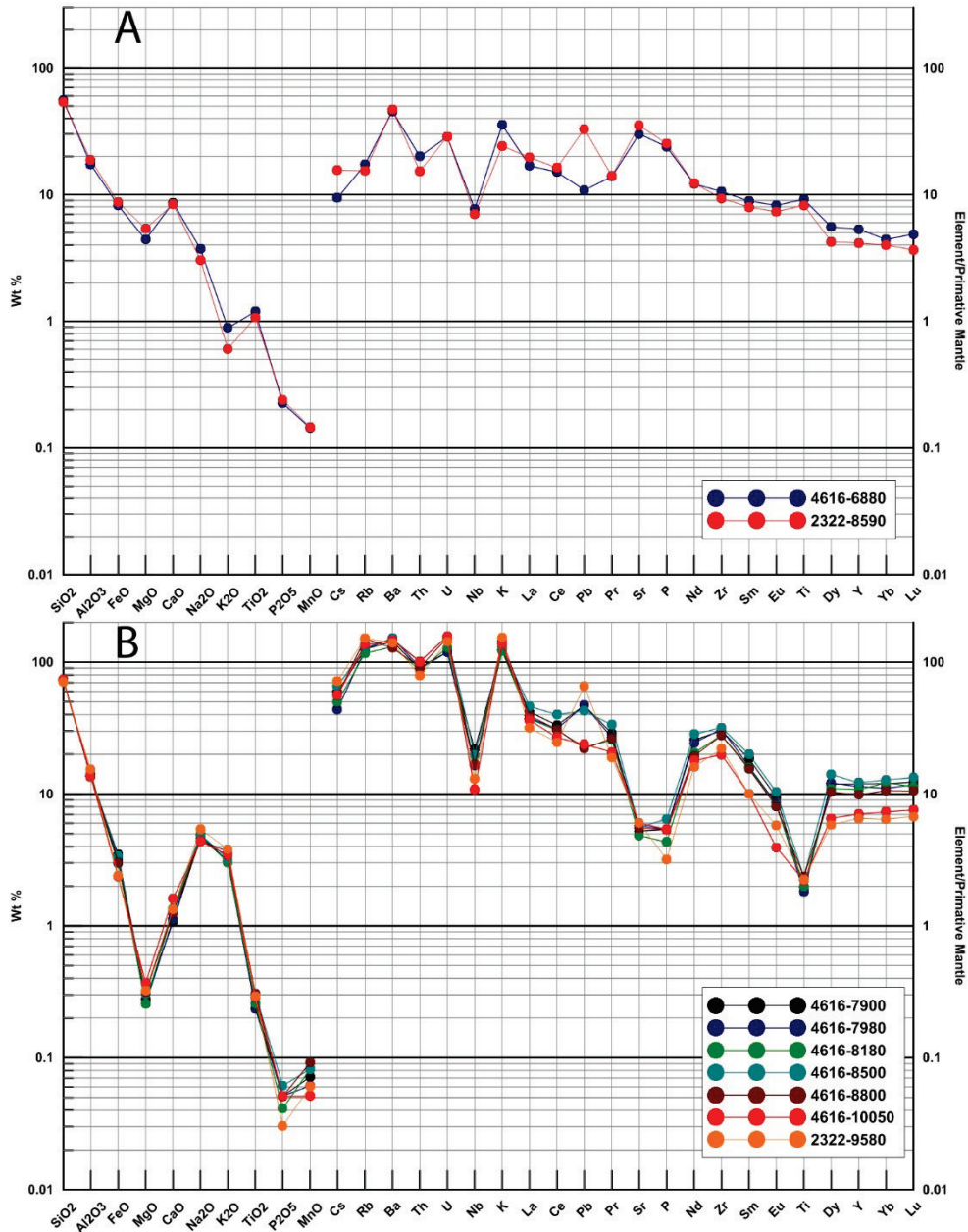


Figure 15 A and B (top and bottom): Geochemical data correlations for NWG 46-16 and CE 23-22. A (top) displays geochemical data for basalts in well NWG 46-16 and CE 23-22. B (bottom) displays tuff correlated with geochemical data from NWG 46-16 and CE 23-22. Oxides are plotted in wt% while trace elements are normalized to primitive mantle.

Within Well NWG 55-29

Within well NWG 55-29, below the -200 m elevation level, there are a number of intrusions as noted in the mud log and cutting descriptions. Included in the intrusive lithologies are a series of 10-70 m thick basaltic andesite to andesite units, these can be divided into 5 groups based on composition. The first two are correlated with units in well NWG 46-16 and were discussed above.

The shallowest of these units (Figure 11, third panel for well 55-29, letter A) is the most chemically evolved with a magnesium value of 37.6, high Ba value, and enriched light rare earth elements (LREE) compared to the other groups. The next group is seen in the well in at least three intervals (Figure 11, third panel for well 55-29, letter B). This group is differentiated from the first group by a higher Mg value of 43.3, lower LREE values, and a lower Rb/Cs ratio. The final group is very similar to the second group, though it has higher heavy rare earth elements (HREE) values, differentiating it from the second group (Figure 11, third panel for well 55-29, letter C). The different geochemical groups are interpreted to be dikes and intrusions from chemically distinct magmas. These intrusions likely originated from deeper intruded magma bodies that are interpreted from positive gravity anomalies on the west flank. The chemical data, gamma ray and lithology logs in well NWG 55-29 show basalt, felsic dikes and micro-granodiorite from -400 m elevation to total depth. The section consists of a mix of older meta-volcanic lithologies, recent and older basalt sub-volcanics, fine crystalline felsic dikes likely associated with granitic intrusives, cryptocrystalline silica metasomatized rock and metasomatic alteration associated with recent basalt sub-volcanic emplacements. Given the complex events which make up this section, it is likely that this interval has undergone multiple strain events and fracturing. Temperature logs recorded during recent EGS injection tests show that at least 5 zones in this portion of the open well that took fluids, which supports this theory.

Well Data and Regional Correlations

Stratigraphic correlation in an area with millions of years of volcanic activity originating from multiple eruptive centers is problematic. Stratigraphy can be complex in volcanic terrains. The geometry of lava flows from any given eruptive center is unpredictable in width, depth, or length because of compositional and viscosity variations, preexisting topography, erosion, re-deposition of volcanic materials, and lithologic similarities between formations of different ages. The stratigraphy underlying Newberry Volcano has been further disrupted by intrusions, deeper lithologic turmoil by volcanic eruptions associated with intrusions, fault offsets, and contact metamorphism. Also compositional variability in both time and space, subsurface stratigraphic correlation, even with geophysical borehole logs, is very difficult (A. Waibel, based on personal observation.).

Unlike correlations between wells within close proximity, regional correlations are more problematic. The following correlations are based on geochemical similarities between well data from the flank of an active volcano and mainly outcrop samples that are from 25 to 100+ km away. With this in mind, the correlations are tentatively proposed, without the confidence to match mapped regional formations to lithologic sections within the wells.

Chemical data for pre-Newberry Volcano formations exposed in central Oregon were referenced for comparison with chemical data from lithologic units in the exploration wells on the flanks of Newberry Volcano. Regional formations span from the Eocene through the Pliocene. The major regional formations include the Clarno (44-40 Ma), John Day (40-20 Ma), Picture Gorge and Prineville Basalts (16 Ma), Mascall (15 Ma), Rattlesnake (7.2 Ma), and the Deschutes (8.8-3.3 Ma). The Clarno, John Day, Mascall, and Rattlesnake formations are comprised primarily of tuffs, volcanoclastic sediments, and lava flows. The Picture Gorge and Prineville Basalts are subsets of the Columbia River Basalts. The Deschutes formation is composed of olivine basalt flows, andesite flows, basaltic ash, debris flows, eroded and re-worked basaltic and andesitic volcanic sediments, and debris flows dating from about 6 to 4 Ma (Smith, 1986). Geochemical data for

each formation comes from various sources. Deschutes data is from Cannon (1984), Smith (1986), McDannel (1989), Lite and Gannett (2002), and unpublished data from Jason McClaughry of the Oregon Department of Geology and Mineral Industries (DOGAMI). Whole rock data for Mascall paleosols and from the Rattlesnake Tuff were digitized from Bestland et al. (2008) and Streck (1994). John Day and Clarno formation data are from Patridge (2010) and unpublished DOGAMI data.

At 660 m above sea level (asl) in well NWG 46-16, a ~10 m thick basalt flow was correlated to basaltic andesite in thermal gradient well N-1 at 1,060 m asl, based on major element composition from Bargar and Keith (1999). Basalts and basaltic andesites above and below formations with geochemical data in N-1 were dated by Swanberg et al. (1988) and given pre-Newberry ages (0.75-0.85 Ma). This correlation was used as a baseline for the boundary between Newberry and pre-Newberry units in well 46-16. An equivalent thin flow is not seen in NWG 55-29. A similar package of basalts and tuffs in 46-16 (650 to 300 m) that occur just below the boundary are seen in NWG 55-29 (650 and 350 m in Figure 11). The top of this package is likely the boundary between Newberry and pre-Newberry lithologies in NWG 55-29. This boundary is less apparent in CE 23-22. The same basalt and tuff sequence is seen on the gamma ray log, but the chemical data do not show as strong a correlation. Rocks encountered above 650 m in wells NWG 46-16 and NWG 55-29 and above 550 m in CE 23-22 are likely to be primarily erupted material from Newberry Volcano and air fall tephra from the High Cascade volcanoes to the west.

Two clear silicic tuff formations are seen in the gamma ray logs from well NWG 46-16 (Figure 11). The first of these begins at 525 m asl, it is about 180 m thick and is interpreted to be tuffs with interbedded lava flows and/or mafic tuffs. These tuffs correlate with geochemical data from tuffs reported by Cannon (1984) and Smith (1986) from the Deschutes formation. Sanidine is noted throughout this section in the mud log for the NWG 46-16 well, and is a prominent mineral in John Day rhyolites and ignimbrites (Smith, 1986; Patridge, 2010). Smith (1986) notes that sanidine in Deschutes volcanoclastic rocks are likely derived from weathering of John Day units. The interval is distinguished from John Day units by a lower ratio of FeO/MgO, lower Nb, and lower REE values.

The second silicic tuff formation begins at about 60 m asl: it is about 225 m thick and consists of a 50 m upper silicic tuff, a 25 m mafic tuff or lava flow, followed by 150 m of silicic tuff with thin (~5-10 m) mafic zones. It is distinguished from John Day tuffs by lower Y, Nb, and LREEs and the lack of sanidine phenocrysts in the cuttings. There is not enough data from this interval to assign it to a regional formation. This interval was not sampled in detail and there is no information on the mafic zones within this formation. Additional sampling through this interval may result in correlation with a regional formation.

As stated earlier, these correlations are based primarily on geochemical correlations with outcrop samples that have been analyzed and published by different authors over the past 40 years. In most of the published data, not all of the same elements were analyzed. In particular the Rare Earth Elements (REE) have limited representation. About 50% of samples reported values for the LREE La and Ce; only 19% of samples reported values for the remaining REE. With no information on the trace element and REE content of many of the formations, correlation or non-correlation was determined primarily from major element data leading to some result ambiguity.

GROUNDWATER HYDROLOGY

Sources for hydrology reports for Newberry Caldera, Newberry Volcano, and the upper Deschutes River Basin include Sammel and Craig (1983), Sammel et al. (1988), Crumrine and Morgan (1994), Caldwell and Truini (1997), and Gannett et al. (2001). These studies provide details regarding precipitation, evaporation, surface water drainage and water chemistry for the Deschutes River Basin and Newberry Volcano.

Groundwater measurements away from the more populated portions of the Deschutes River Basin show only broad regional flow trends without detail or nuance because of the paucity of data. The data base for groundwater hydrology on and adjacent to Newberry Volcano consists of:

- shallow wells in the Deschutes River Basin to the west of Newberry Volcano,
- shallow wells within the caldera,
- two deeper geothermal wells within the caldera,
- temperature gradient wells on the flanks of the volcano,
- four deep geothermal exploration wells on the upper western flank, north of Paulina Creek, and
- three shallow water wells adjacent to the deep exploration wells.

The shallow water wells to the west of Newberry Volcano document the shallow groundwater effects of the large volume of cold Cascade Range precipitation flowing eastward into the Deschutes River Basin. Shallow recreational supply wells within the caldera identify abundant near-surface hot and cold water. The two deeper wells within the caldera show lateral hot and cold water horizons and identify high temperature geothermal fluid within the caldera (Figure 16). Flow testing thru the core rig drill stem at USGS NB2, with a measured bottom-hole temperature of 265°C, was too restricted to quantify the geothermal potential of the system intersected by the hole. The near-by Sandia hole RDO-1, with temperatures over 150°C at 200 m, was not tested (Sammel et al., 1988).

The vadose zone and the water-bearing zones identified in the water wells and temperature gradient wells on the west flank of Newberry Volcano, as depicted by the upper isothermal section of temperature gradient wells (Figure 18 and Figure 19, Temperature Gradient section below), shows meteoric water moving downward to a depth of restricted permeability.

The local groundwater percolation is thought to be more complex than a simple “groundwater mound” model, due to abrupt horizontal and vertical variations in permeability associated with youngvolcanic-flank stratigraphy. The lithologic data from core holes show the western flank (and likely much of the rest of the flank) is composed of ash flows, air-fall tephra beds, mud flows and lava flows. The lava flows can extend for quite some distance (up to tens of km) from the vent area, and have the potential for high fracture permeability. The lithologic data also show beds of strongly clay-altered tuff, ash-flow and debris flows, all with restricted vertical permeability. Sub-horizontal permeability within fractured lava flows and young coarse tephra beds would be quite high, and is the setting for locally perched water-bearing zones on the flanks. On the west flank, north of Paulina Creek, well SF NC-01 shows an isothermal zone extending from 700 ft to an elevation of 5,380 ft. above sea level (asl), underlain by a conductive thermal gradient. One mile to the west, well GEO N-2 shows an isothermal zone of 1,000 ft (to 4,800 ft asl). On the west flank south of Paulina Creek, well GEO N-5 shows an isothermal zone of 1,400 ft (to 4,285 ft asl).

These thick shallow isothermal sections are noted on all of the temperature gradient holes, and reflect a general downward percolation of meteoric water. The top of the underlying thermal conductive gradient indicates a marked reduction in permeability. Please refer to Figure 4 for all well locations.

The three water wells on the upper northwestern flank of the volcano, adjacent to the deep geothermal exploration wells, intersected cold water-bearing zones, all with temperatures near 10°C (50°F), likely perched on lower permeable altered rock.

- The water well drilled by California Energy Company in Section 21 intersected an aquifer at 782 ft with an estimated flow rate of 200 gpm. Upon well completion, the static water level was at 555 ft. depth in the hole, 5,460 ft asl.
- The water well located on the well pad of NWG 55-29 intersected small water-bearing zones at 420 ft, 510 ft and 562 ft. An aquifer estimated to be capable of flowing at least 500 gpm was intersected at 570 ft. Upon well completion the static water level in the well was at 325 ft depth in the hole, 5,475 ft asl.
- The water well located on the well pad of 46-16 intersected the top of an aquifer at 704 ft. After completion the static water level was at 672 ft depth in the hole, 5,518 ft asl. (Oregon Department of Water Resources well files).

The aquifer intersected by the water well on the well pad of 55-29 is located just west of temperature gradient hole GEO N-2. The shallow near-isothermal temperature profile of this temperature gradient well is not obviously disturbed by the shallow aquifer (see GEO N-2 temperature profile, Figure 19 in Temperature Gradient section below). The elevations of the water table observed in the three water wells appear to be in agreement with the elevations of the total depths of the wells. This "falling head with depth" relationship in these wells is characteristic of downward (vertical) movement of groundwater in recharge areas such as Newberry Volcano. The shallow near-isothermal temperature profile of west flank temperature gradient wells is not obviously disturbed by these shallow aquifers (see GEO N-2 and GEO N-5 temperature profiles.)

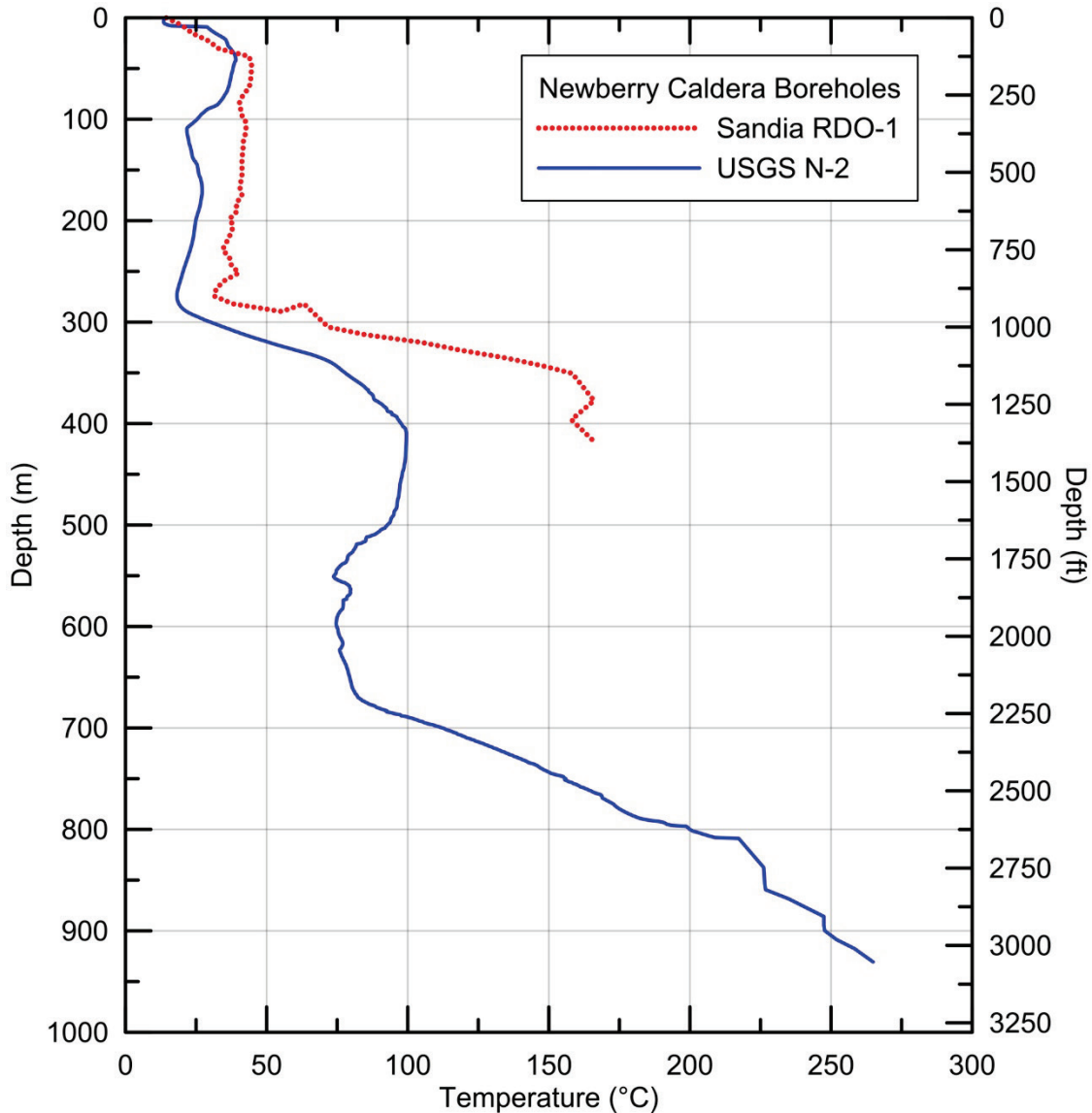


Figure 16: Temperature - Depth plots of two wells inside the caldera logged by the SMU Geothermal Laboratory.

Of the four deep exploration wells, only one provides insight into deeper groundwater hydrology. Wells CE 86-21, CE 23-22, NWG 55-29 and NWG 46-16 were drilled to the 9,000-10,000 ft depth range. CE 86-21, CE 23-22 and NWG 55-29 showed no evidence of extensive fracture permeability and did not have sustained fluid flow. These three wells also showed no evidence of hydrothermal fractures. Well NWG 46-16 was never extensively flow tested due to formation stability problems below the casing shoe. The well intersected hydrothermal veins (Figure 7), and produces a sustained flow of gas from the formation. A water level in well NWG 46-16 of 2070 ft below surface, identified in a temperature-pressure log run about one year after completion, was made while the well was under pressure of about 450 to 500 psi. Compensating for adjustment due to the pressurized condition, the water level in the well would be in the vicinity of 800 to 1000 ft below surface elevation with static non-pressurized conditions. The shallow pressure measurement lacks precision, so this depth is only an estimate.

Temperature gradient wells on Newberry Volcano, by law and by well design, have never been flowed or tested for groundwater data. As pointed out by Swanberg et al. (1988), identifying the top of the water table when drilling core holes can be elusive. However the wells do provide valuable insight into the groundwater conditions on the flanks of the volcano. Thermal profiles produced from measurements in temperature gradient wells drilled on the flanks of Newberry Volcano typically show an upper near-isothermal section, a relatively thick zone where downward-percolating meteoric water and locally laterally-flowing "perched" shallows aquifers dominate the subsurface temperature (Figure 18 and Figure 19, Temperature Gradient section below). GEO temperature gradient well N-3 was drilled on the north flank of the volcano, and was one of two wells used by Sammel et al. (1988) to construct a groundwater model. the driller's log for GEO N-3 well reported twenty feet of standing water in the bottom of the hole at a drilled depth of 540 ft (5,220 ft asl). The temperature of this perched water entry is cold enough to have only minor effect on the isothermal section of the temperature profile. After drilling deeper, the log recorded a static water level in the hole at 1,720 ft. (4,040 ft asl). Toward the bottom of the hole (3,802 ft, 1,958 ft asl) warm water 129°F (54°C) was noted entering the well bore. The temperature profile of the well after completion shows warm water entering the well in the vicinity of the 3,800 ft depth, flowing up the well bore annulus, with possible leakage into the surrounding rock at a depth of 1,980 ft (3,780 ft asl). Thus in well GEO N-3, there appears to be three separate water-bearing zones encountered: one at 5,220 ft asl, another at 4,040 ft asl, and finally a warm water zone intersected 1,958 ft asl with a static water level of 3,780 ft asl. No static water data are available for the two test wells drilled within the caldera, USGS N-2 and RDO-1.

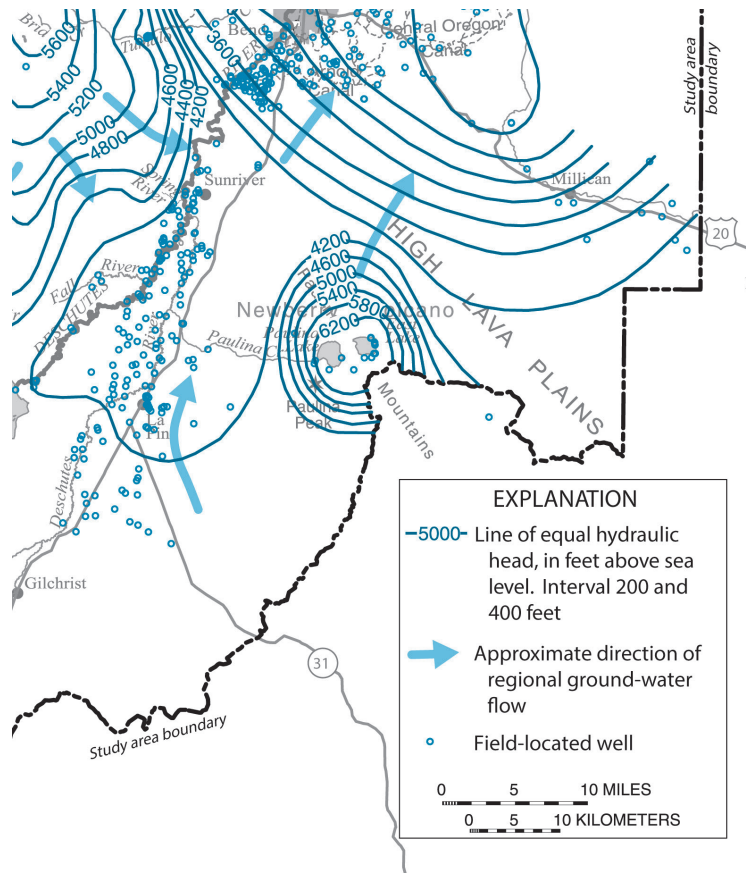


Figure 17: Map of generalized hydrologic head and ground-water flow directions for the area around Newberry Volcano (adapted from Gannett, Lite, Morgan and Collins, 2001, Figure 28, p. 60).

Groundwater Hydrology Interpretation

Static water level measurements from regional wells and from exploration wells on the western and northern flank of the volcano provide interesting glimpses into the hydrology of Newberry Volcano. The data show the static water level in the well that intersected the hydrothermal aquifer to be distinct from that in the cold water -producing zones encountered in other wells. Regional groundwater flow on and in the vicinity of Newberry Volcano is likely one of downward-percolating meteoric water, modified by variable permeability of fractured lava flows, tephra layers and clay-altered ash layers. Increasing clay alteration and lithostatic compression progressively reduces permeability with depth.

The regional groundwater gradient increases very slowly to the south and southeast of the volcano. The gradient begins to drop off more rapidly under the northern half of the volcano (Figure 17). The static cold water level of 4,040 ft asl measured in well GEO N-3 seems to fit the regional groundwater profile. The three water wells on the northwest flank of the volcano encountered cold water aquifers capable of production to satisfy drilling needs in the vicinity of 5,400-5,500 ft asl. GEO N-3 encountered a similar shallow cold aquifer at a depth of 5,220 ft asl. These may all be perched aquifers. The upper isothermal temperature profiles in the vicinities of these water wells

are not able to distinguish these shallow aquifers from the adjacent rock above and below the aquifers.

GEOPHYSICS

Temperature Gradient

Thermal data for twenty-one shallow, intermediate and deep wells are available, two located within the caldera and nineteen located on the volcano flank, outside of the caldera of Newberry Volcano. The data are summarized in Figure 18, Figure 19 and Figure 20. There are temperature logs available for six shallow wells in the range of 190-220 m (600-700 ft), nine wells in the depth range of 615 to 1230 m (2,000 to 4,000 ft) and 2 deep exploration test wells drilled by Davenport, 2 deep exploration test wells drilled by California Energy and two test wells drilled within the caldera (U.S.G.S. and Sandia National Laboratory). The general character of the temperature-depth curves is a low gradient upper zone characterized by the vados or active groundwater zones and a thermally conductive layer below. The only exceptions are the 2 wells in the caldera which show active geothermal fluid flow on several levels, not surprising since there are several warm and cold gas seeps in the caldera as well as an approximately 1,350 year old obsidian flow.

The deep wells drilled by Cal Energy are CE 86-21 and CE 22-23. Little thermal data are available from the 86-21 well although it is clearly very hot (BHT temperature, non-equilibrium, of 315°C (600°F) at 2805 m (9,200 ft)). The CE 22-23 well was logged twice (Spielman and Finger, 1998). Several years after the well was completed, the measured temperature (assumed equilibrium) was 288°C (550°F) at 2,927 m (9,602 ft). The well is for the most part conductive with an equilibrium gradient of about 146 °C/km (8°F/100 ft). There are two zones in the well connected by the drilling that show intra-hole flow (Blackwell and Priest 1996a and 1996b; see Erkan et al., 2008, for a complete discussion of intra-hole flow characteristics). These zones likely do not indicate high permeability between the entry and exit points, but isolated cracks or horizons with only local permeability. Flow within the wellbore is on the order of liters per minute between the connected zones. The two shallower wells document the generally conductive nature of the area below the shallow active groundwater zone seen in both wells.

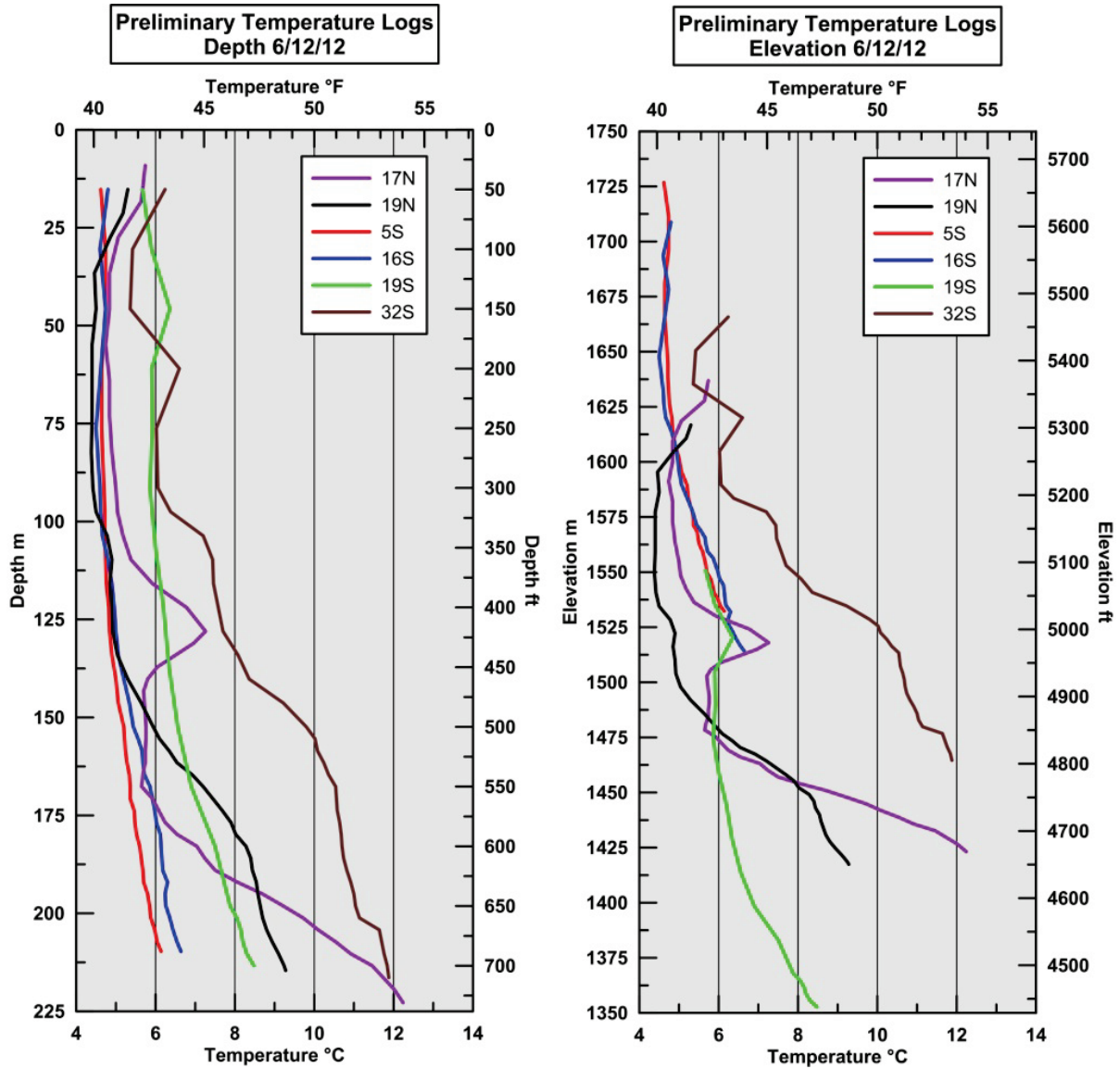


Figure 18: Temperature-depth plots for the six shallow temperature gradient wells on Newberry Volcano that were also used for passive low energy seismic signal monitoring (see Seismic section below).

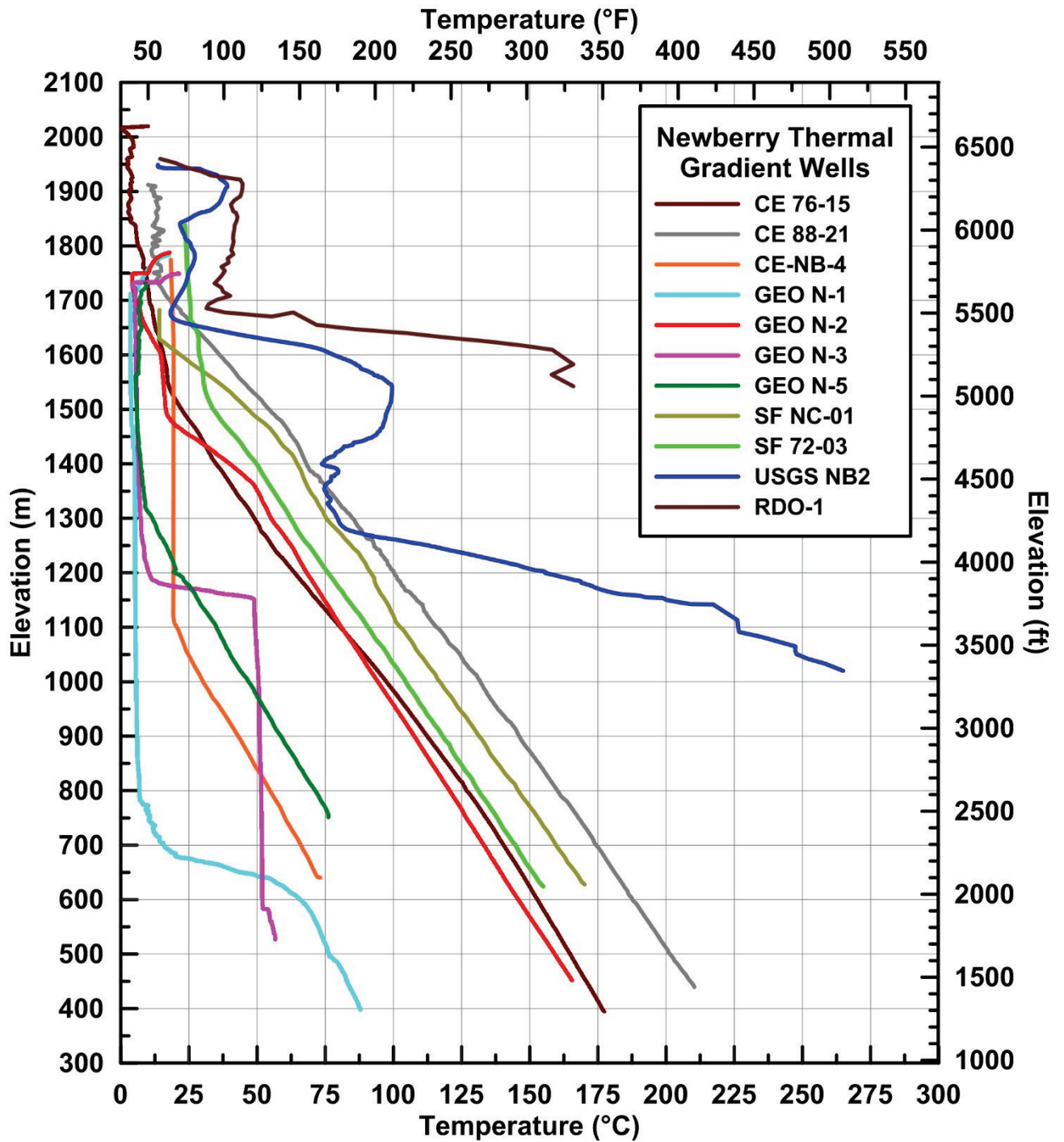


Figure 19: Temperature-depth plots for the temperature gradient wells on Newberry Volcano. RDO-1 and USGS NB2 are located within the caldera.

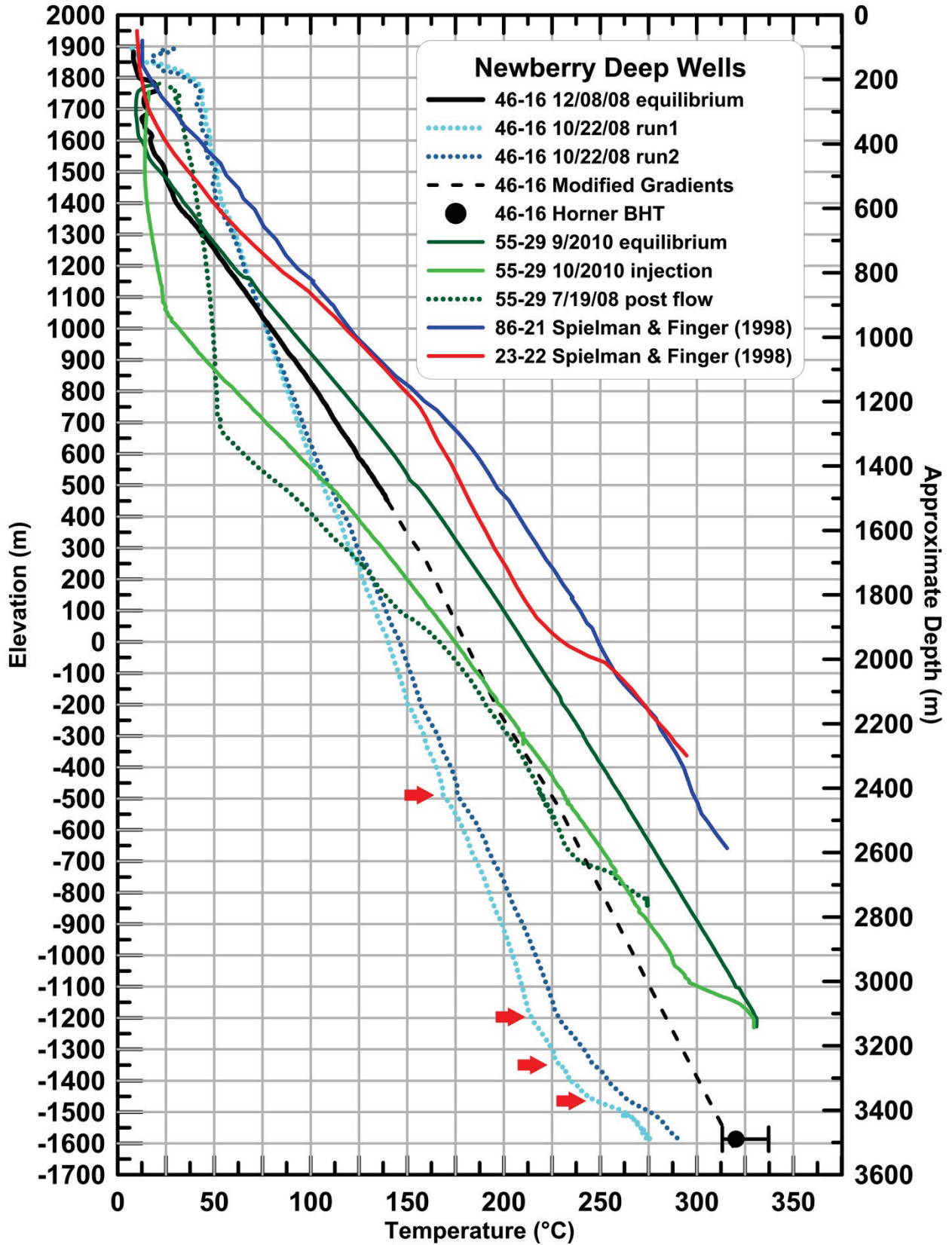


Figure 20: Temperature-depth plots for the deep exploration wells drilled on the west side of Newberry Volcano. The red arrows on run 1 of 46-16 indicate possible fluid loss zones.

Temperature results for all the wells in the area provide the most important and insightful geophysical dataset, and are critical for the geothermal interpretations of other geophysical surveys. Temperature data from the 4 deep wells (Figure 20) are particularly informative as they show glimpses of the deep character underlying the broad thermal anomaly. Several temperature logs were run for each of the deep wells drilled by Davenport Power, and provide high quality data from the wells. The deep thermal data are more complete for the NWG 55-29 well because the NWG 46-16 well bridged at about 1,432 m (~4,700 ft) before a complete equilibrium temperature profile could be obtained. Well NWG 55-29 was logged first by Halliburton on 7/15/08 as part of the open hole logging program. Additional temperature data were collected for well NWG 55-29 in 2010 by AltaRock Energy, including equilibrium and injection temperature logs.

The temperature logs for NWG 46-16 are less comprehensive. The hole was initially logged in the open hole on 20 October 2008 by Baker Atlas. The logging tool failed at the bottom, and only the down-logs were recorded. An attempt to re-log the well on 23 October 2008 was made. The hole had heated up in the interval of time between logging attempts, and the tool instrumentation would not function below 2,835 m (9,300 ft) during this second try. The up-logs above that depth differ significantly from the down-logs of 20 October. Apparently the tool had been damaged by the high temperatures encountered during the second run, rendering the up-logs unreliable. Two successful temperature runs were made by Pacific Process Systems, Inc. on the 22nd and completed on the 23rd of October 2008. A Horner extrapolation was used to predict the equilibrium Bottom Hole Temperature BHT value of 295°C (563°F). This extrapolated temperature may be well below the actual equilibrium temperature at bottom of the well as described in detail in APPENDIX A. Subsequent to the above-mentioned logging runs, well NWG 46-16 bridged below the casing shoe at ~ 1,524 m (5,000 ft), rendering the deepest portion of the hole inaccessible. A near-equilibrium temperature log made on 8 December 2008 was only able to access the well to a depth of 1,430 m (4,700 ft). Based on this December log, and *assuming conductive behavior below 1.5 km (5,000 ft)* (a curve parallel to the one in 55-29) the BHT of the well at 3,500 m (11,500 ft) is projected to be up to 338 °C (640 °F). The temperature would be lower if fracture-hosted convection were occurring near the bottom of the well.

The Davenport temperature gradient well program was halted before completion. The original program called for twelve wells to be drilled, with permitting to 3,000 ft. The wells were located to resolve subsurface temperature anomaly boundary questions on the west flank. Of the original twelve temperature gradient wells proposed in Grant 109, six (Figure 19) were chosen to be included in a microseismic monitoring program (see Low Amplitude Seismic Emission Analysis (LASEA) section). These six wells were drilled with a target depth of 213 m (700 ft), with the exact depth determined at the drill site in order to set the casing shoe in solid rock. These six wells were never completed to the permitted depth as originally planned, and the remaining six proposed temperature gradient wells were never drilled.

Gravity

Two gravity surveys were completed under the direction of the Davenport scientific team, the first in 2007 and the second in 2010. Both surveys were carried out by Zonge International (Waibel et al., 2013). The first gravity survey was centered on the western flank of Newberry Volcano, with the greatest density of stations on the northern part of the western flank. The second gravity survey expanded the coverage to the south, north and east areas of the volcano. The high density of gravity stations of the Davenport surveys were not extended into the

Monument. The resolution of gravity within the Monument, therefore, is markedly poorer than the resolution on the flanks. The data from the Davenport surveys were integrated with data from earlier surveys (Gettings and Griscom, 1988). Figure 21 shows the combined distribution of gravity stations for both surveys done for Davenport Newberry. Figure 22 shows the complete Bouguer Anomaly with a reduction density value of 2.40 gm/cc. The black lines in Figure 22 show the boundary of the Newberry National Volcanic Monument. The blue lines show the perimeters of the two inter-caldera lakes, Paulina Lake and East Lake, and the westward-flowing Paulina Creek.

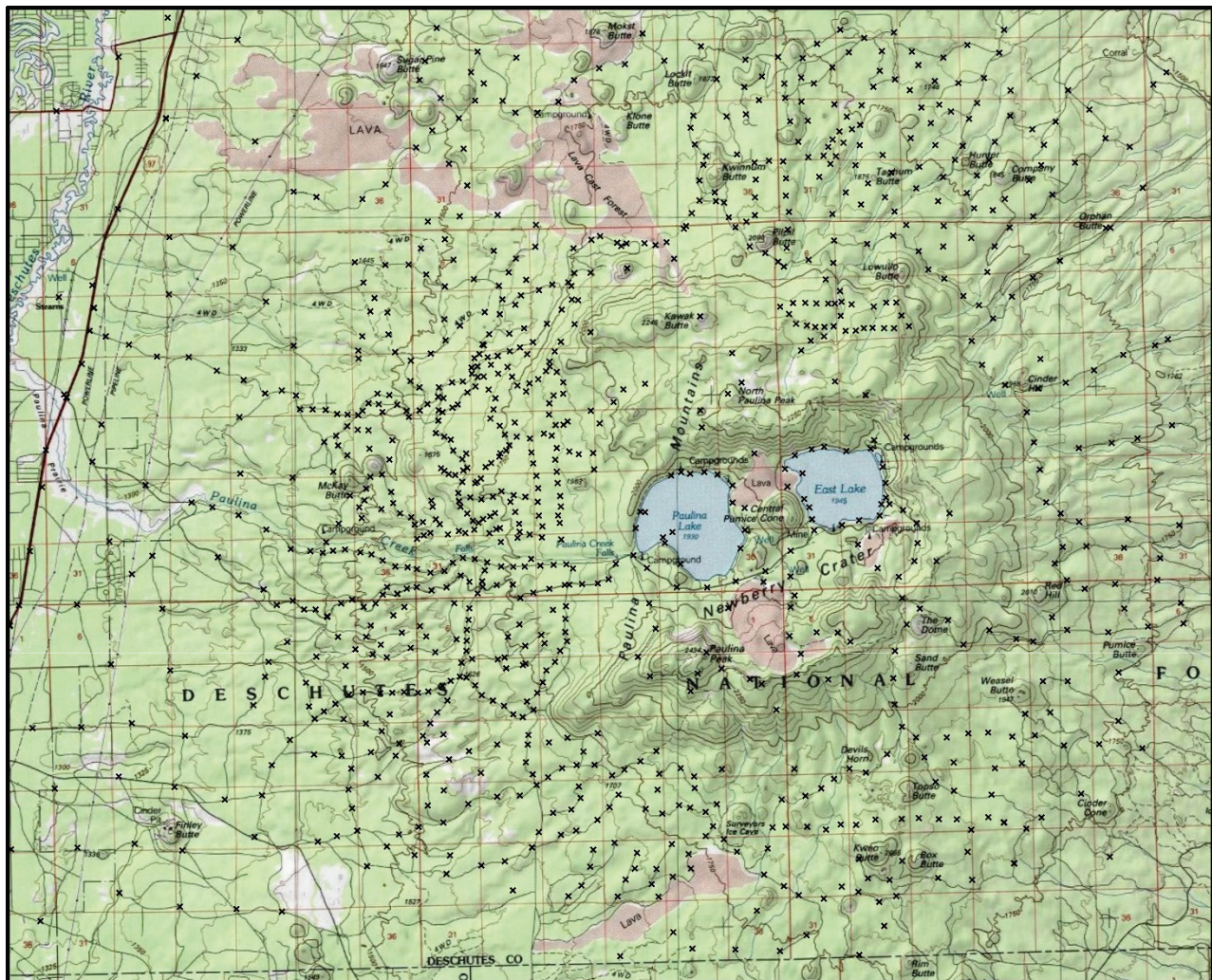


Figure 21: Topographic map of the central and western flank portion of Newberry Volcano. The black dots identify the locations of gravity stations.

The methodology for modeling gravity is relatively straight forward in general application. However the specific modeling of the gravity data on Newberry Volcano is problematic due to the variable nature of volcanic stratigraphy, both vertically and horizontally. The shallower few

thousand feet of volcanic rocks on the flanks of Newberry Volcano range from air-fall tephra to rhyolite and basalt flows. The density of these rocks is 2 grams per cubic centimeter (gm/cc), 2.5 gm/cc, and 2.99 gm/cc respectively. Near-surface lava flows tend to be more abundant on the north and south flanks, while air-fall tephra and pyroclastic flows tend to be more abundant on the eastern and western flanks. Underlying Miocene and older tuffs likely range from a density value similar to clay (2.2 gm/cc) at a shallower less compacted depth, to shale (2.4 gm/cc) with deeper increased compaction. Those areas where the tuff has been recrystallized due to thermal metamorphism related to pluton emplacement would approach a rock density similar to lava flows, or ~2.5 gm/cc. Granodiorite and gabbro plutons have average densities of 2.73 and 3.00 gm/cc respectively. The western flank of the volcano appears to have a shallow upper 2 km layer of mixed lava flows and volcanoclastic rock, with the clastic rock becoming more compacted with depth. Below 2 km the rock is largely a combination of plutons, subvolcanic rock and greenschist-facies metamorphic rock. A complete Bouguer anomaly with a reduction density value of 2.40 gm/cc would serve for the upper 2 km of the west flank and the remaining flank of the volcano (Figure 22). The deeper section of the west flank is better represented by a complete Bouguer anomaly with a reduction density value of 2.60 gm/cc (Figure 23). The reduction density of 2.6 gm/cc shows a reduced size for the high-density gravity anomaly on the west flank.

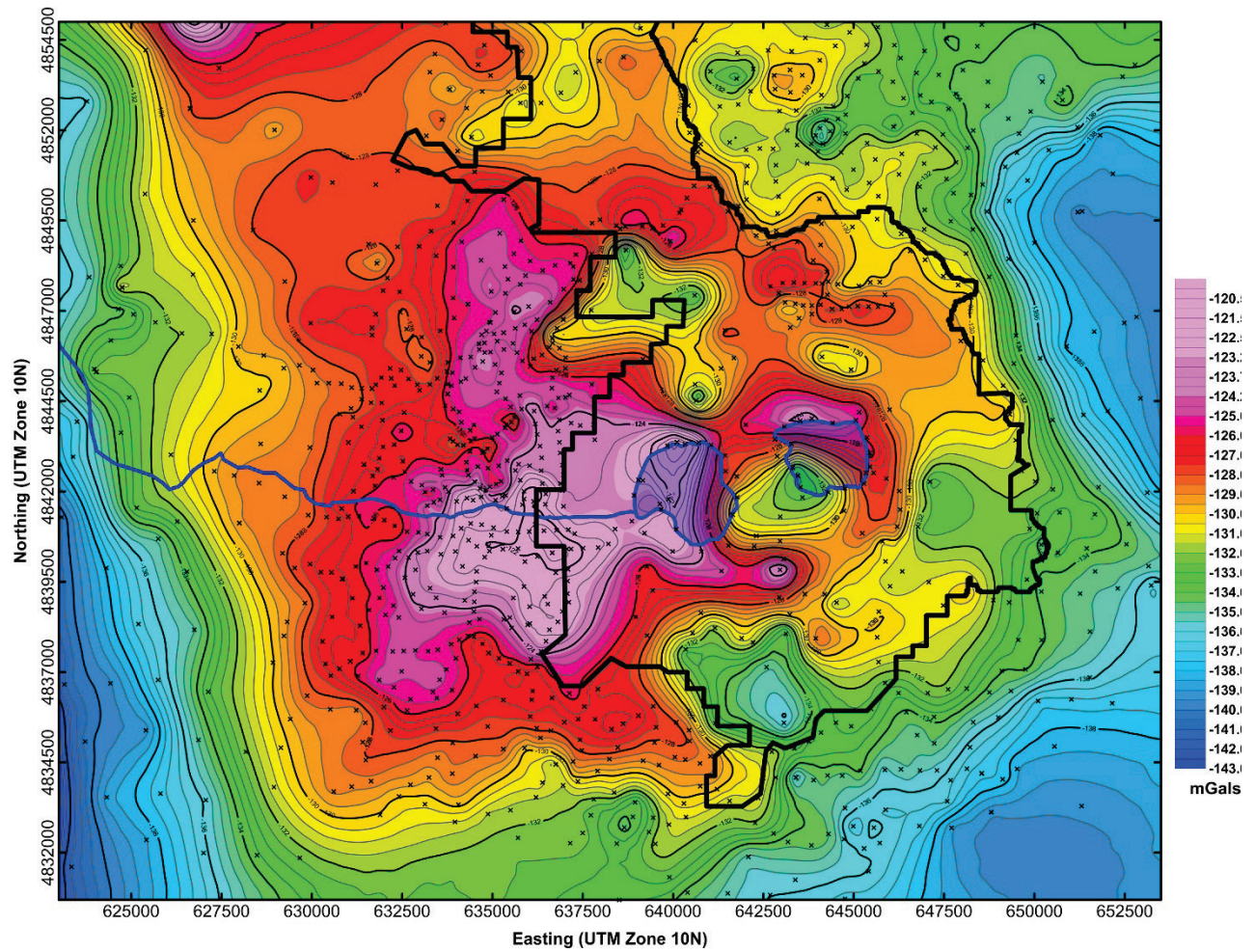


Figure 22: Complete Bouguer Anomaly with a reduction density value of 2.50 gm/cc. East Lake, Paulina Lake and Paulina Creek are shown with blue outlines. The Monument boundary is outlined in black.

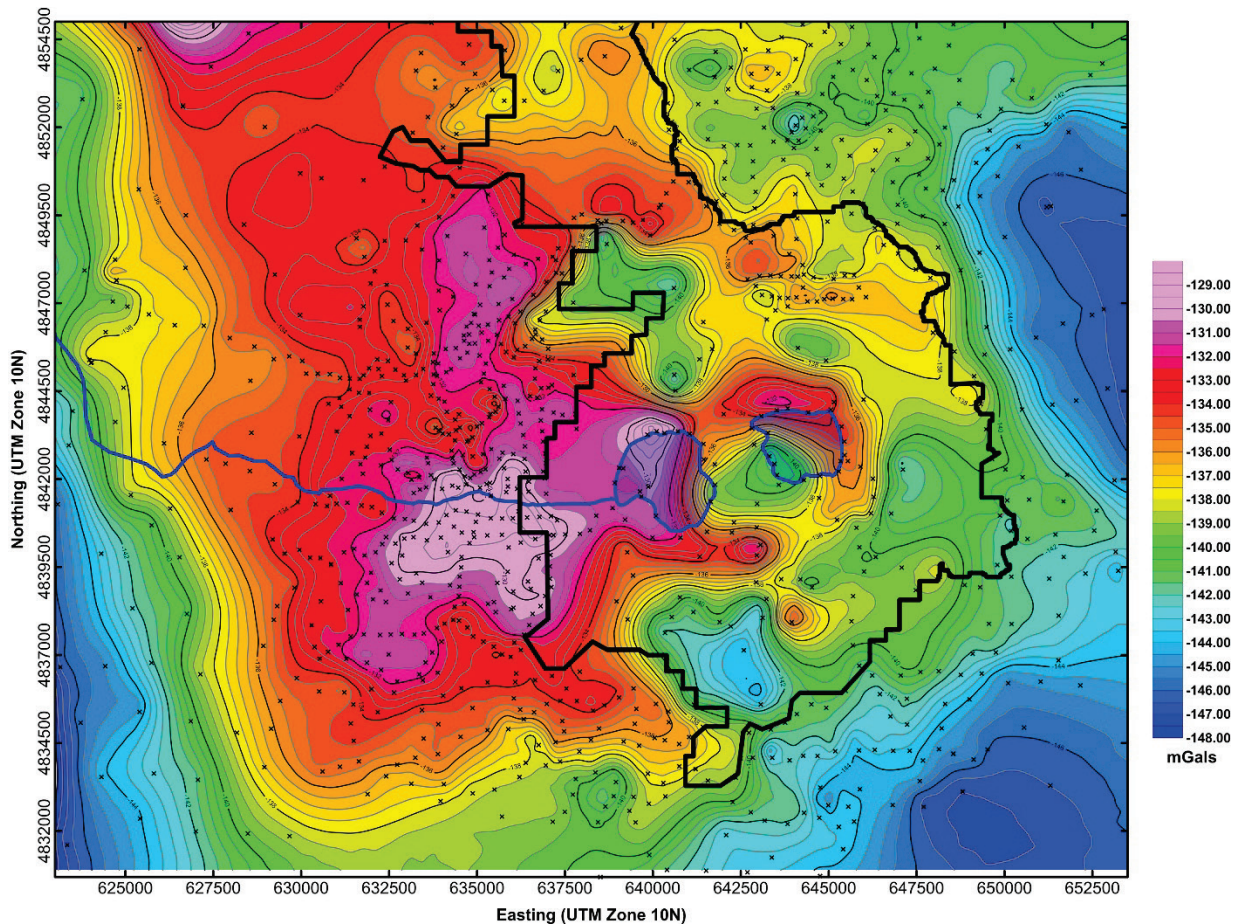


Figure 23: Complete Bouguer Anomaly with a reduction density value of 2.60 gm/cc. East Lake, Paulina Lake and Paulina Creek are shown with blue outlines. The Monument boundary is outlined in black.

The gravity data show the subsurface volcano to be markedly different from the observable topographic edifice. The data also show Newberry Volcano to be located toward the southern end of a larger high-density NNW-trending structural block. The east and west edges of the block trend NNW and the southern edge trends ENE. The southern and eastern flanks of the volcano extend off the gravity edge of this structural block. The positive gravity anomaly (magenta in Figure 22& Figure 23) underlying the western flank and portions of the caldera are interpreted as high-density plutons. This interpretation is supported by granodiorite encountered in wells (CE 86-21 and CE 23-22), and by felsic dikes encountered in well NWG 55-29 (Waibel et al., 2012). High temperature gradients observed in wells on the upper west flank and high temperatures measured in all four deep exploration wells indicate that at least a portion of the plutons underlying the west flank are young enough to still be hot.

Gravity Interpretation

Newberry Volcano (black outline in Figure 24) is located near the tectonic boundary of the Basin and Range province to the south and east, the Blue Mountain province to the north and the Cascade Range to the west. The volcano is positioned on a gravity high block, possibly a segmented fragment of the Blue Mountains province. Newberry Volcano is on the southeast portion of the angular higher-density structural block. The geometry of the block reflects the geometry of the Basin and Range structure. The eastern and western edges of the block strike somewhat west of

due north, complementing the strike of the Holocene fracture and volcanic vent strike on the north flank of the volcano. The lower gravity values at the western edge of the volcano reflect the young sediments of the La Pine basin.

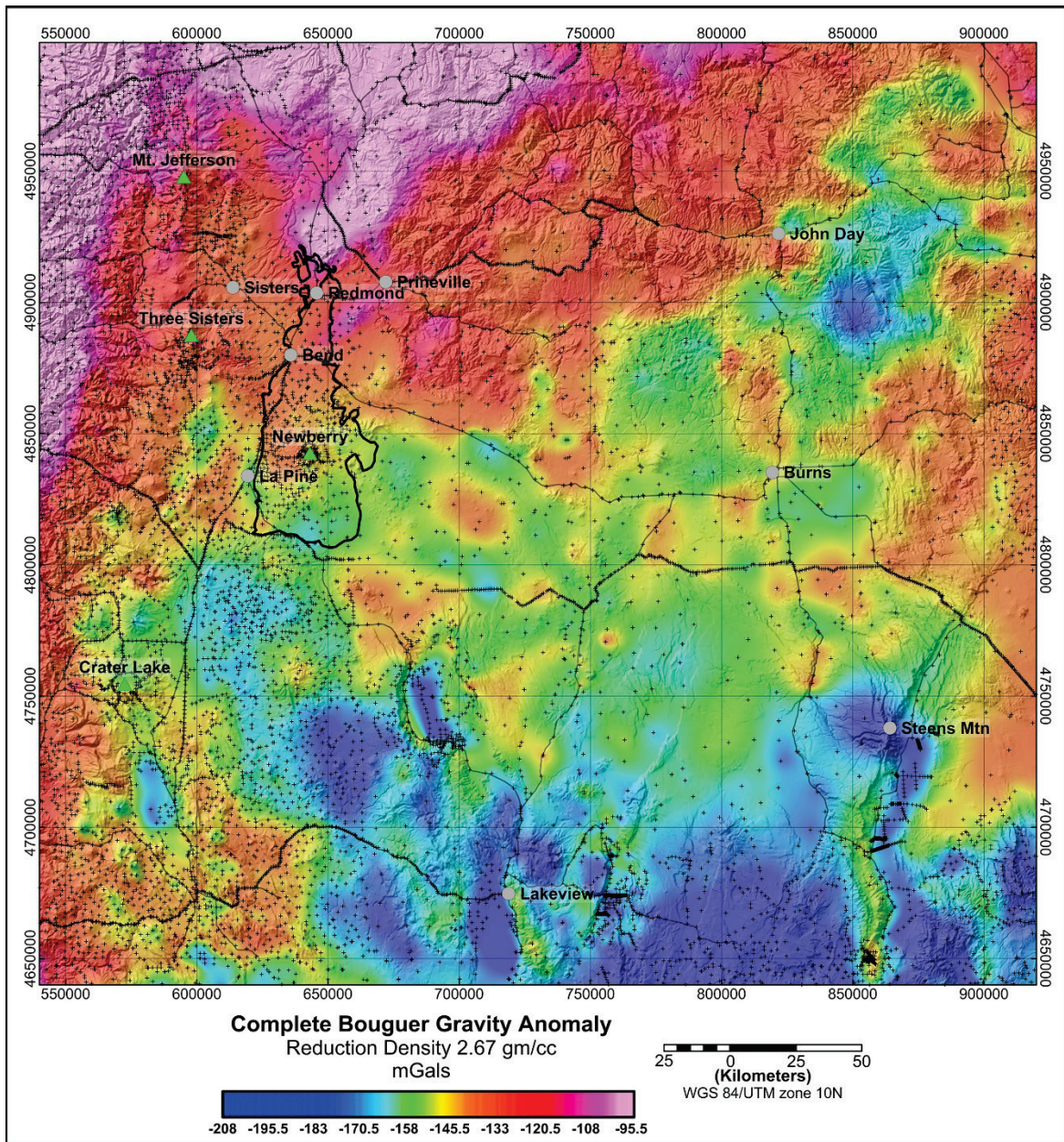


Figure 24: Regional gravity map of southeastern Oregon, Roberts et al., 2008. The black outline shows the maximum extent of lava flows from Newberry Volcano. The location of the caldera is marked by a green triangle. The shield physiographic form of the volcano is localized around the caldera.

One of the more striking features of the gravity data is the asymmetry of the center of the volcano, as reflected by the two lakes located within the caldera, and the location of the deeper plutons (Figure 22 and Figure 23). The high-elevation portions of the volcano, with interior boundaries

forming the pronounced caldera rims, are largely made up of domed silicic lavas. The gravity data, however, do not show these areas to be markedly underlain by a correlative mass of dense plutonic rock. The majority of the cooled subvolcanic magma bodies are located under the western one-third of the caldera and under the upper western flank of the volcano, rather than centered under the caldera. Recent phreatic eruptions and associated clastic rock infilling of the vents could account for a portion of the gravity-low areas within the caldera. The asymmetry of the gravity high and the center of the caldera is not reflected by the surface geology (MacLeod et al., 1995). Arc patterns of volcanic vents to the north of the caldera rim (red curved lines to the north of Paulina Lake in Figure 3) have been interpreted by some as ring fractures/faults (California Energy Co. unpublished document identifying structural drill targets). These interpreted features are not identifiable in either Figure 22 or Figure 23. The NNW-striking fracture zone hosting Holocene basaltic vents is also not identifiable with the gravity data.

Magnetotellurics (MT)

Magnetotelluric is a passive geophysical method, using powerful, naturally-occurring ionospheric current sheets and lightning storms as energy sources. As with many geophysical techniques, the ability to model features is controlled by geometry of both the station density and depth of the feature. Higher density station spacing accommodates higher resolution modeling of shallow variations in resistivity. The resolution of variations in electrical resistivity decreases as depth increases. Local shallow features may show in the near-surface resistive layers but only progressively larger-scale features can be resolved as depth increases. For decades, Magnetotelluric surveys have been a very popular geophysical tool in geothermal exploration. This popularity is based on geophysicists modeling geothermal systems as having electrical resistivity contrasts at depths of several kilometers that can be resolved by MT surface measurements. The popular interpretive MT model for geothermal resources in volcanic terrain is the “mushroom” model (Ussher, et al., 2000). This model assumes a deep, electrically resistive high-temperature hydrothermal up-flow “stem”, overlain by a broad lower-temperature electrically conductive clay alteration “cap”. Temperature attributions for the various electrical resistivity layers are given as 1-10 Ωm corresponds to 70 - 200°C and values greater than 100 Ωm corresponds to 200°C or higher. The assumptions made when applying this model for exploration are that high-temperature electrically resistive greenschist mineral phases at depth are artifacts of, and unique to, a currently active geothermal system, and that an overlying shallow electrically conductive lens or cap is an artifact of, and unique to, discharging geothermal fluid discharging from a geothermal "stem". Morse and McCurry (1997) observe that the low resistivity horizon in the Snake River Plain basalts is associated with secondary calcite, clay, zeolite and the devitrification of volcanic glass. They suggest that a decrease in pH with depth and an increase in temperature with depth may play roles in the increase in electrical conductivity. They do not address possible changes in Eh with depth.

Some of the first MT data were collected at Newberry Volcano by the University of Oregon in 1986 (Urquhart, 1988). Modeling based on these MT data was consistent with the area being a potentially important geothermal resource. The results of this early work have provided the framework for all later work. Subsequent to this early work, two MT surveys were conducted on behalf of Davenport Newberry. The first, centered on the western flank north of Paulina Creek, was carried out by Geosystems in 2006. The second, carried out by Zonge International in 2011, provided in-fill on the western flank and expanded to the north

and south slides of the volcano (Waibel et al., 2013). Figure 25 shows the combined station locations from both surveys. The main emphasis with the MT processing for this study has been to develop an integrated understand of the relationship between the MT, gravity and geology data, and insight into possible structures as indicated by LIDAR.

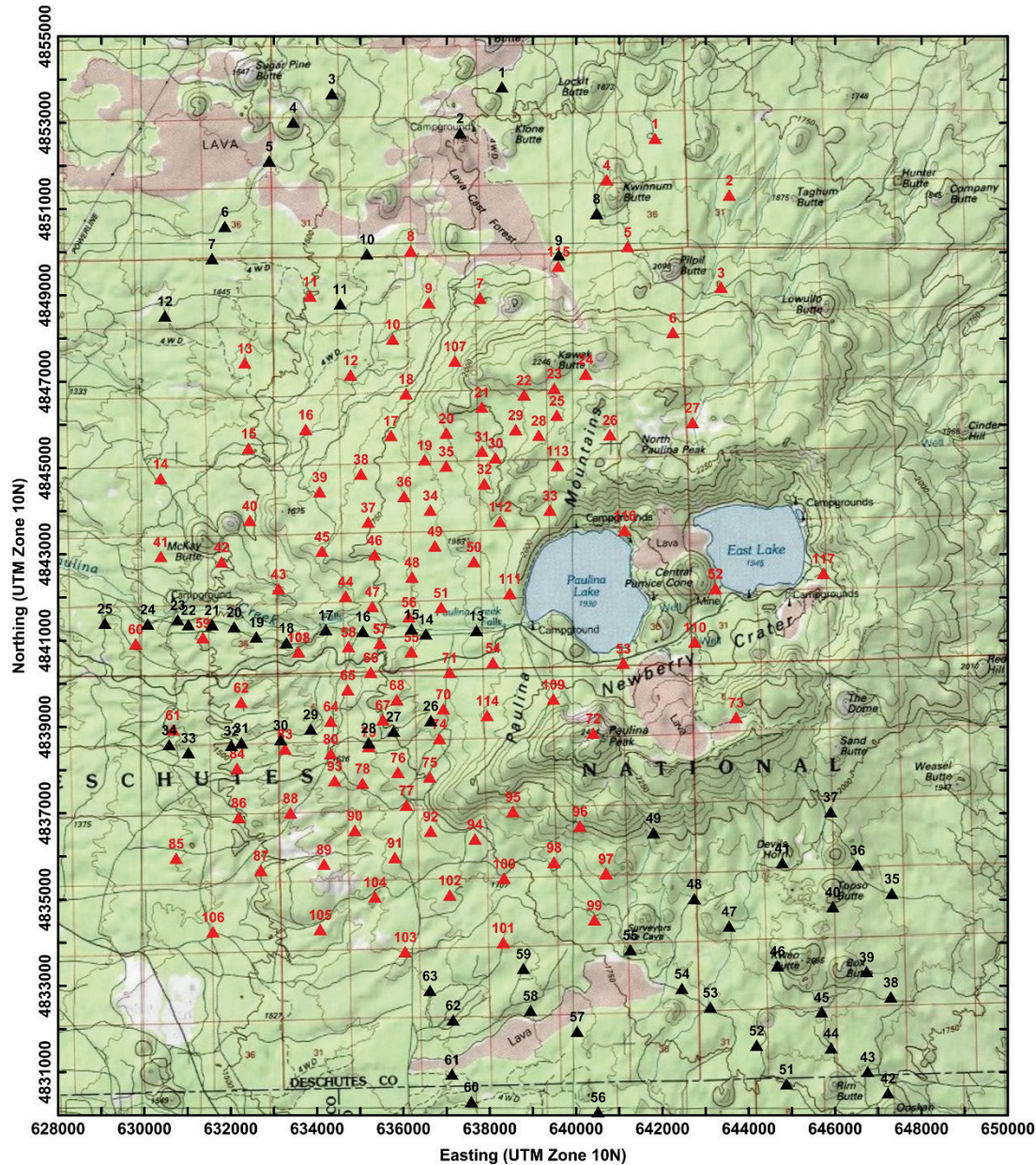


Figure 25: MT station locations, Davenport surveys, on Newberry Volcano. Geosystems 2006 stations are in red and Zonge International 2011 stations are in black (Waibel et al., 2013).

The magnetotelluric survey conducted by Zonge International in the summer of 2011 was designed such that where possible, data were collected along extended lines for 2D inversion. Also, locations were chosen so that data could be integrated with the previous MT survey conducted in 2006 by Geosystems. No MT data could be collected in the caldera because of

National Monument management restrictions. Therefore the resolution of 2-D and 3-D interpretations within the caldera is of very poor quality.

The 2006 MT dataset was reprocessed and presented as a 3-D model. Vertical and horizontal slices were extracted from the 3-D modeling. The MT data processing in 2012 included all available data. The emphasis at this time was to maximize the advantage of relatively high station density. Particular attention was given to the upper two geoelectric layers, the very shallow resistive layer and the underlying shallow highly conductive layer. Figure 26 and Figure 27 show the comparative results of these two efforts along the same vertical slice, line E-W 05. Figure 28 shows the location of this section and of other sections discussed below. The 2012 data processing produced markedly improved resolution within the shallow conductive layer.

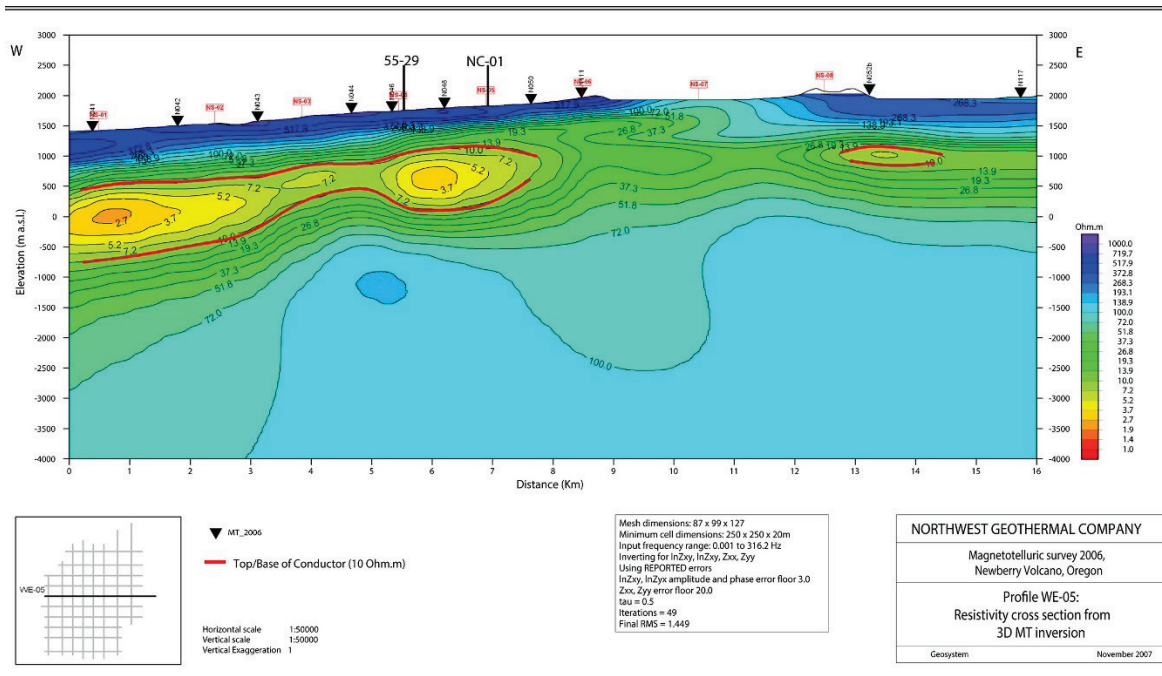


Figure 26: E-W 05 cross section showing the results of the 2008 processing of the 2006 data. The locations of Davenport deep exploration well NWG 55-29 and Santa Fe temperature gradient well NC-01 are identified. The small arrows identify the location of MT stations (Waibel et al., 2013).

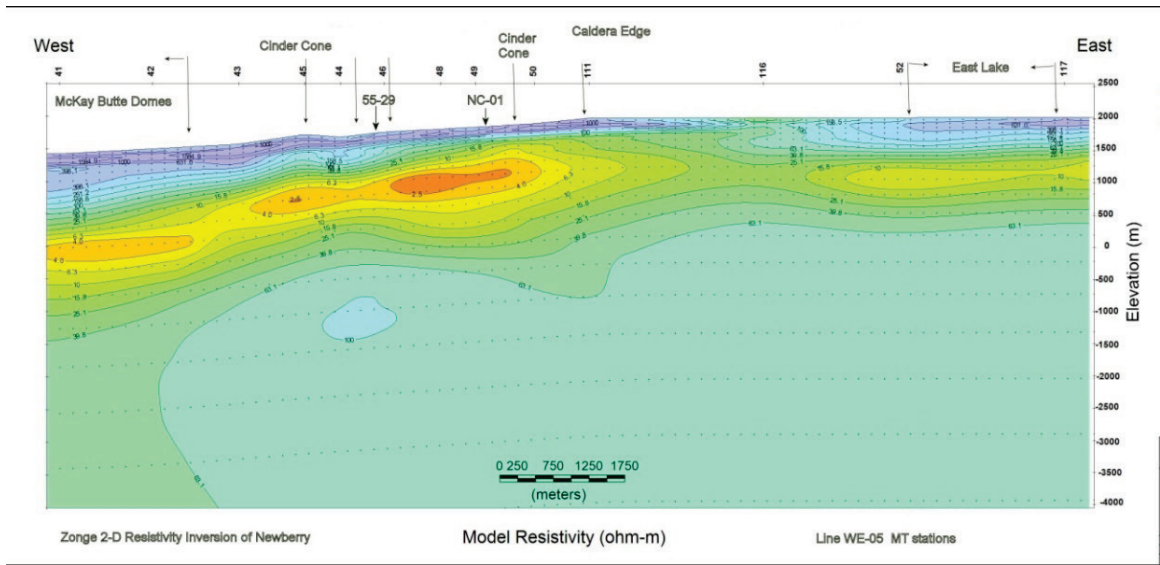


Figure 27: E-W 05 cross section showing the results of 2012 processing. The locations of Davenport deep exploration well NWG 55-29 and Santa Fe temperature gradient well NC-01 are identified. The small arrows identify the location of MT stations. Other geographic points are also identified (Waibel et al., 2013).

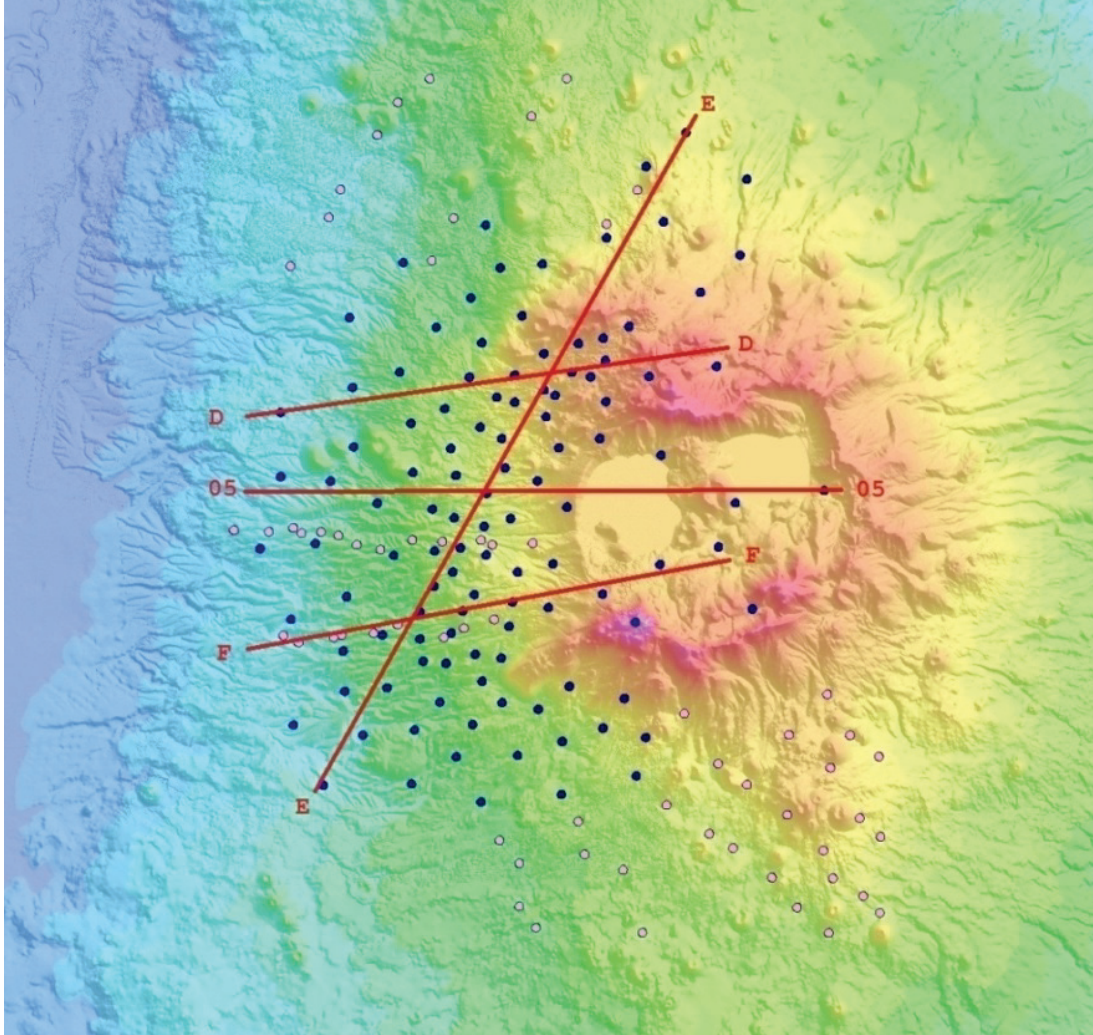


Figure 28: Map of Newberry Volcano showing MT station locations. The red lines show the location of four MT slices of lines 05, D, E, and F. The blue dots identify MT station locations from the 2006 survey. The red circles identify MT station locations from the 2011 survey (Waibel et al., 2013).

MT Discussion

Results from Zonge integrated MT data processing are broadly consistent with the University of Oregon (Urquhart, 1988) and the 2006 Geosystems results. On the flanks of the volcano, 1-D inversions of the MT data consistently image three principal geoelectrical units. Each of the three layers varies in thickness and resistivity. The top layer, which includes the shallow isothermal layer, is resistive, on the order of 1000's of Ωm , and has a thickness of about 1 kilometer. The layer below this is relatively conductive, about 10 Ωm , and varies in thickness and conductivity significantly. Below this the resistivity increases to about 100 Ωm . This modestly resistive third layer may have a thickness of several kilometers. The highest deep electrical resistivity underlies the western flank (e.g. Figures 30 & 31). The extent of this high electrical resistivity does not correspond to either the surface geology (Figure 3) or the geometry of the high rock density (Figure 22) underlying the west flank.

Both Figure 26 and Figure 27 show an upper electrically conductive layer of varying thickness

on the west flank, imaging lenses with highly conductive centers, rather than a more equal-thickness layer. Two data processing events occurred, the 2-D data processing of 2012 and the 3-D data processing done in 2008. Figure 27 shows the results for Line 05 2012 processing with much more detail, and Figure 26 shows the results for the same line done with the older processing technique. Lines D, E and F (Figure 29, Figure 30, & Figure 31, respectively) also show good detail of similar intense electrically conductivity lenses within the upper conductivity layer. Station density is an important constraint when considering the reliability of the shallow conductive lenses identified from data processing. Higher station density provides increased confidence in depicted variations within the shallow conductive layer. The high conductivity lenses defined with one overlying station, or identified between two wide-spaced stations may well be artifacts of the data processing program. Those shallow high conductivity lenses identified by multiple close-spaced stations are more likely to represent actual variations within the shallow conductive horizon.

MT line D strikes approximately north 80° east (Figure 29), and crosses the well NWG 46-16 location. The eastern portion of the line lies to the north of the caldera rim, crossing the Holocene north-northwest volcanic vent trend. Well NWG 46-16 is located between two lenses within the electrically conductive layer. The electrically conductive lens to the west (left) of well 46-16 shows vertical distortion, which is not apparent in other lenses. The electrically conductive layer under the Holocene vent trend shows little variation, though the MT stations are widely separated and would likely not be able to identify short-spaced variations. The deeper electrically resistive layer shows only a very broad trend with no perturbations in the area of well NWG 46-16, which reached a depth of approximately 1,500 m elevation on this slice. The geothermal system intersected by well NWG 46-16 is not identifiable on this image.

MT Line E (Figure 30) strikes N-NE, and intersects wells 55-29, 46-16 and the north-northwest volcanic vent zone. On this line, well NWG 55-29 is shown to be located within a lens of particularly intense low temperature clay alteration as depicted by the very low electrical resistivity. This alteration, as identified on the MT slice, begins at a depth of about 400 m (1,300 ft), and transitions toward the lower electrical conductive greenschist facies alteration at a depth of about 2,200 m (6,400 ft). This agrees with the mineralogy observed in the well cuttings from well 55-29. Well NWG 46-16 is shown located outside of the intense clay alteration lenses. As with Line D (Figure 29), the Holocene north-northwest volcanic vent trend is not recognized in this MT slice, though the MT station spacing is quite wide in this area and may not have been able to identify short spaced perturbations. This figure does show a marked variation in the subsurface character of the volcano from the west flank and the northern flank. The western flank shows a relatively compact shallow conductive layer. The northern flank shows a sloping, ever deepening higher electrical resistivity boundary. This difference may be related to the plutons (inferred from the gravity density anomalies, Figure 22 and Figure 23) and associated eruptive history of the west flank that is not present under the northern flank.

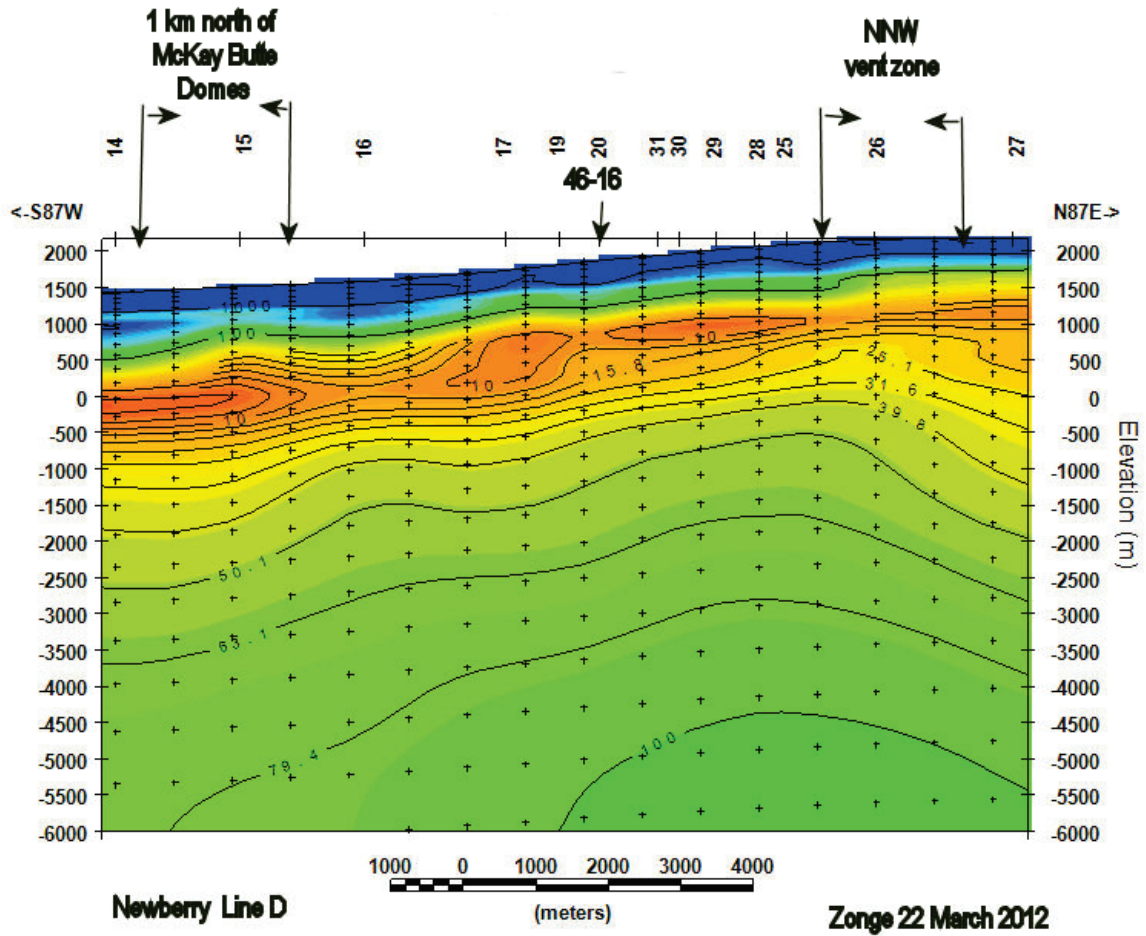


Figure 29: 2-D MT slice Line D. The two digit numbers across the top identify MT stations. This figure is compressed horizontally (Waibel et al., 2013).

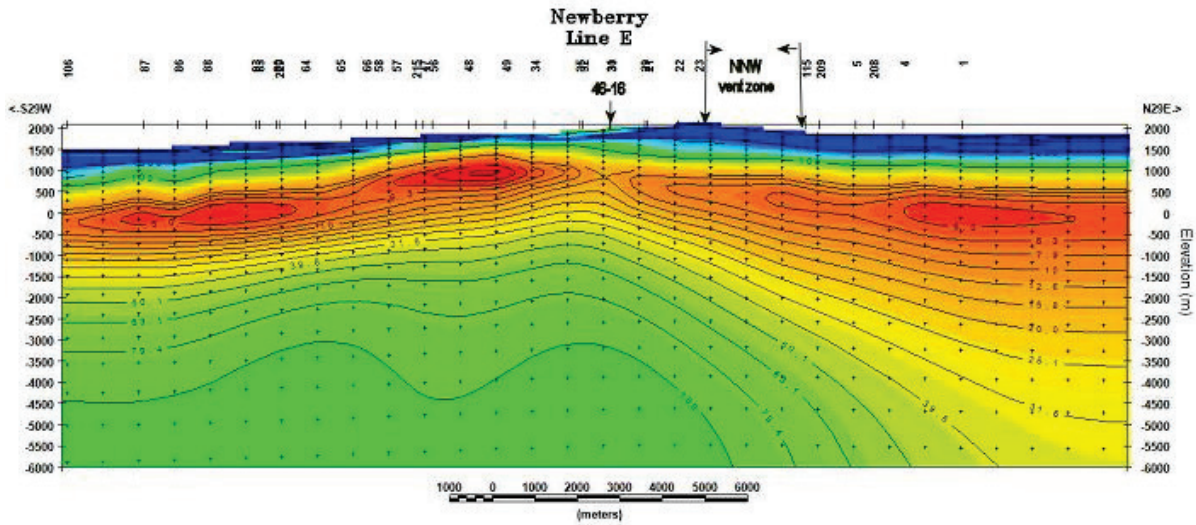


Figure 30: 2-D MT slice Line E. The one, two and three digit numbers across the top identify MT stations.

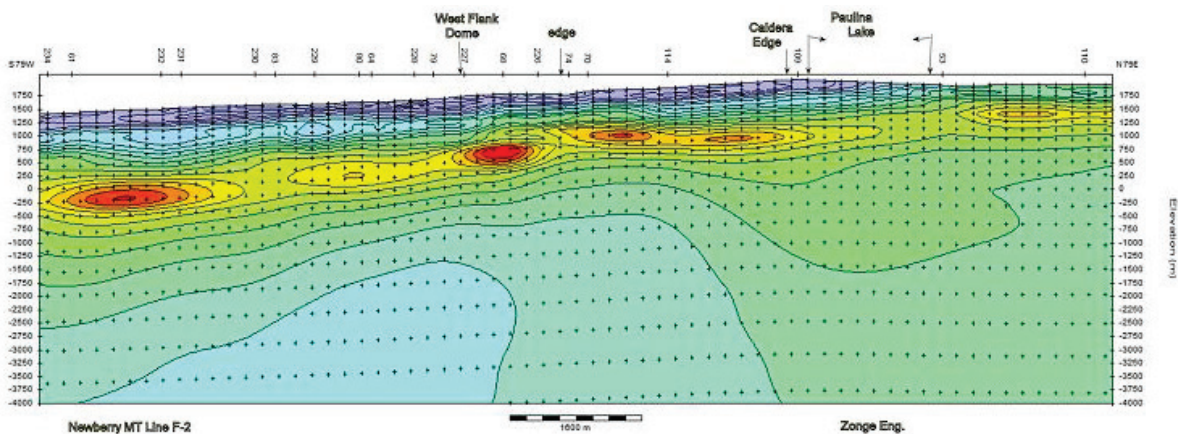


Figure 31: 2-D MT slice Line F. The two and three digit numbers across the top identify MT stations.

MT line F (Figure 31) strikes approximately north 80° east and extends into the caldera along the southern edge of Paulina Lake (Figure 28). It crosses the west flank dome, an arcuate boundary identified on LIDAR and the caldera rim (Figure 36). The western termination of a highly electrically conductive lens ("edge" on Figure 31) matches the location of the arcuate boundary on the LIDAR image. The very deep electrically resistive zone is identified as occurring westward of the highest temperature gradient area.

Many of the highly electrically conductive lenses are documented in the 2-D slices with adequate MT station density to give them credence. Two aspects of these lenses are of particular interest: first is the source of these lens occurrences and second is the apparent vertical off-set within the conductive layer in Line D (Figure 29), just west of well 46-16. The vertical off-set, if not an artifact of computer modeling, may well show vertical structural displacement. The lenses themselves are a bit more challenging. At first glance,

the intense electrically conductive lenses within the conductive second layer in the Newberry MT surveys appear similar to the “mushroom cap” model, which assumes a shallow conductive lenses resulting from clay alteration of rocks by upwelling geothermal fluid. This model can occur in volcanic terrain (i.e., Raharjo et al., 2002); however, the MT survey results from Newberry Volcano demonstrate the inadequacy of the invocation of this model ubiquitously in volcanic terrain. Wells NWG 55-29 and N-2 were drilled through a clay-alteration “mushroom cap”. Well NWG 55-29 was drilled deeper into the “mushroom stem”. Evidence of current or past geothermal fluid circulation has not been observed in any of the data, including core, cuttings and geophysical logs, from wells N-2 and NWG 55-29. In contrast, well NWG 46-16, which is located outside of both intense electrically conductive lenses and deeper electrically resistive "stems", is the only well that intersected active geothermal fluid movement. So, on Newberry Volcano, the wells that drilled into the MT “mushroom” model features found no evidence of present or past geothermal fluid and the well that intersected geothermal fluid was drilled at a location outside any of the MT “mushroom” model features.

The MT data do show a broad shallow electrical conductive layer with interspersed highly electrically conductive lenses (Figure 27, Figure 29, Figure 30 and Figure 31). The temperature gradients on the western flank of Newberry Volcano are high enough to provide some control on the low conductivity layer. The base of the conductive layer does generally correlate with the 150°C temperature isotherm as measured in the wells (Figure 37). The temperature range for clay alteration of volcanic rock is broad enough, and the temperature gradient on the western flank of Newberry Volcano is high enough that the shallow electrically conductive layer is most likely caused by a combination of low-temperature devitrification of volcanic glass shards, diagenetic alteration of volcanic and volcanoclastic rock and low temperature thermal alteration, without recourse to geothermal brine outflow. The very high electrically conductive lenses are areas where these mineral reactions occurred in greater intensity within the shallow conductive layer independent of temperature or geothermal fluid perturbations. This suggests a lithologic variation peculiar to the geometry of the lenses that is not ubiquitous across the flank. One lithologic variation would be localized substantial increases in volcanoclastic content, which would facilitate clay alteration. These lenses may reflect the location of older volcanic eruption craters associated with the underlying older plutons, and now buried by subsequent volcanic and volcanoclastic flows and deposits.

Aeromagnetics

An airborne magnetic survey was carried out by the U.S.G.S. as part of the 1970’s and 1980’s Cascade Range research. This type of survey responds to magnetic masses and is sensitive to mafic igneous rocks which are more iron rich than the silicic rocks. A contour map of the magnetic anomaly field with the Earth’s background field removed and “reduced to pole” is shown in Figure 32. The reduction to pole makes the anomalies on the map correspond more closely with the causing rocks and therefore associations are relatively uncomplicated.

The aeromagnetic data show only occasional and tentative correlations with other datasets. The aeromagnetic pattern shows high values (red) along portions of the upper elevations of the volcano, in part co-located with mapped mafic lava outcrops. It is notable that there is no obvious correlation between the NNW-striking Holocene volcanic vent trend and the aeromagnetic image.

Two areas with a tentative correlation between aeromagnetic lows and gravity lows are located outside the primary area for geothermal exploration, and were not pursued in this study.

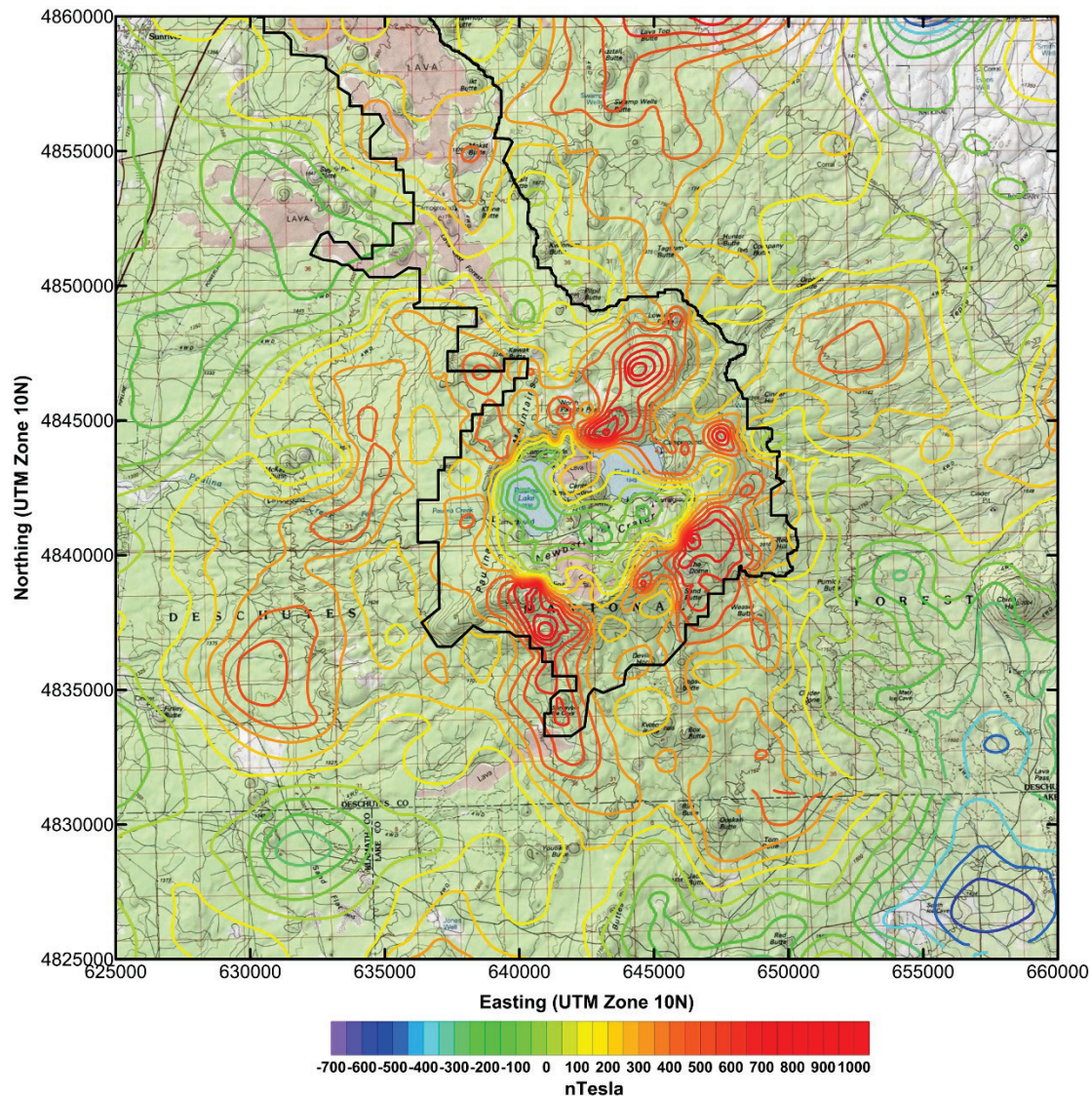


Figure 32: Map of total aeromagnetic field reduced to pole and mean removed. From USGS Survey 1975. The black line outlines the Newberry National Volcanic Monument boundary.

LIDAR

The exploration for geothermal resources on Newberry Volcano has both generated new and taken advantage of existing surface and subsurface imagery of the volcano. LIDAR imagery of

Newberry Volcano became available to Davenport in 2011 (Figure 33). The LIDAR imagery allowed the technical team to see details of topographic features with a resolution that previously had been unavailable with aerial photography and topographic maps. This new imagery should be the catalyst for much research on the volcano, ranging from surface lava flow boundaries to deep regional tectonic structures. This discussion will be confined to how the LIDAR imagery relates to other data in this hydrothermal exploration project. The LIDAR imagery allows interesting comparisons with other datasets. Many of the Quaternary silicic outcrops on the flank of the volcano are identifiable (Figure 34) though there is no surface imagery correlation with the location of plutons underlying the west flank (Figure 35).

A variety of features and patterns are apparent on the LIDAR imagery. These include the nested morphology of the caldera, the NNW and NE structural and vent patterns on the northern flank, the north-trending subsidence breaks along the transition zone between the volcano deposits and the La Pine basin to the west and the surface textural dominance of volcanoclastic deposits on the western and eastern flanks. A comparison of the LIDAR surface imagery with the geologic map (Figure 3 & Figure 33) shows correlation with volcanic vents, younger lava flows and volcanoclastic deposits. Older silicic domes on the west flank of the volcano are able to be identified on the LIDAR imagery when using the geologic map for reference (Figure 34). The four geophysical images of the volcano show little in the way of systematic correlations, as shown in the following figures:

- gravity, Figure 22 and Figure 35
- aeromagnetic, Figure 32
- MT conductor layer, Figure 38
- temperature gradient, Figure 41

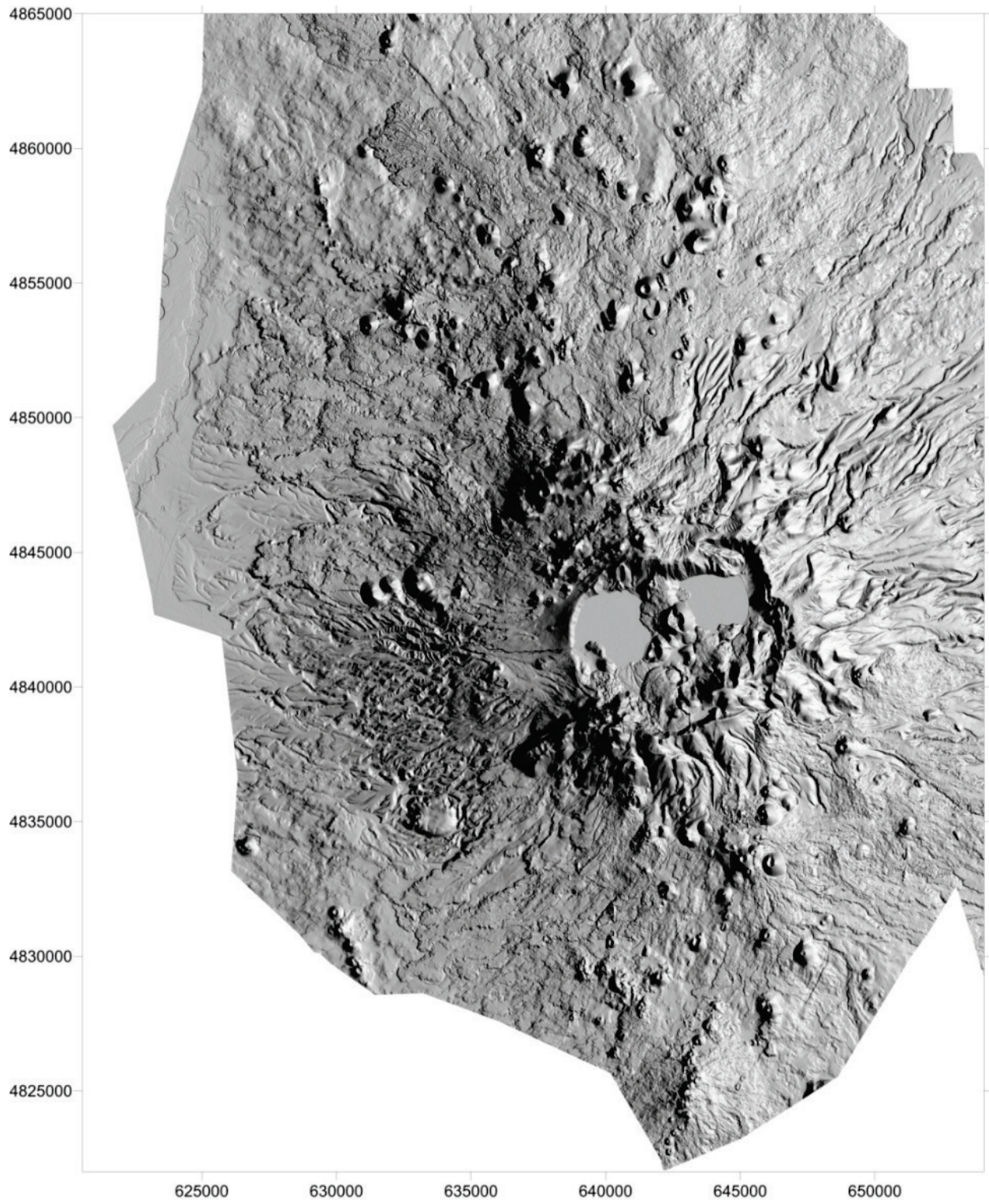


Figure 33: LIDAR image of Newberry Volcano with the illumination at 80 degrees.

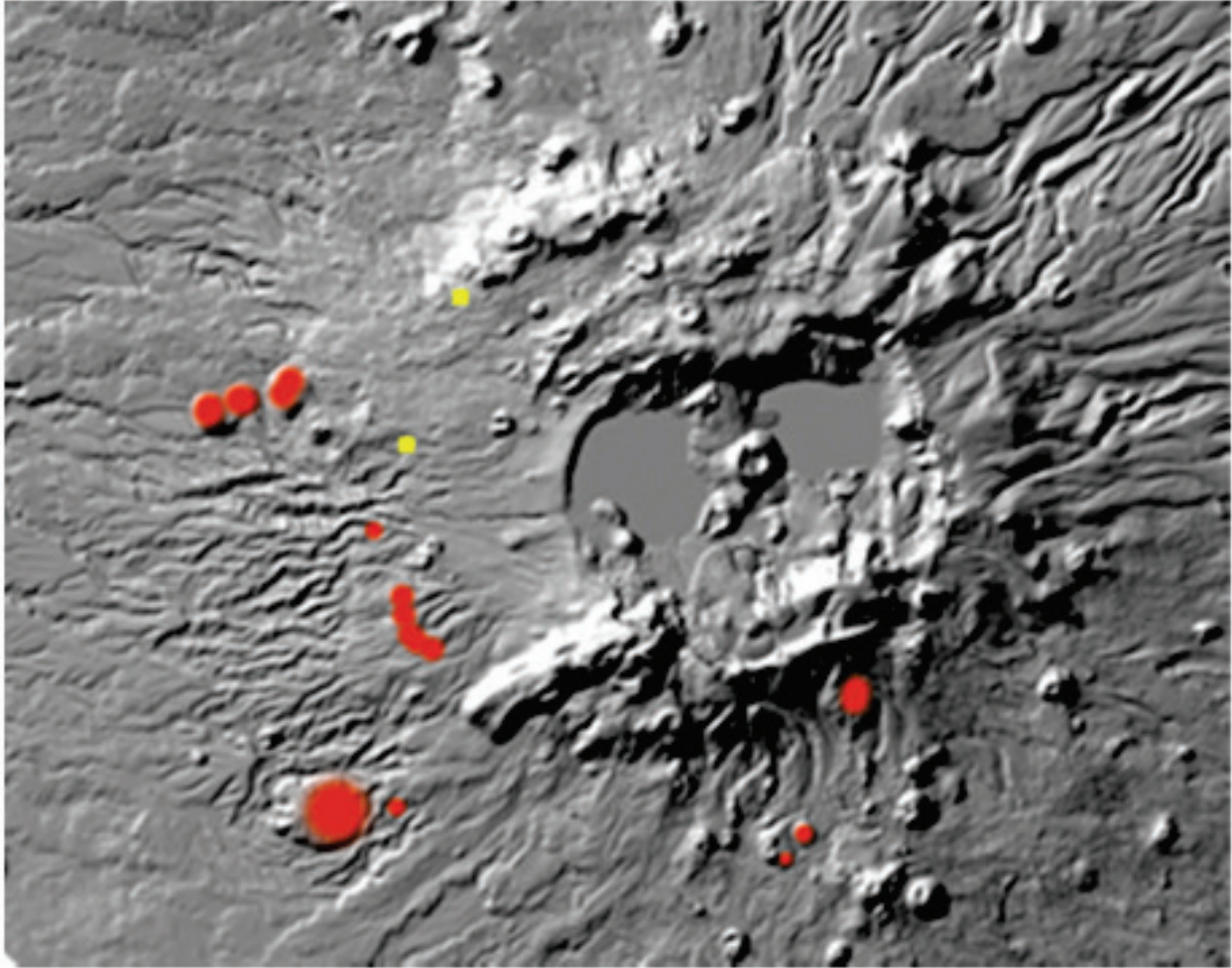


Figure 34: Silicic outcrops on the flank of Newberry Volcano. LIDAR image with the illumination at 320 degrees. The red areas denote the location of Quaternary rhyolite and dacite outcrops on the flank of the volcano (Qer and Qed of MacLeod et al., 1995). The yellow dots identify the two Davenport well sites. The Holocene silicic volcanic outcrops within the caldera are not noted.

The LIDAR imagery does, however, act as a catalyst for considering the volcanic history and how that facilitates interpretations of aspects of the geophysical data. The gravity maps identify areas of high-density rock underlying portions of the west flank (Figure 35). These are inferred to be an accumulation of plutons, an interpretation supported by the lithologies observed in data from deep exploration wells on the west flank (see DEEP EXPLORATION WELLS section above). The temperature data show the heat content of the plutons decreases to the west, implying a decrease in age of the plutons from west to east. It would seem to follow that the location of volcanic eruption sites would likely progress from west to east as the magma emplacement moved from west to east. Evidence of older vent areas on the upper western flank of the volcano are hinted at in the LIDAR imagery. To the west of Paulina Lake is an area of limited surface erosion with an arcuate western boundary (Figure 36). This feature is terminated to the east by the very subtle current west rim of the caldera and by Paulina Lake, in an area where the pronounced cliffs of the northern, eastern and southern caldera rim are missing. Rhyodacite pumice from the ash flow, which forms the modest west rim of the caldera, is estimated to be about 80,000 years old (Jensen,

2006). This ash flow continues to the west, constituting the surface unit in the area of limited erosion within the arcuate boundary. This area lying to the west of Paulina Lake may be the remnant of an older volcanic eruption crater that has since been in-filled, at least in part by the 80,000 y.b.p. tuff. The location of the surface morphology boundary (purple line of Figure 36) corresponds with the western edge of a highly electrically conductive lens observed in MT line F (Figure 31, denoted as “edge”). If the surface morphology of this area observed on the LIDAR imagery does identify the western ruminant of a volcanic eruption creator, the highly electrically conductive lens could be the result of localized aggressive clay alteration of volcanoclastic debris infilling the crater.

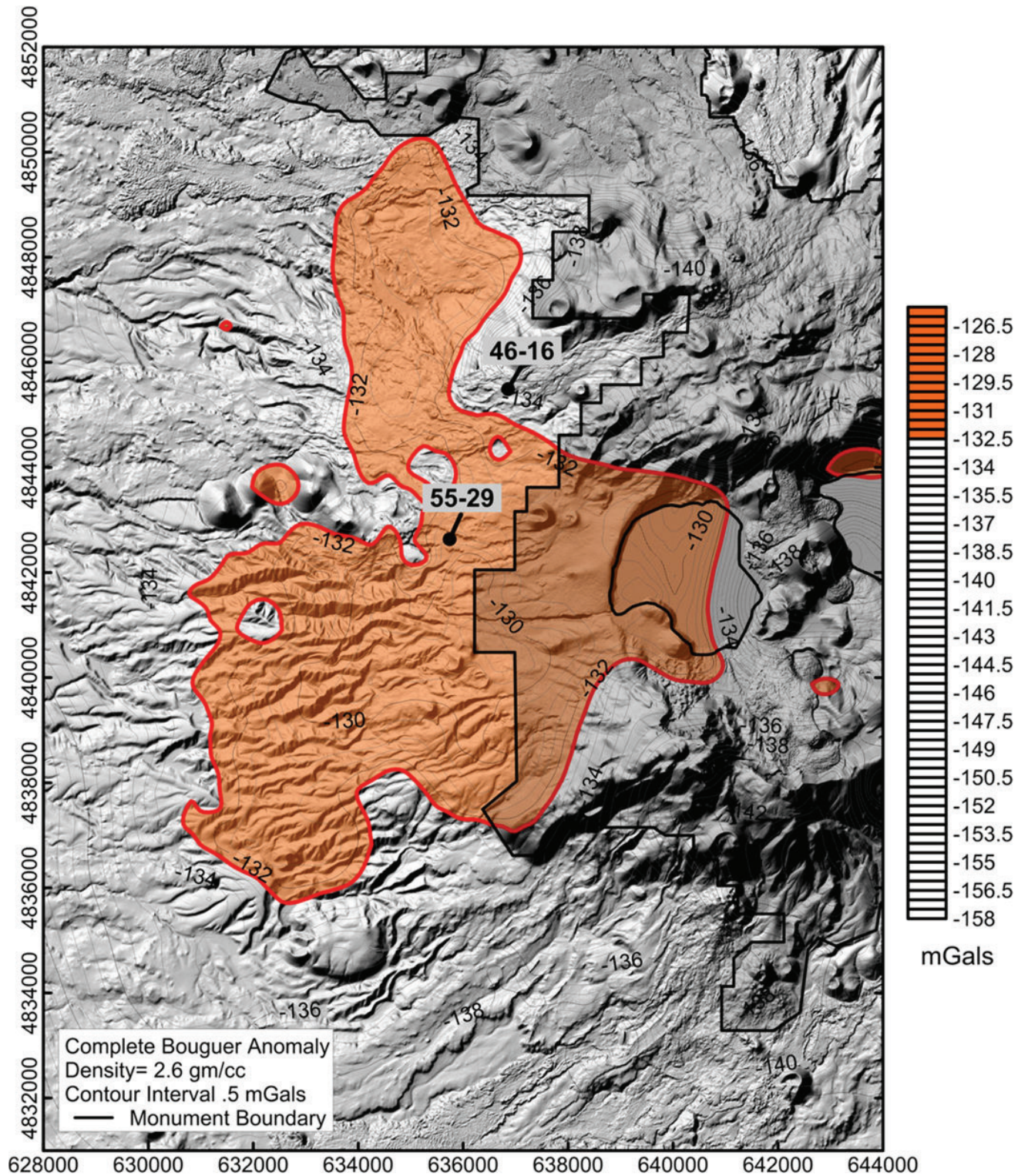


Figure 35: View of LIDAR image of the upper western flank of Newberry Volcano with the high density gravity anomaly overlain. The black line boundary enclosing a shaded area identifies the location of the Newberry National Volcanic Monument.

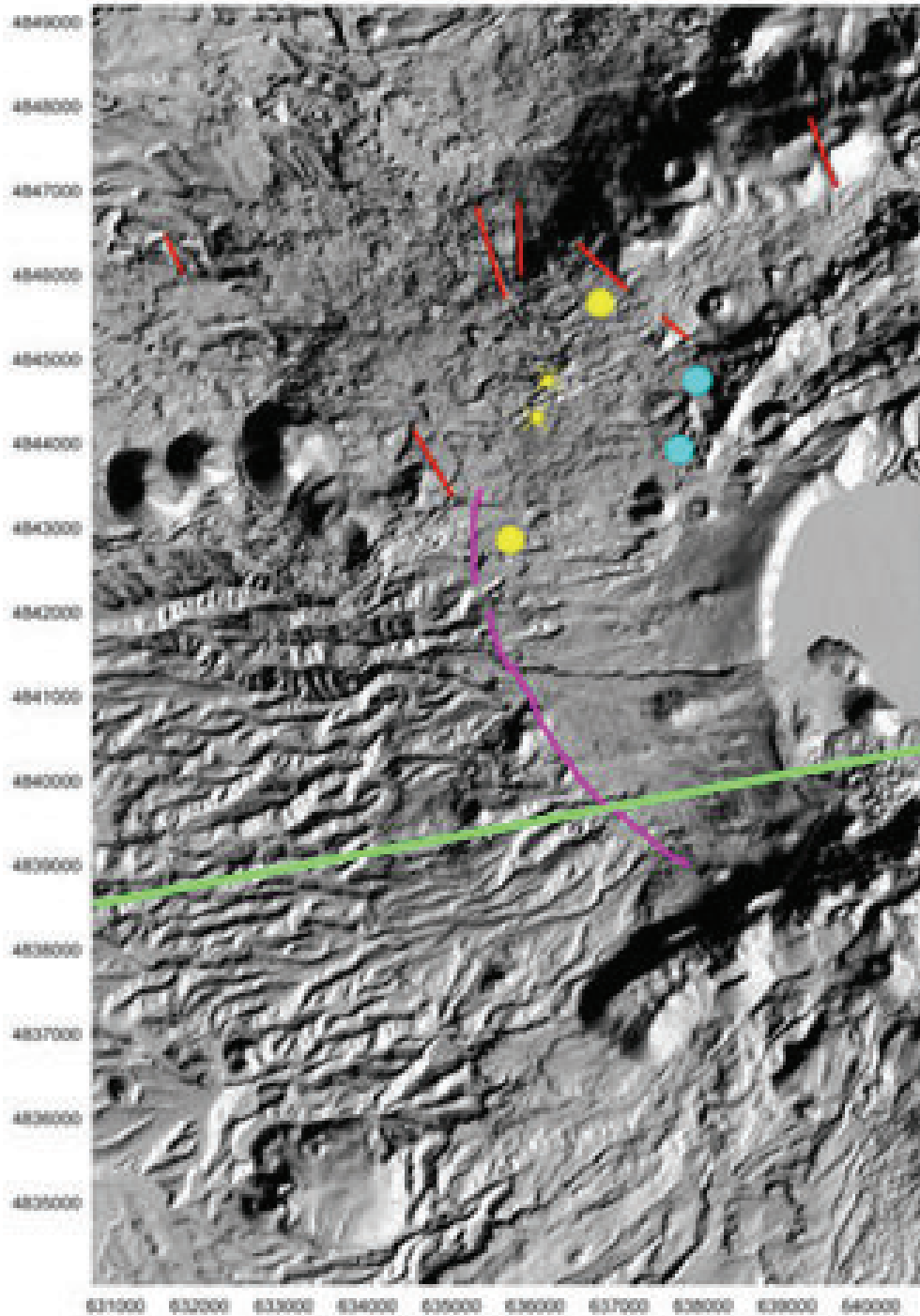


Figure 36: LIDAR image of the west flank of Newberry Volcano. The yellow dots mark Davenport deep exploration wells NWG 46-16 (north) and NWG 55-29 (south). The blue dots mark deep exploration wells CE 23-22 (north) and CE 86-21 (south). The yellow asterisks marks the locations of recently recorded small earthquakes. The purple line marks the arcuate boundary between predominantly unbroken surface area to the east and the more broken surface areas to the west and north. The green line identifies the location of MT line F (Figure 31). The red lines identify a few of the linear patterns, some of which may reflect surface breakage associated with deeper strain.

DISCUSSION

The Western Flank Thermal Anomaly: Temperature at Depth

The heat content calculated beneath the west flank of Newberry Volcano is based on the exploration data developed so far. Temperature data from intermediate and deep wells have demonstrated high gradients (averaging $109\text{ }^{\circ}\text{C}/\text{km}$ ($6^{\circ}\text{F}/100\text{ ft}$) or greater) and temperatures in excess of 260°C (500°F) at depths as shallow as about 1830 m (6,000 ft) the upper western flank of Newberry Volcano. The wells, however, are in a general north-south array on the uppermost accessible portion of the western flank. Hence the west edge of the thermal anomaly and the north-south extensions are not empirically delineated. Two datasets have been compared in an effort to extrapolate temperatures at depth beyond the well locations. Electrical resistivity from the MT surveys that were based on the 3-D MT results, have been compared with the temperature data from the intermediate and deep wells. The comparison suggests that a correlation of the two datasets can be used to extrapolate the temperatures outward from the upper western flank where empirical measurements exist. Two key assumptions that were made to develop the temperature map include:

- 1) The mapped base of the electrical conductor is approximately equal to the 150°C (300°F) isotherm (Figure 38).
- 2) The average gradient in the area is $109^{\circ}\text{C}/\text{km}$ ($6^{\circ}\text{F}/100\text{ ft}$). (Figure 39).

These assumptions are conservative. Temperatures on the lower western flank are predicted to drop sharply, so that in the vicinity of McKay Buttes, temperatures at 3 km (10,000 ft) are predicted to be significantly below 150°C (300°F). The most likely source of the heat for this broad anomaly is plutonic and subvolcanic rock associated with larger-scale eruptions 300,000 years ago and younger (Jensen, 2006). Plutons associated with McKay Buttes on the lower west flank are likely significantly cooler and likely do not contribute toward the thermal anomaly.

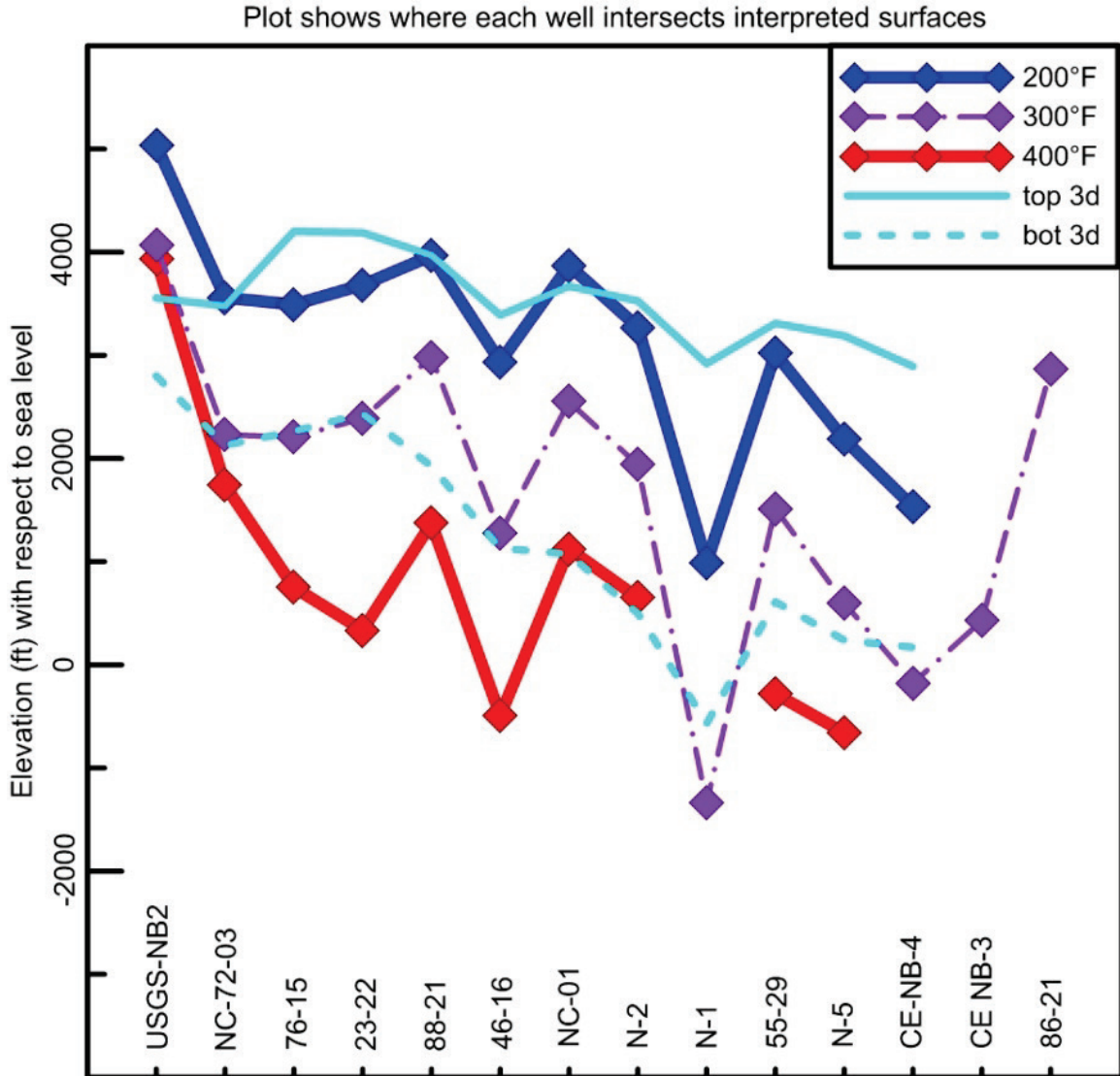


Figure 37: Comparison of the depth to the 200°F, 300 °F, 400°F (93°C, 150°C, 204°C) isotherms and the top of the conductor layer (top) and bottom of the conductor layer (bottom) from the 3-D MT interpretation.

The temperature-depth data for all of the wells in the area were used to obtain depths to isotherms at 10°C (50°F) intervals from the top to the bottom of the well. Since the curves are generally linear, in the case of the shallower wells, the curves were extrapolated (Figure 39) to obtain the depth to the 204°C (400°F) isotherm so that a more complete map could be prepared. Contour maps of the depth to, and elevation of, the 93°C and 204°C (200 and 400°F) isotherms are shown in Figure 40 and Figure 41. Figure 42 shows the anticipated temperature at 3 km (10,000 ft) below ground level, based on the above methodology.

The modeling of temperature at depth has been limited to the western flank of the volcano. The remaining areas of the volcano are not modeled at this time due to the paucity of both temperature gradient wells and MT stations.

An interesting and important feature of the wells with temperature profiles is that they all have similar, and very high, gradients at depth (109°C/km to 146°C/km (6 to 8 °F/100 feet)). The primary factor that causes variation in the depth to the isotherms is not the average deeper gradient, but the thickness of the shallow isothermal zones. Thus the heat source that causes the high gradients appears to be equally strong under a much larger area of the upper west flank than has so far been explored by drilling. So while the elevation of the 204°C (400°F) isotherm, for example, drops over the area from east to west, the drop in the thermal anomaly area is controlled by the thickness of the shallow isothermal section and the change in surface elevation, rather than by the apparent temperature of the deep-seated hot plutonic rock at any given depth.

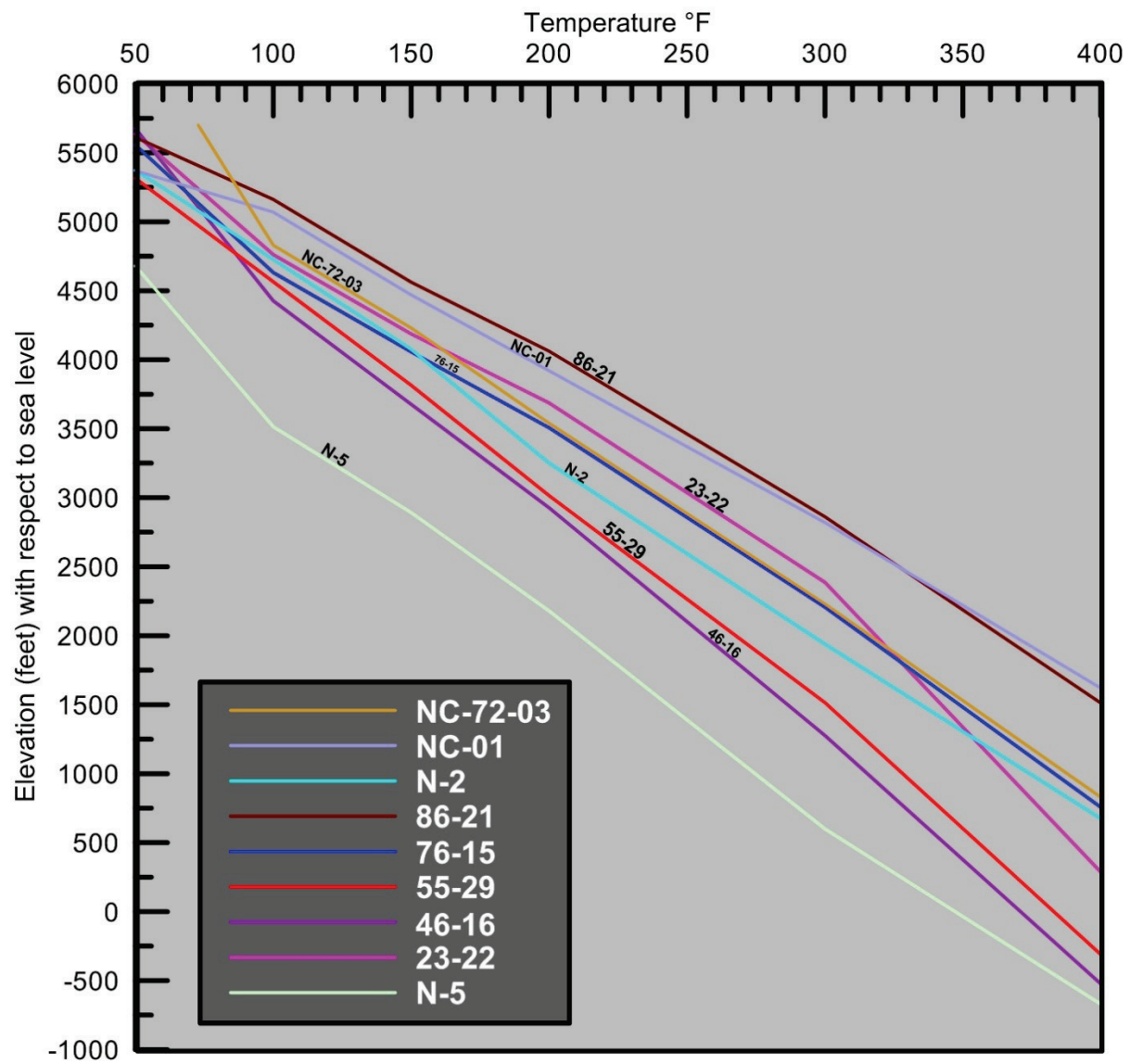


Figure 39: Temperature gradients of TG and deep wells (shown as Current Sites on Figure 40).

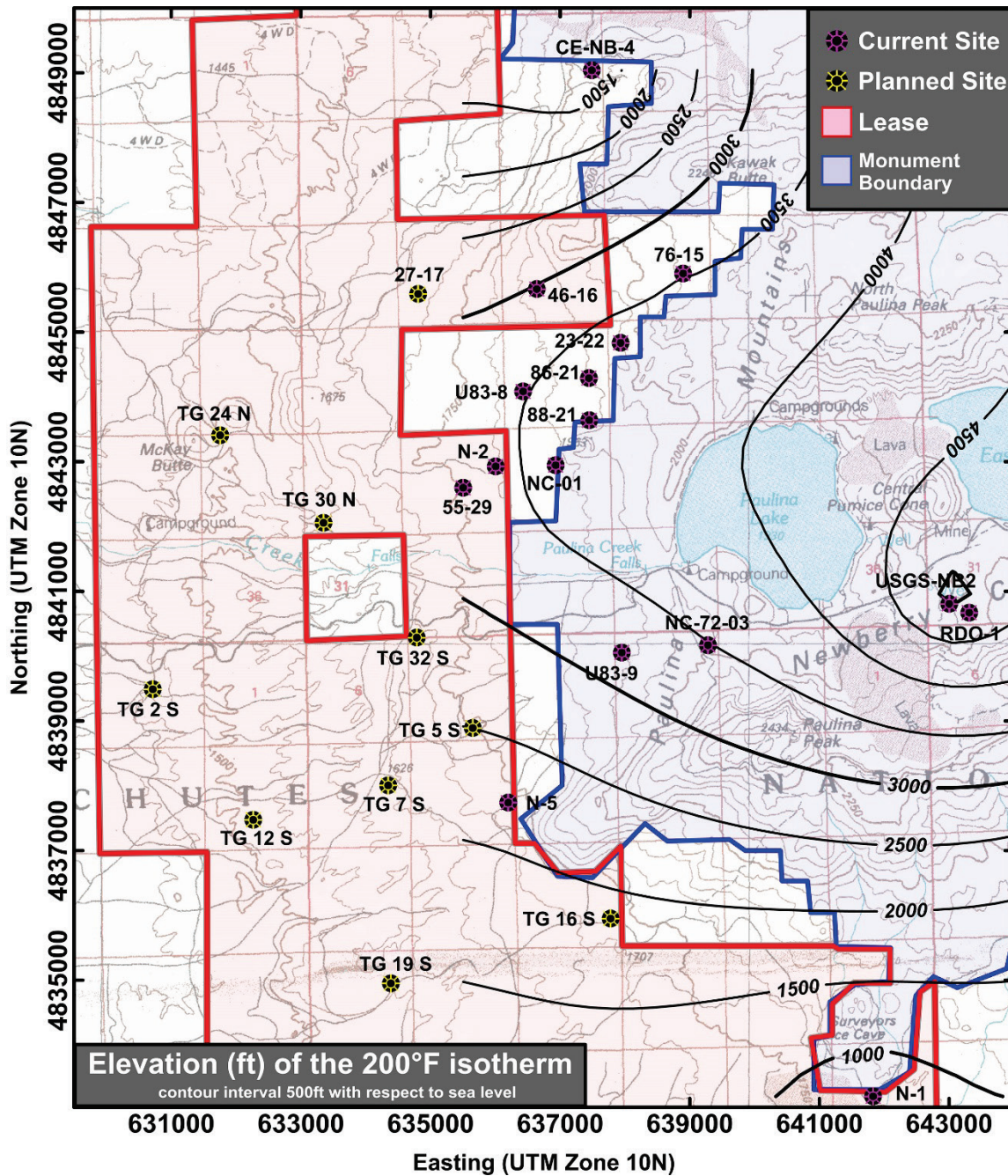


Figure 40: Isotherm map, depth to 200°F (93°C) isotherm from available well data. Note that the "TG" wells marked on the map are not data points, rather permitted but never completed to full depth. Six of these wells were drilled to about 213 m (700 ft) and cased for seismic monitoring purposes. The temperature gradients of these wells are shown in Figure 19.

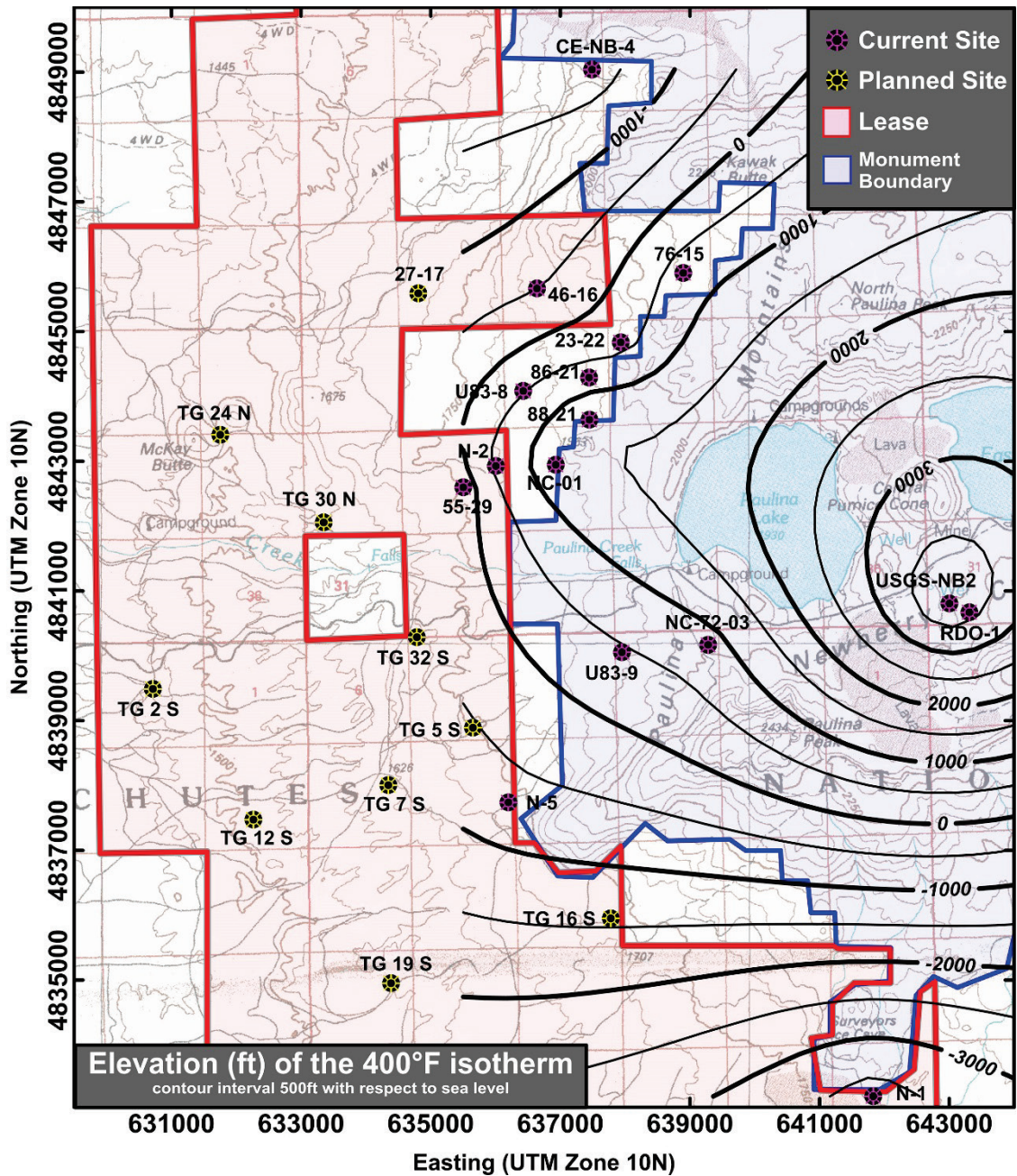


Figure 41: Depth to 400°F (204°C) isotherm from well data. Note that the "TG" wells marked on the map are not temperature data points. They were permitted but never completed.

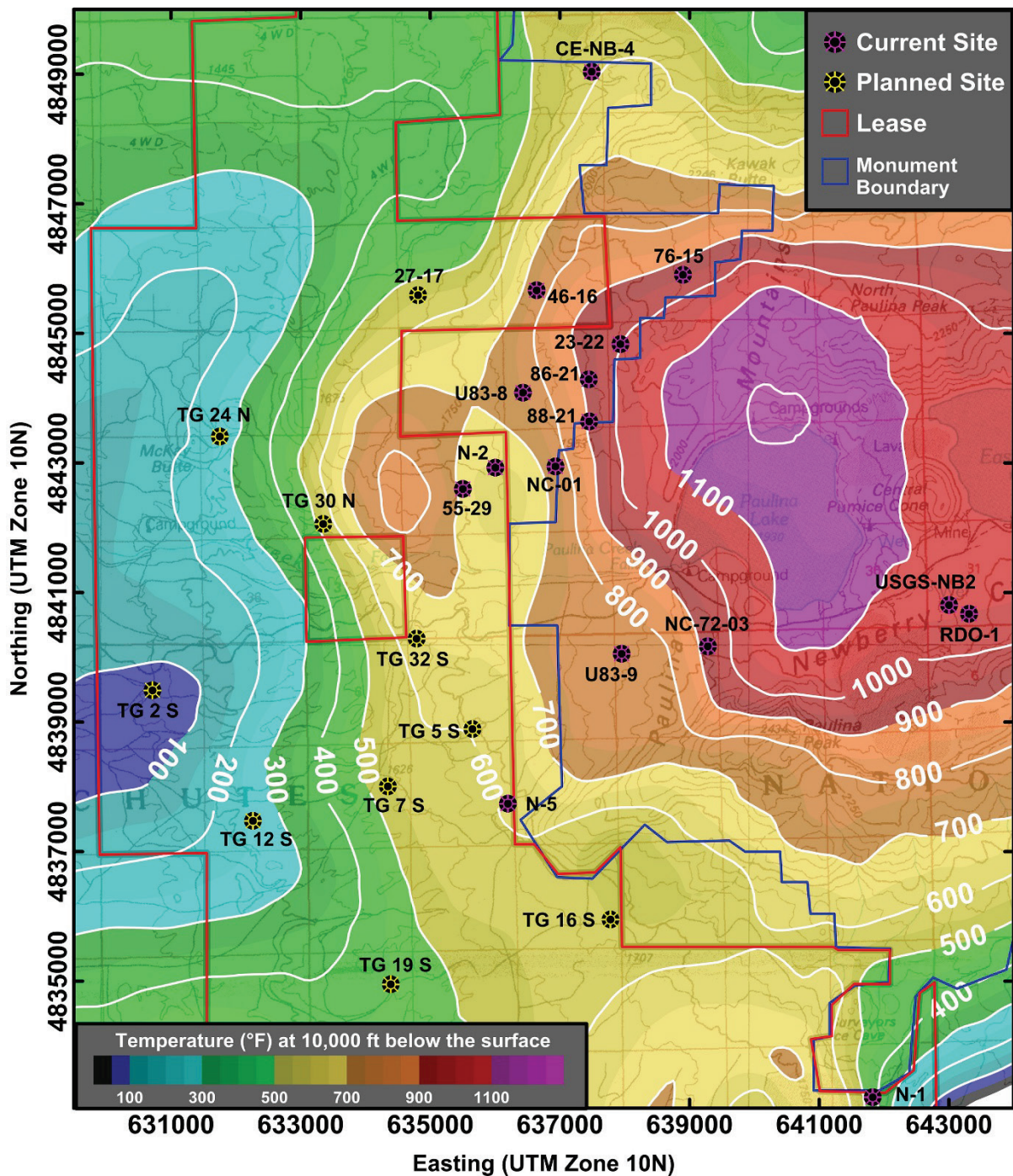


Figure 42: Interpreted temperature at a depth of 3 km (10,000 ft) below the surface. Interpretation method explained in text. The red line identifies the boundaries of the Davenport leases and the royal blue line indicates the monument boundary. Note the contours in the upper and lower left corners are computer-generated artifacts not based on temperature gradient well (Figure 4) or MT station measurements (Figure 25).

One major economic aspect to the west flank thermal anomaly is a determination of how much thermal energy lies at an economically retrievable depth. Based on the above assumptions regarding temperature extrapolations, two volumes were created consisting of the subsurface just on the Davenport lease block (Figure 42) for areas with temperatures over 150°C (300°F). The first volume included the area from the surface to 3 km (10,000 ft) and the second volume from the surface to 3.6 km (12,000 ft). The depths of the volumes are somewhat arbitrary; a greater depth could be accessed based on drilling conditions, cost, and availability of techniques to operate at the very high temperatures. It is predicted for temperatures of over 150°C (300°F) to be encountered in part of the area between 2.4 km to 3 km (8,000 to 10,000 ft). The volume calculated is between 85 to 135 km³. The heat content was calculated in a similar method and with the same physical parameters as used in the “Future of Geothermal Report” (Tester et al., 2006) and EGS protocol of Beardsmore et al. (2010). The calculated heat content beneath the portion of the lease on the west side of Newberry Volcano is 51 EJ³ (exajoules, 10¹⁸ Joules) to a depth of 3 km (10,000 ft) and 88 EJ to a depth of 3.6 km (12,000 ft). These amounts of thermal energy are equivalent to 1,620,000 and 279,000,000 MWy thermal equivalent. An estimate of the recoverable electrical energy from the heat content value is discussed in Tester et al. (2006). Based on that discussion which assumes a recovery factor of 2% (an average temperature drop of about 10°F), and a 20 year life, the electrical potential size calculated from the thermal resource just on the Davenport lease block (Figure 42) is 1,600 and 2,800 MWe for the two depths (Table 1). Regardless of the accessible percentage assumptions, the thermal resource on the upper western flank of Newberry Volcano is substantial. Additional thermal gradient drilling is needed to confirm the analysis of the heat content by corroborating the assumptions made in the temperature calculation as described above. The amount of the thermal resource that can actually be recovered from hydrothermal cells and from EGS development remains to be determined.

Table 1: Estimated EGS potential for Davenport lease area on west side of Newberry Volcano at 10,000 feet and 12,000 feet depths.

Depth	Calculated Heat Content (EJ)	Thermal Energy Estimate (MWy)	Recoverable Electrical Energy Estimate (Assumes 2% recovery factor, 10° F temperature drop, 20 year life.)
10,000 ft.	51 EJ	1,620,000 MWy	1,600 MWe
12,000 ft.	88 EJ	279,000,000 MWy	2,800 MWe

³ The exajoule (EJ) = one quintillion (10¹⁸) Joules. 1 ExaJoule is equivalent to 3.17 x 10⁴ MegaWatt years, [MWy], see APPENDIX A and Tester et al., 2006)

MICROSCEISMIC MONITORING

Davenport was awarded a Department of Energy (DOE) grant 109 to test a combination of traditional and innovative exploration tools for the identification of blind geothermal targets in a volcanic terrain. As one of the tools tested in this program, APEX HiPoint (now Sigma³) proposed conducting a passive microseismic fluid flow analysis using their newly patented low-amplitude seismic emission analysis technique. This has been successfully deployed in the oil and gas industry to identify the location and geometry of fluid flow within induced fractures (Fuller et al., 2007). Evidence of passive seismic monitoring identifying hydrothermal fluid movement through fractures has been noted at Solfatara Volcano, Italy (Bruno et al., 2007). Zucca and Evans (1992) inferred areas of boiling hydrothermal fluid under the western flank and within the caldera of Newberry Volcano, based on interpretations of seismic velocity and attenuation (Figure 43). Davenport's geothermal discovery well, 46-16, complements the conclusions of Zucca and Evans. These published efforts led the Davenport scientific team to consider the possibility of monitoring microseismic patterns to plot the location and geometry of formation fractures hosting hydrothermal fluid movement. Basic technical issues were discussed regarding the application of this untested technique:

- Would microseismic energy be able to travel through the shallow volcanoclastic layers and fractured lava flows?
- What was the detection range of the geophones?
- Would surface natural and cultural microseisms obscure deeper natural signals?

Low Amplitude Seismic Emission Analysis (LASEA)

Beyond these technical issues lay the basic test of the LASEA approach, that is, the ability of the geophones to detect with accuracy the location and geometry of formation fractures hosting hydrothermal fluid movement. Could the LASEA technology identify location and the geometry of the hydrothermal fracture system identified by well 46-16 intersects?

Apex HiPoint worked with the Davenport team to design a test program using their newly patented Low Amplitude Seismic Emission Analysis (LASEA) program. The monitoring and geophone deployment program called for drilling a number of monitoring holes to a depth of approximately 700 ft. Geophones were deployed in each monitoring hole at 50 foot intervals. The monitoring holes were integrated into the temperature gradient program to maximize dual use benefits.

Davenport supplied Sigma³ with well data from NWG wells 46-16 and 55-29, including well completion and condition information. The design and methodology of the test was the result of collaboration between Davenport and APEX HiPoint teams (appears in APPENDIX G: APEX HIPOINT SIGMA³ REPORTS TO DAVENPORT/NEWBERRY, Final Report, beginning on page 187 of Appendix G).

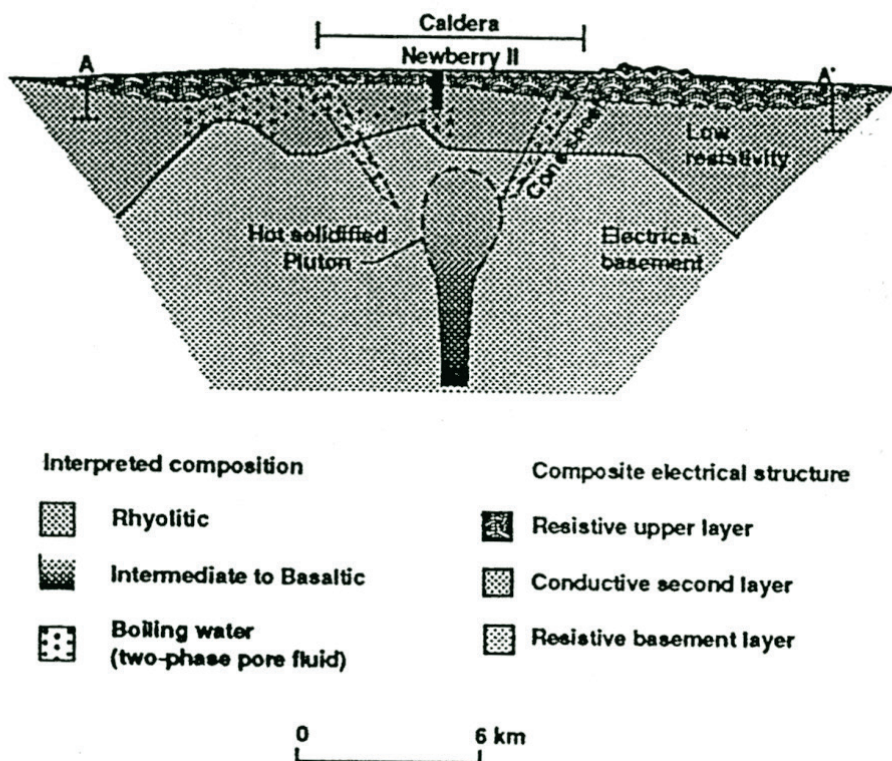


Figure 43: Zucca and Evans inferred two-phase hydrothermal location under the caldera and the west flank of Newberry Volcano, illustrated in this west-east cross-section (Figure from Zucca and Evans, 1992).

Methodology

Davenport rotary-drilled the upper 700 ft. of proposed temperature gradient wells (Figure 44) and cemented casing in each. The location of these wells were originally picked and permitted to resolve subsurface temperature anomaly boundary questions, and were adapted for the seismic monitoring test. One additional well site, to the north of NWG 46-16, was proposed and permitted for seismic monitoring. Funding for this hole was never provided. The APEX HiPoint/ Sigma³ LASEA survey deployed multiple three-component 4.5 Hz digital geophone sondes within the cased wells at 50 ft spacing. The geophones sondes (Figure 45) were manufactured by GeoSpace of Houston, Texas, and are the digital instruments used by Sigma³ for passive microseismic work in the oil and gas industry. Each observation well contained 11, 12, or 13 3-component digital geophone sondes spaced every 50 ft. The survey data were continuously recorded every 0.5 milliseconds but were broken up into records of 10-second units. Each 10-second unit contains all data from each of the geophones for that time period. The contract between Davenport and Sigma³ specified that the signals from 5,000 ft. to 15,000 ft. depth would be processed and the results would be presented in a final report.

The field execution of the LASEA test was divided into two arrays in order to accommodate other activities in the area and equipment availability. The southern array, with four monitoring wells, was located in the southern portion of the western flank (Figure 44, blue dots). A "blind test" area,

it showed no evidence of subsurface fluid flow. Equipment deployment and monitoring in the southern array occurred in December of 2011.

The northern array, with five monitoring wells, was located in the northern portion of the western flank (Figure 44, black dots)). The northern array was located in the vicinity of the two deep exploration wells drilled by Davenport in 2008 (Figure 4, NWG 46-16 and NWG 55-29). It was anticipated by the Davenport scientific team, including APEX HiPoint staff, that the northern array would be a true controlled test of the LASEA microseismic experiment. NWG 46-16 had intersected hydrothermal fractures (Waibel et al., 2012) and had a closed-in well-head pressure of 600 psi. During deployment of the geophones in the northern array, discovery well NWG 46-16 was be opened at specific intervals once a day for three consecutive days (Table 2: 46-16 flow cycle timing). This would create controlled-timing fluid flow within formation fractures intersected by the well and fluid flow up the well and through the venturi created by the formation bridge at 5,000 ft. within the well. The fluid flow through formation fractures into and up the wellbore and the fluid pressure and velocity changes at the venturi provided likely subsurface fluid-flow signals from known source points at known times. The program called for microseismic imagery for time-slices prior to, during and following the well flowing cycles on each of the three days.

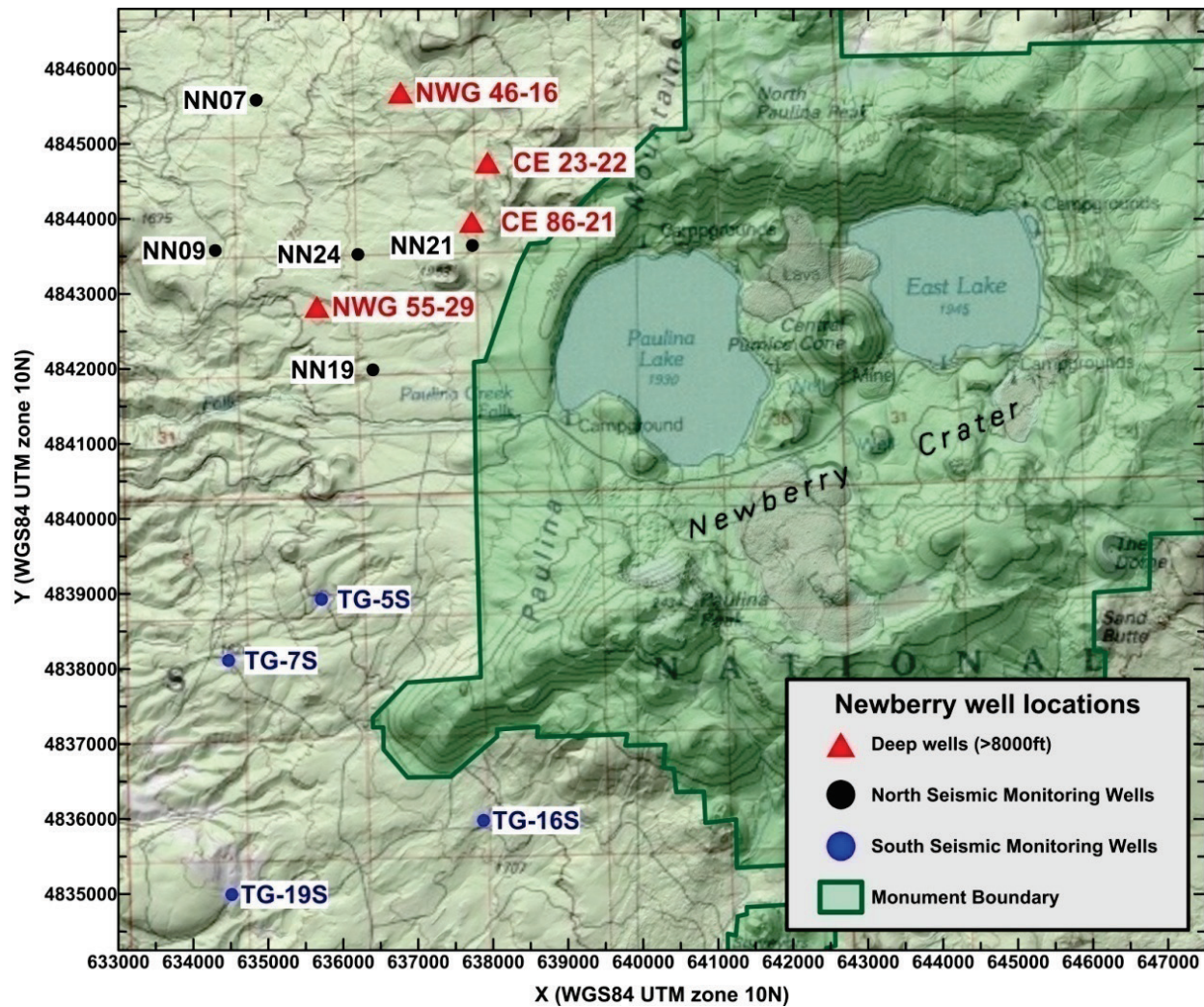


Figure 44: Map of the upper western flank of Newberry Volcano, with seismic monitoring holes and deep exploration holes identified. Paulina Lake and the Big Obsidian Flow in the upper right are within the caldera.



Figure 45: One of the high-grade digital geophones, manufactured by GeoSpace of Houston, Texas, deployed by the APEX HiPoint/ Sigma3 field team in the monitoring wells.

Recording and Analysis

Microseismic monitoring within the four wells of the southern array (Figure 44) began on the 23rd of December 2011 and continued through the 30th of December 2011. The data were processed over the following three months with a grid spacing of 100 m in both north-south and east-west directions. Concerns regarding the ability of the array to receive signals from more than one or two km were alleviated by the dataset showing cultural industrial noise from sources at least 10

km distance (Figure 46). The dataset also showed that processing was dealing with an extremely large volume of signals rather than too few signals. The dominant microseismic signals that were identified on a recurring basis, with a duration period of near 27 hours, clustered around a north-northwest strike (Figure 47).

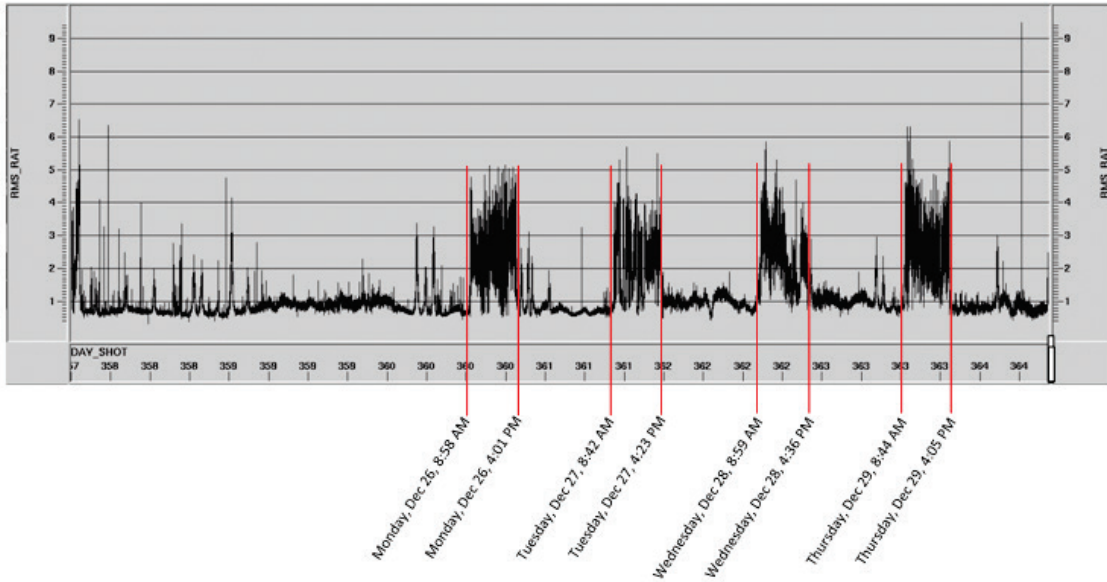


Figure 46: The four highest-amplitude energy clusters are outlined here during the southern array deployment with start and end times of 0900 to 1600. Given the regularity of the start and end times of these periods, they are almost certainly man-made cultural noise related to daily business operating heavy equipment somewhere in the area (Slide 7, APEX HiPoint/ Sigma³ Southern Array Final Report to Davenport).



Figure 47: Southern array shows a dominant trend of episodic microseismic signals observed in the processed data. The four larger blue dots identify the four monitoring hole locations. The smaller dots represent resolved signals. The grid spacing is 100 m (Slide 27, APEX HiPoint/ Sigma³ Southern Array Final Report to Davenport).

Two significant organizational changes occurred between completion of the southern array and the execution of the northern array. APEX HiPoint was acquired by Sigma³. Also an administrative change occurred within Davenport. The Davenport administrative office was closed and the administration of Davenport Holdings was transferred to AltaRock Energy Staff, operator of the EGS program at NWG well 55-29. With this change, primary communications with Sigma³ transferred from the Davenport scientific team to AltaRock Energy staff.

Microseismic monitoring of the wells in the northern array occurred from the 8th to the 15th of September 2013. The geophones were deployed on the 7th and the morning of the 8th of September. Cyclic flowing of NWG 46-16 occurred on the 8th, 9th and 10th. Monitoring continued until the afternoon of the 15 to watch background signals from the NWG 46-16 area, and to continue monitor for the benefit of AltaRock Energy's EGS efforts in well NWG 55-29. NWG Well 46-16 was expected to flow non-condensable gas during the test. The team was pleasantly impressed that the well also flowed liquid, dominated by drilling mud that had been left in the hole (Figure 9 and Figure 10).

Table 2: 46-16 flow cycle timing		
September 8, 2013		
<u>Time (PDT)</u>	<u>Status</u>	<u>Time (GMT)</u>
14:10	opened well, flowing gas phase	21:10
16:05	well started flowing liquid phase	
18:35	shut well in	01:35
September 9, 2013		
<u>Time (PDT)</u>	<u>Status</u>	<u>Time (GMT)</u>
08:45	opened well, flowing gas phase	15:45
11:22	mixed liquid and gas flow	
11:44	liquid phase flow	
17:00	shut well in	00:00
September 10, 2013		
<u>Time (PDT)</u>	<u>Status</u>	<u>Time (GMT)</u>
09:36	opened well, flowing gas phase	16:36
10:17	Oscillating gas and liquid phase flow	
15:15	shut well in	22:15

Northern Array Results

The final report from Sigma³ provided a good comprehensive description of the techniques and theory involved with the LASEA technology. This basic technology discussion provides background insight for the experimental application of the oil and gas field technology to a hydrothermal application (referenced in APPENDIX G: APEX HIPOINT SIGMA³ REPORTS TO DAVENPORT/NEWBERRY). The original intent and the funding was part of the Davenport DOE Grant 109 program, to test the possibility of using this technology as an additional exploration tool to locate blind geothermal resources in volcanic terrain. The application as implemented in the northern array was expanded to benefit a related Davenport/AltaRock Energy/DOE EGS project in the vicinity of NWG well 55-29. Without a significant increase in cost, the survey was expanded to included monitoring formation fracture seismic signals associated with fluid injection into NWG well 55-29.

Four dataset presentations were provided by Sigma³ in an interim report and in their final report. Two slides were identified in an interim report as showing energy level measurements prior to, and immediately after, opening NWG well 46-16 (2014.03.13 46-16 View Of Time Frame Report). The final report presents depictions of large amplitude signal sources, lowest level amplitude signal sources, and the LASEA signal processing of an isolated block around well NWG 46-16.

Figure 48 and Figure 49 show planar views of the northern half of the northern array area. Figure 48 is identified as showing energy measured for a 16 hour period prior to opening well NWG 46-16 for the first time. In this image, NWG 46-16 seems to have been labeled "NM03" by Sigma³. Much supporting information is lacking with these two figures; they do, however, indicate a NE-trending pattern that is repeated in some of the final report figures.

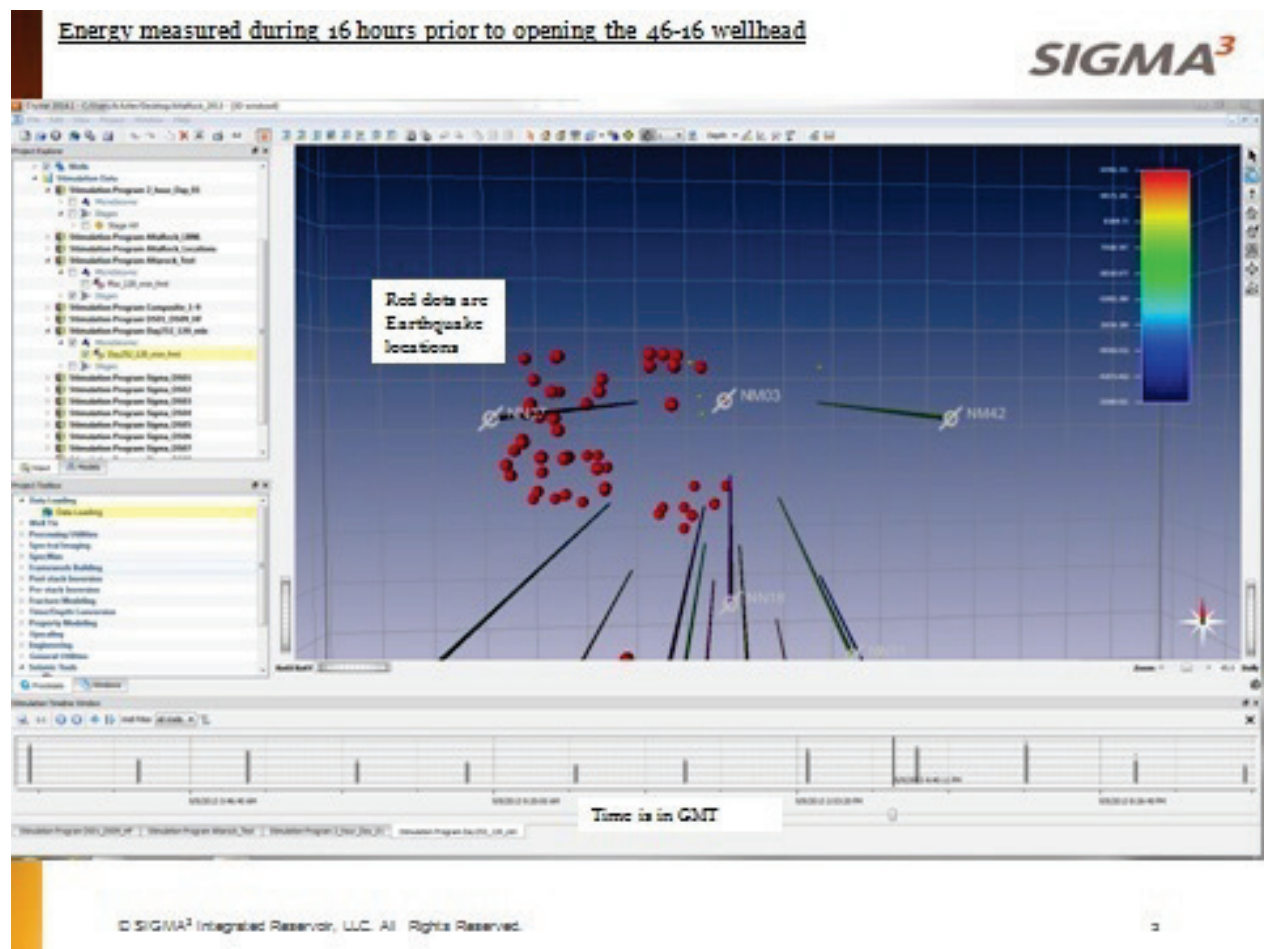


Figure 48: 9 September 2013 16:40 GMT, 09:40:11 AM PDT Sigma³ image identified as a view of energy measured 16 hours prior to opening 46-16 wellhead. The bar toward the bottom of the image shows a dark line labeled "9/9/2013 4:40:11 PM" with image in GMT. This GMT would equate to 09:40:11 AM PDT on 9 September 2013, at which time well 46-16 was flowing gas phase (Table 2, this section). No depth range for signal processing is provided. No depth range for earthquake (red dots) or microseisms

are provided (Sigma³ image, APPENDIX G: APEX HIPOINT SIGMA³ REPORTS TO DAVENPORT/NEWBERRY, March 13, 2014 Quick View of Current Status).

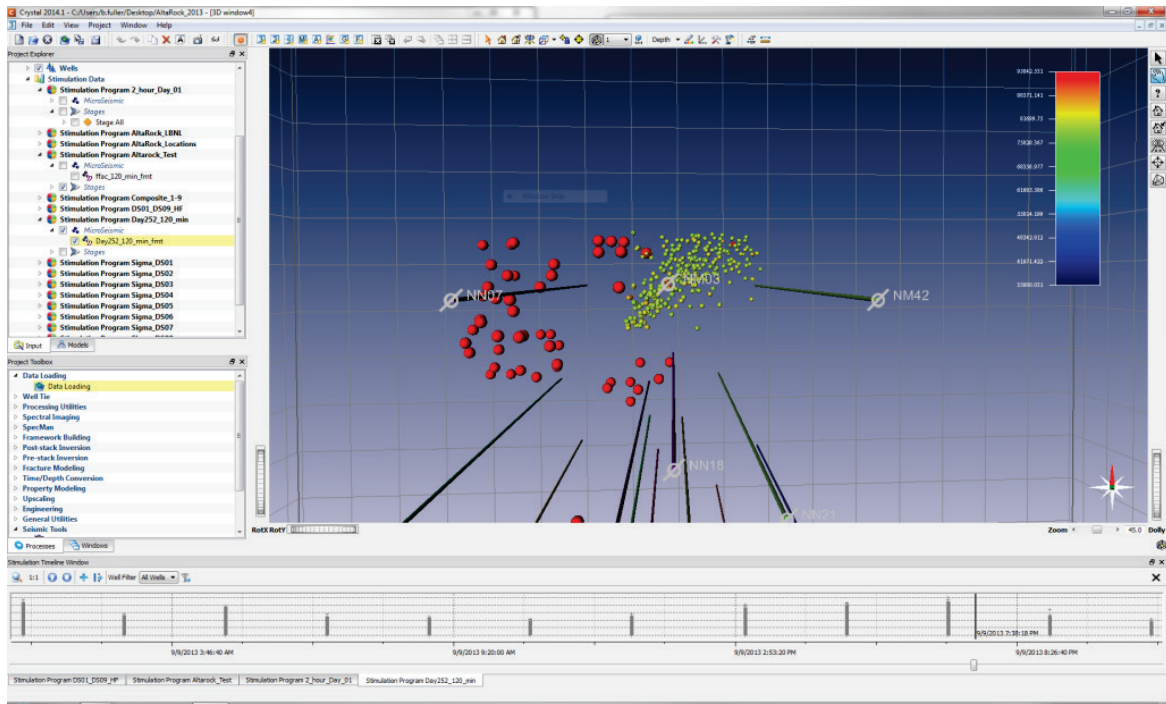
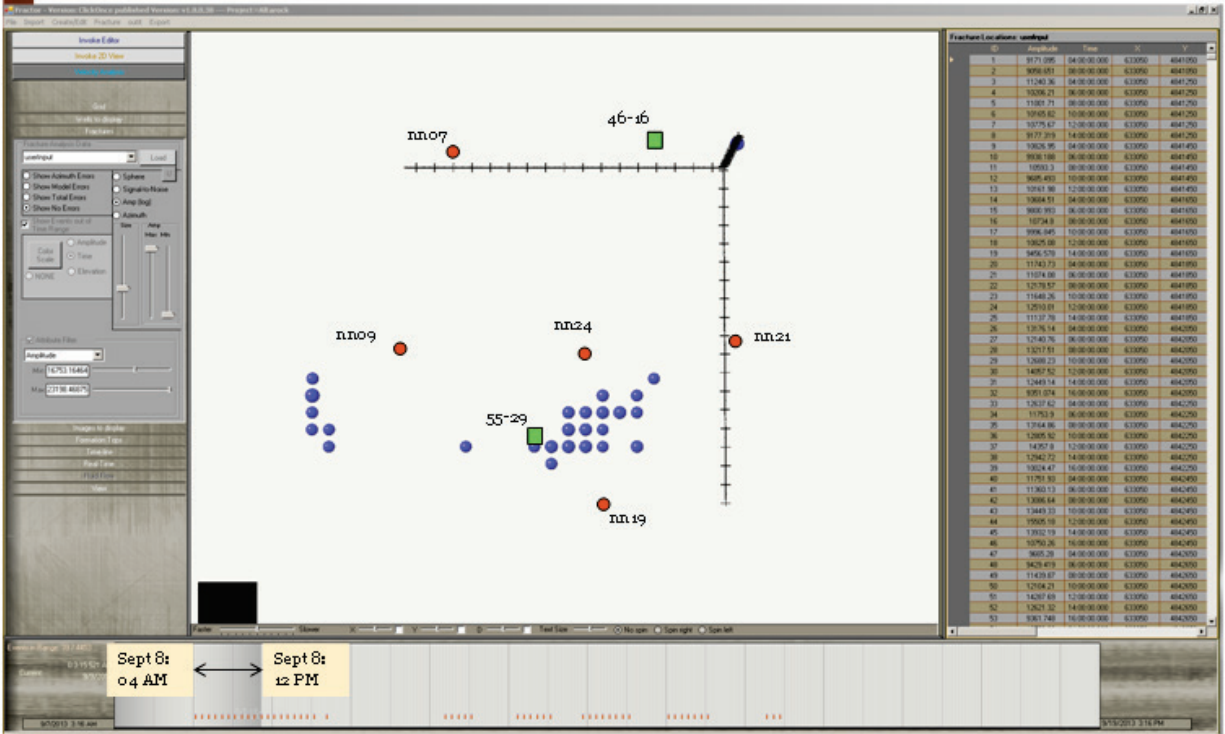


Figure 49: Sigma³ image identified as a view of energy measured 2 hours immediately after opening 46-16 wellhead. The bar toward the bottom of the image shows a dark line labeled "9/9/2013 7:38:18 PM" with image time in GMT. This GMT would equate to 12:38:18 PM PDT on 9 September 2013, at which time well 46-16 was flowing liquid phase (Table 2, this section). No depth range for signal processing is provided. No depth range for earthquake (red dots) or microseisms are provided. (Sigma³ image, APPENDIX G: APEX HIPOINT SIGMA³ REPORTS TO DAVENPORT/NEWBERRY, March 13, 2014 Quick View of Current Status).

The initial seismic energy computations were made for a single horizontal plane at an elevation of -1250 m (-4,101 ft) relative to average sea level. This corresponds to approximately 10,000 ft. below the mean surface elevation in the area of interest. The size of the grid spacing for the northern array data processing is 200 m in both north-south and east-west directions (the spacing for the southern array was 100 m). The grid plane was 6 km by 6 km centered near the middle of the 5 observation wells, placing well NWG 46-16 at the northern boundary of the grid. This selected horizontal plane misses the major potential signal target depths associated with the discovery well NWG 46-16; hydrothermal fractures between 9,000 and 9500 ft. depth and the in-well flow velocity changes within the venturi created by the partial bridge at 5,000 ft. depth.

Figure 50, Figure 51 and Figure 52 are examples of large amplitude signals, planar view at a depth of approximately 10,000 ft. below the surface (Section 4, Sigma³ Final Report). These signals show a NE-trending pattern in the vicinity of NWG well 55-29, signals to the west, and no signal cluster identification in the vicinity of NWG well 46-16. The presentation time increments of these figures spans from prior to, during, and subsequent to flowing of NWG well 46-16.

Largest amplitudes: Active time period 1

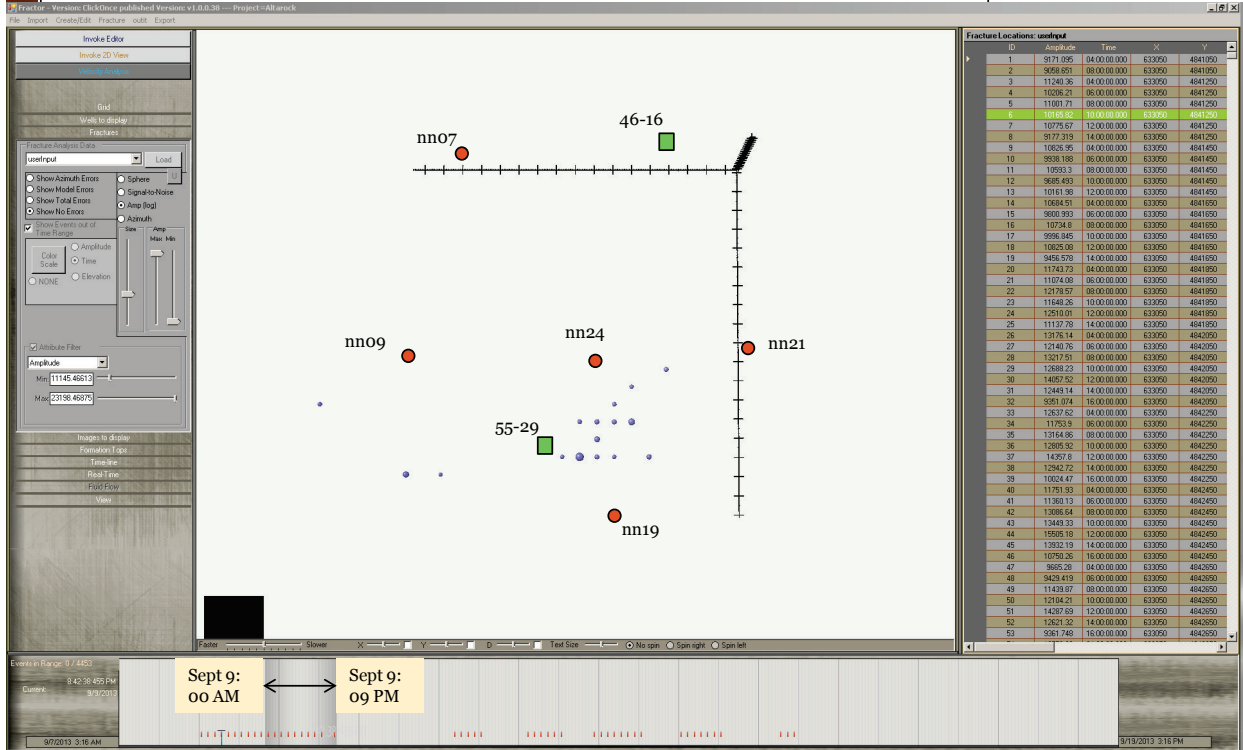


© SIGMA³ Integrated Reservoir, LLC. All Rights Reserved.

7

Figure 50: Large amplitude signals detected by the northern array for a 20 hour period prior to, during and after the first flowing of well NWG 46-16, 8 September 2013. (Sigma³, 2014 Newberry Final Report, Figure 30).

Largest Amplitudes: Active time period 2: similar to period 1 but with lower amplitude

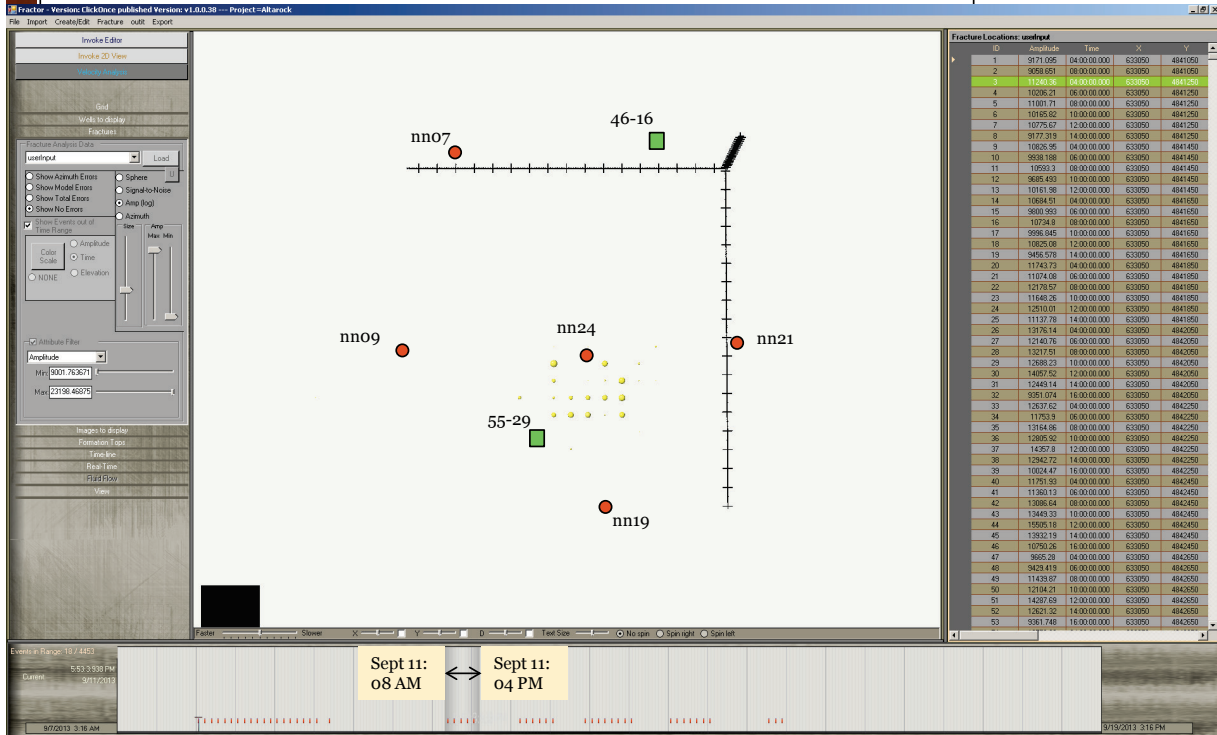


© SIGMA³ Integrated Reservoir, LLC. All Rights Reserved.

8

Figure 51: Large amplitude signals in the northern array for a 21 hour span on 9 September 2013, including prior to, during, and after flowing of well NWG 46-16 (Sigma³, 2014 Newberry Final Report, Figure 31).

Largest Amplitudes: Active time period 3: Lower amplitudes continue but move to the NE



© SIGMA³ Integrated Reservoir, LLC. All Rights Reserved.

9

Figure 52: Large amplitude signals detected by the northern array one day after the last flow test of well NWG 46-16 flow tests, 11 September 2013. (Sigma³, 2014 Newberry Final Report, Figure 32).

Figure 53 through Figure 57 are examples of the lowest level amplitude signals, planar view at a depth of approximately 10,000 ft. below the surface (Section 4, Sigma³ Final Report). The presentation time increments of these figures spans from prior to, during, and subsequent to flowing of NWG well 46-16.

The signal patterns identified in these figures show regional patterns that appear to be independent of activity in either wells NWG 46-16 or 55-29. The progressively expanding regional pattern that has no correlation with the flow cycles of NWG well 46-16. No origin of source or comments regarding these patterns is offered by Sigma³. The signal pattern may reflect local geological variations and variations in rock physics to transmit or reflect signals. Perhaps of equal interest to the location of signal patterns is the area from NWG well 46-16 west and southwest past monitoring well TG-17N (AltaRock Energy designated nn07) where there is an absence of signals. At this time there is no unique hypothesis explaining the lowest level amplitude signals identified in this survey.

Lowest Amplitudes: September 08 – The well was opened at 14:10 local time This plot shows the amplitudes prior to opening the flow.

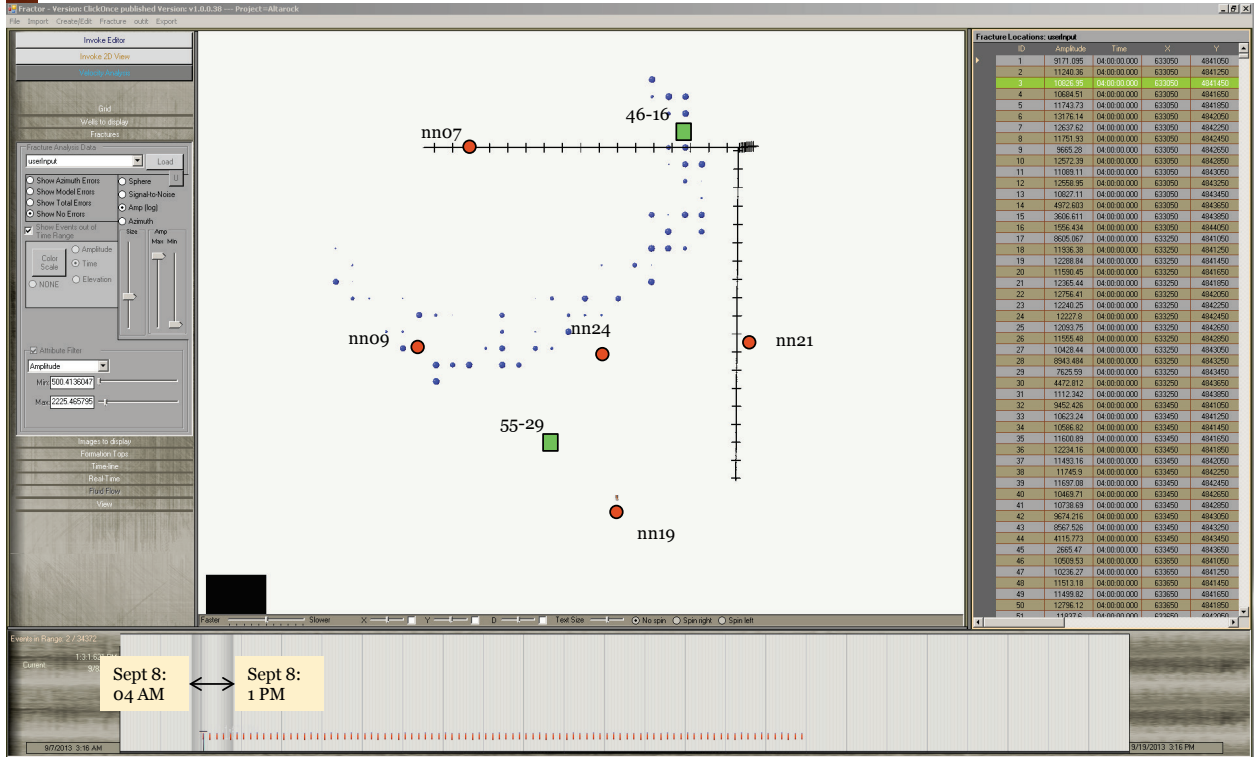
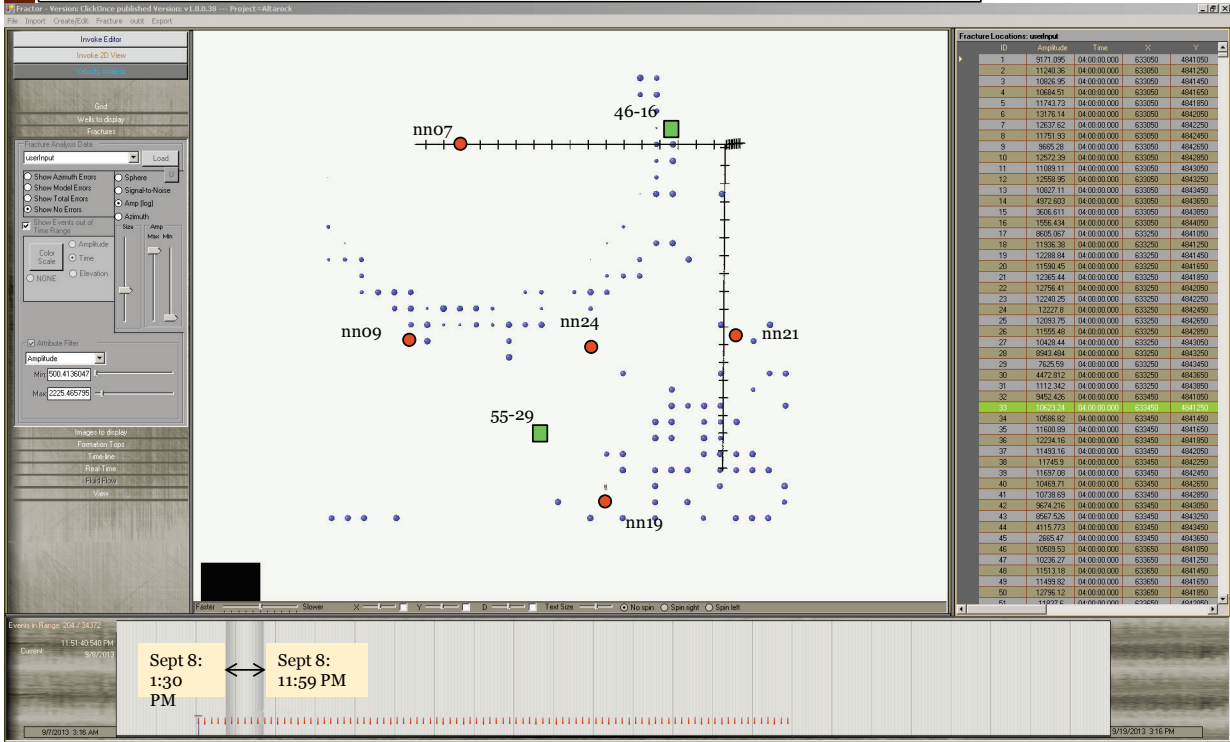


Figure 53: Lowest level of seismic amplitude activity detected in the northern array prior to opening well NWG 46-16, 8 September 2014 (Sigma³, 2014 Newberry Final Report, Figure 37).

Lowest Amplitudes: September 08 – The well was opened at 14:10 local time This plot shows the amplitudes after opening the flow at 14:10 until midnight on Sept 08. Activity near the 46-16 does not change in an obvious way in response to the first day of flowing the well.

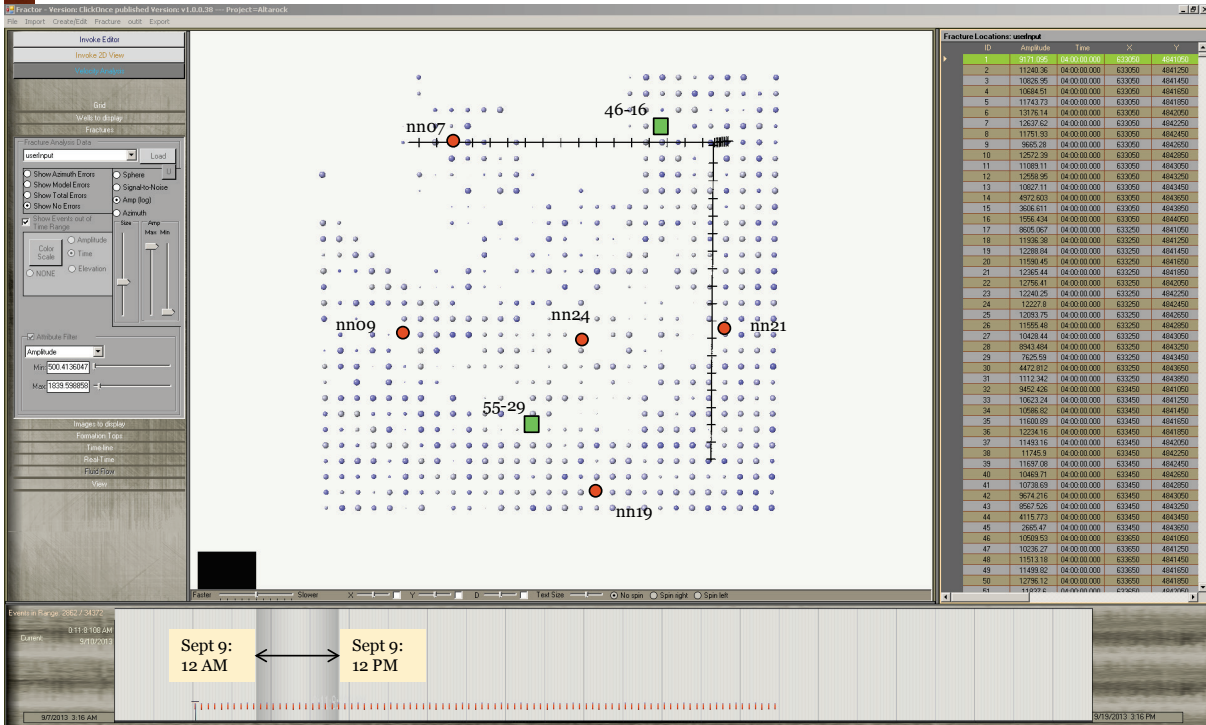


© SIGMA³ Integrated Reservoir, LLC. All Rights Reserved.

17

Figure 54: Lowest level of seismic amplitude activity detected in the northern array during and subsequent to flowing of well NWG 46-16 on 8 September 2014 (Sigma³, 2014 Newberry Report, Figure 38).

Lowest Amplitudes: September 09 – General activity increases throughout the area and in particular near observation well nn07 which had previously been a particularly quiet location.



© SIGMA³ Integrated Reservoir, LLC. All Rights Reserved.

18

Figure 55: Lowest level of seismic amplitude activity detected in the northern array for a 24 hour period, prior to, during and after during flowing of well NWG 46-16 on 9 September 2014 (Sigma³, 2014, Newberry Report, Figure 39).

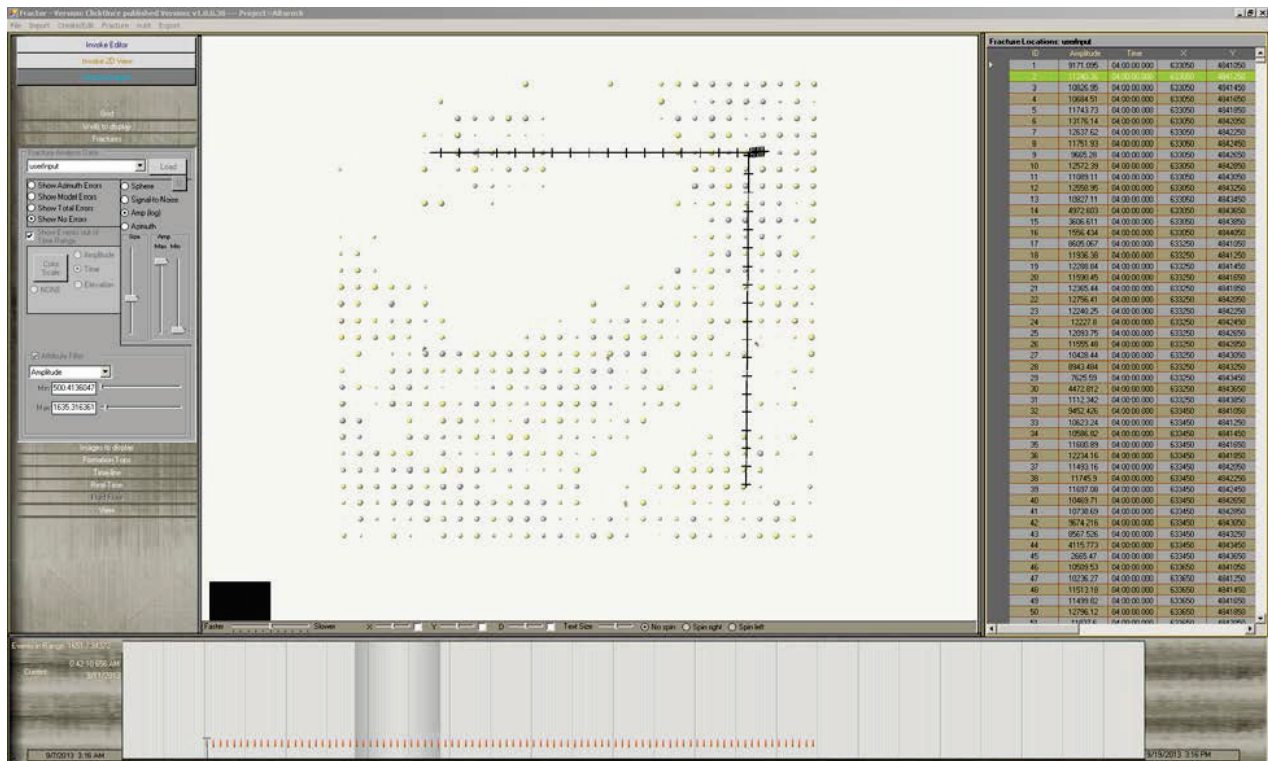


Figure 56: Lowest level of seismic amplitude activity detected in the northern array for a 24 hour period, prior to, during and after during flowing of well NWG 46-16 on 10 September 2014 (Sigma³, 2014 Newberry Report, Figure 40).

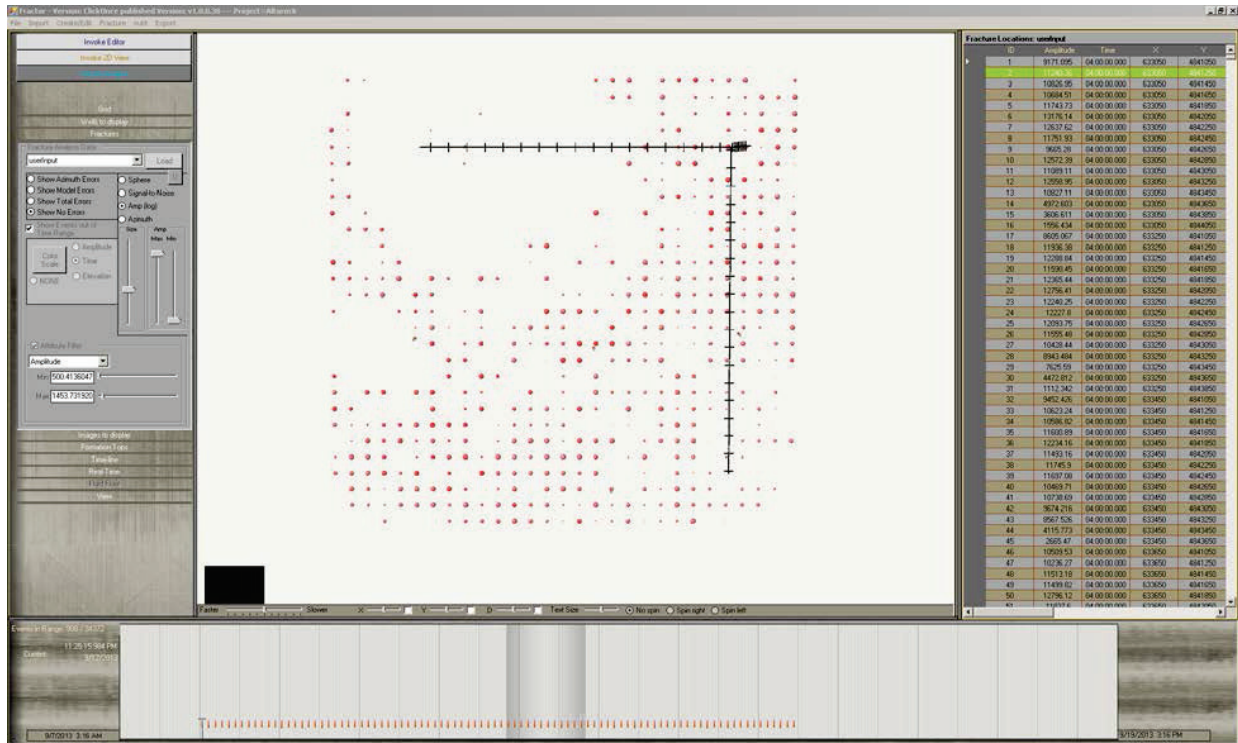


Figure 57: Lowest level of seismic amplitude activity detected in the northern array for a 24 hour period, prior to, during and after during flowing of well NWG 46-16 on 12 September 2014 (Sigma³, 2014 Newberry Report, Figure 42).

Signals from a confined block in the immediate vicinity of NWG well 46-16 underwent LASEA signal processing in a more detailed manner than of the entire northern seismic array block (Section 3, Sigma³, 2014 Newberry Report). Figure 58 through Figure 63 are selections of data processing imagery for the NWG well 46-16 block. The final report (full version available APPENDIX G: APEX HIPOINT SIGMA³ REPORTS TO DAVENPORT/NEWBERRY, starting page 187 of Appendix G) describes the methodology:

"...a technical analysis outlining how LASEA was used to characterize the flow paths around 46-16 using the signal from venting gas from the well on three separate days. To help evidence the technical analysis this section contains several 2D images, both planar and vertical, of the LASEA results in the region around well 46-16. This includes results during at least two separate well flowing events and two interlude events, to show reproducibility (or lack thereof). "

(Sigma³, 2014 Newberry Report)

"The grid node spacing for computations was 50 m. The velocity field was taken from previous work in Table 19 of an unpublished report titled "Report to AltaRock Energy Inc. Newberry Calibration Shot Project" by Gillian R. Foulger, of Foulger Consulting, dated October 09, 2010. The dots shown on the LASEA display are effectively the result of a series of cross correlations and sums that include input from thirty (30) minutes of

continuously recorded data (over 3 gigabytes of data). An additional data smoother was also applied such that for any given grid node in the volume, the data sample that is displayed is an average of the LASEA value for that 30 min periods. The time smoothing provides way to diminish the effect of anomalous amplitudes, both large and small."

(Sigma³, 2014 Newberry Report)

The final report also makes some observation regarding Sigma³ "hotspot" processing of signals:

" Without "Hotspot", microseismic events that are roughly in the same position as each other will overlap and obscure their neighbors from view and making analysis more difficult. "Hotspot" is using an effect called "Additive Blending" which, instead of obscuring its overlapping neighbors, adds the overlapping microseismic events, or cumulative coherent LASEA amplitudes colors together so you can see a cumulative cloud of values. This view can allow a user to quickly spot high energy locations as opposed to simply being able to identify areas of high microseismic or LASEA event occurrence."

(Sigma³, 2014 Newberry Report)

"The analysis will focus on the 30 minutes stack as the 3D viewer is currently incapable of handling the volume of data for the 15 minutes stack."

(Sigma³, 2014 Newberry Report)

"The provided annotations to each figure are logically integrated with the imagery. Each of these views are orthographic projections as follows:

- 1) Left pane is North up in map / plan view
- 2) Top Right pane is depth view looking west
- 3) Bottom right is depth view looking North"

(Sigma³, 2014 Newberry Report)

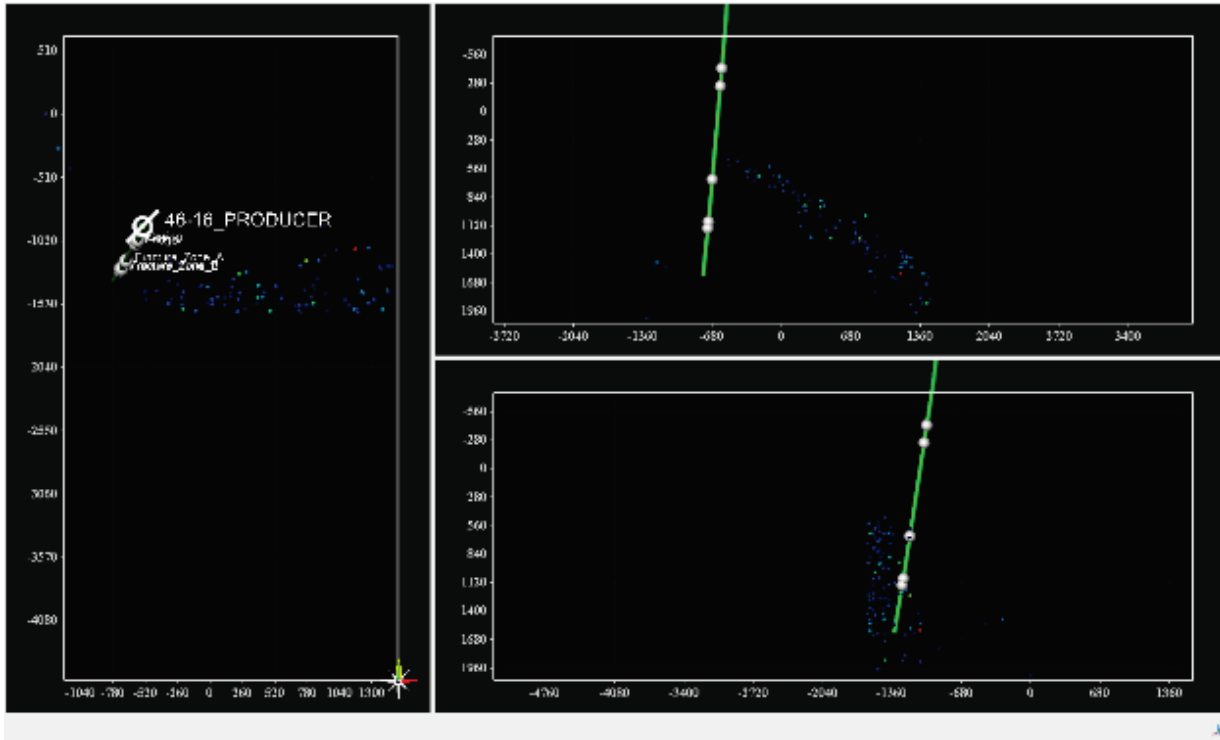


Figure 58: 11:53 PDT 8 September 2013, prior to flowing NWG 46-16. (Sigma³, 2014 Newberry Report).

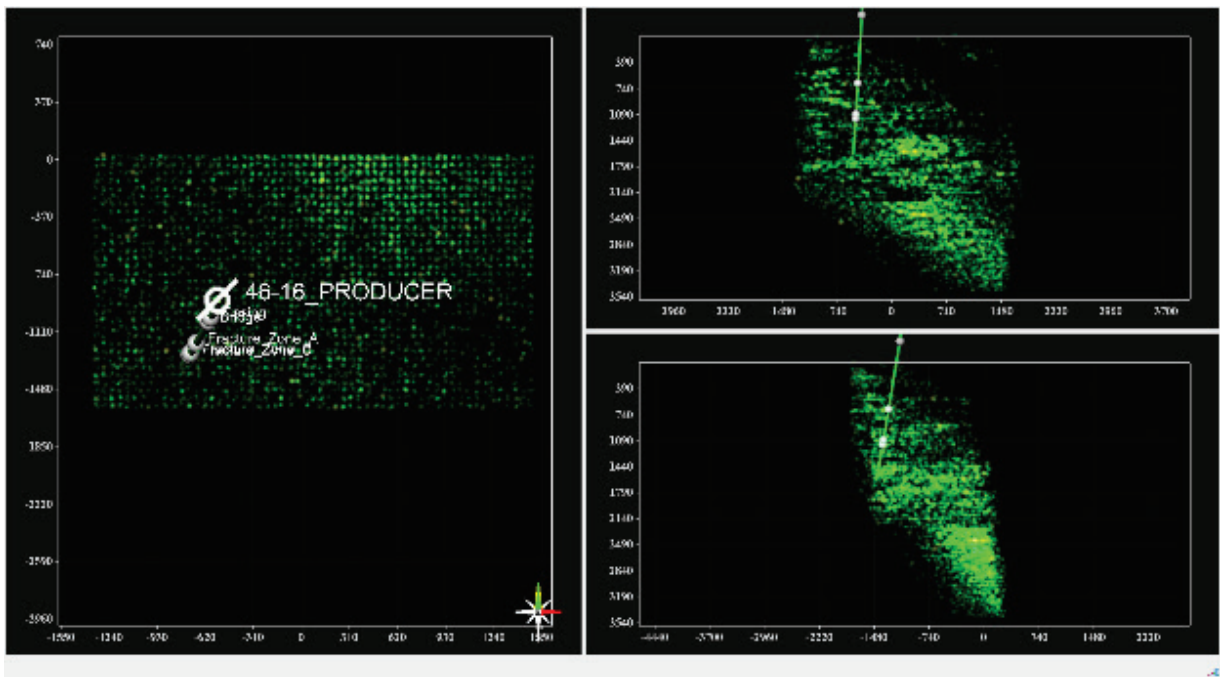


Figure 59: 14:53 PDT 8 September 2013, well flowing "Figure 9 - 14:53 local time. Perspective is North Up. Same as Figure 13, however only the top 50% of energy is imaged. This corresponds to time 43 minutes after opening of the valves. One notes from this perspective that there is a consistent LASEA response. We see activity at Fracture Zones A, B & C." (From Sigma³ Newberry Report)

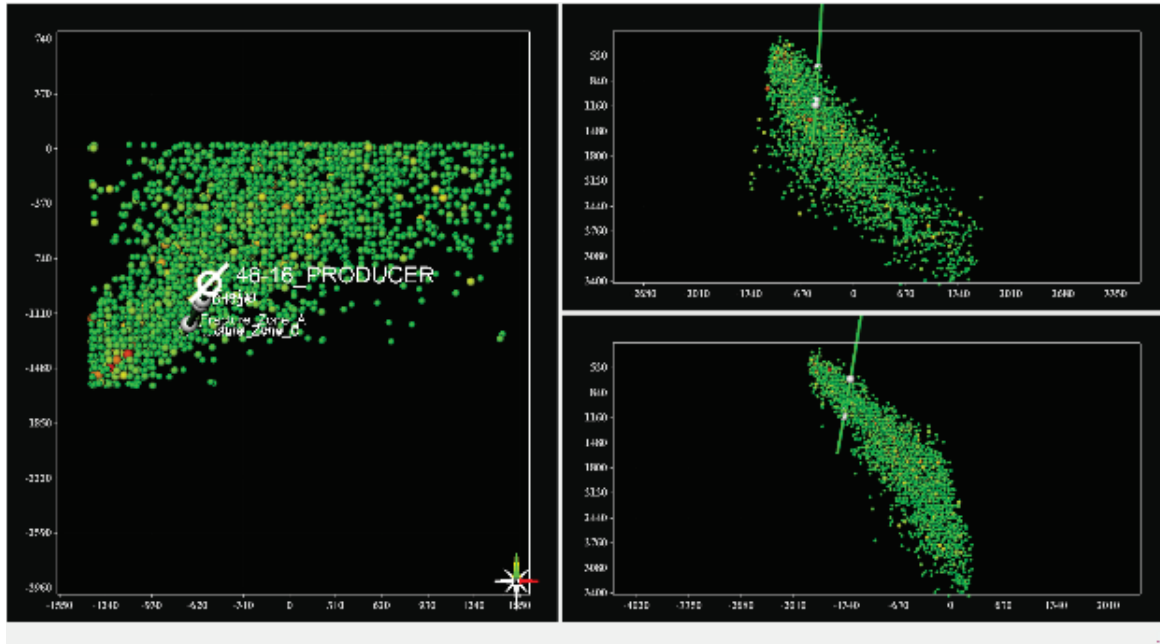


Figure 60: 14:53 PDT 8 September 2013, well flowing. "Figure 10 - 14:53 local time. Perspective is North Up. Same perspective as Figure 14, however visualized using conventional spheres with gridded amplitudes colored by relative intensity of coherent amplitudes. This corresponds to time 43 minutes after opening of the valves. One notes from this perspective that there is a consistent LASEA response. We see activity at Fracture Zones A, B & C." (Sigma³, 2014 Newberry Final Report)

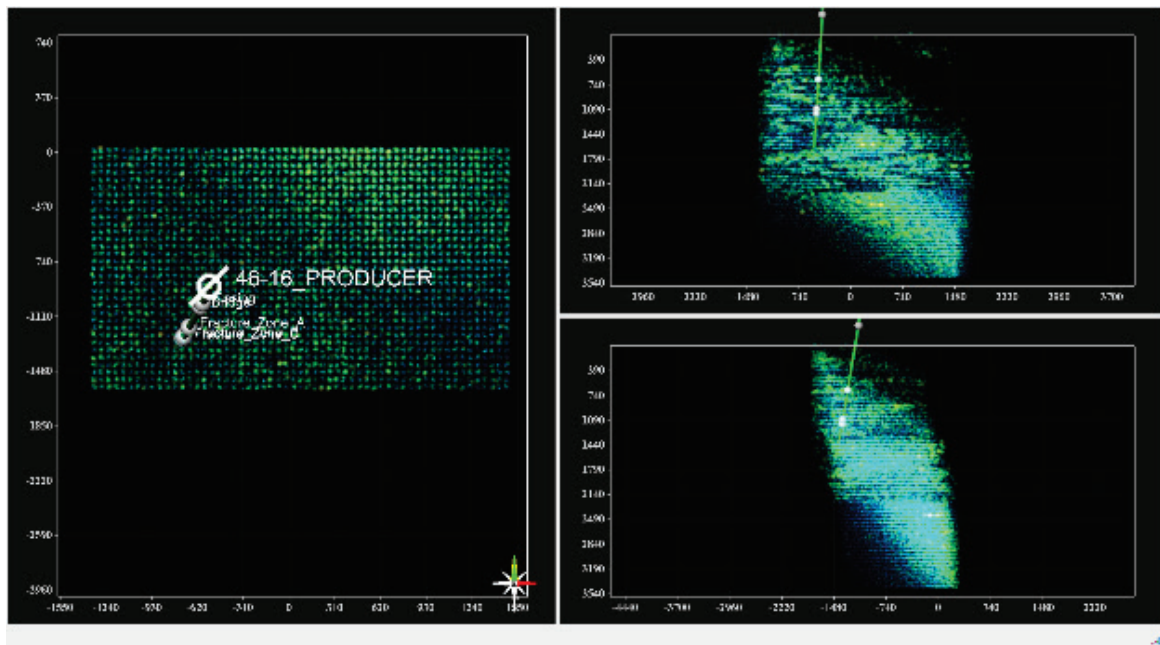


Figure 61: 14:53 PDT 8 September 2013, well flowing, Figure 8 - 14:53 – local time. Perspective is North Up. Visualized using Hotspot technology. This corresponds to time 43 minutes after opening of the valves. One notes from this perspective that there is a significant rise in LASEA response. We see activity at Fracture Zones A, B & C." (Sigma³, 2014 Newberry Final Report).

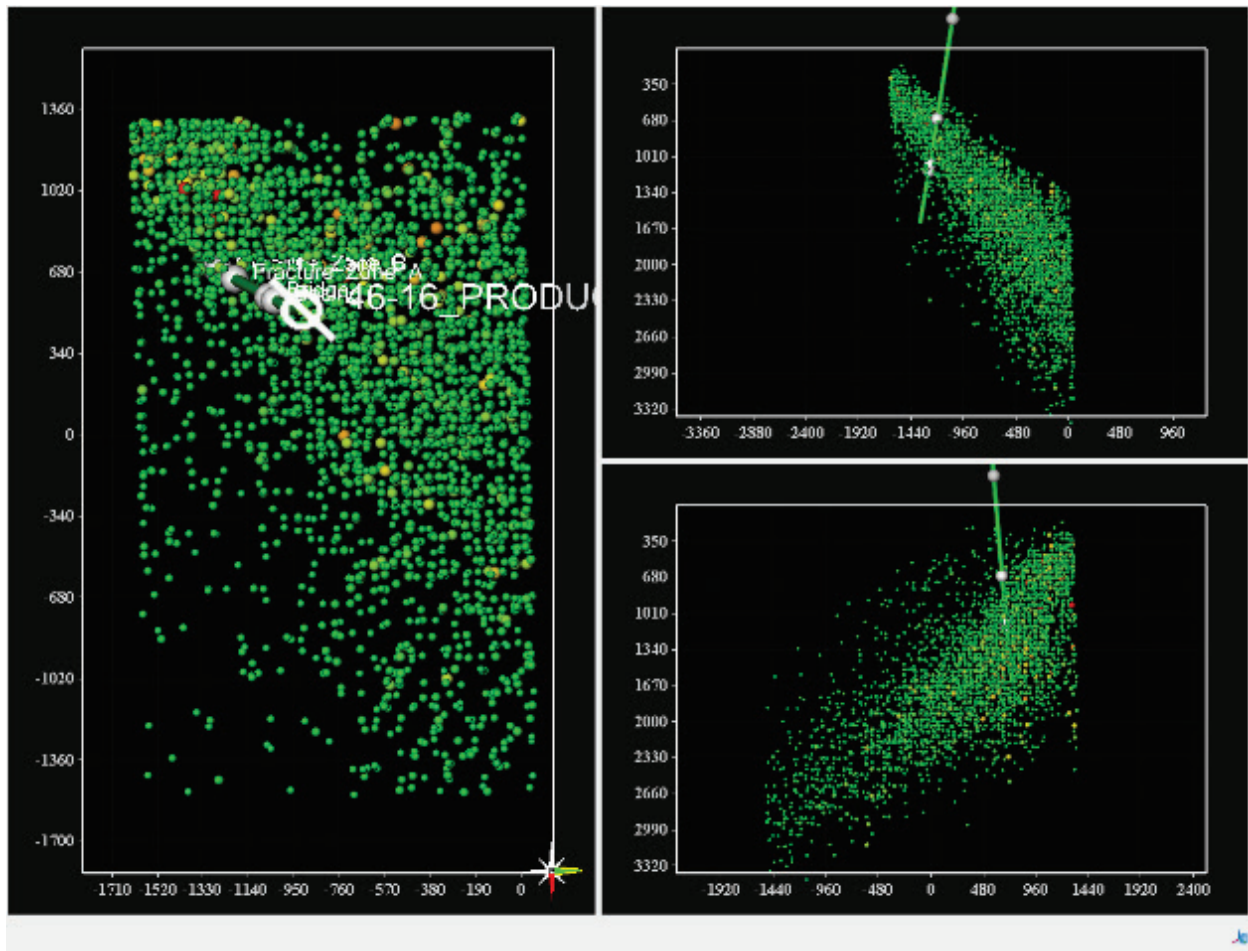


Figure 62: 22:24 PDT 8 September 2013, well shut in at 18:35 PDT, Figure 16 - 22:24 Local time. Perspective is West Up. Visualized using conventional technology. This corresponds to the LASEA response four (4) hours after of shut-in (18:35) local. One clearly sees the highest intensity response at Fracture Zones B & C, with some connectivity to Zone A." (Sigma³, 2014 Newberry Report) Comparison of this figure with Figure 60 shows the left panel is rotated to west rather than north being up, and is noted. The lower right panel is supposed to be providing a view to the north. The directional trace of the well is to the south and west. The lower right panel may actually be presenting a view to the south, with west to the right, rather than a view to the north.

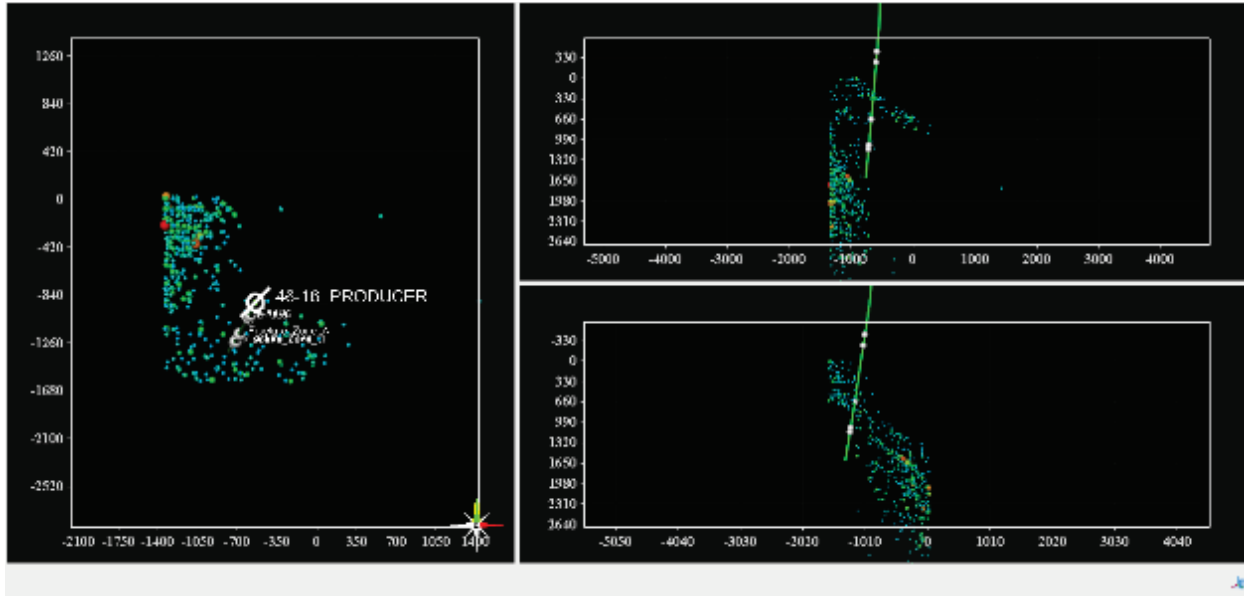


Figure 63: 14:34 PDT 10 September 2013, well flowing “Figure 21 - 14:34. Shut well in at 14:14 to attach gas sample bottle. North Up. Top 50% energy” (Sigma³, 2014 Newberry Report).

Figure 58, Figure 60, Figure 62 and Figure 63, (right panels) show in horizontal slices a broad pattern of signals dipping to the NW in the vicinity of NWG well 46-16. However in the planer view (left panel) only Figure 60 and Figure 62 show the signals in the immediate vicinity of the well. Figure 59 and Figure 61 show signal patterns that appear to be regional rather than peculiar to fluid movement through fractures in the vicinity of the well. Variations in the regional vs. well-related signals may be an artifact of data processing methods.

Ambiguity and deficiencies with the Sigma³ northern array partial and interim reports were noted by the Davenport scientific team. Requests for clarification were mostly addressed in the final report. Much is still left for the reader to infer, which leaves open the potential for incorrect assumptions.

Data from the southern array identified a recurring linear pattern (Figure 47 and 12-12-2012 Final Report Southern Array). The most subscribed interpretation by the Davenport scientific team is that the pattern represents a linear structural boundary that is reflecting signals along the structural linear plane. It is possible that the linear signal pattern might be indentifying fluid movement along a geological structure. This latter interpretation is considered to be a less likely interpretation without corroboration from other exploration techniques (e.g. temperature gradient profiles). No indication of structure of a similar strike was observed in the area of the northern array.

The northern array was designed to have been a good controlled source test for evaluation of LASEA as a potential hydrothermal exploration tool. Key to the test was to have monitoring wells located to provide good geometric coverage around well MWG 46-16. A key monitoring well located to the north of the well 46-16 was never drilled. All of the completed monitoring wells are to the south of the well, providing coverage for only a 120 degree arc, leaving a 240 degree arc around the important discovery well uncovered.

Unlike the results of the southern array, the data processing from the northern array showed three generalized patterns. The first is the pattern identified in the large amplitude signals in the vicinity and to the west of NWG well 55-29 (Section 4, Sigma³ Final Report). The second is the regional patterns shown in the lowest amplitude signals and the inferred regional patterns shown in the immediate vicinity of NWG well 46-16 (Section 4, Sigma³ Final Report). The third pattern shows a general trend of signals adjacent to NWG well 46-16 dipping to the northeast.

Brian Fuller, formerly of APEX HiPoint and now with Sigma³, wrote the following comments regarding the results of LASEA in the vicinity of NWG well 46-16:

"The LASEA (Low Amplitude Seismic Emissions Analysis) response observed in the survey was consistent with results observed in oil and gas operations. In other words opening the wellhead to flow at the very least caused a pressure change near the open hole section and a combination of pressure change and possibly fluid movement resulted in a LASEA response. The LASEA calculation was designed to detect low-amplitude signals that are persistent over long periods of time where "long periods of time" can be on the order of minutes to hours to days in time length but are all "long" time periods compared with the time duration of microseismic rock breaking events that last on the order of 10 ms (1/100th of a second). The LASEA response seen in the Oregon survey was consistent with oil and gas operations in two important ways. First, the response was correlated in time with flowing and shut in of the wellhead. And secondly, the response was not limited to the spatial area within a few meters of the wellbore. Instead the response was spread to greater distance (possibly as much as 100 m from the well). The microseismic industry has observed for over a decade that reservoir stimulation, either by injection or production of fluids, can result in stress changes within the reservoir up to hundreds of meters from the injection/production point and that those changes can produce observable microseismic events."

(B. Fuller, personal communication.)

The primary purpose for including LASEA in the Davenport/DOE Grant 109 program was to test the technique in a controlled setting for its value as a tool to be included for exploration of blind geothermal resources in volcanic terrain. In this task it has not proven to be of value. The unconstrained variables in signal patterns and irresolvable sources for signals preclude use of this technique for primary exploration at this time. The secondary purpose for applying LASEA was to attempt to identify hydrothermal fluid flow through natural formation fractures feeding into the geothermal discovery well NWG 46-16 under controlled flow testing.

The signal pattern identified in some of the images near NWG well 46-16 are intriguing, though not definitive. The signal clusters in the vicinity of and intersecting the well may be related to fluid movement. This pattern is identified only in some of the interpretive presentations. The Davenport scientific team views these results with hopeful caution. Since the northeast-trending signal pattern depicted in Figure 49, Figure 60 and Figure 62 could be interpreted as the result of fluid flow through natural fractures, it should be taken into consideration when formulating next-step strategies related to the hydrothermal resource intersected by NWG well 46-16.

EVALUATION OF EXPLORATION METHODS FOR BLIND GOETHERMAL RESOURCES IN VOLCANIC TERRAIN

Davenport was the recipient of a grant from the U.S.D.O.E. in 2010 to test a combination of exploration tools, both traditional and innovative, for their ability to identify a "blind" geothermal resource in volcanic terrain. The site for this test was the western flank of Newberry Volcano. A large subsurface thermal anomaly was outlined underlying the upper western flank from temperature gradient data. The flank has no surface evidence of the underlying heat, thus making it an ideal location to test exploration techniques that, if successful, could be transferred to other volcanic terrains.

The term "blind" in reference to a geothermal resource refers to a subsurface thermal anomaly with no surface thermal, fluid, or chemical reaction evidence of the presence of the underlying thermal energy. The efforts to advance the geothermal industry forward from exploring for resources in areas with surface evidence of the underlying thermal energy to the point of understanding how to explore for geothermal resources in areas lacking surface evidence is akin to the transition in the oil industry transitioning from drilling oil seeps to exploring for subsurface oil reservoirs which lack any surface seepage of the underlying oil. The U.S. D.O.E. grant 109 funding for the Davenport Newberry Volcano geothermal project was designed to test and evaluate a combination of traditional and experimental exploration techniques with regard to their ability to delineate geothermal resources in a "blind" setting. The western flank of Newberry Volcano afforded an unusually favorable setting for this testing in that the earlier drilling had identified a large area of the upper flank to be underlain by hot rock, as described above.

Each of the exploration methods have been discussed in detail above. Following are brief comments regarding the value of each component study, both those employed as part of the Grant 109 activities, and those used that were not specifically part of the Grant 109 package.

Geological maps were available from the USGS and from unpublished mapping done previously by the first author. The geologic maps provided a valuable and necessary base volcanic context for the area, including the ages and composition of lavas and tephra. The maps provided little detail in the way of tectonic structure and recent faulting other than that directly reflected in the location of volcanic vents. Volcanic rocks dated as part of the geologic mapping provided valuable data on the volcanic history of the Newberry Volcano, unusually long for a Cascade Range volcano.

Temperature gradient data have been indispensable to the entire geothermal exploration on Newberry Volcano. Temperature gradient measurements are the only geophysical exploration tool that uniquely measures the sought-after target, a geothermal resource. Other geophysical techniques provide non-unique models that may be interpreted to represent heat, geothermal fluid, rock variations, etc. Without the data from temperature gradient holes there would have been only very weak justification for funding of geothermal exploration on the flanks of this volcano. Most of the temperature gradient holes that were drilled, and those sites permitted to be drilled, on the flank of the volcano were designed to be drilled from 3,000 to 4,000 ft. deep, with consideration of the unusually thick shallow isothermal section. Temperature gradient data were the only data that uniquely identified a thermal anomaly underlying the west flank of the volcano.

Gravity surveys, with a high density of stations on the western flank of Newberry Volcano, provided a key contribution to the geothermal exploration program. The combined results of all of the gravity surveys were integrated, providing a rather detailed view of location and geometry of density anomalies underlying the volcano. Gravity data cannot uniquely be interpreted for heat content. The goal for using this tool was to look for structures and to look at the shape and boundaries of high density, probably plutonic rock related to the volcano. The gravity anomaly pattern does show the location and geometry of plutons underlying the volcano, data critical to understanding the volcanic history and the source of heat underlying the western flank. Both of the two Davenport deep exploration well locations were picked based on temperature gradient and gravity data. Both of the wells intersected high heat, and one intersected active hydrothermal fractures.

Magnetotelluric (MT) survey data were not able to contribute to identifying hydrothermal resources. Even with the discovery well drilled, the data could not be massaged to identify the location. The decades-old accepted and popular "mushroom" model provided no insight into the location of hydrothermal resources. The quality of the shallow MT data was very good, however, and was of great value in that the final processing by provided valuable structural and volcanology insight. The first of two MT surveys was designed by Greg Ussher for the Davenport scientific team. It had close station spacing on the northwestern flank of the volcano, which turned out to be key for the final modeling. The second survey, which expanded the survey area coverage, was laid out by the Davenport team and executed by Zonge International. These two survey designs served the project very well, and have been the core base for all data processing. The results of the initial 3-D modeling were smoothed, showing only broad changes, none of which could be interpreted as geothermal targets. At a team meeting at the Zonge International offices the discussions turned to the high station density and the associated resolution that could be produced by reprocessing the shallow (<2 km) layers in 2-D slices. The change in product was marked. Vertical off-sets in the shallow electrically conductive layer were now observed, and there was a correlation between the 2-D vertical slices with features identified on LIDAR. There was also observed a correlation with the well lithologies. At no point did the MT data identify the area near well 46-16 as having any MT character that has been the standard "signature" of a geothermal system. The broad shallow electrically conductive layer associated with secondary clay did match a temperature horizon in the well data on the upper part of the west flank of the volcano, but had no other contribution regarding temperature or hydrothermal activity. Ultimately the MT proved to be a valuable tool in part for clues of shallow younger tectonic and volcanic structure on the western flank that is obscured on the surface by the most recent Holocene and late Pleistocene tephra deposits.

Major and trace element geochemistry from cuttings and core have turned out to be very valuable in understanding the lack of deeper rock type correlations in the two Davenport wells. Visual review of the well cuttings proved inadequate to identify many age and lithology boundaries. Therefore lithologic correlation between wells was not possible without the geochemical contribution.

LIDAR has proven to be an extremely valuable exploration tool. The subtle topographic details provided with LIDAR far exceed that of topographic maps and aerial photography. This high-resolution surface imagery greatly improves the insight into possible relationships between surface topography and models of subsurface geophysics.

Low Amplitude Seismic Emission Analysis (LASEA), or fluid flow analysis, has been carried out on only one of two areas to date. The second monitoring array is scheduled to be carried out in the August-September time frame of this year. The first array was located in the southern part of the west flank, in an area with no supporting evidence of fluid flow. It was a true blind test in a blank area. The results showed a north-northwest linear pattern of signals. The second array was to be located in the vicinity of well NWG 46-6, an area with known hydrothermal fractures and fluid movement. These results as discussed above are ambiguous and give no additional insights into the geothermal or fluid flow conditions. The results of both the southern and northern arrays have provided tantalizing interpretations that deserve future investigation. The results of this program, however, have not shown this technique capable of uniquely identifying subsurface hydrothermal fluid movement.

Aeromagnetic data collected by the U.S.G.S. in the 1970s were reprocessed. It did not show any detailed structure. The data do reflect the surface geology to some degree. These data have not been found to have contributed toward evaluating the geothermal potential of Newberry Volcano. However the authors suggest that it should not be dismissed, and should be tested elsewhere in volcanic terrains; given other chances at different locations.

CONCLUSIONS AND RECOMMENDATIONS

Geological and geophysical assessments conducted by the Davenport team indicate that there is a minimum 15 square mile area on the upper western flank of Newberry Volcano outside the Monument underlain by 400°F (200°C) to > 600°F (>315°C) rock at less than 3 km (10,000 ft) depth. One hydrothermal system has been encountered to date by deep exploration test drilling done on a limited portion of the west flank thermal anomaly. One area ideal for EGS research has also been confirmed by deep exploration test drilling.

In a pecking order of value, the tools that worked best for siting the hydrothermal and EGS wells were temperature gradient and gravity. LIDAR, not part of the original proposal, became available and was integrated into the program, and turned out to also be of critical importance. MT, as interpreted by the geothermal community for decades (the "mushroom" model), would have led to wells drilled in areas with no potential for hydrothermal discovery. The problem with the application of MT is not with the quality of data, but with questions that MT surveys are asked to resolve. The structural type of hydrothermal resource that MT is capable of identifying likely does not exist under the west flank of Newberry Volcano. The MT survey, with a relatively high station density, modeling 2-D vertical slices instead of 3-D modeling, produced extremely valuable shallow (<1.5 km) structural data. This dataset, integrated with LIDAR and lithologic and mineralogical data from existing wells, really changed the understanding of the volcano, and provided valuable insight into older volcanic vent locations associated with earlier Newberry Volcano plutons to the west of the current nested caldera.

The crowning achievement of the Davenport exploration program is the hydrothermal discovery well NWG 46-16. However, with well stability problems below the casing shoe, the well has never been, nor can be, fully flow tested without resolution of the stability issue. Two possible strategies have been discussed as to resolving the problem. The first would be to re-enter the well, clean out the bridge, and run the 9 5/8th inch casing as per the original well design. The second would be to set a plug in the well just above the casing shoe and side-track out the casing, parallel to the first

leg, and complete the well with a casing program similar to the original well design. Both approaches have advantages and disadvantages.

Option one, re-entering the existing hole and stabilizing the unstable zone, could potentially be done quickly, and, therefore, at a relatively lower cost than a side-track. There are two potential draw-backs with this option. First, the hole may not stabilize easily and the budget (of both time and money) would be essentially open-ended, with no guarantee of success. The second is that, if the first phase were completed successfully and the well was unable to sustain flow, it would not be known if the low flow rate were due to the flow potential of the fractures or due to well damage due to the substantial amount of rock fragments and cuttings pushed into formation fractures from cleaning out the bridge.

The side-track would provide a cleaner well with only standard risk of fracture damage. The goal would be to parallel the original hole with the anticipation of intersecting the same fractures encountered in the first leg. This could be done within a fairly predictable budget and knowledge of minimal formation fracture damage. The budget would, however, likely run higher than a ‘best-case-scenario’ outcome for cleaning out the bridge (that is, stabilized quickly and the casing run without any problems). The microseismic monitoring in the area near well 46-16 has not been completed. If this experimental survey should prove capable of identifying geothermal fluid movement in formation fractures in the vicinity of well 46-16, a better target might become available for drilling a side-track leg to the hole, rather than just paralleling the first leg.

ACKNOWLEDGEMENTS

We want to thank Kenneth E. Lite of the Oregon Water Resources Department for his review and contributions to the section on Groundwater and Hydrology. The final version of this report was improved during editing by Cathy Chickering Pace of the SMU Huffington Department of Earth Sciences. We appreciate the efforts of Trenton Cladouhos of AltaRock Energy, Inc. in facilitating the final project completion. Thank you.

BIBLIOGRAPHY

- APEX HiPoint, 2012, Data processing results: Davenport Newberry Volcano project. Unpublished report submitted to Davenport Newberry.
- Arestad, J.E. and R.W. Potter II, 1988, Stratigraphic test drilling in the Newberry Crater KGRA, Oregon: Geothermal Resources Council Bull., November, pp. 3-8.
- Bargar, Keith.E. and Terry E.C. Keith, 1999, Hydrothermal Mineralogy of Core from Geothermal Drill Holes at Newberry Volcano, Oregon, USGS Professional Paper 1578.
- Beardsmore, G., L. Rybach, D. Blackwell, and C. Baron, 2010, A Protocol for Estimating and Mapping Global EGS Potential, GRC Transactions, Vol. 34.
- Bestland, E. A., M.S. Forbes, E.S. Krull, G.J. Retallack, and T. Fremd, 2008. Stratigraphy, paleopedology, and geochemistry of the middle Miocene Mascall Formation (type area, central Oregon, USA). *PaleoBios*, 28, 41-61.
- Beyer, Robert Lee, 1973, Magma differentiation at Newberry Crater in central Oregon. University of Oregon Ph.D. Dissertation, 84 p.
- Blackwell, D.D., R.G. Bowen, D.A. Hull, J. Riccio, and J.L. Steele, Heat flow, volcanism and subduction in northern Oregon, *J. Geophys. Res.*, 87, 8735-8754, 1982
- Blackwell, D. D. and G. R. Priest, 1996, Comment on “Rates and patterns of groundwater flow in the Cascade Range volcanic arc and the effect on subsurface temperatures” by S.E. Ingebritsen, D.R. Sherrod, and R.H. Mariner, *J. Geophys Res.*, Vol. 101, pp. 17,561-17,568.
- Blackwell, D. D. and G. R. Priest, 1996, Comment on “Heat flow from four new research holes in the Western Cascades, Oregon, USA” by S.E. Ingebritsen, M.A. Scholl, and D.R. Sherrod, *Geothermics*, Vol. 25, pp. 707-713.
- Blackwell, David D., John L. Steele, Michael K. Frohme, Charles F. Murphy, George R. Priest and Gerald L. Black, 1990, Heat flow in the Oregon Cascade Range and its correlation with regional gravity, Curie point depths, and geology. *Jour. Geophys. Res.*, Vol. 95, No. B12, pp. 19,475-19,494.
- Bruno, Pier Paolo G., Giovanni P. Ricciardi, Zaccaria Petrillo, Vincenzo Di Fiore, Antonio Troiano and Giovanni Chiodini, 2007, Geophysical and hydrogeological experiments from a shallow hydrothermal system at Sulfatara Volcano, Campi Flegrei, Italy: Response to caldera unrest. *Jour. Geophys. Res.*, Vol. 112, No. B6, B6201, 17 pp.
- Caldwell, Rodney R. and Margot Truini, 1997, Ground-water and water-chemistry data for the Upper Deschutes Basin, Oregon. U.S.G.S. Open-File Report 97-197. 77 pp.
- Cannon, D.M., 1984, The Stratigraphy, Geochemistry, and Mineralogy, of Two Ash-Flow Tuffs in the Deschutes Formation, Central Oregon, M.S. Thesis, Oregon State University, Department of Geology.

- Catchings, R.D. and W.D. Mooney, 1988, Crustal structure of east central Oregon: Relation between Newberry Volcano and regional crustal structure. *Jour. Geophys. Res.*, Vol. 93, No. B9, pp 10081-10094.
- Crumrine, Milo D. and David S. Morgan, 1994, Hydrologic, water-quality and meteorologic data for Newberry Volcano and vicinity, Deschutes County, Oregon, 1991-1993. U.S.G.S. Open-File Report 94-122, 70 p.
- Davies, K.G. and A.M. Johnson, ed., 1961, Peter Skene Ogden's Snake Country journal, 1826-1827. Hudson's Bay Record Society, Vol. XXIII, 255 pp.
- DOGAMI (Oregon Department of Geology and Mineral Industries) on-line data, Newberry Volcano files.
- Epoch, 2008, Final Well Report - NWG 46-16. Unpublished well report.
- Epoch, 2008, Final Well Report - NWG 55-29. Unpublished well report.
- Erkan, Kamil, Gwen Holdmann, Walter Benoit and David Blackwell, 2008, Understanding The Chena Hot Springs, Alaska, geothermal system using temperature and pressure data from exploration boreholes. *Geothermics*, (2008), doi: 10.1016/j.geothermics.2008.09.001.
- Finger, John T., Ronald D. Jacobson and Paul B. Spielman, 1977, Newberry exploration slimhole. *Geothermal Res. Council Trans.*, Vol. 21, pp. 97-102.
- Fitterman, David V., 1988, Overview of the structure and geothermal potential of Newberry Volcano, Oregon. *Jour. Geophys. Res.*, Vol. 93, No. B9, pp 10059-10066.
- Fitterman, D.V., W.D. Stanley and R.J. Bisdorf, 1988, Electrical structure of Newberry Volcano, Oregon. *Jour. Geophys. Res.*, Vol. 93, No. B9, pp 10119-10134.
- Foulger, Gillian R., 2010, Report to AltaRock Energy Inc. Newberry Calibration Shot Project. unpublished report to AltaRock Energy.
- Frone, Zachary S., 2014, Heat flow, thermal modeling and whole rock geochemistry of Newberry Volcano, Oregon and heat flow modeling of the Appalachian Basin, West Virginia, Dissertation, Southern Methodist University, Dallas, Texas 75275, 267 p.
- Frone, Zachary, Al Waibel and David Blackwell, 2014, Thermal modeling and EGS Potential of Newberry Volcano, central Oregon, Proceeding, 39th Workshop on Geothermal Reservoir Engineering, Stanford University, Stanford, California, February 24-26, 2014, SGP-TR-202. 10 p.
- Fuller, Brian, Les Engelbrecht, Rich Van Dok and Marc Sterling, 2007, Diffraction processing of downhole passive monitoring data to Image hydrofracture locations. *Proceedings SEG San Antonio Annual Meeting*, pp. 1297-1301.
- Gannett, Marshall W., Kenneth E. Lite Jr., David S. Morgan and Charles A. Collins, 2001, Groundwater hydrology of the Upper Deschutes Basin, Oregon. U.S.G.S. Water Resources Investigations Report 00-4162, 77 pp.

- Geosystem, 2007, Magnetotelluric survey Newberry Volcano, Oregon, USA: Report for Northwest Geothermal Company, 16 pp. Geosystem Sri, Viale Abruzzi 17, Milano, Italy.
- Geotronics Corp., 1979, Magnetotelluric survey in the Newberry Caldera of central Oregon for SUNOCO Energy Development Co. unpublished, 17 p.
- Gettings, M.E., and A. Griscom, 1988, Gravity model studies of Newberry Volcano, Oregon, *Jour. Geophys. Res.*, Vol. 93, No. B9, pp 10109-10118.
- Higgins, Michael W., 1973, Petrology of Newberry Volcano, central Oregon. *Geol. Soc. America Bull.* February, 1973, Vol. 84, no. 2, pp 455-488.
- Ingebritsen, S. E., D. R. Sharrod and R. H. Mariner, 1989, Heat flow and hydrothermal circulation in the Cascade Range, north-central Oregon. *Science*, Vol. 243, No. 4897, pp. 1458-1462.
- Jensen, Robert A., 2006, Roadside guide to the geology of Newberry Volcano. *Fourth edition*, CenOreGeoPub, Bend, Oregon, 182 p.
- Jensen, R.A., Donnelly-Nolan, J.M., and McKay, D.M., 2009, A field guide to Newberry Volcano, Oregon, in O'Connor, J.E., Dorsey, R.J., and Madin, I.P., eds., *Volcanoes to Vineyards: Geologic Field Trips through the Dynamic Landscape of the Pacific Northwest: Geological Society of America Field Guide 15*, p. 53–79, doi: 10.1130/2009.fl d015(03).
- Keith, Terry E.C. and Keith E. Bargar, 1988, Petrology and hydrothermal mineralogy of U.S. Geological Survey Newberry 2 drill core from Newberry Caldera, Oregon. *Jour. Geophys. Res.*, Vol. 93, No. B9, pp 10174-10190.
- Keith, T.E.C., M.W. Gannett, J.C. Eichelberger and A.F. Waibel, 1986, Lithology and hydrothermal alteration of drill hole RDO- 1, Newberry Caldera, Oregon. *Oregon Geology*, Vol. 48, pp 103-110.
- Keith, T.E.C., R.H. Mariner, K.E. Bargar, W.C. Evans and T.S. Presser, 1984, Hydrothermal alteration in Oregon's Newberry Volcano no. 2: fluid chemistry and secondary-mineral distribution. *Geothermal Res. Council Bull*, Vol. 13, pp 9-17.
- Knott, J.R., Sarna-Wojcicki, A.M., Montañez, I.P., Wan, E. (2007). Differentiating the Bishop ash bed and related tephra layers by elemental-based similarity coefficients of volcanic glass shards using solution inductively coupled plasma-mass spectrometry (S-ICP-MS). *Quaternary International*, Volume 166, Issue 1, May 2007, Pages 79-86.
- Kuehn, Stephen C., 2002, Stratigraphy, Distribution, and Geochemistry of the Newberry Volcanic Tephra: Washington State University Ph.D. dissertation, Department of Geology, August 2002, 701 p.
- Linneman, Scott R., 1990,. The Petrologic Evolution of the Holocene Magmatic System of Newberry Volcano, Central Oregon, Ph.D. diss., University of Wyoming, Department of Geology and Geophysics.

- Lite, Kenneth E., Jr., and Marshall W. Gannett, 2002, Geologic framework of the regional ground-water flow system in the upper Deschutes Basin, Oregon: U.S. Geological Survey Water-Resources Investigations Report 02-4015, p. 44.
- Lowe, D.J., 2011, Tephrochronology and its application: A review, *Quaternary Geochronology*, Volume 6, Issue 2, April 2011, Pages 107-153, ISSN 1871-1014.
- MacLeod, Norman S., George W. Walker and Edwin H. McKee, 1975, Geothermal significance of eastward increase in age of upper Cenozoic rhyolite domes in southeastern Oregon. *in* Proceedings, Second United Nations Symposium on the Development and Use of Geothermal Resources, San Francisco, California, USA, Vol. 1, pp 465-474.
- MacLeod, Norman S., David R. Sherrod, Lawrence A. Chitwood and Edwin H. McKee, 1979, Newberry Volcano, Oregon - Geologic summary and field trip guidebook. Unpublished, 35 p.
- MacLeod, Norman S., David R. Sherrod and Lawrence A. Chitwood, 1982, Geologic map of Newberry Volcano, Deschutes, Klamath, and Lake Counties, Oregon. U.S. Geological Survey Open-File Report 82-847, 27 p., with map.
- MacLeod, N. S., Sherrod, D. R., Chitwood, L. A. & Jensen, R. A. (1995). Geologic Map of Newberry Volcano, Deschutes, Klamath, and Lake Counties, Oregon. *U.S. Geological Survey Miscellaneous Investigations Map*, I-2455, 2 maps.
- McClaughry, J.D., Ferns, M.L., and Gordon, C.L., 2009, Field trip guide to the Neogene stratigraphy of the Lower Crooked Basin and the ancestral Crooked River, Crook Counties, Oregon. *Oregon Geology*, vol. 69, no. 1, Fall 2009.
- McDannel, Angela K., 1989, Geology of the Southernmost Deschutes Basin, Tumalo Quadrangle, Deschutes County, Oregon., M.S. Thesis, Oregon State University, Department of Geology.
- Mckay, Daniele, Julie M. Donnelly-Nolan, Robert A. Jensen, and Duane E. Champion, , 2009, The post-Mazama northwest rift zone eruption at Newberry Volcano, Oregon, in O'Connor, J.E., Dorsey, R.J., and Madin, I.P., eds., *Volcanoes to Vineyards: Geologic Field Trips through the Dynamic Landscape of the Pacific Northwest: Geological Society of America Field Guide 15*, p. 91-110, doi: 10.1130/2009.fl d015(05).
- Morgan, David S., Dwight Q. Tanner and Milo D. Crumrine, 1997, Hydrologic and water-quality conditions at Newberry Volcano, Deschutes County, Oregon, 1991-1995. U.S.G.S. Water-Resources Investigations Report 97-4008, 66 p.
- Morse, Lee H. and Michael McCurry, 1997, Possible correlations between basalt alteration and the effective base of the Snake River Plain aquifer at the Idaho National Engineering and Environmental Laboratory. Proceedings 32nd Symposium Engineering Geology and Geotechnical Engineering. 13 pp.
- Muffler, L.J.P., 1979, Assessment of geothermal resources of the United States -- 1978. U.S. Geol. Survey Cir. 790, 163 p

- Osborn, William L., Susan Petty, Laura L. Norziger and Douglas Perry, 2010, Geothermal Resources Transaction, Vol. 34, p. 413-418.
- Patridge, K.A. (2010). Geochemistry and Petrogenesis of John Day Ash Flows near Prineville, Oregon. M.S. Thesis, Washington State University, School of Earth and Environmental Sciences.
- Phillips, Kenneth N., 1968, Hydrology of Crater, East and Davis Lakes, Oregon. U.S.G.S. Water-Supply Paper 1859-E, 60 p.
- Raharjo, I., P. Wannamaker, R. Allis, and D. Chapman, 2002, Proceedings of the 27th Stanford Workshop on Geothermal Reservoir Engineering, 7 pp Roberts, Carter W., Robert P. Kucks, and Patricia L. Hill, 2008, Oregon magnetic and gravity maps and data—A website for distribution of data: U.S. Geological Survey Data Series 355.
- Robinson, P. T., Walker, G. W., and McKee. E. H., 1990, Eocene(?), Oligocene and lower Miocene rocks of the Blue Mountains region: in Walker, G. W., ed., Geology of the Blue Mountains region of Oregon, Idaho, and Washington: U.S. Geological Survey Professional Paper 1437, p. 29–62.
- Russell, Israel C., 1905, Preliminary report on the geology and water resources of central Oregon: U.S. Geological Survey Bull. 252, 138 p.
- Sammel, Edward A. and Robert W. Craig, 1983, Hydrology of the Newberry Volcano Caldera, Oregon. U.S.G.S. Water Resources Investigation. Report 83-4091.
- Sammel, E.A., S.E. Ingebritsen and R.H. Mariner, 1988, The hydrothermal system at Newberry Volcano, Oregon. Jour. Geophys. Res., Vol. 93, No. B9, pp 10149-10162.
- Sarna-Wojcicki, A. M.; Bowman, H. R.; Meyer, C. E.; Russell, P. C.; Woodward, M. J.; McCoy, Gail; Rowe, J. J., Jr.; Baedeker, P. A.; Asaro, Frank; Michael, Helen, (1984). Chemical analyses, correlations, and ages of upper Pliocene and Pleistocene ash layers of east-central and Southern California. USGS Professional Paper: 1293
- Sherrod, David R., Edward M. Taylor, Mark L. Ferns, William E. Scott, Richard M. Conrey, and Gary A. Smith, 2004, Geologic map of the Bend 30-x60-minute quadrangle, central Oregon; U.S. Geol. Survey Geologic Investigations Series 1-2683.
- Sherrod, David R., Larry G. Mastin, William E. Scott and Steven P. Schilling, 1997, Volcano hazards at Newberry Volcano, Oregon. U.S.G.S. Open-File Report 97-513, 14 p.
- Sigma³, 2014, A report for the 2013 Newberry low-amplitude passive seismic monitoring project. Unpublished report to AltaRock Energy.
- Smith, G.A., 1986, Stratigraphy, sedimentology, and petrology of Neogene rocks in the Deschutes basin, central Oregon: a record of continental-margin volcanism and its influence on fluvial sedimentation in an arc-adjacent basin: Corvallis, Oregon State Univ., Ph.D. dissertation, 467p.

- Spielman, Paul B. and John T. Finger, 1998, Well test results of exploration drilling at Newberry Crater, Oregon. *in*: Proceedings, 23rd Workshop on Geothermal Reservoir Engineering, pp. 21-26.
- Stauber, Douglas A., Susan M. Green and H.M. Iyer, 1988, Three-dimensional *P* velocity structure of the crust below Newberry Volcano, Oregon. *Jour. Geophys. Res.*, Vol. 93, No. B9, pp 10095-10108.
- Steele, J.L., and D.D. Blackwell, 1982, Heat flow in the vicinity of the Mount Hood volcano, Oregon, p. 31-42, in, *Geology and Geothermal Resources of the Mount Hood Area, Oregon*, ed.G.R. Priest and B.F. Vogt, Oregon Dept Geol. Min. Ind. Special Paper 14.
- Streck, M. J. , 1994, *Volcanology and Petrology of the Rattlesnake Ash-Flow Tuff, eastern Oregon*. Ph.D. Diss, Oregon State University, Department of Geology.
- Sun, S.S., and W.F. McDonough, 1989, *Chemical and Isotopic Systematics of Oceanic Basalts: Implications for Mantle Composition and Processes*. Geological Society, London, v. 42: p. 313-345.
- Swanberg, C.A., W.C. Walkey, J. Combs, 1988, Core Hole Drilling and the “Rain Curtain” Phenomenon at Newberry Volcano, Oregon. *Journal of Geophysical Research*, Vol. 93, NO. B9, pg 10,163-10,173.
- Tester, J. W., Anderson, B., Batchelor, A., Blackwell, D., DiPippo, R., Drake, E., Garnish, J., Livesay, B., Moore, M.C., Nichols, K., Petty, S., Toksoz, N., Veatch, R., Augustine, C., Baria, R., Murphy, E., Negraru, P., Richards, M., 2006, *The future of geothermal energy: Impact of enhanced geothermal systems (EGS) on the United States in the 21st century*. Massachusetts Institute of Technology, DOE Contract DE-AC07-05ID14517 Final Report, 209 p.
- Urquhart, Scott Allen, 1988, *A magnetotelluric investigation of Newberry Volcano, Oregon*. MSc thesis, Univ. of Oregon, 75 p.
- Ussher, Greg, 2006, *Reprocessed geophysical data informally provided to Davenport Power, LLC, as preliminary to designing an expansive MT program*.
- Ussher, G., C. Harvey, R. Johnstone, and E. Anderson, 2000, *Understanding the resistivities observed geothermal systems: Proceedings of the World Geothermal Congress, Kyushu-Tohoku, Japan*, pp. 1915-1920.
- Waibel, A.F., 1979, *Geologic map of Newberry Volcano*. Unpublished report to Sunedco, released to the public in 1985.
- Waibel, A.F., 1979, *Soil geochemistry survey of the Breitenbush and Newberry Caldera areas of Oregon*. Unpublished report to Sunedco, released to the public in 1985.
- Waibel, Al, Les Beard and Gary Oppliger, 2013, *The evolving role of MT in geothermal exploration at Newberry Volcano, Oregon*. PROCEEDINGS, Thirty-Eighth Workshop on Geothermal Reservoir Engineering Stanford University, Stanford, California, SGP-TR-198

- Waibel, Albert F., Zachary Frone and Todd Jaffe, 2012, Geothermal exploration at Newberry Volcano, central Oregon. *Geothermal Resources Transactions*, Vol. 36, pp. 803-810.
- Williams, Howell, 1935, Newberry Volcano of central Oregon: *Geological Society of America Bull.*, vol. 46, no. 2, pp 253-304.
- Williams, H., 1957, A geological map of the Bend Quadrangle, Oregon, and a reconnaissance geologic map of the central portions of the High Cascade Mountains. State of Oregon Department of Geology and Mineral Industries Map.
- Zonge Geosciences Inc., 2007, Gravity survey on the Newberry project for Davenport Resources LLC. 38 pp.
- Zucca, John J. and John R. Evans, 1992, Active high-resolution compressional wave attenuation tomography at Newberry Volcano, central Cascade Range. *Jour. Geophys. Res.*, vol. 97, No. B7, pp 11047-11055.

APPENDIX A: TEMPERATURE DATA FOR WELLS 55-29 and 46-16

Dr. Zachary Frone and Dr. David D. Blackwell
Southern Methodist University

Temperature and Heat Flow Data

Data for Well 55-29

Equilibrium temperature data were collected from the wellhead to 3,000 m (9,843.6 ft) true vertical depth on 9/22/2010. Samples were collected for thermal conductivity analysis from 14 intervals in the well. Cuttings were taken every 15 m (50 ft) from each interval and mixed; this resulted in an averaged lithology for the interval. Thermal conductivity values of the cuttings were measured using the divided bar technique (Blackwell and Spafford, 1987; Sass et al. 1971). Measured thermal conductivity values were corrected for the *in situ* temperature using data from Birch and Clark, 1940. An average gradient was calculated for each sampled interval and multiplied by the corrected thermal conductivity value resulting in an interval heat flow. For the final well value all the intervals were averaged (Table 1).

Appendix A, Table 3 Heat flow for well 55-29.

Depth Interval (Tvd)		Measured Thermal Conductivity (W/m*K)	Log Temperature (°C)	Temperature Corrected Thermal Conductivity (W/m*K)	Interval gradient (°C/km)	Heat flow (mW/m ²)	Corrected Heat flow (mW/m ²)
Top (m)	Bottom (m)						
1126	1289	1.46	136.6	1.46	121.4	177.1	177.2
1454	1544	1.85	175.8	1.85	110.3	203.9	204.1
1544	1648	2.87	185.9	2.47	108.6	311.9	268.2
1693	1797	2.19	201.9	2.09	102	222.9	213.2
1812	1885	2.37	214.4	2.09	103.8	245.8	216.9
1885	1930	2.62	222.3	2.30	110.3	289.1	253.7
1945	2094	2.27	228.8	1.99	95.1	215.6	189.2
2094	2243	2.43	243.2	1.99	100.8	244.6	200.6
2258	2287	2.92	260.0	2.30	99.5	290.6	228.9
2332	2436	2.93	267.2	2.30	99.1	290.3	227.9
2510	2570	2.17	285.0	1.99	97.4	211.0	193.8
2585	2645	2.89	292.3	2.26	98.5	284.7	222.6
2765	2808	2.89	310.1	2.26	95	274.5	214.7
2910	2983	2.36	324.9	1.99	79.9	188.8	159.0
						246.5 ± 11.7	212.2 ± 7.6

Data for Well 46-16

Equilibrium temperature data were collected for three intervals in the shallower portion of the well, to the bridge in the well at 1,432 m (~4,700 ft). For these upper intervals, equilibrium temperature measurements and thermal conductivity samples were used to calculate heat flow using the process described above for well 55-29. Below the bridge, thermal conductivity samples were available and measured, but the gradient values were calculated based on the upper portion of the wellbore, rather than measured. Table two shows results for the upper, measured portion of the well; table three provides the estimated temperatures for the lower portion.

Appendix A, Table 4: Thermal Conductivity, Equilibrium Temperature Measurements, and Heat flow for well 46-16

Depth Interval (TvD)		Measured Conductivity (W/m*K)	Logged Temperature (°C)	Temperature Corrected Conductivity (W/m*K)	Interval Gradient (°C/km)	Heat flow (mW/m ²)	Corrected Heat flow (mW/m ²)
Top (m)	Bottom (m)						
1054	1204	1.68	108.8	1.76	102.6	172.4	180.3
1234	1340	1.575	125.5	1.63	107.7	169.7	175.8
1355	1506	1.85	140.8	1.92	96.9	179.3	186.6
						173.8 ± 2.3	180.9 ± 2.6

Appendix A, Table 5: Thermal conductivity results and calculated heat flow for 46-16. Calculated interval gradients assume constant heat flow with depth (note the heat flow value of 180.9 used to calculate the gradient is from Table 2 above).

Depth Interval (TvD)		Measured Conductivity (W/m*K)	Estimated Average Temperature (°C)	Temperature Corrected Conductivity (W/m*K)	Heat flow (mW/m ²)	Calculated Interval Gradient
Top (m)	Bottom (m)					
1521	1611	1.72	155*	1.61	180.9	112.4
1821	1881	2.79	187*	2.30	180.9	78.6
2106	2256	2.00	223*	1.77	180.9	102.3
2406	2566	2.66	256*	2.22	180.9	81.4
2716	2865	2.76	289*	2.18	180.9	83.0
3005	3155	2.52	322*	2.14	180.9	84.6

* temperatures estimated from gradient extrapolation

Temperature Interpretation for Well 46-16

An estimate of the bottom-hole temperature (BHT) is important to get a better idea of the thermal resource in 46-16. Three different estimates of the BHT for this well are shown and described below.

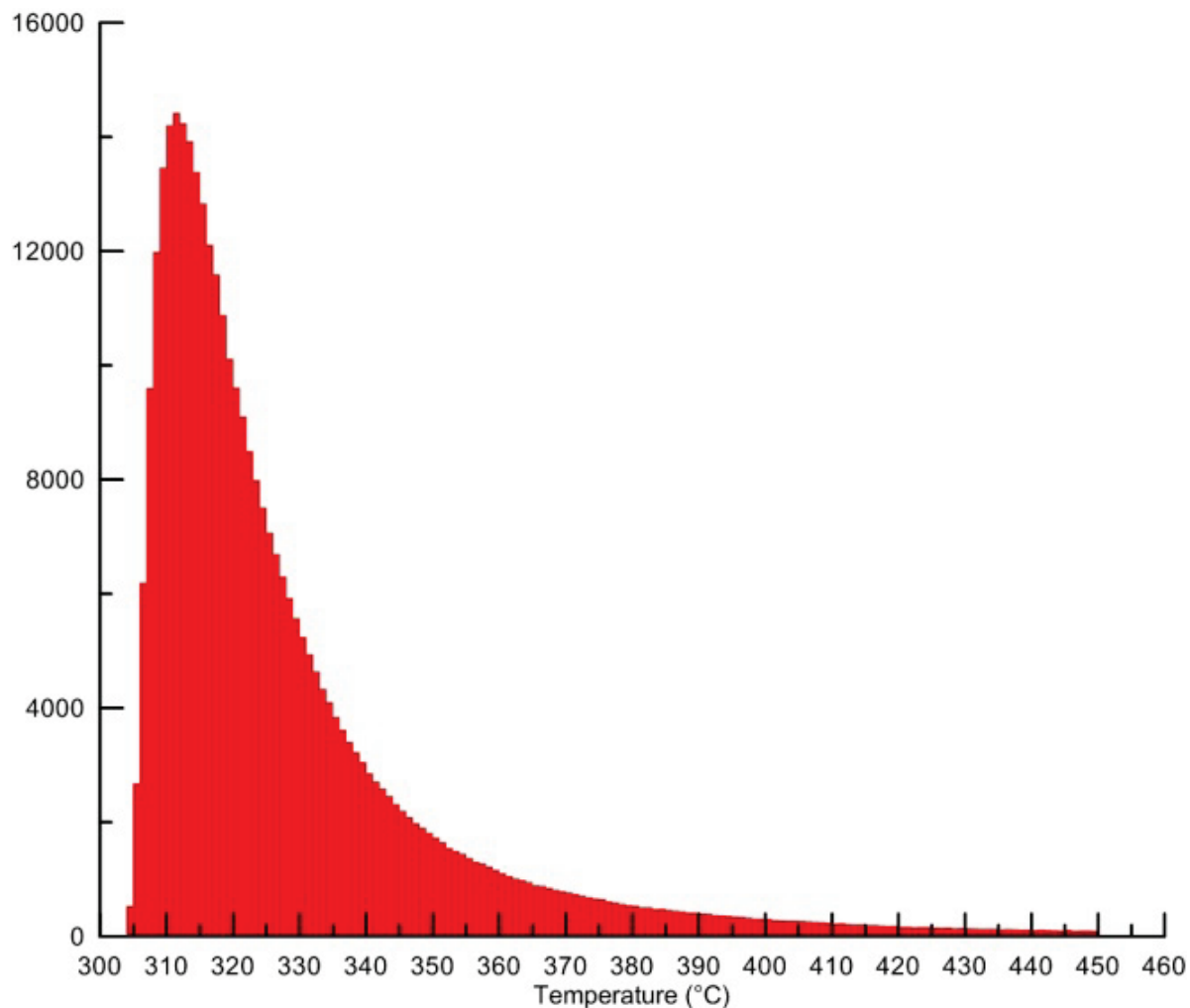
The first estimate is based solely on the extrapolation of the equilibrium gradient of 108°C/km from the upper 1,432 m (4,700 ft) of the well to the bottom-hole depth. At first a linear gradient to total depth looks reasonable based on data from other deep wells that show a high conductive gradient to total depth. This results in a calculated BHT of 362°C (685°F) at 3,484 m (11,430 ft) true vertical depth.

A second estimate of the BHT is based on the three non-equilibrium logs that were collected 3-4 days after drilling was completed, but prior to the bridge forming. Two of the logs were collected on 10/22/2008 and the third on 10/23/2008. The BHT from each of these logs were used to calculate a Horner Corrected BHT which is based on the time since circulation (TSC) and the amount of thermal recovery since the completion of drilling (Deming and Chapman, 1988). The correction requires data on the TSC and the circulation time (t_c) from which the following equation is calculated for each log:

Appendix A, Equation 1

$$\ln\left(1 + \frac{t_c}{TSC}\right)$$

The results from Appendix A, Equation 1 are plotted versus temperature and a best fit line is extrapolated to infinite time (y-intercept), the intercept is the Horner temperature. An example of the correction is shown in Appendix A, Figure 3. No time stamps were found with the log files so estimates of the TSC were used for the correction. Ranges for the circulation time and the TSC for the 3 logs were estimated from the logging dates. Using a Monte Carlo methodology, over 1 million iterations were calculated, but only the values with an r^2 value greater than 0.9 on the best fit line were kept. The peak of the calculated temperature distribution is 311°C; this value is plotted in Appendix A, Figure 4 and Appendix A, Figure 5 below with error bars from 307-334°C (based on Appendix A, Figure 1 histogram bin values >4,000).



Appendix A, Figure 64: Histogram of the Monte Carlo method calculated Horner temperatures for r^2 values between 0.9 and 1.0. Left axis is the number of occurrences.

The third estimate of the BHT in 46-16 is based on heat flow calculated for the upper portion of the well. Heat flow was assumed to be constant with depth. Using the heat flow value of 180.9 mW/m² and the thermal conductivity measurements from the lower portion of the well, gradients were calculated for each interval. A corrected temperature was then calculated. For portions of the well with no thermal conductivity measurements the gradient for the zone above it was used. There is a noticeable increase in the conductivity values below 1,830 m (6,000 ft), which is likely due to changing stable mineral phases with increasing temperature. The calculated gradient was used to calculate a theoretical equilibrium temperature depth curve for the well. The calculated BHT for this method is 319°C (606°F), which is in good agreement with the value from the Horner Correction value at 311°C.

Based on these results, the BHT in well 46-16 is likely in the range of 310-330°C (590-625°F). Temperature depth plots below show the results of the three methods (Appendix A, Figure 4 and Appendix A, Figure 5).

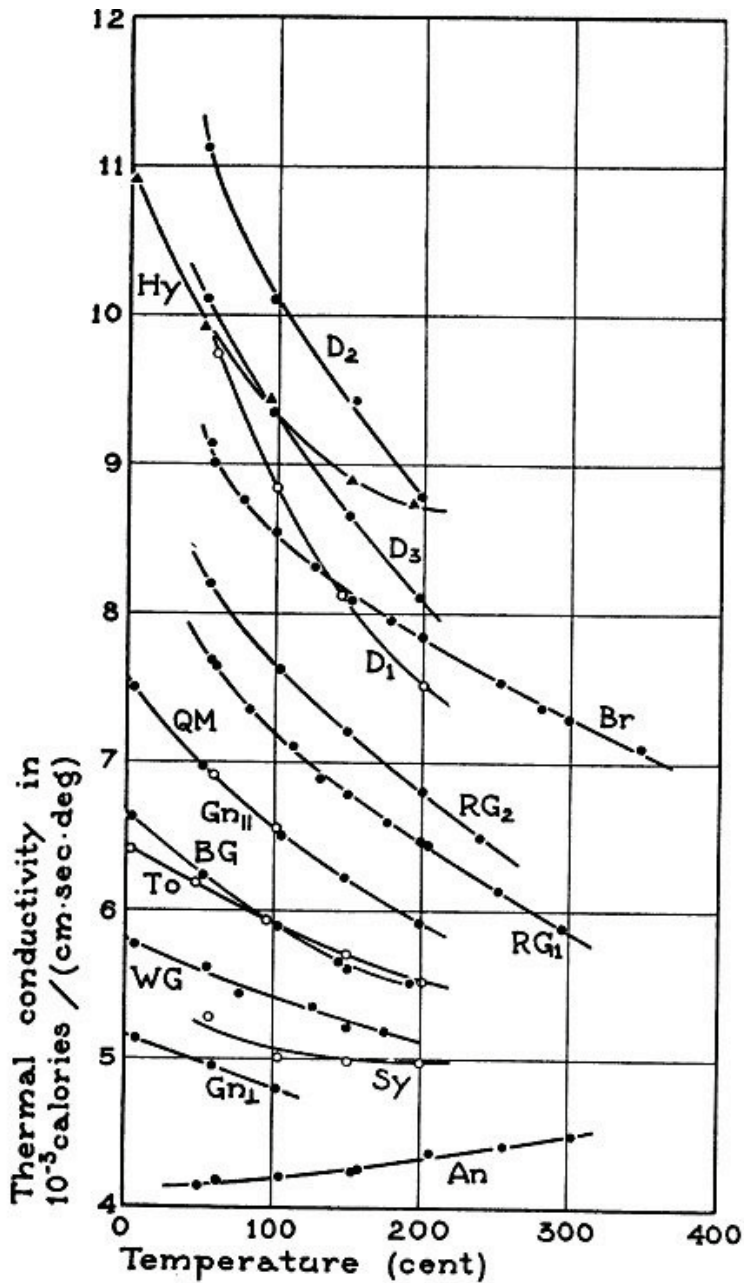
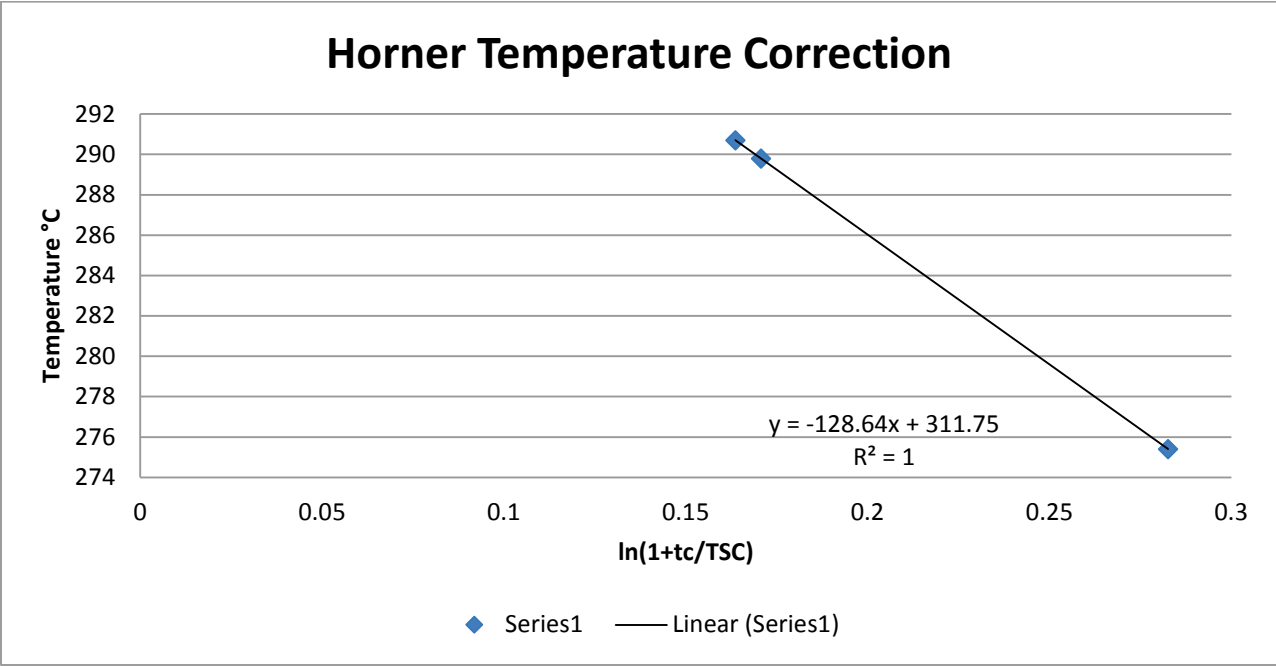


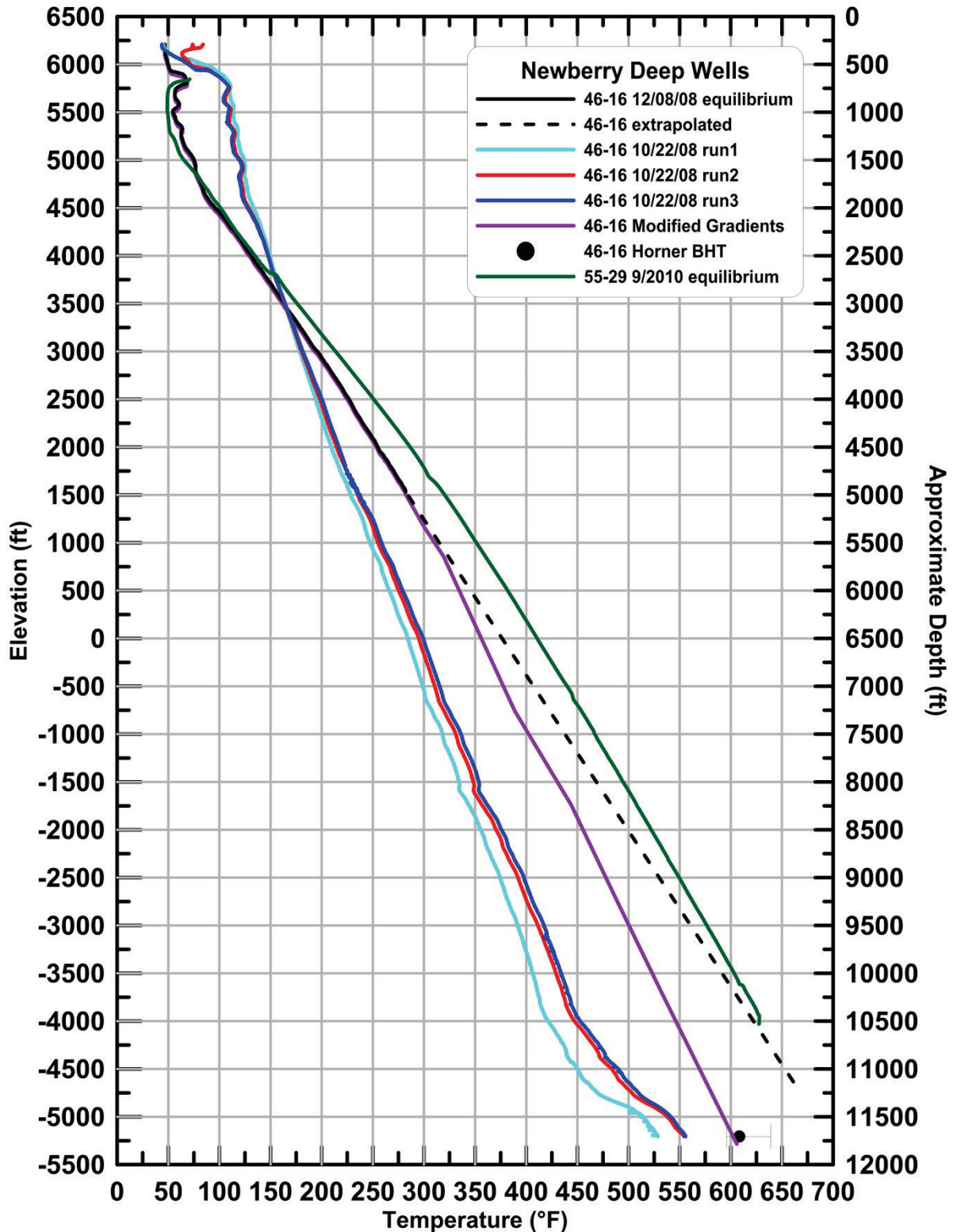
Fig. 4. Thermal conductivity of holocrystalline rocks.

An	Anorthosite, Quebec.	RG ₁	Rockport Granite 1.
Gn ₁	Gneiss, Pelham, ⊥ bed-plane.	RG ₂	Rockport Granite 2.
Gn ₂	Gneiss, Pelham, bed-plane.	Br	Bronzitite.
Gn ₃	Gneiss, Pelham, bed-plane.	Hy	Hypersthene.
Sy	Syenite, Ontario.	D ₁	Dunite 1.
WG	Westerly Granite.	D ₂	Dunite 3.
To	Tonalite, Calif.	D ₃	Dunite 2.
BG	Barre Granite.		
QM	Quartz monzonite, Calif.		

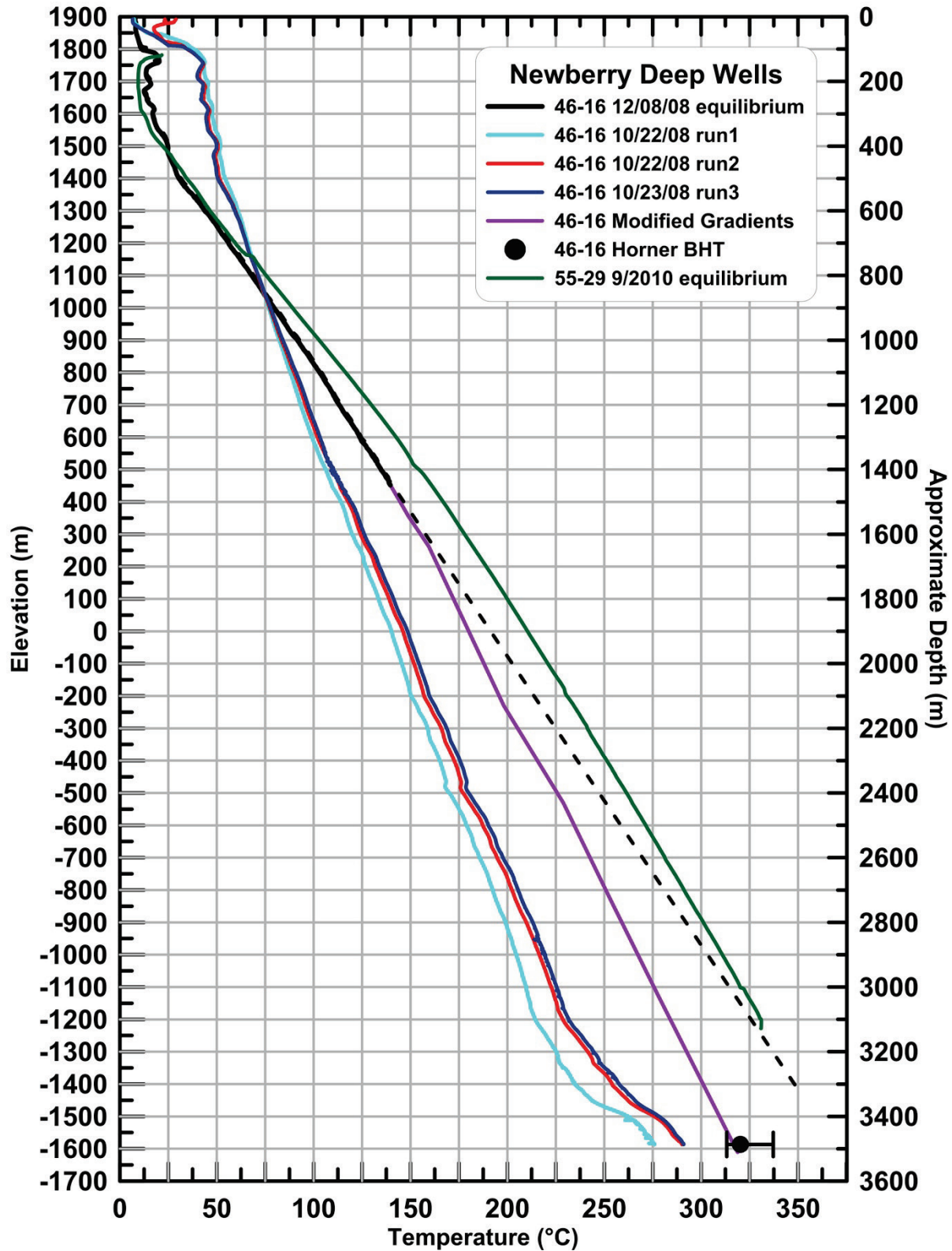
Appendix A, Figure 65: From Birch and Clark, 1940, Figure 4. The temperature dependent thermal conductivity of various rock types is shown. Note units on this figure are in Cal/cm*sec*deg and Appendix A Tables 1-3 are in W/m*K.



Appendix A, Figure 66: Example of Horner temperature corrections. The y-intercept of 311.75 represents the corrected temperature.



Appendix A, Figure 67: Temperature depth data from 46-16 in feet and °F. The black dashed line is from method 1 (constant gradient extrapolation), the black dot is from method 2 (Horner correction), purple curve is from method 3 (thermal conductivity calculated gradients). The equilibrium temperature data from 55-29 is plotted for reference.



Appendix A, Figure 68: Temperature depth data from 46-16 in meters and °C. The black dashed line is from method 1 (constant gradient extrapolation), the black dot is from method 2 (Horner correction), purple curve is from method 3 (thermal conductivity calculated gradients). The equilibrium temperature data from 55-29 is plotted for reference.

Appendix A - References

Birch, F. and H. Clark, 1940, The Thermal Conductivity of Rocks and its Dependence Upon Temperature and Composition, *Am. Jour. Sc.*, Vol. 238, No. 8, August, 1940.

Blackwell, D.D. and R.E. Spafford, 1987, Experimental methods in continental heat flow. In: Sammis and Henyey, (Eds.), *Methods of Experimental Physics*, vol. 24. Academic Press, New York, Chapter 14, pp. 189-226.

Deming, D. and D.S. Chapman, 1988, Heat Flow in the Utah-Wyoming Thrust Belt From Analysis of Bottom-Hole Temperature Data Measured in Oil and Gas Wells, *J. Geophys. Res.*, 93(B11), 13657–13672, doi: 10.1029/JB093iB11p13657.

Sass, J.H., A.H. Lachenbruch, and R.J. Munroe, 1971, Thermal conductivity of rocks from measurements on fragments and its application to heat-flow determinations, *J. Geophys. Res.*, 76(14), 3391–3401, doi: 10.1029/JB076i014p03391.

APPENDIX B: Geochemistry Data Analysis

This Appendix contains 2 datasets.

1. 'Cuttings' geochemical data collected by ICP-ES for major elements and ICP-MS for trace and Rare Earth Elements (REE). The analysis was performed by Acme Labs. The values in the tables are the lab reported values.
2. 'Core' XRF data collected by Dr. Zachary Frone using a handheld Bruker Tracer XRF. All XRF data are from core samples. Each core was analyzed in three spots and the average composition of the three spots was averaged for the final reported value. The standard deviation of the three points of each core is also reported in the tables. The data have been corrected for XRF peak overlaps, as described in the text (Core Samples).

Appendix B Table of Contents

'Cuttings' geochemical data collected	Appendix B, Page 2
'Core' XRF data collected	Appendix B, Page 38

APPENDIX C: Geologica Reports to Davenport Power

This
label

geologica

Innovative Strategies for Environmental and
Natural Resource Management

To: Todd Jaffe, Davenport Newberry Holdings
Al Waibel, Columbia Geoscience
From: Jill Robinson Haizlip, Geologica
Date: 4 February 2010

Re: Gas Analysis of Newberry wells

Analyses of gasses produced from high temperature geothermal systems have been used to understand the relationship between gas phases, liquid phases and solid (mineral) phases. This has led to the formulation of chemical geothermometers based on gas populations.

Chemical geothermometers are based on the understanding of chemical reactions and chemical equilibria between gas, liquid and/or solid phases. Gas geothermometry techniques are applicable under three types of conditions. The first considers only gas-gas equilibrium. The second considers gas-mineral equilibrium using H₂S, CH₄ and H₂. The third uses gas analysis from well production fluid and requires measurement of a gas-water ratio. The most comprehensive and useful gas geothermometers are based on substantive gas-water well test samples where partial pressures of gasses and gas-water ratios can be reliably estimated. These geothermometers work well for samples collected at hot springs, boiling springs, and flowing geothermal wells. These sites provide constraints on temperature, pressure, and relationships between steam and non-condensable gasses.

Well and sampling conditions at well 46-16 present some significant limitations with regard to gas geothermometry interpretations. The well reached TD, and was cooled by circulation of water and remnant drilling fluid, in preparation to running a suite of geophysical logs. A process was then initiated to unload the hole, to test production potential from promising zones within the well bore. As the fluid pressure within the well bore was decreased, a section of tuff just below the casing shoe bridged the hole. Multiple attempts to clear the bridge were unsuccessful, and flow test efforts were suspended. No fluid samples from a flowing well were possible. Currently the hole remains bridged at and below the casing shoe. The water left in the well bore was a combination of fresh water from a shallow coldwater well and remnant drilling fluid. When the well was shut in for the season the water level was at the well head.

5 Third Street Suite 224
San Francisco, CA 94103

Phone (415) 597-7881 • Fax (415) 597-7880

jhaizlip@geologica.net
www.geologica.net

A visit to the 46-16 well site in the spring of 2009 noted gas under pressure venting from the well head. The well head pressure gage registered 600 psi. The pressure was bled off and the leaking well head was repaired. The well head pressure built back up to 600 psi within a matter of hours. In October of 2009 samples of the gas were collected and a Temperature/Pressure log was run. The static water level was observed to be at 2070 ft. The well was bridged at 5000 ft., about 200 ft. below the casing shoe. A maximum temperature was recorded at the bridge of 304°F, though the water was observed to be slowly circulating within the well bore.

The depth(s) of gas entries and corresponding formation temperature(s) for well 46-16 could not be measured at this time due to the bridge as the geothermal gas is entering the well bore at some depth below the bridge. The gas is percolating upward thru the water in the well bore, possibly chemically shifting with reactions with the well bore water, and then accumulating in the well head. The source depth of the gas entry is unknown, though one notable possibility is around 9,000-10,000 foot depth, particularly between 9100 and 9400 ft. This zone produced marked gas entries during drilling, with CO₂ values exceeding 15,000 ppm. Temperature data for the well below the bridge are minimum temperatures in that the temperature survey was run with other geophysical logs after the hole had been intentionally cooled to protect the instrumentation.

Geophysical logs show a temperature of about 410°F at 9000 ft. on run 1, and about 450°F on run 2. These temperatures are similar to that observed in well 55-29 taken under comparable conditions and timing. Due to bridging, no thermal equilibrated temperatures are available for well 46-16. With well 55-29 the final equilibrated temperature at that point was about 590°F at 9,000 ft. and above 600°F at 10,000 ft. Therefore all that can be said for well 46-16 is that the minimum formation temperature at 9,000 ft. is 450°F, with a likelihood of the actual formation temperature being 100°F higher than the measured temperature.

This all results in the limited application of gas geothermometry on samples collected in October of 2009. There are, however, some qualifying conclusions that can be made.

Geologica has reviewed results from recent gas sampling (by Geologica) and analysis of gas (by Thermochem) accumulated in well Newberry Geothermal Well #46-16. The gas sampling was performed in October 2009 during the venting of gas built up at the wellhead. During sampling, the gas did not include significant amounts of water and therefore no gas/water ratios were available. The analytical results presented below are compared with those collected during the flow test of 55-29 and evaluated for temperature indications based on gas composition.

geologica

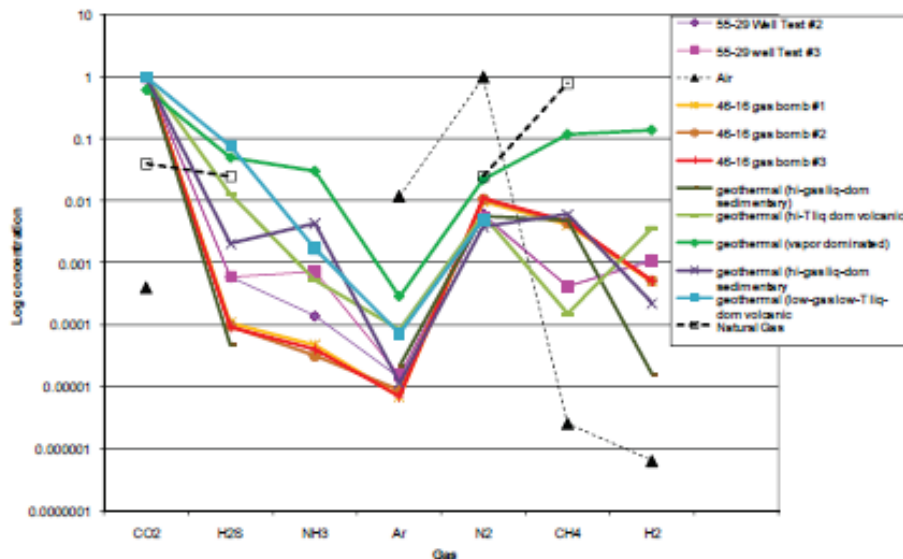
Noncondensable Gas Analysis

Well-Sample	Date-Time	carbon dioxide, CO2	hydrogen sulfide, H2S	ammonia, NH3	argon, Ar	oxygen, O2	nitrogen, N2	methane, CH4	hydrogen, H2
		ps % by volume	% by volume	% by volume	% by volume	% by volume	% by volume	% by volume	% by volume
NWG-46-16	10/25/2009 13:10	98.6	0.0107	0.004715	0.000695	0.00791	0.951	0.412	0.0491
NWG-46-16	10/25/2009 13:50	98.4	0.00952	0.00314	0.000867	0.0109	1.06	0.442	0.0509
NWG-46-16	10/25/2009 14:05	98.4	0.00913	0.004	0.000689	0.00459	1.08	0.47	0.0508
NWG-55-29 FT	7/19/2008 0:00	99.2	0.0589	0.0137	0.00138	0.0234	0.622	0.042	0.113
NWG-55-29 FT	7/19/2008 0:36	99.2	0.0601	0.072	0.00151	0.0028	0.562	0.0408	0.106

A comparison of gas analyses indicates that the gas collected at the end of the attempted flowing of well 55-29 and the gas collected recently from 46-16 were similar but not identical in composition. As shown in the Schoeller diagram below, relative concentration patterns of major noncondensable gas samples from the Newberry wells (carbon dioxide (CO₂), hydrogen sulfide (H₂S), ammonia (NH₃), argon (Ar), nitrogen (N₂), methane (CH₄) and hydrogen (H₂) are within the range of geothermal gases from other geothermal systems. The composition of geothermal gas is distinct from air, which has negligible hydrogen sulfide and ammonia and from natural gas which is almost all carbon dioxide and has negligible amounts of ammonia, argon and hydrogen.

The composition of gas samples from both wells appear to be hydrothermal (geothermal) gas similar to that from known liquid-dominated geothermal systems hosted in volcanic rocks. In addition to the proportions of major noncondensable gas, the hydrothermal character of these gases is indicated by the ratio of nitrogen and argon (N₂/Ar) which averages almost 1400 in 46-16 and over 400 in 55-29 (although in 55-29 it may probably lowered by air contamination). The average N₂/Ar in air saturated meteoric water is 38. The average N₂/Ar ratio in magmatic "andesitic" gas typical of gas discharges from geothermal and volcanic centers is between 800 and 2000.

Newberry Deep Wells Noncondensable Gas



geologica

The hydrothermal nature of the gases indicates that they have interacted with water at high temperatures. The composition of the gases is consistent with origin as magmatic gas which subsequently interacted with water. This may allow the application of gas geothermometers: temperatures estimated from temperature-dependent gas reactions. Because no water was produced with the gas, the gas/water ratio is unknown, preventing the application of geothermal industry standard gas geothermometers. When applying the gas geothermometers which are independent of water, results indicate that these gases may originate at a range of from 458°F up to 617°F (well 44-16) and 535 to 590°F (55-29). Assuming these gases have equilibrated in the presence of water as would be expected in a hydrothermal system, and some assumptions are made regarding the water pressure it appears that the temperature of this system averages around 470°F (ranging between 420-492 in 46-16 (dry gas sample from wellhead) and 458-529F in 55-29 (dry gas sample during flow test)). This range of temperatures may reflect differences in equilibrium of various gas reactions or they represent a mixture of gases from different zones which vary in liquid water saturation and temperature.

In summary, based on the analysis of gas sampled from 46-16 and 55-29, it appears there is evidence that geothermal fluid exists in the vicinity of the wellbores. The temperature of these fluids is in the range of the measured temperatures.

In order to improve confidence of and possibly expand on these tentative conclusions the following tests should be conducted:

1. Helium and helium isotope measurements to assess the magmatic contribution to these gases;
2. Comparison of gas results to alteration mineralogy in order to select optimum geothermometers;
3. Additional analyses to speciate sulfur and sulfur isotopes.
4. Comparison with gas analysis of fumaroles within the caldera.

Please feel free to call if you have questions.

Jill Robinson Haizlip
Geologica Inc.
5 3rd St. Suite 224
San Francisco, CA 94103
(415) 597-7801-o (415) 722-3628-c

geologica

44-16 Gas Temperature Estimated from Gas Geothermometers

Estimated Total Pressure	Ptot=PCO2 by DAM-P=10 bar PCO2= Ptot-by mineral equilibria=Max. WHP=600 psi/g=42 bar		sat water@550F=72 bar		=BHP-hydrostatic@550F=138bar	
	°C	°F	°C	°F	°C	°F
Estimated Temperature						
Empirical (D'Amore & Panichi 1980)	169	335	171	341	200	392
Pyrite-Magnetite (Giggenbach 1980)	179	354	181	358	205	402
Pyrite-Pyrrhotite (Giggenbach 1980)*	236	456	236	456	236	456
H2S (Giggenbach 1987)	167	333	170	338	200	392
Ammonia Breakdown (Giggenbach 1980)	147	296	151	303	192	377
H2/Ar (Giggenbach 1981)*	288	550	288	550	288	550
H2/Ar-CO2/Ar-gtd (Powell 2000)*	325	617	325	617	325	617
Average of Select Geothermometers (*independent of gas/water)	283	541				
Average of All Geothermometers	227	440				

geologica

55-29 Flow Test Subsurface Temperature Estimated from Gas Geothermometers

Estimated Total Pressure	P _{tot} =PCO ₂ by D/Am-P=10 bar		PCO ₂ = P _{tot} by mineral equilibria		sat water @ 50 F=72 bar		=BHP-hydrostatic @ 550 F=130 bar	
	°C	°F	°C	°F	°C	°F	°C	°F
Estimated Temperature								
Empirical (D'Amore & Panichi 1980)	225	438	229	445	248	479	265	509
Pyrite-Magnetite (Giggenbach 1980)	223	434	226	439	255	482	269	516
Pyrite-Pyrrhotite (Giggenbach 1980)*	279	535	279	535	279	535	279	535
H ₂ S (Giggenbach 1987)	209	408	213	415	248	479	265	509
Ammonia Breakdown (Giggenbach 1980)	117	242	120	248	155	311	172	341
H ₂ /Ar (Giggenbach 1991)*	291	556	291	556	291	556	291	556
H ₂ /Ar-CO ₂ /Argid (Powell 2000)*	310	590	310	590	310	590	310	590
Average of Select Geothermometers (*Independent of gas/water)	293	560						
Average of All Geothermometers	258	495						

geologica

APPENDIX D: Well 44-16 Notes and Information

This appendix contains supplementary information on well 44-46. Specifically, notes compiled by Al Waibel on September 12, 2013 following three days of testing activity, the summary page of the well report covering October 24-November 6, 2008, and the well survey information. Much of this information was contained in lengthier communications between Al Waibel and APEX HiPoint Sigma³.

Well 46-16 Time Sequence Flowing of Well, 8, 9, 10 September 2013

8 Sept. 2013

1410	Opened valves, pressure gage reading 550 psi, strong flow of non-condensable gas
1500	Pressure gage reading 400 psi.
1515	Pressure gage reading 300 psi.
1605	Well starting to flow liquid, dark brown, low flow rate
1620	Flow rate increased from low to strong fountain flow.
1745	Oscillating liquid and gas flow with gradually more gas.
1812	Oscillating liquid and gas flow, dominated by gas.
1835	Shut well in.

9 Sept. 2013

0845	Pressure gage reading 550 psi.
0940	Cleaning sample port tube in preparation for collecting gas sample.
1010	Open well to moderate flow to purge line and sample bottle.
1017	Completed gas sampling and secured sample bottle, and opening well. Strong flow of non-condensable gas.
1027	Pressure gage reading 500 psi.
1047	Pressure gage reading 480 psi.
1050	Very small puffs of liquid occasionally occurring with the gas flow.
1115	Pressure gage reading 400 PSI.
1122	Transition from gas to gas with occasional light water spray.
1144	Total liquid flow.
1230-1700	Oscillating gas and liquid flow, becoming mostly gas over time with short low-flow burps of very thick drilling fluid.
1700	Shut in well.

10 Sept. 2013

0936	Pressure gage reading 425 psi. Open well to flow.
1005	Pressure gage reading 150 PSI.
1017	Transition from 100% gas to mixed gas and dilute drilling fluid.
1125	Strong liquid flow, increasingly more muddy.
1226	Transition from liquid to gas.
1246-1413	Gas flow with intermittent flows of thick mud.
1413	Shut well in to attach gas sample bottle.
1416	Opened well to flush and fill gas sample bottle.
1420	Shut in well just as muddy water started to mix with gas flow.
1421	Opened well, flowing muddy water.
1428	Transition to gas flow.
1441	Flow rate of gas dropping off to such a slow rate that ear plugs are not needed.
1451-1515	Very low gas flow rate with occasional burps of very thick mud.
1515	Shut well in.

Additional Notes on Sequence of Flow, September 8-10, 2013

The valves on the well were opened at 14:09 in order to release the gas pressure that had built up. This was done as part of the Apex microseismic monitoring program, to see if fluid movement within formation fractures could be detected by the Apex array. The gas flowed out a horizontal 4-inch pipe with a 90 degree elbow at the end, pointing the flow upward. Gas flowed for almost 2 hours, and the pressure gage showed a reading of 300 psi. At approximately 16:05 the flow changed abruptly from gas to water. The water was dark, and appeared to be made up of drilling fluid, containing mud and polymers. This flow continued, jetting 20 to 30 feet above the discharge pipe. The temperature of the discharge started out as slightly warm, increasing over time to quite warm, though not really hot. By 17:20 the flow started to shift from predominantly water to water with short bursts of gas. The periods of gas flow was under one minute at first, and increased over time. The gas was likely non-condensable gas, as it cooled the pipe. By 18:00 the flow consisted of gas with shorter spurts of dark-colored water. The well was shut in at 18:00. The pressure gage after shut-in read 100 psi, the lowest mark on the gage.

The stabilized water level in well 46-16 has been measured during logging at 2,070 ft below the surface, 3,745 ft asl. The first open fractures observed below 7,000 ft. The major observations of open hydrothermal veins were in a zone below 9,000 ft. (see graph in Appendix D, Figure 1 below), associated with significant gas kicks. This would place a static column of water in the well, at open-well conditions, of over 7,000 ft. above the major hydrothermal mineral-bearing fractures. The well is bridged in the 5,000 ft. area. The gas entries in the well would have to flow through the bridge in order to accumulate and build pressure within the well-head. It is very unlikely that any fracture-hosted liquid-phase would be able to make it through the bridge with any significant flow rate. The fluid pressure within fluid-bearing fractures in well 46-16 is reflected by the static

water level within the well, 2,070 ft. below the surface. The flow from the well appears to have been largely gas driven, though the water was coming from deep enough to contain some heat.

At this time we have no insight as to the condition of the bridge. If any of the rock within the bridge were moved around due to this flow, the noise should have been detected by the Apex array. At this time there is no way to estimate how much fracture-hosted fluid entered the well bore during this short 4-hour flow. With the bridge in place, the short-term flow from the formation fractures reaching the upper part of the well would be largely gas-phase. The liquid phase would be more constricted by the bridge and would have a slower flow rate. This lower flow rate would likely be unable to sustain a liquid flow rate to the surface, regardless of fluid temperature within the formation because of higher rates of thermal energy loss relative to the volume of fluid flow. If the well were to be capable of liquid-phase flow often enough, the drilling fluid within the well bore would progressively be replaced by fluid from the fractures.

Initial Rough Calculations:

- Estimate flow for Sunday (8 Sept) and Monday (9 Sept), 3,000 gal. each day
- Estimate flow for Tuesday (10 Sept), 4,000 gal.
- 13 3/8" casing, 0.8818 cu. ft. per linear ft, a bit over 6.6 gal/linear ft.

Ergo – total displacement of well-bore could be about 1,500 ft, or about 1/2 of the liquid volume between the top of the static water (2,070 ft BGL with 600 psi well-head pressure) and the bridge (5,000 ft BGL); total flow volume far less than the liquid volume above the bridge. Regardless of the accuracy of these estimates, it is clear that not enough fluid has been discharged to equal the volume of fluid above the bridge.

Any fluid flowing from the well originating below the bridge would have to pass through the bridge and pass up through a substantial column of thermally equilibrated water/drilling mud (300°F at the bridge depth of 5,000 ft, please see temperature chart in Appendix D, Figure 2). The limited flow volumes for these three days would hardly be enough to heat up the well bore or produce hot discharge.

The liquid during each flow period ranged from dirty water to thick mud. At this time one could only speculate as to the dilute mud fraction. Is it a result of mud flocculation in between flow episodes, or is there a component of hydrothermal water seeping through the bridge?

NOTE: Drilling mud viscosity was raised to 80, then to 120 in an attempt to clear the hole of bridge during rig flow test attempt, on November 2, 2008 (see Excerpt of 46-16 Well Summary Report below). The mud column was flushed and replaced with water from a depth of 4,700 ft. before closing in the well. This procedure actually progressively dilutes the drilling fluid, rather than replacing it. The flow of non-condensable gas and any liquid phase from deep hydrothermal fractures would have to ascend thru the bridge at around 5,000 ft and through drilling mud. If much of the 80 to 120 viscosity mud reached the deeper portions of the hole and entered smaller fractures, it would have been baked by the high formation temperatures. The bentonite would have been altered to illite, and would be difficult to remove from the fractures.

There has been some speculation that water entries into the well at this time could be from fractures in the rock between the casing shoe and the bridge. There is no empirical evidence for any fractures

at this depth from any of the well data. The rock at this depth in well 46-16, as with well 55-29, has been altered to very low-grade greenschist facies, dominated by phyllosilicates (clays, chlorite, etc.). The mechanical aspects of this rock under strain would result in plastic deformation rather than rock failure (breaking, fracturing). As with well 55-29, the grade of thermal metamorphism in the rock would have to reach the albite-epidote greenschist facies to become brittle enough to host fractures.

Well 46-16 Status & History as Regarding Flow Tests of September 2013

Well 46-16, which was drilled approximately 1 mile WNW of CalEnergy Exploration's well 23-22, encountered greenschist facies metamorphosed volcanic rock at a depth of 7,200 ft. The well was drilled in a southerly direction to explore an east-west gravity boundary with the thought that this boundary may represent a tectonic structure. The well was drilled depth of 11,600 ft, and had an estimated bottom-hole temperature of between 600°F and 700°F. Druze epidote and epidote-quartz crystal clusters, formed in open fractures from geothermal fluid, were observed in the cuttings at:

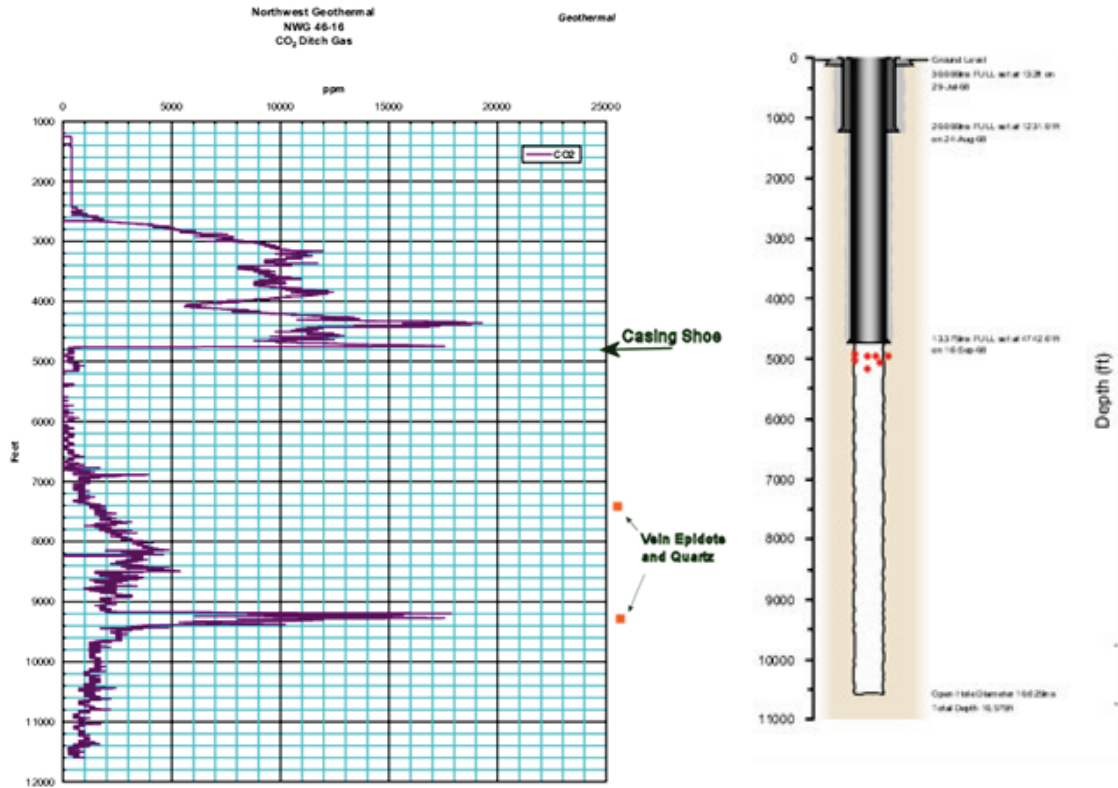
- 7,330 ft
- 7,360-70 ft,
- 9,280 ft,
- 9,350 ft, and
- 9,400 ft.

No precipitated pyrite or other sulphur-bearing minerals were observed associated with these fractures. Significant increases in gasses were observed during drilling, particularly pronounced in the 9,000-9,500 ft. range (Appendix D, Figure 1). Temperature survey logs show significant perturbations indicative of formation fluid flow affecting the temperature profile of the well. The rock had been thermally metamorphosed to the greenschist facies, and is mechanically brittle, capable of hosting fractures when stressed. No major fluid loss was encountered, though many small fracture zones were observed.

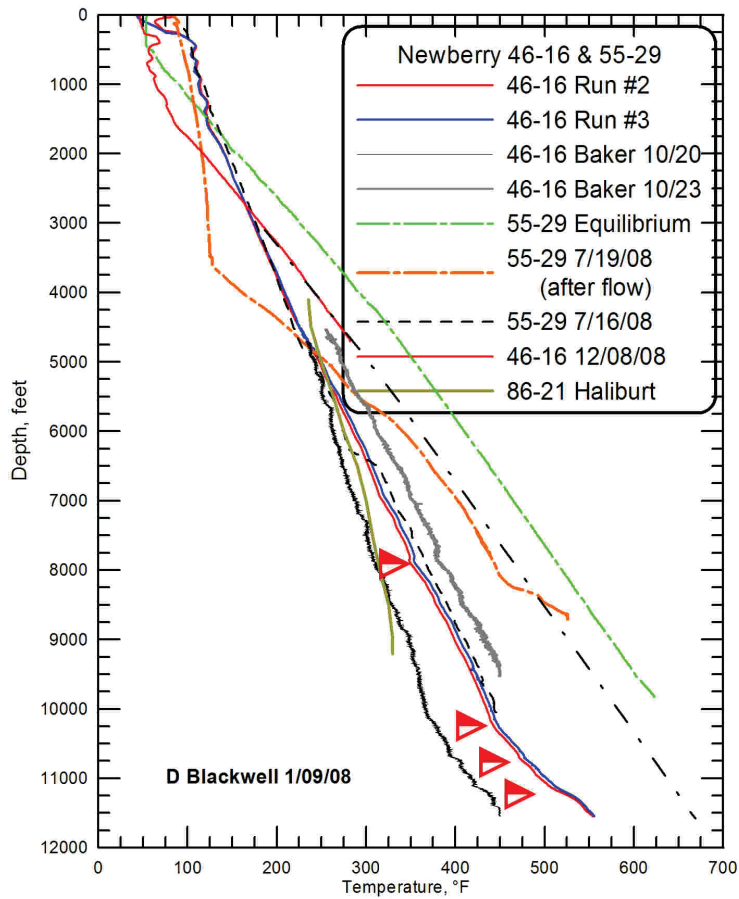
2012 GRC Newberry paper extract

Well 46-16 intersected high temperature, open fractures hosting hydrothermal minerals and a shut-in well-head pressure of approximately 600 psi. Until the bridged section of the well is resolved, no flow test or complete sampling of both liquid and gas phases of the hydrothermal fluid from the fractures is possible. This well was directionally drilled to the south to cross a gravity boundary. The well data provide prima facie evidence that an active hydrothermal system was intersected.

2012 GRC Newberry paper extract



Appendix D, Figure 1: A graph showing CO₂ values measured by Epoch Mudlogging during drilling of well 46-16. The depth of the casing shoe and the location of hydrothermally precipitated druse quartz and epidote observed in the drill cuttings are noted on the right of the graph. On the well profile diagram, red dots indicate the general location of the bridge. Note, the static water level in well 46-16 was measured at 2070 ft. below surface during T/P logging.



Appendix D, Figure 2: The temperature gradient profiles of three of the deep exploration wells, 46-16, 55-29 and 86-21. The equilibrium temperature profile for well 55-29 (bright green) shows a good straight conductive gradient without formation fluid flow. This matches well-site data observed while the hole was being drilled. The profiles for well 46-16 (red and blue lines) show significant perturbations indicative of formation fluid flow affecting the temperature profile of the well. The red arrows are locations where Dr. David D. Blackwell observed evidence in the temperature profiles of formation fluid flow.

Excerpt of 46-16 Well Summary Report

Well Summary Report

page 8 of 8

Well ID: 46-16

NORTHWEST GEOTHERMAL

NWG 46-16 Well Name: Northwest Geothermal 46-16

Field: Newberry Sect: 16 Town: T21S Rng: R12E County: Deschutes State: OR

24-Oct-08 Current Depth (ft): 11,600

Comments: Run formation logs (DIP & Express) - RIH with drill pipe to 1,980 ft - Attempt to displace well with air, no good - Change out valve on flow line - Monitor well

25-Oct-08 Current Depth (ft): 11,600

Comments: Stagged in hole displacing well bore with air to 5,476 ft - Pipe string plugged - Pulled out hole to find plug in pipe.

26-Oct-08 Current Depth (ft): 11,600

Comments: Laid out plugged drill pipe - Make up BHA , stage in hole unloading wellbore to 3,056 ft - POOH change BHA, picked up 10 5/8" bit , stagged in hole unloading wellbore to 4,801 ft - Ream from 4,801 ft to 5,106 ft with air and foam.

27-Oct-08 Current Depth (ft): 11,600

Comments: Reamed from 5,106 ft to 5,298 ft -(pipe stuck @ 5,290 ft) - Work stuck pipe, set up to circulate with fluid and filled the hole with water. Cleaned formation out of test unit and weir box.

28-Oct-08 Current Depth (ft): 11,600

Comments: Attempt to work pipe free while waiting on back off unit and fishing tools - mixed pit of mud - held safety meeting, rig up and run free point tool

29-Oct-08 Current Depth (ft): 11,600

Comments: Ran free point and string shot and backed off stuck pipe at 4665 ft - POH. Break and inspect all box and pins on 8" Drill collars - all look good. Pick up and make up fishing

tools. Rig down and move out air compressors , nipple down gas busters - tear out air lines , nipple down flow line to muffler , rig down tie down lines to muffler while waiting on xo sub.

30-Oct-08 Current Depth (ft): 11,600

Comments: RIH with fishing BHA. Screw into fish at 4850 ft. Jar on fish. (slowly coming free) Fish came free at 4650 ft. POOH with fish. Lay down fishing tools. RIH with clean out assembly checking all connections.

31-Oct-08 Current Depth (ft): 11,600

Comments: Finish running in hole with 10 5/8 inch bit and BHA. ream from 4765 ft. T/5239 ft. Hole packing off. Pulled up to shoe. Bring mud visc. up to 55. RIH and reamed to 4956 ft.

pumping sweeps as necessary. Short trip to shoe.

01-Nov-08 Current Depth (ft): 11,600

Comments: Reamed 12 1/4 inch hole with 10 5/8 inch bit F/4765 ft. T/5428 ft. Pumping sweeps and making short trips to shoe as necessary. Brought mud visc up from 55 to 80. Hole still trying to pack off.

02-Nov-08 Current Depth (ft): 11,600

Comments: Short trip to shoe, build mud volume, Reamed to 5052 ft. Brought mud visc. from 80 to 120. Reamed T/5616 ft. Mud started to flash. Short trip to shoe, circulating to keep well full. (lost 110 bbls of mud splashing over shakers. Reamed to 5676 ft. cooling well with little or no fill.

03-Nov-08 Current Depth (ft): 11,600

Comments: Reamed 12 1/4 inch hole F/5816 ft. T/6863 ft. Pumping high visc sweeps as necessary.

04-Nov-08 Current Depth (ft): 11,600

Comments: Reamed fill F/6275 ft T/6939 ft. RIH to 7223 ft. Reamed T/7318 ft. RIH to 8175 ft. Stopped there to circulate DP full of water. Had tight hole and pumped out first stand, then POH OK. POH laying down DP.

05-Nov-08 Current Depth (ft): 11,600

Comments: POH and laying down drillpipe, change hole over from mud to water at 4700 ft. POH and laying down drillpipe, heavy weight, drill collars, and bit. Close master valve.

06-Nov-08 Current Depth (ft): 11,600

Comments: Dump mud pits, take on water, flush 3rd part mud systems, Nipple down and remove BOPs, blanket wellhead, and dump water and give final rinse on mud pitts. RIG RELEASE AT 24:00 HOURS ON 11/06/2008. (FINAL REPORT)

46-16 Well SURVEY INFORMATION

<i>Data Courtesy of Scientific Drilling</i>							
Measured Depth	Inclination	Azimuth	TVD	Vertical	Coordinates		DLS
(Feet)	(Degrees)	(Degrees)	(Feet)	(Section)	N(+)/S(-)	E(+)/W(-)	(Deg/100 ft.)
-	0.00	0.00	0.0	0.0	0.0	0.0	0.00
112	0.00	0.00	112.0	0.0	0.0	0.0	0.00
234	0.92	91.40	234.0	-0.4	0.0	1.0	0.75
525	1.12	99.22	542.9	-2.1	-0.5	6.1	0.08
725	2.17	110.80	724.9	-2.9	-2.2	11.6	0.55
1,025	1.57	155.22	1024.7	-0.7	-7.9	18.6	0.51
1,180	1.66	171.31	1179.7	2.6	-12.1	19.9	0.30
1,393	1.58	186.08	1392.6	7.9	-18.1	20.0	0.20
1,613	2.19	189.15	1612.5	14.8	-25.2	19.0	0.28
1,768	1.98	173.83	1767.4	20.0	-30.8	18.8	0.38
1,892	2.01	161.17	1891.3	23.4	-35.0	19.8	0.36
1,955	2.00	146.37	1954.2	24.7	-37.0	20.7	0.82
2,019	2.19	165.17	2018.2	26.3	-39.1	21.7	1.11
2,050	2.56	169.99	2049.2	27.3	-40.3	21.9	1.36
2,082	2.79	172.83	2081.1	28.5	-41.8	22.2	0.83
2,173	3.03	172.02	2172.0	32.4	-46.4	22.8	0.27
2,269	3.28	176.40	2267.9	37.0	-51.6	23.3	0.36
2,332	3.50	182.08	2330.8	40.3	-55.4	23.3	0.64
2,426	3.88	180.04	2424.6	45.8	-61.4	23.2	0.43
2,521	4.26	191.24	2519.3	52.2	-68.1	22.5	0.93
2,614	5.09	189.03	2612.0	59.5	-75.5	21.2	0.91
2,710	5.68	189.36	2707.6	68.2	-84.4	19.8	0.62
2,805	5.92	193.32	2802.1	77.5	-93.8	17.9	0.49
2,899	6.89	195.90	2895.5	87.8	-104.0	15.2	1.08
2,993	7.38	205.64	2988.8	99.4	-114.8	11.1	0.72
3,088	8.02	206.68	3082.9	112.1	-126.3	5.4	0.84
3,151	7.87	208.97	3145.3	120.8	-134.0	1.4	0.74
3,246	8.36	208.78	3239.4	134.2	-145.7	-5.1	0.82
3,340	8.68	206.70	3332.3	148.1	-158.0	-11.6	0.73
3,433	9.07	204.88	3424.2	162.5	-171.0	-17.8	0.64
3,528	9.32	209.74	3518.0	177.6	-184.4	-24.8	1.72
3,624	9.55	207.44	3612.7	193.3	-198.2	-32.3	1.58
3,720	10.52	209.22	3707.2	210.0	-213.0	-40.2	0.68
3,784	10.55	209.63	3770.2	221.7	-223.2	-46.0	1.30
3,815	10.29	209.08	3800.7	227.3	-228.0	-48.7	0.70
4,068	9.60	204.72	4049.9	270.9	-267.0	-68.5	1.48
4,195	9.39	206.64	4175.1	291.9	-285.8	-77.6	0.88
4,315	8.76	208.82	4293.6	310.8	-302.6	-86.4	0.07
4,410	8.87	208.06	4387.5	325.3	-315.4	-93.4	0.00
4,502	8.53	206.84	4478.4	339.2	-327.7	-99.8	0.88
4,596	8.67	206.63	4571.4	353.2	-340.3	-106.1	1.91
4,680	8.25	206.05	4654.5	365.6	-351.4	-111.6	0.31
4,837	7.45	202.08	4810.0	387.0	-370.9	-120.3	0.62
4,931	8.68	202.98	4903.1	400.2	-383.1	-125.4	1.32
5,025	8.82	202.77	4996.0	414.5	-396.3	-131.0	0.15
5,117	9.16	204.47	5086.8	428.9	-409.4	-136.7	0.47
5,212	9.51	206.40	5180.6	444.3	-423.4	-143.4	0.49
5,308	9.74	206.74	5275.2	460.3	-437.7	-150.5	0.25

(Continued on next page)

Appendix D Table 1 Data courtesy of Scientific Drilling. It is continued on the next page.

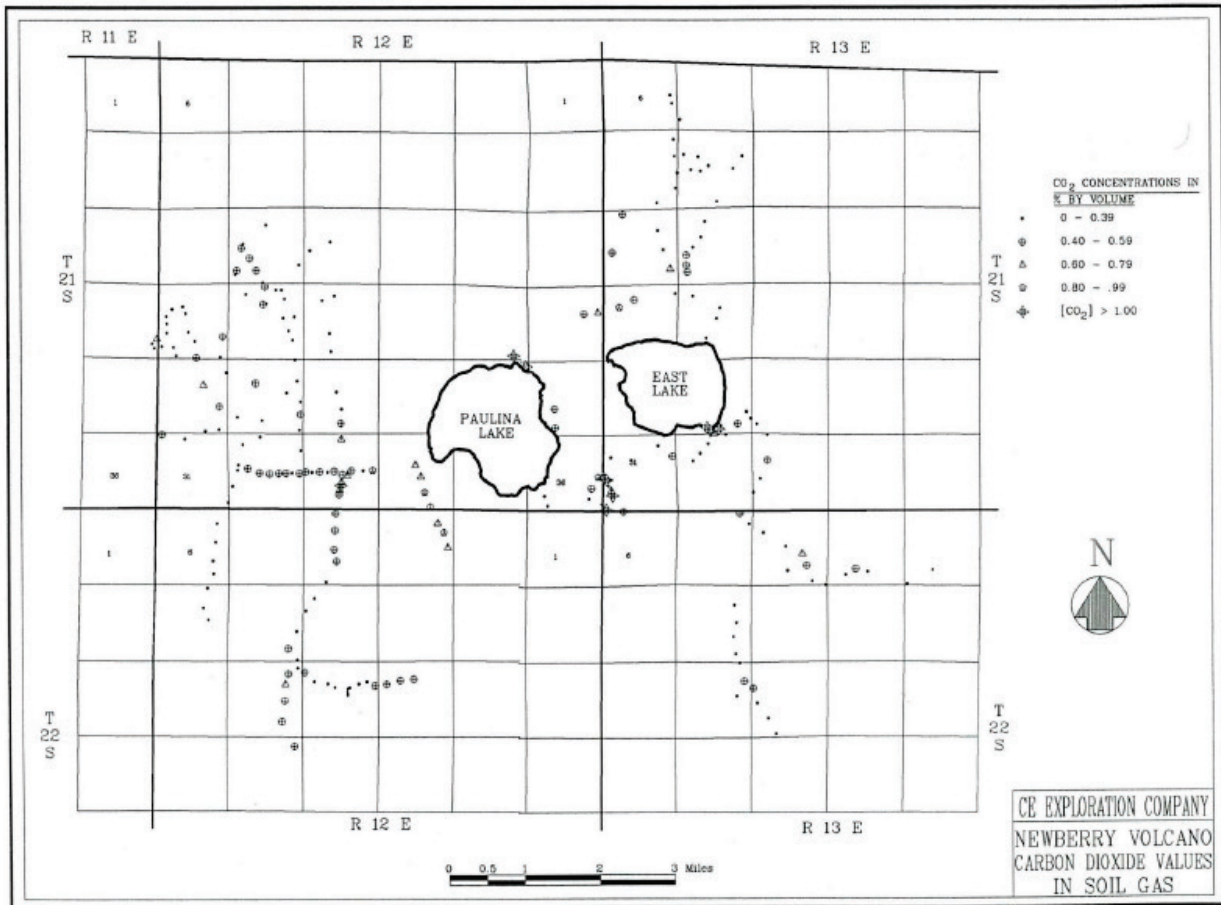
(Continued from previous page)							
Measured Depth (Feet)	Inclination (Degrees)	Azimuth (Degrees)	TVD (Feet)	Vertical (Section)	Coordinates		DLS (Deg/100 ft.)
					N(+)	S(-) E(+)/W(-)	
5,402	9.72	206.88	5367.9	476.2	-451.9	-157.7	0.03
5,495	9.85	206.27	5459.5	492.0	-466.0	-164.8	0.18
5,590	9.90	206.16	5553.1	508.3	-480.6	-172.0	0.06
5,684	9.46	206.74	5645.8	524.1	-494.8	-179.0	0.48
5,777	9.55	206.70	5737.5	539.4	-508.5	-185.9	0.10
5,872	9.45	205.52	5831.2	555.1	-522.6	-192.8	0.23
5,966	9.42	205.22	5923.9	570.5	-536.5	-199.4	0.06
6,057	9.78	206.28	6013.6	585.7	-550.2	-206.0	0.44
6,184	9.69	207.70	6138.8	607.2	-569.3	-215.8	0.20
6,246	9.88	208.73	6199.9	617.7	-578.6	-220.7	0.42
6,341	10.07	209.35	6293.5	634.1	-593.0	-228.7	0.23
6,436	10.20	208.74	6387.0	650.8	-607.6	-236.8	0.18
6,531	10.47	211.38	6480.5	667.7	-622.3	-245.4	0.57
6,626	10.48	212.60	6573.9	684.9	-637.0	-254.5	0.23
6,720	10.58	209.76	6666.3	702.0	-651.7	-263.4	0.56
6,815	10.49	208.88	6759.7	719.3	-666.8	-271.9	0.19
6,916	9.01	203.64	6859.2	736.4	-682.1	-279.5	1.71
7,012	9.68	206.50	6954.0	751.9	-696.2	-286.1	0.85
7,105	9.14	206.55	7045.7	767.1	-709.8	-292.9	0.58
7,201	9.29	209.77	7140.5	782.5	-723.4	-300.2	0.56
7,295	10.30	210.22	7233.1	798.4	-737.2	-308.2	1.08
7,387	10.39	213.20	7323.6	814.8	-751.3	-316.9	0.59
7,482	10.52	216.20	7417.0	831.8	-765.5	-326.7	0.59
7,577	10.51	211.72	7510.4	848.9	-779.8	-336.4	0.86
7,673	10.38	209.76	7604.8	866.2	-794.8	-345.3	0.39
7,768	10.19	209.00	7698.3	883.1	-809.6	-353.6	0.25
7,861	10.18	210.10	7789.8	899.5	-823.9	-361.7	0.21
8,051	10.02	211.40	7976.9	932.7	-852.5	-378.7	0.15
8,242	9.90	210.91	8165.0	965.5	-880.8	-395.8	0.08
8,434	10.20	212.08	8354.1	998.8	-909.3	-413.3	0.19
8,530	10.91	214.30	8448.5	1016.2	-924.0	-423.0	0.85
8,624	10.80	214.44	8540.8	1033.7	-938.6	-433.0	0.12
8,719	10.76	214.20	8634.1	1051.2	-953.3	-443.0	0.06
9,084	11.28	212.72	8992.5	1119.2	-1010.1	-482.2	0.00
9,206	11.22	214.73	9112.2	1142.8	-1029.9	-495.4	0.33
9,375	11.30	214.50	9277.9	1175.3	-1057.1	-514.1	0.05
9,471	11.15	212.67	9372.1	1193.8	-1072.6	-524.5	0.40
9,593	11.17	212.84	9491.8	1217.2	-1092.5	-537.2	0.03
9,750	11.15	215.30	9645.8	1247.2	-1117.6	-554.2	0.30
9,845	11.14	212.13	9739.0	1265.3	-1132.9	-564.4	0.64
9,939	11.45	212.48	9831.2	1283.6	-1148.5	-574.3	0.34
10,032	11.43	213.78	9922.3	1301.8	-1163.9	-584.4	0.28
10,124	11.32	212.82	10012.5	1319.8	-1179.1	-594.3	0.24
10,328	11.37	212.09	10212.6	1359.6	-1213.0	-615.9	0.07
10,575	11.45	212.00	10454.7	1408.1	-1254.4	-641.8	0.03
10,702	11.05	210.05	10579.2	1432.7	-1275.6	-654.6	0.43
10,798	11.51	209.95	10673.4	1451.4	-1291.9	-663.9	0.48
10,893	11.52	210.27	10766.5	1470.3	-1308.3	-673.5	0.07
10,988	11.18	210.12	10859.6	1488.9	-1324.4	-682.9	0.36
11,083	10.98	209.59	10952.8	1507.1	-1340.3	-691.9	0.24
11,274	10.54	207.47	11140.5	1542.7	-1371.6	-709.0	0.31
11,369	9.97	206.01	11234.0	1559.6	-1386.7	-716.6	0.66
11,534	9.90	210.77	11396.5	1588.0	-1411.7	-730.1	0.50
*11599.0 *Survey Projected	9.90	210.77	11460.5	1599.1	-1421.3	-735.8	0.00

Appendix D Table 2: Continuation of previous table.

APPENDIX E: USGS Well Gas Chemistry Data, September 25, 2013

USGS Gas Chemistry Data , September 25, 2013			
2013.09.25	Newberry 46-16	Newberry 46-16	Newberry 46-16
	9/6/2013	9/9/2013	9/10/2013
vol-%			
He	0.0014	0.0002	0.0002
H2	<0.0002	0.0327	0.0418
Ar	0.0012	0.0013	0.0008
O2	0.0006	0.0335	0.0023
N2	4.4861	0.7393	0.6969
CH4	2.0361	0.2695	0.3251
CO2	92.2157	98.5465	98.5737
C2H6	0.0003	0.0003	<0.0002
H2S	<0.0005	0.0077	<0.0005
CO	<0.001	<0.001	<0.001
C3H8	<0.0005	<0.0005	<0.0005
C4H10	<0.0005	<0.0005	<0.0005
Sum	98.7414	99.6311	99.6408
N2/Ar	3842.8	589.6	889.1
air-cor.	3930.8	-2558.1	1008.2
N2/O2	7486.37	22.06	307.52
t(D'A,P)	na	113	na
CO2 term	na	1	na
d13C-CO2	-4.58	-5.84	-5.98
d13C-CH4			

APPENDIX F: Map of CO₂ in Soil Gas for Newberry Volcano



APPENDIX G: APEX HIPOINT SIGMA³ REPORTS TO DAVENPORT/NEWBERRY

This appendix contains eight presentations and/or communications from APEX/HiPoint/Sigma³. They are presented from oldest to newest, with the exception of the first item, a release from Sigma³.

Appendix G Table of Contents (page numbers refer to this Appendix G)

Letter authorizing release of information, 11/18/2014, 1 pp.....	Appendix G, page 2
Proposal of Work and Strategy, 5/13/2011, 13 pp.....	Appendix G, page 3
Interim Report Data Processing Results, 3/27/2012, 50 pp.....	Appendix G, page 16
Final Report Passive Seismic Monitoring Project, 12/13/2012, 46 pp...	Appendix G, page 66
Interim Report 2013 Low-amplitude Passive Seismic Monitoring Project, 1/2/2014, 25 pp	Appendix G, page 112
Quick View of Current Status, 3/13/2014, 3 pp.....	Appendix G, page 137
Draft Version (Rev. 4) Final Project Report, 4/27/2014, 47 pp	Appendix G, page 140
Final Version (Rev. 6) of Final Project Report, 9/10/2014, 63 pp.....	Appendix G, page 187

This release letter below was provided by John Ughetta, through Brian Fuller, to Al Wiabel and Trenton Cladouhos, as indicated by the email record at right.

Forwarded Message:

> To: Trenton Cladouhos <tcladouhos@altarockenergy.com>, Al
Waibel<awaibel@hevanet.com>
> From: Brian Fuller <b.fuller@sigmacubed.com>
> Subject: FW: AltaRock Data Release Nov 2014.docx
> Date: Tue, 25 Nov 2014 06:17:29 +0000
> -----
> Al,
> Here is the data release form.
> Brian
>
> From: John Ughetta
<j.ughetta@sigmacubed.com<mailto:j.ughetta@sigmacubed.co> m>>
> Date: Tue, 18 Nov 2014 08:00:48 -0700
> To: Brian Fuller
<b.fuller@sigmacubed.com<mailto:b.fuller@sigmacubed.com>>
> Subject: AltaRock Data Release Nov 2014.docx
>

November 18, 2014

Trenton Cladouhos, PhD, LG
Senior Vice President R&D
AltaRock Energy, Inc.
4010 Stone Way North, Suite 400
Seattle, WA 98103

Dear Trenton,

This letter serves as a release of any confidentiality data, information, intellectual property, or trade secrets provided in the Sigma Cubed final report for the Davenport Energy 109 Grant by the US Department of Energy (“DOE”) determining if Sigma Cubed Inc. proprietary Low-Amplitude-Emission Analysis (“LASEA”) technique has utilitarian value for geothermal exploration to Davenport Newberry Holdings, AltaRock Energy, and the Department of Energy.

Sincerely,

John A. Ughetta
EVP Sales and Business Development
Sigma Cubed Inc.
4700 West Sam Houston Parkway S.
Suite 150
Houston, TX 77041

APEX HiPoint

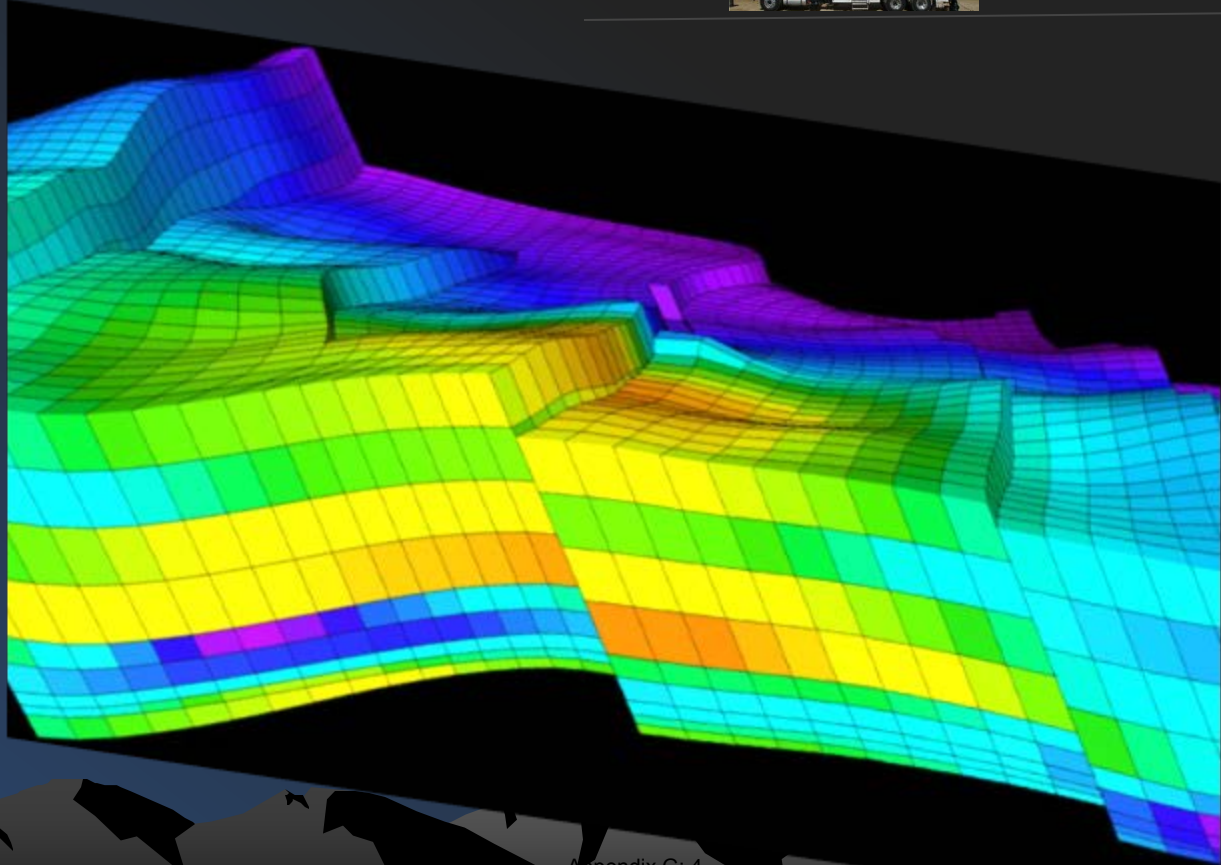
Fracture Mapping and 3D VSP

Passive Seismic Data Acquisition and Analysis Plans for Newberry Geothermal Project



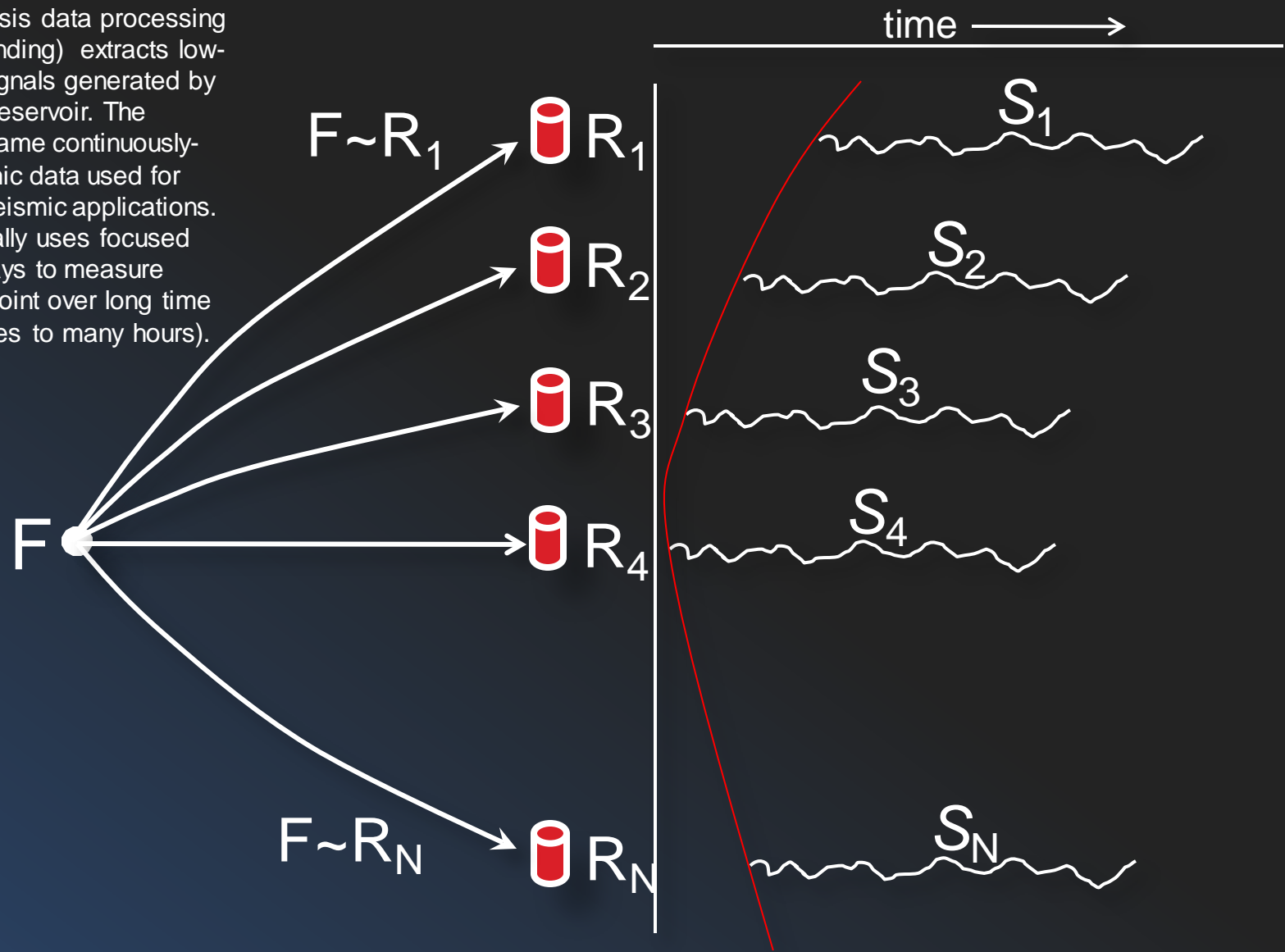
Reservoir Production Monitoring with Fluid Flow Analysis

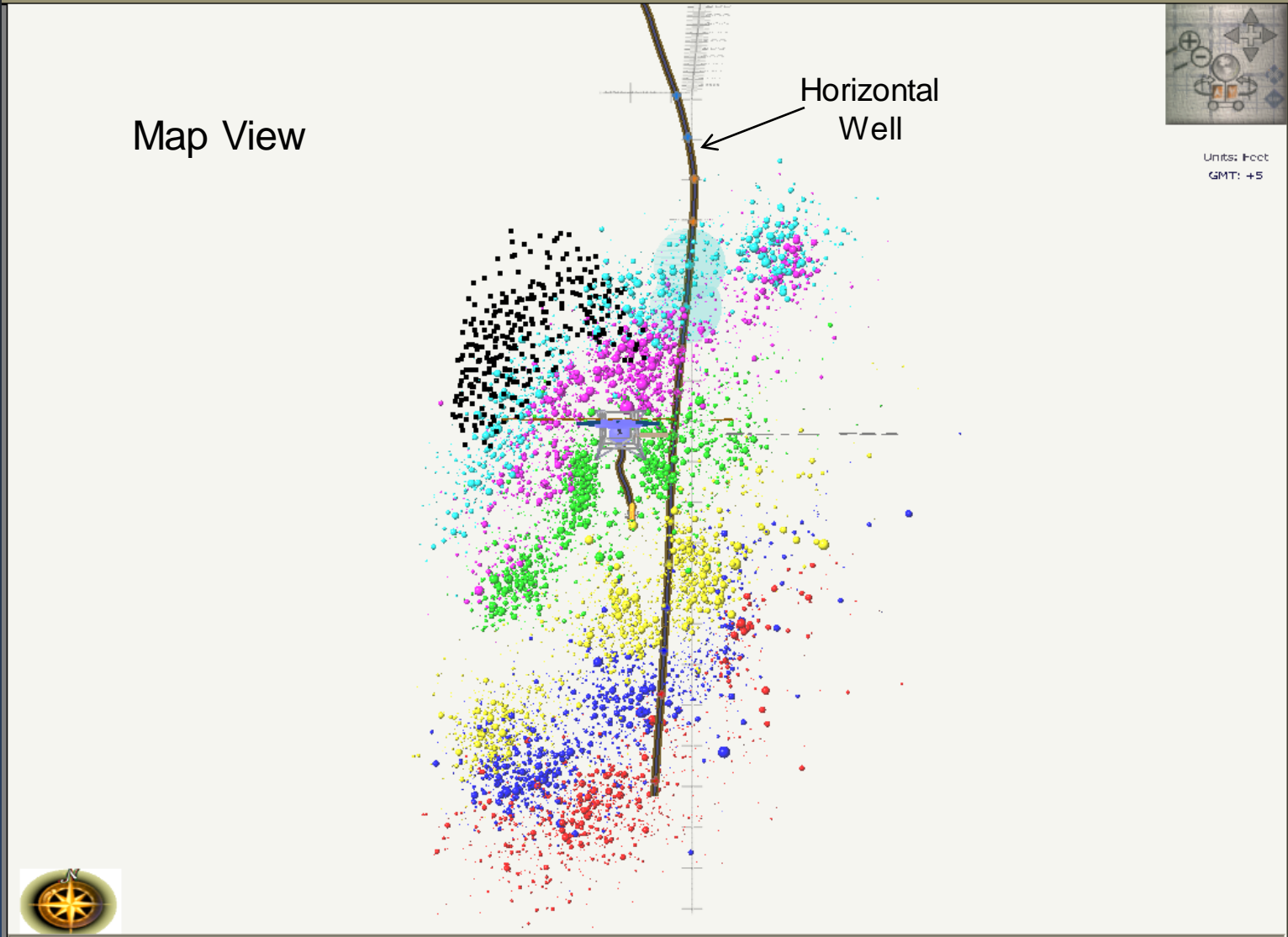
Fluid Flow Analysis can be used to monitor production from producing fields to determine where fluids are being produced. Combined with reservoir simulators, this information could provide the most accurate means currently available to estimate reservoir capacity and accessible reserves in place.

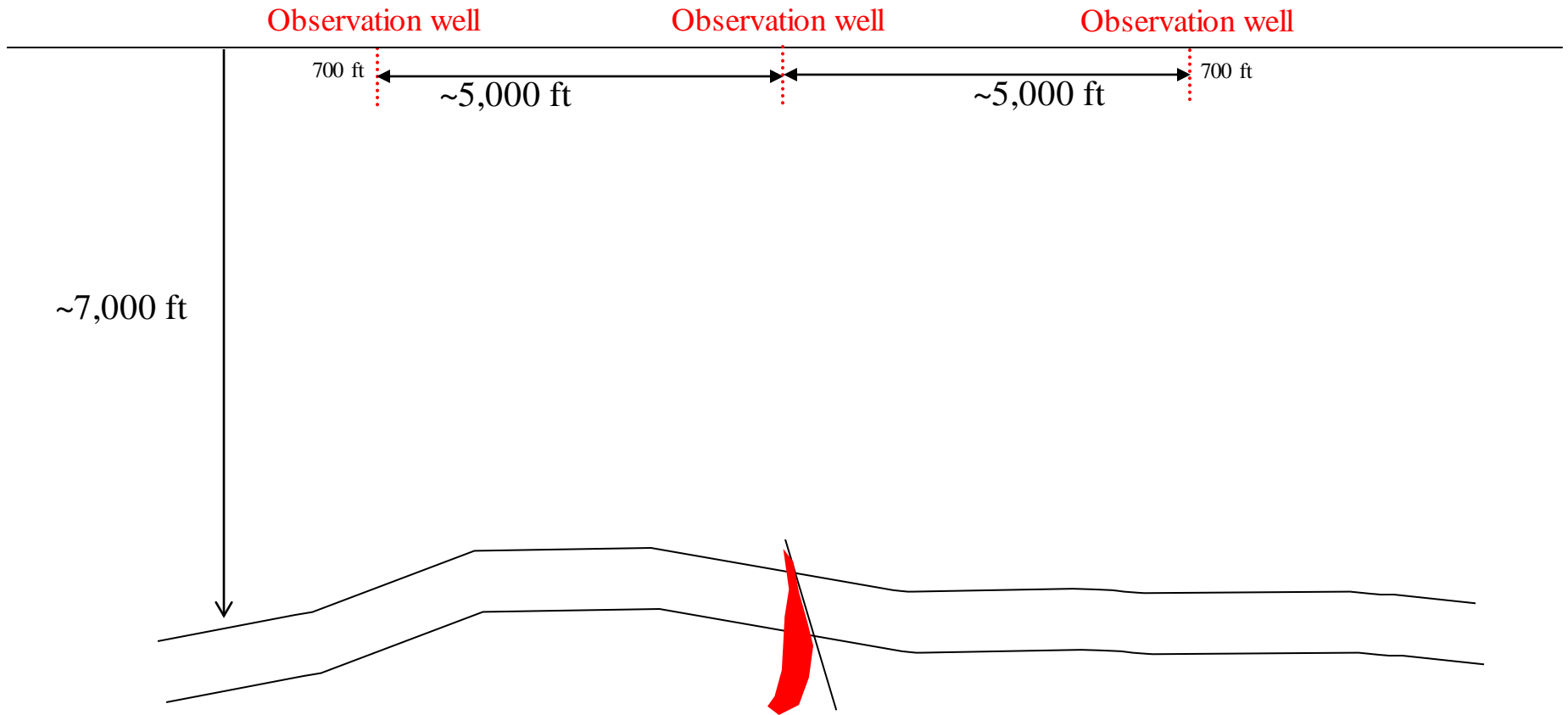


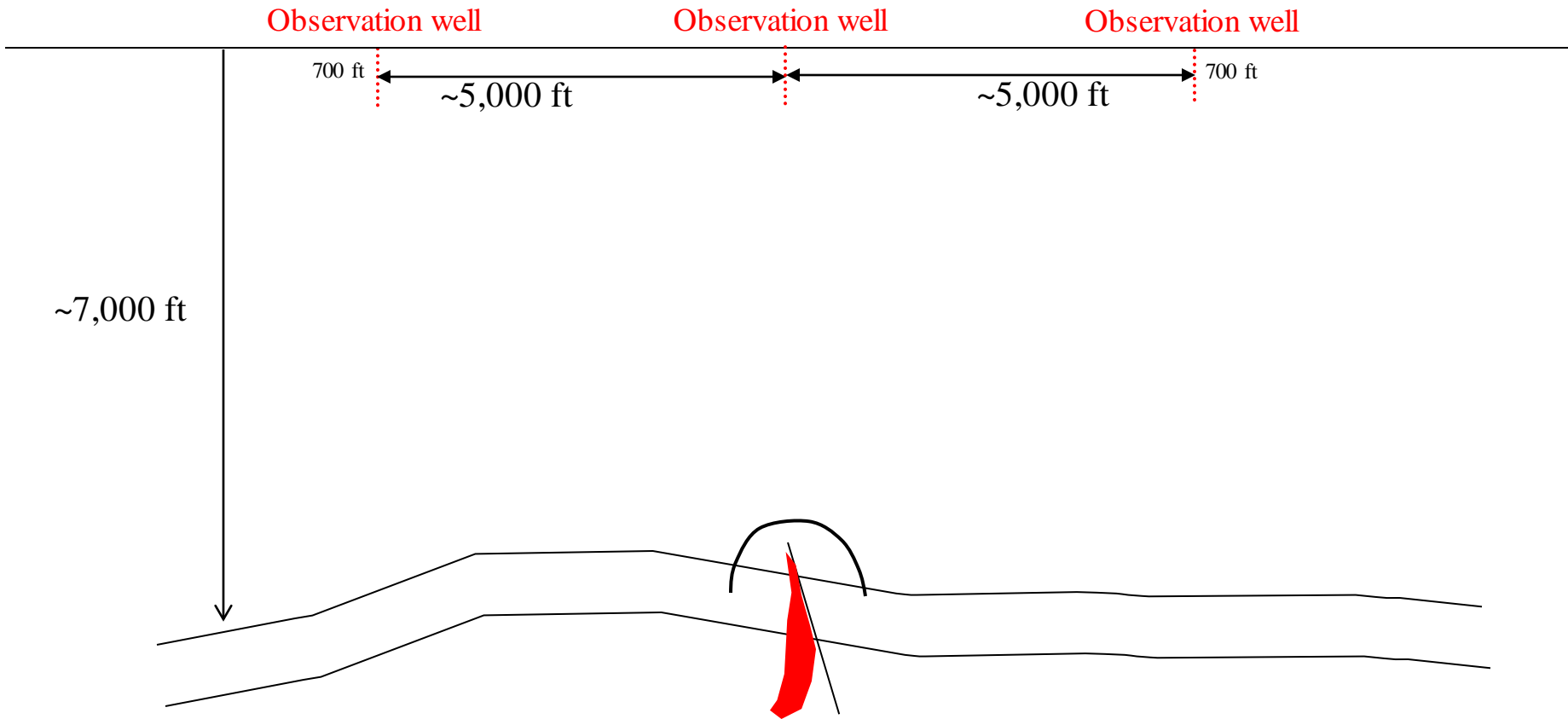


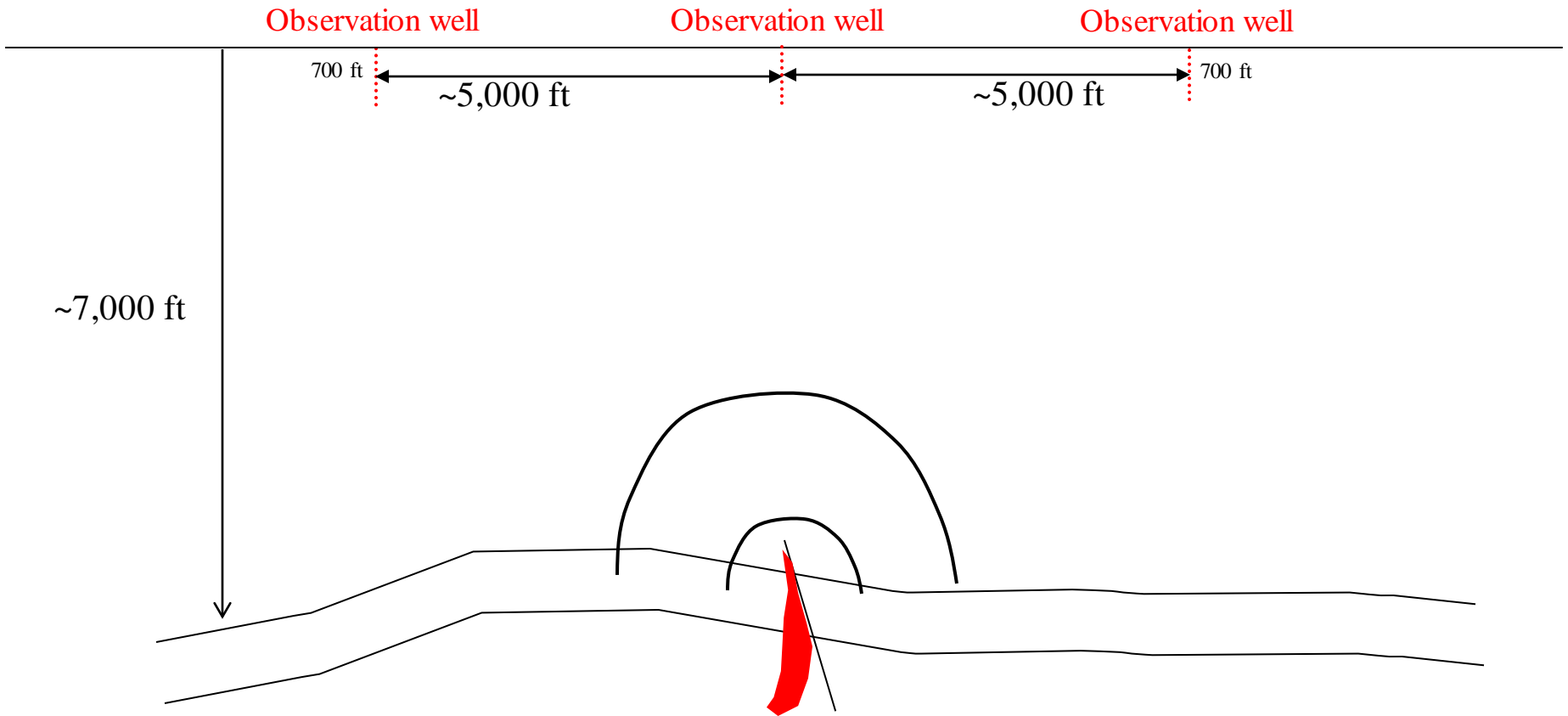
Our Fluid Flow Analysis data processing algorithm (patent pending) extracts low-amplitude seismic signals generated by fluids flowing in the reservoir. The algorithm uses the same continuously-recorded microseismic data used for conventional microseismic applications. The method essentially uses focused seismic receiver arrays to measure energy flow from a point over long time periods (many minutes to many hours).

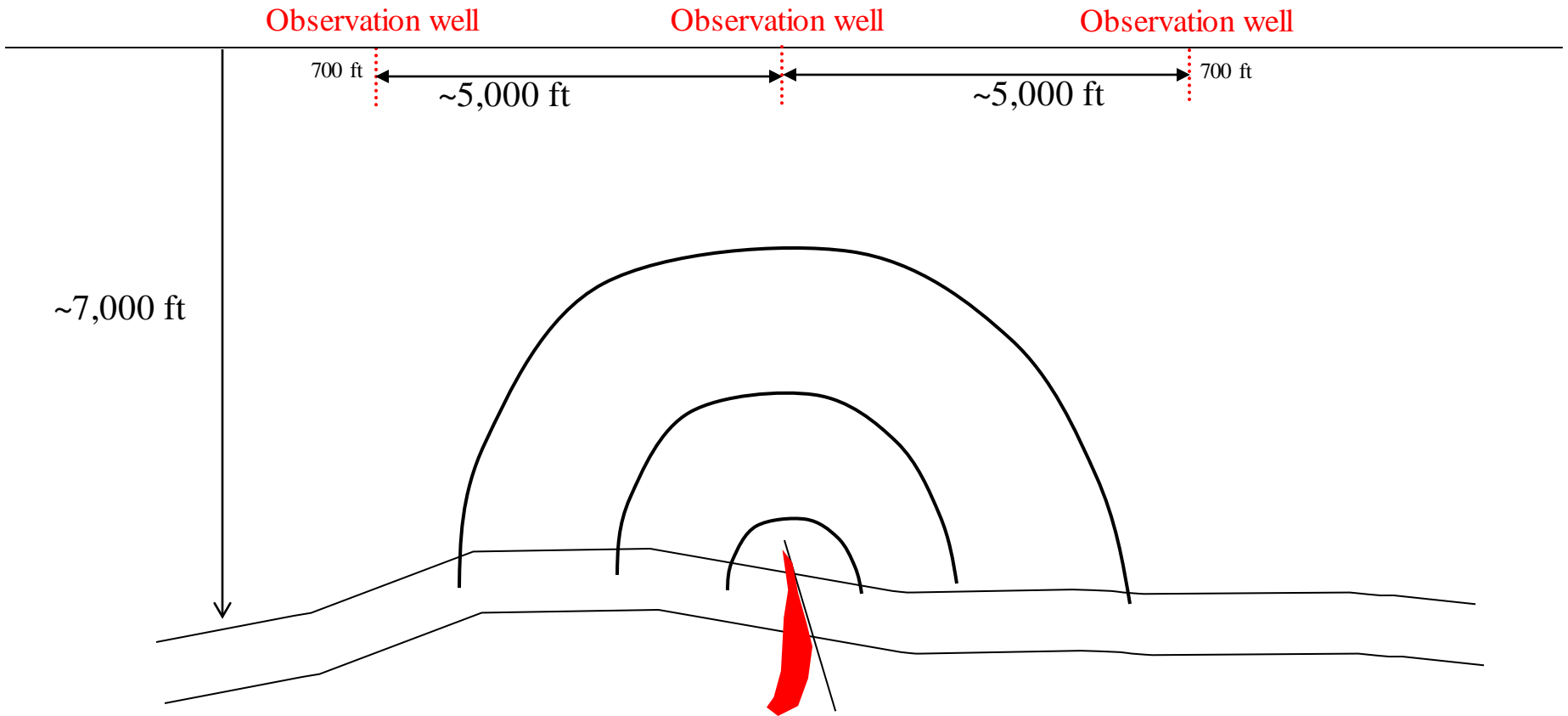


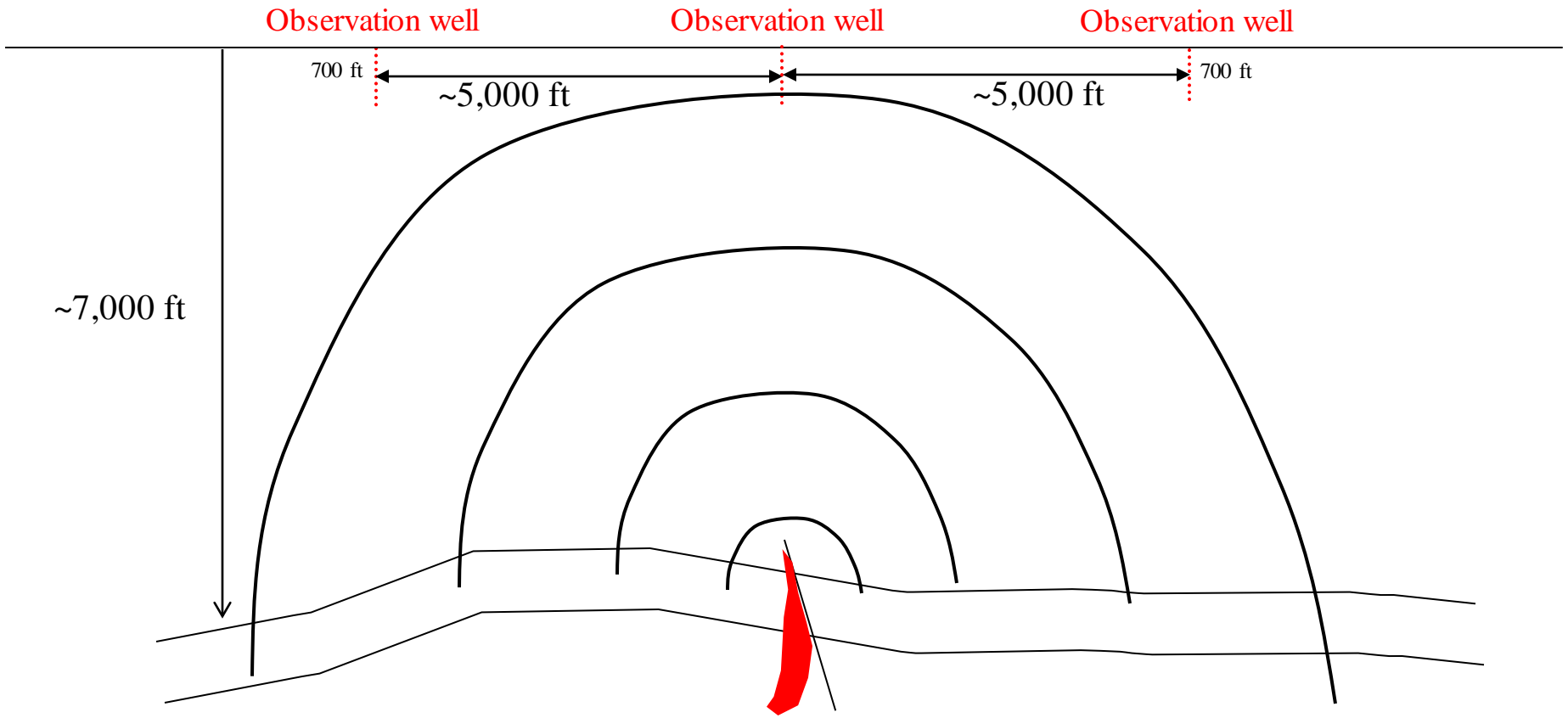


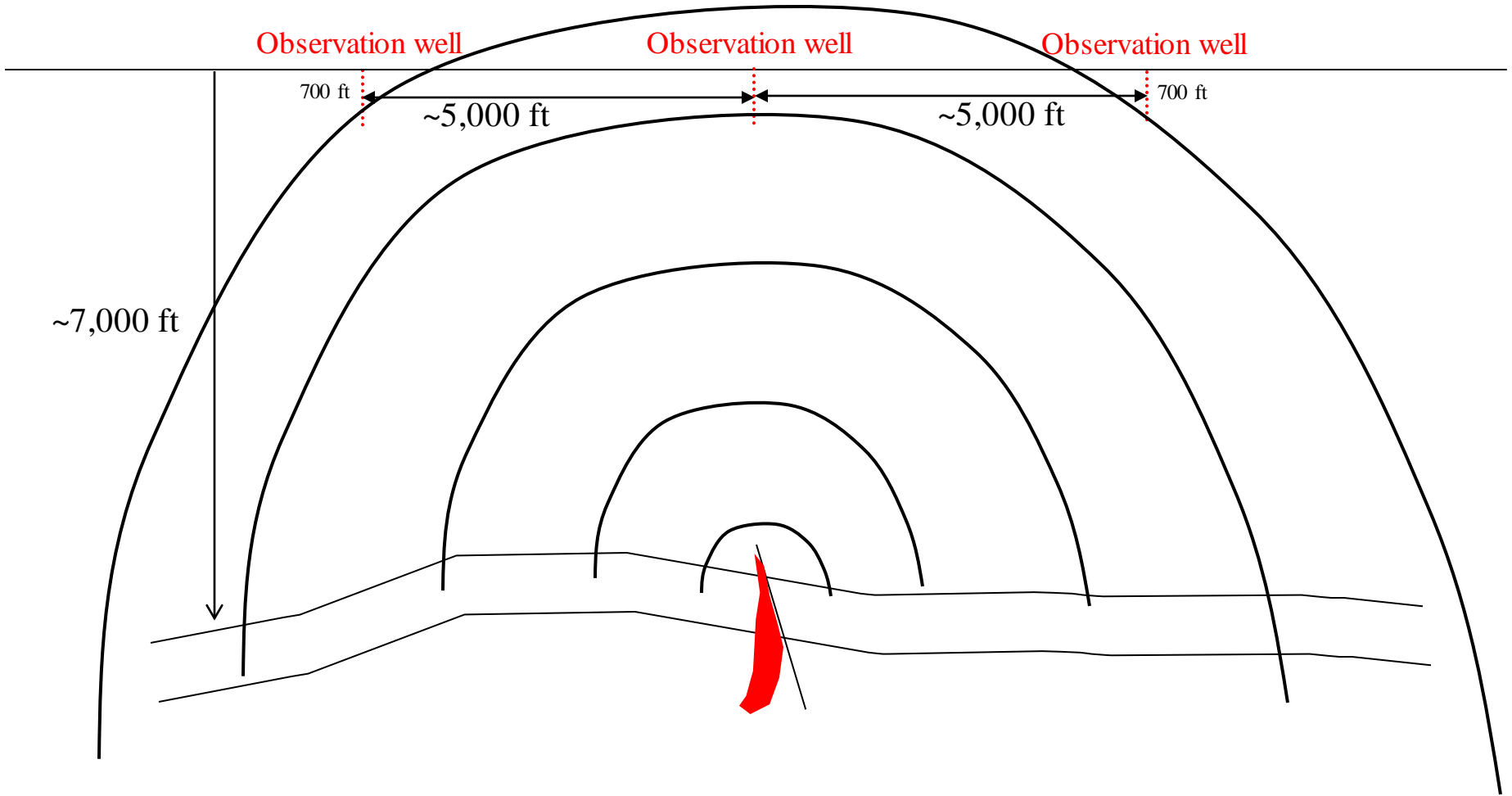












Acquisition - Seismic

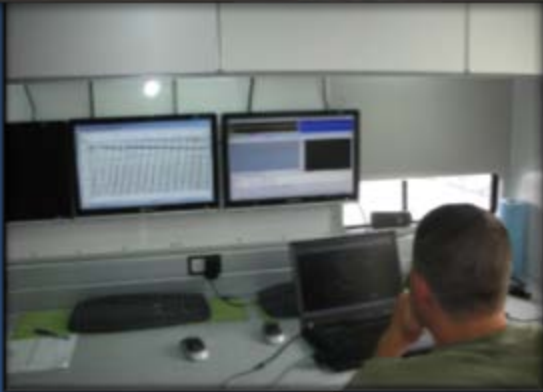


Geospace BSR Array

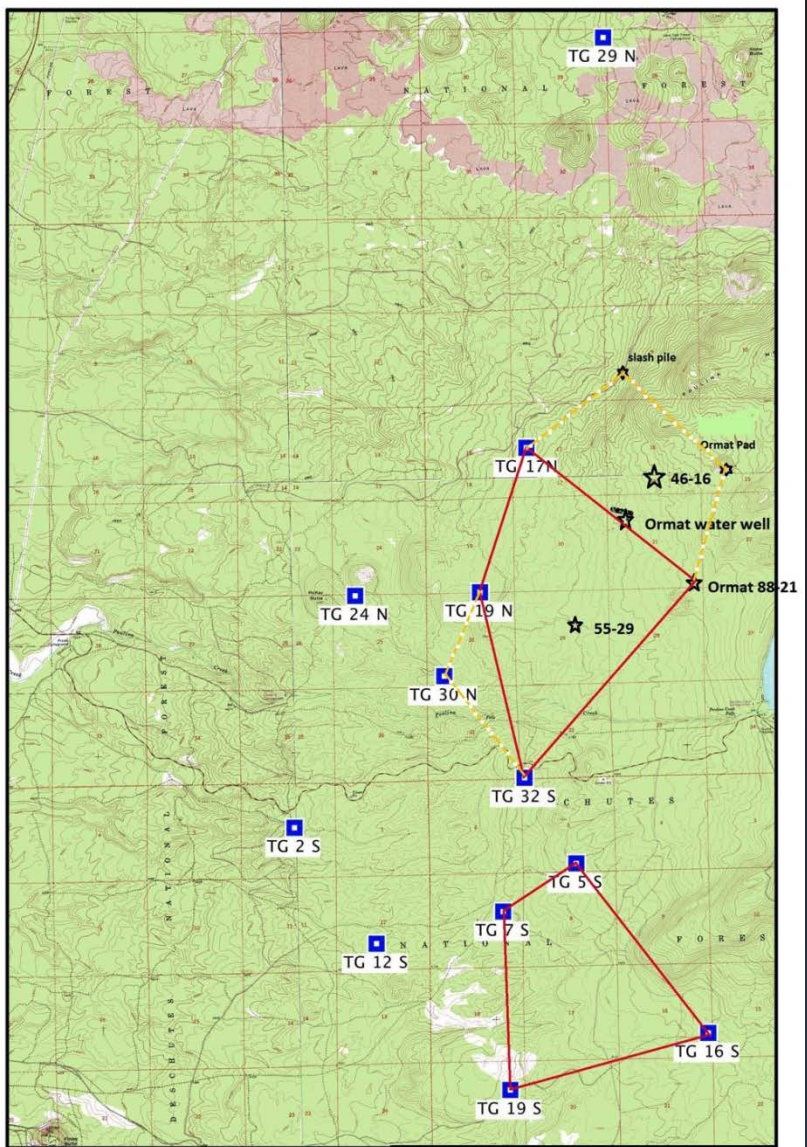
- 3 Component Geophone Sondes
- Lightweight
- Large Receiver Array
- Real-Time, High Bandwidth Data Transmission
- 10 sondes per well, 50 ft apart in each borehole



The same data acquisition equipment and continuously-recorded data that is used for normal microseismic data acquisition is used for Fluid Flow Analysis. Older datasets can be re-analyzed via Fluid Flow Analysis to obtain new reservoir insights.



Newberry Geothermal Project area – available wells for seismic data acquisition.



Newberry Geothermal Project
Figure 2: Drill Site Location Map
Prepared by PLS Environmental, LLC
Version 2 7-29-09





Data processing result:
Davenport Newberry volcano project

March 27, 2012

Project History

Passive seismic data was continuously recorded by APEX HiPoint, LLC in each of 4 instrumented observation wells for 6 days and 17 hours between December 23, 2011 and December 30, 2011. Maps of the well locations are shown on the following two slides. Each observation well contained 11, 12, or 13 3-component digital geophone sondes spaced at 50 ft. The geophones sondes were manufactured by GeoSpace of Houston, TX and are high-grade digital instruments used by APEX HiPoint, LLC for passive microseismic work in the oil and gas industry. The purpose of recording the data was to determine 1) if areas of anomalously high levels of seismic energy could be detected and located and 2) if such areas could be detected, what would the characteristics of the anomaly be such as spatial extent, time variance of amplitude, and seismic frequency dependence.

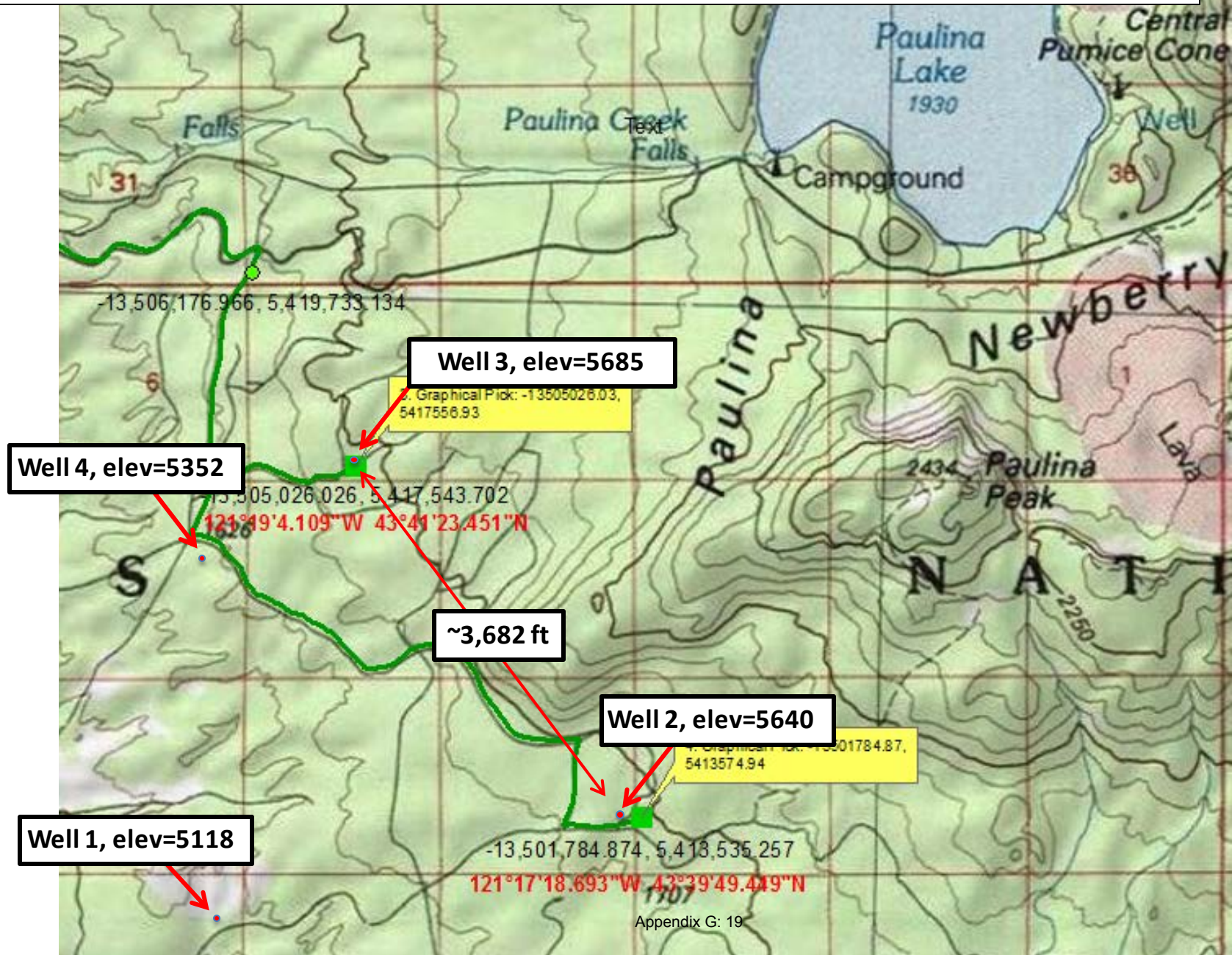
APEX HiPoint's data processing technology including "Low Amplitude Seismic Emission Analysis" previously known as "Fluid Flow Analysis" is being employed to achieve the goals of the survey. A basic assumption is that areas of anomalously high persistent seismic wave emission are probably associated with subsurface fluid movement or high variations in heat flow that cause stress changes in the rock mass and thus seismic emissions. The expected depth range of activity is between 6,000 and 12,000 ft.

We begin the presentation with some observations about the data that were made prior to the main LASEA (Low Amplitude Seismic Emission Analysis) work.

Satellite view with instrument well locations (Well 1,2,3&4).



Topographic map at approximate alignment with satellite view and well locations.



Presurvey Geophysical Expectations Versus What We Observe

Prior to the survey our understanding was that previous ground-base (earthquake type) seismic observations made it seem unlikely that obvious seismic activity would be observed. Our analysis of the data thus far however shows at least three distinct types of activity that register on our seismometers, two of which are significant.

- 1) The first type of activity shows significantly elevated amplitudes from approximately 9:00 AM to 4:00 PM on the four working days (non-holiday, non-weekend) during the survey. This type of activity is almost assuredly due to some man-made source such as a gravel pit, mining, or heavy equipment operations somewhere in the area. If no sources of heavy equipment can be identified then these time periods may merit further consideration.
- 2) The second type of activity also shows elevated seismic amplitudes but they occur at random times and for time periods of a few minutes. Given that many of these time periods are in the middle of the night or otherwise outside working hours, are of short time periods, and affect all of the observation wells it is likely that the seismic source is naturally occurring.
- 3) The third type of seismic activity worth noting is that of actual low-amplitude upgoing seismic events that can be observed on one or more observation wells. These events clearly originate at depth but their precise depth and X,Y coordinates of origin have not yet been identified.

Basic Information About the Seismic Data

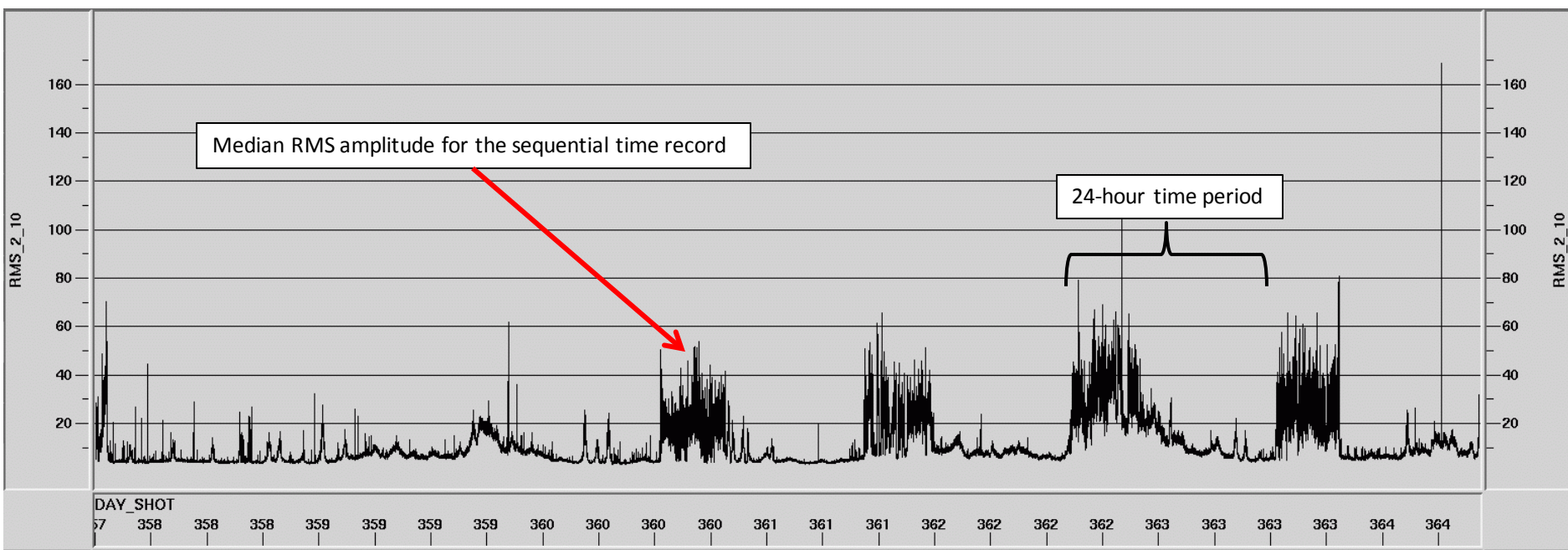
The survey data was continuously recorded but broken up into records of 10-seconds in length for convenience in handling the data. The last sample of one record is followed by the first sample of the next record and the sequential samples are recorded precisely 0.5 milliseconds apart. Each 10-second record contains a 10-second long data trace for EACH of the 141 geophones (47 3-component geophone sondes) that was deployed. The start time of each data trace is precisely synchronized to the same time. The record times are synchronized with a GPS satellite and is accurate to within a fraction of a microsecond.

Basic Seismic Measurements in the Following Slides

Early analysis of this dataset showed that there were large amplitude variations throughout the time length of the survey. In order to understand these variations we computed a basic and very robust measurement of amplitude and plotted these amplitudes for the entire survey as a function of time at 10 second intervals. We first computed the Root Mean Squared (RMS*) amplitude of every individual data trace and then computed the median of the RMS trace amplitudes for each 10-second record. The median computation avoids having a small number of noise bursts dominate the amplitude measurement. We then plotted the Median RMS value at a 10-second interval for the entire 6+ days of the survey to find intervals of anomalous amplitudes so that we could understand these intervals better. The following slide shows the Median RMS amplitude for the entire survey computed after application of a bandpass filter that preserved frequencies in the bandwidth 2-10 Hz.

*RMS=square root of the mean of squared data trace amplitudes

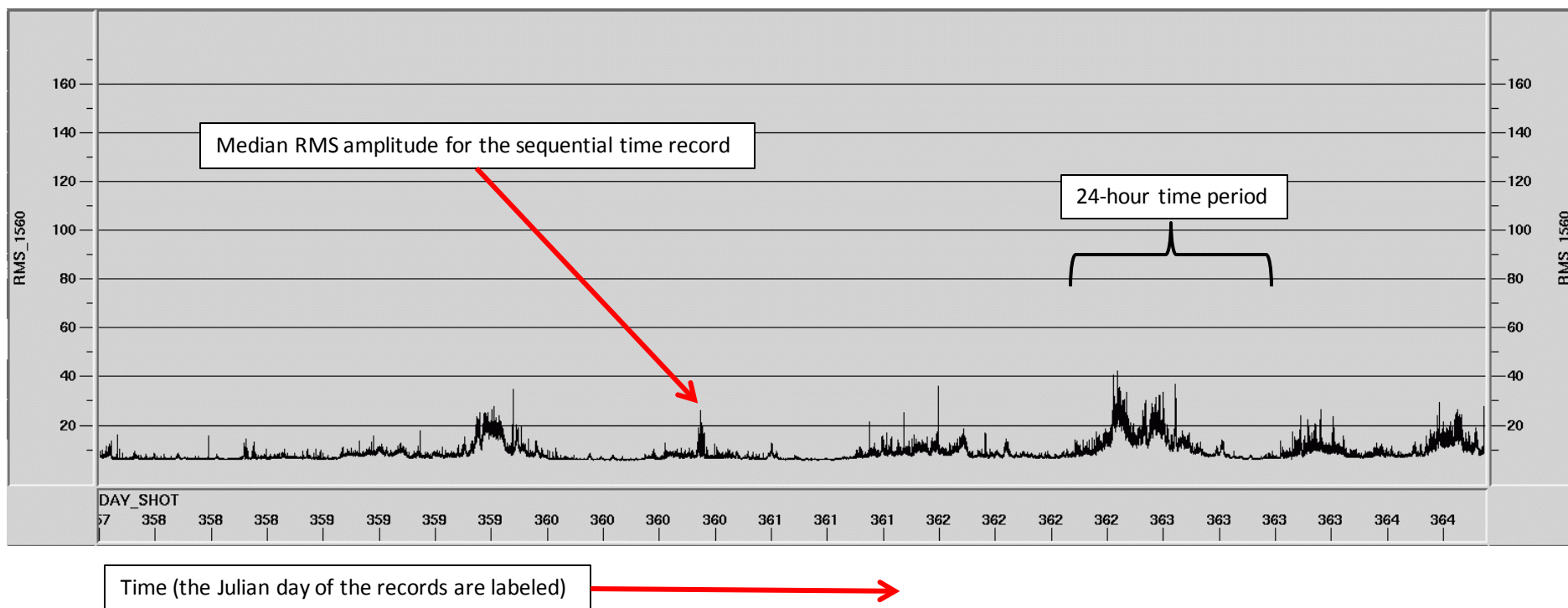
Root Mean Squared (RMS) amplitude 2-10 Hz for entire duration of survey



Time (the Julian day of the records are labeled) →

We see immediately that there is a high degree of Median RMS amplitude throughout the survey and that they are not entirely randomly distributed but are in some cases clustered around a time frame.

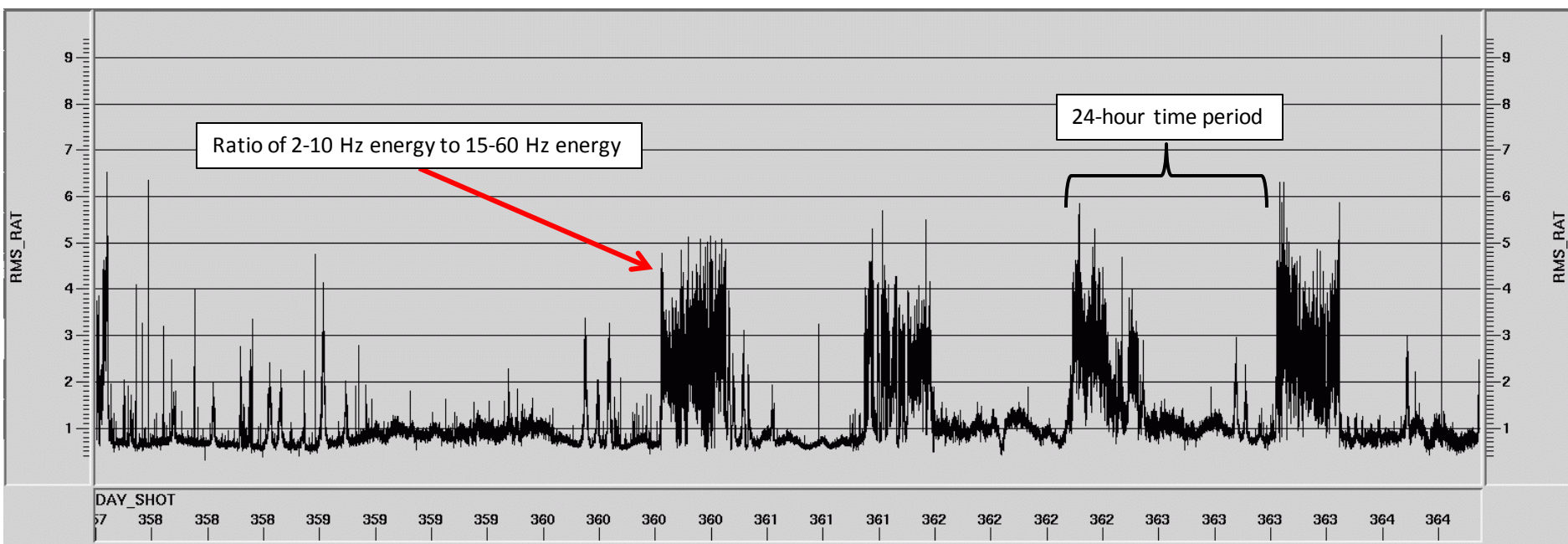
Root Mean Squared (RMS) amplitude 15-60 Hz for entire duration of survey



We repeated the calculations from the previous slide using data to which a bandpass filter that preserved frequencies between 15 and 60 Hz had been applied. The plot above is on the same scale as the previous slide (2-10 Hz preserved) from which we can see that there is a significant amount more energy in the 2-10 Hz bandwidth than the 15-60 Hz bandwidth during the high-amplitude periods. The rest of the time there is about the same amount of energy in these two bandwidths.

Note that even though this band includes 60 Hz signal it is not necessary to assume that the contribution at 60 Hz is due to 60 Hz electrical noise (the frequency at which US electrical power operates). The equipment used to record the data is nearly immune to 60-cycle electrical noise because digitization of the signal is done within the geophone sonde itself and the length of wire over which analog signal is carried within the geophone sonde is on the order of a few centimeters rather than a copper strand that carries signal to the surface along with picking up 60-cycle interference.

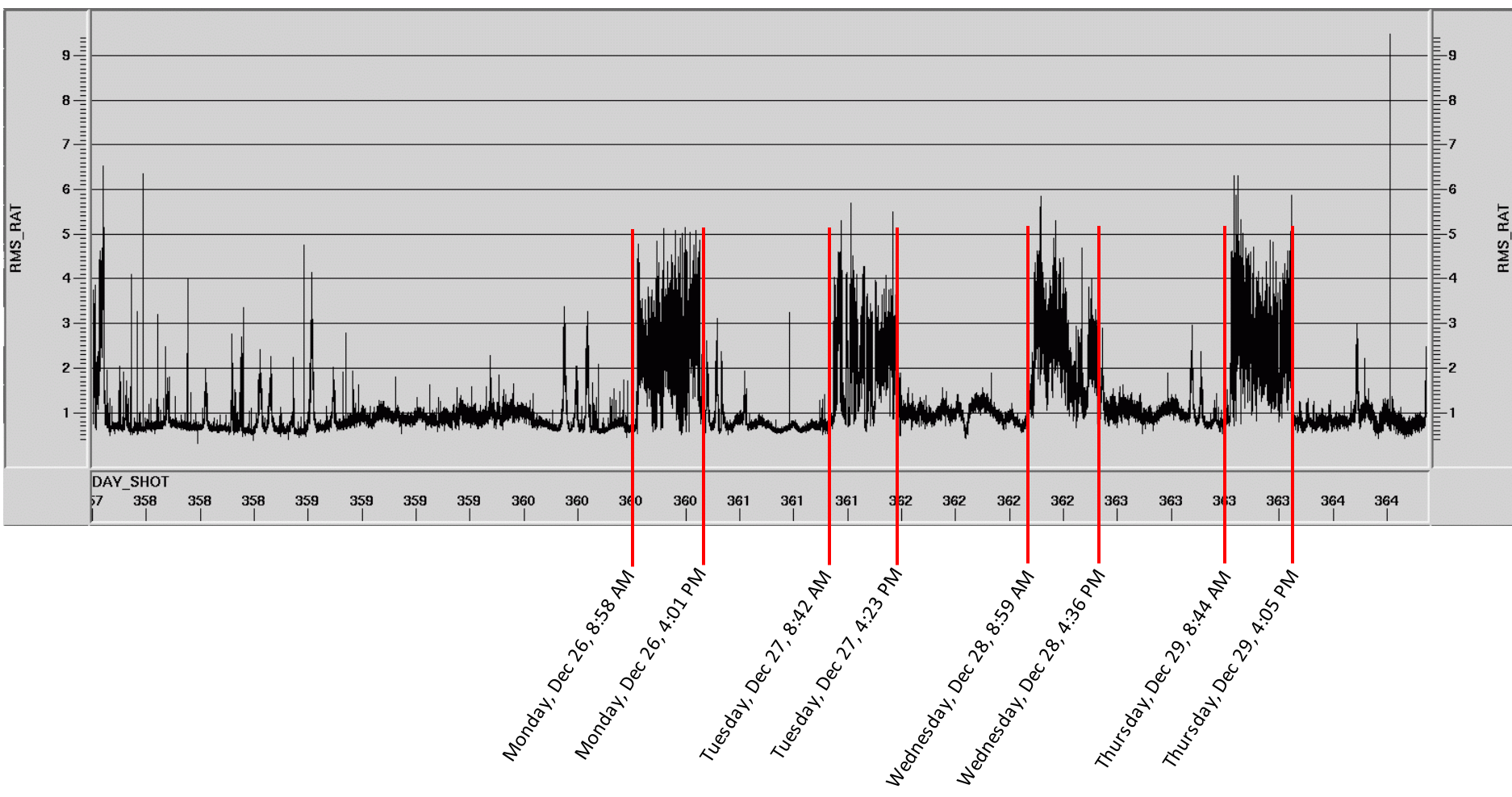
Ratio of Root Mean Squared amplitude 2-10 Hz/15-60 Hz for entire duration of survey



Time (the Julian day of the records are labeled) →

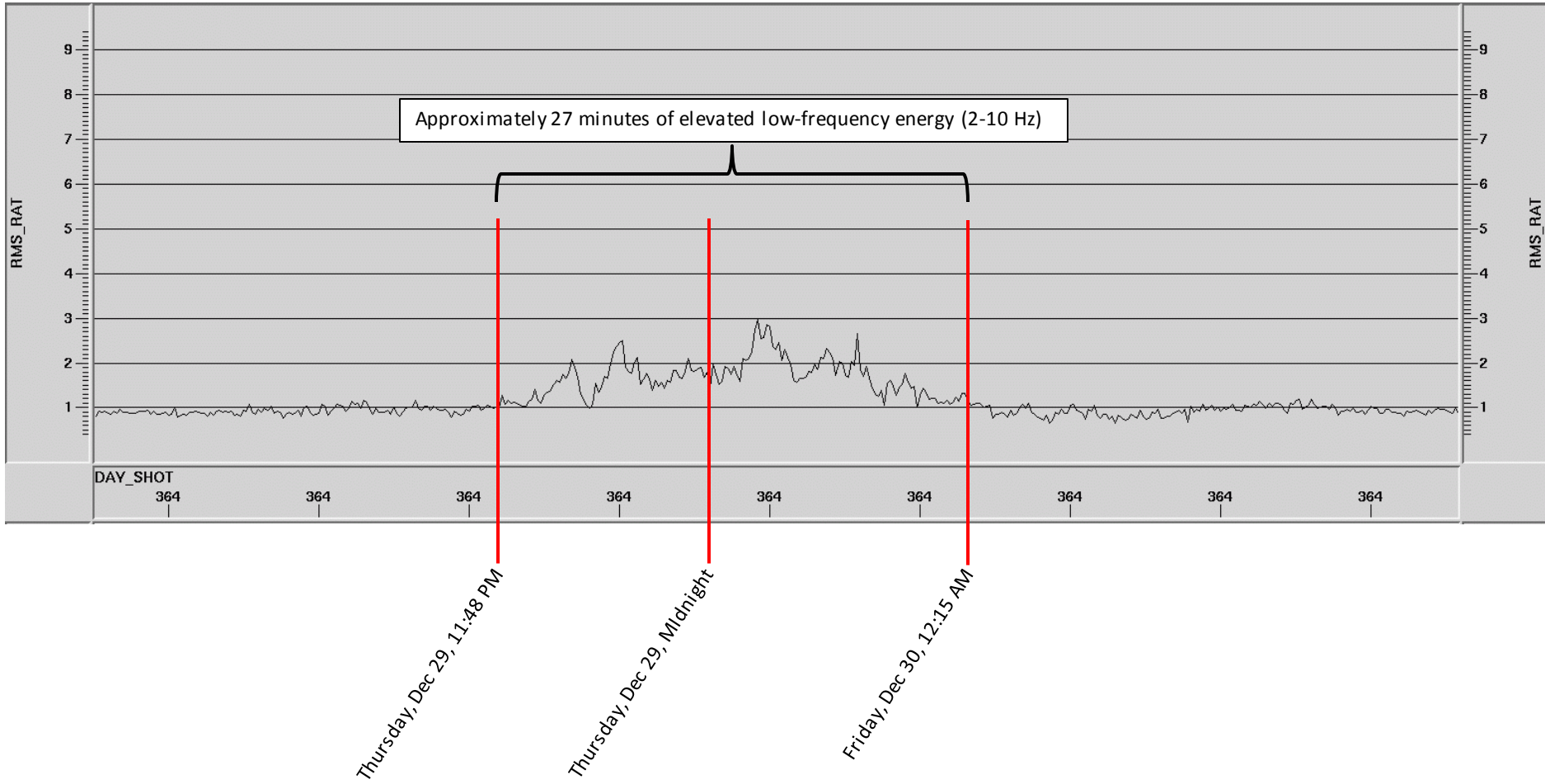
We computed the ratio of energy in the 2-10 Hz bandwidth and the 15-60 Hz bandwidth to accentuate the time frame of the high-energy periods.

Ratio of Root Mean Squared amplitude 2-10 Hz/15-60 Hz for entire duration of survey



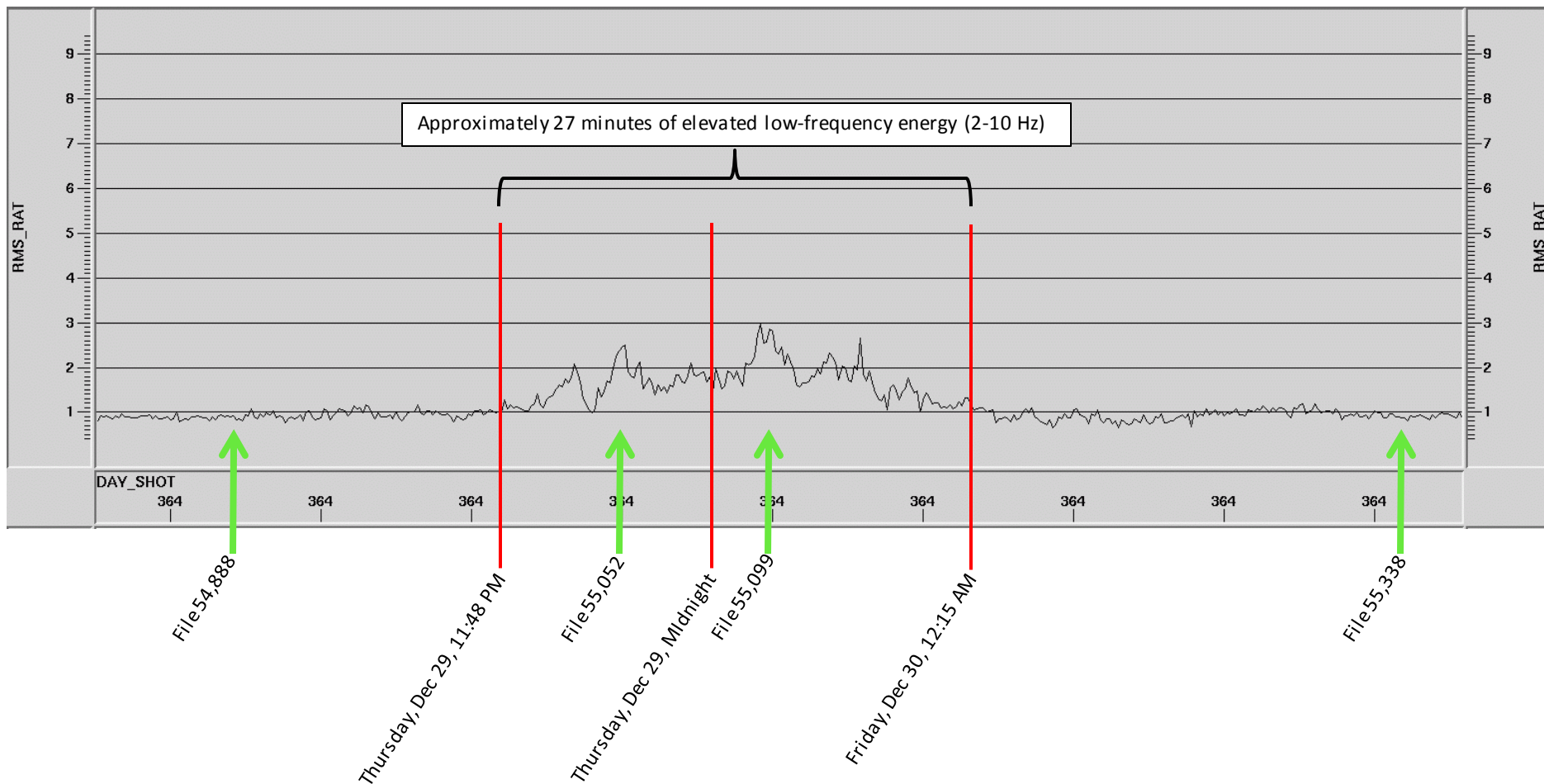
The four highest-amplitude energy clusters are outlined here with start and end times shown. Given the regularity of the start and end times of these periods they are almost certainly man-made cultural noise related to “9-to-5” business operating heavy equipment somewhere in the area. A wood chip plant has been tentatively identified as source of the seismic energy.

Ratio of Root Mean Squared amplitude 2-10 Hz/15-60 Hz for limited time



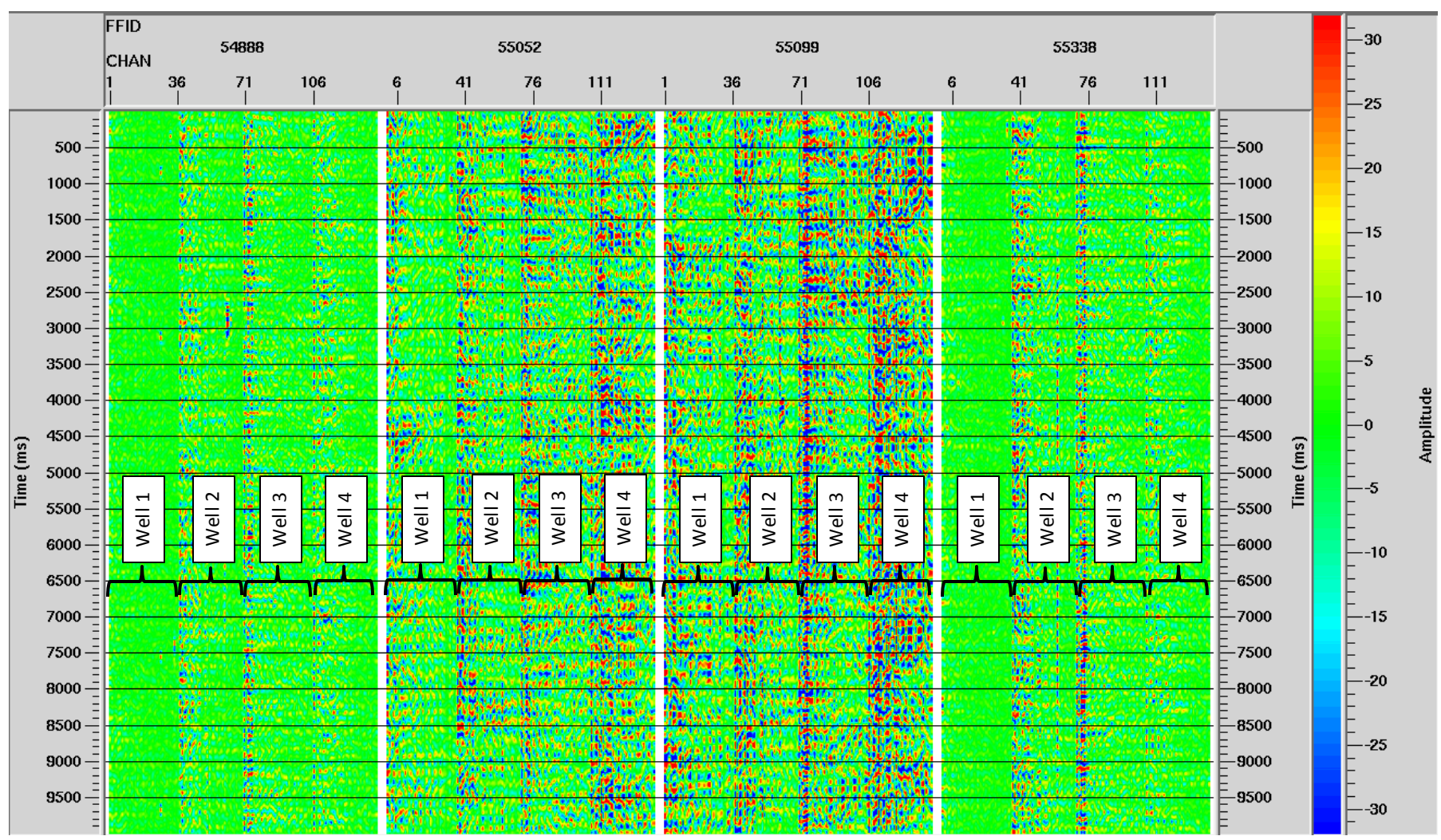
There are, however, multiple time periods such as the 27 minute time period shown above at approximately midnight on the night of December 29, 2011 that are unlikely to be mining, gravel, or timbering operations. It is unlikely man-made due to the short time duration of the amplitudes (industrial operations are sustained) and the time of day. Most outdoor industrial operations do not run at night due to safety restrictions and worker availability.

Green arrows point to records shown on the following slide



We selected seismic records at the times of the four green arrows shown above and plotted their amplitudes on the next slide to verify that the background amplitude increase was ubiquitous across all of the observation wells.

Seismic records showing amplitudes before, during, and after the 25 minute high amplitude period

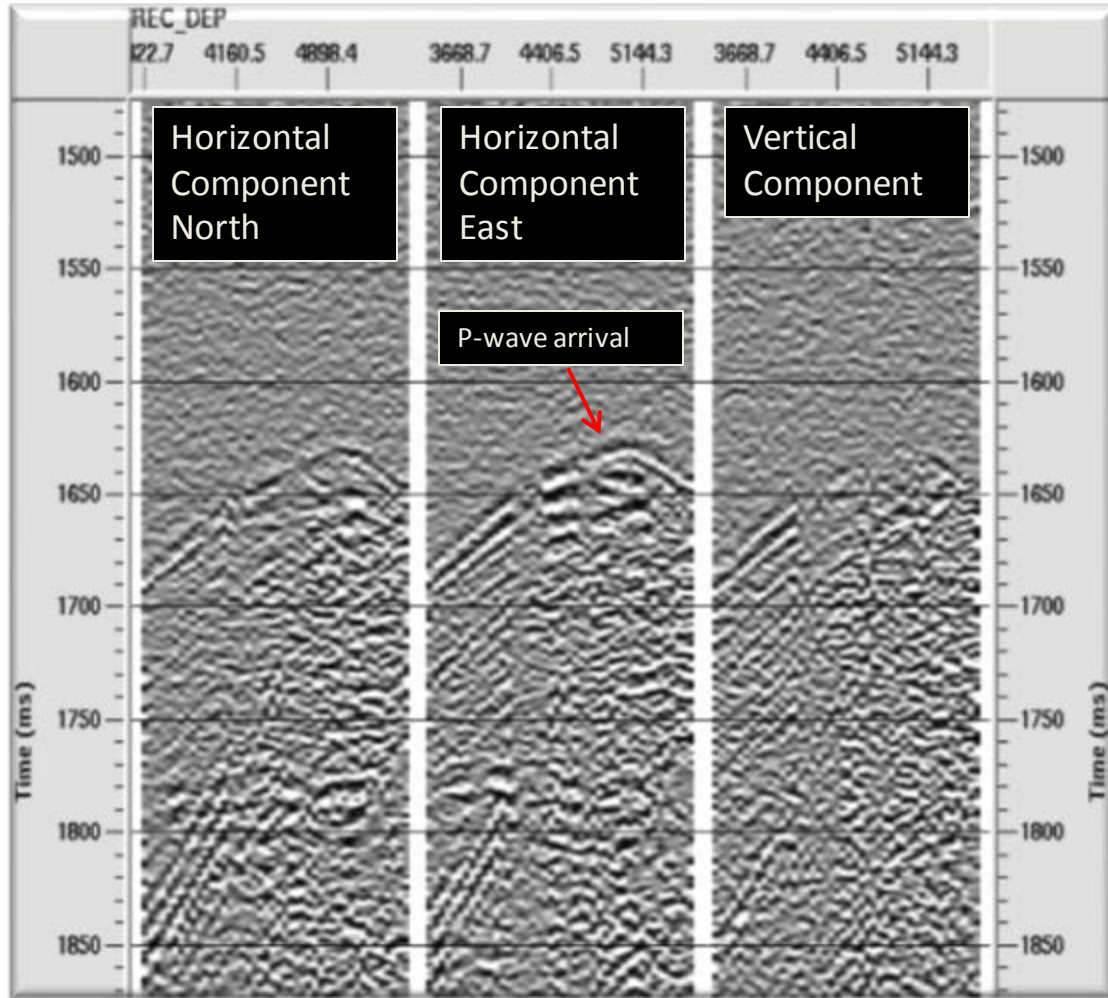


The four seismic records annotated in the previous slide are shown here after bandpass filter of 2-10 Hz with entire-screen scaling, which means that amplitudes can be directly compared to one another. Red and blue colors indicate that the data trace has high amplitude and green means low amplitude. Thus, it is easy to see that the two center records (55,052 and 55,099) that were recorded during the high-amplitude midnight period on the previous slide do, in fact, have a larger amplitude than the two records recorded outside the 25 minute time period. There are numerous short time periods within the survey time period that should be investigated as possibly having a naturally occurring source. The fact that all four wells see elevated amplitude indicate that the effect of the source is widespread throughout the area.

Overview of LASEA concept

The following four slides discuss the concept of LASEA (Low Amplitude Seismic Emission Analysis). This discussion is followed by results from the Newberry Volcano project.

Explanation of Low Amplitude Seismic Emission Analysis (LASEA)



Conventional microseismic methods focus on analysis of high-amplitude short duration seismic events like the one shown in the figure to the left. Events like this one originate when rocks break in response to injection of hydraulic stimulation fluids or changes in stress due to large temperature variations. They are generally very small earthquakes with magnitude on the order of -3 to -1.

In contrast to the large-amplitude short-duration events, there are also situations in which seismic energy is generated over long periods of time but with even lower amplitudes than the event shown in the figure to the left.

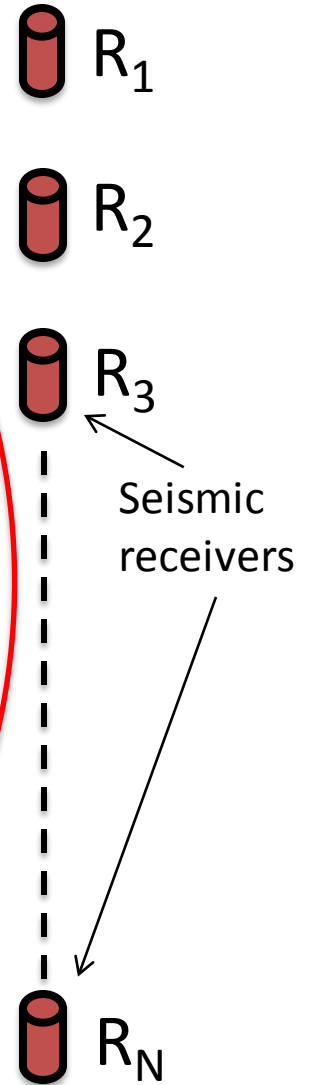
APEX HiPoint has developed a method that we call LASEA (Low Amplitude Seismic Emission Analysis) that provides a direct measure of seismic energy output from points in a volume of earth over time. Anomalously large amplitude values may correspond to locations in the earth where fluids are moving, stress is changing due to temperature fluctuations, or the points are in direct connection with a source of variable pressure, even when rocks do not break in response to the pressure/stress changes.

Seismic waves

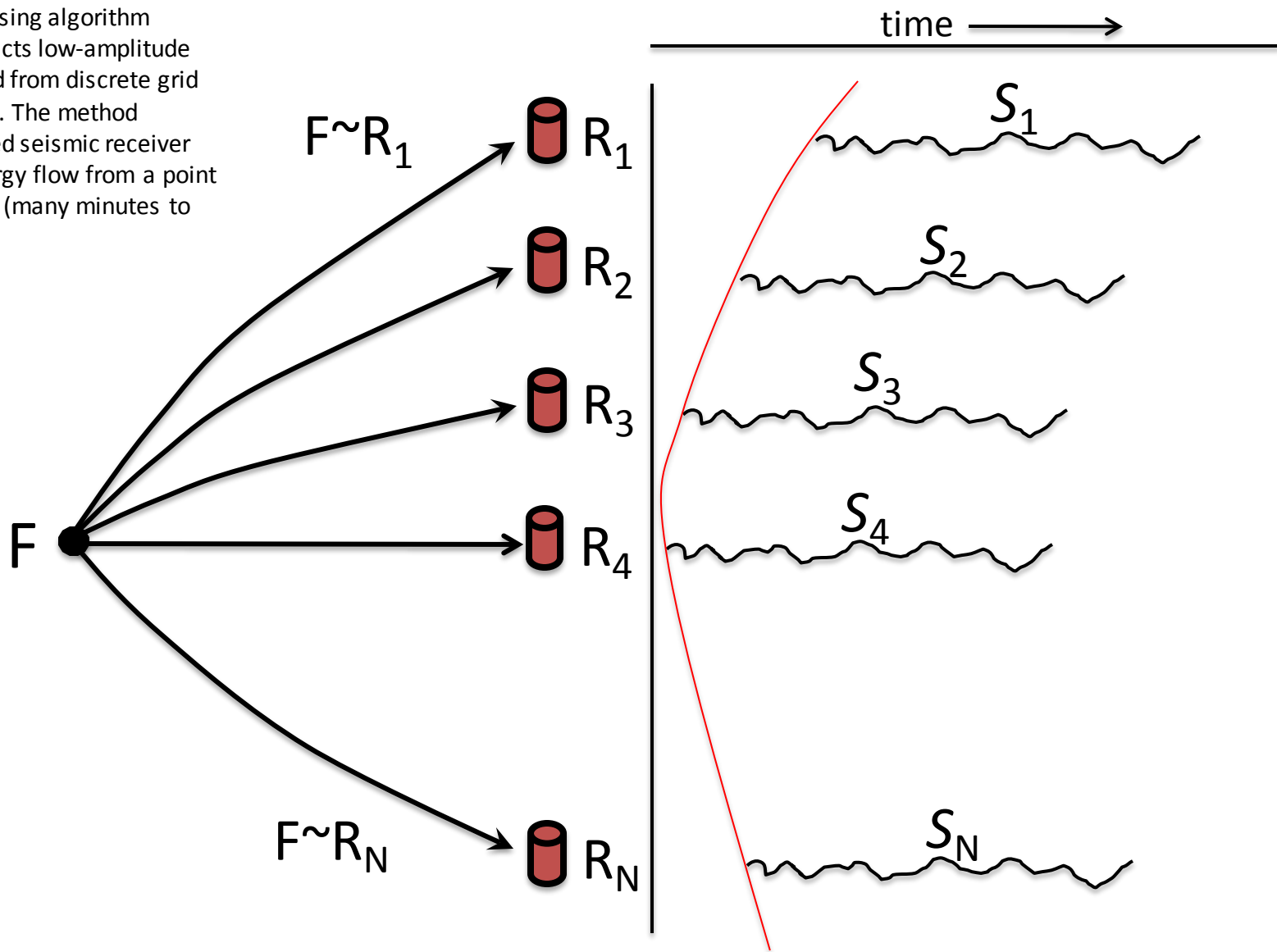
When fluids in natural fractures are subjected to varying pressure from fluid sources or changing temperature, the fluids push on the adjacent rock walls generating low-amplitude vibrations that can be recorded by geophones. These vibrations can be persistent over long periods of time. Natural processes such as volcanic activity for example, can continue for millennia. The LASEA method takes advantage of persistent seismic signals in spite of relatively small amplitudes of magnitude of -3 or smaller.



Fluid within fractures transmits energy in the form of pressure to the adjacent rock walls to generate seismic waves.



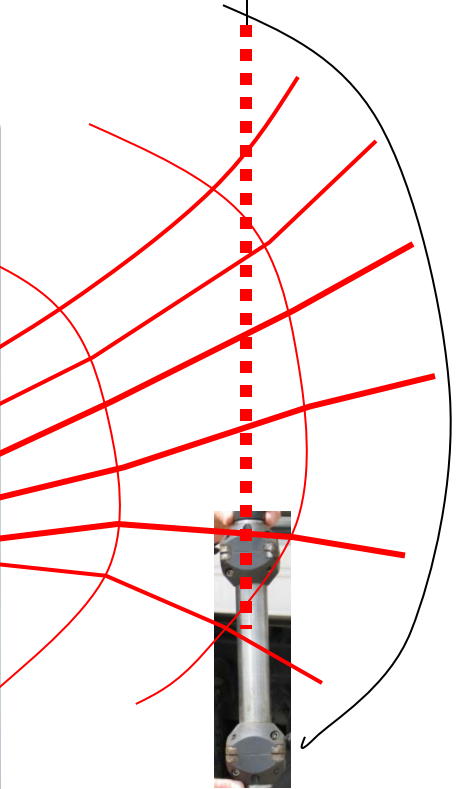
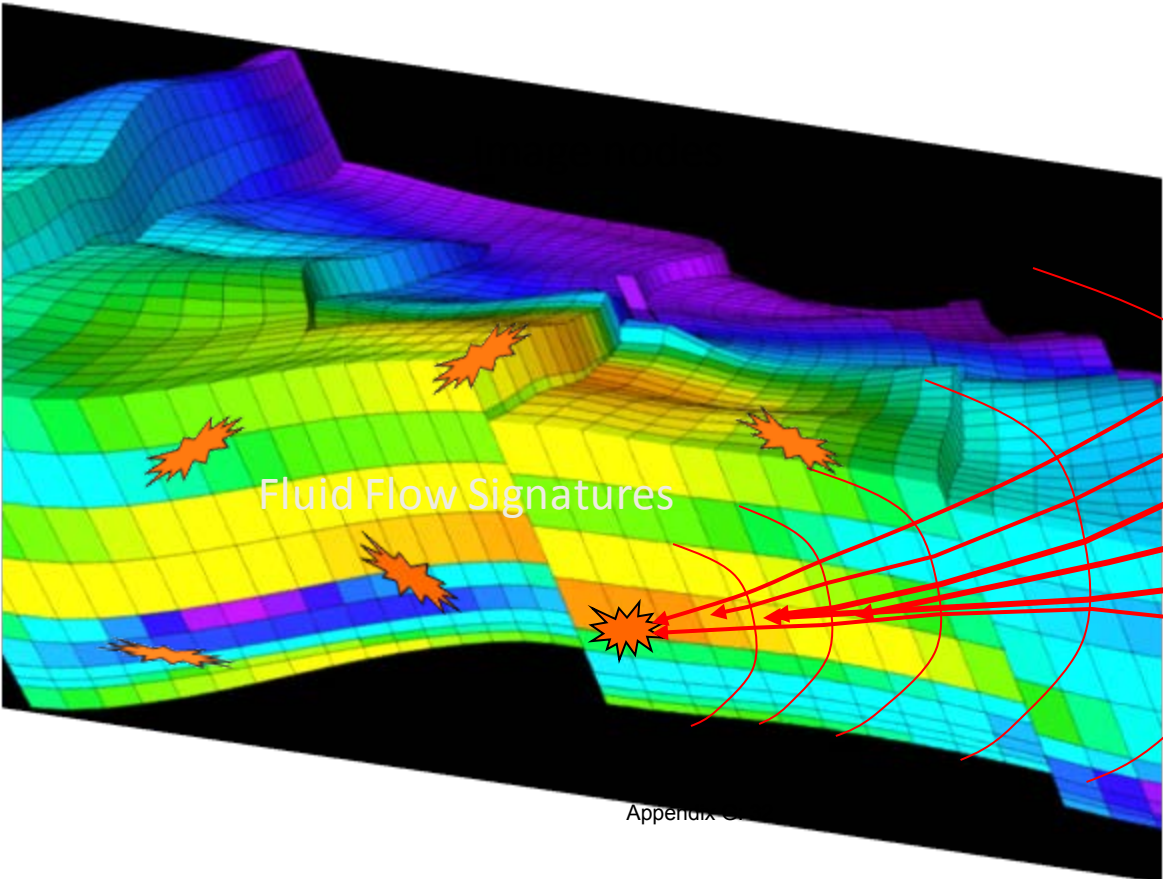
The LASEA data processing algorithm (patent pending) extracts low-amplitude seismic signals emitted from discrete grid nodes within the earth. The method essentially uses focused seismic receiver arrays to measure energy flow from a point over long time periods (many minutes to many hours).



The LASEA algorithm essentially uses an array of 3-component geophones as an antenna to measure seismic energy flux from each grid node in a 3D volume somewhere near the observation wells. The algorithm is much more focused and precise than a simple energy measurement as it employs elements of Kirchhoff Depth Migration, virtual source concepts, and other technologies. The algorithm is computationally intensive but computers with sufficient computational capacity can be employed to efficiently calculate results.

Reservoir Production Monitoring with LASEA

LASEA can be used to monitor production from producing fields to determine where fluids are being produced or for subsurface hydrothermal activity. Combined with reservoir simulators, this information could provide the most accurate means currently available to estimate reservoir capacity and accessible reserves in place.

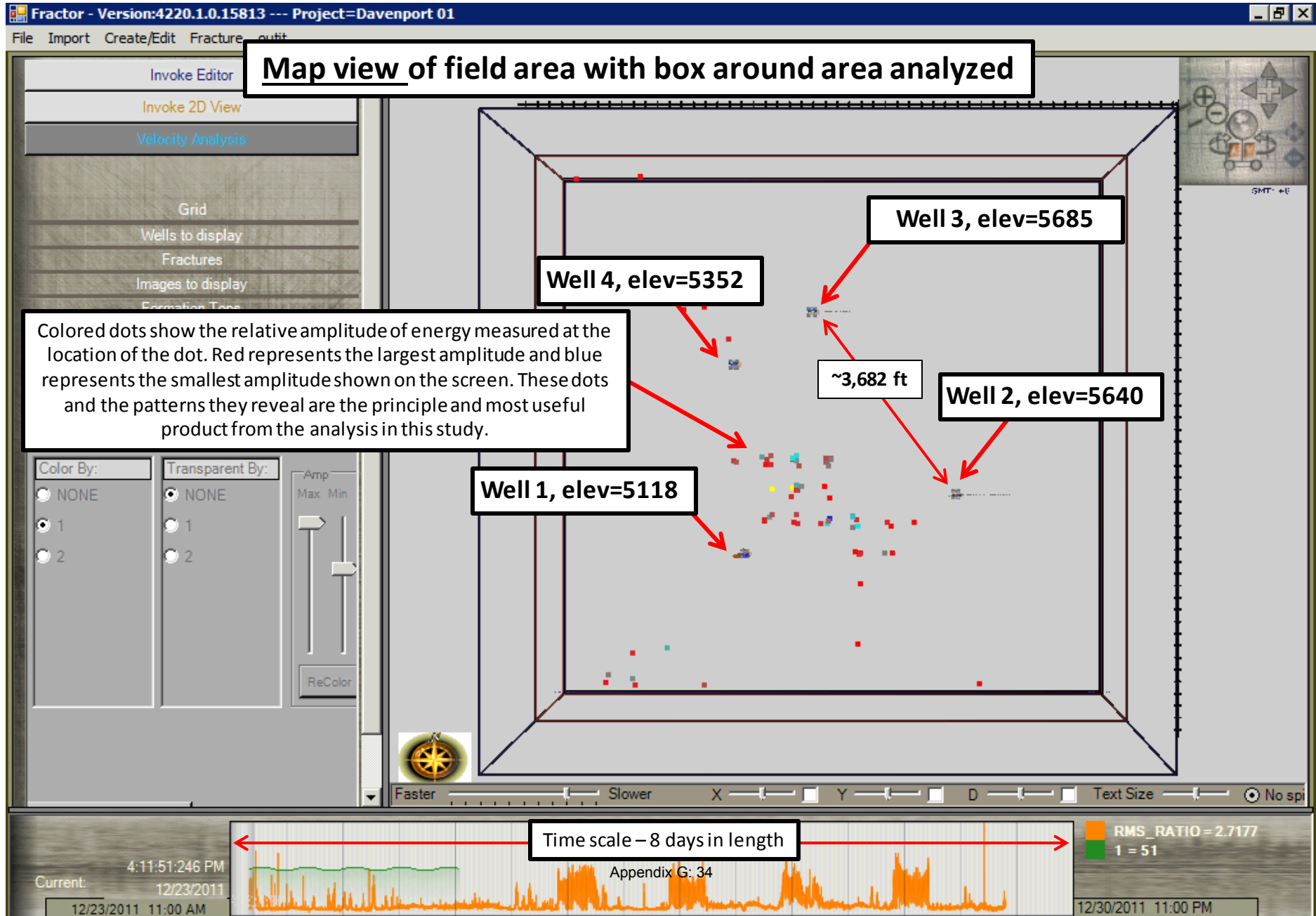


LASEA Output

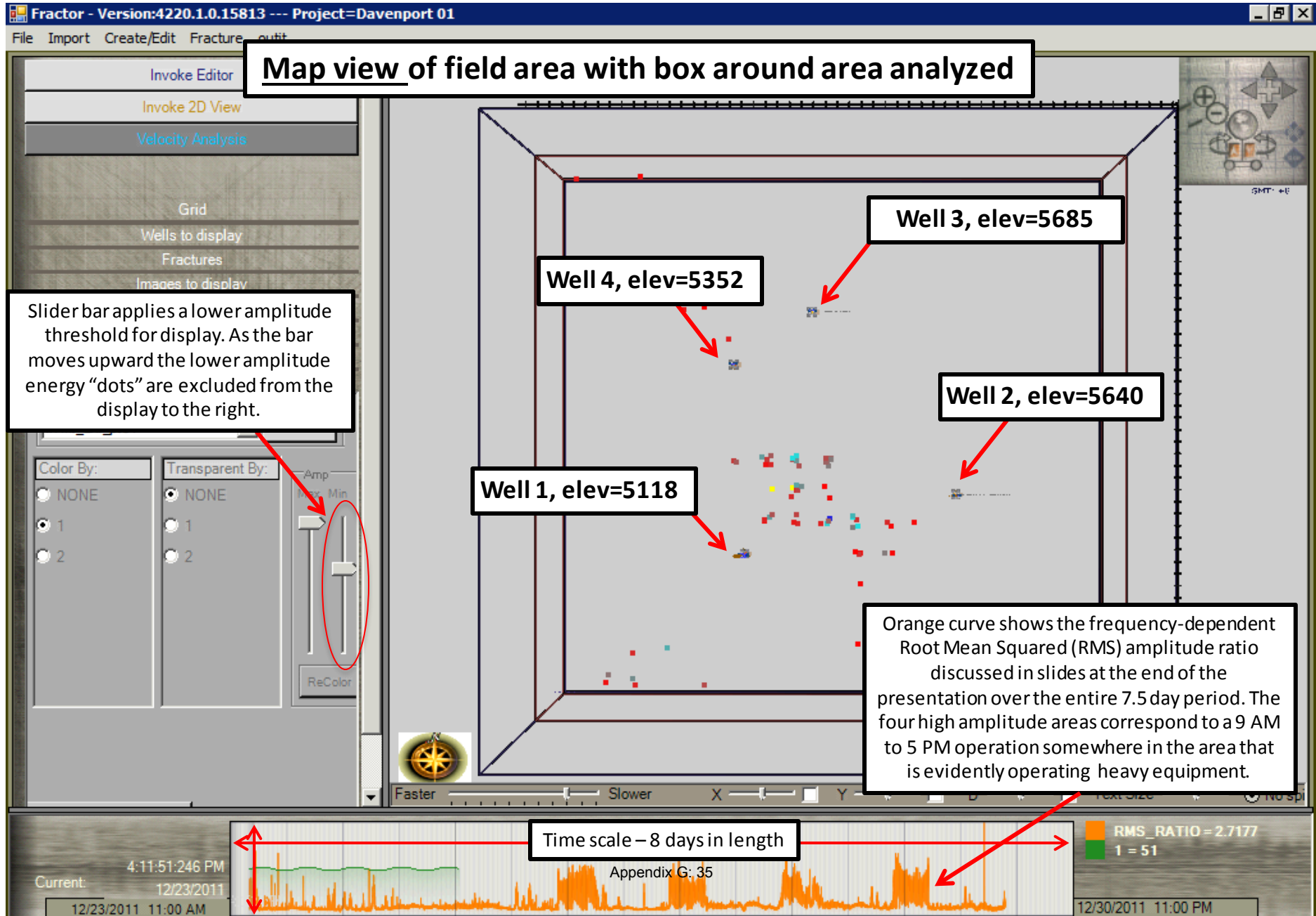
LASEA scans a full 3D volume of the earth at some grid interval and computes the amount of seismic energy detected from that location over some time period, normally on the order of a few minutes to hours. LASEA then outputs a number corresponding to the energy measurement for that grid node and time. The grid node energy measurements can then be viewed in a 3D viewer to observe trends in the energy.

The following three slides show a view of the 3D seismic viewing package developed by APEX HiPoint called Fractor. The results are from the Davenport Newberry Volcano project.

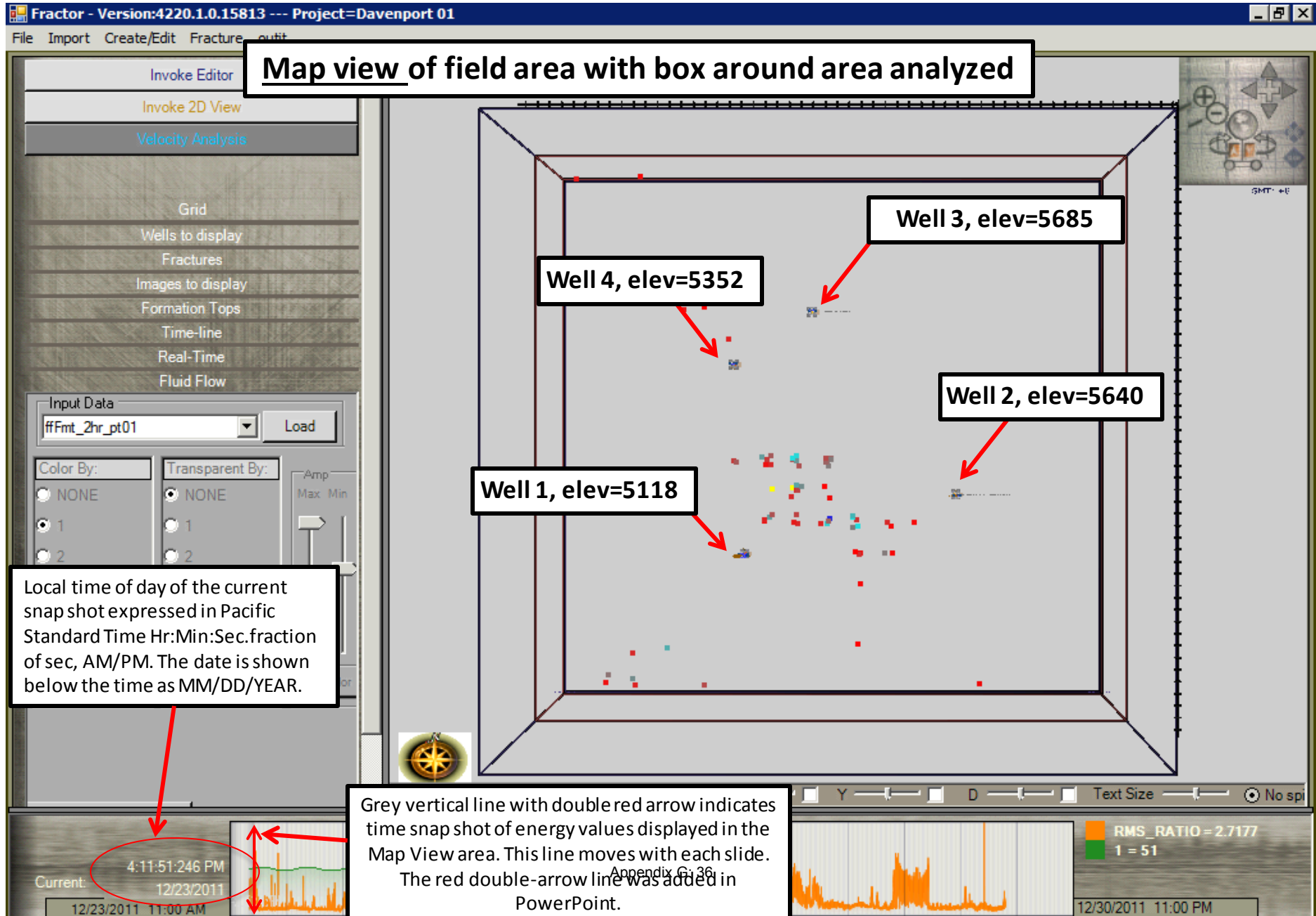
Viewing software features



Viewing software features continued



Viewing software features continued



Map view of field area with box around area analyzed

Well 4, elev=5352

Well 3, elev=5685

Well 2, elev=5640

Well 1, elev=5118

Local time of day of the current snapshot expressed in Pacific Standard Time Hr:Min:Sec.fraction of sec, AM/PM. The date is shown below the time as MM/DD/YEAR.

Grey vertical line with double red arrow indicates time snapshot of energy values displayed in the Map View area. This line moves with each slide. The red double-arrow line was added in PowerPoint.

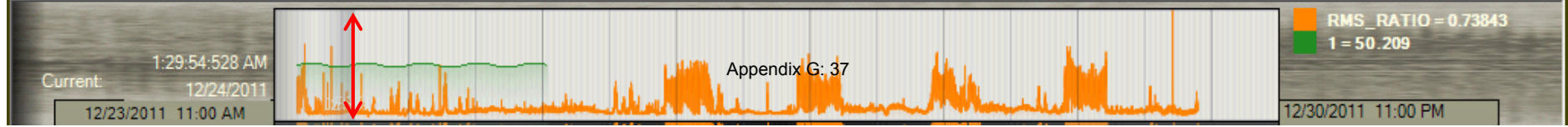
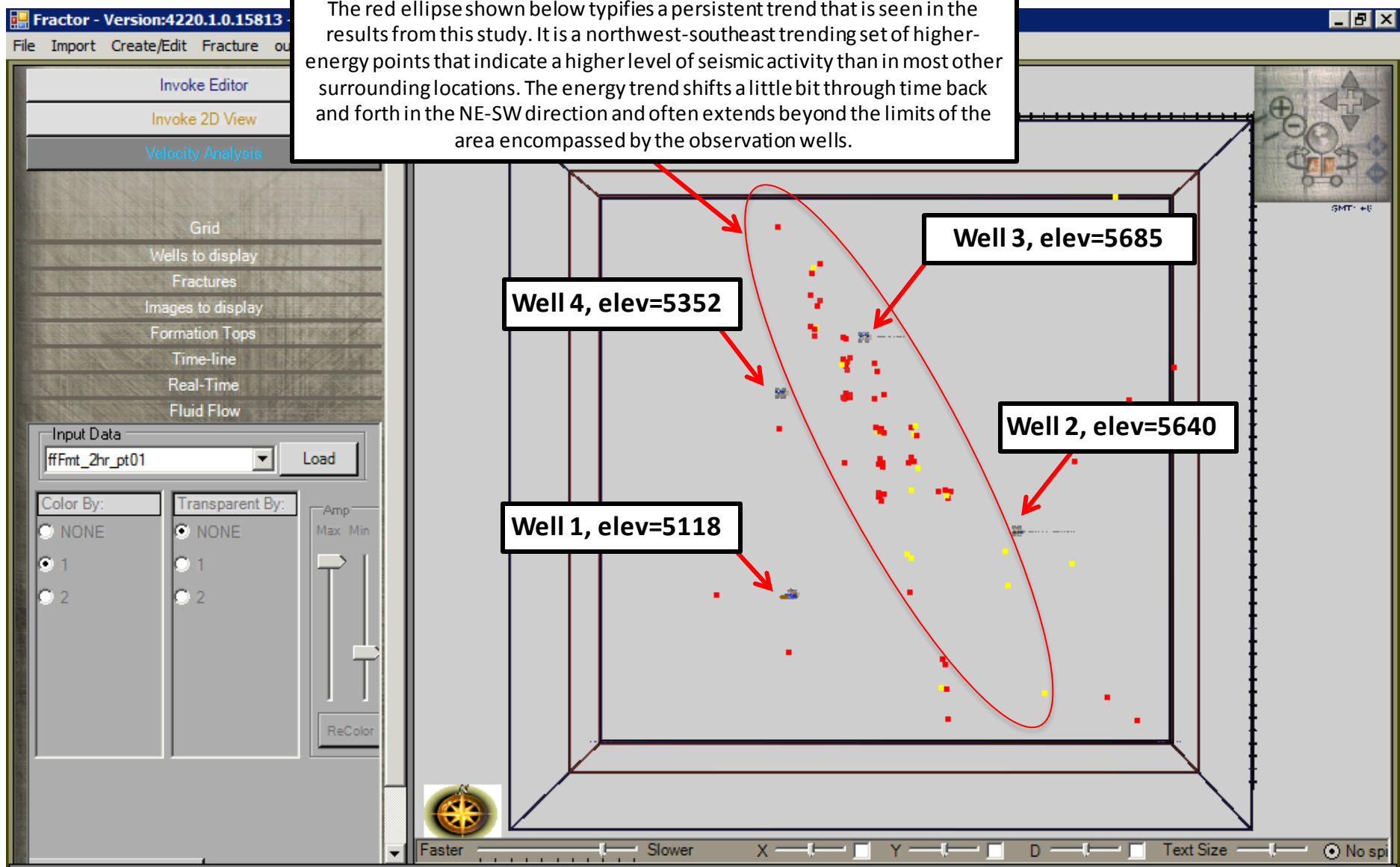
Current: 4:11:51:246 PM
12/23/2011

RMS_RATIO = 2.7177
1 = 51

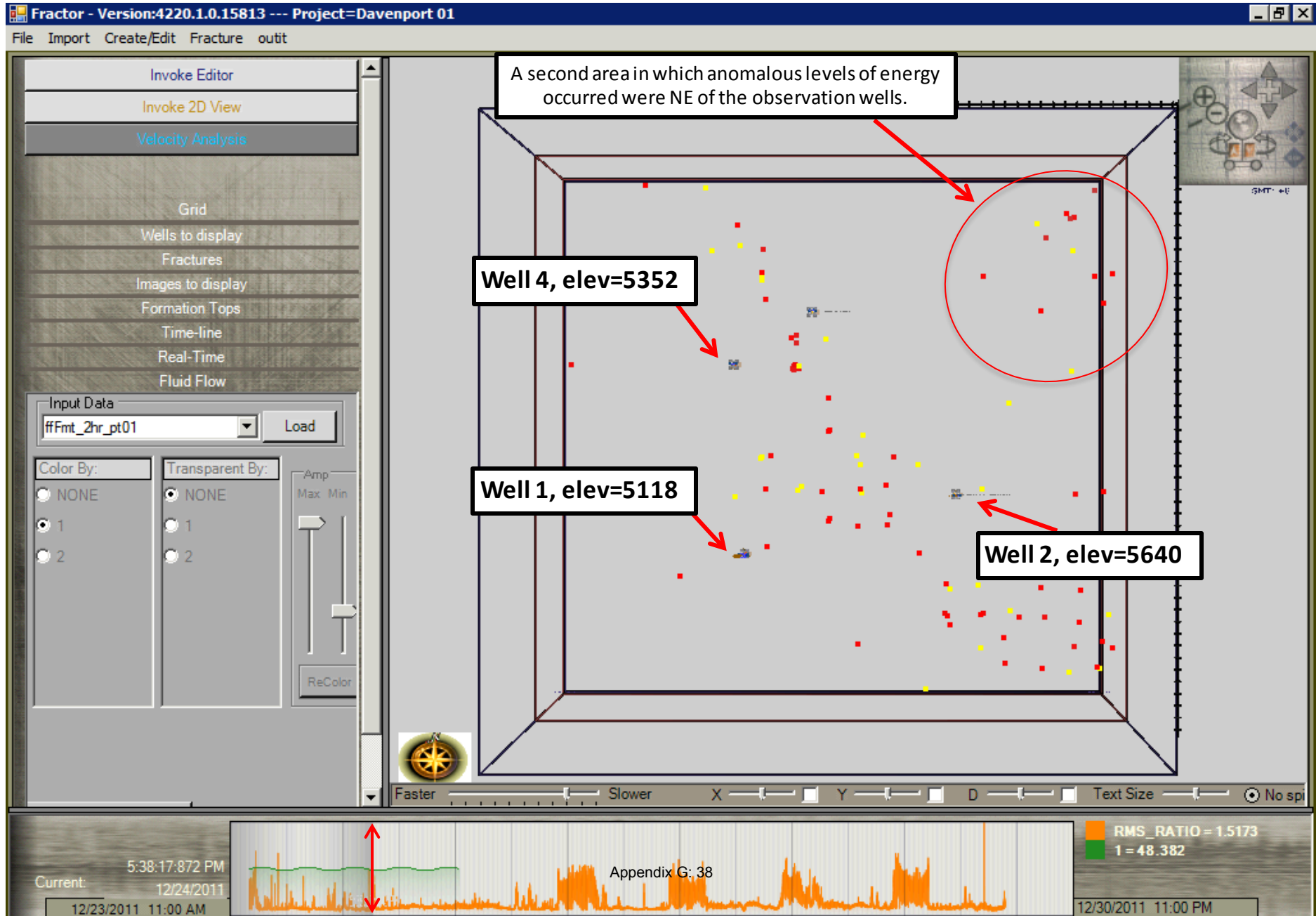
12/30/2011 11:00 PM

Preview of main conclusions

The red ellipse shown below typifies a persistent trend that is seen in the results from this study. It is a northwest-southeast trending set of higher-energy points that indicate a higher level of seismic activity than in most other surrounding locations. The energy trend shifts a little bit through time back and forth in the NE-SW direction and often extends beyond the limits of the area encompassed by the observation wells.



Preview of main conclusions continued



Time snapshots: map view

The following 17 slides show map view images of LASEA output from the Davenport Newberry Volcano project at sequential time periods from the beginning of the project to the end.

Side views are supplied following the map view to give a feeling for the vertical extent of anomalous energy measurements.

Begin recording time.

Fractor - Version:4220.1.0.15813 --- Project=Davenport 01

File Import Create/Edit Fracture outit

Invoke Editor
Invoke 2D View
Velocity Analysis

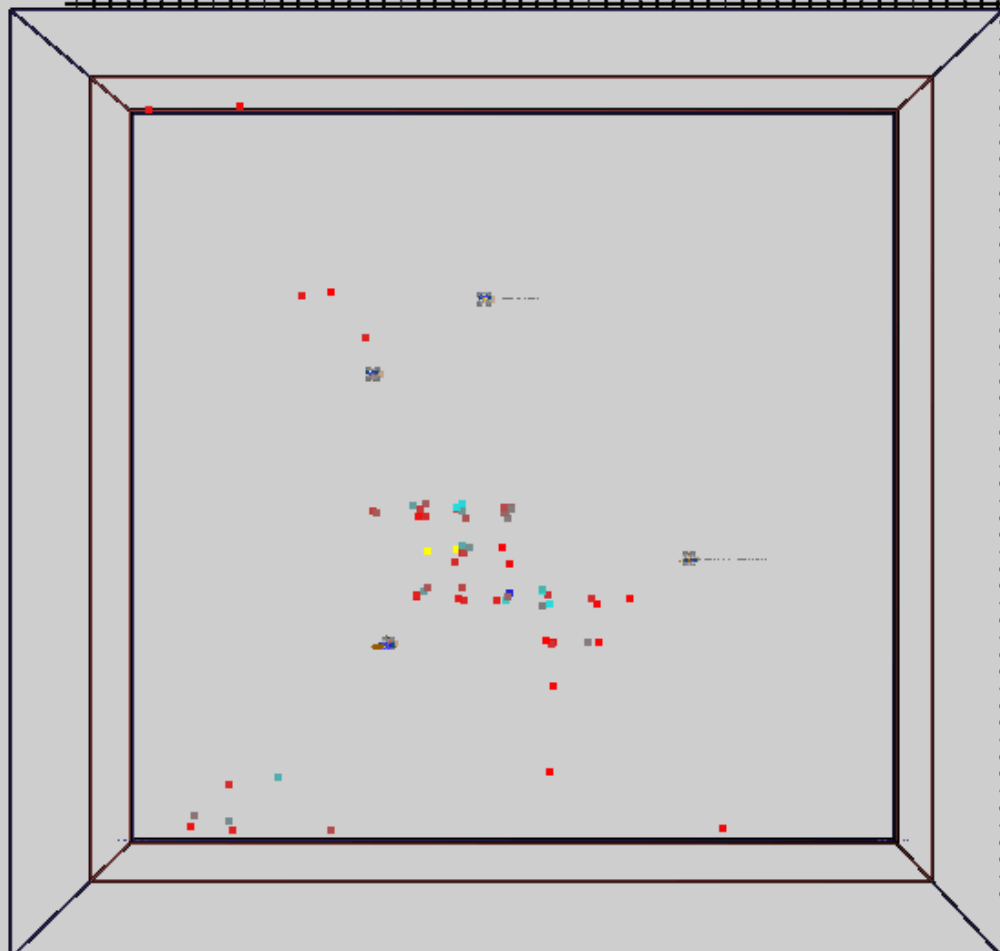
Grid
Wells to display
Fractures
Images to display
Formation Tops
Time-line
Real-Time
Fluid Flow

Input Data
ffFmt_2hr_pt01 Load

Color By:
 NONE
 1
 2

Transparent By:
 NONE
 1
 2

Amp
Max Min
ReColor



Faster Slower X Y D Text Size No spi

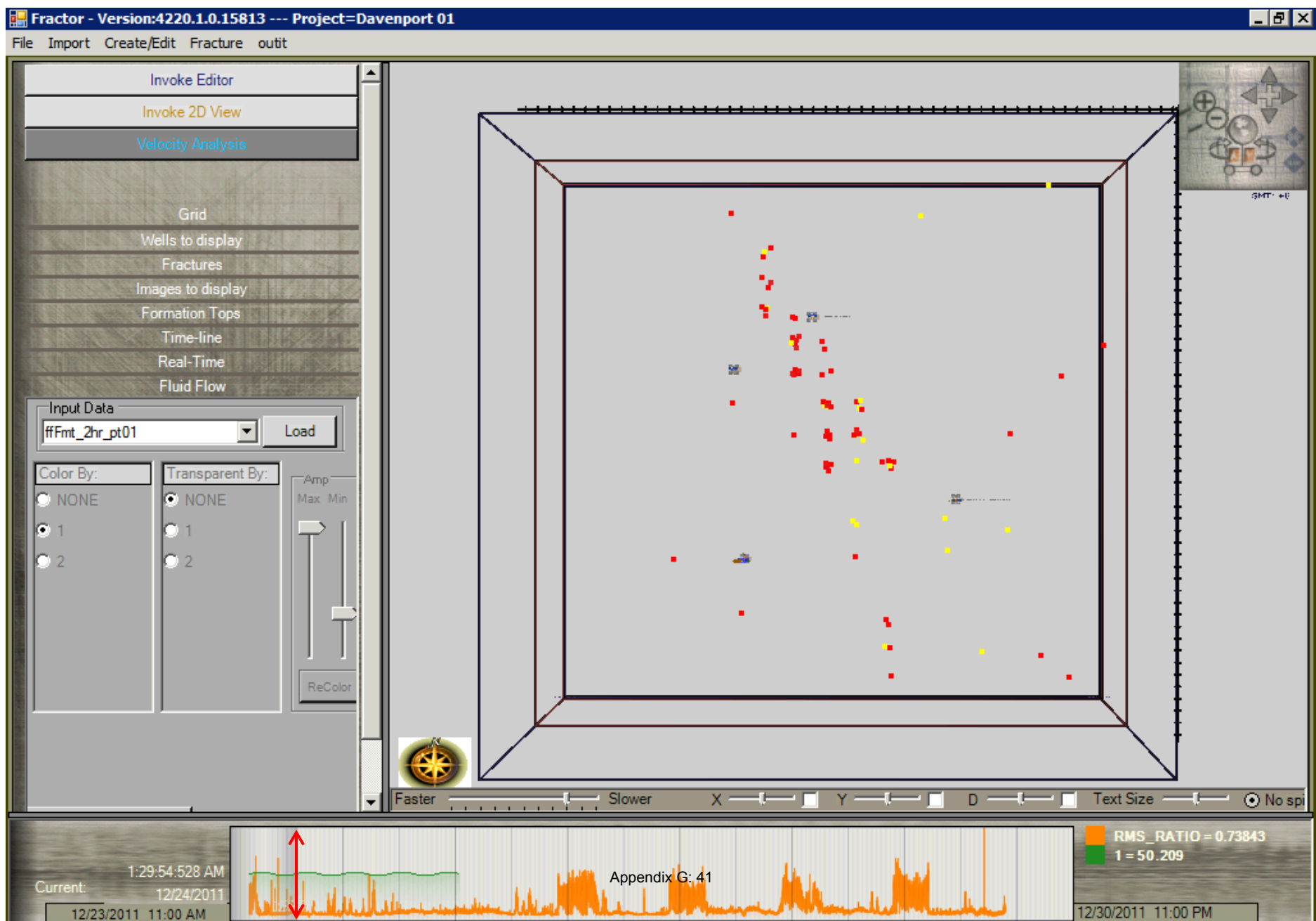
Current: 4:11:51:246 PM
12/23/2011
12/23/2011 11:00 AM

Appendix G: 40

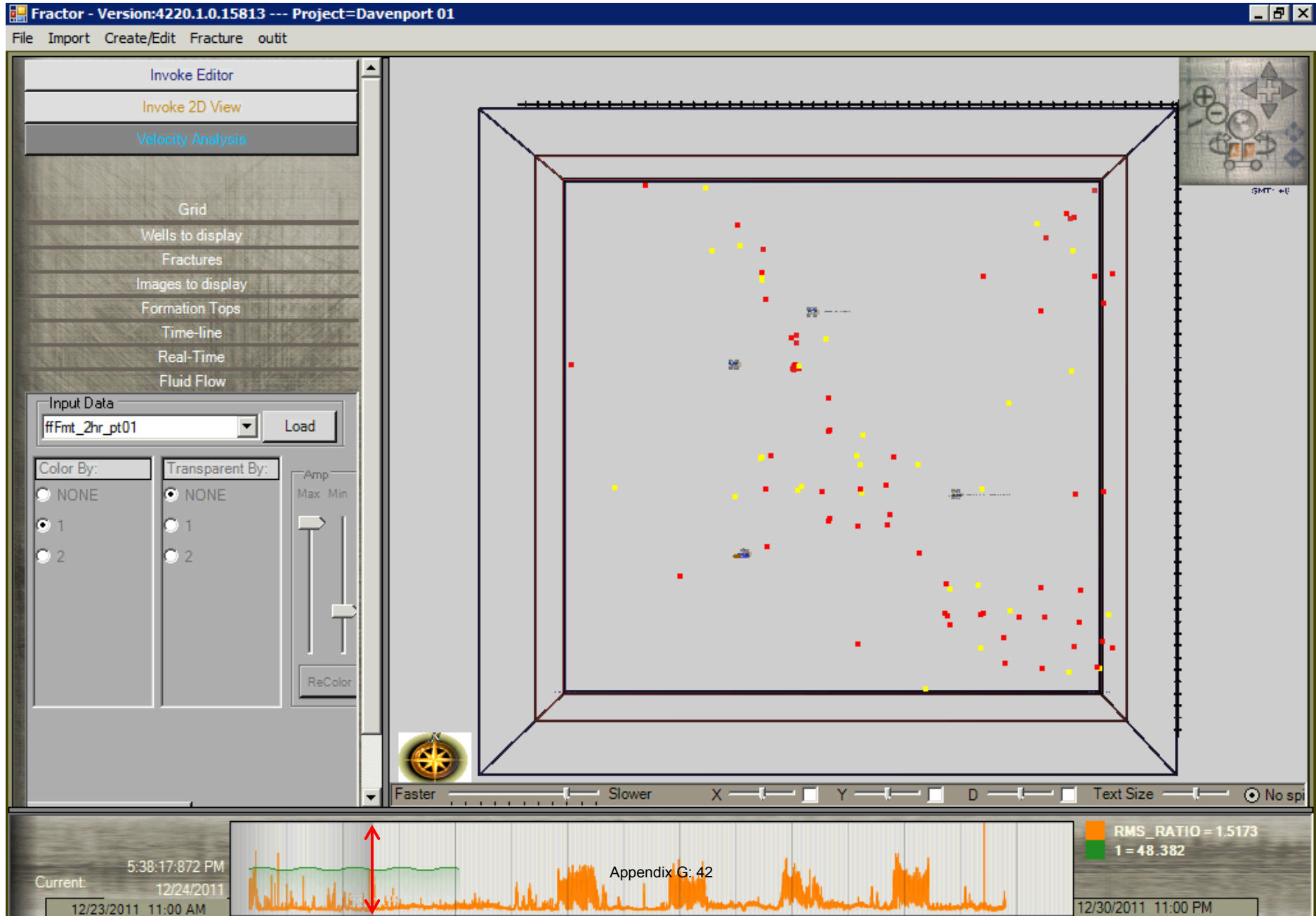
RMS_RATIO = 2.7177
1 = 51

12/30/2011 11:00 PM

This time frame shows the strong NW-SE trend.



This time frame shows the strong NW-SE trend with extension to the SE and some energy in the NE.



Invoke Editor

Invoke 2D View

Velocity Analysis

Grid

Wells to display

Fractures

Images to display

Formation Tops

Time-line

Real-Time

Fluid Flow

Input Data

ffFmt_2hr_pt01

Load

Color By:

NONE

1

2

Transparent By:

NONE

1

2

Amp

Max Min

ReColor



Faster

Slower

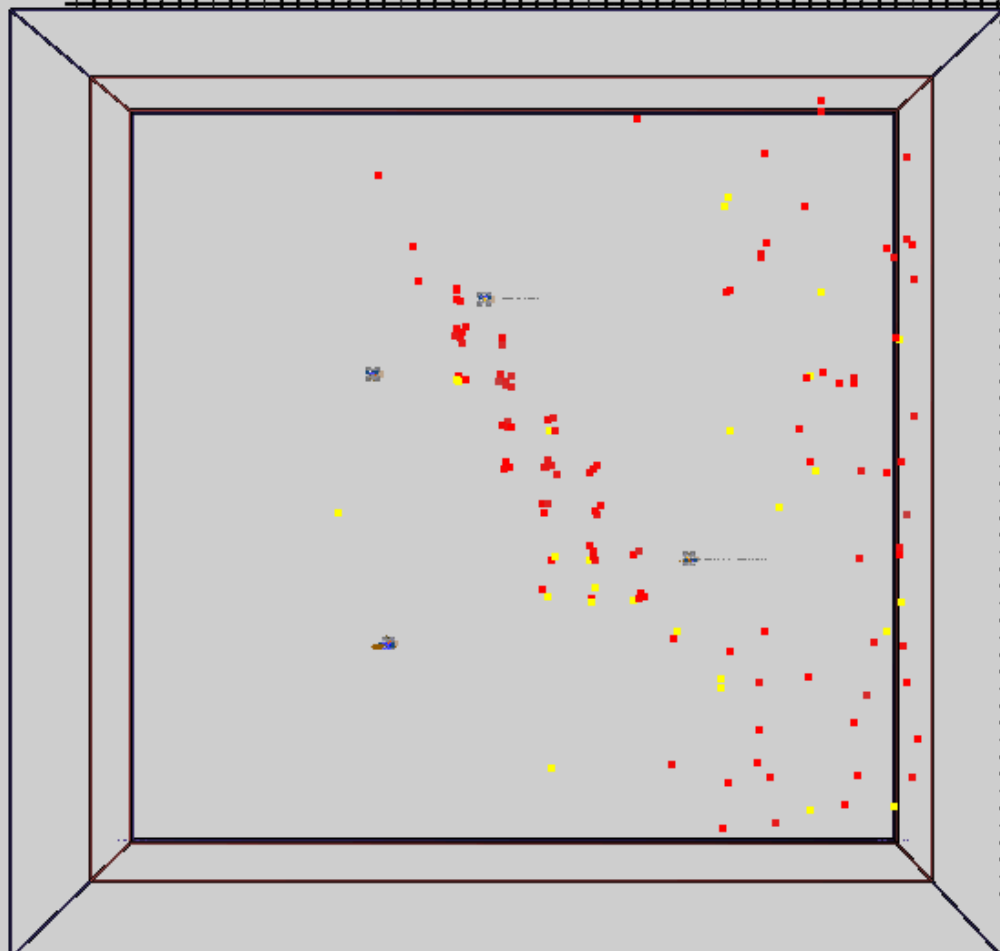
X

Y

D

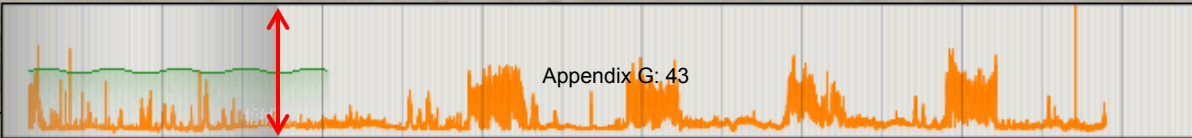
Text Size

No sp



SMT +E

Current: 4:34:49.969 AM
12/25/2011
12/23/2011 11:00 AM



Appendix G: 43

RMS_RATIO = 0.82208
1 = 48.268

12/30/2011 11:00 PM

Invoke Editor

Invoke 2D View

Velocity Analysis

Grid

Wells to display

Fractures

Images to display

Formation Tops

Time-line

Real-Time

Fluid Flow

Input Data

ffFmt_2hr_pt02

Load

Color By:

NONE

1

2

Transparent By:

NONE

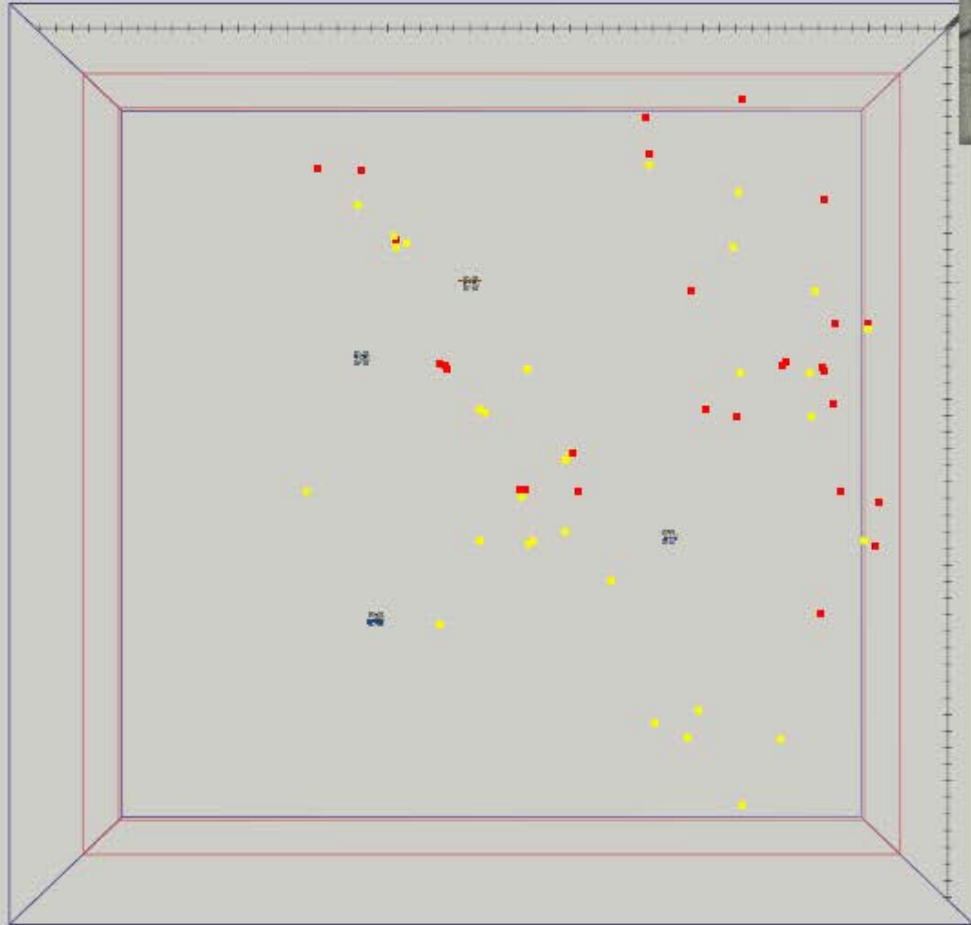
1

2

Amp

Max. Min

ReColor



Faster

Slower

X

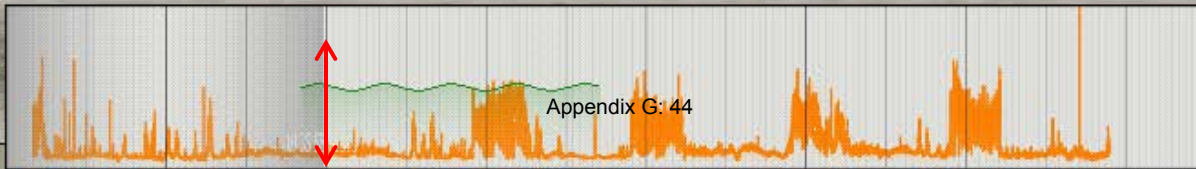
Y

D

Text Size

No sp

Current: 10:35:55:623 AM
12/25/2011



RMS_RATIO = 0.73572

12/23/2011 11:00 AM

12/30/2011 11:00 PM

Invoke Editor

Invoke 2D View

Velocity Analysis

Grid

Wells to display

Fractures

Images to display

Formation Tops

Time-line

Real-Time

Fluid Flow

Input Data

ffFmt_2hr_pt02

Load

Color By:

NONE

1

2

Transparent By:

NONE

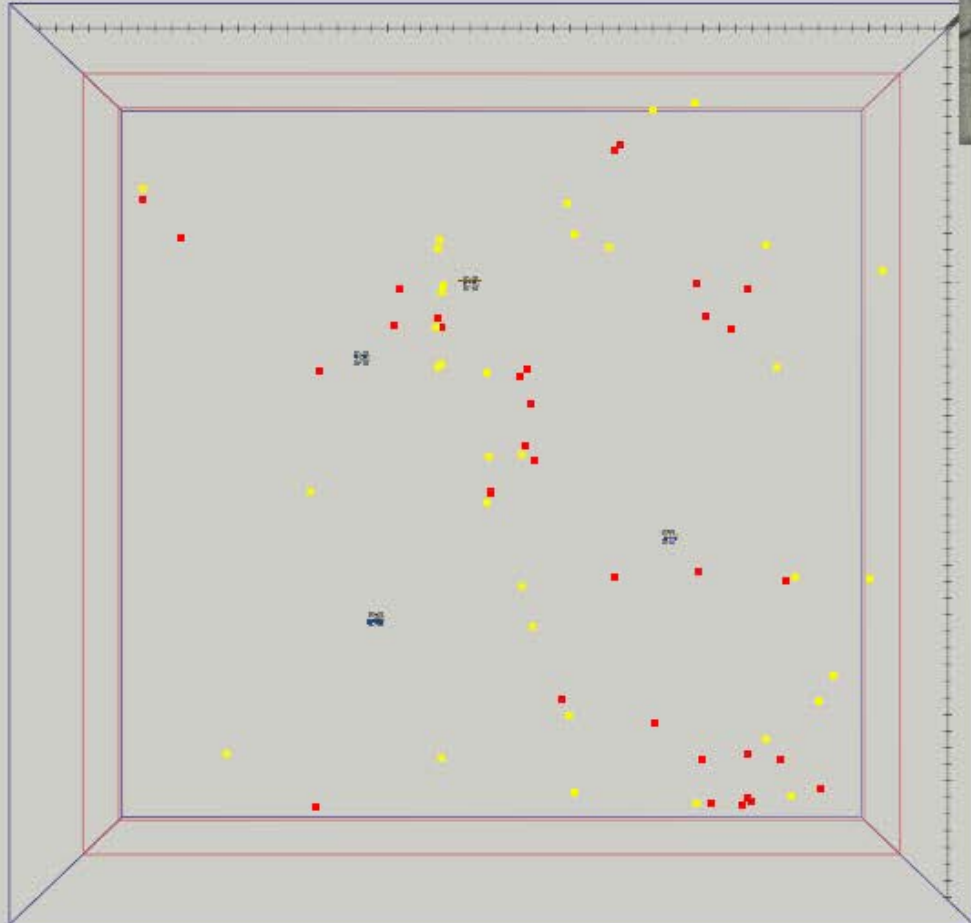
1

2

Amp

Max. Min

ReColor



Faster

Slower

X

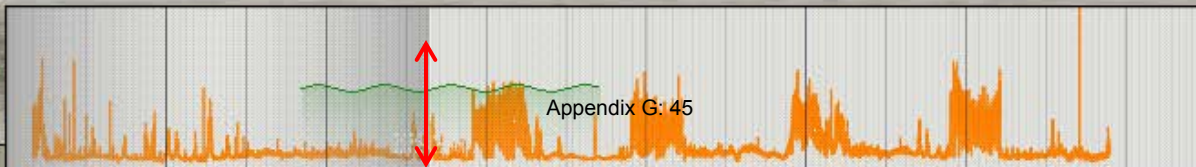
Y

D

Text Size

No sp

Current: 2:27:54:164 AM
12/26/2011

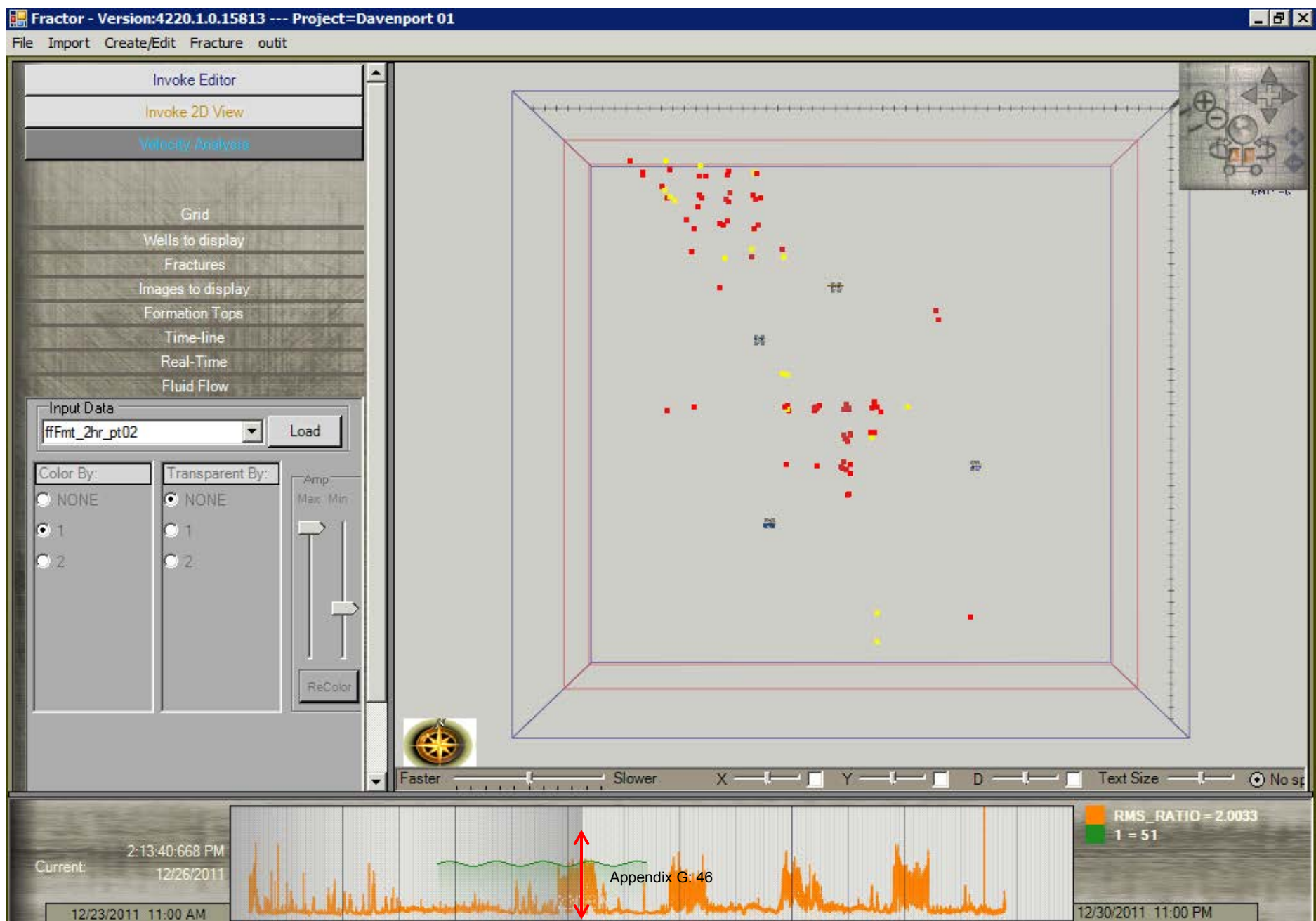


RMS_RATIO = 0.79803
1 = 48.662

12/23/2011 11:00 AM

12/30/2011 11:00 PM

This time frame shows the NW-SE trend. It is also in the 9AM-to-5PM time frame of the industrial operation that is suspected.



Invoke Editor

Invoke 2D View

Velocity Analysis

Grid

Wells to display

Fractures

Images to display

Formation Tops

Time-line

Real-Time

Fluid Flow

Input Data

ffFmt_2hr_pt02

Load

Color By:

NONE

1

2

Transparent By:

NONE

1

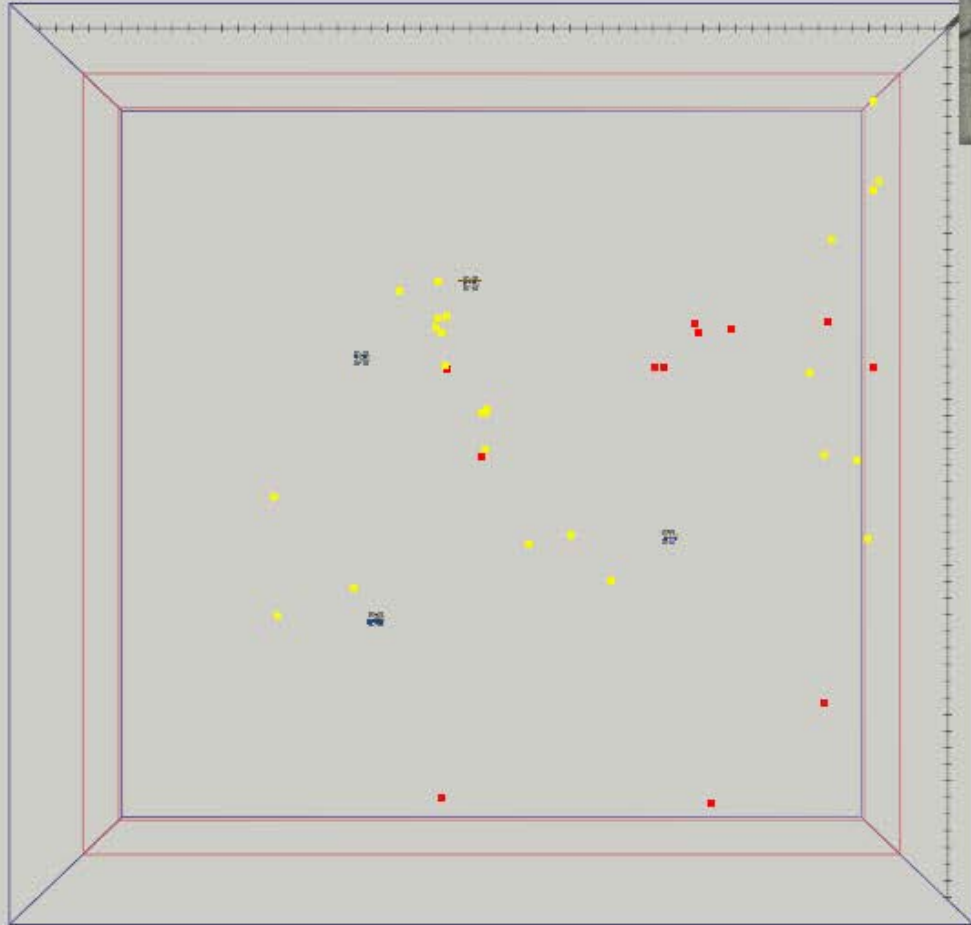
2

Amp

Max Min



ReColor



Faster

Slower

X

Y

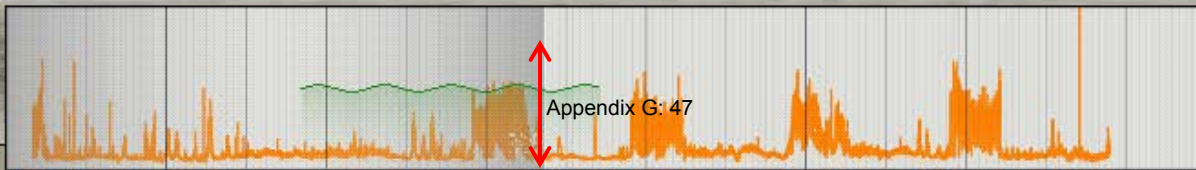
D

Text Size

No sp

Current: 7:41:56.717 PM
12/26/2011

12/23/2011 11:00 AM



RMS_RATIO = 0.72532
1 = 48.514

12/30/2011 11:00 PM

Invoke Editor

Invoke 2D View

Velocity Analysis

Grid

Wells to display

Fractures

Images to display

Formation Tops

Time-line

Real-Time

Fluid Flow

Input Data

ffFmt_2hr_pt03

Load

Color By:

NONE

1

2

Transparent By:

NONE

1

2

Amp

Max. Min



ReColor



Faster

Slower

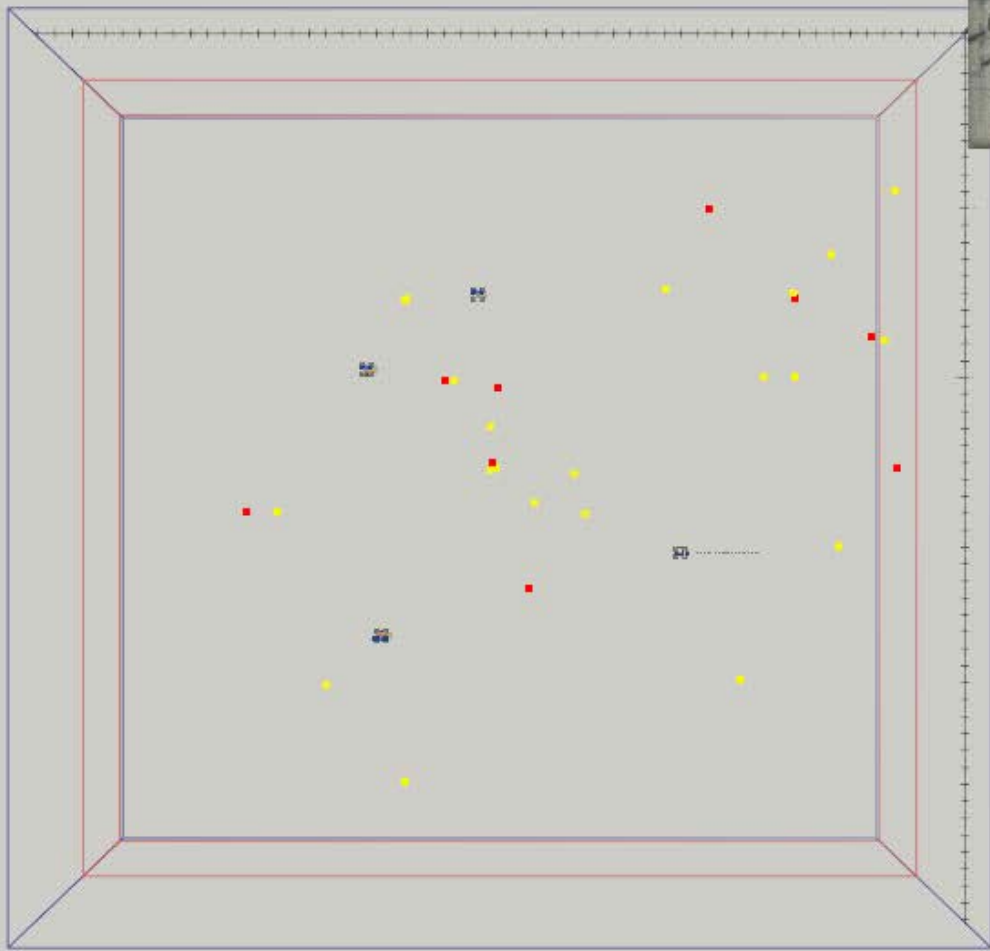
X

Y

D

Text Size

No sp

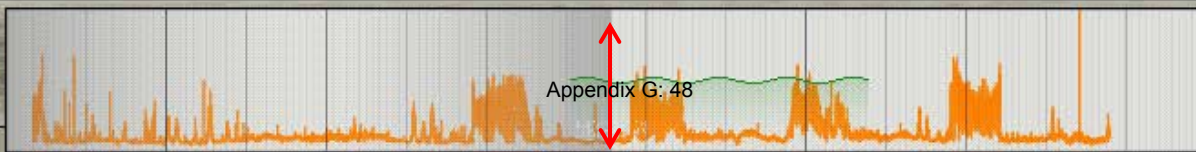


GMT: -6

Current: 5:49:14:407 AM

12/27/2011

12/23/2011 11:00 AM



Appendix G: 48

RMS_RATIO = 0.71187
1 = 48.662

12/30/2011 11:00 PM

Invoke Editor

Invoke 2D View

Velocity Analysis

Grid

Wells to display

Fractures

Images to display

Formation Tops

Time-line

Real-Time

Fluid Flow

Input Data

ffFmt_2hr_pt03

Load

Color By:

NONE

1

2

Transparent By:

NONE

1

2

Amp

Max. Min

ReColor



Faster

Slower

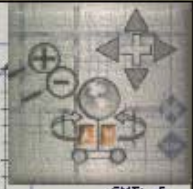
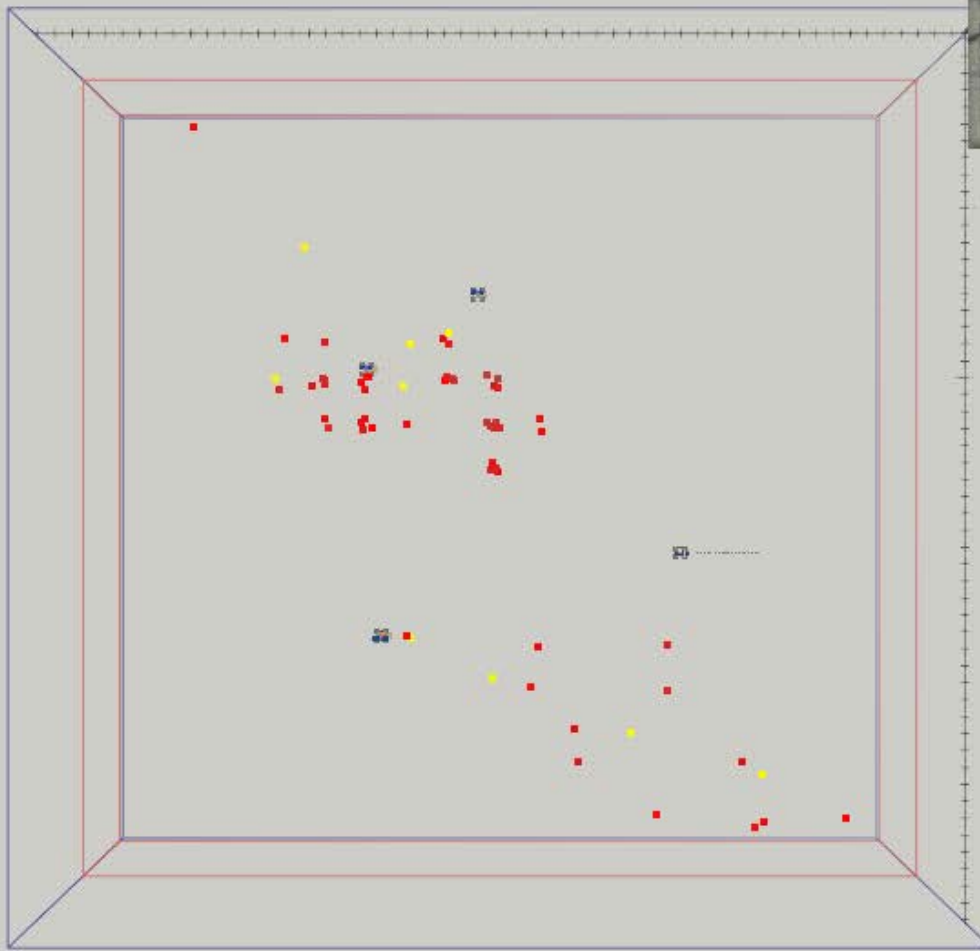
X

Y

D

Text Size

No sp

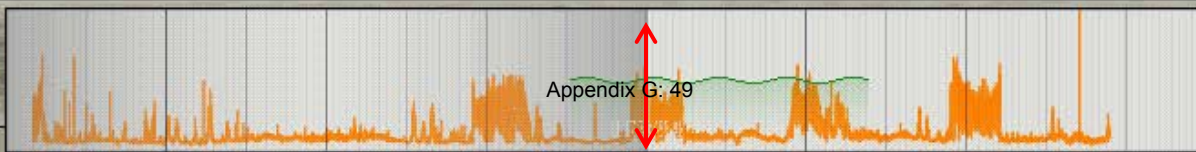


GMT: -6

Current: 11:17:30:455 AM

12/27/2011

12/23/2011 11:00 AM



RMS_RATIO = 0.86044
1 = 51.732

12/30/2011 11:00 PM

Invoke Editor

Invoke 2D View

Velocity Analysis

Grid

Wells to display

Fractures

Images to display

Formation Tops

Time-line

Real-Time

Fluid Flow

Input Data

ffFmt_2hr_pt03

Load

Color By:

NONE

1

2

Transparent By:

NONE

1

2

Amp

Max. Min

ReColor



Faster

Slower

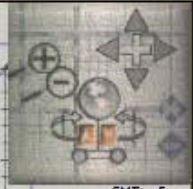
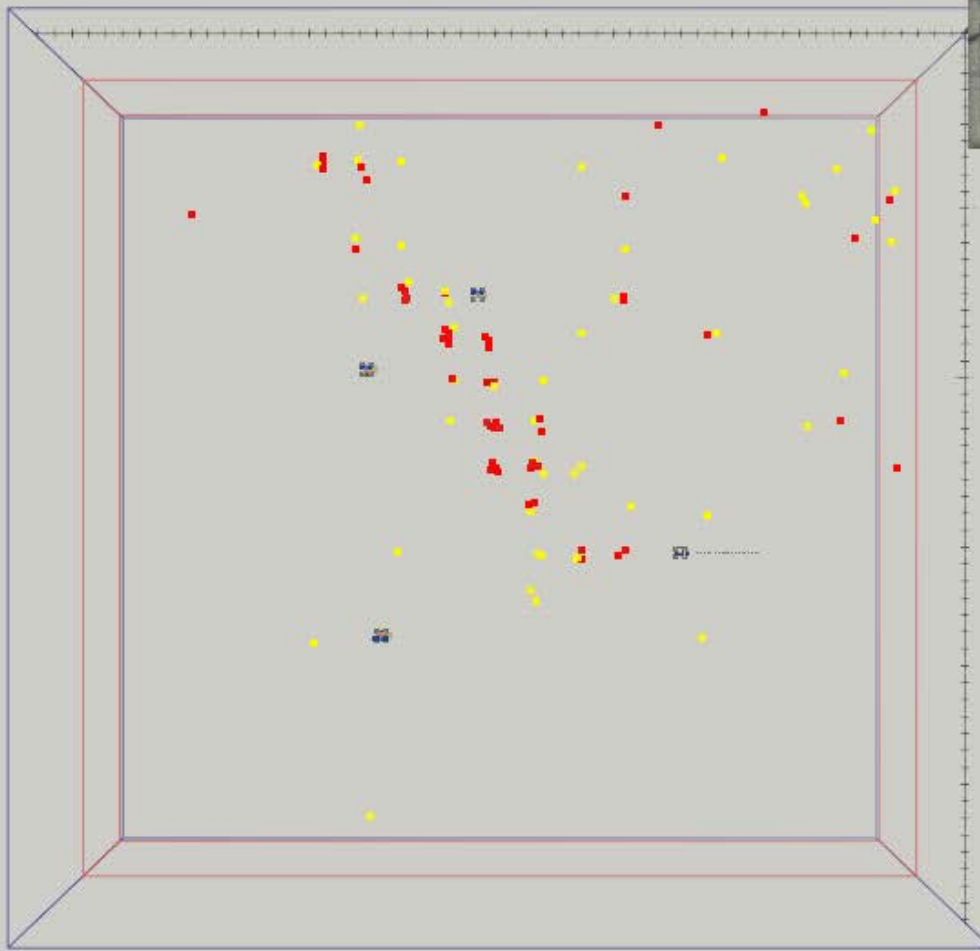
X

Y

D

Text Size

No sp

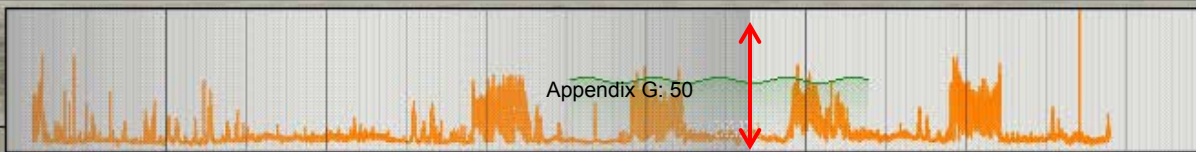


GMT: -6

Current: 2:36:39.392 AM

12/28/2011

12/23/2011 11:00 AM



RMS_RATIO = 1.1379
1 = 48.268

12/30/2011 11:00 PM

Invoke Editor

Invoke 2D View

Velocity Analysis

Grid

Wells to display

Fractures

Images to display

Formation Tops

Time-line

Real-Time

Fluid Flow

Input Data

ffFmt_2hr_pt03

Load

Color By:

NONE

1

2

Transparent By:

NONE

1

2

Amp

Max Min

ReColor



Faster

Slower

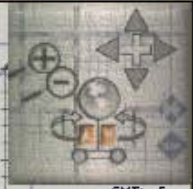
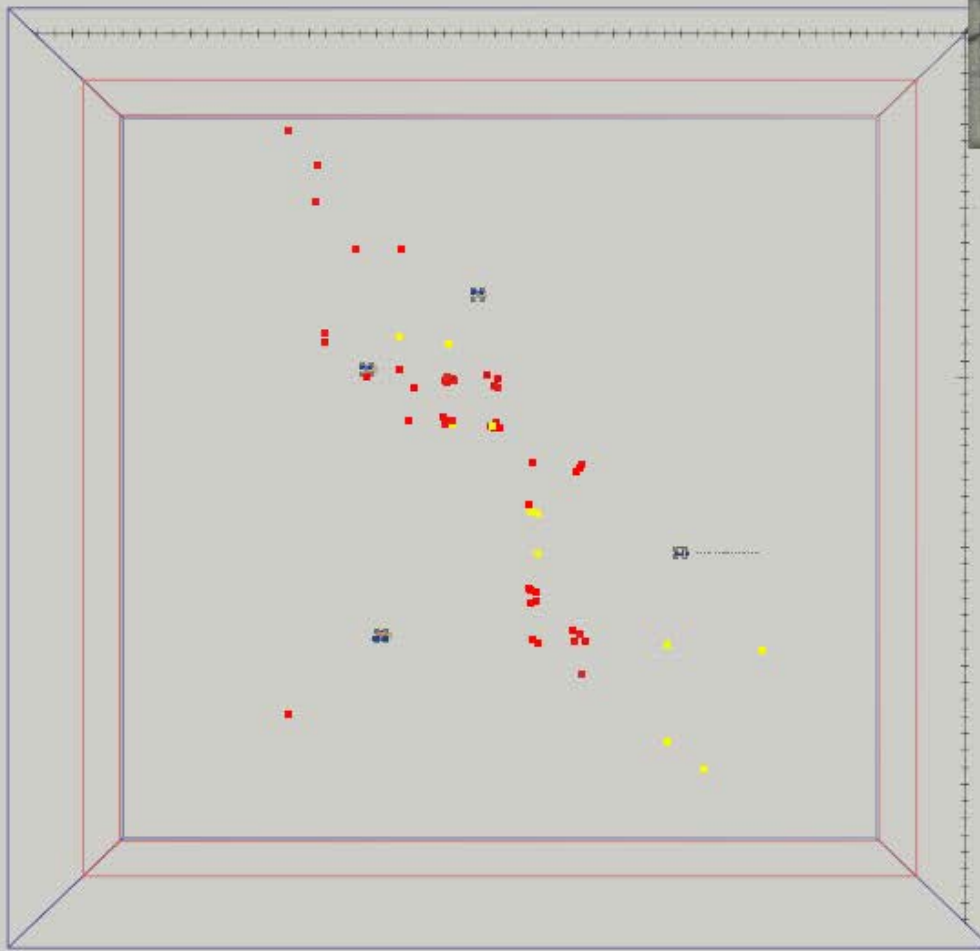
X

Y

D

Text Size

No sp

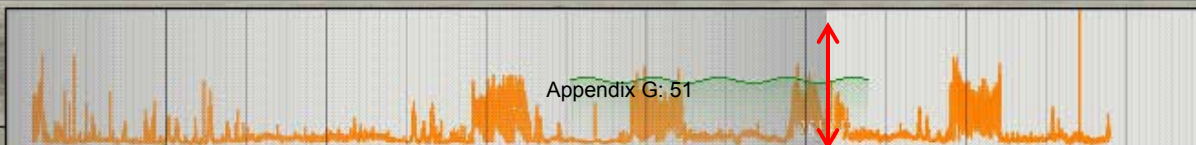


GMT: -6

Current: 2:6:1:94 PM

12/28/2011

12/23/2011 11:00 AM



Appendix G: 51

RMS_RATIO = 1.0522
1 = 48.514

12/30/2011 11:00 PM

Invoke Editor

Invoke 2D View

Velocity Analysis

- Grid
- Wells to display
- Fractures
- Images to display
- Formation Tops
- Time-line
- Real-Time
- Fluid Flow

Input Data

ffFmt_2hr_pt04

Color By:

NONE

1

2

Transparent By:

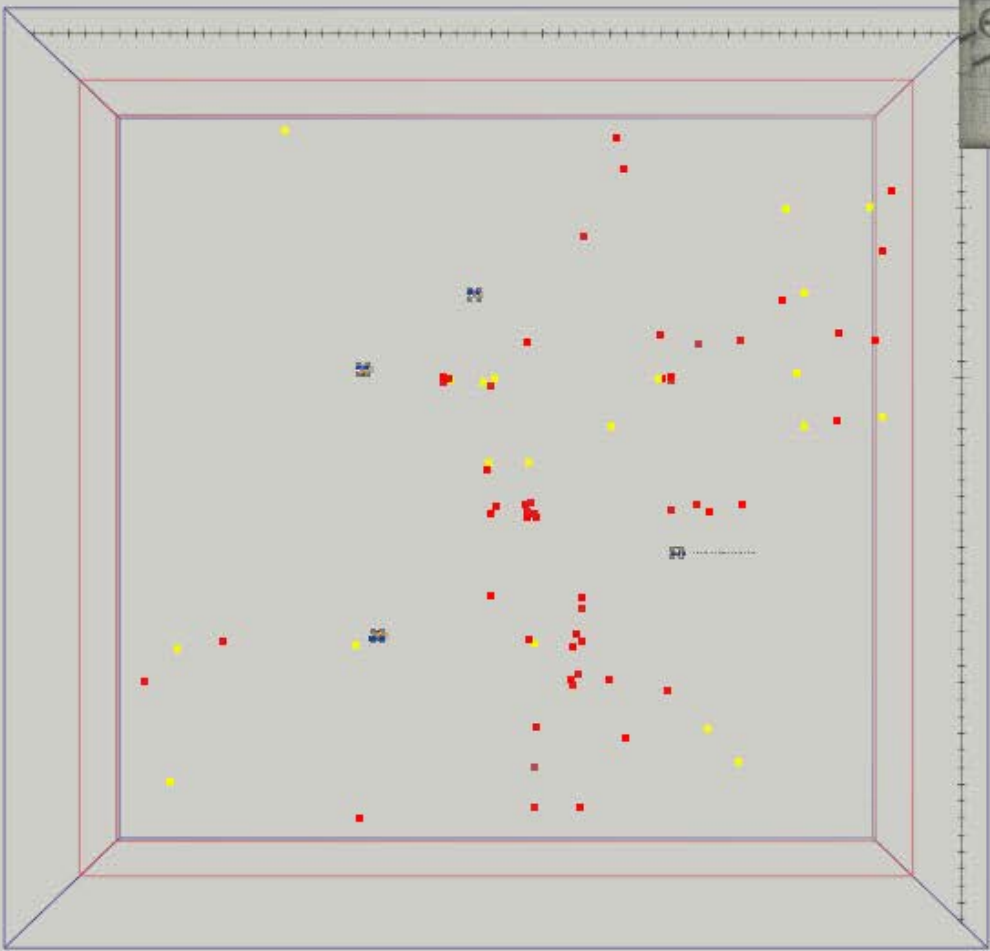
NONE

1

2

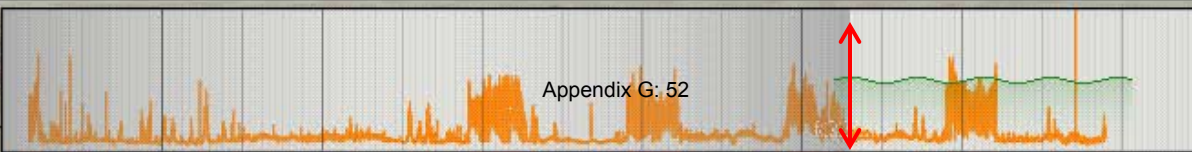
Amp

Max Min



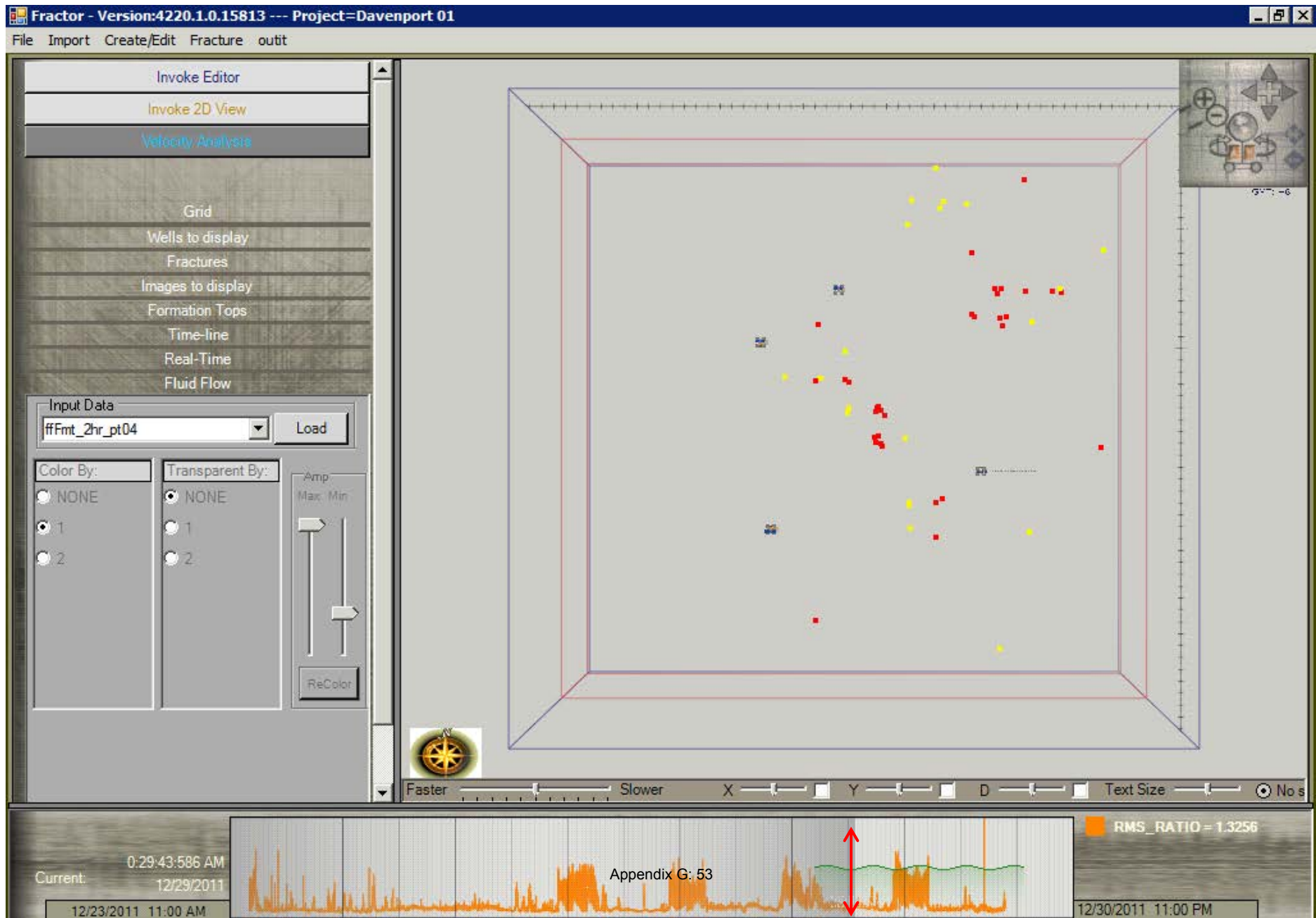
Faster Slower X Y D Text Size No s

Current: 6:12:13:130 PM
12/28/2011
12/23/2011 11:00 AM



RMS_RATIO = 1.1023
1 = 51.176
12/30/2011 11:00 PM

This time frame shows the NE activity at a relatively high level.



Invoke Editor
Invoke 2D View
Velocity Analysis

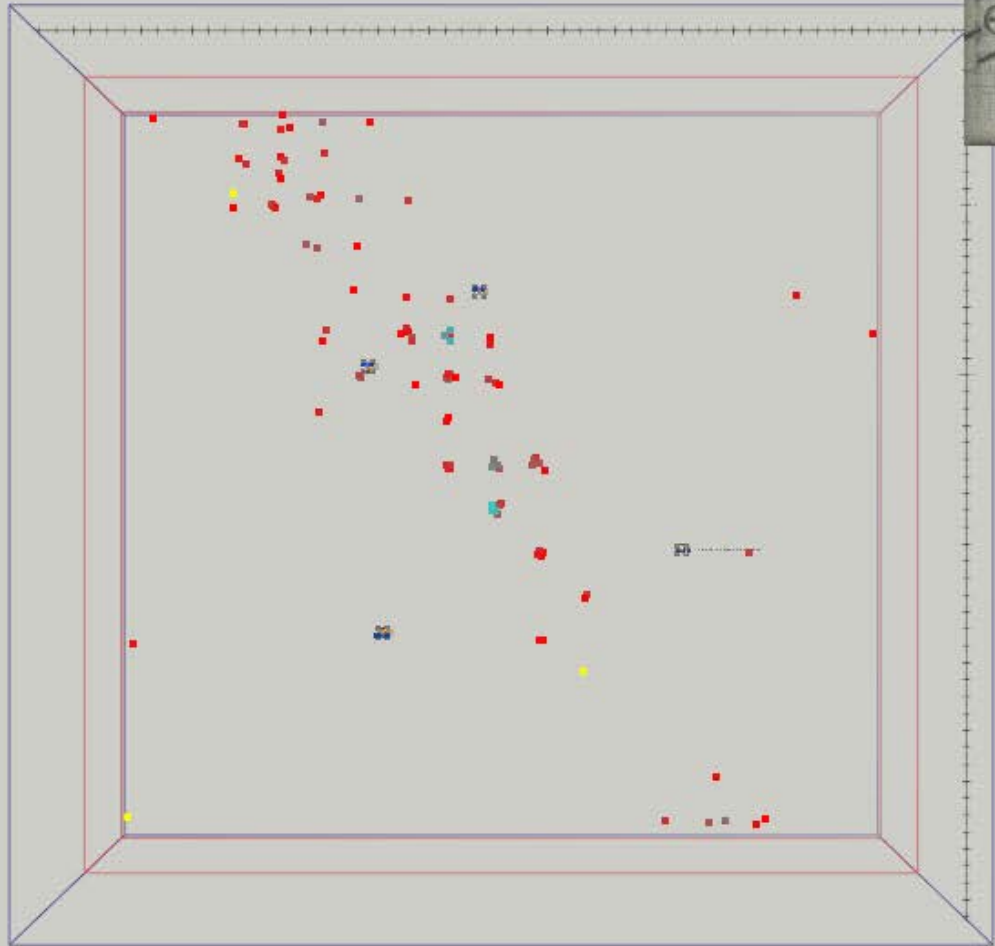
Grid
Wells to display
Fractures
Images to display
Formation Tops
Time-line
Real-Time
Fluid Flow

Input Data
ffFmt_2hr_pt04 Load

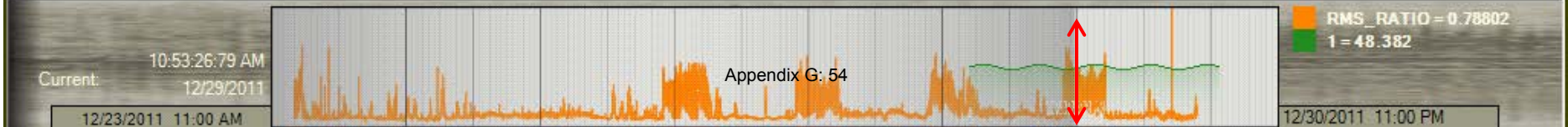
Color By:
 NONE
 1
 2

Transparent By:
 NONE
 1
 2

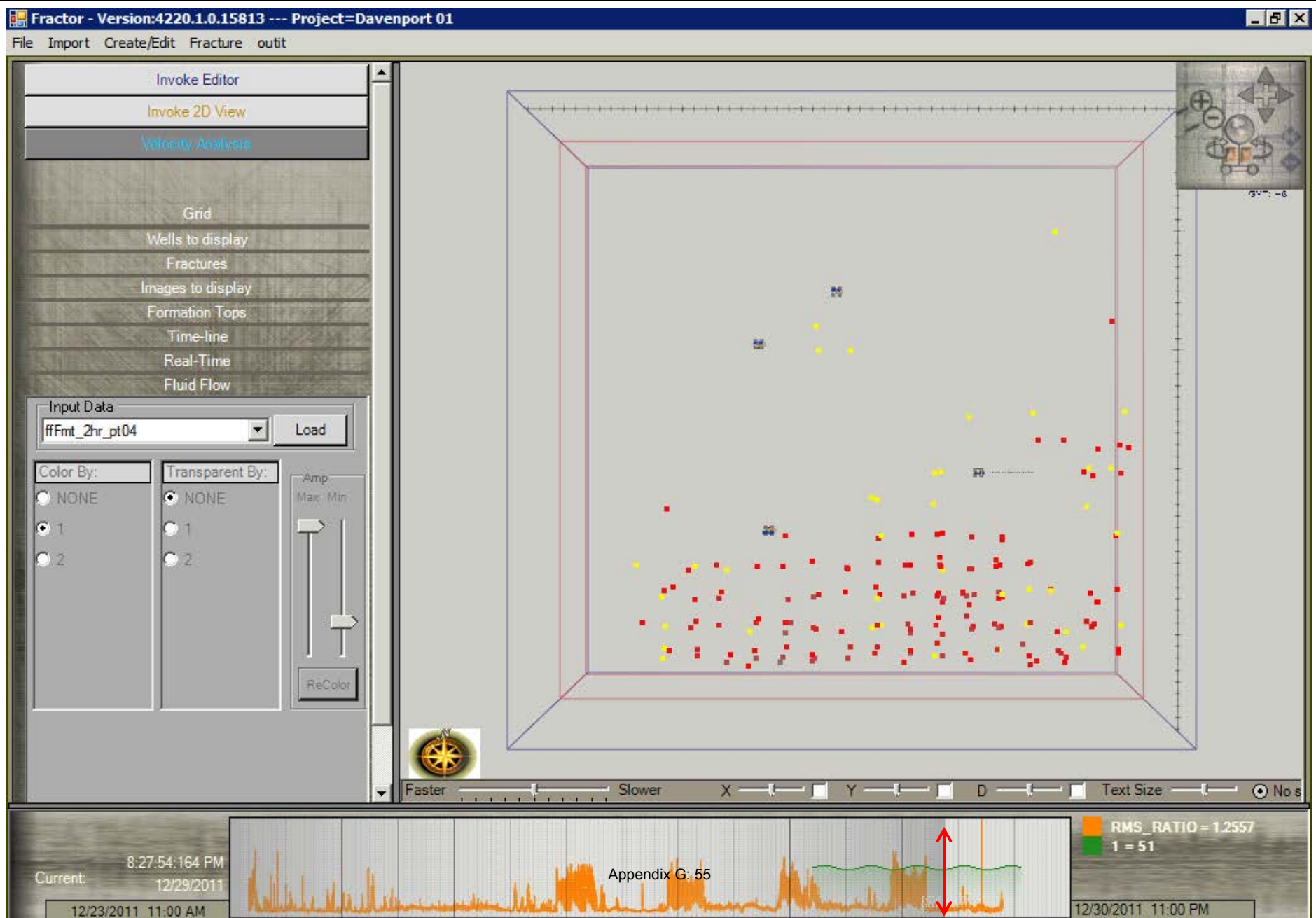
Amp
Max Min
ReColor



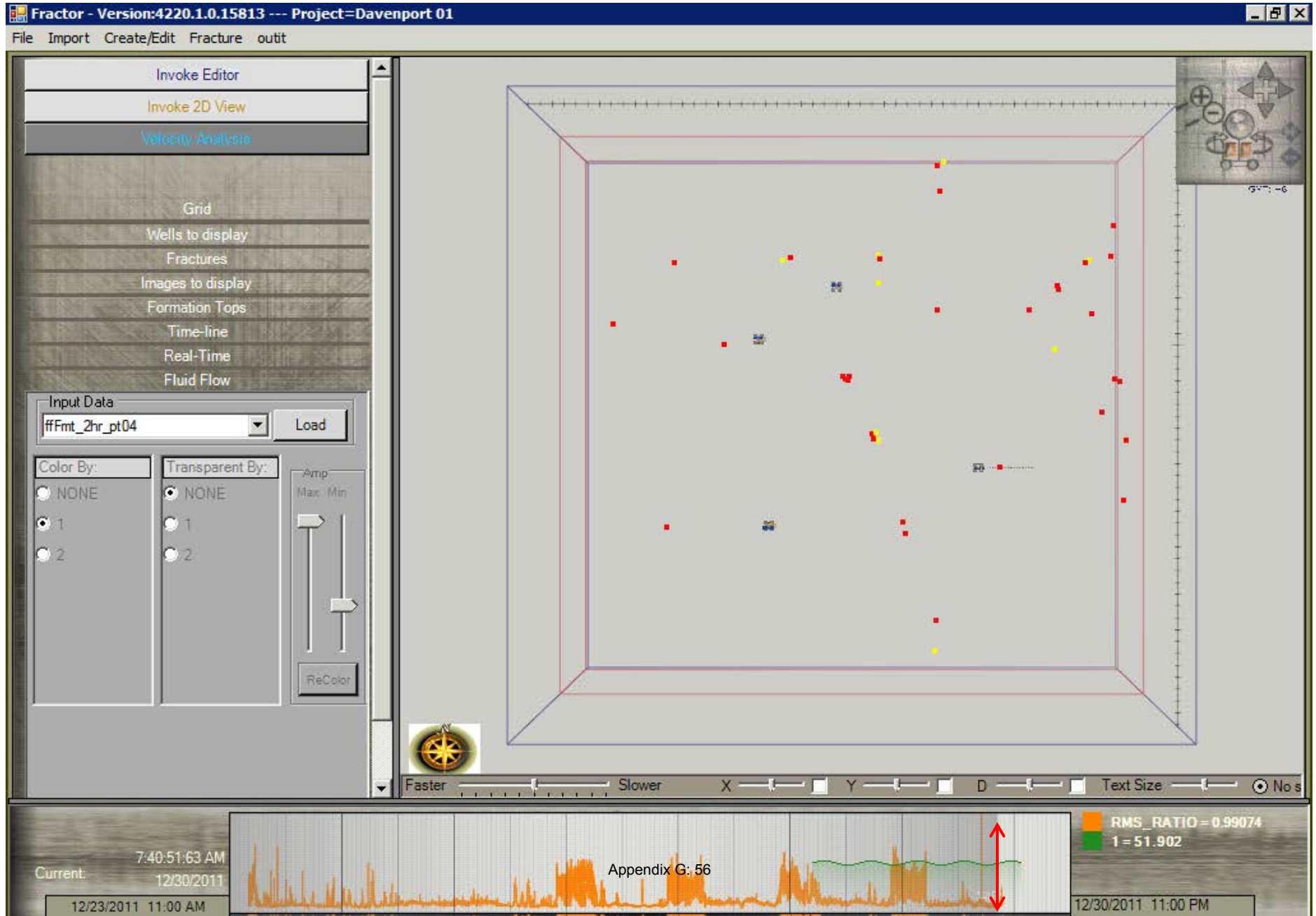
Faster Slower X Y D Text Size No s



Apparently there was some interference from the south that occurred for several hours. It is not obvious from the field data what the source of the energy was but it dominated the image.



The final frame of the survey shows a return to the NW-SE trend at some level with continued energy in the NE quadrant.



Time snapshots: side view

The following five slides show a combination of map and side view images of LASEA output from the Davenport Newberry Volcano project at sequential time periods near the beginning of the survey. The map view for each time frame is shown just before the slide that contains the side view. The views are time-equivalent within a few seconds of one another.

Side views show the vertical extent of the most anomalously high energy measurements.

Pay attention to the caption at the top of each slide for the date and time and an explanation of what is shown.

Invoke Editor
Invoke 2D View
Velocity Analysis

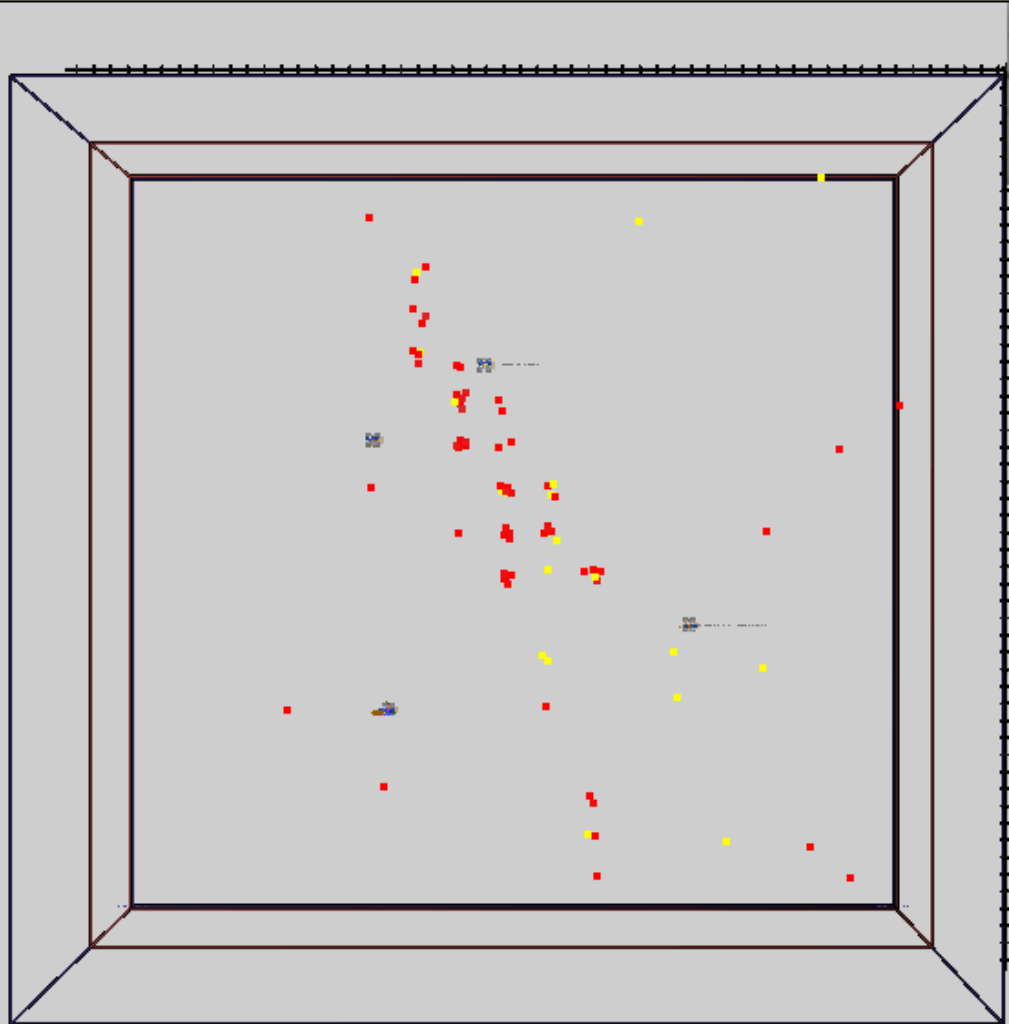
Grid
Wells to display
Fractures
Images to display
Formation Tops
Time-line
Real-Time
Fluid Flow

Input Data
ffFmt_2hr_pt01 Load

Color By:
 NONE
 1
 2

Transparent By:
 NONE
 1
 2

Amp
Max Min
ReColor



Faster Slower X Y D Text Size No spi

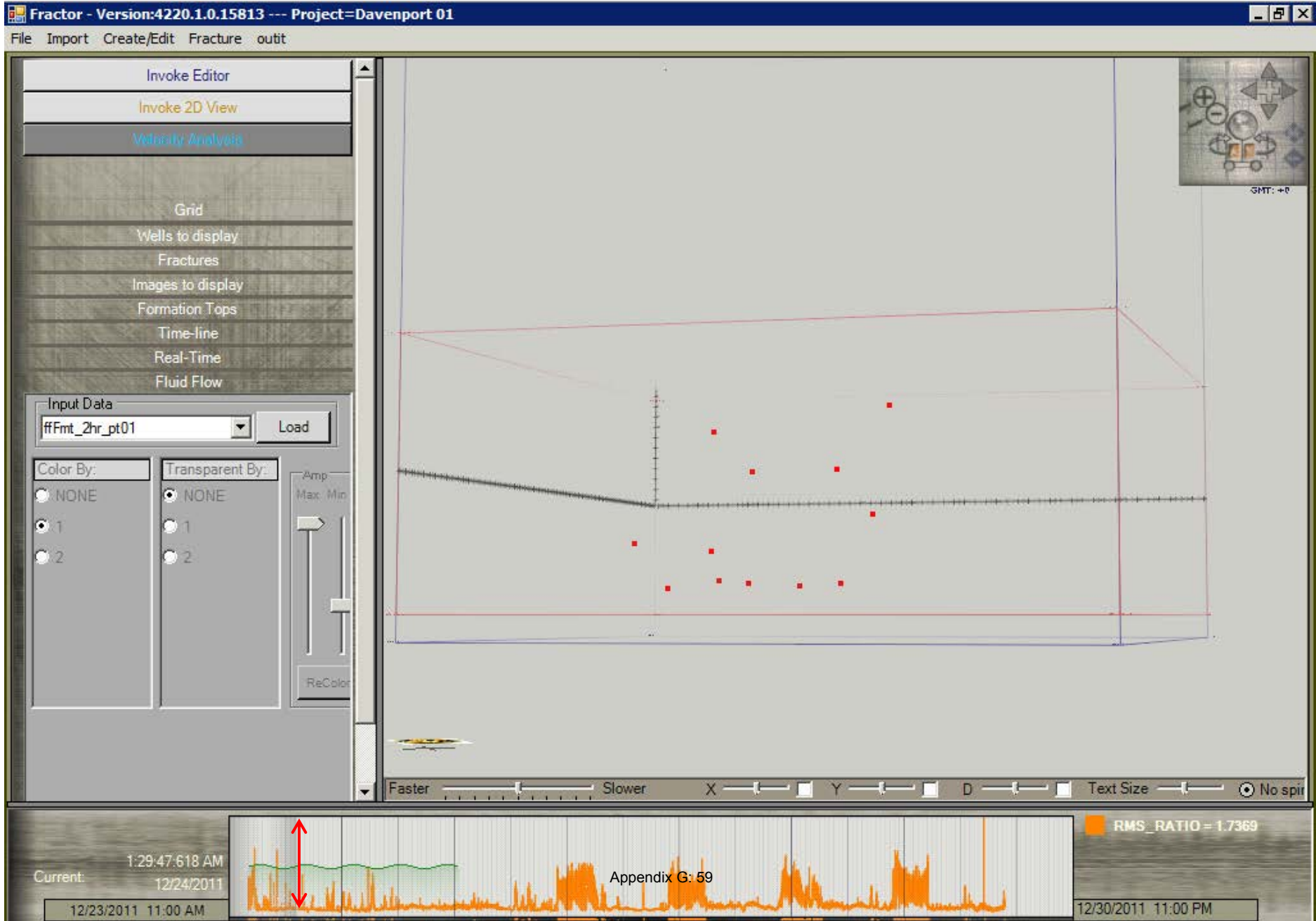
Current: 1:29:54.528 AM
12/24/2011
12/23/2011 11:00 AM

Appendix G: 58

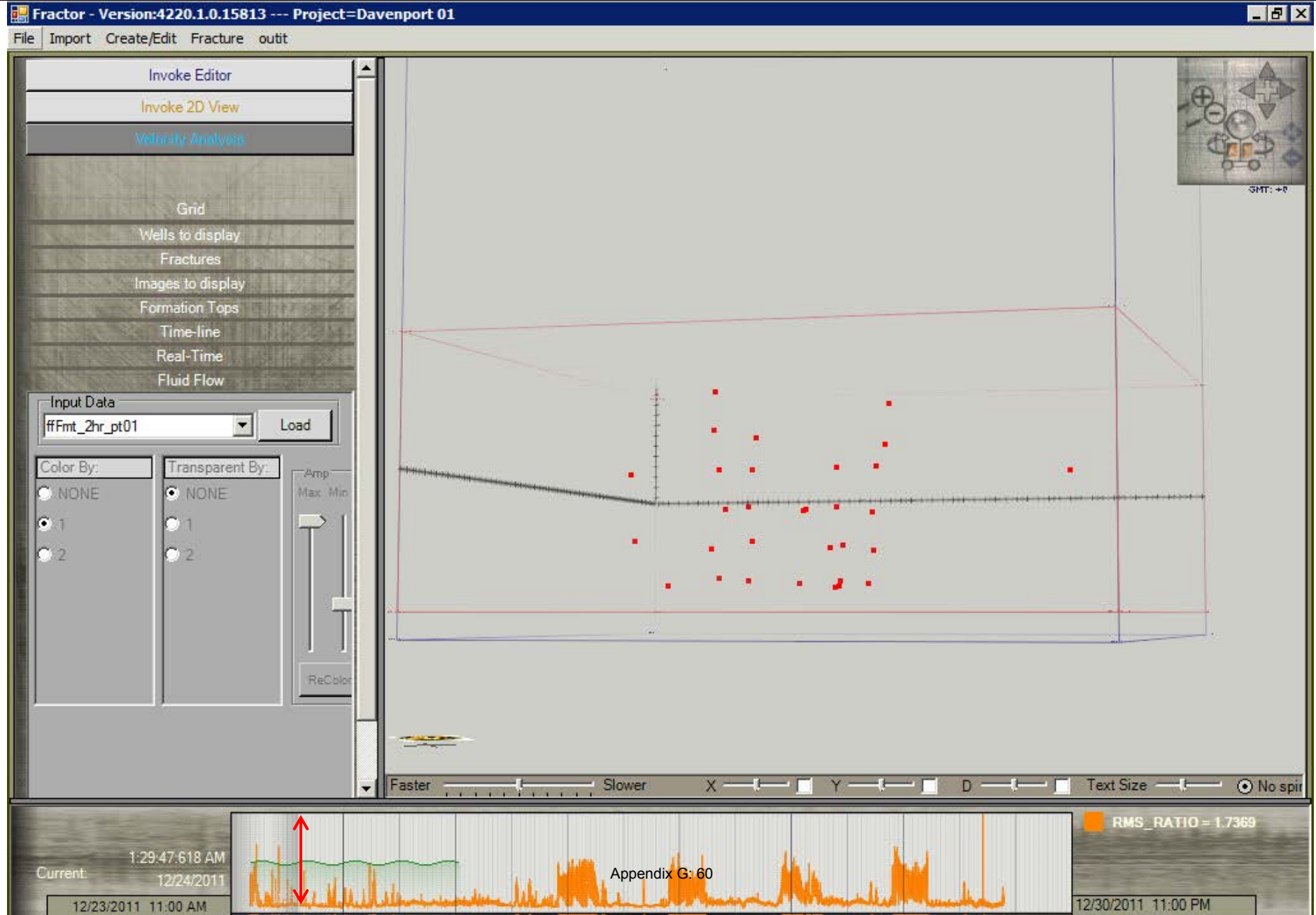
RMS_RATIO = 0.73843
1 = 50.209

12/30/2011 11:00 PM

The bottom section contains a real-time data plot with an orange waveform and a green horizontal line. A red double-headed arrow indicates the amplitude of the waveform. The plot is labeled 'Appendix G: 58'. To the right, there are two colored squares (orange and green) with associated numerical values: 'RMS_RATIO = 0.73843' and '1 = 50.209'. The bottom right corner shows the date and time '12/30/2011 11:00 PM'. The bottom left corner shows the current time '1:29:54.528 AM' and date '12/24/2011', along with a timestamp '12/23/2011 11:00 AM'.



Side view December 24, 1:29 AM – edited to include more of the highest energy points. In other words this view includes all of the points from the previous slide plus some lower energy points than the previous slide.



Invoke Editor
Invoke 2D View
Velocity Analysis

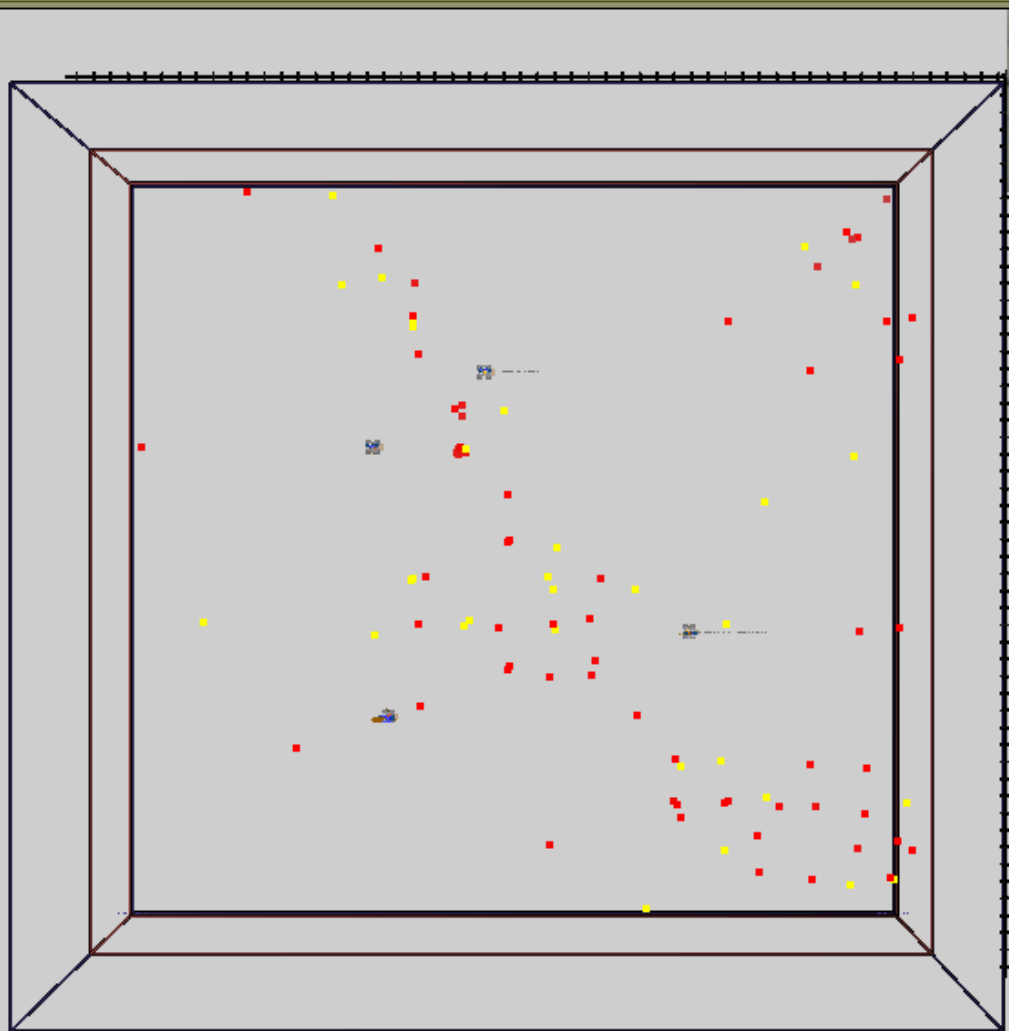
Grid
Wells to display
Fractures
Images to display
Formation Tops
Time-line
Real-Time
Fluid Flow

Input Data
ffFmt_2hr_pt01 Load

Color By:
 NONE
 1
 2

Transparent By:
 NONE
 1
 2

Amp
Max Min
ReColor

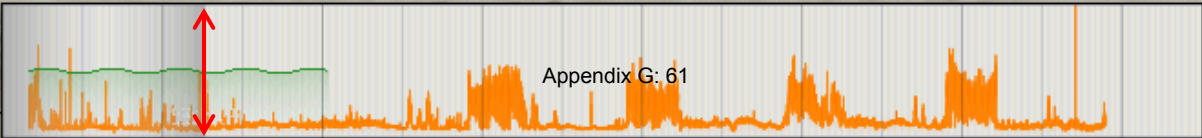


SMT +E

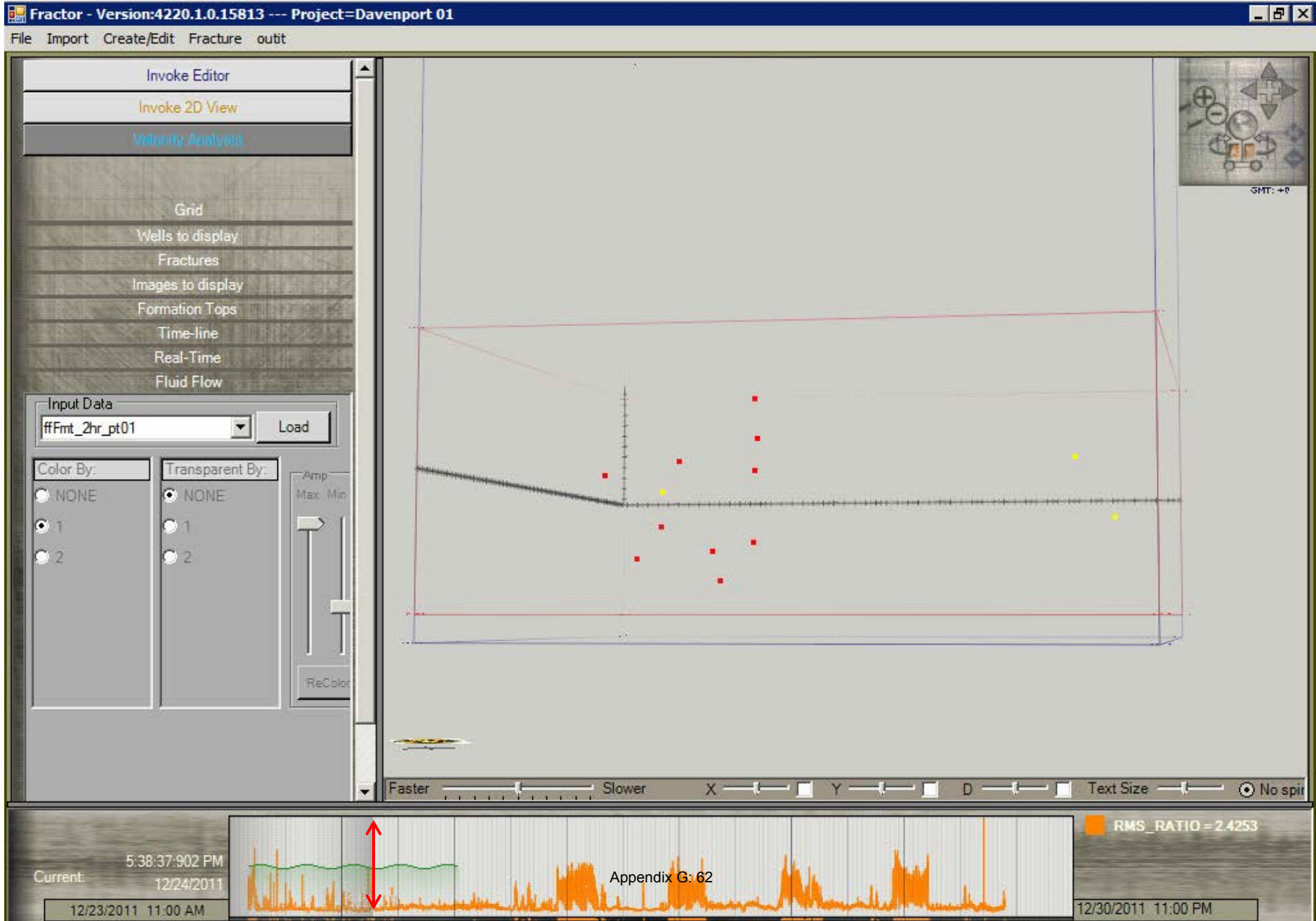


Faster Slower X Y D Text Size No spi

Current: 5:38:17:872 PM
12/24/2011
12/23/2011 11:00 AM

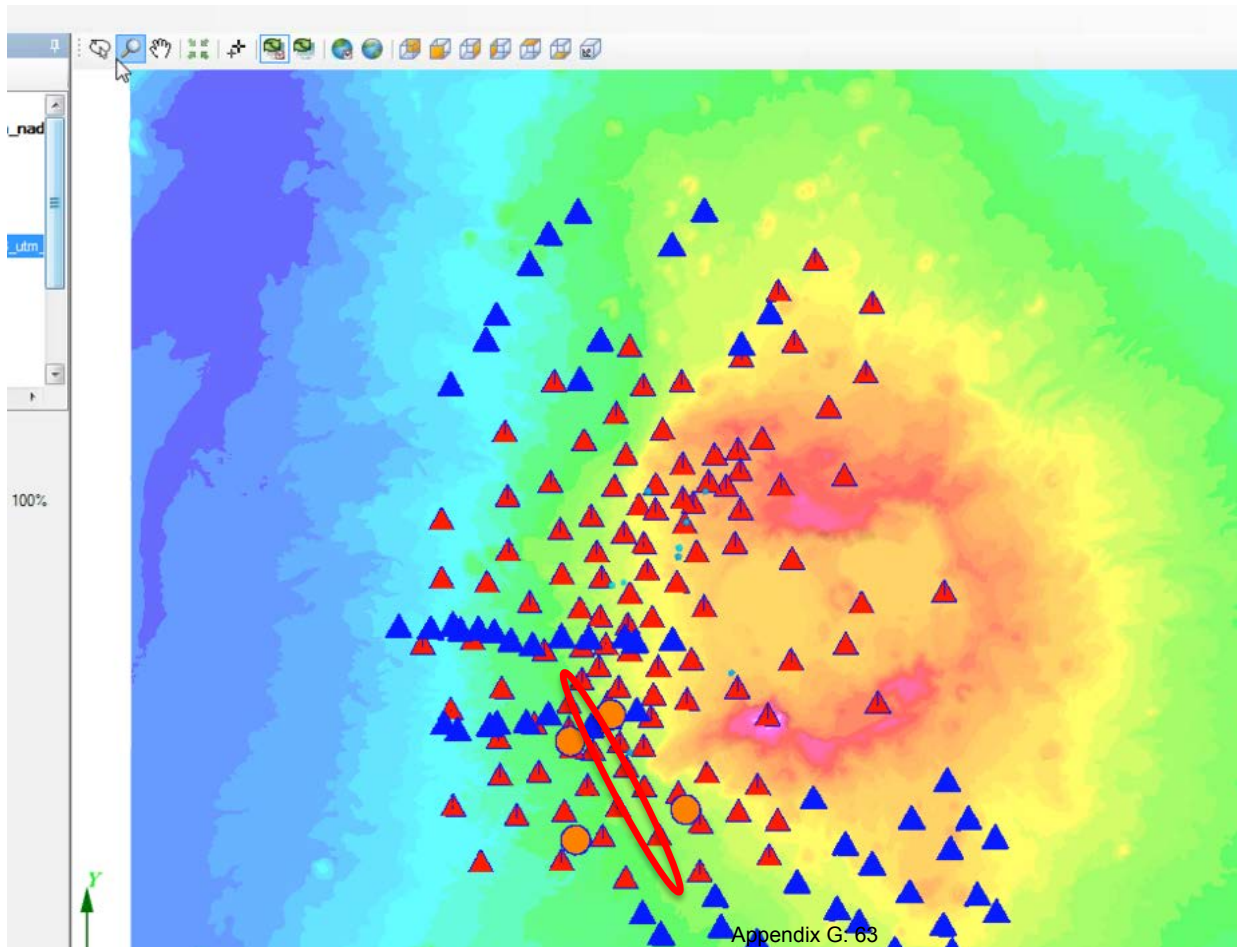


RMS_RATIO = 1.5173
1 = 48.382
12/30/2011 11:00 PM



Comments from data analyst

Geophysical data is rarely definitive in explaining or expressing the entire geological story of a particular location. A more complete picture is always obtained by integration of multiple datasets and observations. Multiple independent datasets that show similar features provide some level of confidence in the results of individual datasets. The MT result for example is shown below with the observation well locations (orange dots) and the orientation of the NW-SE seismic energy trend as a red ellipse. The seismic ellipse is largely in alignment with the MT contours. Both MT and seismic alignments are tangential to the crater outline which one might expect faulting related to the volcanic crater to exhibit as in ring faults that surround Calderas in Colorado for example.



Comments from data analyst continued

Further work of this kind would appear to be warranted in terms of results. There are clearly subsurface zones that have substantially higher passive seismic energy output as a function of time. These may be zones that are more likely to yield high levels of heat and/or hot water under the assumption that the anomalous seismic activity is related to volcanic activity.

Anticipated future data processing work

The completion of data acquisition (December, 2011), delivery of the data processing report, raw field data, and ASCII list of high amplitude energy locations completes the terms of the contract. We at APEX HiPoint find this project to be interesting and want to continue contributing to the result in at least the following ways:

- 1) LASEA (Low Amplitude Seismic Emission Analysis) analysis of the data in different frequency bands.
- 2) Investigation of specific 20-30 minute high-energy time periods during which there is elevated RMS amplitude but that are outside normal times when man-made seismic noise is expected. These may be time periods more likely to be naturally occurring events without man-made seismic interference.
- 3) Possible improved 3D visualization of energy locations. In the past week our company has become a member of the Sigma³ group of companies <http://www.msnbc.msn.com/id/46807453>. The Sigma³ companies have some excellent visualization tools which we have already begun integrating into the LASEA workflow. We hope to be able to provide displays from these tools using the Davenport data within a few months.
- 4) Higher resolution calculations from the same dataset that may include improved focusing and smaller grid spacing. The current grid spacing is 600 ft. With improved display tools we should be able to shrink that spacing to 100 ft or less.

PROTECTED RIGHTS NOTICE

These protected data were produced under agreement no. DE-EE-0002833 with the U.S. Department of Energy and may not be published, disseminated, or disclosed to others outside the Government until five (5) years from the date the data were generated, unless express written authorization is obtained from the recipient. Upon expiration of the period of protection set forth in this Notice, the Government shall have unlimited rights in this data. This Notice shall be marked on any reproduction of this data, in whole or in part. Protected to: 12/13/2017

Final Report Davenport Newberry Volcano Passive Seismic Monitoring

December 13, 2012



Now a SIGMA³ Company

SIGMA³

Project History

Davenport Newberry Holdings hired APEX HiPoint, LLC (now a SIGMA³ company) to record and process passive seismic data at the Newberry Volcanic area near Bend, Oregon (central Oregon). Continuous seismic data was recorded in each of 4 instrumented observation wells for 6 days and 17 hours between December 23, 2011 and December 30, 2011. Maps of the well locations are shown on the following two slides. Each observation well contained 11, 12, or 13 3-component digital geophone sondes spaced at 50 ft. The geophones sondes were manufactured by GeoSpace of Houston, TX and are high-grade digital instruments used by the APEX group of SigmaCubed for passive microseismic work in the oil and gas industry. The purpose of recording the data was to determine 1) if areas of anomalously high levels of seismic energy could be detected and located and 2) if such areas could be detected, what would the characteristics of the anomaly be such as spatial extent, time variance of amplitude, and seismic frequency dependence.

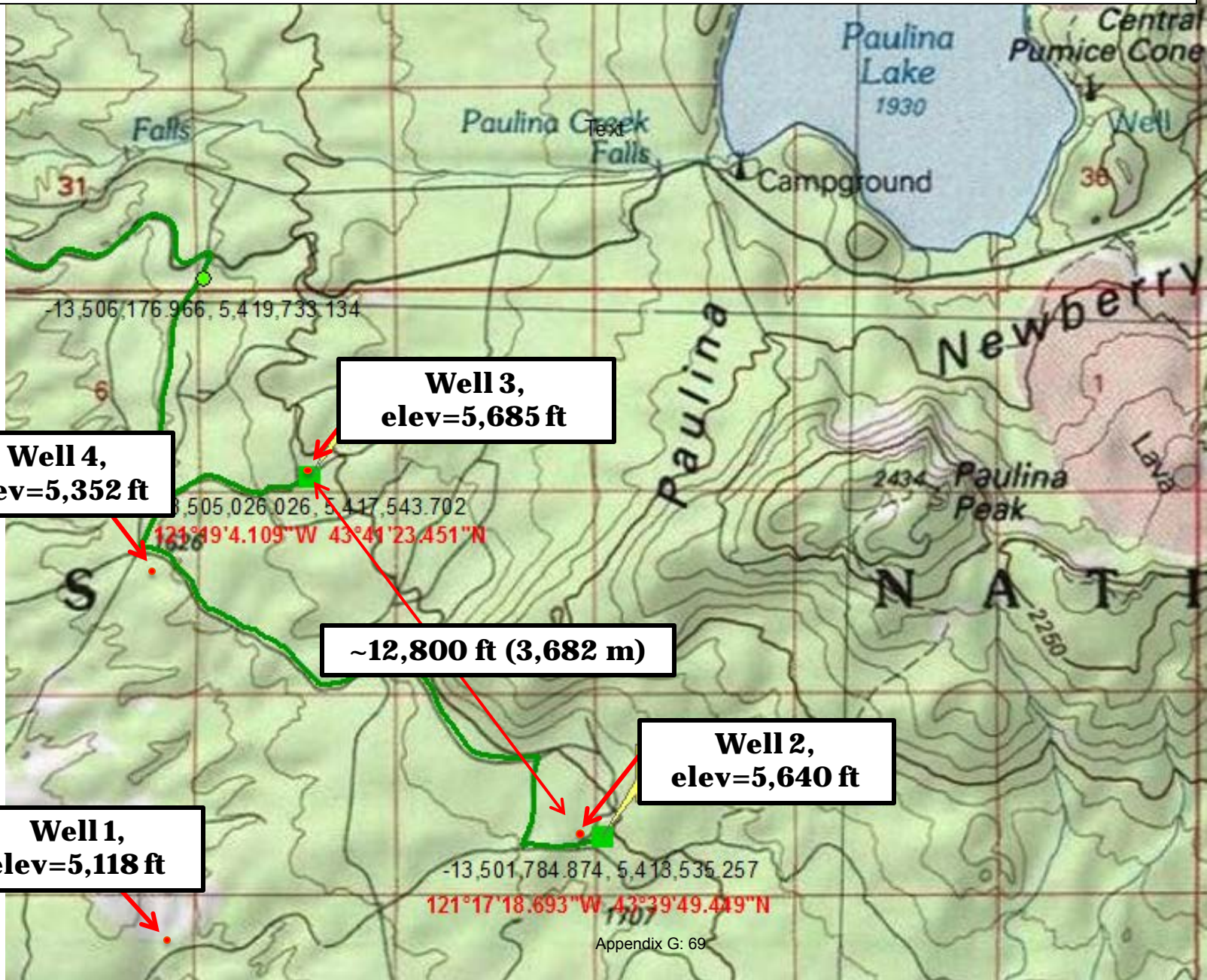
APEX's data processing technology, including "Low Amplitude Seismic Emission Analysis" (LASEA) previously known as "Fluid Flow Analysis", was employed to achieve the goals of the survey. A basic assumption is that areas of anomalously high persistent seismic wave emission are probably associated with subsurface fluid movement or high variations in heat flow that cause stress changes in the rock mass and thus seismic emissions. The acronym "LASEA" was adopted as we recognized that Fluid Flow or fluid movement is probably not the only source of persistent low-amplitude seismic wavefields.

The first LASEA analysis was completed in April, 2011 with an initial grid volume from 5,000 ft depth to 11,000 ft depth. However, Davenport requested that the analysis volume be increased to include from 3,000 ft depth to 20,000 ft depth so the calculations were repeated with a larger volume. The second set of calculations include application of a new data filter that suppresses noise based on adaptive filtering between vertical and horizontal geophone components. The filter improved the clarity of the NW-SE energy trend that was evident in the first pass of data processing.

Satellite view with instrument well locations (Well 1,2,3&4).



Topographic map at approximate alignment with satellite view and well locations.



Appendix G: 69

Basic Information About the Seismic Data

The survey data was continuously recorded but broken up into records of 10-seconds in length for convenience in handling the data. The last sample of one record is followed by the first sample of the next record and the sequential samples are recorded precisely 0.5 milliseconds apart. Each 10-second record contains a 10-second long data trace for EACH of the 141 geophones (47 3-component geophone sondes) that was deployed. The start time of each data trace is precisely synchronized to the same time. The record times are synchronized with a GPS satellite and is accurate to within a fraction of a microsecond.

Information for absolute comparisons of recorded data amplitudes

Seismic data amplitudes can carry important information. Data amplitudes as recorded by seismic instruments are a function of the instrument design and gain (amplitude multipliers) that are applied to data before being recorded. Specifications for the recording instruments used are given below with the information needed by seismologists to be able to directly compare amplitudes recorded by varying instruments.

Specifications

Frequency	4.5 Hz	8 Hz
Natural Frequency (Fn) ±.75 Hz	4.5 Hz	8 Hz
Fn tolerance at tilt	± 1.25 Hz	± 1.25 Hz
Tilt, vertical geophone	10°	20°
Tilt, horizontal geophone	±1.25°	±3.5°
Resistance		
Standard Coil Resistance	380 Ω ±5%	
Distortion		
Harmonic Distortion with coil to case velocity of 0.7 in/s (1.8 cm/s) p-p	N.S.	<0.20% @12 Hz
Sensitivity		
Intrinsic Voltage Sensitivity (G)	.81 V/in/s, (.32 V/cm/s) ± (10%)	
Normalized Transduction Constant	.0416 √DCR V/in/s. (.0164 √DCR V/cm/s)	
Damping		
Open Circuit Damping (Bo)	.34 ±20%	.39 ±10%
Damping Constant (B _c R _t)	762	602

Specifications at 25°C. Orientation is operating position (vertical or horizontal) unless otherwise

Internal to the sonde, there were actually two geophones for each component wired in parallel. The impedance is ½ of the value shown and sensitivity is 2 times the value shown. Voltage sensitivity is 1.62 V/in/s and Normalized Transduction Constant is 0.832 V/in/s.

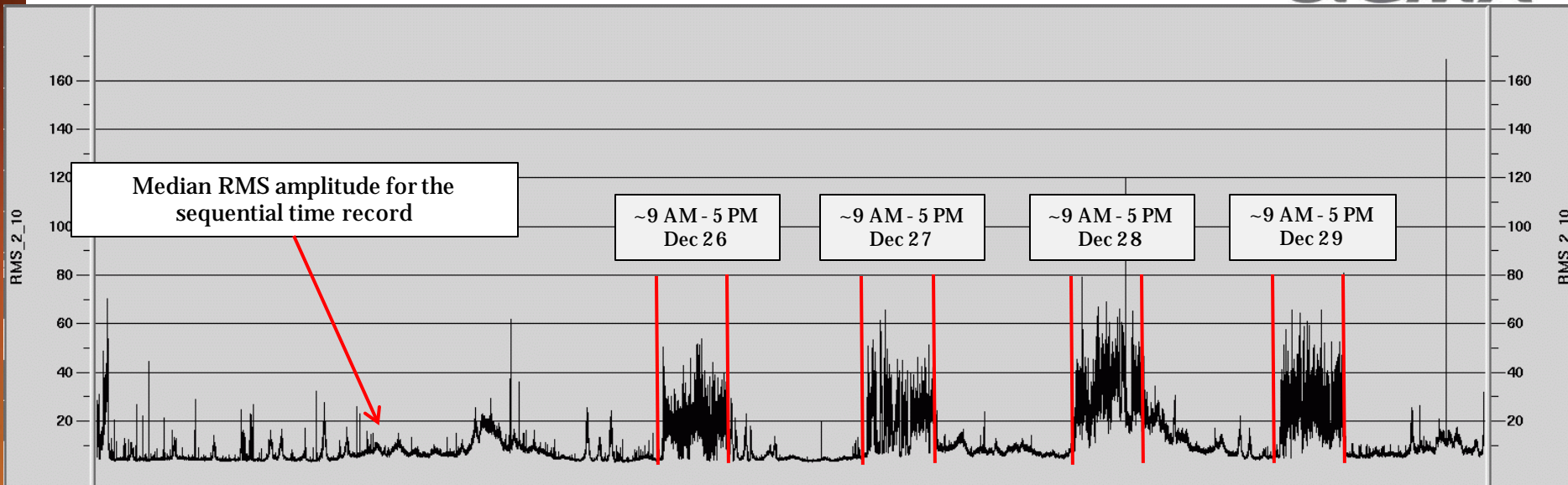
Ambient Seismic Measurements

Variations through time in ambient (background) seismic energy can be useful in understanding components of cultural and naturally-occurring seismic energy sources. The Root Mean Squared (RMS*) amplitude of the data was computed for the entire time length of the of the survey and plotted as one of the data attributes. The following slide shows the Median RMS amplitude computed at 10-second intervals for the entire 6 day, 17 hour survey. A bandpass filter of 2-10 Hz (this filter preserves frequencies in the band 2-10 Hz) was applied to the data before computation of the RMS amplitude. A second computation was also done for a higher frequency band and is discussed later.

*The Root Mean Squared (RMS) amplitude is computed at 10 second intervals for this dataset in the following way. First, the sum of squared data trace amplitudes was computed for each 10-second long data trace in a data record. The square root of the summed squared values was then computed. For example, for this dataset each 10-second data record contained 138 data traces (46 sondes times 3 data traces per sonde). Each of the data traces in a 10-second record contained 20,000 data samples. The RMS value (square root of the sum of squared amplitudes) was computed for each data trace in the 10-second record, thus this part of the operation resulted in 138 RMS values, one for each respective input data trace.

The second step in the operation was to compute the median RMS value from the 138 RMS values derived above. The median computation results in a single output value that represents the RMS amplitude of the 10-second data record from which the RMS value was derived. The median computation avoids having a small number of noise bursts dominate the amplitude measurement.

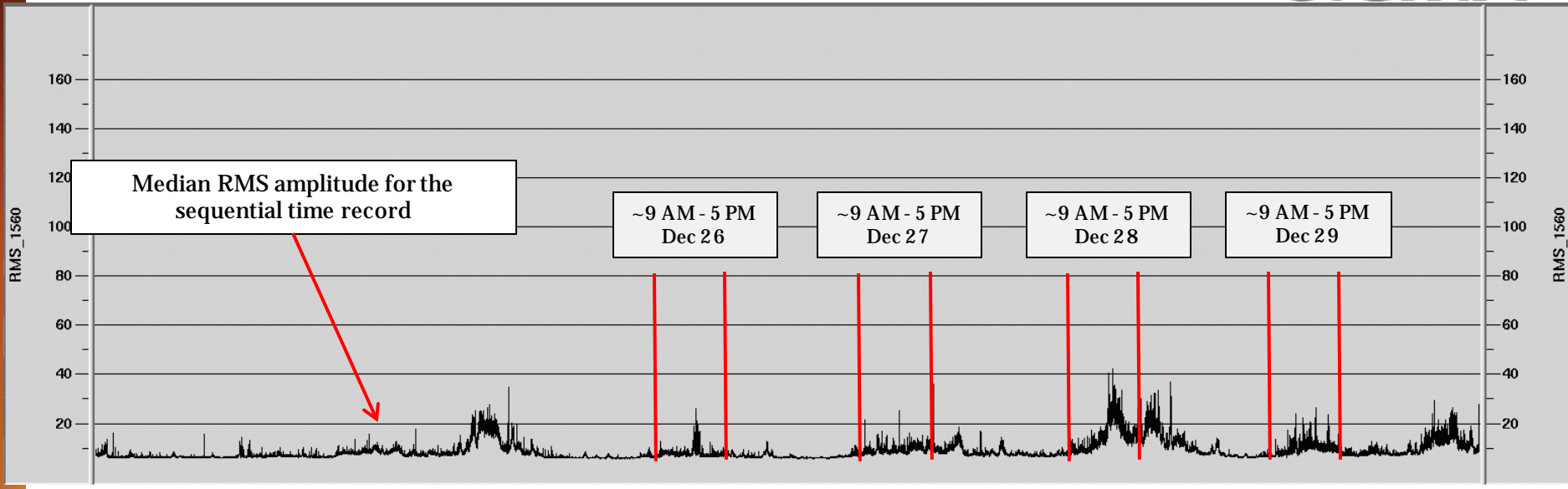
Root Mean Squared (RMS) amplitude 2-10 Hz for entire duration of survey



Julian day (GMT) →

In the 2-10 Hz frequency bandwidth, there is a significant rise in ambient RMS amplitude that is in the 9:00 AM to 5:00 PM time frame which is clearly cultural. Interestingly, the nearest significant human population to the field site is La Pine, Oregon which is 12 miles away from the field site and with a population of only 1,700.

Root Mean Squared (RMS) amplitude 15-60 Hz for entire duration of survey

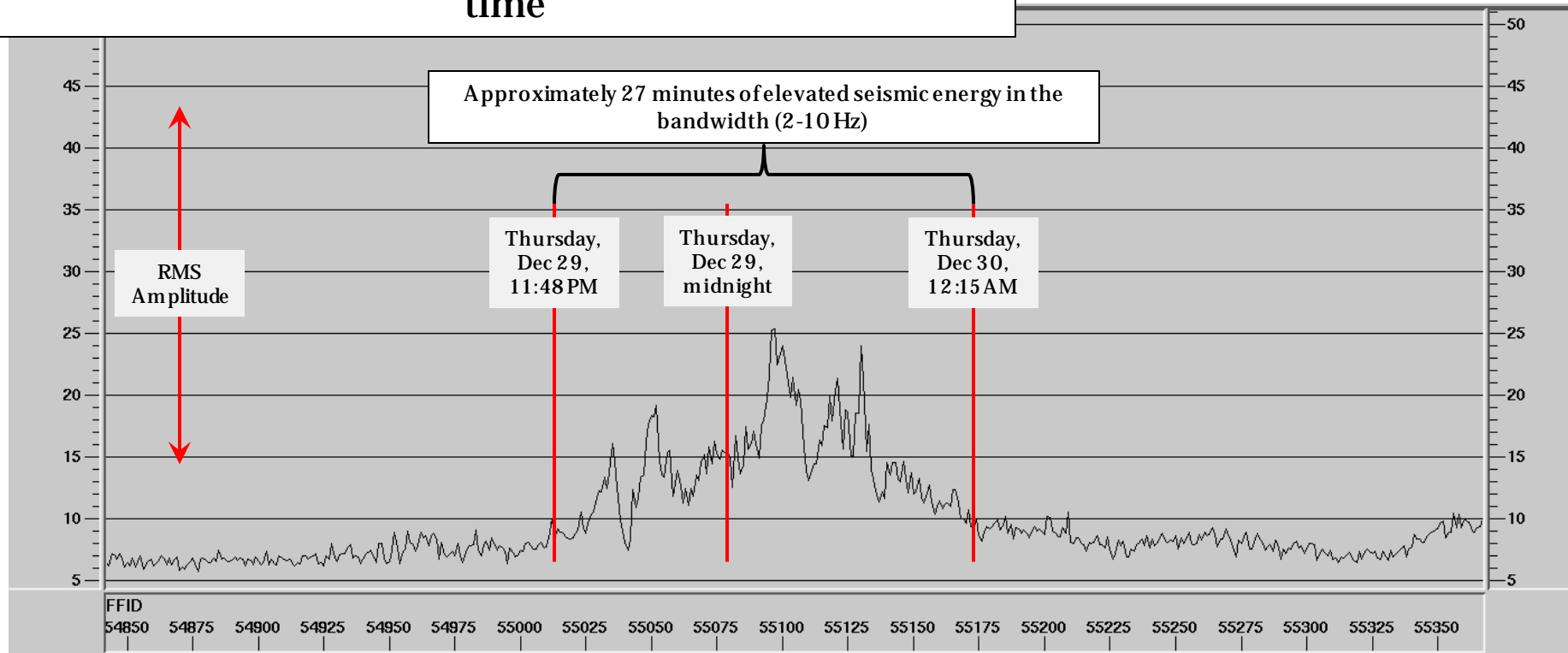


Time (the Julian day of the records are labeled)

We repeated the calculations from the previous slide using data to which a bandpass filter that preserved frequencies between 15 and 60 Hz had been applied. The plot above is on the same scale as the previous slide (2-10 Hz preserved) from which we can see that there is a significant amount more energy in the 2-10 Hz bandwidth than the 15-60 Hz bandwidth during the high-amplitude periods. The rest of the time there is about the same amount of energy in these two bandwidths. The LASEA analysis of the data was conducted on the data with 15-60 Hz bandpass filter to avoid interference from low-frequency cultural noise in the 2-10 Hz bandwidth.

Note that even though this band includes 60 Hz signal it is not necessary to assume that the contribution at 60 Hz is due to 60 Hz electrical noise (the frequency at which US electrical power operates). The equipment used to record the data is nearly immune to 60-cycle electrical noise because digitization of the signal is done within the geophone sonde itself and the length of wire over which analog signal is carried within the geophone sonde is on the order of a few centimeters rather than a copper strand that carries signal to the surface along with picking up 60-cycle interference.

Root Mean Squared amplitude 2-10 Hz for limited time

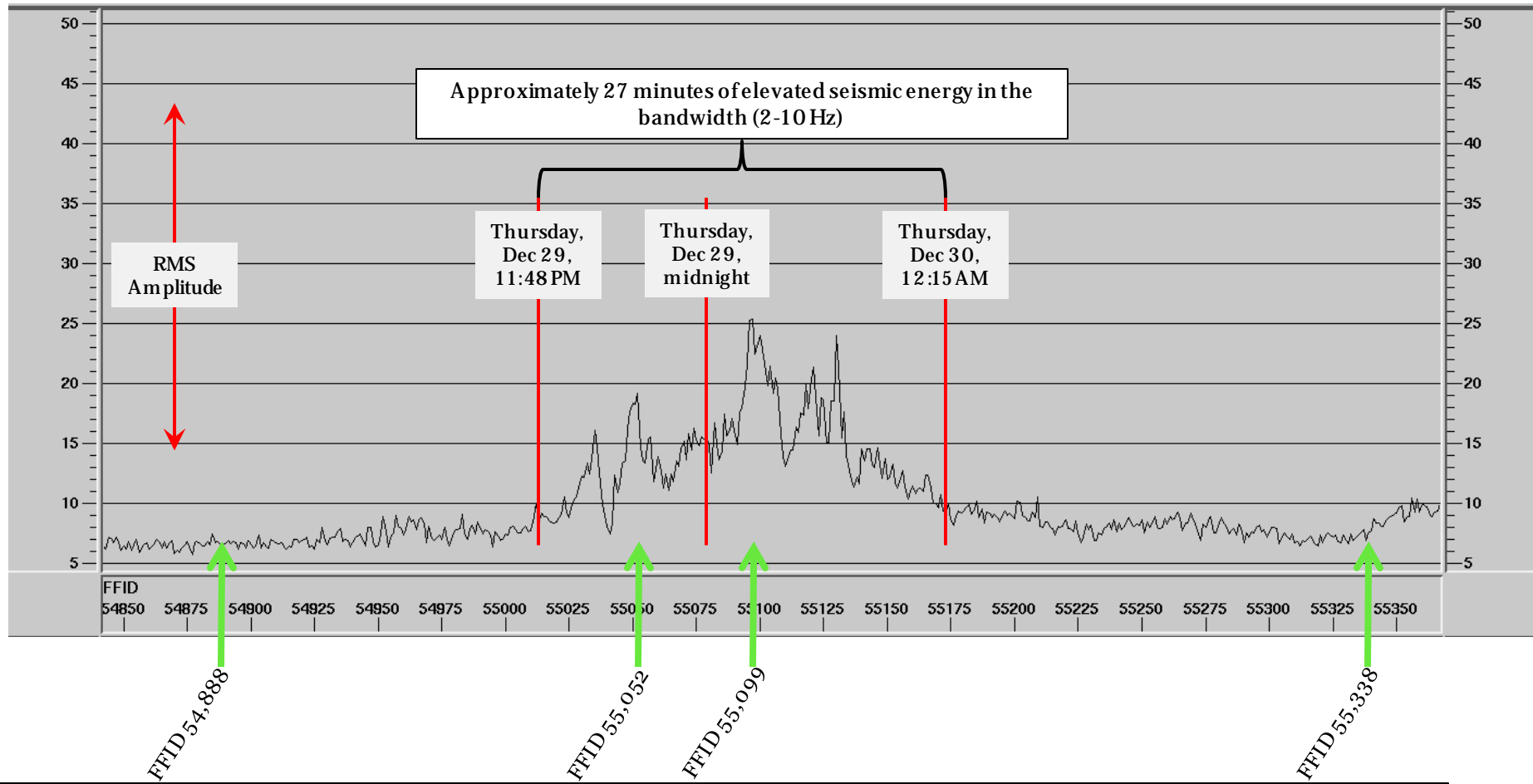


Plots in the previous slides show that the seismic frequency band 2-10 Hz contains more ambient seismic signal than the 15-60 Hz bandwidth. The 2-10 Hz bandwidth does not strictly contain cultural seismic signals however. The data above shows RMS amplitude in the 2-10 Hz bandwidth for a time period of approximately 1.5 hours centered around midnight, December 29, 2011. In the center of the time period shown there is a 27-minute time period in which there is an elevated RMS amplitude from 12 minutes before midnight until 15 minutes after midnight in which RMS amplitude increases by a factor of 2 to 4 over the time period before or after the 27-minute period.

There are multiple time periods such as the 27 minute time period shown that are unlikely to have a cultural source such as mining, gravel, or timbering operations because of the short time duration (industrial operations are sustained) and the time of day. Most outdoor industrial operations do not run at night due to safety restrictions and worker availability. See continued discussion on the next two slides.

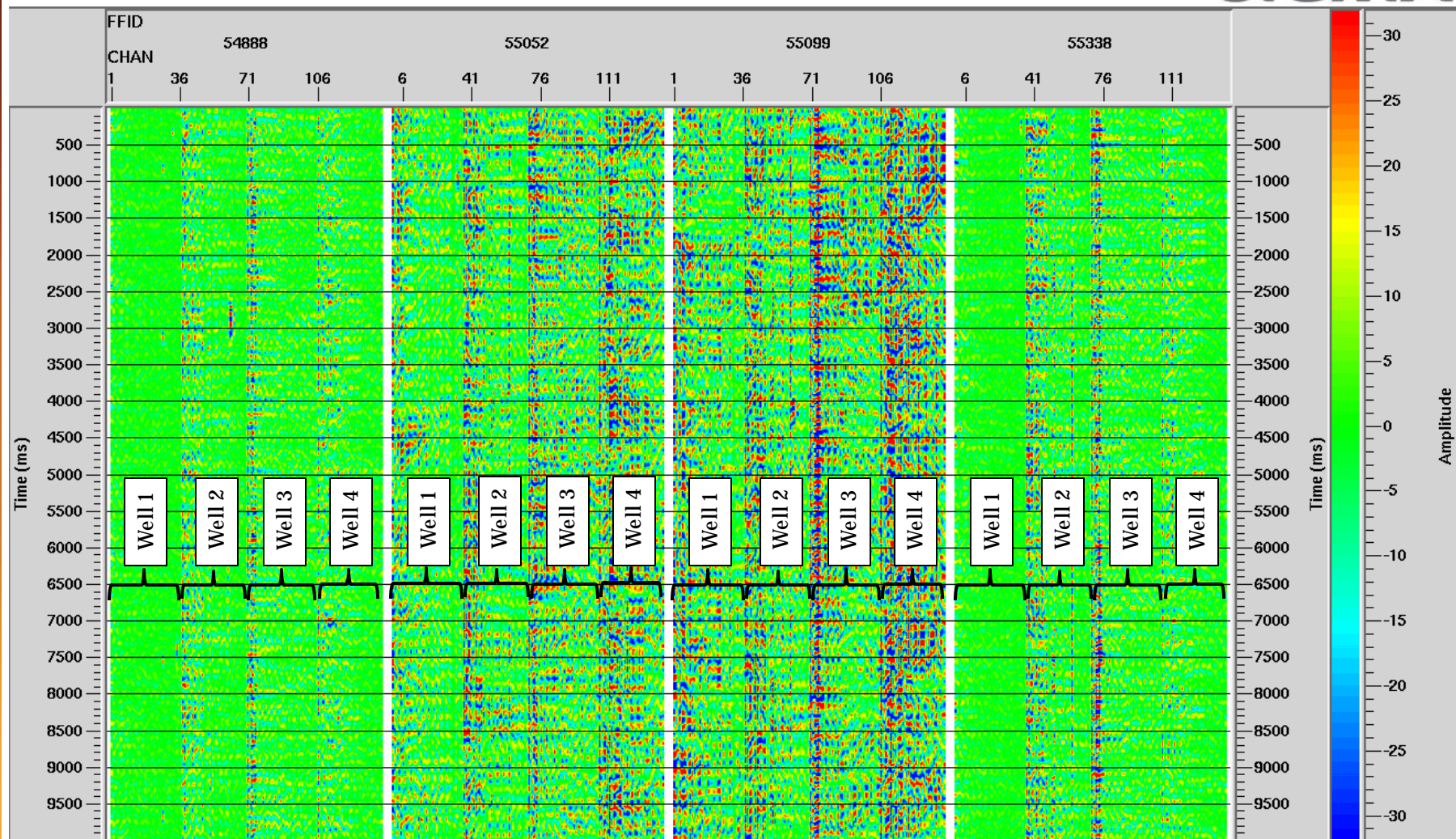
Note: the horizontal axis in this plot is labeled "FFID" which stands for "Field File Identification" and is a standard seismic terminology indicating a unique number that is assigned to each field record. For this dataset FFID values are sequential and incremented by 1 with each new 10-second record. See continued discussion on the next slide.

Green arrows point to records shown on the following slide



Seismic records at the times of the four green arrows shown above were extracted and plotted on the next slide to verify that the background amplitude increase was ubiquitous across all of the observation wells.

Seismic records showing amplitudes before, during, and after the 27 minute high amplitude period



The four seismic records annotated in the previous slide are shown here after bandpass filter of 2-10 Hz with entire-screen scaling, which means that amplitudes can be directly compared to one another. Red and blue colors indicate that the data trace has high amplitude and green means low amplitude. Thus, it is easy to see that the two center records (55,052 and 55,099) that were recorded during the high-amplitude midnight period on the previous slide do, in fact, have a larger amplitude than the two records recorded outside the 27 minute time period. The fact that all four wells see elevated amplitude indicate that the effect of the source is widespread throughout the area. There are numerous short time periods within the survey time period that likely have a naturally occurring source since they are in time periods unlikely to have a cultural/man-made origin such as industrial activity.

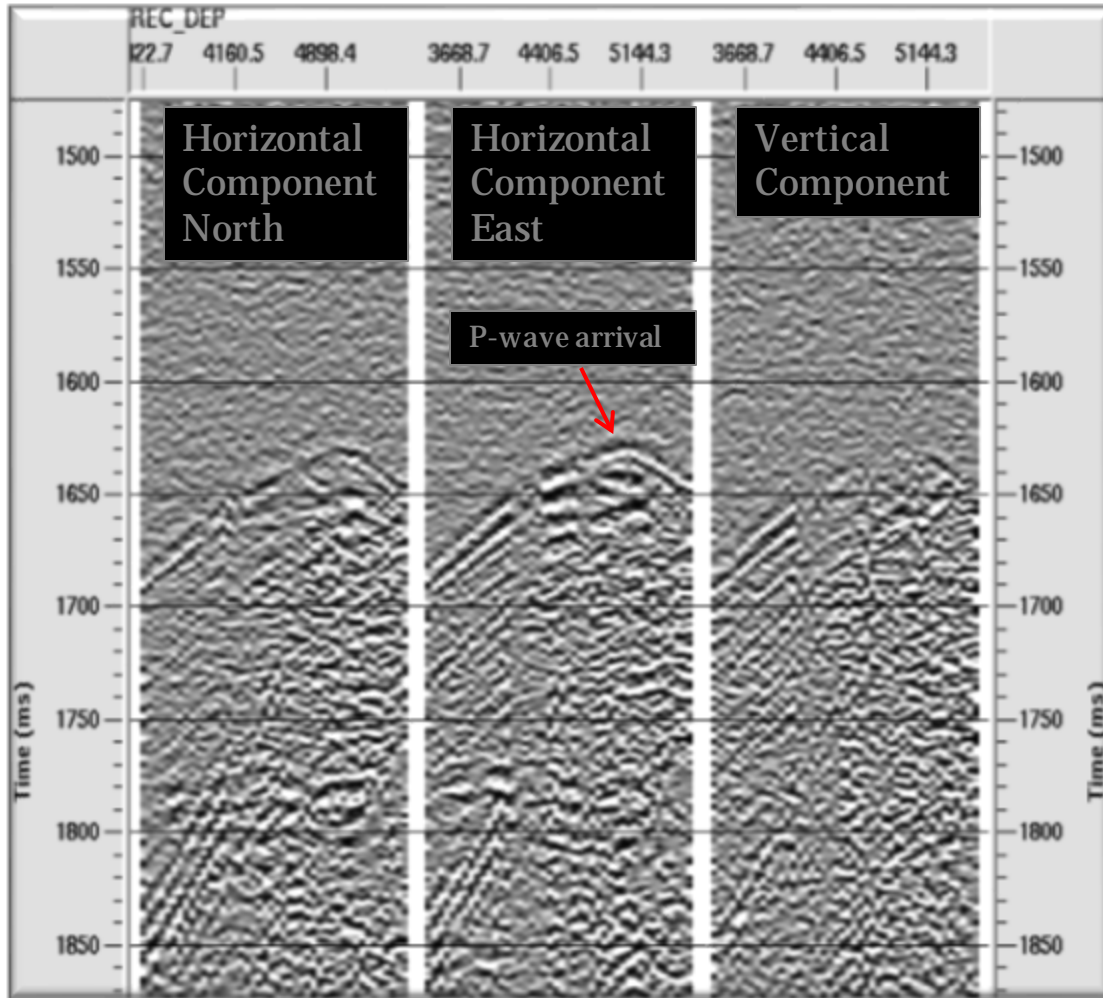
Overview of LASEA concept and data processing

Before proceeding into the next section that describes the major findings of this study, we discuss the fundamental calculations that are the basis of LASEA or Low Amplitude Seismic Emission Analysis. The following eight slides discuss the LASEA method and method of displaying the result. Results from the Newberry Volcano project then follow.

Use of P-waves

The data processing applied to the Davenport Newberry dataset is specifically for P-waves (compressional waves). Shear waves, or S-waves, were not considered for three reasons. First, we do not have S-wave velocity information for this location and velocity information is a critical element in LASEA calculations. Second, we have observed that S-waves in the seismic frequency band that we consider do not propagate through the upper few hundred meters of the earth as well as they do at depth. While our observations are for sedimentary formations, we have no evidence at this location to contradict our observation, hence S-waves may not even be present in the recorded data. Finally, we have never done LASEA analysis with S-waves due in part to the complexity in the polarity of S-waves and S-wave splitting. P-waves are much more predictable than S-waves and therefore more reliable for LASEA computations.

Explanation of Low Amplitude Seismic Emission Analysis (LASEA)



Conventional microseismic methods focus on analysis of relatively high-amplitude short duration seismic events like the one shown in the figure to the left. Events like this one originate when rocks break in response to injection of hydraulic stimulation fluids or changes in stress due to large temperature variations. They are generally very small earthquakes with magnitude on the order of -3 to -1.

In contrast to the large-amplitude short-duration events, there are also situations in which seismic energy is generated over long periods of time but with smaller amplitudes than the event shown in the figure to the left.

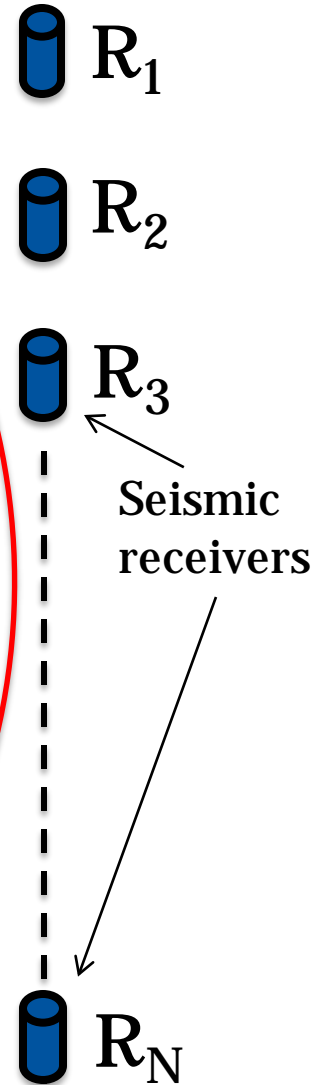
SigmaCubed has developed a method that we call LASEA (Low Amplitude Seismic Emission Analysis) that provides a direct measure of seismic energy output from points in a volume of earth over time. Anomalously large amplitude values may correspond to locations in the earth where fluids are moving, stress is changing due to temperature fluctuations, or the points are in direct connection with a source of variable pressure, even when rocks do not break in response to the pressure/stress changes.

Seismic waves

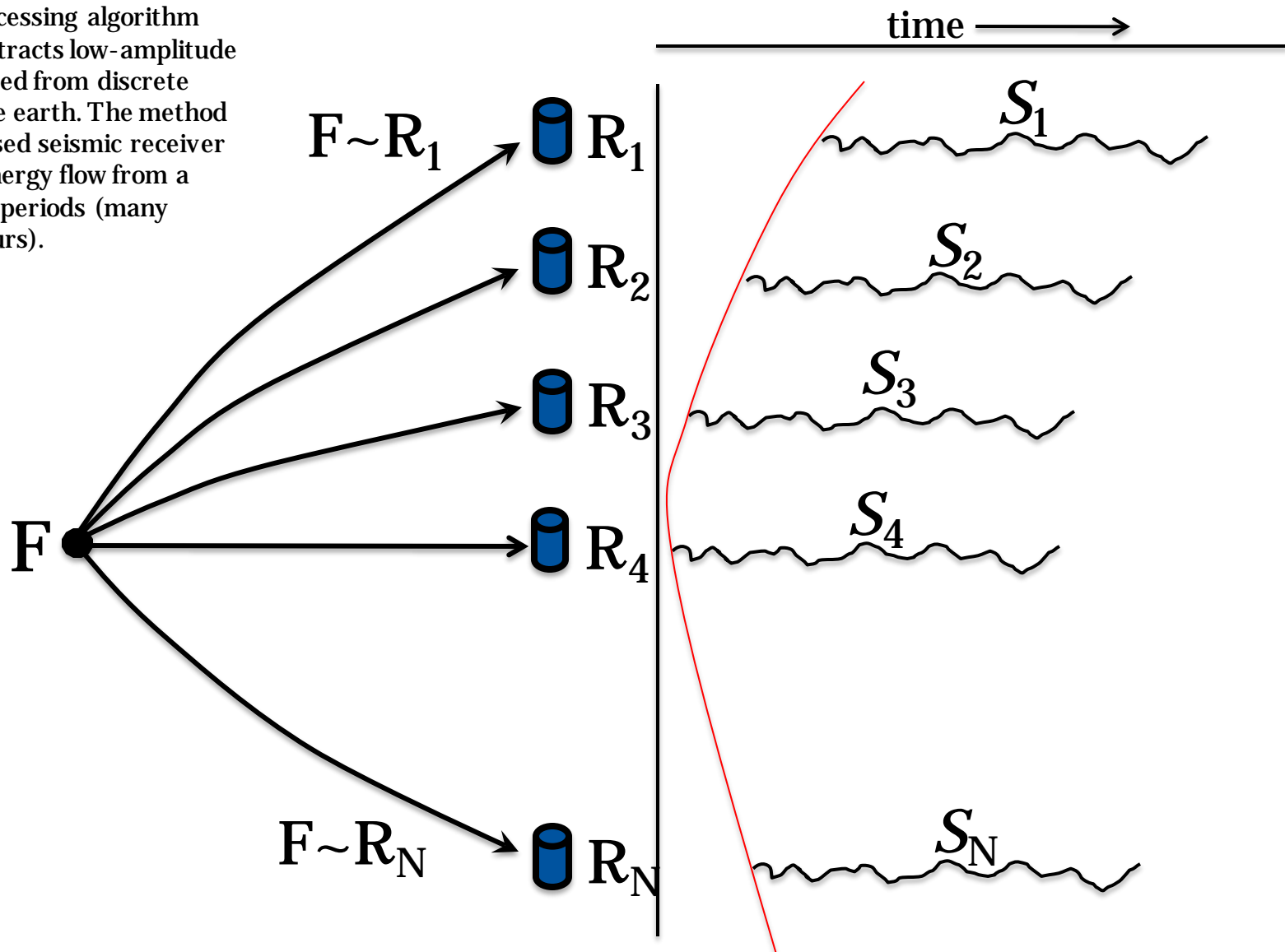
When fluids in natural fractures are subjected to varying pressure from fluid sources or changing temperature, the fluids push on the adjacent rock walls generating low-amplitude vibrations that can be recorded by geophones. Rocks can also fracture in response to stress changes related to temperature variations. These vibrations can be persistent over long periods of time. Natural processes such as volcanic activity can continue for millennia. The LASEA method takes advantage of persistent seismic signals in spite of relatively small amplitudes of magnitude of -3 or smaller.



Fluid within fractures transmits energy in the form of pressure to the adjacent rock walls to generate seismic waves. Energy transfer can also be in the form of conductive heat transfer that could cause stress and rock fractures.



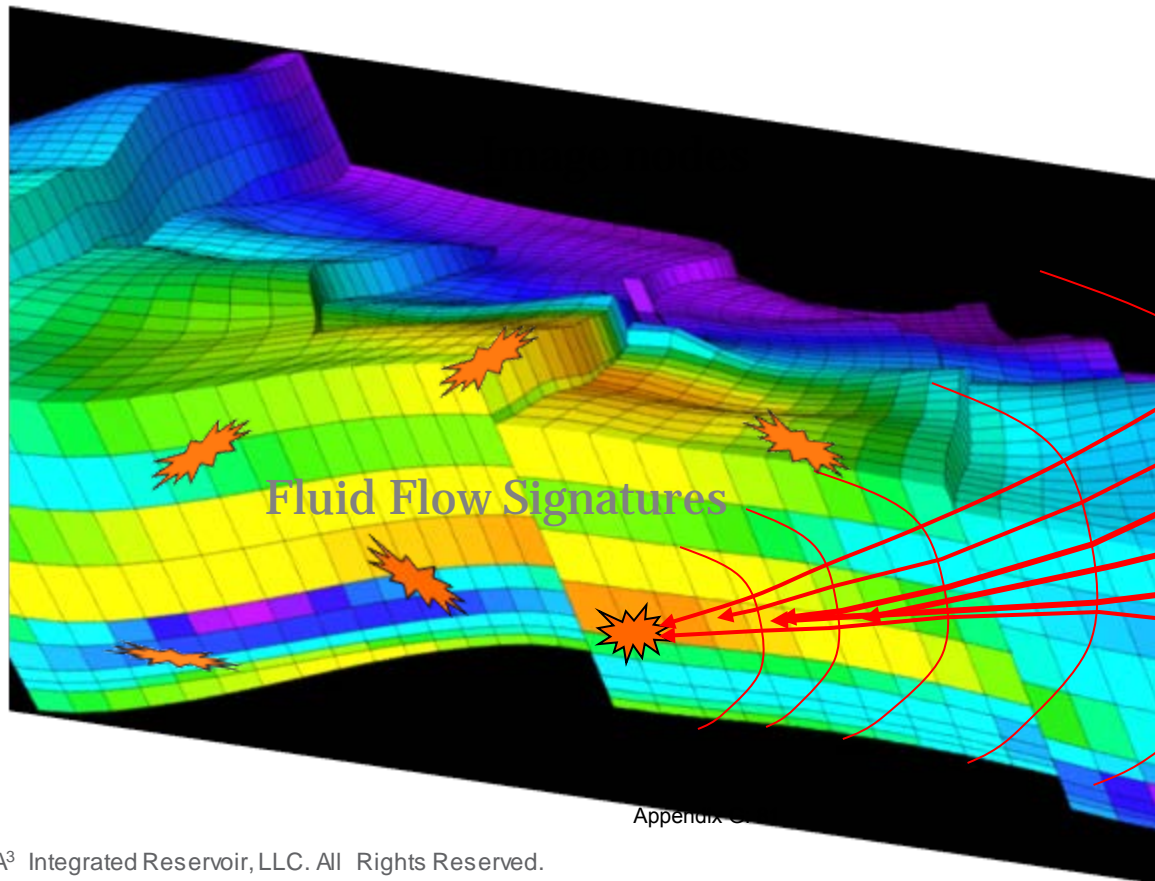
The LASEA data processing algorithm (patent pending) extracts low-amplitude seismic signals emitted from discrete grid nodes within the earth. The method essentially uses focused seismic receiver arrays to measure energy flow from a point over long time periods (many minutes to many hours).



The LASEA algorithm essentially uses an array of 3-component geophones as an antenna to measure seismic energy flux from each grid node in a 3D volume somewhere near the observation wells. The algorithm is much more focused and precise than a simple energy measurement as it employs elements of Kirchhoff Depth Migration, virtual source concepts, and other technologies. The algorithm is computationally intensive but computers with sufficient computational capacity can be employed to efficiently calculate results. The output from the algorithm is an estimate of energy output from each grid node in a volume defined by the user. Amplitudes of output sample values are comparable to one another but at this time the output is not computed or reported in standard energy or power output measures such as watts.

Reservoir Production Monitoring with LASEA

LASEA can be used to monitor production from producing fields to determine where fluids are being produced or for monitoring subsurface hydrothermal activity. Combined with reservoir simulators, this information could provide the most accurate means currently available to estimate reservoir capacity and accessible reserves in place. The idealized image below would require structural information and specialized software such as a SigmaCubed software product called Crystal.

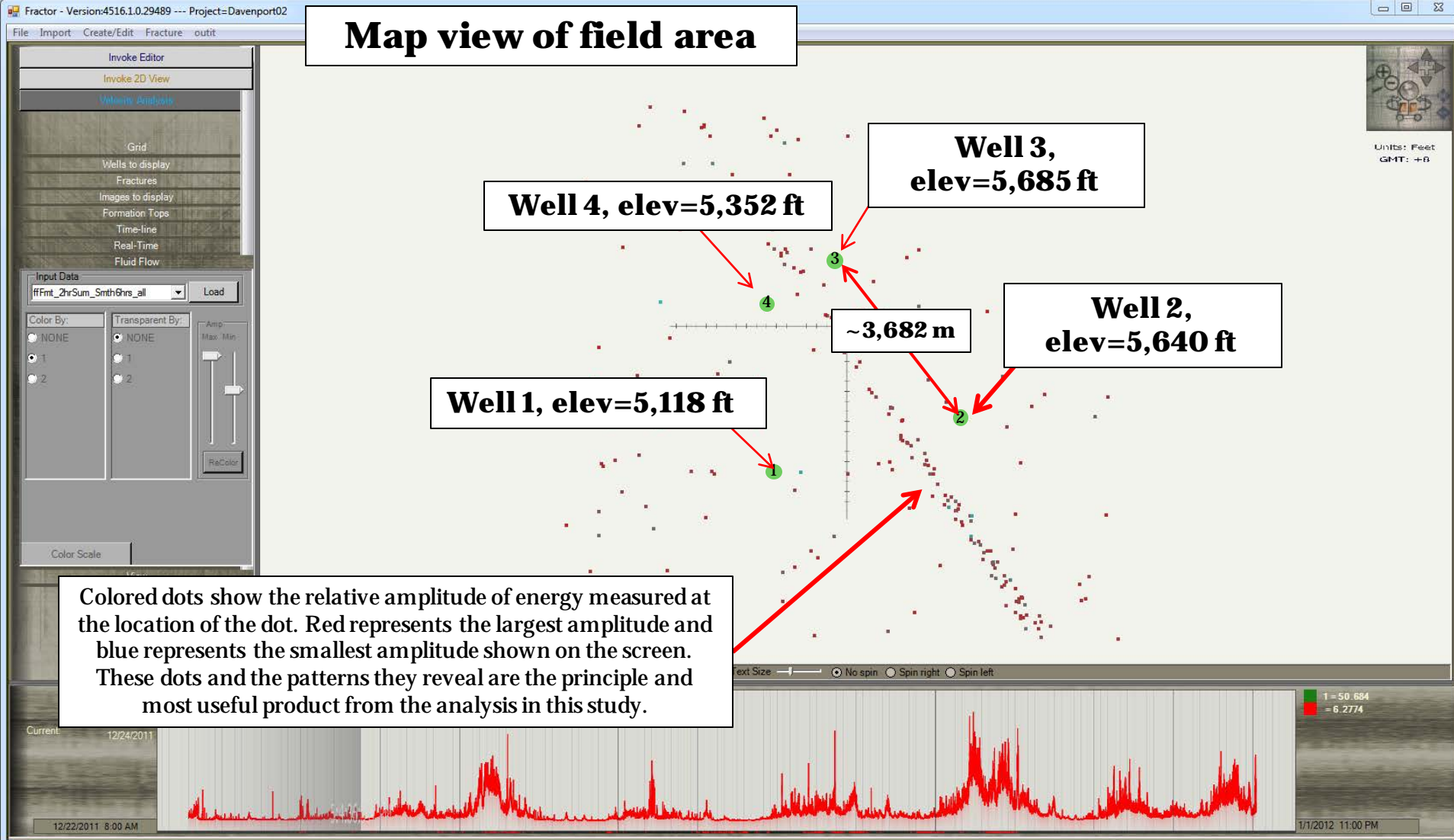


Appendix C

LASEA Output

LASEA scans a full 3D volume of the earth at a user-specified grid interval and computes the amount of seismic energy detected from that location over some time period, normally on the order of a few minutes to hours. LASEA then outputs a number corresponding to the energy measurement for that grid node and time. The grid node energy measurements can then be viewed in a 3D viewer to observe trends in the energy.

The following three slides show a view of the 3D seismic viewing package developed by APEX HiPoint called Fractor. The results are from the Davenport Newberry Volcano project.



Map view of field area

Well 4, elev=5,352 ft

Well 3, elev=5,685 ft

Well 2, elev=5,640 ft

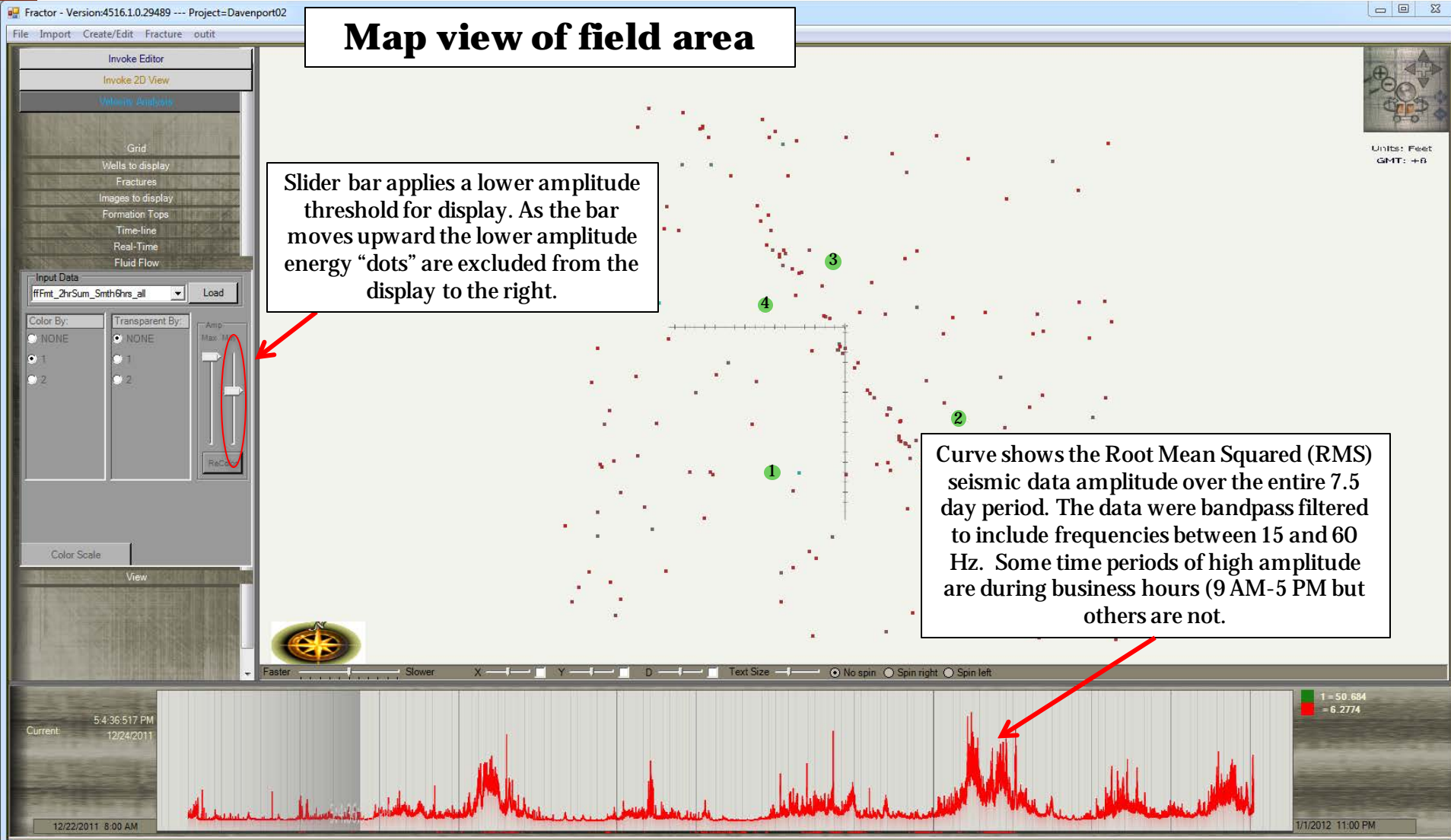
Well 1, elev=5,118 ft

~3,682 m

Colored dots show the relative amplitude of energy measured at the location of the dot. Red represents the largest amplitude and blue represents the smallest amplitude shown on the screen. These dots and the patterns they reveal are the principle and most useful product from the analysis in this study.

Time scale – 8 days in length

Viewing software features continued



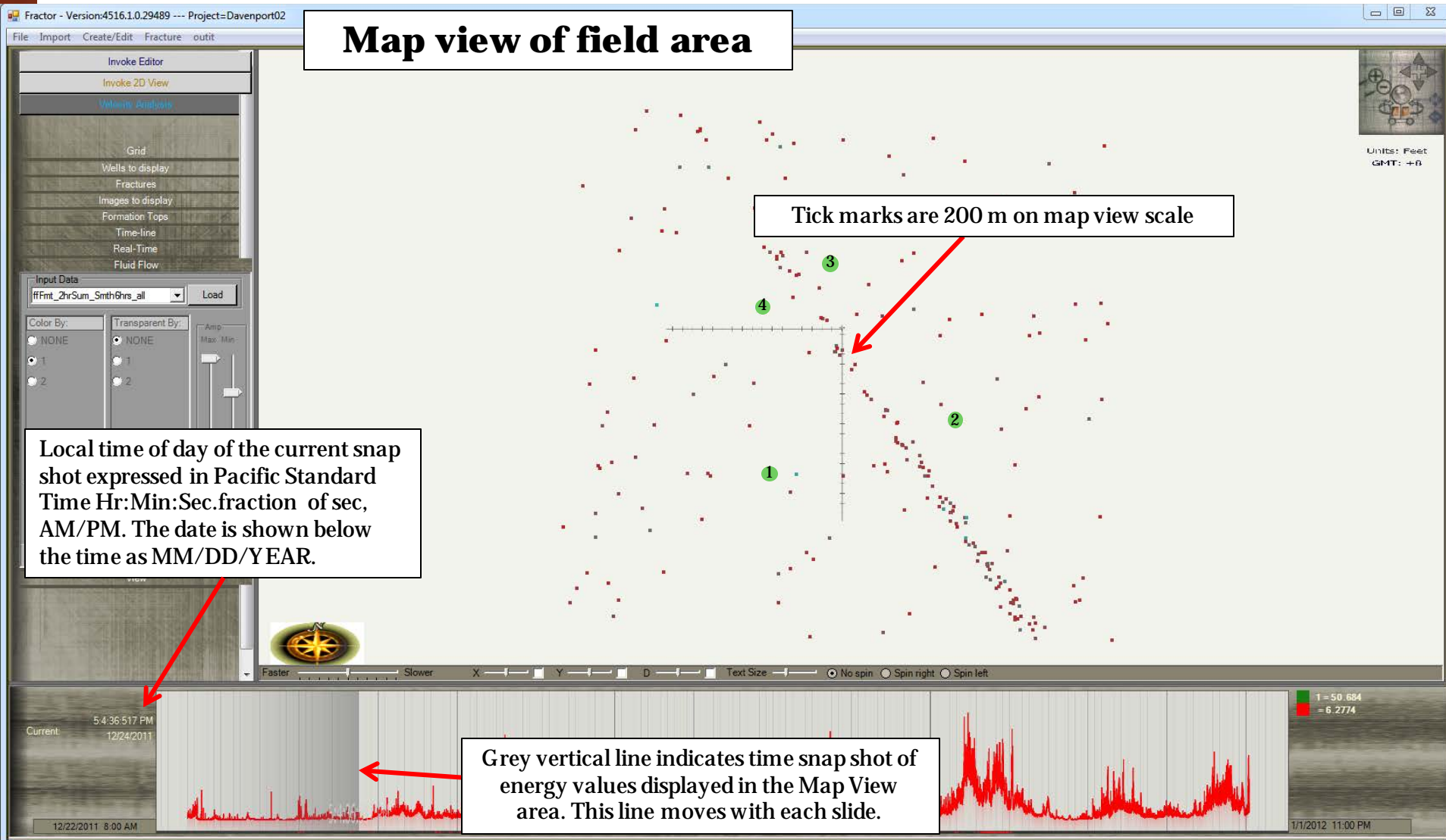
Map view of field area

Slider bar applies a lower amplitude threshold for display. As the bar moves upward the lower amplitude energy "dots" are excluded from the display to the right.

Curve shows the Root Mean Squared (RMS) seismic data amplitude over the entire 7.5 day period. The data were bandpass filtered to include frequencies between 15 and 60 Hz. Some time periods of high amplitude are during business hours (9 AM-5 PM but others are not.

Time scale – 8 days in length

Viewing software features continued



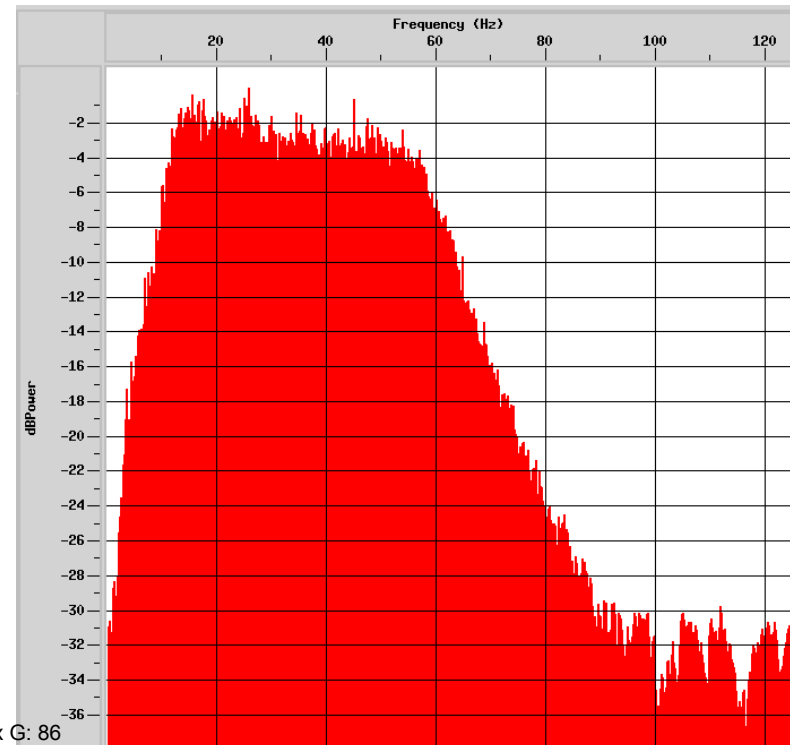
Data Processing Steps Applied Prior to LASEA

The data processing steps applied to the Davenport Newberry data prior to being input to the LASEA process are shown below:

- 1) Load data from field disks to ProMAX data format (ProMAX is a leading industry seismic data processing software package)
- 2) Apply geometry assignment to all data (receiver X, Y, and elevation)
- 3) Determine horizontal geophone component orientation and apply rotation to Vertical, North, and East directions
- 4) Bandpass filter (Butterworth bandpass 12 Hz, 18 dB/Oct, 60 Hz, 45 dB/Oct - discussed below)
- 5) Noise suppression via 3-Component filter (discussed below)

Steps 4 and 5 were done to maximize signal quality with respect to “noise” where “noise” is defined as seismic energy that is not of interest to this project and that may interfere with the signal quality of the desired data. Examples of seismic energy not of interest to this project are high frequency background noise and culturally generated noise.

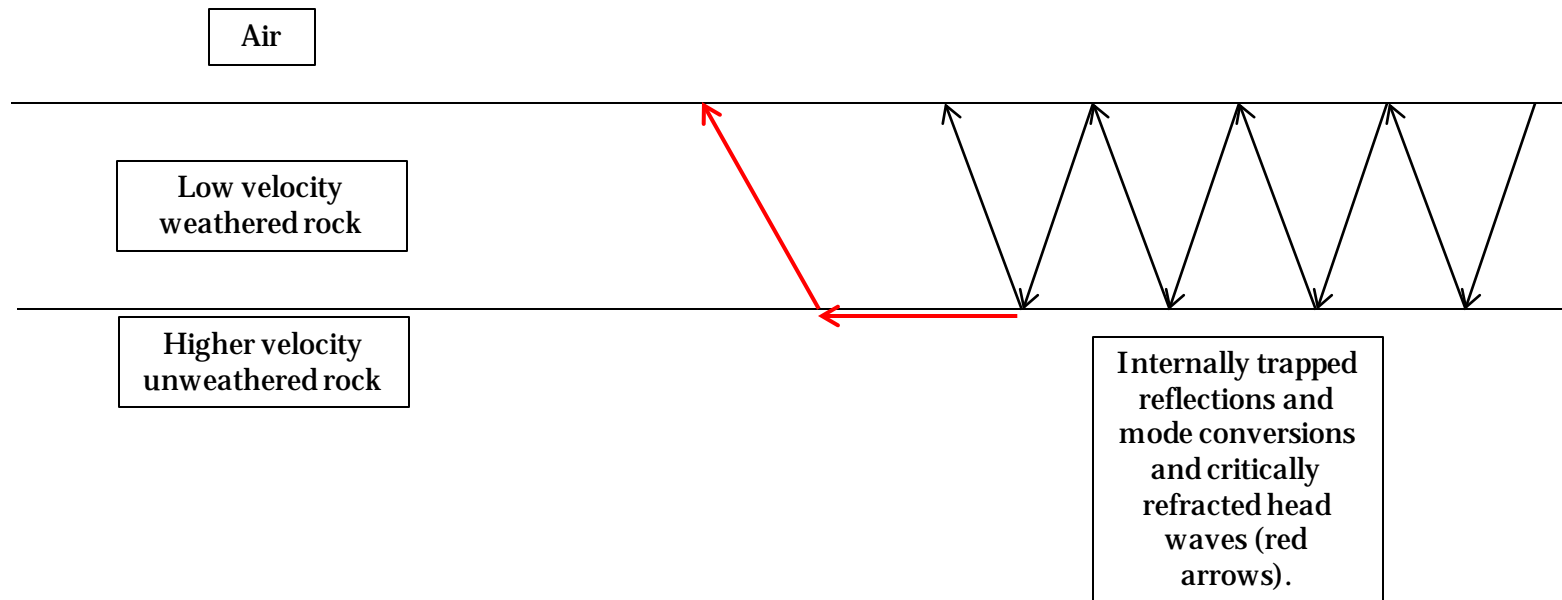
The amplitude spectrum and filter panel displays of the data were analyzed and it was found that below 15 Hz there is a significant amount of coherent energy in the near-surface waveguide (more later on this subject) and a significant random noise component enters the data above 60 Hz. We therefore applied a Butterworth bandpass filter with the following parameters 12 Hz, 18 dB/Octave slope, 60 Hz, 45 dB/Octave slope. The spectrum of a typical record after the filter is shown to the right.



Appendix G: 86

Data Processing Steps Applied Prior to LASEA (continued)

Step 5 in the data processing flow discussed above is titled “Noise suppression via 3-Component filter”. The filter applied was developed by SigmaCubed geophysicists after it was noticed that in nearly every location we have tested, it appears that the near-surface (approximately upper 1,000 ft of the earth) acts a waveguide. The waveguide effect occurs when there are large velocity variations in a vertical direction and wave modes become trapped as depicted in the sketch below. Near-surface velocity effects are well known in seismology and are related to weathering and compressional stress unloading of rocks and is what drives the need for refraction statics in reflection seismology.

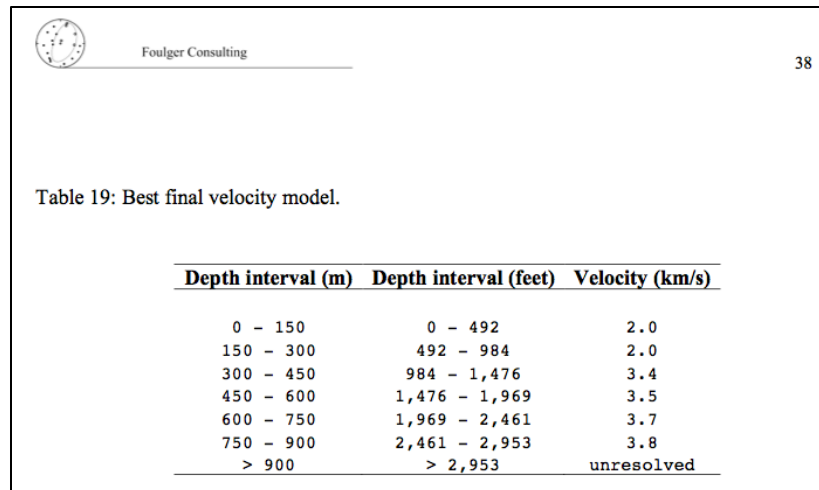


Data Processing Steps Applied Prior to LASEA (continued)

The near-surface waveguide effects described above act as a source of seismic interference for our desired seismic signals from depth. The desired signals from depth arrive at the surface with a strong bias toward traveling vertically upward due to the wavefield being refracted toward the normal of the velocity gradient. Our 3-component noise filter takes advantage of the known wavefield characteristics of both the desired signals and the undesired signals and suppresses the undesired part of the observed wavefield.

LASEA Processing Specifics

The grid node spacing for computations was 100 m. The velocity field was taken from previous work in Table 19 of an unpublished report titled “Report to AltaRock Energy Inc. Newberry Calibration Shot Project” by Gillian R. Foulger, of Foulger Consulting, dated October 09, 2010. The table directly from the report is shown below:



Foulger Consulting 38

Table 19: Best final velocity model.

Depth interval (m)	Depth interval (feet)	Velocity (km/s)
0 - 150	0 - 492	2.0
150 - 300	492 - 984	2.0
300 - 450	984 - 1,476	3.4
450 - 600	1,476 - 1,969	3.5
600 - 750	1,969 - 2,461	3.7
750 - 900	2,461 - 2,953	3.8
> 900	> 2,953	unresolved

Depths greater than 900 m were unresolved in the Foulger report and for the LASEA analysis were assumed to be 3.8 km/s via extension of the deepest velocity determined in Table 19.

Further refinement of the velocity field may be possible with seismic sources that may be generated by upcoming fracture stimulation at the Newberry site.

Additional velocity information

A table of interval velocity as a function of depth derived from the shallow instrument wells is presented below. The measurements are taken from nearby source points shot with a small surface seismic source provided by APEX-HiPoint (now SIGMA³). The table is for depths greater than 73 m. Depths shallower than 73 m exhibited highly variable velocities but are generally in the range of 1,800 m/s indicating a variable weathering layer. Wells 1, 2, and 3 had a consistent velocity at depths between 73 and 195 m and Well 4 had a lower velocity. All of the above variations are consistent with observed spatial variations that are well-documented and in commercial seismic data analyses such as surface seismic reflection imaging.

Well Number (see map in Slide 4 above)	Velocity in m/s in the interval 73-195 m depth
1	3,123
2	3,230
3	3,299
4	2,566

LASEA Processing Specifics continued

Depths greater than 900 m were unresolved in the Foulger report and for the LASEA analysis were assumed to be 3.8 km/s via extension of the deepest velocity determined in Table 19. Further refinement of the velocity field may be possible with seismic sources that may be generated by upcoming fracture stimulation at the Newberry site.

The dots shown on the LASEA display are effectively the result of a series of cross correlations and sums that include input from two hours of continuously recorded data (over 1.9 gigabytes of data). An additional data smoother was also applied such that for any given grid node in the volume, the data sample that is displayed is an average of the 2-hour LASEA value for that 2-hour time period AND the prior and subsequent two hour periods. The time smoothing provides way to diminish the effect of anomalous amplitudes, both large and small.

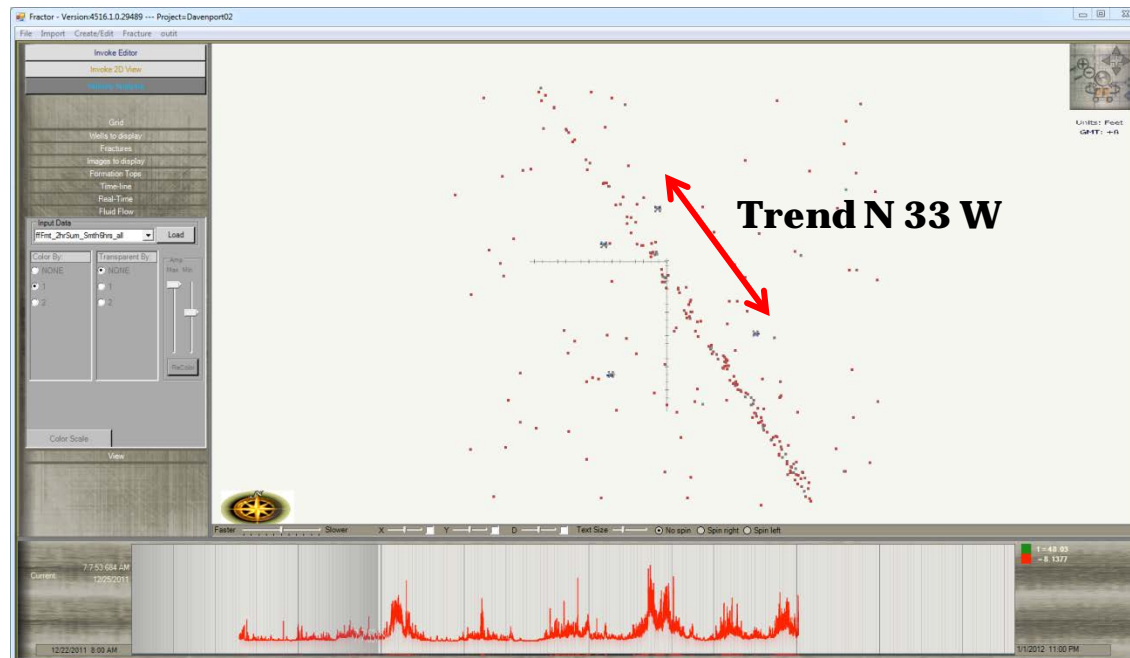
LASEA Results for Newberry Volcano Study

The following slides show highlights from the LASEA results for Newberry Volcanic Area.

Linear Trend Activity – a principle discovery

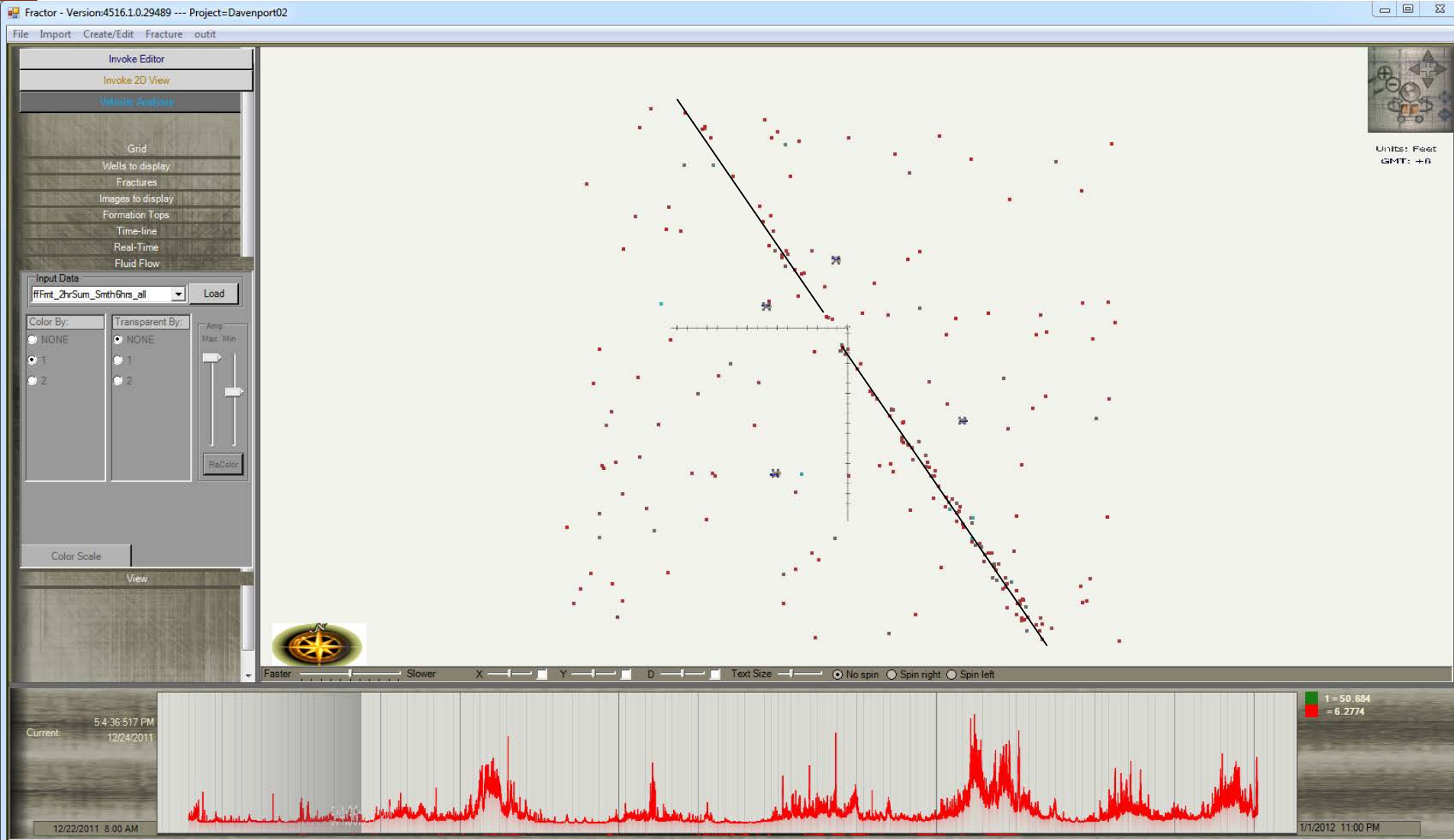
Two separate time periods of seismic activity resulted in a strongly linear trend being illuminated. “Strongly linear” is a qualitative phrase but the NW-SE linear trend stands out against the background seismic activity as shown in the example below which was recorded during the first period of activity at 07:07 am, 12/25/2011. The begin and end times of the two time periods are in the table below. The second activity period followed the first by 3 days and 5 hours. The first period lasted ~22 hours and the second ~31 hours though the second may have lasted longer but recording ceased near the end of the second period. Both time periods show activity at the same locations. The linear trend probably continues beyond the mapping area shown as the NW and SE ends of the trend are at the edges of the investigation area.

Begin	End	Comment
12/24 5:10 pm	12/25 7:00 pm	Consistently present
12/29 00:15 am	12/30 07:00 am	Intermittent, consistently present but variable in amplitude relative to ambient background levels



Appendix G: 92

Linear Trend Activity – possible variation in direction



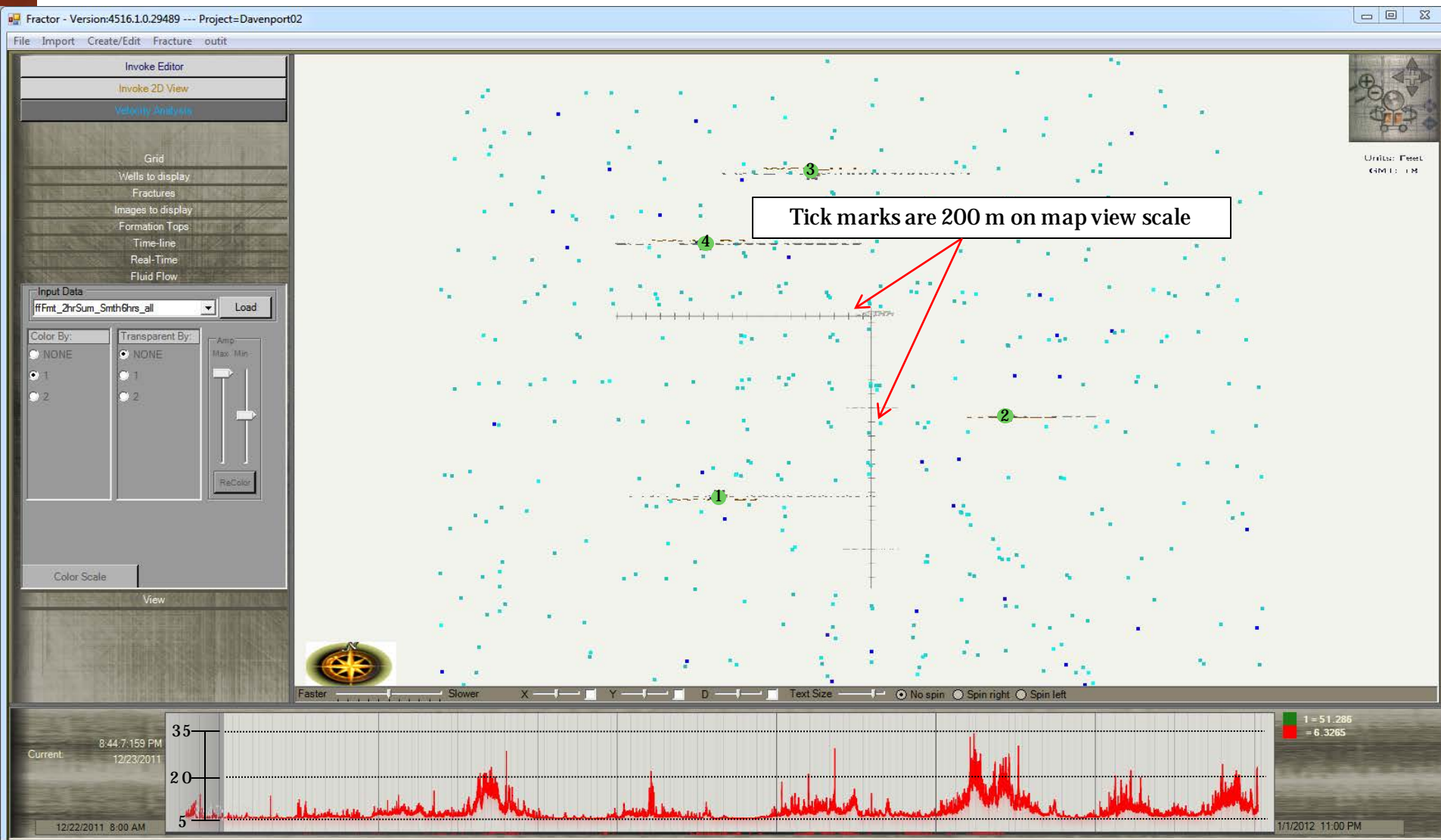
While further analysis is warranted, the linear trend appears to vary somewhat between the NW and SE segments of the trend. The difference is only a few degrees but is visually perceptible. The two line segments drawn above were fit by eye.

Important time intervals in the following slides

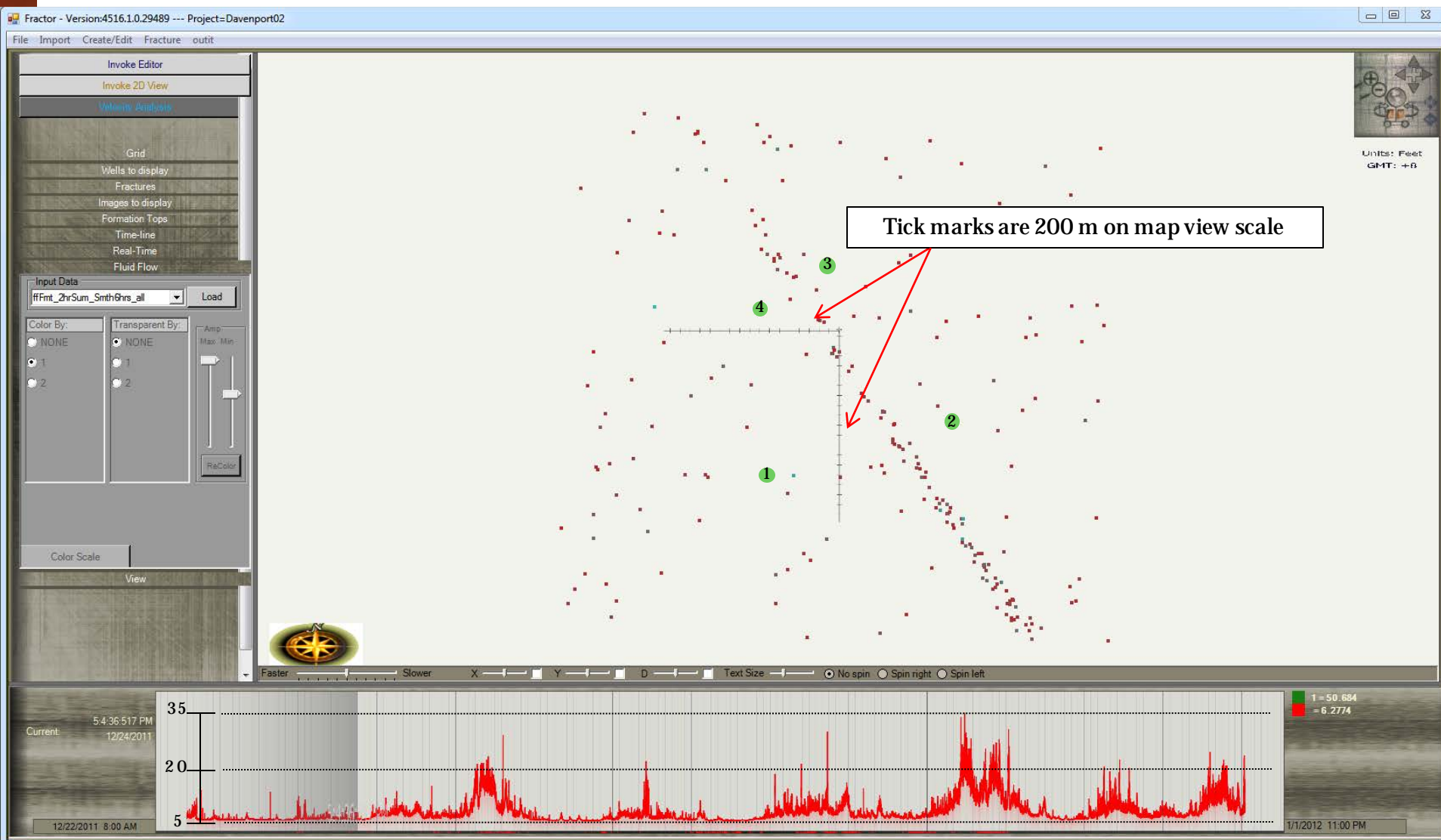
The following slides show the LASEA results at various sequential time steps throughout the 6 day-17 hour recording time period. These slides were selected and annotated to show typical results but also times of interest. The amplitude threshold slider bar was set in each display to optimize information that can be derived from each slide. Setting the slider bar is an interpretive process. Davenport and its agents may wish to set slider bars at different levels to discover other results.

The first slide shown is December 23 at 8:44 PM. The first approximately 27 hours of operation showed primarily indistinct energy patterns and was typified by generally low background (RMS) seismic amplitudes. The second slide shows the energy field December 24 at 5:04 PM when the first of two time periods displaying linear trends appears on the data.

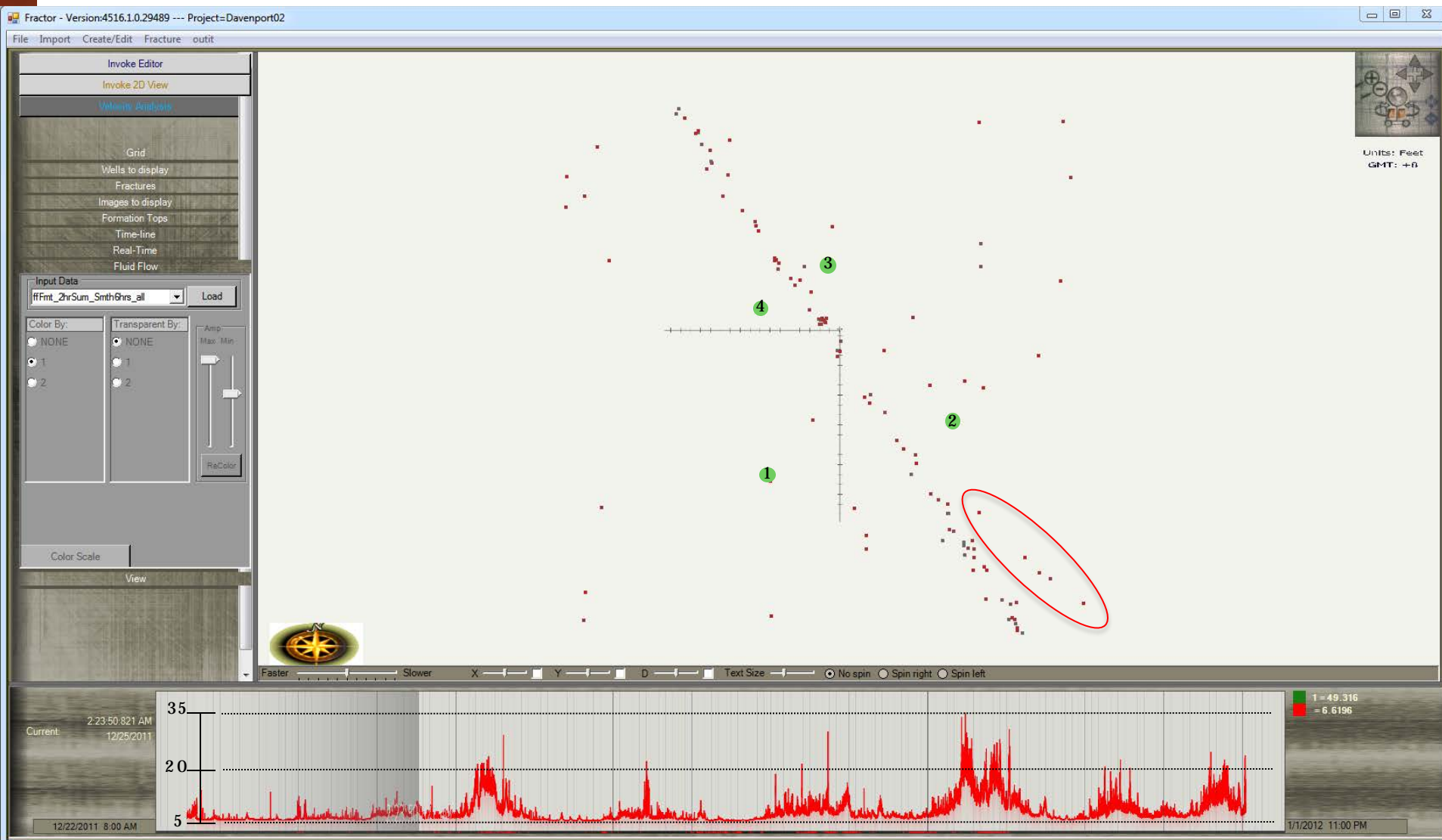
On the first two slides there is an annotation showing that there are 200 m between adjacent tick marks on a scale that is on the plot. The scale remains consistent at 200 m between tick marks for all map view slides shown henceforth.



The first approximately 27 hours of operation is typified by relatively low background energy (RMS curve in red above) and indistinct energy patterns, though there is a hint of the linear trend even in this figure, but it does not stand out against the general background amplitudes.

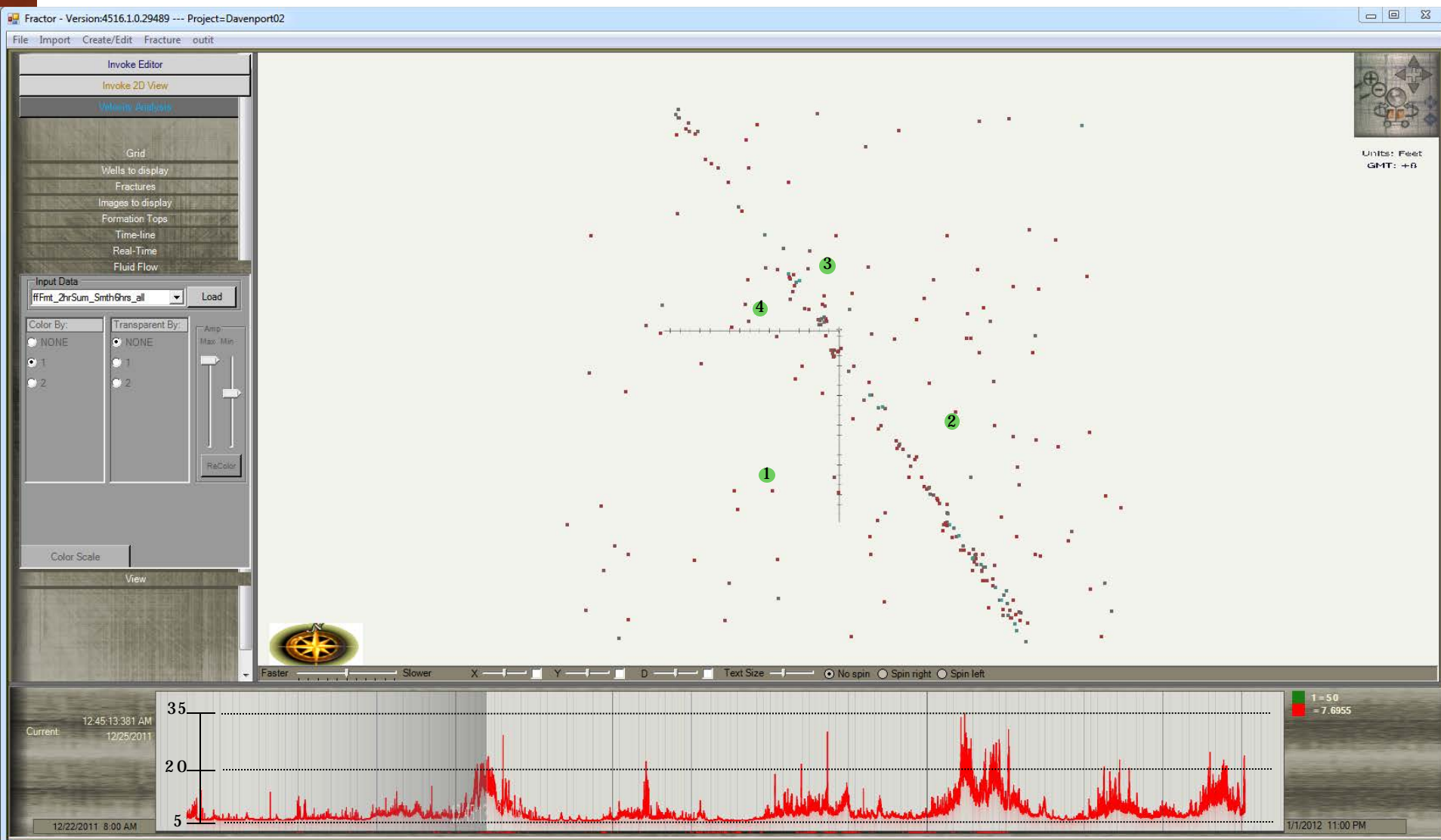


The linear trend becomes apparent at this point in time standing out as a clear trend above the ambient seismic energy.

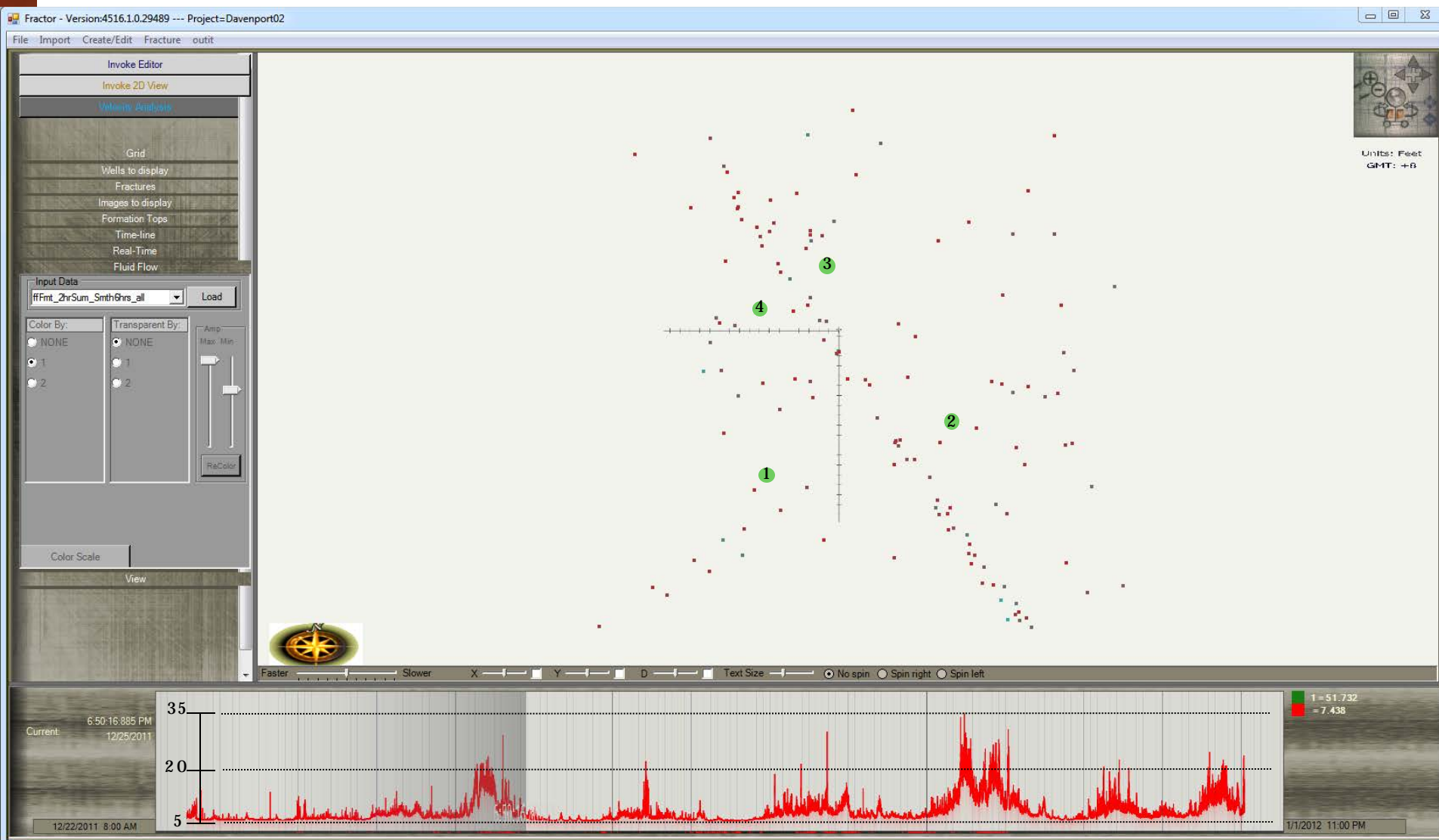


The linear trend continues with an interesting “splay” to the SE which is visible from time to time. This trend has a slightly different orientation than the main trend in the SE part of the field area.

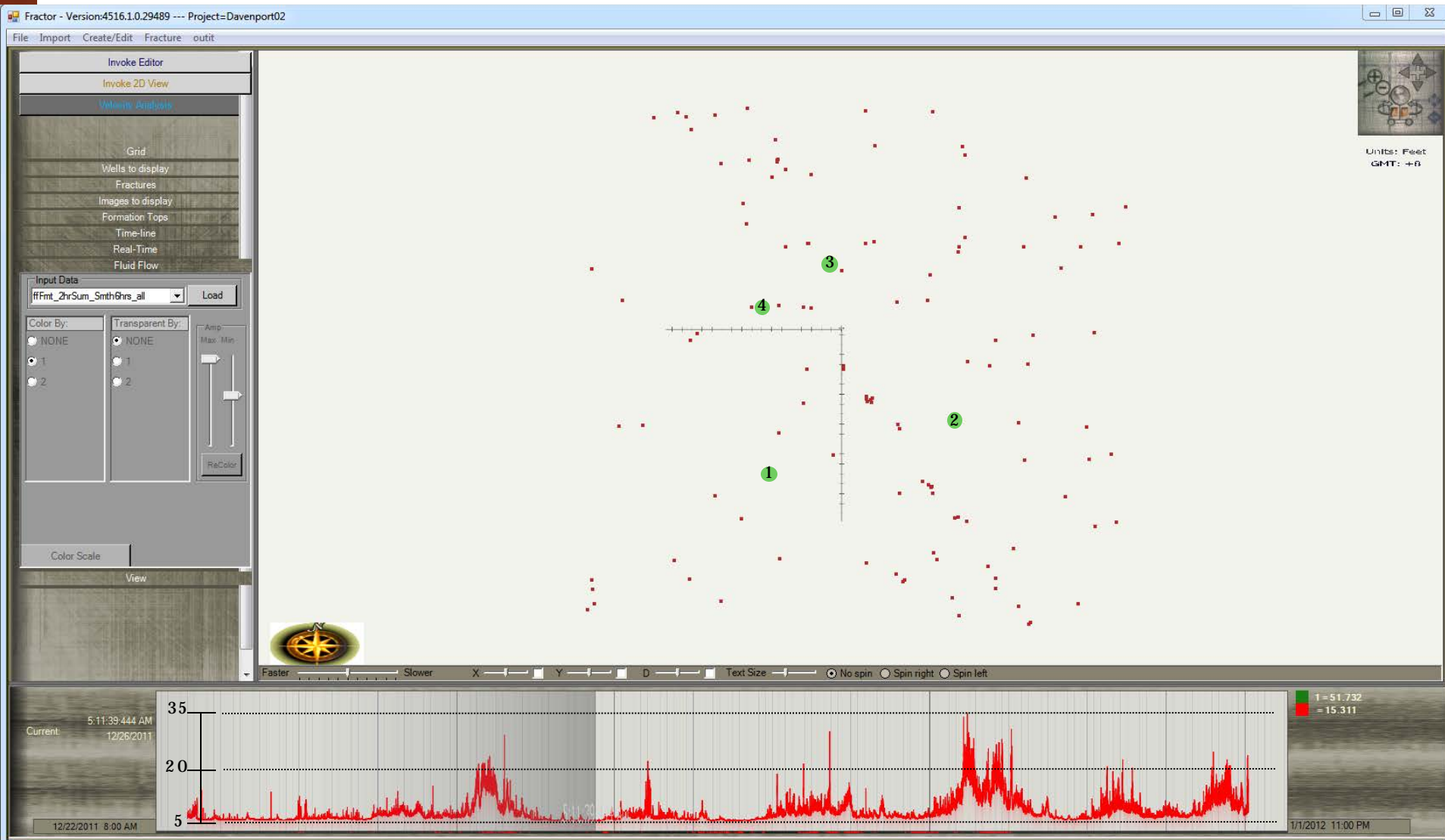
Appendix G: 97



The linear trend continues. Note that the software displays the hour directly afternoon as “AM” but we know from the context of the display and from moving the pointer to before 12:00 and after 1:00 that this plot is 45 minutes after noon and should be considered “PM” rather than AM.



The linear trend continues until this time then stops as the ambient RMS amplitude decays. Note that the time shown is a national holiday in the United States (Christmas day) and we do not expect industrial activity to have occurred anywhere within the region, thus the RMS amplitude decay at this point in time along with the cessation of the linear trend points to the linear trend and ambient noise levels being related to one another.

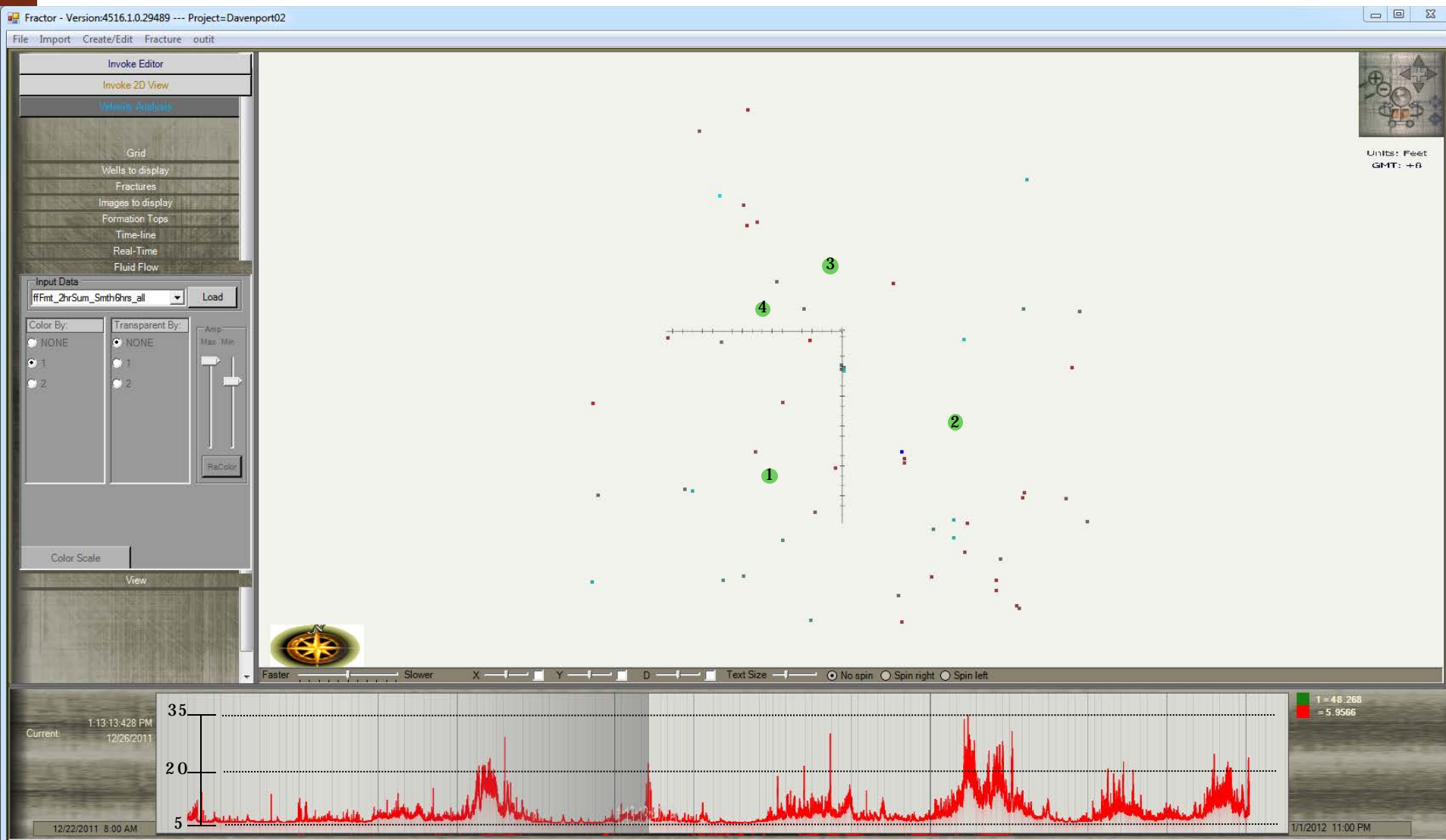


During this quiet ambient background period, the linear trend is still somewhat present, but near the same amplitude of the largest ambient background.

Appendix G: 100

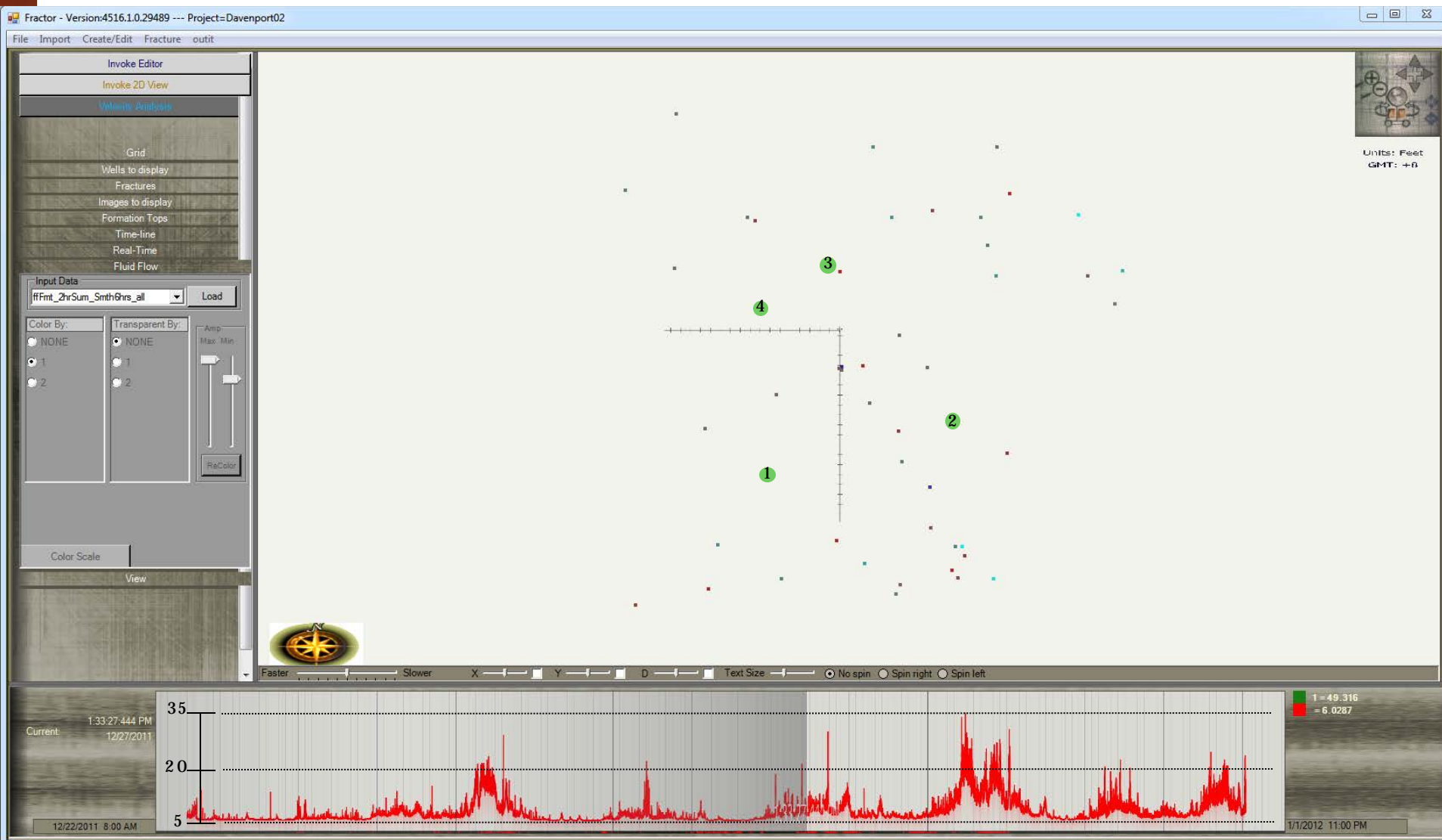


During this quiet ambient background period, the linear trend is still somewhat present, but near the same amplitude of the largest ambient background. During this time the “splay” area returns, though it is in a different position than in the previous slide on Dec 25 at 2:23 AM.



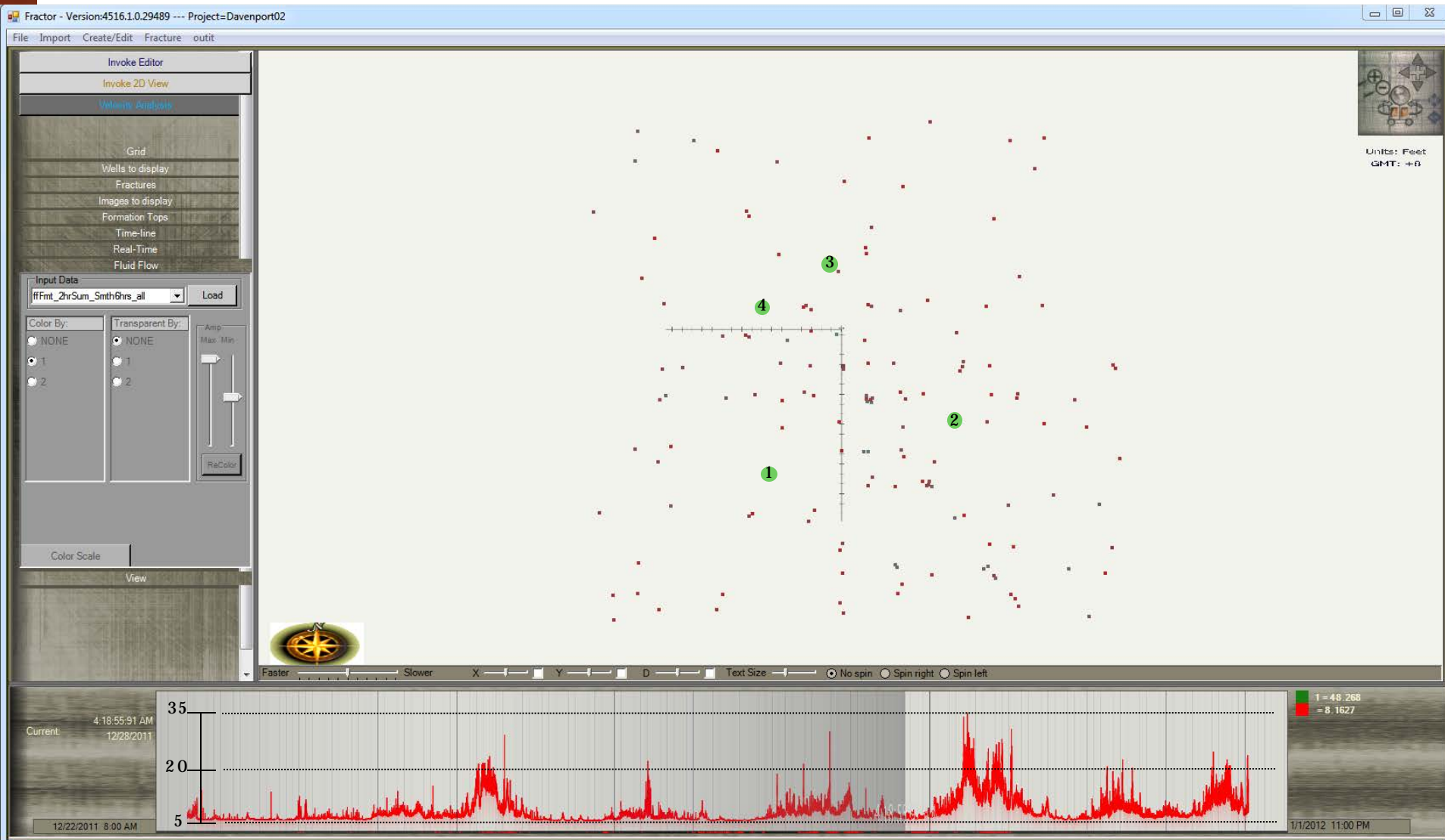
During this quiet ambient background period, the linear trend is still somewhat present, but near the same amplitude the largest ambient background.

Appendix G: 102

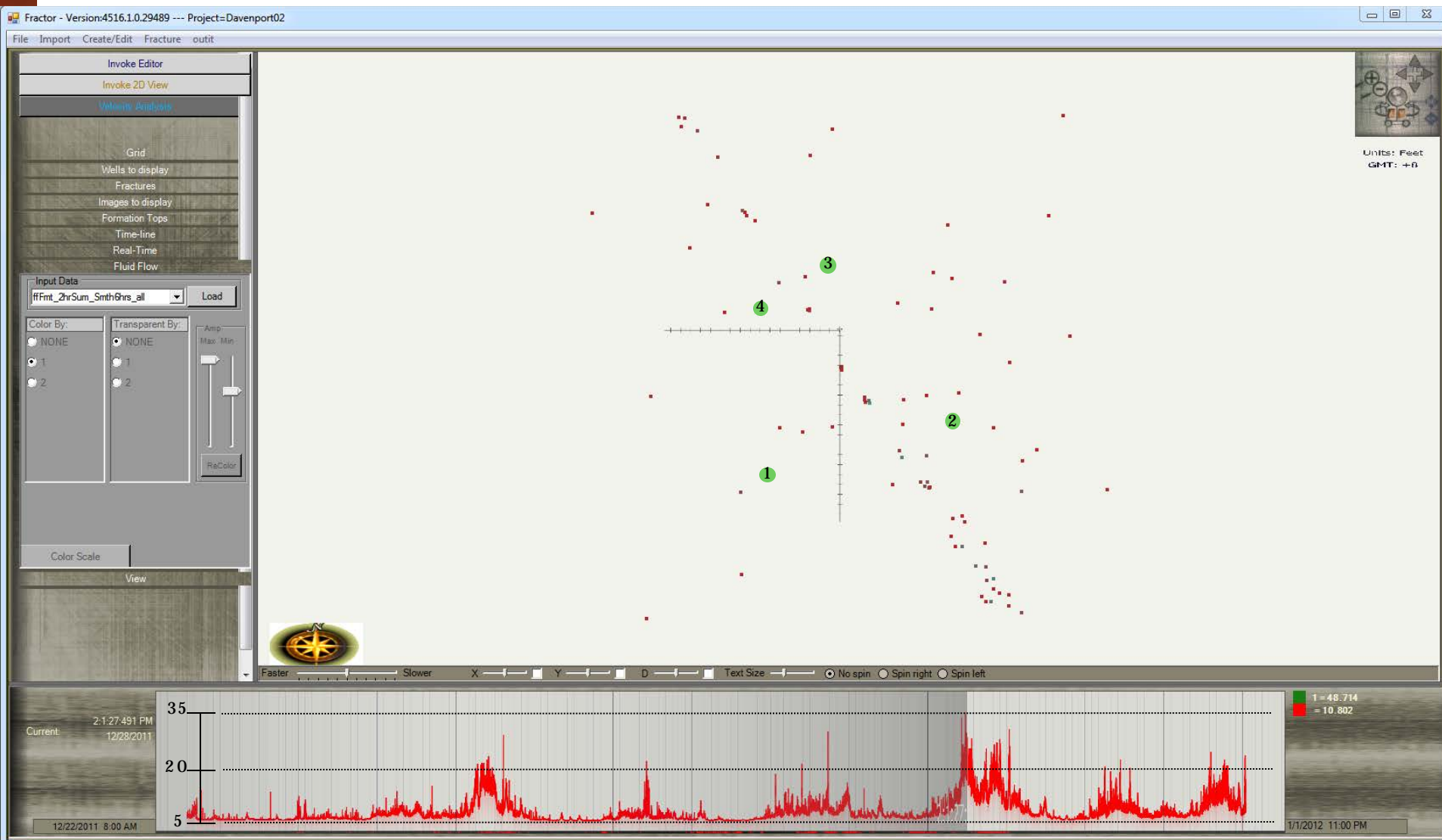


During this quiet ambient background period, the linear trend is still somewhat present, but near the same amplitude the largest ambient background.

Appendix G: 103

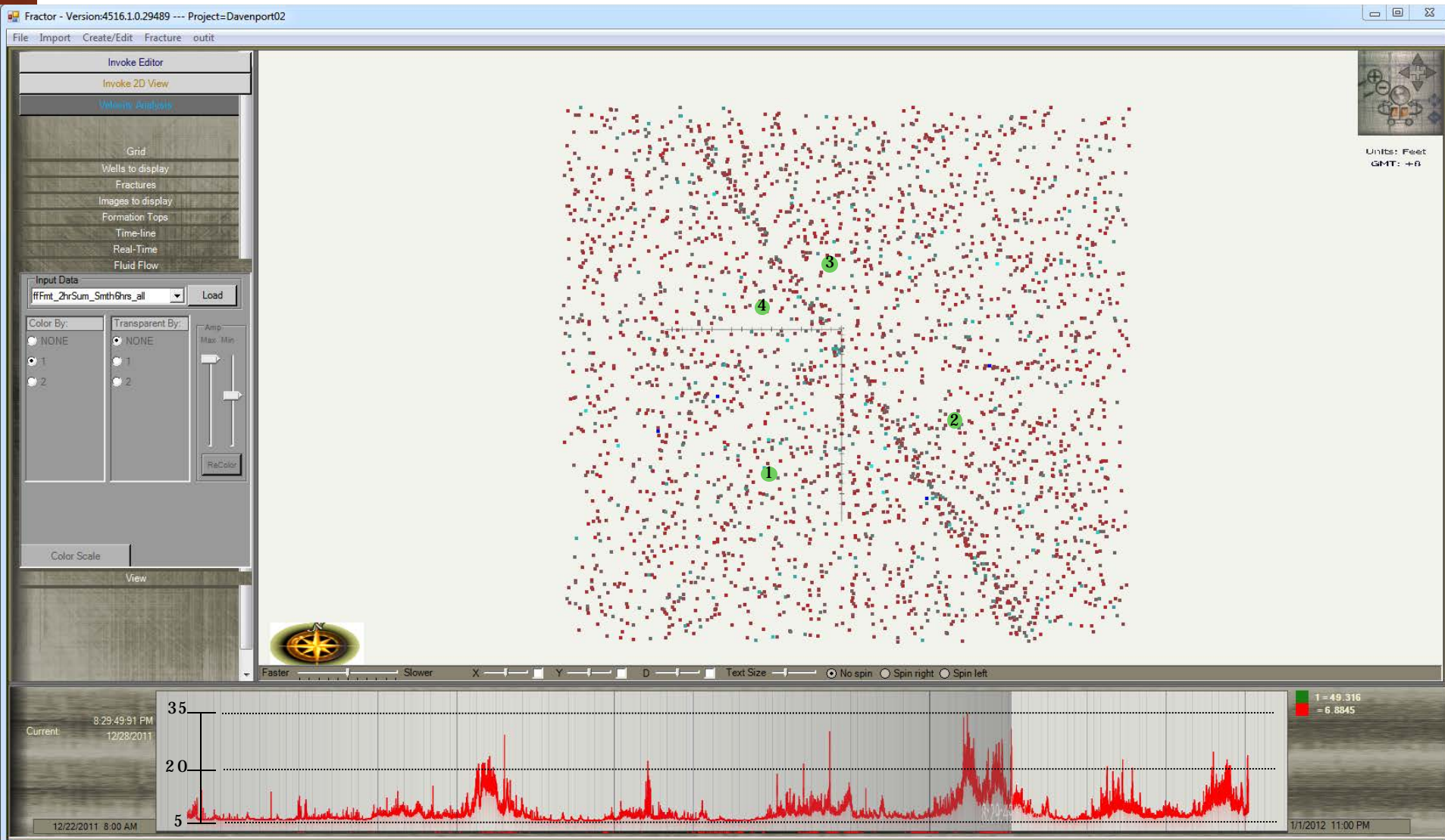


During this quiet ambient background period, there is not an immediately discernible pattern to the energy.



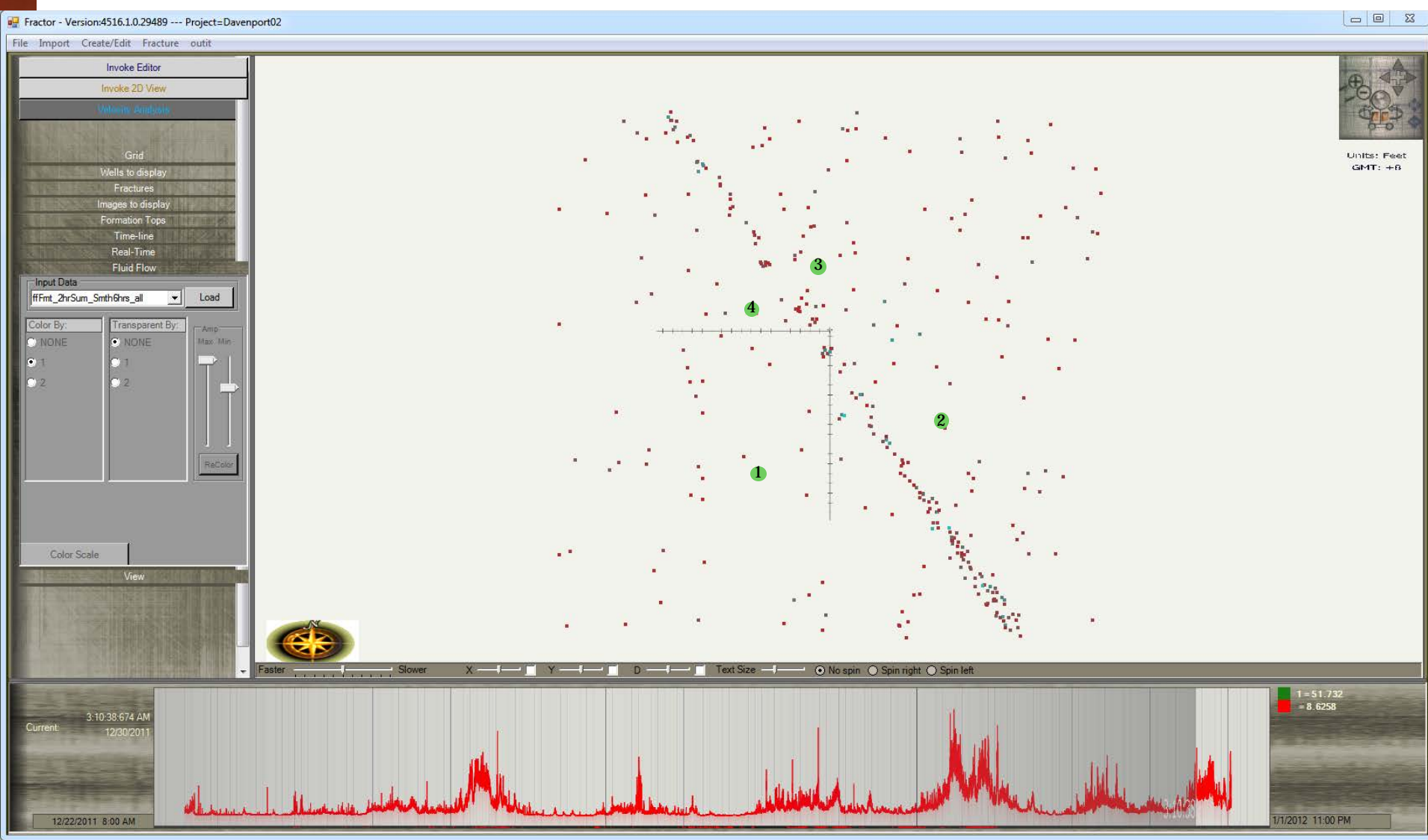
The linear trend restarts at this point during a high ambient background increase which is coincidental with mid-day, so part of the ambient energy is due to cultural sources.

Appendix G: 105

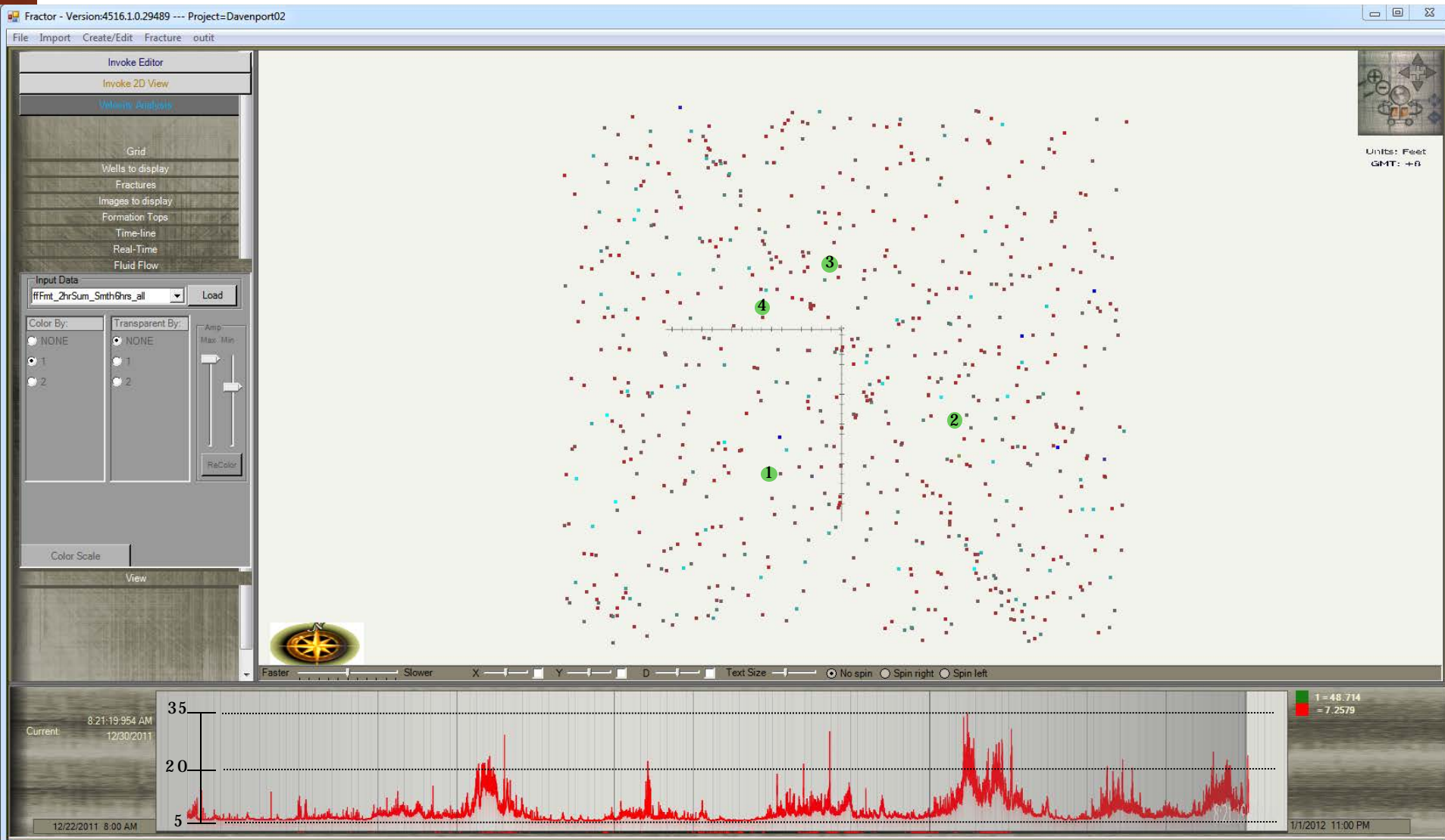


The linear trend continues but there is also relatively high ambient energy.

Appendix G: 106



The linear trend continues.



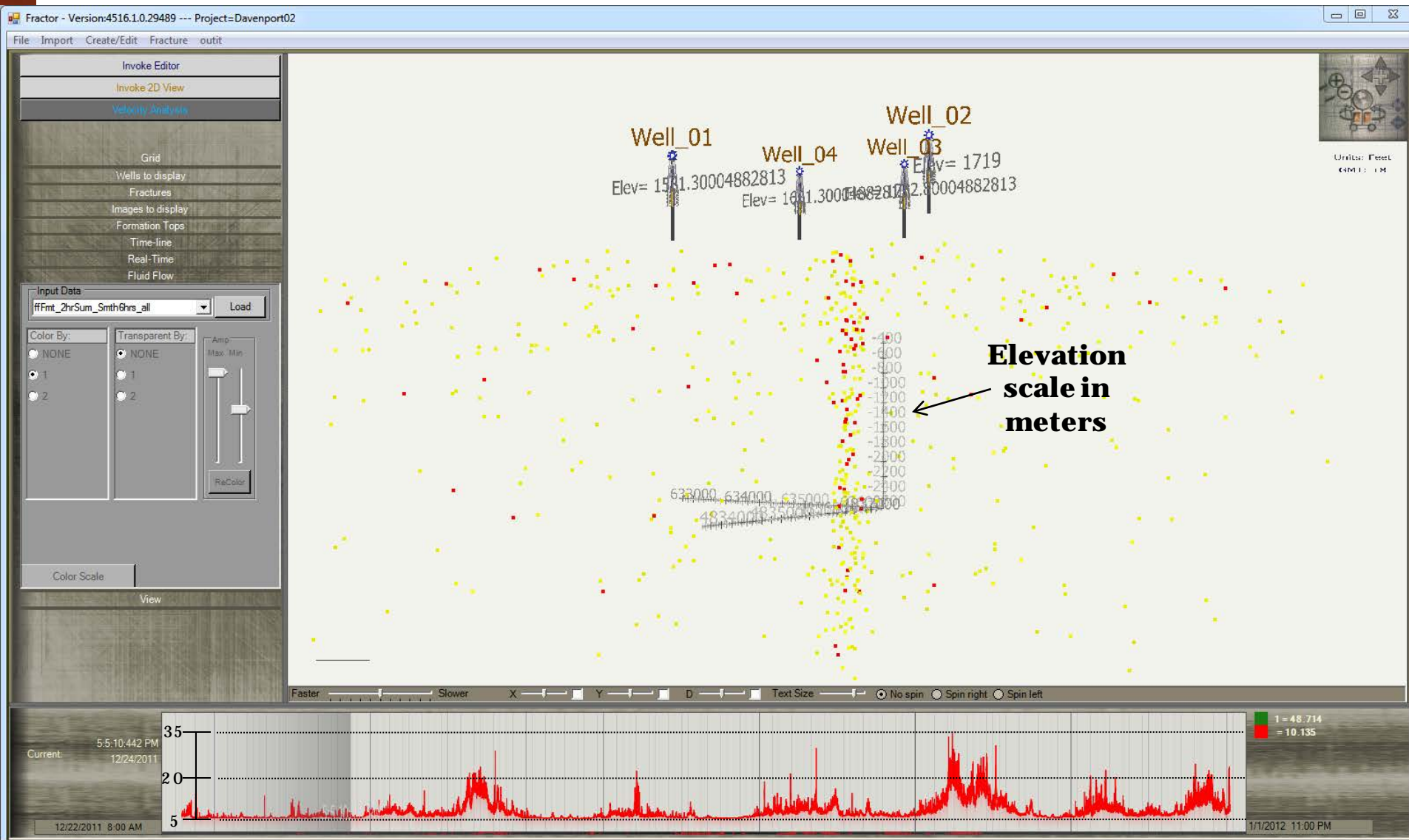
This frame is at the end of the recording period. The linear trend is still present at this time.

Depth of the high amplitude LASEA signal

The following slides show the LASEA results as a side view from the southeast looking along the strong NW-SE lineation. The first slide shows the results with a low threshold amplitude set which reveals that the lineation extends above the expected depth of maximum activity (10,000 ft = ~3,050 m) and well into the shallow section.

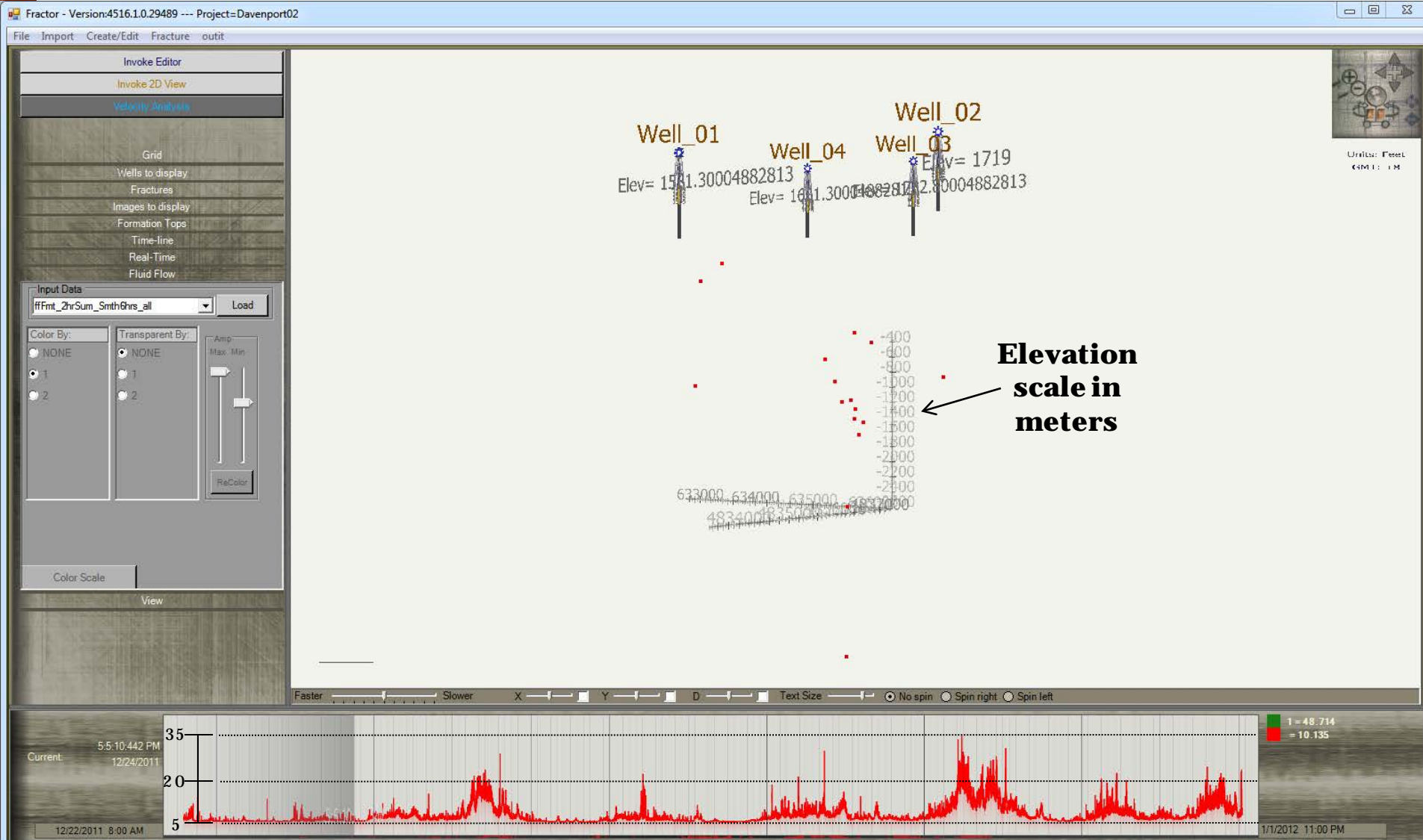
The next slide however shows the same scene only with the low-amplitude threshold slider set to a higher level. The measurement tool in the figure shows elevation in meters. The highest-amplitude parts of the lineation are at an elevation of about -1,400 m or a depth of 3,100 m (~10,000 ft) relative to the surface of the earth. The well head elevations are also shown on the plot.

The presence of the lineation at shallower depths may or may not have geologic significance, but it is our opinion that they are an artifact of the actual signal coming from depth and being incorrectly imaged by the algorithm *because the geometry of the observation wells is not well suited to imaging shallow seismic activity in combination with the data processing algorithm.* We would need wells much closer together to image shallow seismic activity. The fact that the highest amplitude energy mapping comes from depth, where the recording wells geometry *IS* favorable, is an indication that the energy from depth is real but that the shallower energy is an artifact. We do not see a way to draw an exact line separating artifact from real image data.



A low threshold value is set for the energy and it can be seen that some energy is mapped for a large depth range for the linear feature. The next slide however shows a different story.

Appendix G: 110



This slide is identical to the previous slide except that the display threshold has been raised showing that the predominant energy is mapped in the depth range of 3,000 m (elevation at the surface is ~1600-1700 m). Energy mapped at shallower depths is probably due to the receiver well geometry being unfavorable for shallow mapping and there for those shallow values are probably processing artifacts. The higher amplitude energy is concentrated at the SE end of the linear trend.



An interim report for the 2013 Newberry low-amplitude passive seismic monitoring project

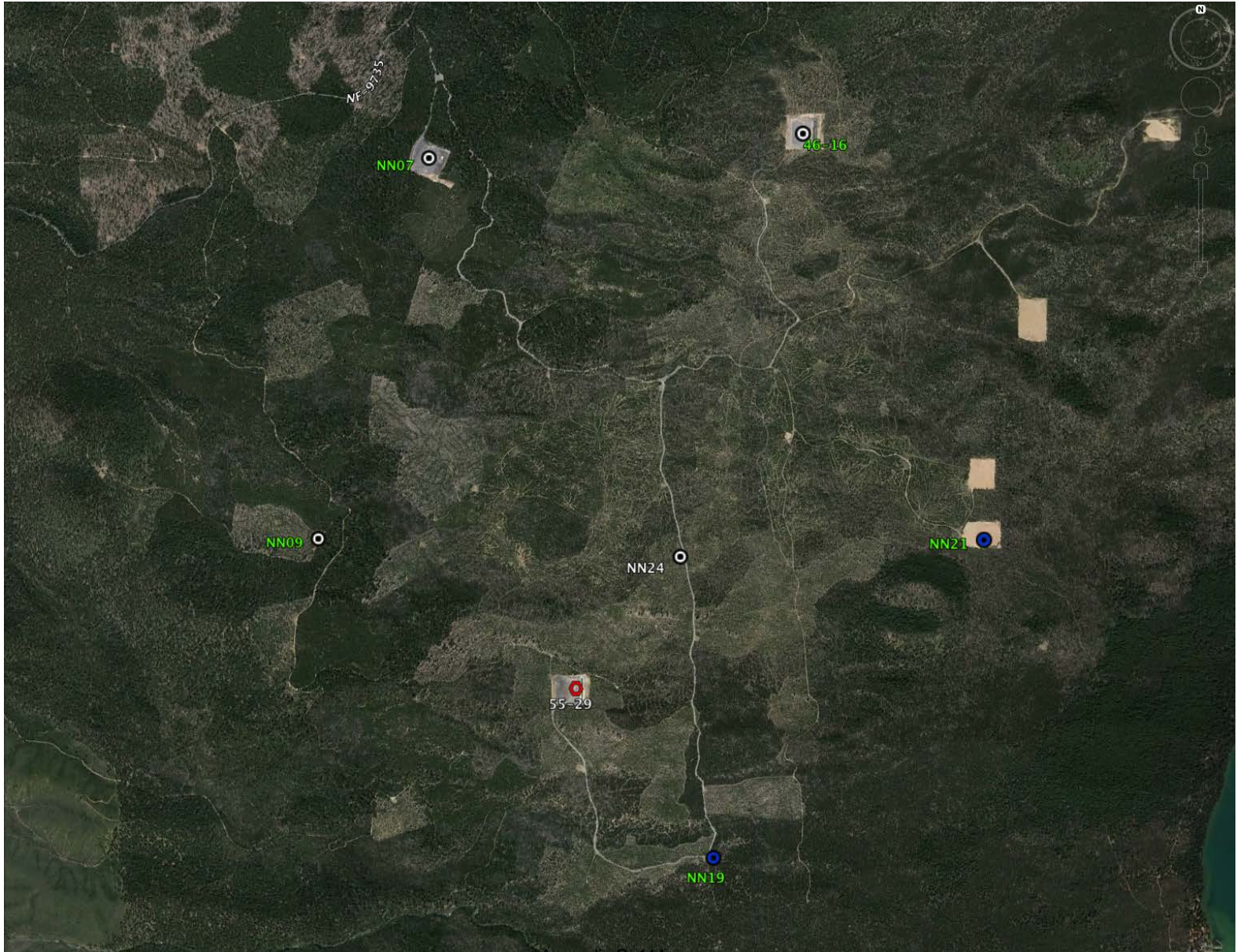
Altarock Energy, Inc

Jan 02, 2014
Author, Brian Fuller

SIGMA³

Introduction

This report is an interim discussion of partial results for the Newberry passive seismic project conducted for Altarock in September, 2013 by SigmaCubed. Seismic energy computations were made for a single horizontal plane an elevation of -1250 m (-4101 ft) relative to mean sea level . This elevation equates to approximately 10,000 ft below the mean surface elevation in the area of interest. The final full 3-dimensional energy calculations were completed January 01 and the results are being prepared for insertion into a 3D viewer to finalize the report. We expect there will be some back-and-forth discussion with Altarock and its agents regarding the report. For example, a brief discussion with Al Waibel this morning lead to this updated interim report that shows interesting seismic activity around the 46-16 well at a lower amplitude than was detected around the 55-29 well.

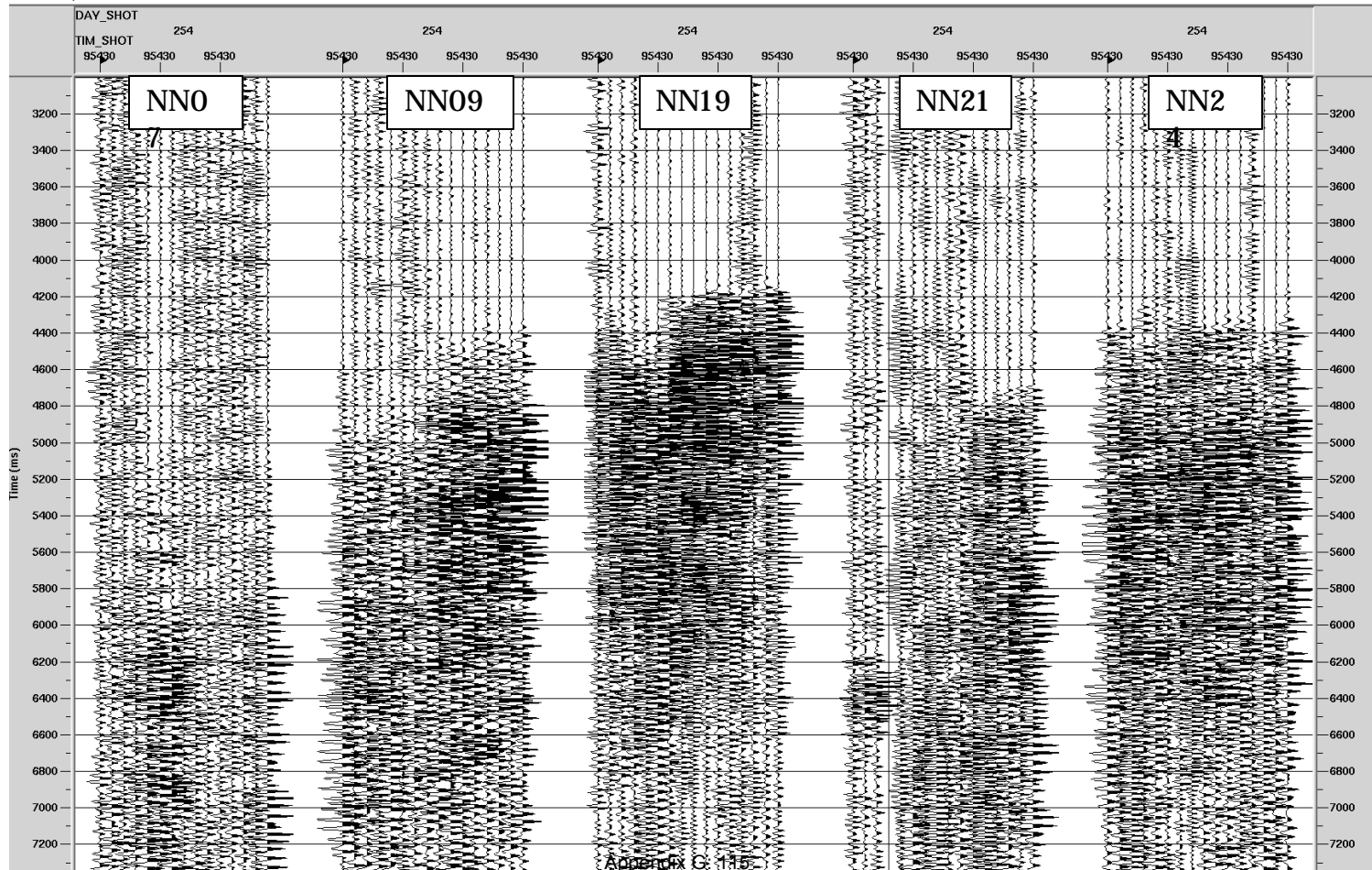


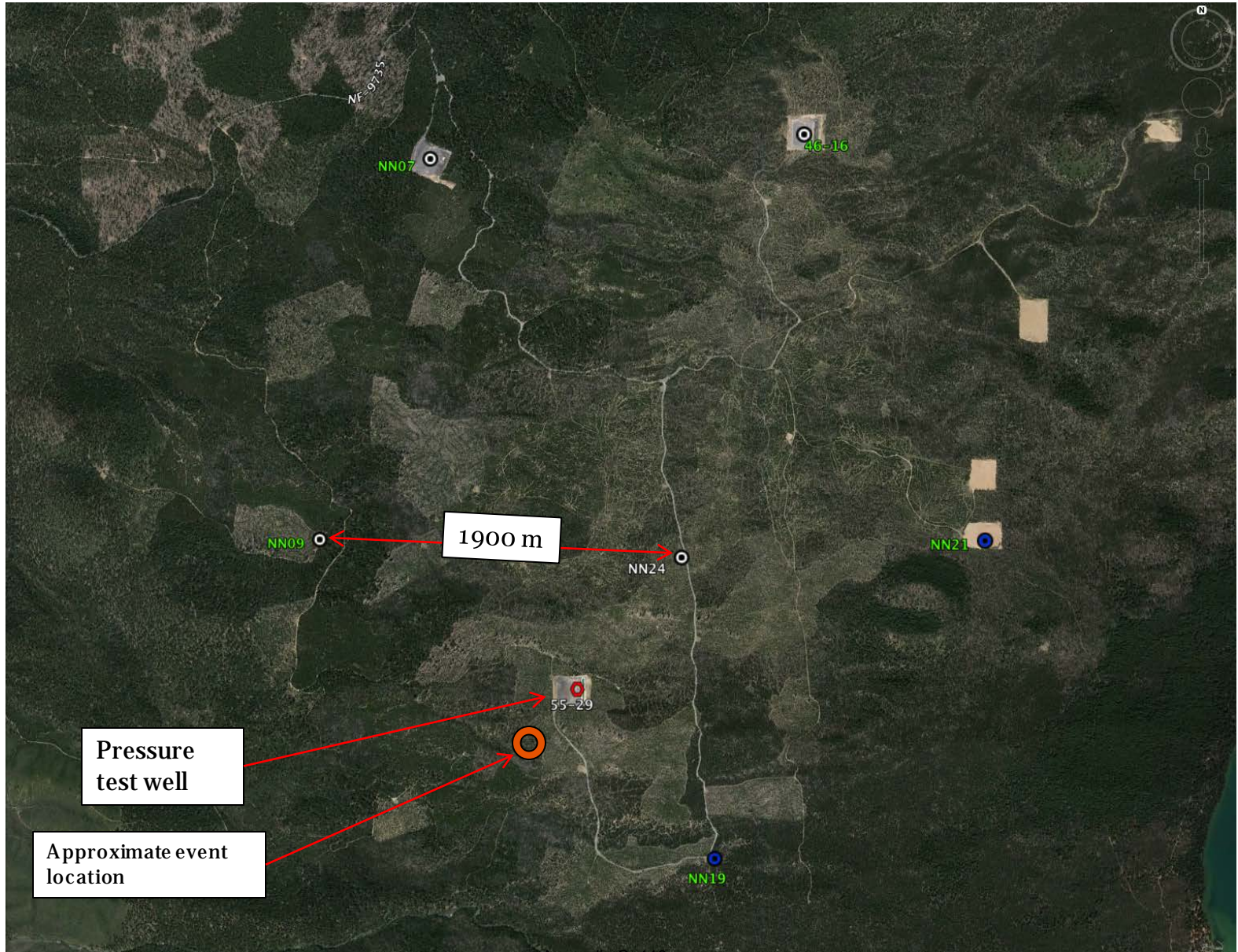
Appendix G. 114

Pressure test event

This event occurred September 11, 2013 at 54 minutes after midnight local time (09:53 GMT) near the 55-29 well. Water injection had been underway in the 46-16 well for the previous 16 hours when this event occurred. The water injection rate was about 138 gpm and surface pressure 400 psi at the time of the event. It is unlikely that this event is related to water injection in the 46-16 well because of the proximity of these wells and because of the already high level of seismic activity near the 55-29 well documented in this report.

The data shown is the vertical component with an Ormsby bandpass filter applied with parameters 15-21-36-48 Hz. While the arrivals are indistinct relative to arrivals we see in oil and gas microseismic data, the travel times are precise enough to see that this event occurred nearest to well NN19. A first order estimate of the location is shown on the next slide. The differences in event arrival times indicates that this event occurred at less than 1,000 m depth (subject to review).





Appendix G. 116

Seismic energy measurement result for elevation -1250 m msl
(-4101 ft msl or ~10,000 ft depth relative to surface in the area of interest)

The following slides show 7 separate time periods in which the **highest level** of seismic activity occurred in the study area measured at an elevation of -1250 m (msl). The analysis was carried out on a 2D grid plane at elevation -1250 m with a 200 m grid spacing in both the North-South and East-West direction. The grid plane was 6 km by 6 km centered near the middle of the 5 observation wells.

The highest seismic activity zones are mostly located near the 55-29 well though there are some variations.

The time periods of the 7 period of highest activity are shown on the time scale at the bottom of each display. The radius of spheres on the following displays are proportional to the energy measured within each time period shown. The values plotted range from 9,000-24,000 energy units that are internally consistent but the number range itself is arbitrary. In other words there is no meaning in comparing these numbers to any other power or energy measurement in seismology outside of this dataset.

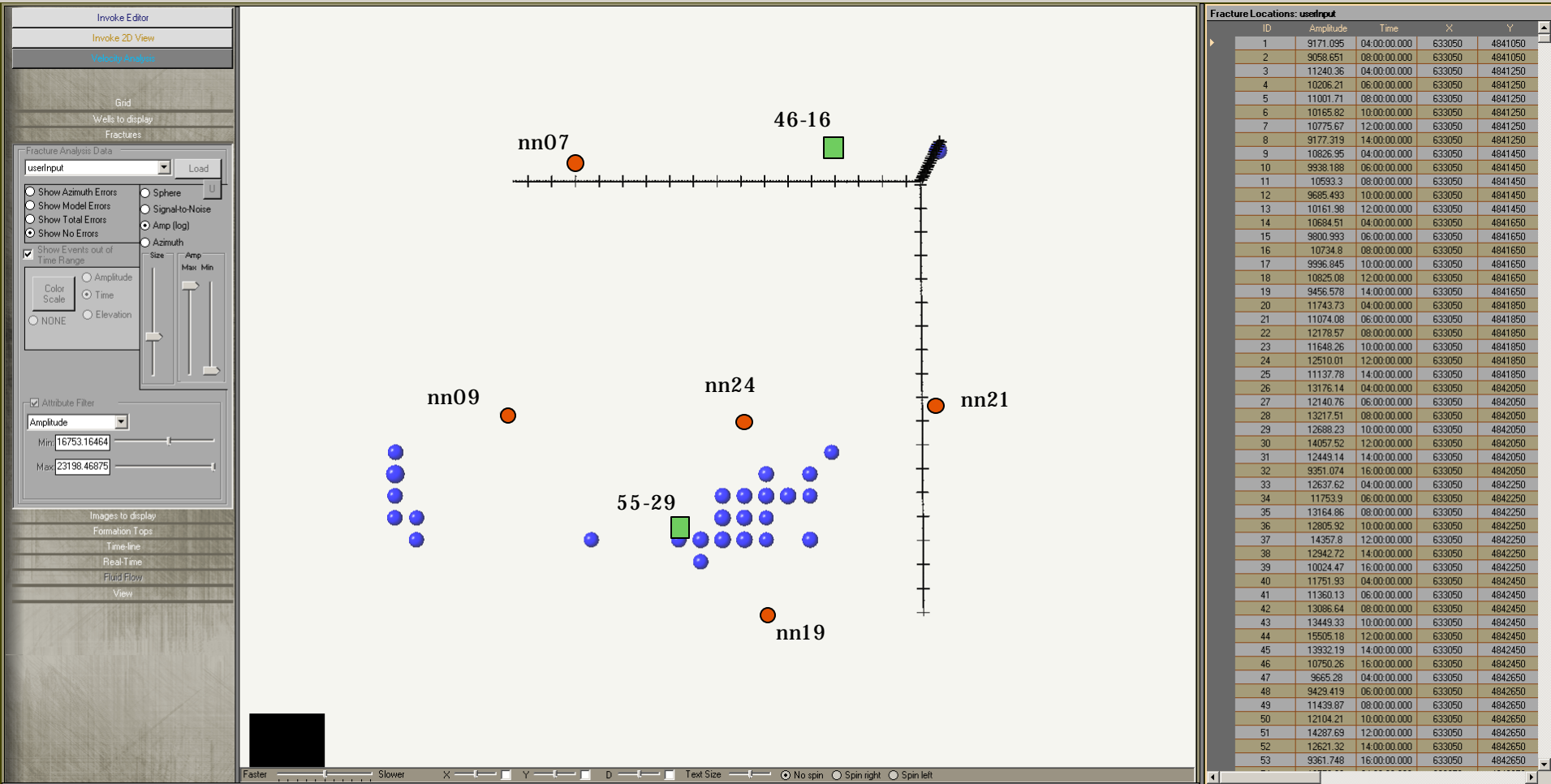
When the spheres are large there was a larger amount of seismic energy detected at the grid node during the time frame and when they are small there is a smaller amount of energy detected in the time frame. The smallest amounts of energy detected on some grid nodes approached zero so the grid nodes shown showed energy levels that were many-fold over the lowest amplitudes.

The grid nodes change color in the following displays. At the current time the color of the grids has no meaning.

Largest amplitudes: Active time period 1

Fractor - Version: ClickOnce published Version: v1.0.0.38 --- Project=Altarock

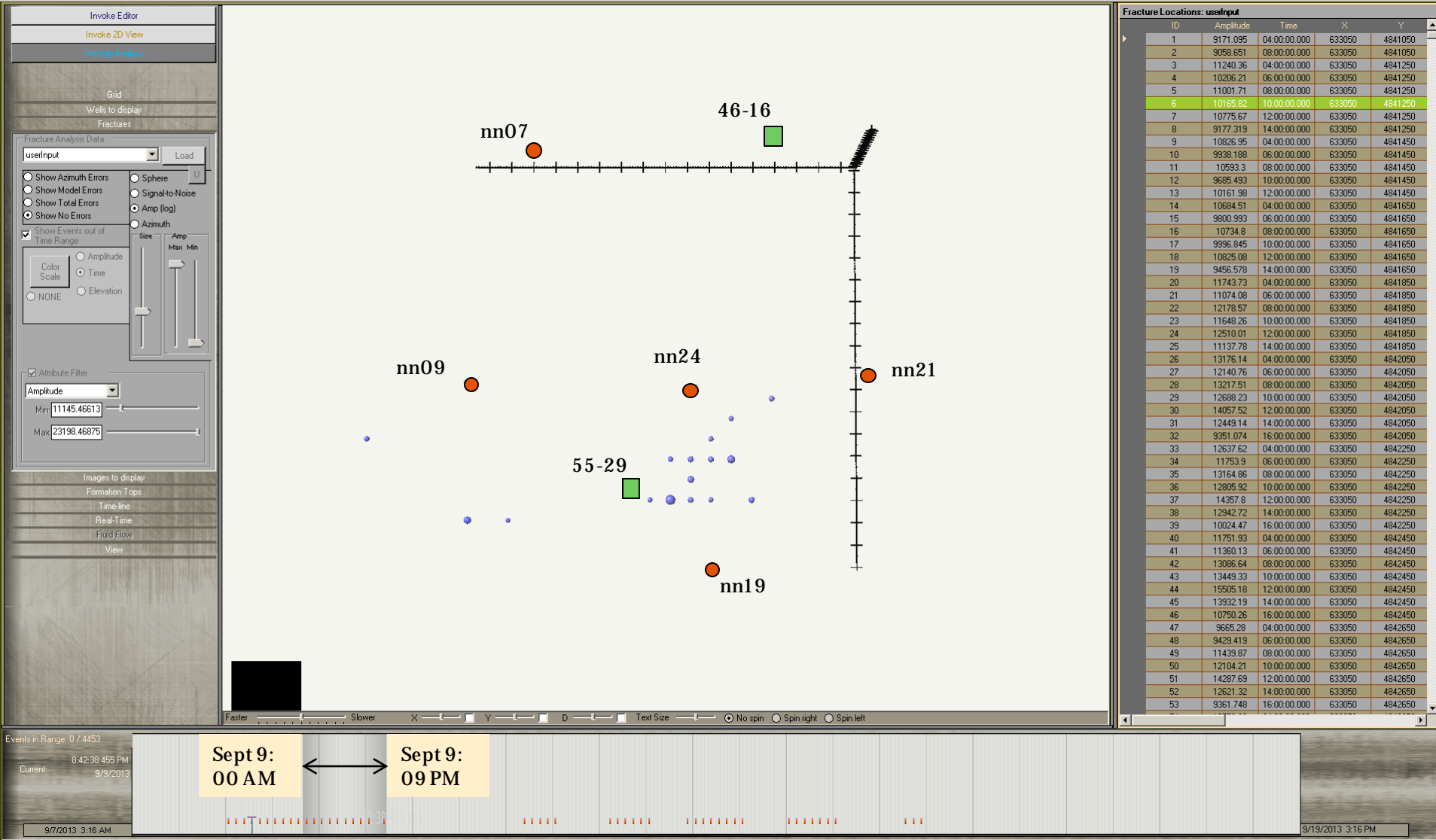
File Import Create/Edit Fracture outbit Export



Largest Amplitudes: Active time period 2: similar to period 1 but with lower amplitude

Fractor - Version: ClickOnce published Version: v1.0.0.38 --- Project=Altarock

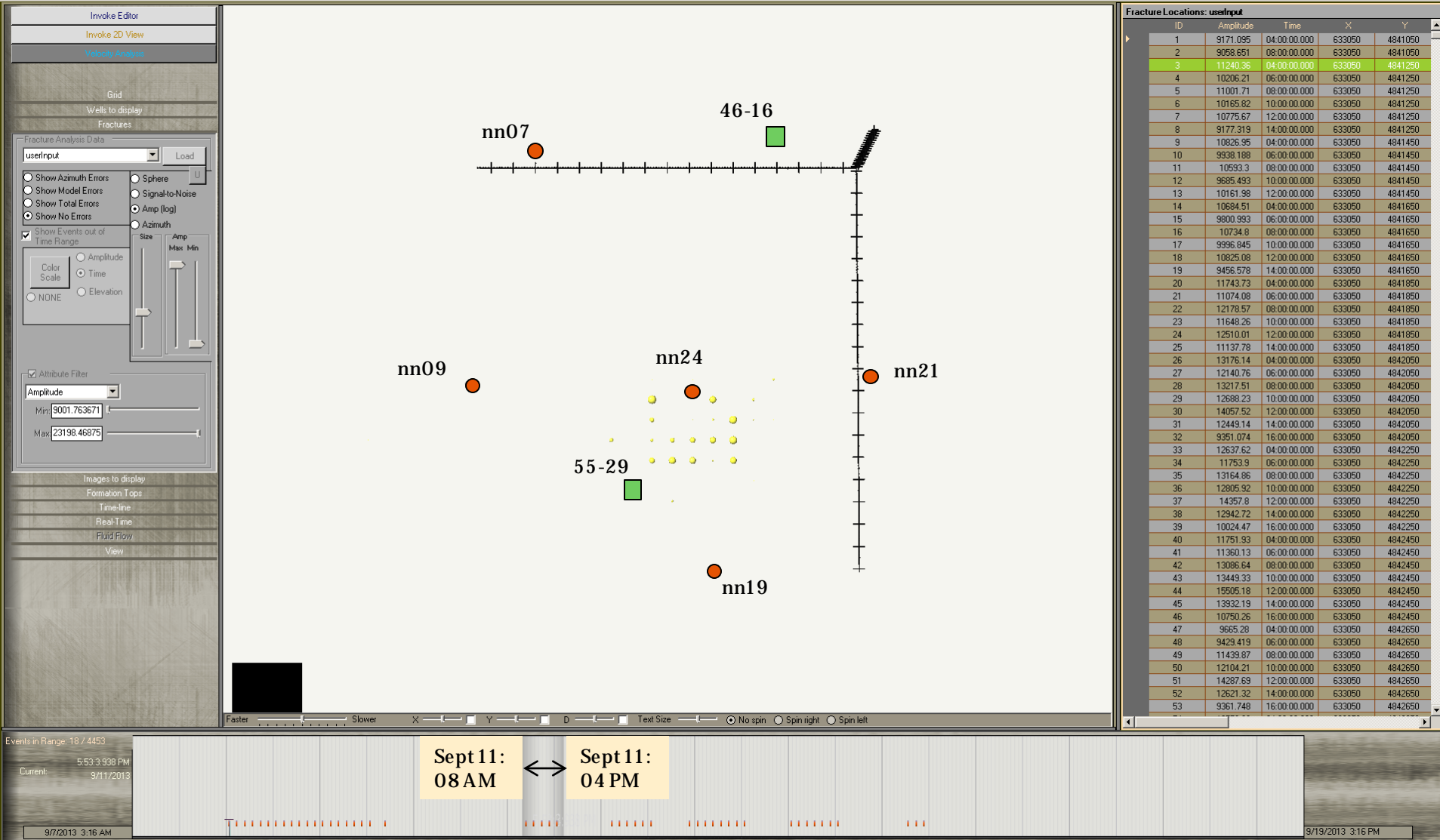
File Import Create/Edit Fracture outbit Export



Largest Amplitudes: Active time period 3: Lower amplitudes continue but move to the NE

Fractor - Version: ClickOnce published Version: v1.0.0.38 --- Project=Altarock

File Import Create/Edit Fracture outit Export



Largest Amplitudes: Active time period 4: Amplitudes increase and remain to NE of 55-29

Fractor - Version: ClickOnce published Version: v1.0.0.38 --- Project=Altarock

File Import Create/Edit Fracture outbit Export

Invoke Editor
Invoke 2D View
View Only Analysis

Grid
Wells to display
Fractures

Fracture Analysis Data
userinput Load

Show Azimuth Errors
 Show Model Errors
 Show Total Errors
 Show No Errors

Show Events out of Time Range

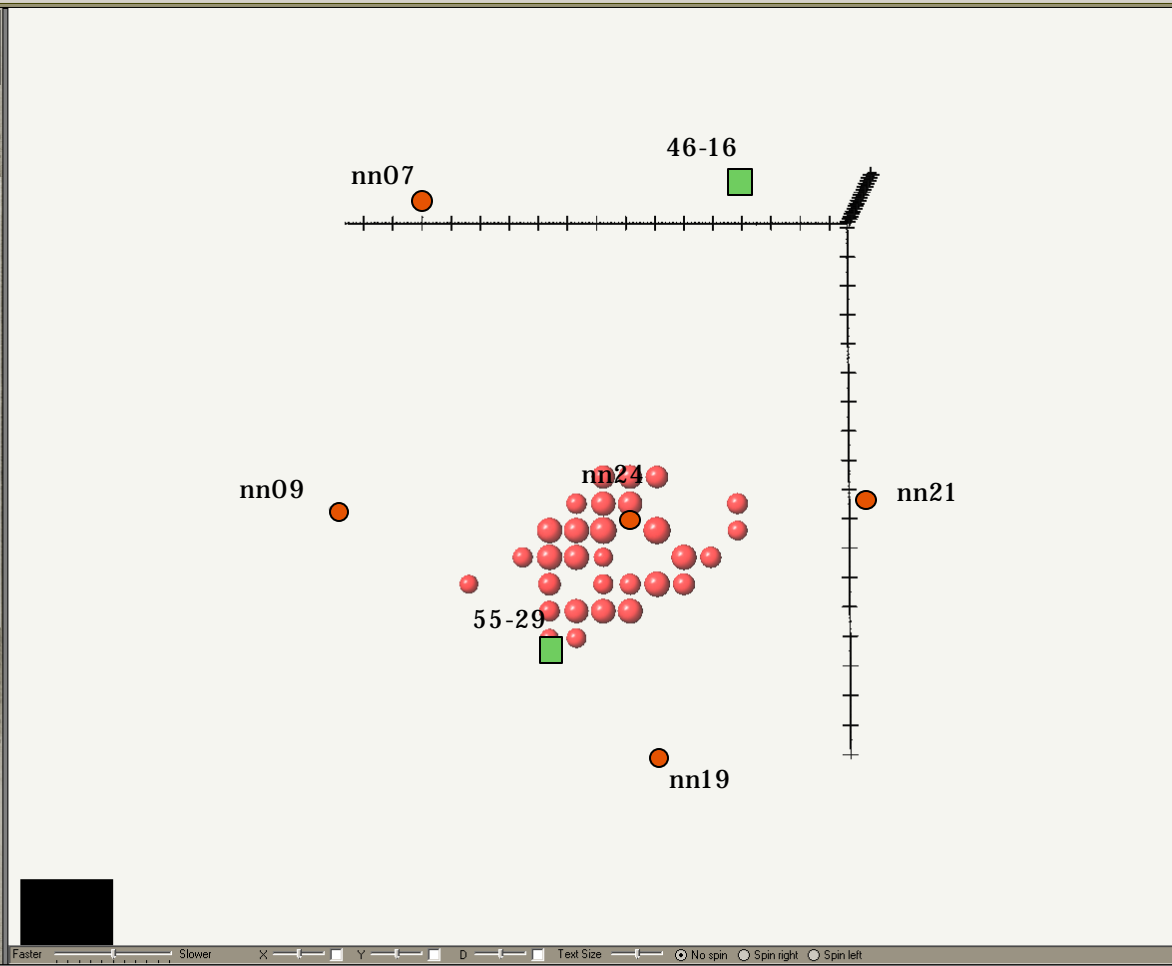
Amplitude
 Time
 NONE

Sphere
 Signal-to-Noise
 Amp (log)
 Azimuth

Size
 Amp Max Min

Attribute Filter
 Amplitude
 Min: 16880.93499
 Max: 23198.46875

Images to display
 Formation Tops
 Time-line
 Real-Time
 Fluid Flow
 View



Fracture Locations: userinput

ID	Amplitude	Time	X	Y
1	9171.095	04:00:00.000	633050	4841050
2	9068.651	08:00:00.000	633050	4841050
3	11240.36	04:00:00.000	633050	4841250
4	10206.21	06:00:00.000	633050	4841250
5	11001.71	08:00:00.000	633050	4841250
6	10165.82	10:00:00.000	633050	4841250
7	10775.67	12:00:00.000	633050	4841250
8	9177.319	14:00:00.000	633050	4841250
9	10826.95	04:00:00.000	633050	4841450
10	9938.188	06:00:00.000	633050	4841450
11	10593.3	08:00:00.000	633050	4841450
12	9685.493	10:00:00.000	633050	4841450
13	10161.98	12:00:00.000	633050	4841450
14	10684.51	04:00:00.000	633050	4841650
15	9900.993	06:00:00.000	633050	4841650
16	10734.8	08:00:00.000	633050	4841650
17	9996.845	10:00:00.000	633050	4841650
18	10825.08	12:00:00.000	633050	4841650
19	9456.578	14:00:00.000	633050	4841650
20	11743.73	04:00:00.000	633050	4841850
21	11074.08	06:00:00.000	633050	4841850
22	12178.57	08:00:00.000	633050	4841850
23	11648.26	10:00:00.000	633050	4841850
24	12510.01	12:00:00.000	633050	4841850
25	11137.78	14:00:00.000	633050	4841850
26	13176.14	04:00:00.000	633050	4842050
27	12140.76	06:00:00.000	633050	4842050
28	13217.51	08:00:00.000	633050	4842050
29	12688.23	10:00:00.000	633050	4842050
30	14057.52	12:00:00.000	633050	4842050
31	12449.14	14:00:00.000	633050	4842050
32	9351.074	16:00:00.000	633050	4842050
33	12637.62	04:00:00.000	633050	4842250
34	11753.9	06:00:00.000	633050	4842250
35	13164.86	08:00:00.000	633050	4842250
36	12805.92	10:00:00.000	633050	4842250
37	14357.8	12:00:00.000	633050	4842250
38	12942.72	14:00:00.000	633050	4842250
39	10024.47	16:00:00.000	633050	4842250
40	11751.93	04:00:00.000	633050	4842450
41	11360.13	06:00:00.000	633050	4842450
42	13086.64	08:00:00.000	633050	4842450
43	13449.33	10:00:00.000	633050	4842450
44	15505.18	12:00:00.000	633050	4842450
45	13932.19	14:00:00.000	633050	4842450
46	10750.26	16:00:00.000	633050	4842450
47	9665.28	04:00:00.000	633050	4842650
48	9429.419	06:00:00.000	633050	4842650
49	11439.87	08:00:00.000	633050	4842650
50	12104.21	10:00:00.000	633050	4842650
51	14287.69	12:00:00.000	633050	4842650
52	12621.32	14:00:00.000	633050	4842650
53	9361.748	16:00:00.000	633050	4842650



Largest Amplitudes: Active time period 5: Similar to period 4

Fractor - Version: ClickOnce published Version: v1.0.0.38 --- Project=Altarock

File Import Create/Edit Fracture outbit Export

Invoke Editor
Invoke 2D View
Visually Analyze

Grid
Wells to display
Fractures

Fracture Analysis Data
userinput Load

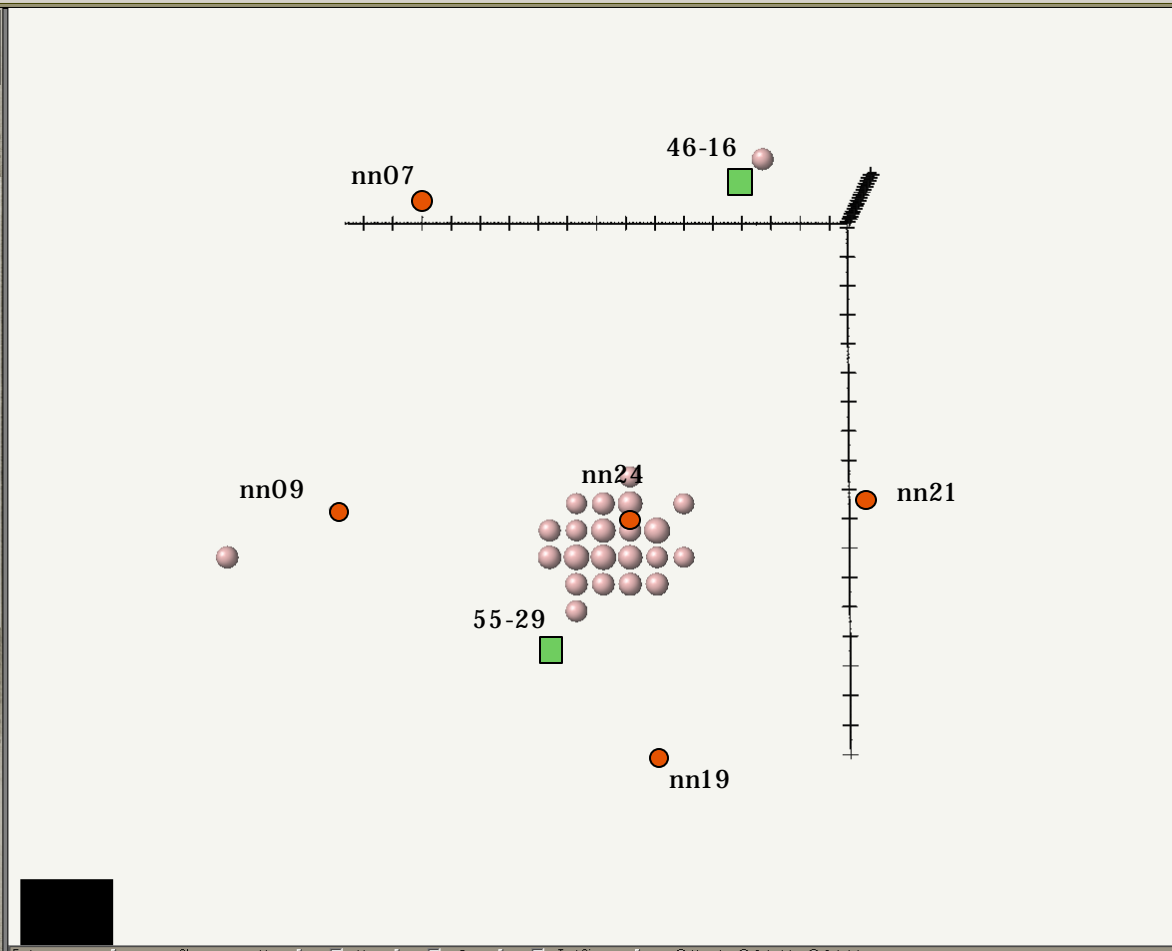
Show Azimuth Errors
 Show Model Errors
 Show Total Errors
 Show No Errors

Show Events out of Time Range

Color Scale
 Amplitude
 Time
 NONE
 Elevation

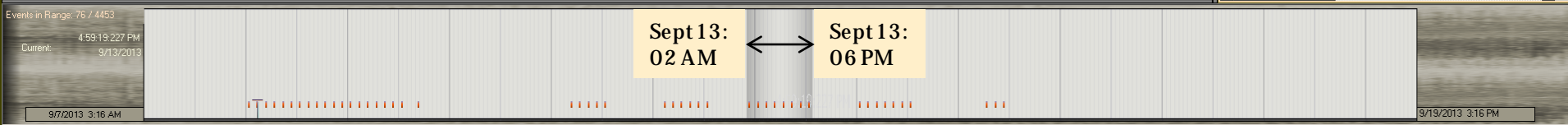
Attribute Filter
 Amplitude
 Min: 18428.37584
 Max: 23198.46875

Images to display
 Formation Tops
 Time-line
 Real-time
 Fluid Flow
 View



Fracture Locations: userinput

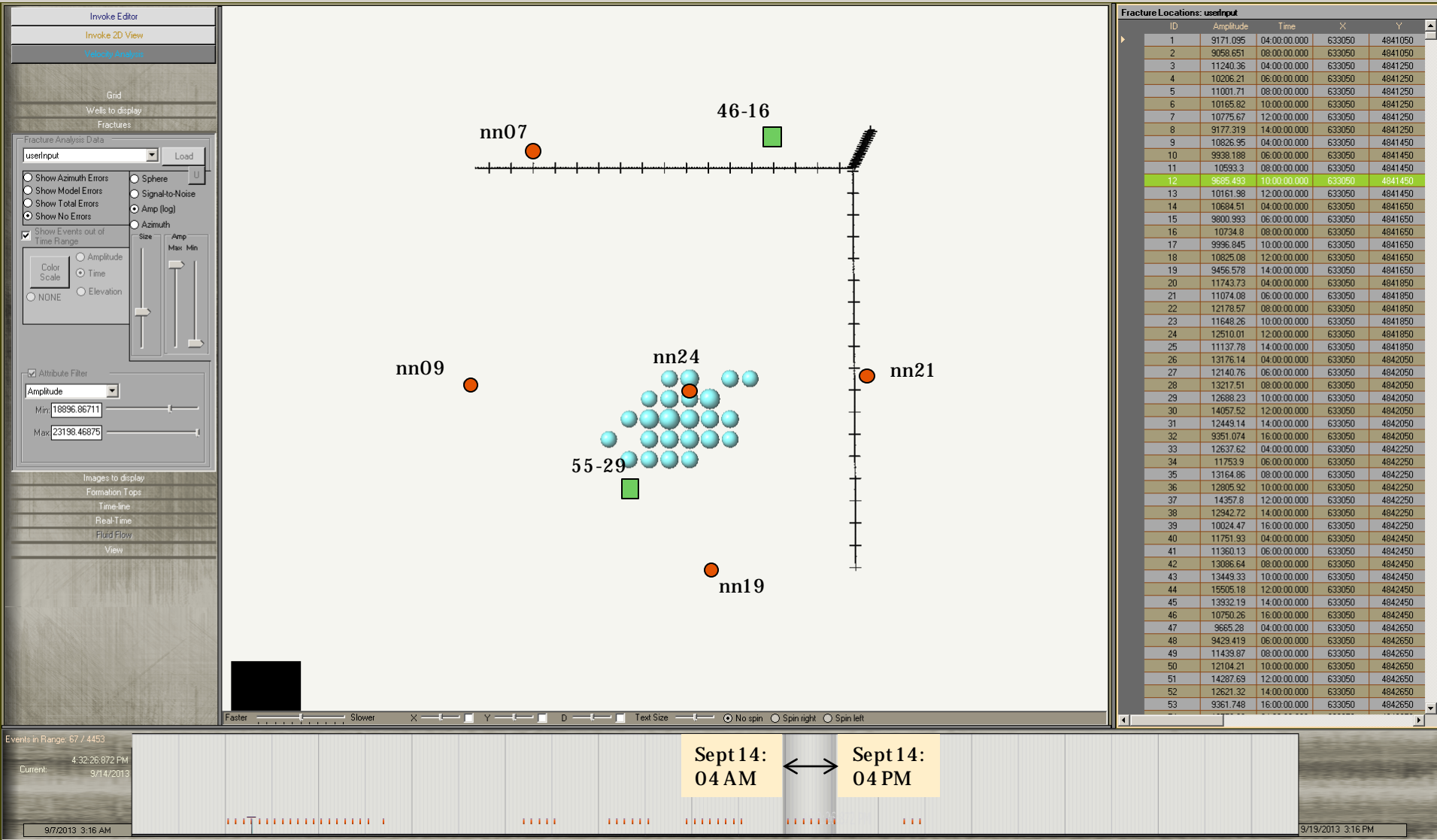
ID	Amplitude	Time	X	Y
1	9171.095	04:00:00.000	633050	4841050
2	9058.651	08:00:00.000	633050	4841050
3	11240.36	04:00:00.000	633050	4841250
4	10206.21	06:00:00.000	633050	4841250
5	11001.71	08:00:00.000	633050	4841250
6	10165.82	10:00:00.000	633050	4841250
7	10775.67	12:00:00.000	633050	4841250
8	9177.319	14:00:00.000	633050	4841250
9	10826.95	04:00:00.000	633050	4841450
10	9938.188	06:00:00.000	633050	4841450
11	10593.3	08:00:00.000	633050	4841450
12	9685.493	10:00:00.000	633050	4841450
13	10161.98	12:00:00.000	633050	4841450
14	10684.51	04:00:00.000	633050	4841650
15	9900.993	06:00:00.000	633050	4841650
16	10734.8	08:00:00.000	633050	4841650
17	9996.845	10:00:00.000	633050	4841650
18	10825.08	12:00:00.000	633050	4841650
19	9456.578	14:00:00.000	633050	4841650
20	11743.73	04:00:00.000	633050	4841850
21	11074.08	06:00:00.000	633050	4841850
22	12178.57	08:00:00.000	633050	4841850
23	11648.26	10:00:00.000	633050	4841850
24	12510.01	12:00:00.000	633050	4841850
25	11137.78	14:00:00.000	633050	4841850
26	13176.14	04:00:00.000	633050	4842050
27	12140.76	06:00:00.000	633050	4842050
28	13217.51	08:00:00.000	633050	4842050
29	12688.23	10:00:00.000	633050	4842050
30	14057.52	12:00:00.000	633050	4842050
31	12449.14	14:00:00.000	633050	4842050
32	9351.074	16:00:00.000	633050	4842050
33	12637.62	04:00:00.000	633050	4842250
34	11753.9	06:00:00.000	633050	4842250
35	13164.86	08:00:00.000	633050	4842250
36	12805.92	10:00:00.000	633050	4842250
37	14357.8	12:00:00.000	633050	4842250
38	12942.72	14:00:00.000	633050	4842250
39	10024.47	16:00:00.000	633050	4842250
40	11751.93	04:00:00.000	633050	4842450
41	11360.13	06:00:00.000	633050	4842450
42	13086.64	08:00:00.000	633050	4842450
43	13449.33	10:00:00.000	633050	4842450
44	15505.18	12:00:00.000	633050	4842450
45	13932.19	14:00:00.000	633050	4842450
46	10750.26	16:00:00.000	633050	4842450
47	9665.28	04:00:00.000	633050	4842650
48	9429.419	06:00:00.000	633050	4842650
49	11439.87	08:00:00.000	633050	4842650
50	12194.21	10:00:00.000	633050	4842650
51	14287.69	12:00:00.000	633050	4842650
52	12621.32	14:00:00.000	633050	4842650
53	9361.748	16:00:00.000	633050	4842650



Largest Amplitudes: Active time period 6: continued energy NE of 55-29

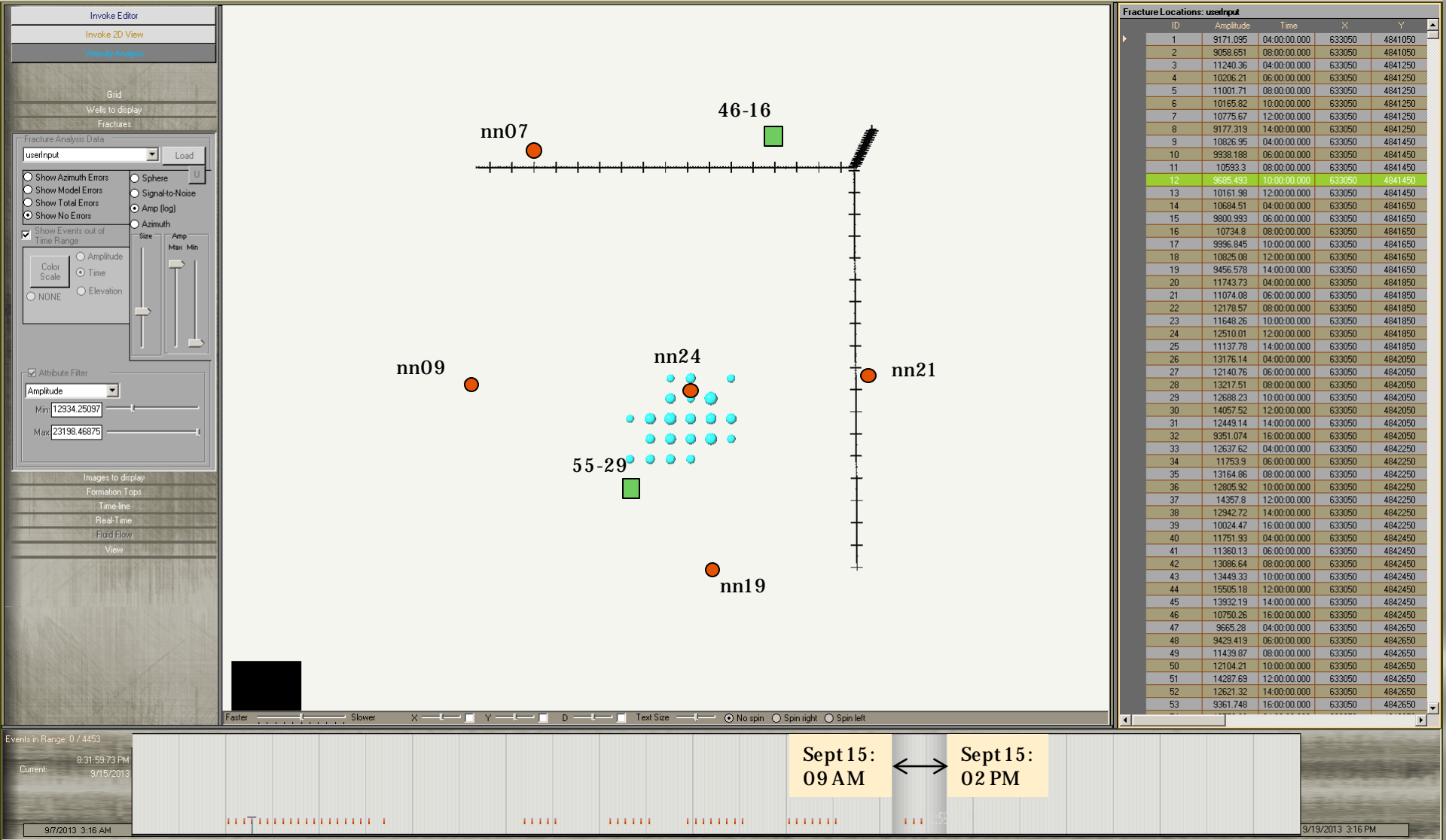
Fractor - Version: ClickOnce published Version: v1.0.0.38 --- Project=Altarock

File Import Create/Edit Fracture outbit Export



Largest Amplitudes: Active time period 7: continued energy NE of 55-29, end of survey

Fractor - Version: ClickOnce published Version: v1.0.0.38 --- Project=Altarock



A possible implication of plots above

Although engineering activity had already been underway in the 55-29 well prior to this seismic survey, the measured seismic energy increased significantly around the 55-29 well on September 12 in response to active injection in the 55-29 well starting September 10. The seismic activity between Sept 08-11 moved decidedly to the Northeast of the 55-29. Seismic activity increased around noon on Sept 12.

One might speculate* that this result indicates the fracture energy from the injection moved primarily northeast from the 55-29 well and that uptake wells might most profitably be drilled northeast of the 55-29 well.

*These comments are speculation and will require more in-depth analysis by engineering experts familiar with the geology and engineering properties of the field location.

Analysis of the lower amplitudes

The following slides show time periods in which the ***lowest level*** of seismic amplitude activity occurred in the study area and in particular the analysis is focused on the area around the 46-16 well. As in the slides above, these computations were done for a constant horizontal plane at an elevation of -1250 m (msl). The analysis was carried out on a 2D grid plane at elevation -1250 m with a 200 m grid spacing in both the North-South and East-West direction. The grid plane was 6 km by 6 km centered near the middle of the 5 observation wells.

The highest seismic activity zones were shown in the slides above and they dominated the amplitude spectrum but a primary question of this survey is whether this type of survey can detect the seismic response related to fluid flowing in fractures near the 46-16. Fluids were produced from the 46-16 Sept 08, 09, and 10 so we focus in the following analysis on amplitudes that are lower than the dominant amplitudes measured near the 55-29 well. Note that seismic energy might be due to the fluid motion itself or might be due to rocks breaking in response to stress changes as the fluid pressures change in the rock. We make no claim at this time that we can differentiate the direct cause of the seismic energy that is measured.

The grid nodes change color in the following displays. At the current time the color of the grids has no meaning.

Lowest Amplitudes: September 08 – The well was opened at 14:10 local time This plot shows the amplitudes prior to opening the flow.

Fractor - Version: ClickOnce published Version: v1.0.0.38 --- Project=Alkarock

File Import Create/Edit Fracture outlook Export

Invoke Editor
Invoke 2D View
History Analysis

Grid
Wells to display
Fractures

Fracture Analysis Data
uselinput Load

Show Azimuth Errors
 Show Model Errors
 Show Total Errors
 Show No Errors
 Show Events out of Time Range

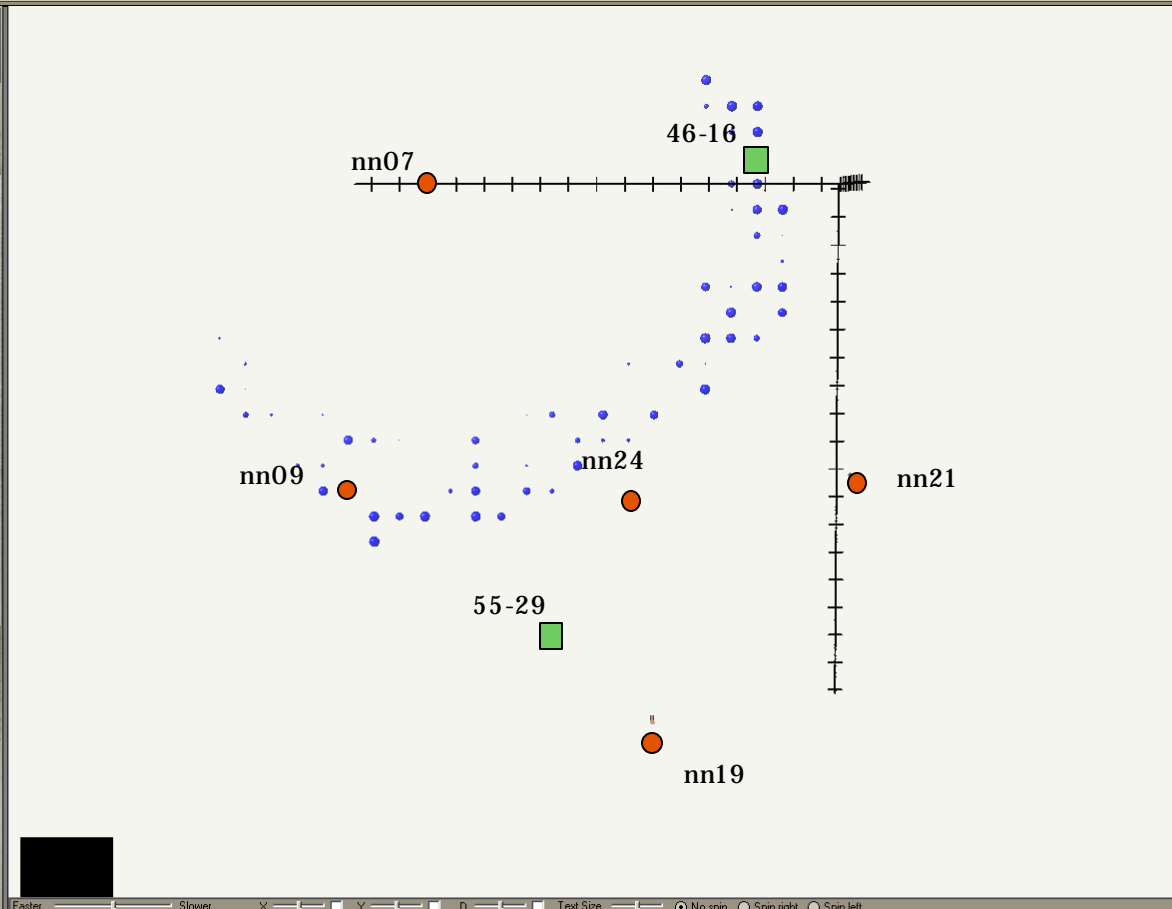
Sphere
 Signal-to-Noise
 Amp (log)
 Azimuth

Amplitude
 Time
 Elevation

Color Scale
NONE

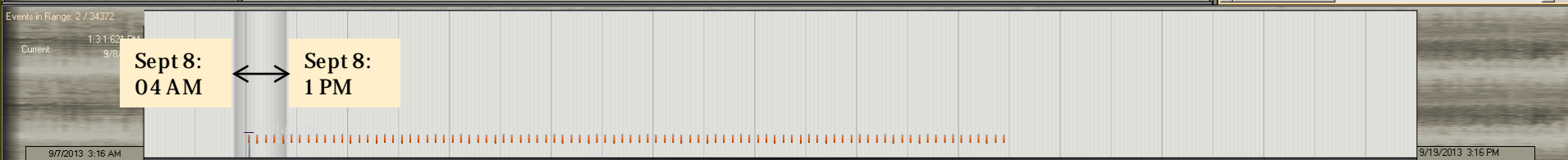
Attribute Filter
 Amplitude
 Min: 500.4136047
 Max: 2225.465795

Images to display
Formation Tops
Time-line
Real-Time
Fluid Flow
View



Fracture Locations: uselinput

ID	Amplitude	Time	X	Y
1	9171.095	04:00:00.000	633050	4941050
2	11240.36	04:00:00.000	633050	4941250
3	10836.95	04:00:00.000	633050	4941450
4	10884.51	04:00:00.000	633050	4941650
5	11743.73	04:00:00.000	633050	4941850
6	13176.14	04:00:00.000	633050	4942050
7	12637.62	04:00:00.000	633050	4942250
8	11751.93	04:00:00.000	633050	4942450
9	9665.28	04:00:00.000	633050	4942650
10	12572.39	04:00:00.000	633050	4942850
11	11089.11	04:00:00.000	633050	4943050
12	12558.95	04:00:00.000	633050	4943250
13	10827.11	04:00:00.000	633050	4943450
14	4972.603	04:00:00.000	633050	4943650
15	3606.611	04:00:00.000	633050	4943850
16	1956.434	04:00:00.000	633050	4944050
17	8605.067	04:00:00.000	633250	4941050
18	11936.38	04:00:00.000	633250	4941250
19	12288.84	04:00:00.000	633250	4941450
20	11590.45	04:00:00.000	633250	4941650
21	12365.44	04:00:00.000	633250	4941850
22	12756.41	04:00:00.000	633250	4942050
23	12240.25	04:00:00.000	633250	4942250
24	12227.8	04:00:00.000	633250	4942450
25	12093.75	04:00:00.000	633250	4942650
26	11555.48	04:00:00.000	633250	4942850
27	10428.44	04:00:00.000	633250	4943050
28	8943.484	04:00:00.000	633250	4943250
29	7625.59	04:00:00.000	633250	4943450
30	4472.812	04:00:00.000	633250	4943650
31	1112.342	04:00:00.000	633250	4943850
32	9452.426	04:00:00.000	633450	4941050
33	10623.24	04:00:00.000	633450	4941250
34	10586.82	04:00:00.000	633450	4941450
35	11600.89	04:00:00.000	633450	4941650
36	12234.16	04:00:00.000	633450	4941850
37	11493.16	04:00:00.000	633450	4942050
38	11745.9	04:00:00.000	633450	4942250
39	11697.08	04:00:00.000	633450	4942450
40	10469.71	04:00:00.000	633450	4942650
41	10738.69	04:00:00.000	633450	4942850
42	9674.216	04:00:00.000	633450	4943050
43	8567.526	04:00:00.000	633450	4943250
44	4115.773	04:00:00.000	633450	4943450
45	2665.47	04:00:00.000	633450	4943650
46	10509.53	04:00:00.000	633650	4941050
47	10236.27	04:00:00.000	633650	4941250
48	11513.18	04:00:00.000	633650	4941450
49	11499.82	04:00:00.000	633650	4941650
50	12796.12	04:00:00.000	633650	4941850
51	11297.6	04:00:00.000	633650	4942050



Lowest Amplitudes: September 08 – The well was opened at 14:10 local time This plot shows the amplitudes after opening the flow at 14:10 until midnight on Sept 08. Activity near the 46-16 does not change in an obvious way in response to the first day of flowing the well.

Fractor - Version: ClickOnce published Version: v1.0.0.38 --- Project: Alkarock

File Import Create/Edit Fracture outlook Export

Invoke Editor
Invoke 2D View
History Analysis

Grid
Wells to display
Fractures

Fracture Analysis Data
usetInput Load

Show Azimuth Errors
 Show Model Errors
 Show Total Errors
 Show No Errors
 Show Events out of Time Range

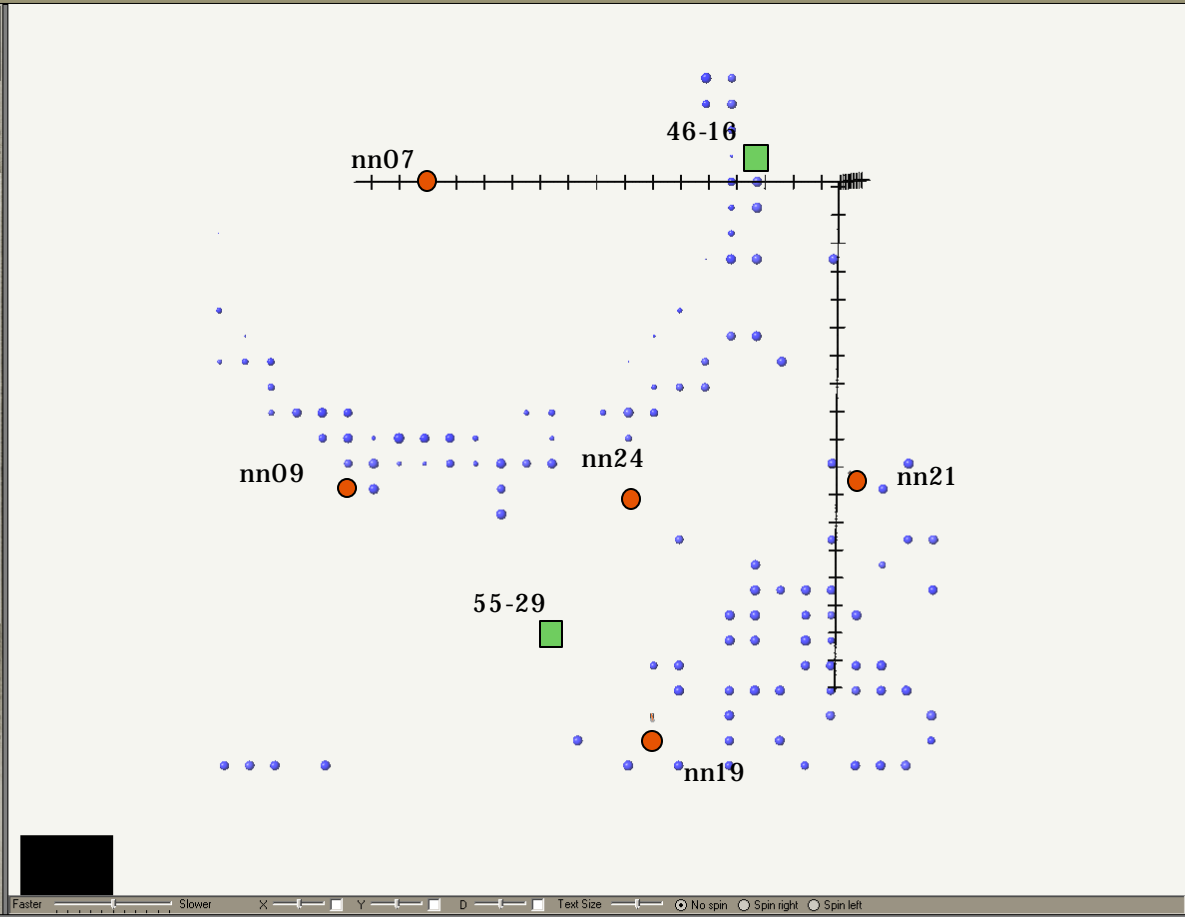
Sphere
 Signal-to-Noise
 Amp (log)
 Azimuth

Amplitude
 Time
 Elevation

NONE

Attribute Filter
 Amplitude
 Min: 500.4136047
 Max: 2225.465795

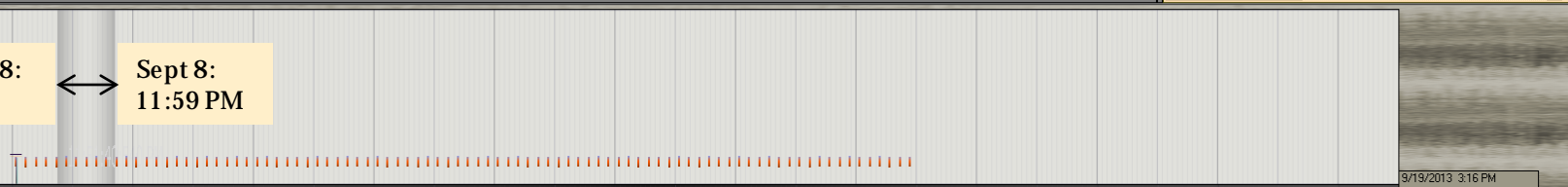
Images to display
 Formation Tops
 Time-line
 Real-Time
 Fluid Flow
 View



Fracture Locations: usetInput

ID	Amplitude	Time	X	Y
1	9171.095	04:00:00.000	633050	4941050
2	11240.36	04:00:00.000	633050	4941250
3	10826.95	04:00:00.000	633050	4941450
4	10684.51	04:00:00.000	633050	4941650
5	11743.73	04:00:00.000	633050	4941850
6	13176.14	04:00:00.000	633050	4942050
7	12637.62	04:00:00.000	633050	4942250
8	11751.93	04:00:00.000	633050	4942450
9	9665.28	04:00:00.000	633050	4942650
10	12572.39	04:00:00.000	633050	4942850
11	11089.11	04:00:00.000	633050	4943050
12	12558.95	04:00:00.000	633050	4943250
13	10827.11	04:00:00.000	633050	4943450
14	4972.603	04:00:00.000	633050	4943650
15	3606.611	04:00:00.000	633050	4943850
16	1956.434	04:00:00.000	633050	4944050
17	8605.067	04:00:00.000	633250	4941050
18	11936.38	04:00:00.000	633250	4941250
19	12288.84	04:00:00.000	633250	4941450
20	11590.45	04:00:00.000	633250	4941650
21	12365.44	04:00:00.000	633250	4941850
22	12756.41	04:00:00.000	633250	4942050
23	12240.25	04:00:00.000	633250	4942250
24	12227.8	04:00:00.000	633250	4942450
25	12093.75	04:00:00.000	633250	4942650
26	11555.48	04:00:00.000	633250	4942850
27	10428.44	04:00:00.000	633250	4943050
28	8943.484	04:00:00.000	633250	4943250
29	7625.59	04:00:00.000	633250	4943450
30	4472.812	04:00:00.000	633250	4943650
31	1112.342	04:00:00.000	633250	4943850
32	9452.426	04:00:00.000	633450	4941050
33	10623.24	04:00:00.000	633450	4941250
34	10586.82	04:00:00.000	633450	4941450
35	11600.89	04:00:00.000	633450	4941650
36	12234.16	04:00:00.000	633450	4941850
37	11493.16	04:00:00.000	633450	4942050
38	11745.9	04:00:00.000	633450	4942250
39	11697.08	04:00:00.000	633450	4942450
40	10469.71	04:00:00.000	633450	4942650
41	10738.69	04:00:00.000	633450	4942850
42	9674.216	04:00:00.000	633450	4943050
43	8567.526	04:00:00.000	633450	4943250
44	4115.773	04:00:00.000	633450	4943450
45	2665.47	04:00:00.000	633450	4943650
46	10509.53	04:00:00.000	633650	4941050
47	10236.27	04:00:00.000	633650	4941250
48	11513.18	04:00:00.000	633650	4941450
49	11499.82	04:00:00.000	633650	4941650
50	12796.12	04:00:00.000	633650	4941850
51	11297.6	04:00:00.000	633650	4942050

Events in Range: 204 / 34372
 11:51:40:540 PM
 Current: 9/8/2013
 9/7/2013 3:16 AM



Lowest Amplitudes: September 09 – General activity increases throughout the area and in particular near observation well nn07 which had previously been a particularly quiet location.

Fractor - Version: ClickOnce published Version: v1.0.0.38 --- Project=Alkarock

File Import Create/Edit Fracture Output Export

Invoke Editor
Invoke 2D View
History Analysis

Grid
Wells to display
Fractures

Fracture Analysis Data
usetInput Load

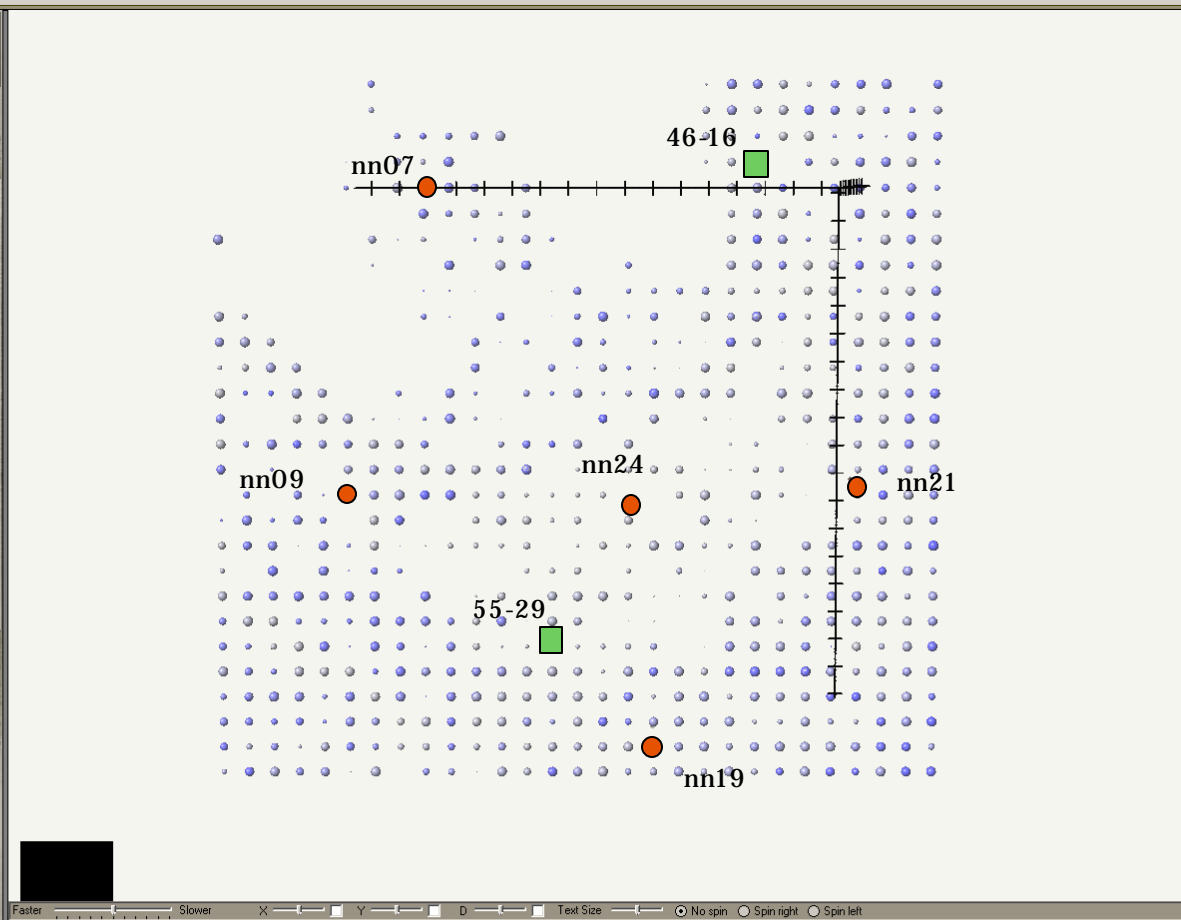
Show Azimuth Errors
 Show Model Errors
 Show Total Errors
 Show No Errors
 Show Events out of Time Range

Sphere
 Signal-to-Noise
 Amp (log)
 Azimuth

Amplitude
 Time
 Elevation
 NONE

Attribute Filter
 Amplitude
 Min: 500.4136047
 Max: 1839.598858

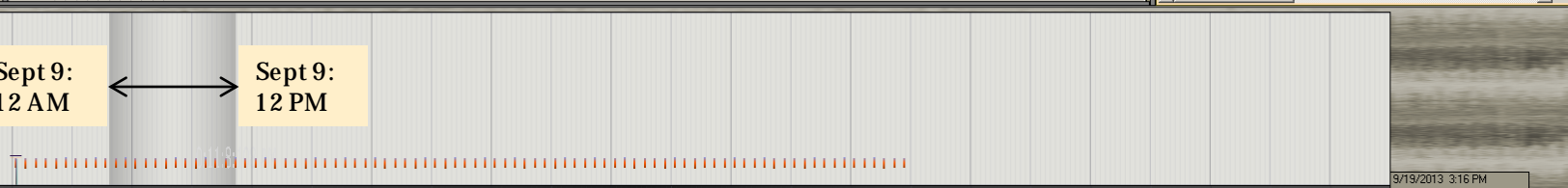
Images to display
Formation Tops
Time-line
Real-Time
Fluid Flow
View



Fracture Locations: useInput

ID	Amplitude	Time	X	Y
1	9171.095	04:00:00.000	633050	4841050
2	11240.36	04:00:00.000	633050	4841250
3	10826.95	04:00:00.000	633050	4841450
4	10684.51	04:00:00.000	633050	4841650
5	11743.73	04:00:00.000	633050	4841850
6	13176.14	04:00:00.000	633050	4842050
7	12637.62	04:00:00.000	633050	4842250
8	11751.93	04:00:00.000	633050	4842450
9	9665.28	04:00:00.000	633050	4842650
10	12572.39	04:00:00.000	633050	4842850
11	11089.11	04:00:00.000	633050	4843050
12	12558.95	04:00:00.000	633050	4843250
13	10827.11	04:00:00.000	633050	4843450
14	4972.603	04:00:00.000	633050	4843650
15	3606.611	04:00:00.000	633050	4843850
16	1956.434	04:00:00.000	633050	4844050
17	8605.067	04:00:00.000	633250	4841050
18	11936.38	04:00:00.000	633250	4841250
19	12288.84	04:00:00.000	633250	4841450
20	11590.45	04:00:00.000	633250	4841650
21	12365.44	04:00:00.000	633250	4841850
22	12756.41	04:00:00.000	633250	4842050
23	12240.25	04:00:00.000	633250	4842250
24	12227.8	04:00:00.000	633250	4842450
25	12093.75	04:00:00.000	633250	4842650
26	11555.48	04:00:00.000	633250	4842850
27	10428.44	04:00:00.000	633250	4843050
28	8943.484	04:00:00.000	633250	4843250
29	7625.59	04:00:00.000	633250	4843450
30	4472.812	04:00:00.000	633250	4843650
31	1112.342	04:00:00.000	633250	4843850
32	9452.426	04:00:00.000	633450	4841050
33	10623.24	04:00:00.000	633450	4841250
34	10586.82	04:00:00.000	633450	4841450
35	11600.89	04:00:00.000	633450	4841650
36	12234.16	04:00:00.000	633450	4841850
37	11493.16	04:00:00.000	633450	4842050
38	11745.9	04:00:00.000	633450	4842250
39	11697.08	04:00:00.000	633450	4842450
40	10469.71	04:00:00.000	633450	4842650
41	10738.69	04:00:00.000	633450	4842850
42	9674.216	04:00:00.000	633450	4843050
43	8567.526	04:00:00.000	633450	4843250
44	4115.773	04:00:00.000	633450	4843450
45	2665.47	04:00:00.000	633450	4843650
46	10509.53	04:00:00.000	633650	4841050
47	10236.27	04:00:00.000	633650	4841250
48	11513.18	04:00:00.000	633650	4841450
49	11499.82	04:00:00.000	633650	4841650
50	12796.12	04:00:00.000	633650	4841850
51	11297.6	04:00:00.000	633650	4842050

Events in Range: 2862 / 34372
 0:11:8:108 AM
 Current: 9/10/2013
 9/7/2013 3:16 AM



Lowest Amplitudes: September 10 – Flow continues in the 46-16 and general energy level remains near levels of the previous day. The well is shut in at 15:15 local time on this day.

Fractor - Version: ClickOnce published Version: v1.0.0.38 --- Project=Alkarock

File Import Create/Edit Fracture outlook Export

Invoke Editor
Invoke 2D View
History Analysis

Grid
Wells to display
Fractures

Fracture Analysis Data
usetInput Load

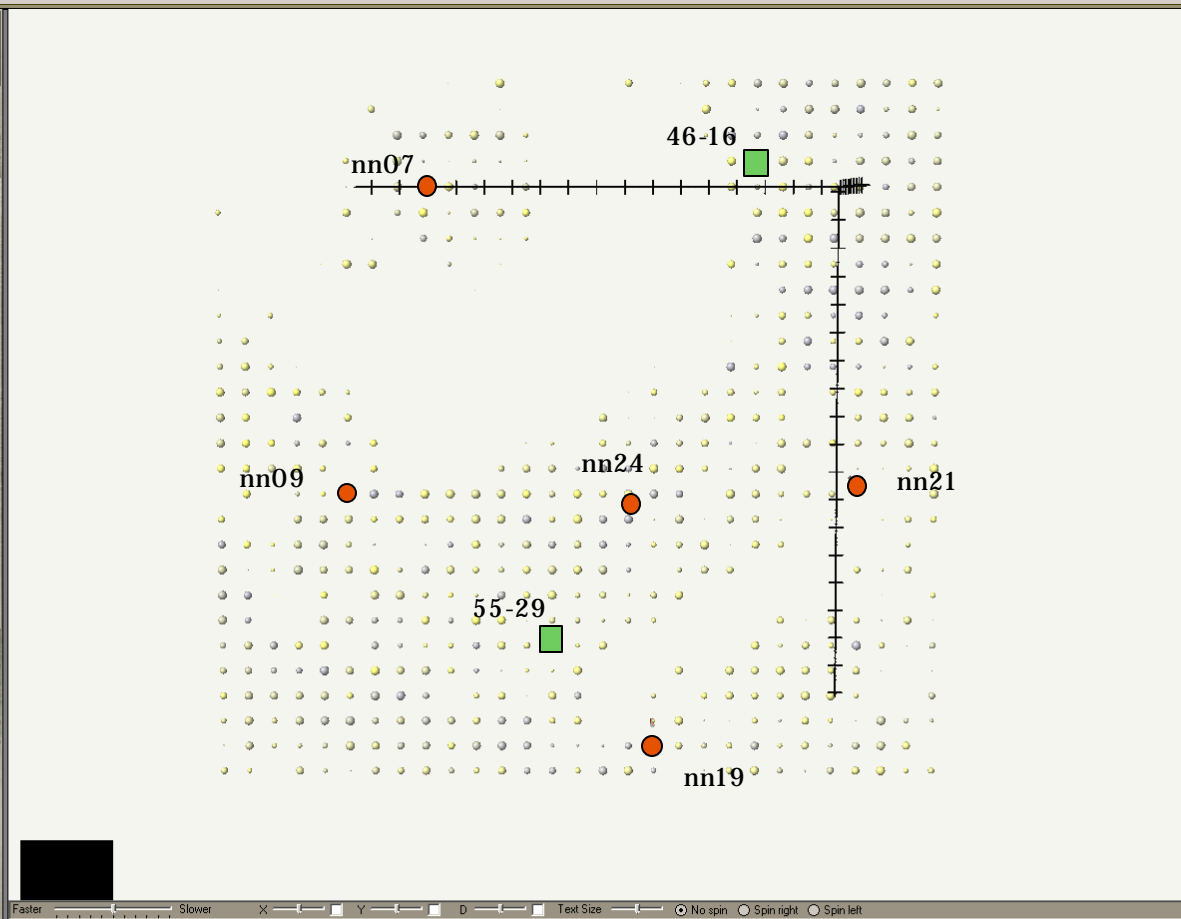
Show Azimuth Errors
 Show Model Errors
 Show Total Errors
 Show No Errors
 Show Events out of Time Range

Sphere
 Signal-to-Noise
 Amp (log)
 Azimuth

Amplitude
 Time
 Elevation
 NONE

Attribute Filter
 Amplitude
 Min: 500.4136047
 Max: 1635.316361

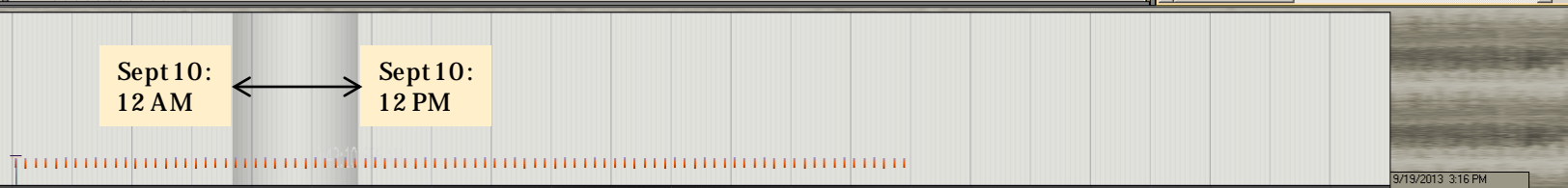
Images to display
Formation Tops
Time-line
Real-Time
Fluid Flow
View



Fracture Locations: usetInput

ID	Amplitude	Time	X	Y
1	9171.095	04:00:00.000	633050	4841050
2	11240.36	04:00:00.000	633050	4841250
3	10826.95	04:00:00.000	633050	4841450
4	10684.51	04:00:00.000	633050	4841650
5	11743.73	04:00:00.000	633050	4841850
6	13176.14	04:00:00.000	633050	4842050
7	12637.62	04:00:00.000	633050	4842250
8	11751.93	04:00:00.000	633050	4842450
9	9665.28	04:00:00.000	633050	4842650
10	12572.39	04:00:00.000	633050	4842850
11	11089.11	04:00:00.000	633050	4843050
12	12558.95	04:00:00.000	633050	4843250
13	10827.11	04:00:00.000	633050	4843450
14	4972.603	04:00:00.000	633050	4843650
15	3606.611	04:00:00.000	633050	4843850
16	1956.434	04:00:00.000	633050	4844050
17	8605.067	04:00:00.000	633250	4841050
18	11936.38	04:00:00.000	633250	4841250
19	12288.84	04:00:00.000	633250	4841450
20	11590.45	04:00:00.000	633250	4841650
21	12365.44	04:00:00.000	633250	4841850
22	12756.41	04:00:00.000	633250	4842050
23	12240.25	04:00:00.000	633250	4842250
24	12227.8	04:00:00.000	633250	4842450
25	12093.75	04:00:00.000	633250	4842650
26	11555.48	04:00:00.000	633250	4842850
27	10428.44	04:00:00.000	633250	4843050
28	8943.484	04:00:00.000	633250	4843250
29	7625.59	04:00:00.000	633250	4843450
30	4472.812	04:00:00.000	633250	4843650
31	1112.342	04:00:00.000	633250	4843850
32	9452.426	04:00:00.000	633450	4841050
33	10623.24	04:00:00.000	633450	4841250
34	10586.82	04:00:00.000	633450	4841450
35	11600.89	04:00:00.000	633450	4841650
36	12234.16	04:00:00.000	633450	4841850
37	11493.16	04:00:00.000	633450	4842050
38	11745.9	04:00:00.000	633450	4842250
39	11697.08	04:00:00.000	633450	4842450
40	10469.71	04:00:00.000	633450	4842650
41	10738.69	04:00:00.000	633450	4842850
42	9674.216	04:00:00.000	633450	4843050
43	8567.526	04:00:00.000	633450	4843250
44	4115.773	04:00:00.000	633450	4843450
45	2665.47	04:00:00.000	633450	4843650
46	10509.53	04:00:00.000	633650	4841050
47	10236.27	04:00:00.000	633650	4841250
48	11513.18	04:00:00.000	633650	4841450
49	11499.82	04:00:00.000	633650	4841650
50	12796.12	04:00:00.000	633650	4841850
51	11297.6	04:00:00.000	633650	4842050

Events in Range: 1651 / 34372
Current: 0:42:10.656 AM
9/11/2013



Lowest Amplitudes: September 11 – Low amplitudes are diminished from the previous day. Injection begins on the 55-29.

Fractor - Version: ClickOnce published Version: v1.0.0.38 --- Project=Alkarock
 File Import Create/Edit Fracture outlook Export

Invoke Editor
 Invoke 2D View
 History Analysis

Grid
 Wells to display
 Fractures

Fracture Analysis Data
 useInput Load

Show Azimuth Errors
 Show Model Errors
 Show Total Errors
 Show No Errors
 Show Events out of Time Range

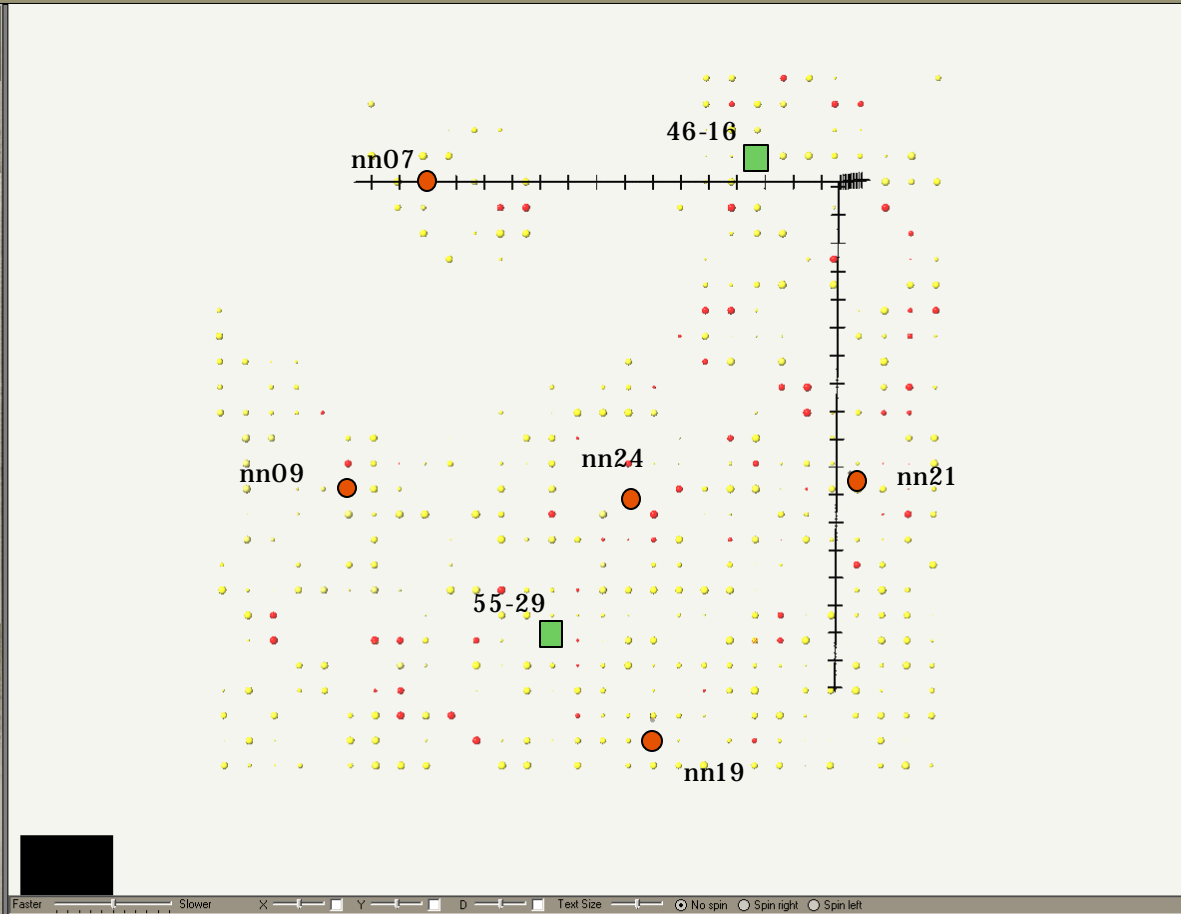
Sphere
 Signal-to-Noise
 Amp (log)
 Azimuth

Amplitude
 Time
 Elevation

Color Scale
 NONE

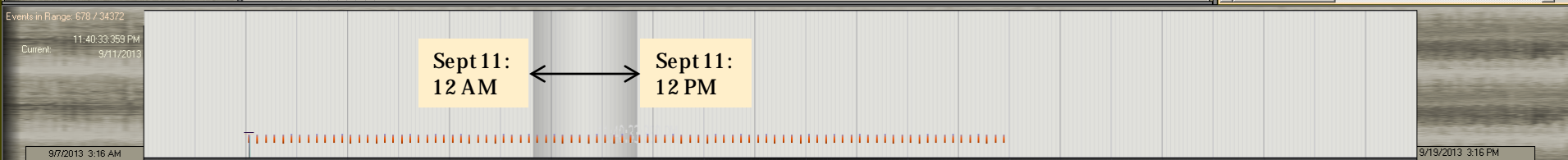
Attribute Filter
 Amplitude
 Min: 500.4136047
 Max: 1453.731920

Images to display
 Formation Tops
 Time-line
 Real-Time
 Fluid Flow
 View



Fracture Locations: useInput

ID	Amplitude	Time	X	Y
1	9171.095	04:00:00.000	633050	4941050
2	11240.36	04:00:00.000	633050	4941250
3	10826.95	04:00:00.000	633050	4941450
4	10684.51	04:00:00.000	633050	4941650
5	11743.73	04:00:00.000	633050	4941850
6	13176.14	04:00:00.000	633050	4942050
7	12637.62	04:00:00.000	633050	4942250
8	11751.93	04:00:00.000	633050	4942450
9	9665.28	04:00:00.000	633050	4942650
10	12572.39	04:00:00.000	633050	4942850
11	11089.11	04:00:00.000	633050	4943050
12	12558.95	04:00:00.000	633050	4943250
13	10827.11	04:00:00.000	633050	4943450
14	4972.603	04:00:00.000	633050	4943650
15	3606.611	04:00:00.000	633050	4943850
16	1956.434	04:00:00.000	633050	4944050
17	8605.067	04:00:00.000	633250	4941050
18	11936.38	04:00:00.000	633250	4941250
19	12288.84	04:00:00.000	633250	4941450
20	11590.45	04:00:00.000	633250	4941650
21	12365.44	04:00:00.000	633250	4941850
22	12756.41	04:00:00.000	633250	4942050
23	12240.25	04:00:00.000	633250	4942250
24	12227.8	04:00:00.000	633250	4942450
25	12093.75	04:00:00.000	633250	4942650
26	11555.48	04:00:00.000	633250	4942850
27	10428.44	04:00:00.000	633250	4943050
28	8943.484	04:00:00.000	633250	4943250
29	7625.59	04:00:00.000	633250	4943450
30	4472.812	04:00:00.000	633250	4943650
31	1112.342	04:00:00.000	633250	4943850
32	9452.426	04:00:00.000	633450	4941050
33	10623.24	04:00:00.000	633450	4941250
34	10586.82	04:00:00.000	633450	4941450
35	11600.89	04:00:00.000	633450	4941650
36	12234.16	04:00:00.000	633450	4941850
37	11493.16	04:00:00.000	633450	4942050
38	11745.9	04:00:00.000	633450	4942250
39	11697.08	04:00:00.000	633450	4942450
40	10469.71	04:00:00.000	633450	4942650
41	10738.69	04:00:00.000	633450	4942850
42	9674.216	04:00:00.000	633450	4943050
43	8567.526	04:00:00.000	633450	4943250
44	4115.773	04:00:00.000	633450	4943450
45	2665.47	04:00:00.000	633450	4943650
46	10509.53	04:00:00.000	633650	4941050
47	10236.27	04:00:00.000	633650	4941250
48	11513.18	04:00:00.000	633650	4941450
49	11499.82	04:00:00.000	633650	4941650
50	12796.12	04:00:00.000	633650	4941850
51	11297.6	04:00:00.000	633650	4942050



Lowest Amplitudes: September 12 – Low amplitudes return to levels nearer pre-injection in the 46-16, particularly near the nn07 observation well.

Fractor - Version: ClickOnce published Version: v1.0.0.38 --- Project=Alkarock

File Import Create/Edit Fracture outlook Export

Invoke Editor
Invoke 2D View
History Analysis

Grid
Wells to display
Fractures

Fracture Analysis Data
usetInput Load

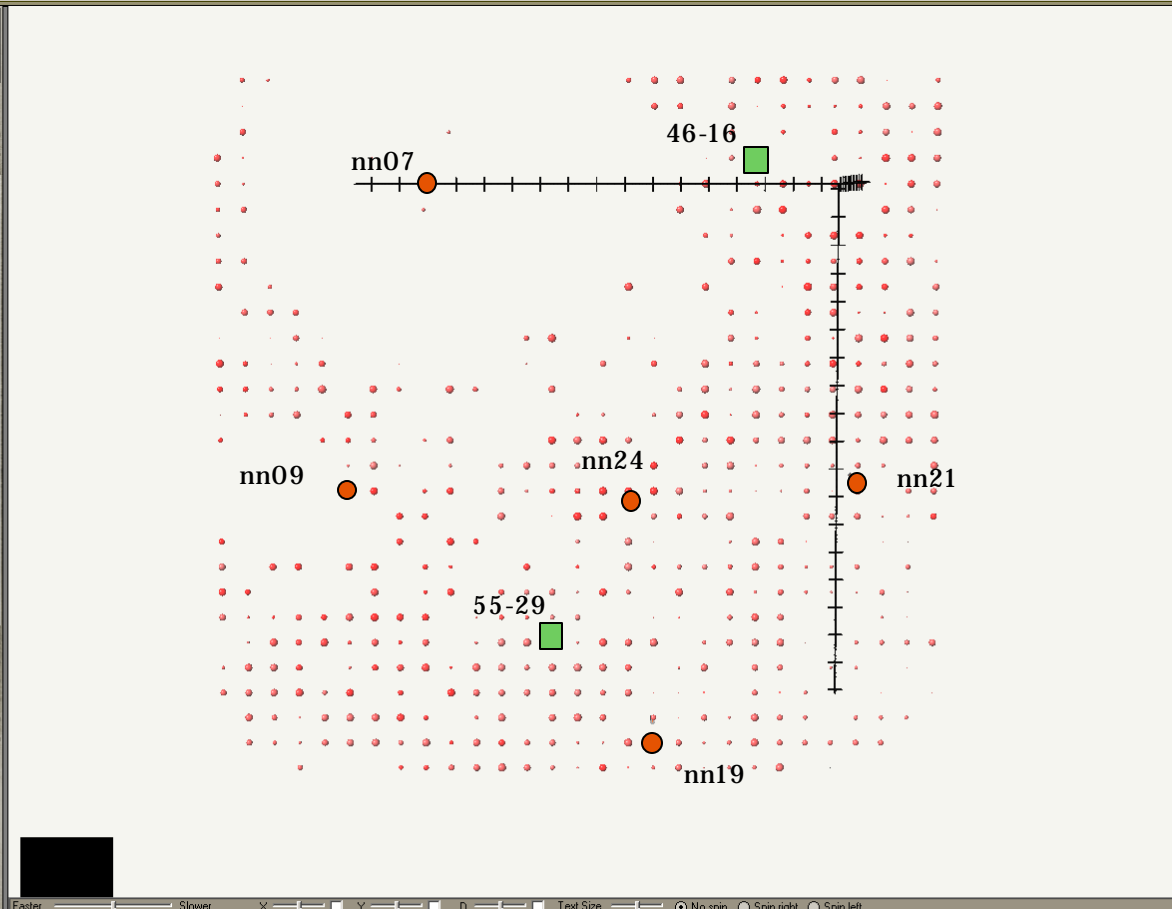
Show Azimuth Errors
 Show Model Errors
 Show Total Errors
 Show No Errors
 Show Events out of Time Range

Sphere
 Signal-to-Noise
 Amp (log)
 Azimuth

Amplitude
 Time
 Elevation
 NONE

Attribute Filter
 Amplitude
 Min: 500.4136047
 Max: 1453.731920

Images to display
 Formation Tops
 Time-line
 Real-Time
 Fluid Flow
 View



Fracture Locations: useInput

ID	Amplitude	Time	X	Y
1	9171.095	04:00:00.000	633050	4941050
2	11240.36	04:00:00.000	633050	4941250
3	10826.95	04:00:00.000	633050	4941450
4	10684.51	04:00:00.000	633050	4941650
5	11743.73	04:00:00.000	633050	4941850
6	13176.14	04:00:00.000	633050	4942050
7	12637.62	04:00:00.000	633050	4942250
8	11751.93	04:00:00.000	633050	4942450
9	9665.28	04:00:00.000	633050	4942650
10	12572.39	04:00:00.000	633050	4942850
11	11089.11	04:00:00.000	633050	4943050
12	12558.95	04:00:00.000	633050	4943250
13	10827.11	04:00:00.000	633050	4943450
14	4972.603	04:00:00.000	633050	4943650
15	3606.611	04:00:00.000	633050	4943850
16	1956.434	04:00:00.000	633050	4944050
17	8605.067	04:00:00.000	633250	4941050
18	11936.38	04:00:00.000	633250	4941250
19	12288.84	04:00:00.000	633250	4941450
20	11590.45	04:00:00.000	633250	4941650
21	12365.44	04:00:00.000	633250	4941850
22	12756.41	04:00:00.000	633250	4942050
23	12240.25	04:00:00.000	633250	4942250
24	12227.8	04:00:00.000	633250	4942450
25	12093.75	04:00:00.000	633250	4942650
26	11555.48	04:00:00.000	633250	4942850
27	10428.44	04:00:00.000	633250	4943050
28	8943.484	04:00:00.000	633250	4943250
29	7625.59	04:00:00.000	633250	4943450
30	4472.812	04:00:00.000	633250	4943650
31	1112.342	04:00:00.000	633250	4943850
32	9452.426	04:00:00.000	633450	4941050
33	10623.24	04:00:00.000	633450	4941250
34	10586.82	04:00:00.000	633450	4941450
35	11600.89	04:00:00.000	633450	4941650
36	12234.16	04:00:00.000	633450	4941850
37	11493.16	04:00:00.000	633450	4942050
38	11745.9	04:00:00.000	633450	4942250
39	11697.08	04:00:00.000	633450	4942450
40	10469.71	04:00:00.000	633450	4942650
41	10738.69	04:00:00.000	633450	4942850
42	9674.216	04:00:00.000	633450	4943050
43	8567.526	04:00:00.000	633450	4943250
44	4115.773	04:00:00.000	633450	4943450
45	2665.47	04:00:00.000	633450	4943650
46	10509.53	04:00:00.000	633650	4941050
47	10236.27	04:00:00.000	633650	4941250
48	11513.18	04:00:00.000	633650	4941450
49	11499.82	04:00:00.000	633650	4941650
50	12796.12	04:00:00.000	633650	4941850
51	11297.6	04:00:00.000	633650	4942050

Events in Range: 908 / 34372
 Current: 11:25:15.984 PM
 9/12/2013



Lowest Amplitudes: September 13 – Low amplitudes return to levels near pre-injection in the 46-16, particularly near the nn07 observation well.

Fractor - Version: ClickOnce published Version: v1.0.0.38 --- Project: Alkarock

File Import Create/Edit Fracture Output Export

Invoke Editor
Invoke 2D View
History Analysis

Grid
Wells to display
Fractures

Fracture Analysis Data
usetinput Load

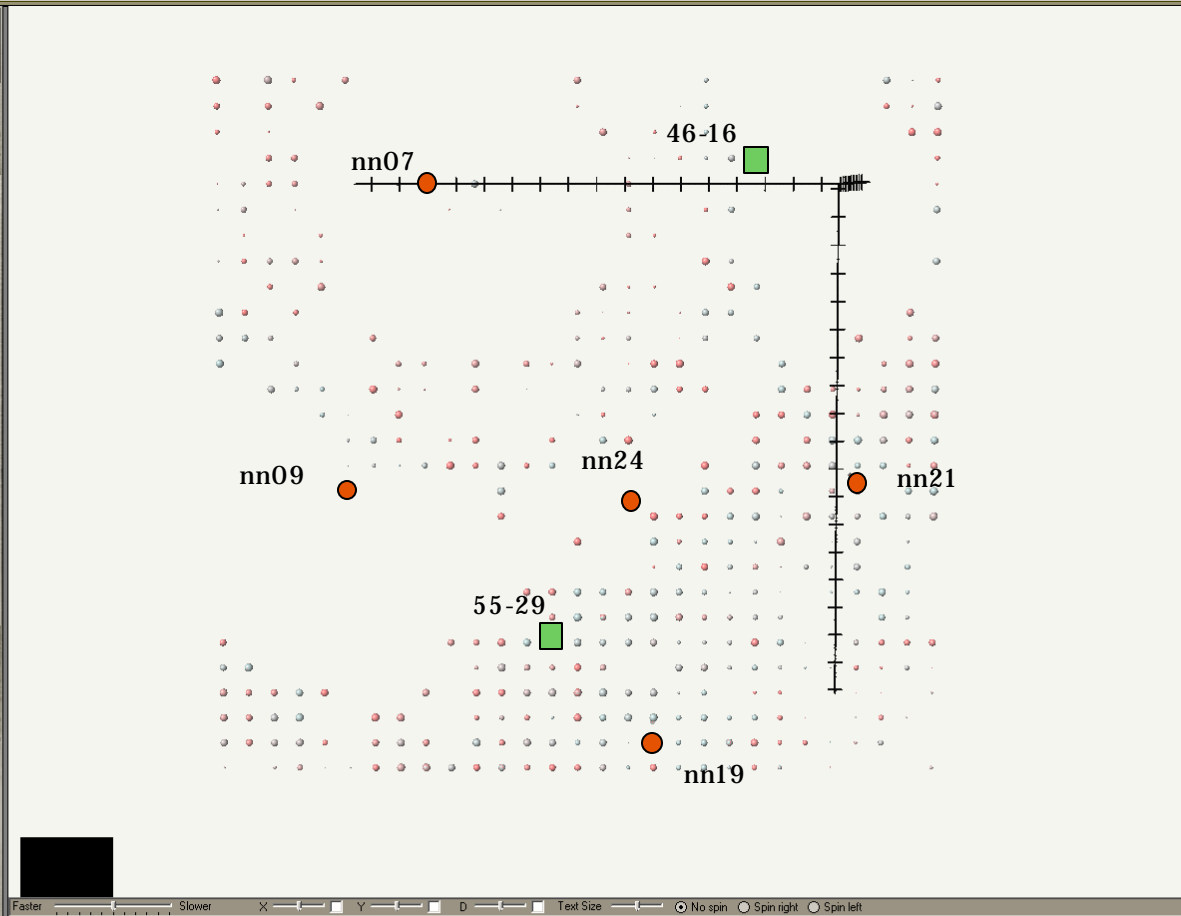
Show Azimuth Errors
 Show Model Errors
 Show Total Errors
 Show No Errors
 Show Events out of Time Range

Sphere
 Signal-to-Noise
 Amp (log)
 Azimuth

Amplitude
 Time
 Elevation
 NONE

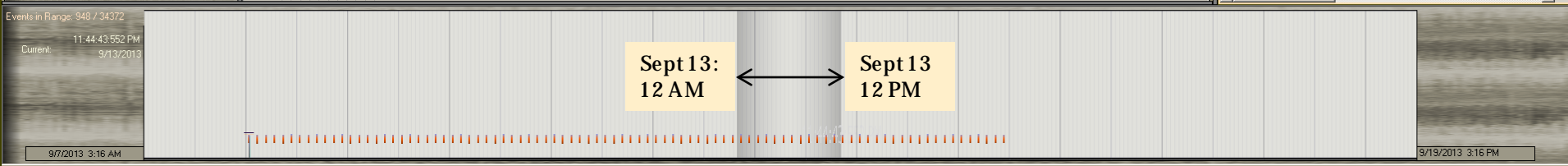
Attribute Filter
 Amplitude
 Min: 500.4136047
 Max: 1453.731920

Images to display
 Formation Tops
 Time-line
 Real-Time
 Fluid Flow
 View



Fracture Locations: usetinput

ID	Amplitude	Time	X	Y
1	9171.095	04:00:00.000	633050	4841050
2	11240.36	04:00:00.000	633050	4841250
3	10826.95	04:00:00.000	633050	4841450
4	10884.51	04:00:00.000	633050	4841650
5	11743.73	04:00:00.000	633050	4841850
6	13176.14	04:00:00.000	633050	4842050
7	12637.62	04:00:00.000	633050	4842250
8	11751.93	04:00:00.000	633050	4842450
9	9665.28	04:00:00.000	633050	4842650
10	12572.39	04:00:00.000	633050	4842850
11	11089.11	04:00:00.000	633050	4843050
12	12558.95	04:00:00.000	633050	4843250
13	10827.11	04:00:00.000	633050	4843450
14	4972.603	04:00:00.000	633050	4843650
15	3606.611	04:00:00.000	633050	4843850
16	1956.434	04:00:00.000	633050	4844050
17	8605.067	04:00:00.000	633250	4841050
18	11936.38	04:00:00.000	633250	4841250
19	12288.84	04:00:00.000	633250	4841450
20	11590.45	04:00:00.000	633250	4841650
21	12365.44	04:00:00.000	633250	4841850
22	12756.41	04:00:00.000	633250	4842050
23	12240.25	04:00:00.000	633250	4842250
24	12227.8	04:00:00.000	633250	4842450
25	12093.75	04:00:00.000	633250	4842650
26	11555.48	04:00:00.000	633250	4842850
27	10428.44	04:00:00.000	633250	4843050
28	8943.484	04:00:00.000	633250	4843250
29	7625.59	04:00:00.000	633250	4843450
30	4472.812	04:00:00.000	633250	4843650
31	1112.342	04:00:00.000	633250	4843850
32	9452.426	04:00:00.000	633450	4841050
33	10623.24	04:00:00.000	633450	4841250
34	10586.82	04:00:00.000	633450	4841450
35	11600.89	04:00:00.000	633450	4841650
36	12234.16	04:00:00.000	633450	4841850
37	11493.16	04:00:00.000	633450	4842050
38	11745.9	04:00:00.000	633450	4842250
39	11697.08	04:00:00.000	633450	4842450
40	10469.71	04:00:00.000	633450	4842650
41	10738.69	04:00:00.000	633450	4842850
42	9674.216	04:00:00.000	633450	4843050
43	8567.526	04:00:00.000	633450	4843250
44	4115.773	04:00:00.000	633450	4843450
45	2665.47	04:00:00.000	633450	4843650
46	10509.53	04:00:00.000	633650	4841050
47	10236.27	04:00:00.000	633650	4841250
48	11513.18	04:00:00.000	633650	4841450
49	11499.82	04:00:00.000	633650	4841650
50	12796.12	04:00:00.000	633650	4841850
51	11297.6	04:00:00.000	633650	4842050



Fractor - Version: ClickOnce published Version: v1.0.0.38 --- Project=Alkarock
 File Import Create/Edit Fracture outlook Export

Invoke Editor
 Invoke 2D View
 History Analysis

Grid
 Wells to display
 Fractures

Fracture Analysis Data
 useInput Load

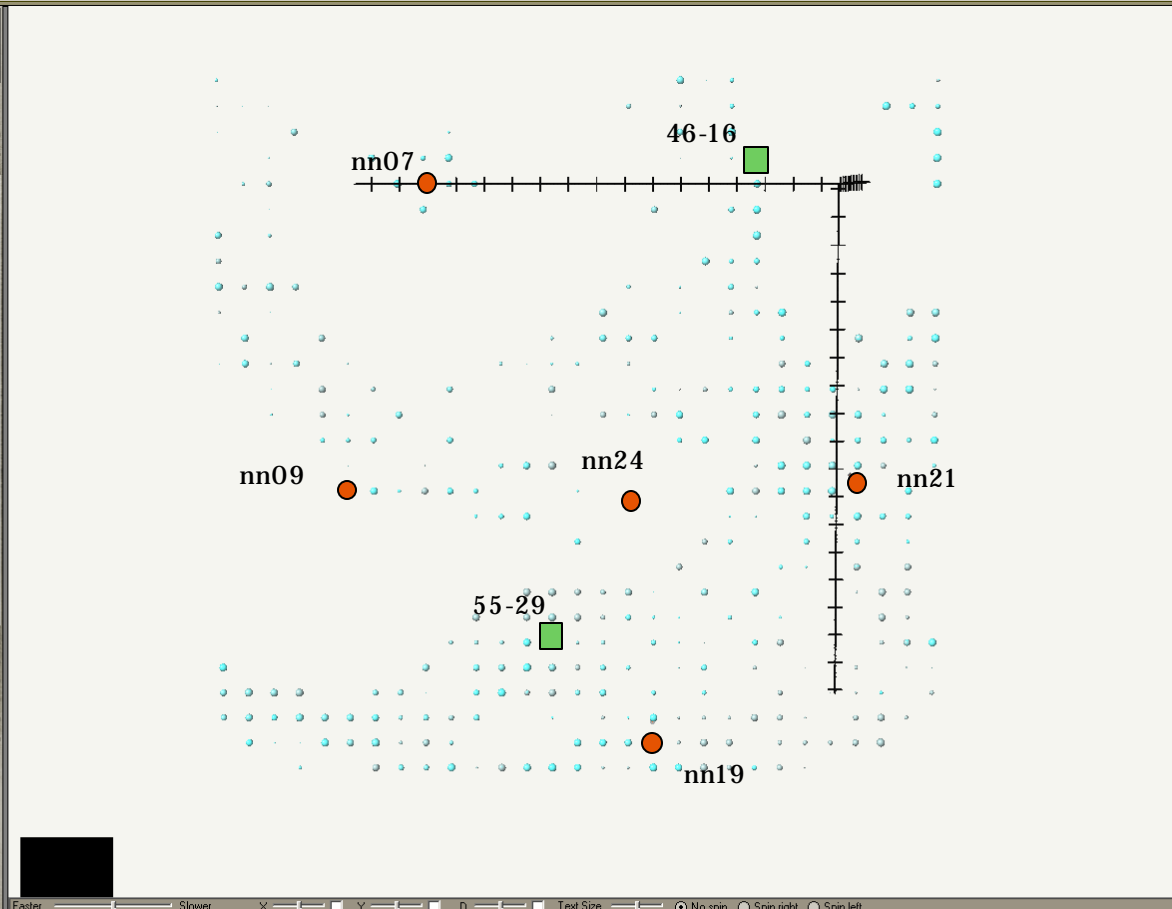
Show Azimuth Errors
 Show Model Errors
 Show Total Errors
 Show No Errors
 Show Events out of Time Range

Sphere
 Signal-to-Noise
 Amp (log)
 Azimuth

NONE
 Amplitude
 Time
 Elevation

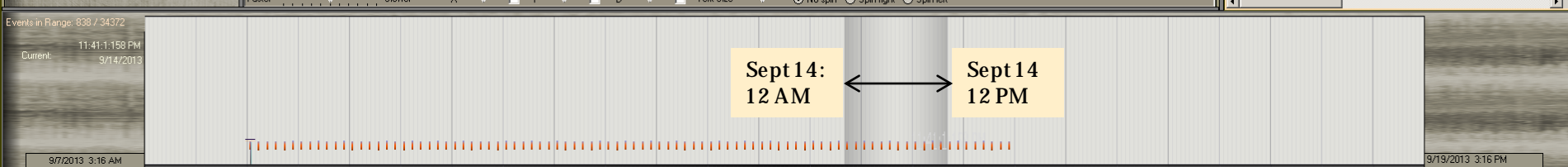
Attribute Filter
 Amplitude
 Min: 500.4136047
 Max: 1272.147479

Images to display
 Formation Tops
 Time-line
 Real-Time
 Fluid Flow
 View



Fracture Locations: useInput

ID	Amplitude	Time	X	Y
1	9171.095	04:00:00.000	633050	4941050
2	11240.36	04:00:00.000	633050	4941250
3	10826.95	04:00:00.000	633050	4941450
4	10684.51	04:00:00.000	633050	4941650
5	11743.73	04:00:00.000	633050	4941850
6	13176.14	04:00:00.000	633050	4942050
7	12637.62	04:00:00.000	633050	4942250
8	11751.93	04:00:00.000	633050	4942450
9	9665.28	04:00:00.000	633050	4942650
10	12572.39	04:00:00.000	633050	4942850
11	11089.11	04:00:00.000	633050	4943050
12	12558.95	04:00:00.000	633050	4943250
13	10827.11	04:00:00.000	633050	4943450
14	4972.603	04:00:00.000	633050	4943650
15	3606.611	04:00:00.000	633050	4943850
16	1956.434	04:00:00.000	633050	4944050
17	8605.067	04:00:00.000	633250	4941050
18	11936.38	04:00:00.000	633250	4941250
19	12288.84	04:00:00.000	633250	4941450
20	11590.45	04:00:00.000	633250	4941650
21	12365.44	04:00:00.000	633250	4941850
22	12756.41	04:00:00.000	633250	4942050
23	12240.25	04:00:00.000	633250	4942250
24	12227.8	04:00:00.000	633250	4942450
25	12093.75	04:00:00.000	633250	4942650
26	11555.48	04:00:00.000	633250	4942850
27	10428.44	04:00:00.000	633250	4943050
28	8943.484	04:00:00.000	633250	4943250
29	7625.59	04:00:00.000	633250	4943450
30	4472.812	04:00:00.000	633250	4943650
31	1112.342	04:00:00.000	633250	4943850
32	9452.426	04:00:00.000	633450	4941050
33	10623.24	04:00:00.000	633450	4941250
34	10586.82	04:00:00.000	633450	4941450
35	11600.89	04:00:00.000	633450	4941650
36	12234.16	04:00:00.000	633450	4941850
37	11493.16	04:00:00.000	633450	4942050
38	11745.9	04:00:00.000	633450	4942250
39	11697.08	04:00:00.000	633450	4942450
40	10469.71	04:00:00.000	633450	4942650
41	10738.69	04:00:00.000	633450	4942850
42	9674.216	04:00:00.000	633450	4943050
43	8567.526	04:00:00.000	633450	4943250
44	4115.773	04:00:00.000	633450	4943450
45	2665.47	04:00:00.000	633450	4943650
46	10509.53	04:00:00.000	633650	4941050
47	10236.27	04:00:00.000	633650	4941250
48	11513.18	04:00:00.000	633650	4941450
49	11499.82	04:00:00.000	633650	4941650
50	12796.12	04:00:00.000	633650	4941850
51	11297.6	04:00:00.000	633650	4942050



Fractor - Version: ClickOnce published Version: v1.0.0.38 --- Project=Alkarock

File Import Create/Edit Fracture outlook Export

Invoke Editor
Invoke 2D View
History Analysis

Grid
Wells to display
Fractures

Fracture Analysis Data
useInput Load

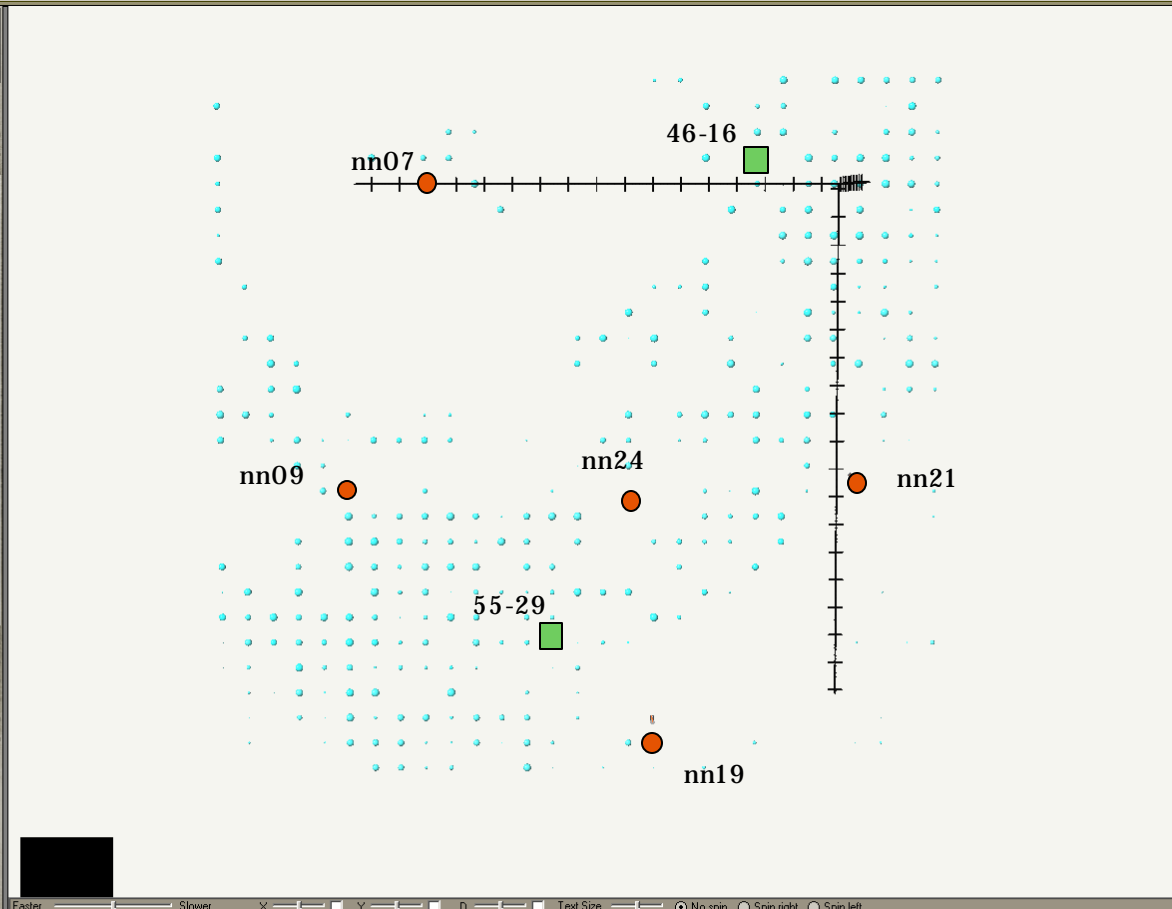
Show Azimuth Errors
 Show Model Errors
 Show Total Errors
 Show No Errors
 Show Events out of Time Range

Sphere
 Signal-to-Noise
 Amp (log)
 Azimuth

Amplitude
 Time
 Elevation
 NONE

Attribute Filter
 Amplitude
 Min: 500.4136047
 Max: 1272.147479

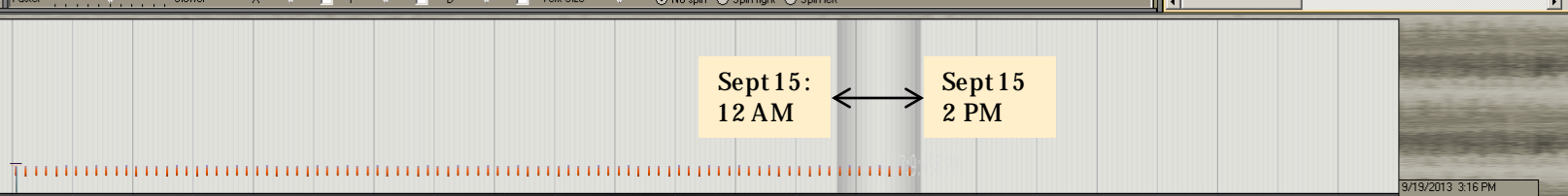
Images to display
Formation Tops
Time-line
Real-Time
Fluid Flow
View



Fracture Locations: useInput

ID	Amplitude	Time	X	Y
1	9171.095	04:00:00.000	633050	4941050
2	11240.36	04:00:00.000	633050	4941250
3	10836.95	04:00:00.000	633050	4941450
4	10884.51	04:00:00.000	633050	4941650
5	11743.73	04:00:00.000	633050	4941850
6	13176.14	04:00:00.000	633050	4942050
7	12637.62	04:00:00.000	633050	4942250
8	11751.93	04:00:00.000	633050	4942450
9	9665.28	04:00:00.000	633050	4942650
10	12572.39	04:00:00.000	633050	4942850
11	11089.11	04:00:00.000	633050	4943050
12	12558.95	04:00:00.000	633050	4943250
13	10827.11	04:00:00.000	633050	4943450
14	4972.603	04:00:00.000	633050	4943650
15	3606.611	04:00:00.000	633050	4943850
16	1956.434	04:00:00.000	633050	4944050
17	8605.067	04:00:00.000	633250	4941050
18	11936.38	04:00:00.000	633250	4941250
19	12288.84	04:00:00.000	633250	4941450
20	11590.45	04:00:00.000	633250	4941650
21	12365.44	04:00:00.000	633250	4941850
22	12756.41	04:00:00.000	633250	4942050
23	12240.25	04:00:00.000	633250	4942250
24	12227.8	04:00:00.000	633250	4942450
25	12093.75	04:00:00.000	633250	4942650
26	11555.48	04:00:00.000	633250	4942850
27	10428.44	04:00:00.000	633250	4943050
28	8943.484	04:00:00.000	633250	4943250
29	7625.59	04:00:00.000	633250	4943450
30	4472.812	04:00:00.000	633250	4943650
31	1112.342	04:00:00.000	633250	4943850
32	9452.426	04:00:00.000	633450	4941050
33	10623.24	04:00:00.000	633450	4941250
34	10586.82	04:00:00.000	633450	4941450
35	11600.89	04:00:00.000	633450	4941650
36	12234.16	04:00:00.000	633450	4941850
37	11493.16	04:00:00.000	633450	4942050
38	11745.9	04:00:00.000	633450	4942250
39	11697.08	04:00:00.000	633450	4942450
40	10469.71	04:00:00.000	633450	4942650
41	10738.69	04:00:00.000	633450	4942850
42	9674.216	04:00:00.000	633450	4943050
43	8567.526	04:00:00.000	633450	4943250
44	4115.773	04:00:00.000	633450	4943450
45	2665.47	04:00:00.000	633450	4943650
46	10509.53	04:00:00.000	633650	4941050
47	10236.27	04:00:00.000	633650	4941250
48	11513.18	04:00:00.000	633650	4941450
49	11499.82	04:00:00.000	633650	4941650
50	12796.12	04:00:00.000	633650	4941850
51	11297.6	04:00:00.000	633650	4942050

Events in Range: 492 / 34372
4:17:9.498 PM
Current: 9/15/2013
9/7/2013 3:16 AM



Analysis of the lower amplitudes

Opening the 46-16 well appears to have increased the energy measurement in the entire area but particularly near the nn07 which may have tantalizing implications. It is possible that a repetition of this analysis with different seismic frequency bands will yield more information about the question of detecting fluid flow in the subsurface. That calculation will require several days of computer time and so cannot be done tonight. The full 3D display may also yield more information.



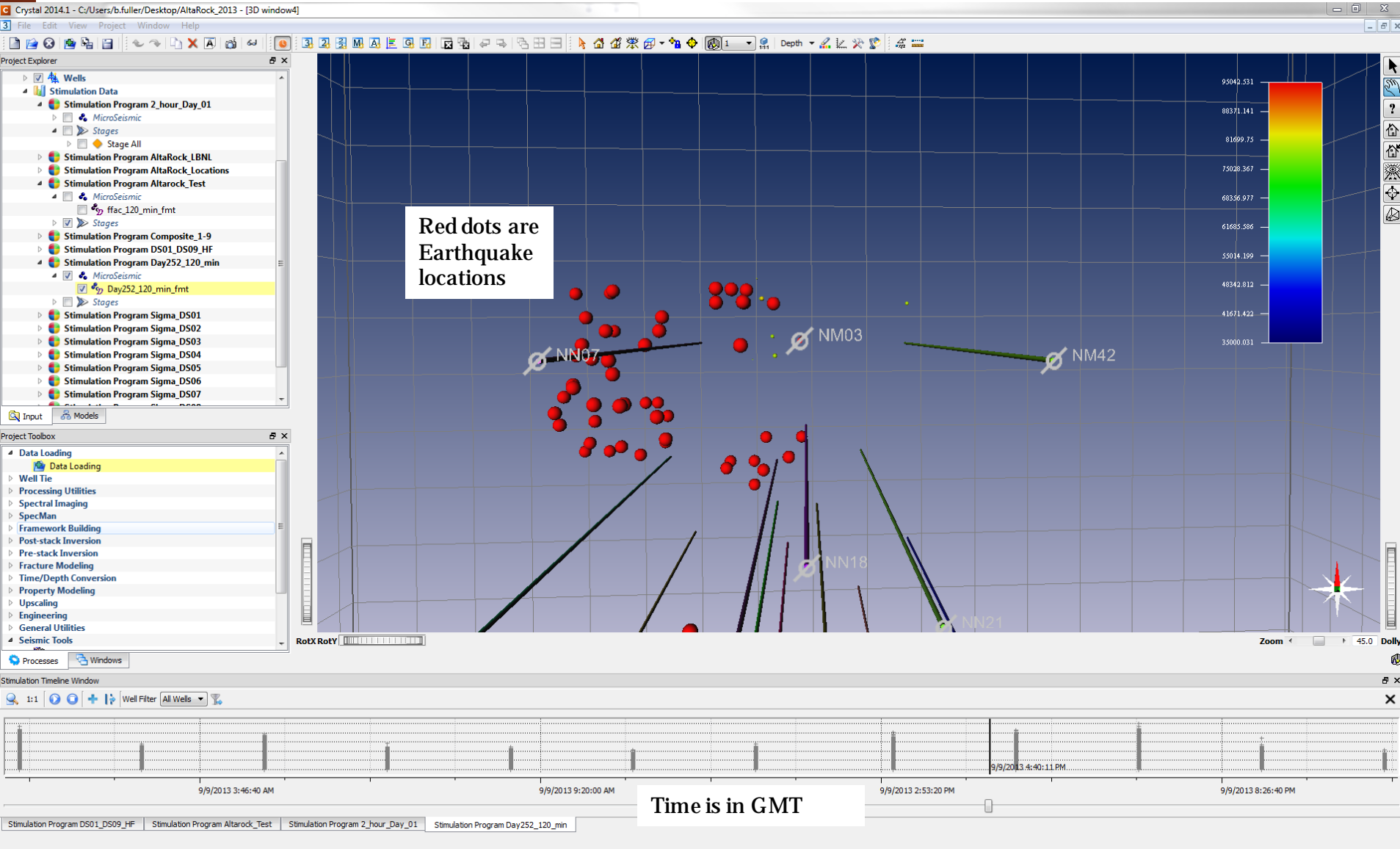
Quick view of current status

Altarock Energy, Inc

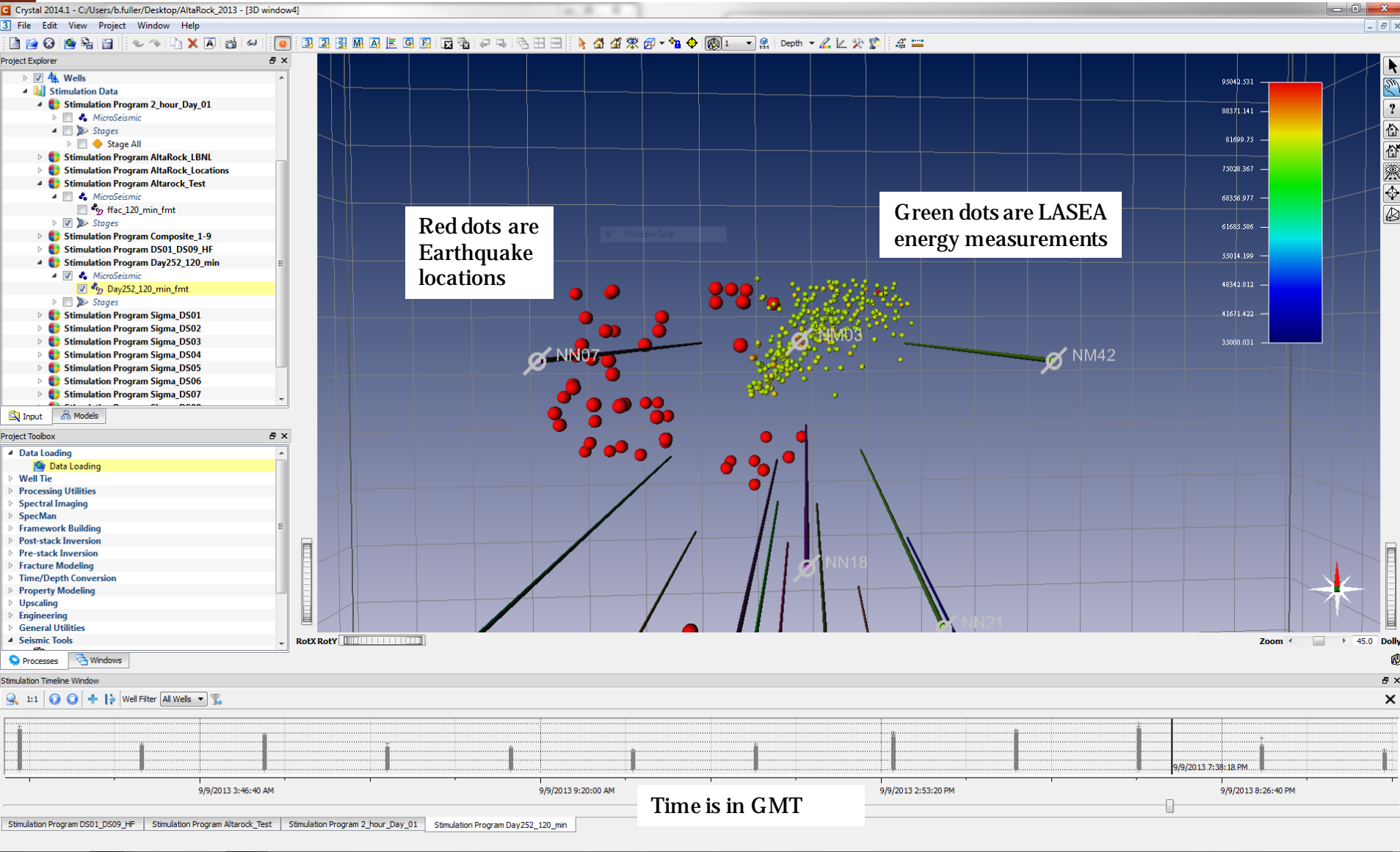
March 13, 2014 Author, Brian Fuller

SIGMA³

Energy measured during 16 hours prior to opening the 46-16 wellhead



Energy measured in the 2 hours immediately after opening the wellhead. Amplitudes on this slide and the previous slide are at the same scale and can be compared.



FINAL PROJECT REPORT



RELEASE RECORD				
REVISION	SECTION	COMPANY	RECIPIENT	DATE
4	ALL	ALTAROCK ENERGY, INC	TRENTON CLADOUHOS	4/27/14

Trenton Cladouhos, PhD, LG
Senior Vice President R&D
AltaRock Energy, Inc.
4010 Stone Way North, Suite 400
Seattle, WA 98103
tcladouhos@altarockenergy.com



This document contains trade secret and other proprietary information that is owned by Sigma³ and is protected by intellectual property rights under common law and applicable statute. This information, either through the use of this document or through other use of the technology contained herein, is strictly prohibited unless you have the express written permission of Sigma³.

REVISION RECORD				
REVISION	SECTION	AUTHOR	SUMMARY OF CHANGE	DATE
A0	ALL	Scott Taylor	Template	7/31/13
1	ALL	Brian Fuller	First pass LASEA	11/20/13
2	ALL	Brian Fuller	Updated LASEA volume	12/30/13
3	ALL	Brian Fuller	Updated LASEA volume	1/10/14
4	ALL	Scott Taylor	Input fine resolution LASEA run	4/27/14
5	ALL	Scott Taylor	Crystal images	5/28/14



Sigma Cubed, Inc.
4700 West Sam Houston Parkway North, Suite 150,
Houston, TX, 77041
Ph: +1.281.363.8500

COPYRIGHT © 2014 Sigma Cubed Integrated Reservoir Solutions, Inc. (“Sigma³”)
ALL RIGHTS RESERVED

This document contains trade secret and other proprietary information that is owned by Sigma³ and is protected by intellectual property rights under common law and applicable statute. This information, either through the use of this document or through other use of the technology contained herein, is strictly prohibited unless you have the express written permission of Sigma³.

DOCUMENT NO: S3-REP-01-5-ALTAROCK_REDUX	REVISION NO: 05	REVISION DATE: 29/04/2014	Page 2 of 47	PM APPROVAL: SCOTT TAYLOR
---	---------------------------	-------------------------------------	--------------	-------------------------------------

Table of Contents

1	executive summary.....	4
1.1	program objectives.....	4
2	PAD 46-16 ANALYSIS.....	5
2.1	LASEA ANALYSIS.....	44
3	Pad 55-29 Injection ANALYSIS.....	46
3.1	Pad 55-29 Injection SUMMARY	46

DOCUMENT NO: S3-REP-01-5-ALTAROCK_REDUX	REVISION NO: 05 Appendix G: 142	REVISION DATE: 29/04/2014	Page 3 of 47	PM APPROVAL: SCOTT TAYLOR
---	--	-------------------------------------	--------------	-------------------------------------

1 EXECUTIVE SUMMARY

The Sigma Cubed (“S3”) portion of the Davenport Energy 109 Grant by the US Department of Energy (“DOE”) was to determine if this technique had any utilitarian value for geothermal exploration. The critical test with controls was the well 46-16 intermittent flowing. The plan as laid out was to compare signals resulting from fluid flow within near well bore fractures prior to, during, and after each of the three well-flowing episodes. With each flow episode there was significant fluid discharge, both gas and liquid phases. S3 has been supplied with the timing and durations for each of the flow events.

DOE is expecting a paper specifically addressing the results of the Sigma3 test, as it applies to value as a geothermal exploration tool.

1.1 PROGRAM OBJECTIVES

Imaging injection activity on the 46-16 well is the primary goal of the project and imaging the activity on the 55-29. For each well the primary objective is to determine if areas of anomalously high levels of seismic energy can be detected and located. Secondary Objectives are contingent upon detection and localization of anomalously high levels of coherent seismic energy. For valid localized coherent seismic energy Sigma Cubed shall attempt to define the characteristics of the anomaly such as:

- spatial extent,
- time variance of amplitude,
- and seismic frequency dependence

DOCUMENT NO: S3-REP-01-5-ALTAROCK_REDUX	REVISION NO: 05 Appendix G: 143	REVISION DATE: 29/04/2014	Page 4 of 47	PM APPROVAL: SCOTT TAYLOR
---	--	-------------------------------------	--------------	-------------------------------------

2 PAD 46-16 ANALYSIS

12 September 2013 notes and information

AW

Well 46-16

Sequence Flowing of Well, 8, 9, 10 September 2013

8 Sept. 2013

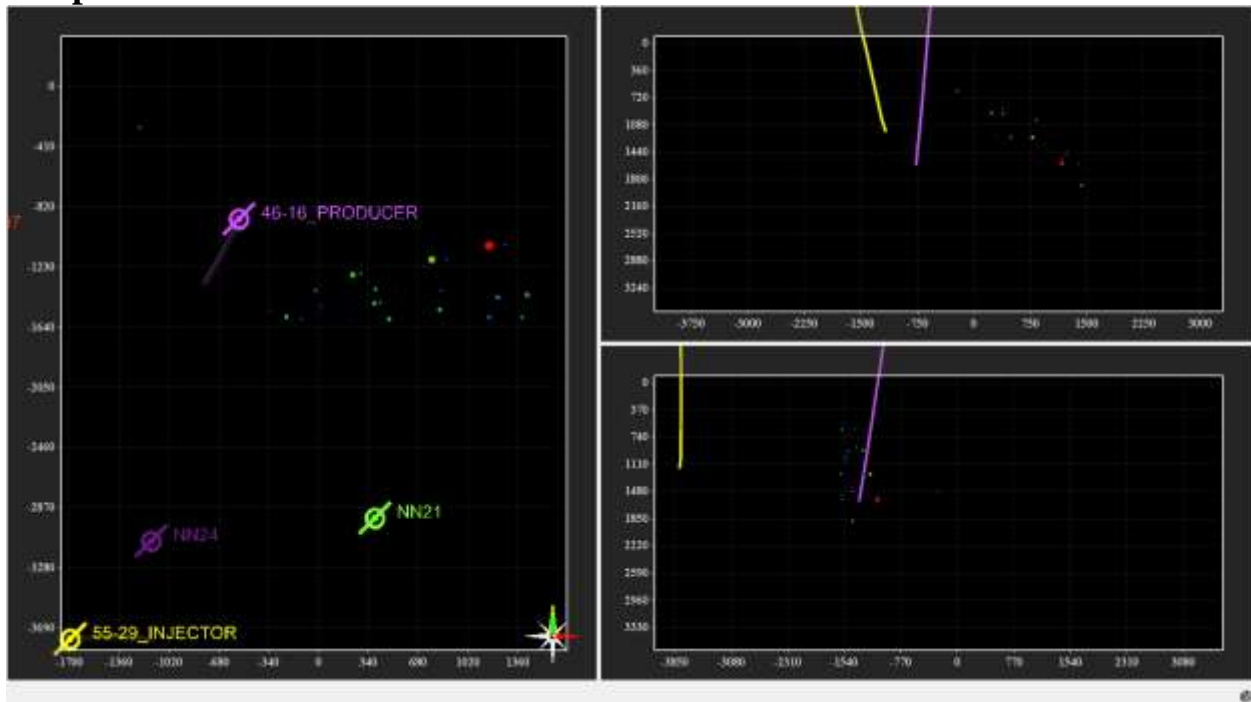


Figure 1 - 11:53

DOCUMENT NO: S3-REP-01-5-ALTAROCK_REDUX	REVISION NO: 05 Appendix G: 144	REVISION DATE: 29/04/2014	Page 5 of 47	PM APPROVAL: SCOTT TAYLOR
--	---------------------------------------	------------------------------	--------------	------------------------------

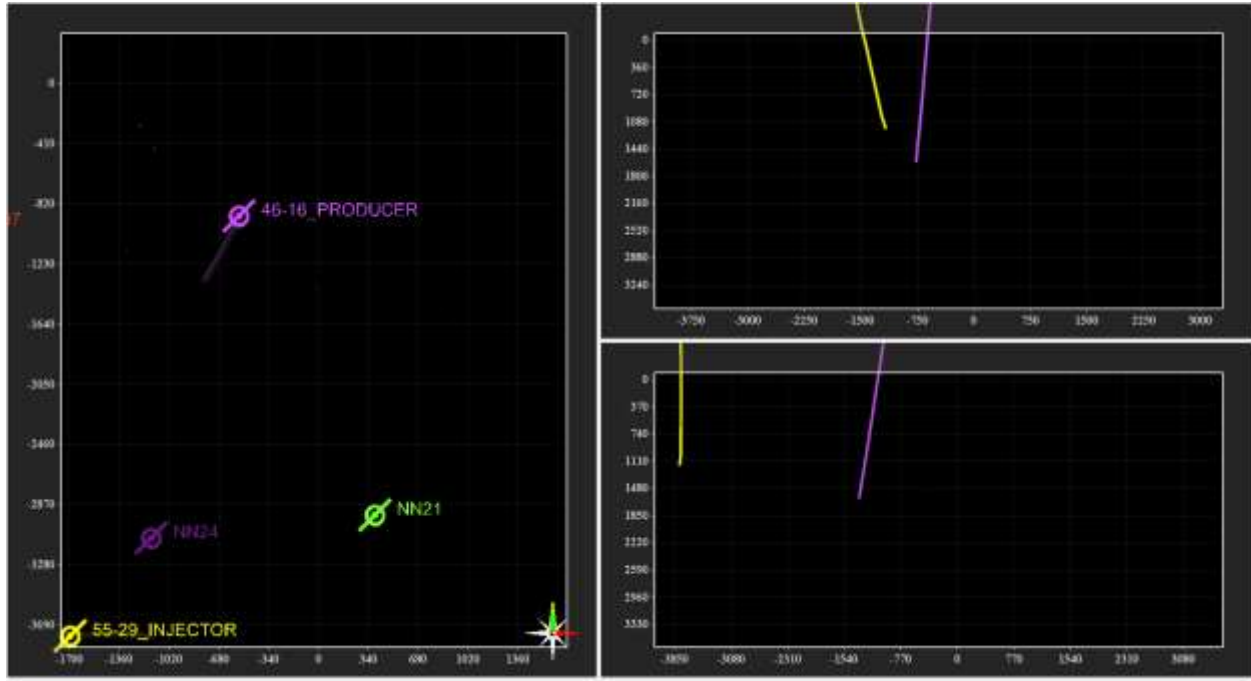


Figure 2 - 12:23

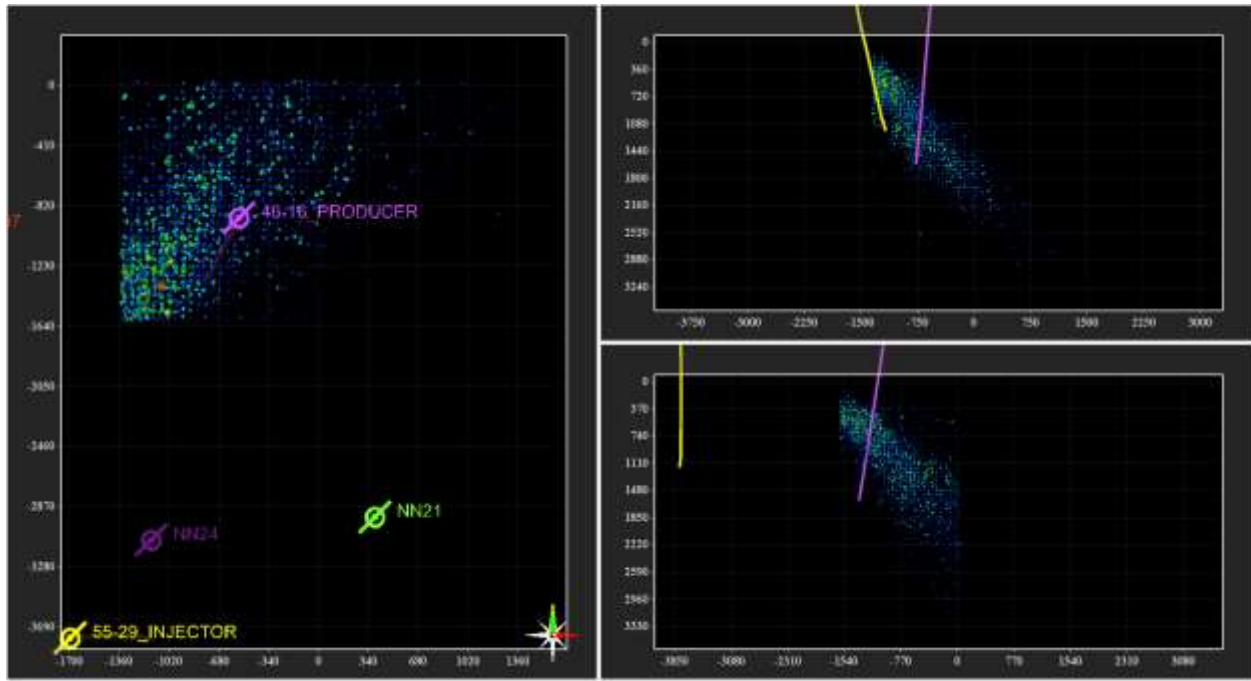


Figure 3 - 12:53

DOCUMENT NO: S3-REP-01-5-ALTAROCK_REDUX	REVISION NO: 05 Appendix G: 145	REVISION DATE: 29/04/2014	Page 6 of 47	PM APPROVAL: SCOTT TAYLOR
--	---------------------------------------	------------------------------	--------------	------------------------------

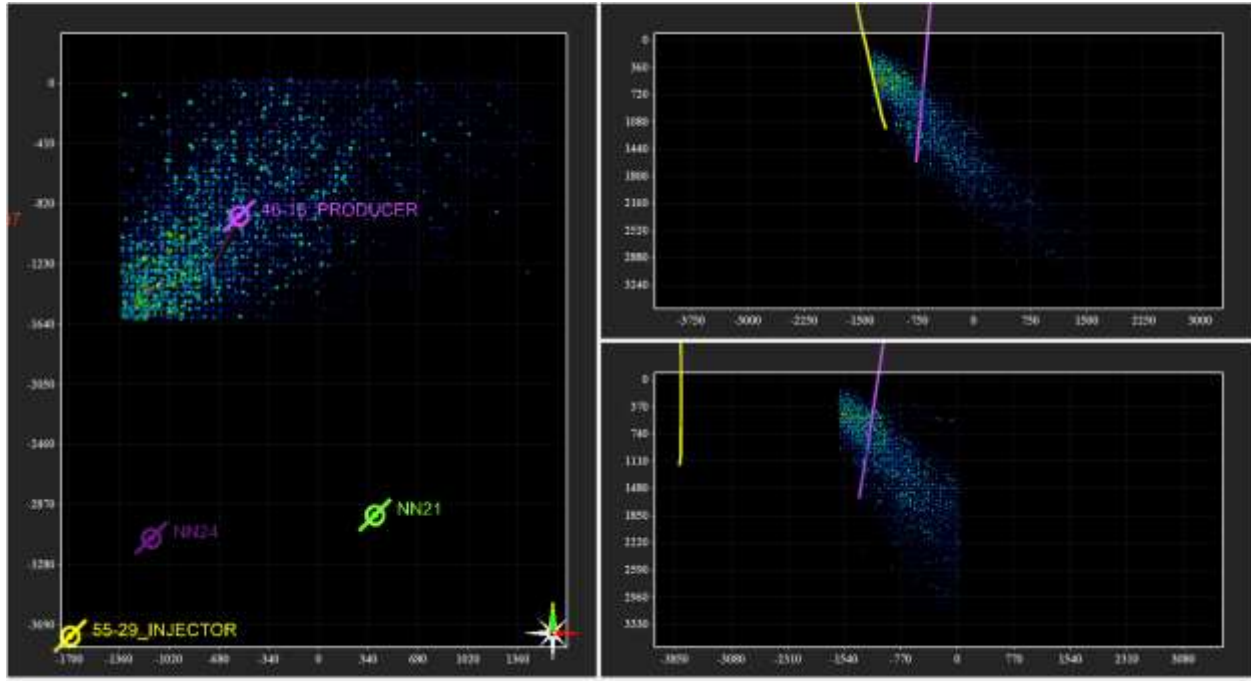


Figure 4 - 13:23

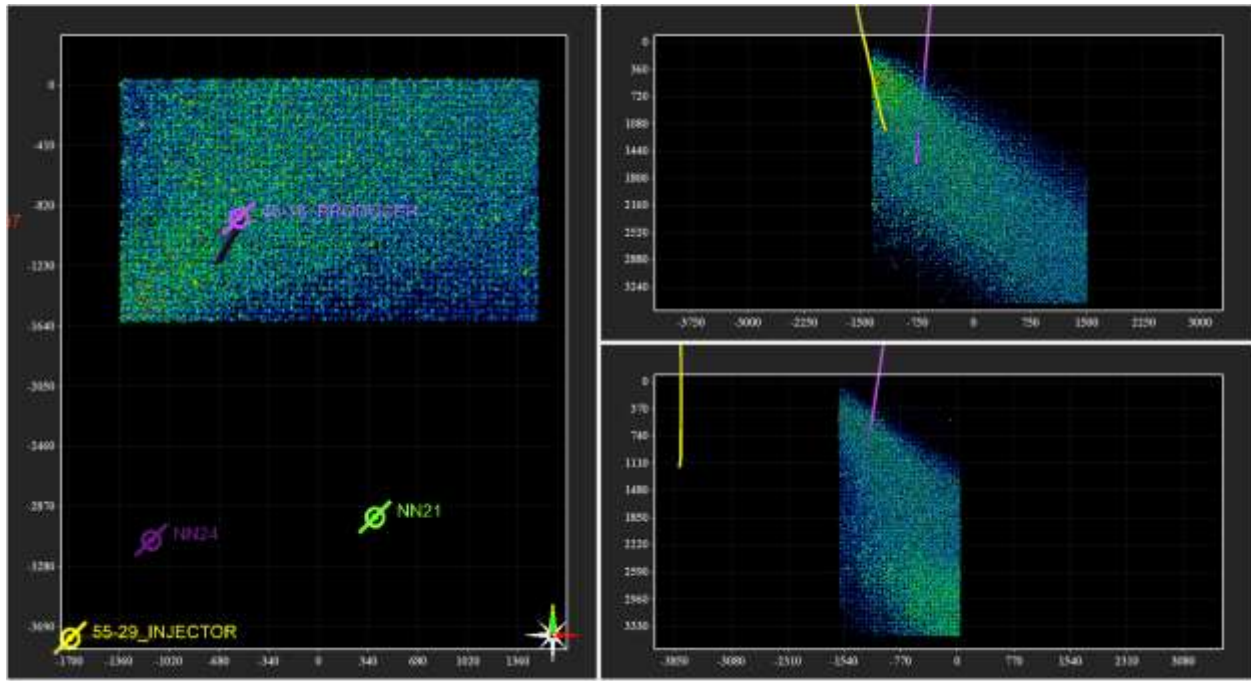


Figure 5 - 13:53

1410

Opened valves, pressure gage reading 550 psi, strong flow of non-condensable gas

DOCUMENT NO: S3-REP-01-5-ALTAROCK_REDUX	REVISION NO: 05 Appendix G: 146	REVISION DATE: 29/04/2014	Page 7 of 47	PM APPROVAL: SCOTT TAYLOR
--	---------------------------------------	------------------------------	--------------	------------------------------

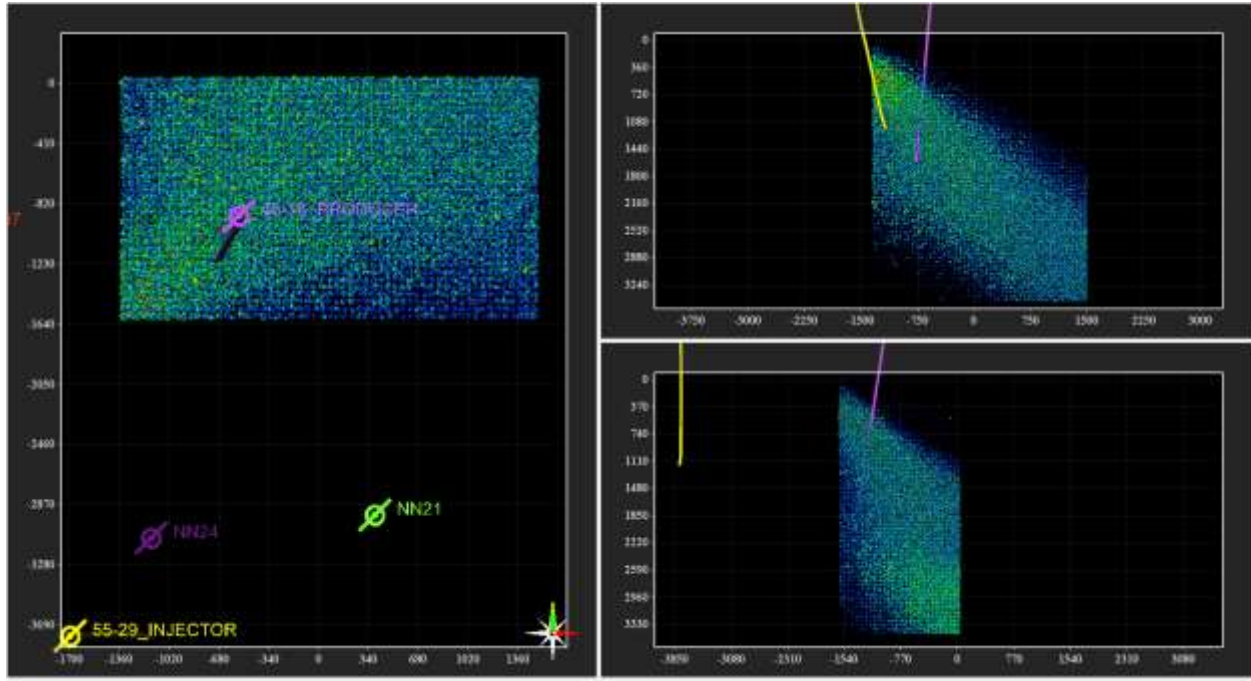


Figure 6 - 14:23

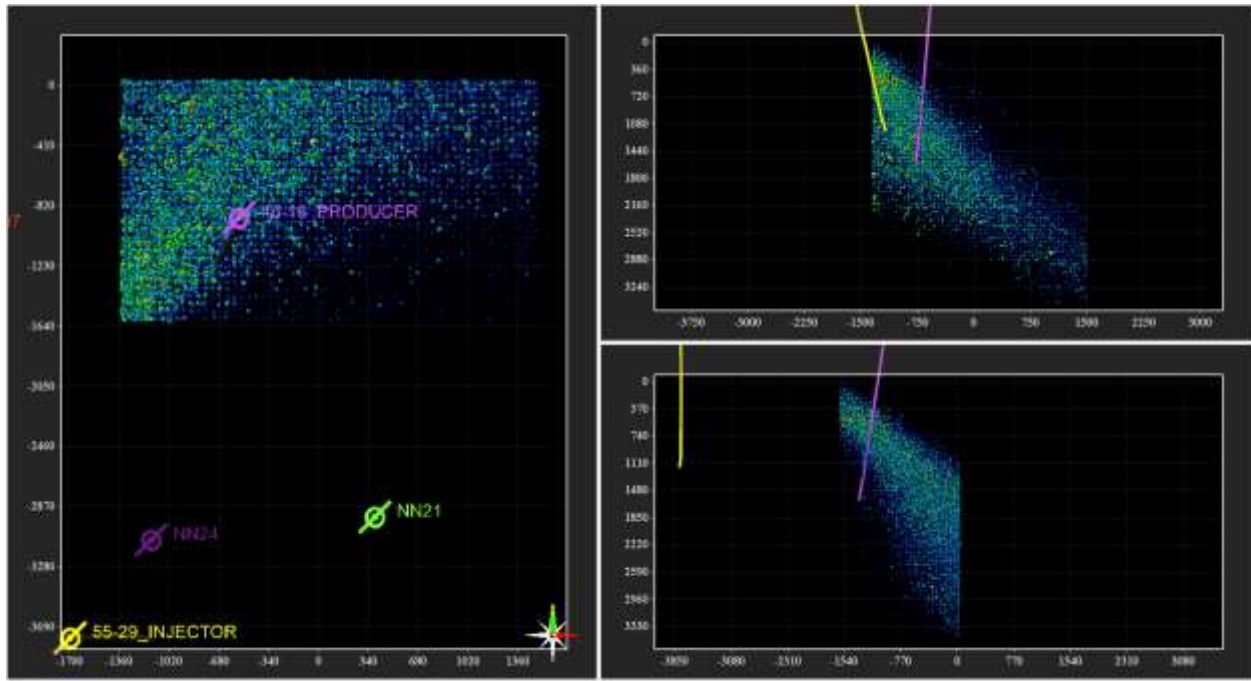


Figure 7 - 14:53

1500 Pressure gage reading 400 psi.
 1515 Pressure gage reading 300 psi.

DOCUMENT NO: S3-REP-01-5-ALTAROCK_REDUX	REVISION NO: 05 Appendix G: 147	REVISION DATE: 29/04/2014	Page 8 of 47	PM APPROVAL:
				SCOTT TAYLOR

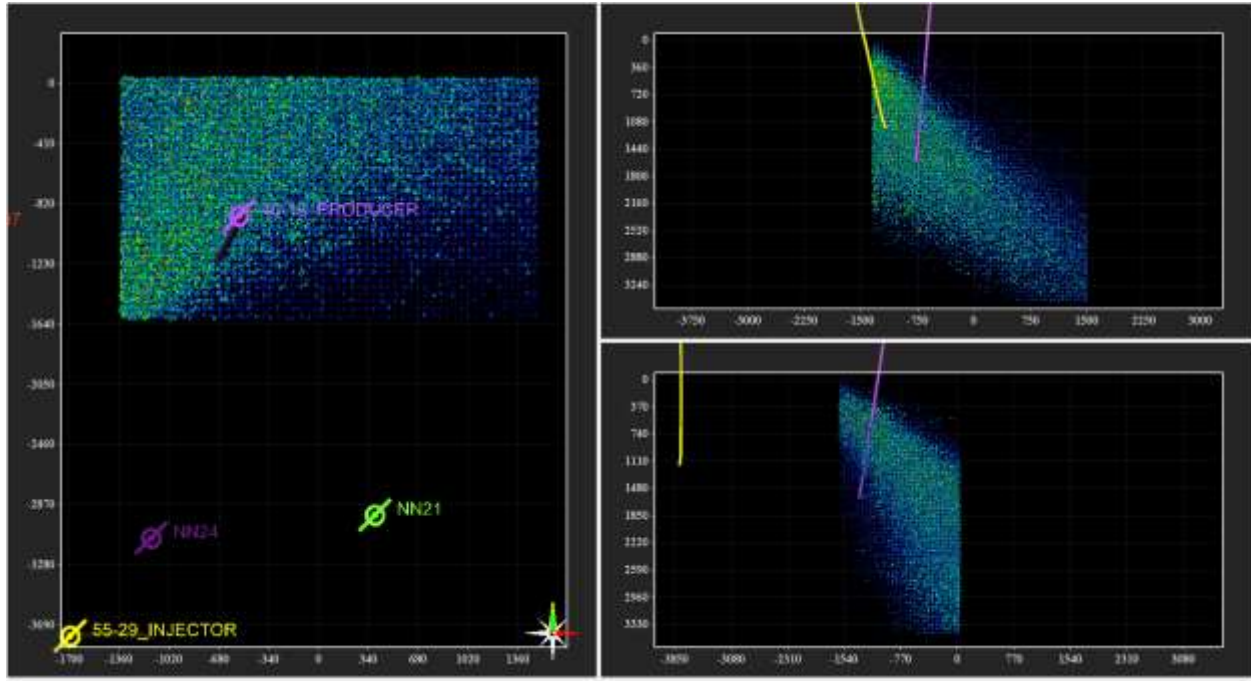


Figure 8 - 15:23

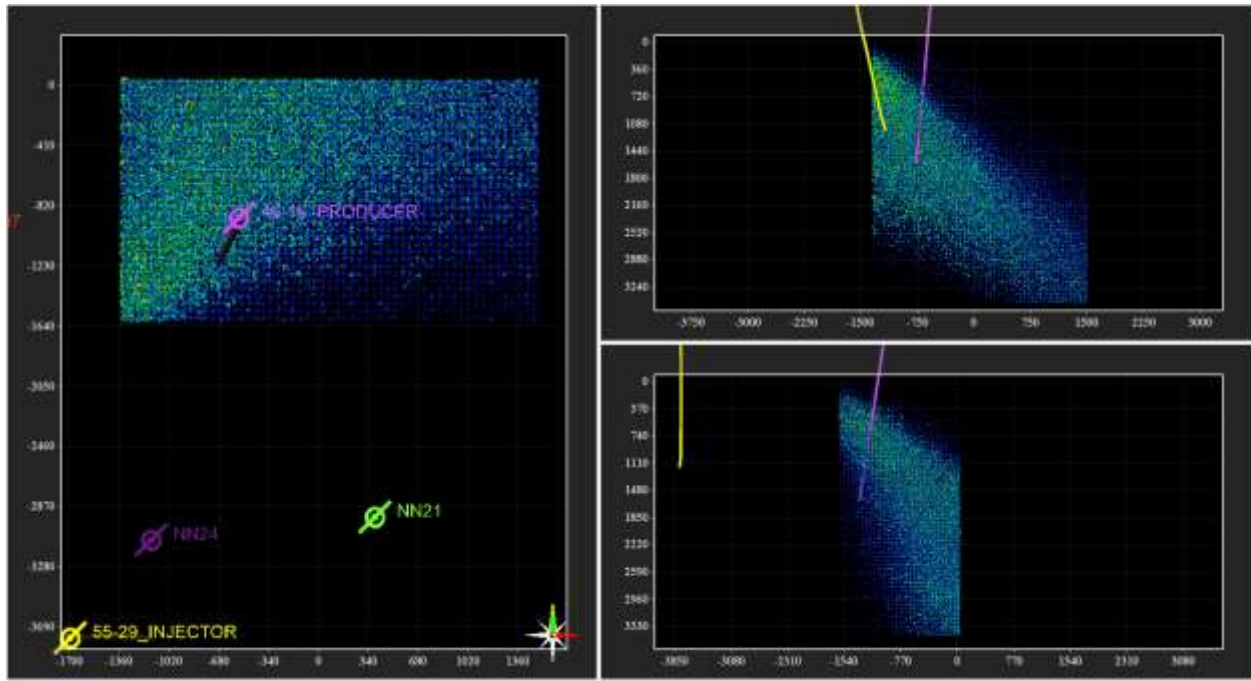


Figure 9 - 15:53

1605
1620

Well starting to flow liquid, dark brown, low flow rate
Flow rate increased from low to strong fountain flow.

DOCUMENT NO: S3-REP-01-5-ALTAROCK_REDUX	REVISION NO: 05 Appendix G: 148	REVISION DATE: 29/04/2014	Page 9 of 47	PM APPROVAL: SCOTT TAYLOR
--	---------------------------------------	------------------------------	--------------	------------------------------

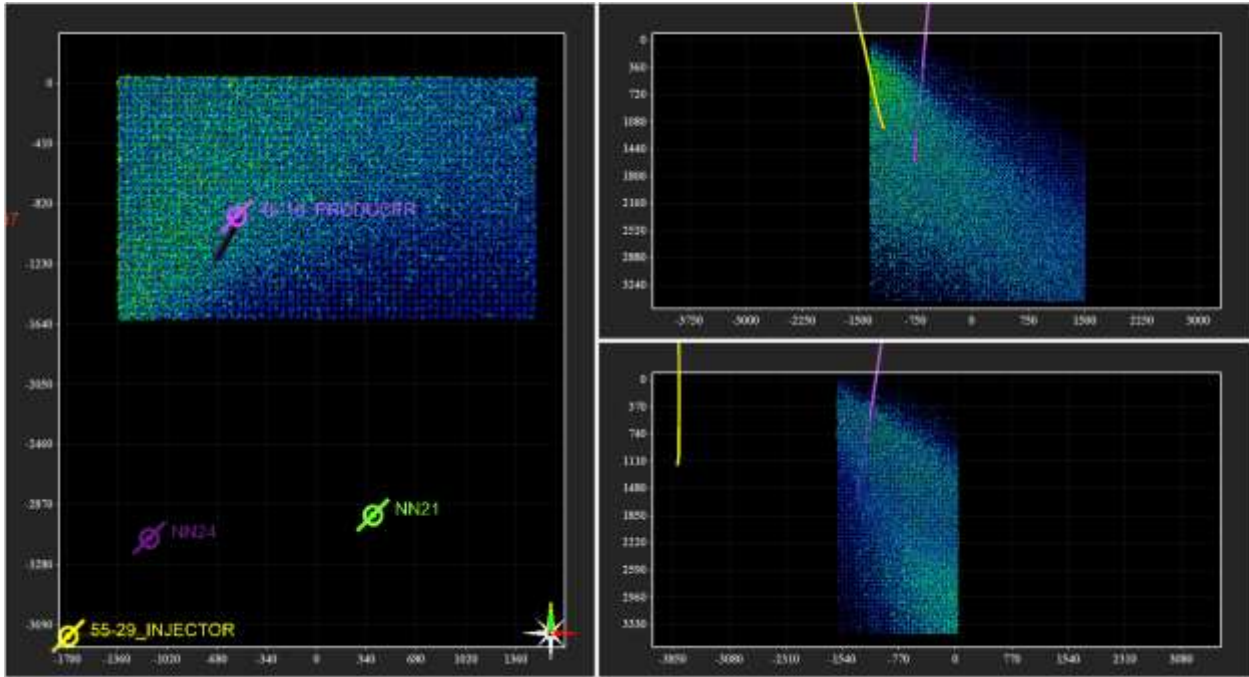


Figure 10 - 16:23

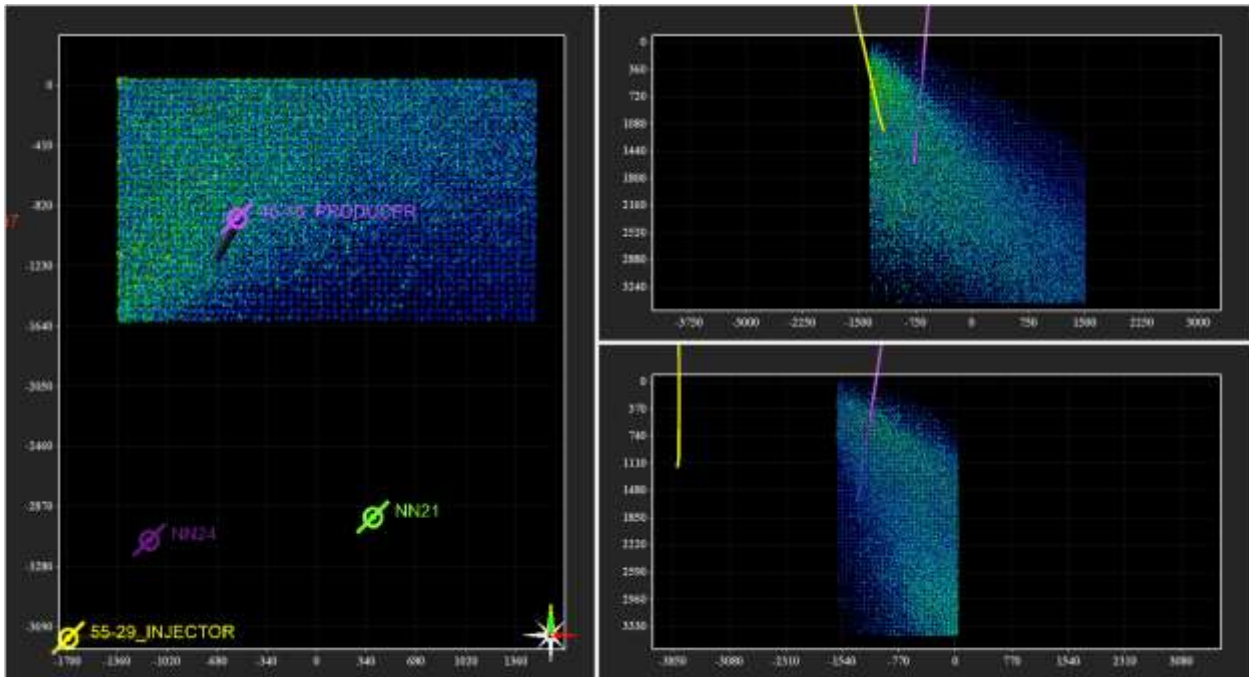


Figure 11 - 16:53

<p>DOCUMENT NO: S3-REP-01-5-ALTAROCK_REDUX</p>	<p>REVISION NO: 05 Appendix G: 149</p>	<p>REVISION DATE: 29/04/2014</p>	<p>Page 10 of 47</p>	<p>PM APPROVAL: SCOTT TAYLOR</p>
---	---	---	----------------------	---

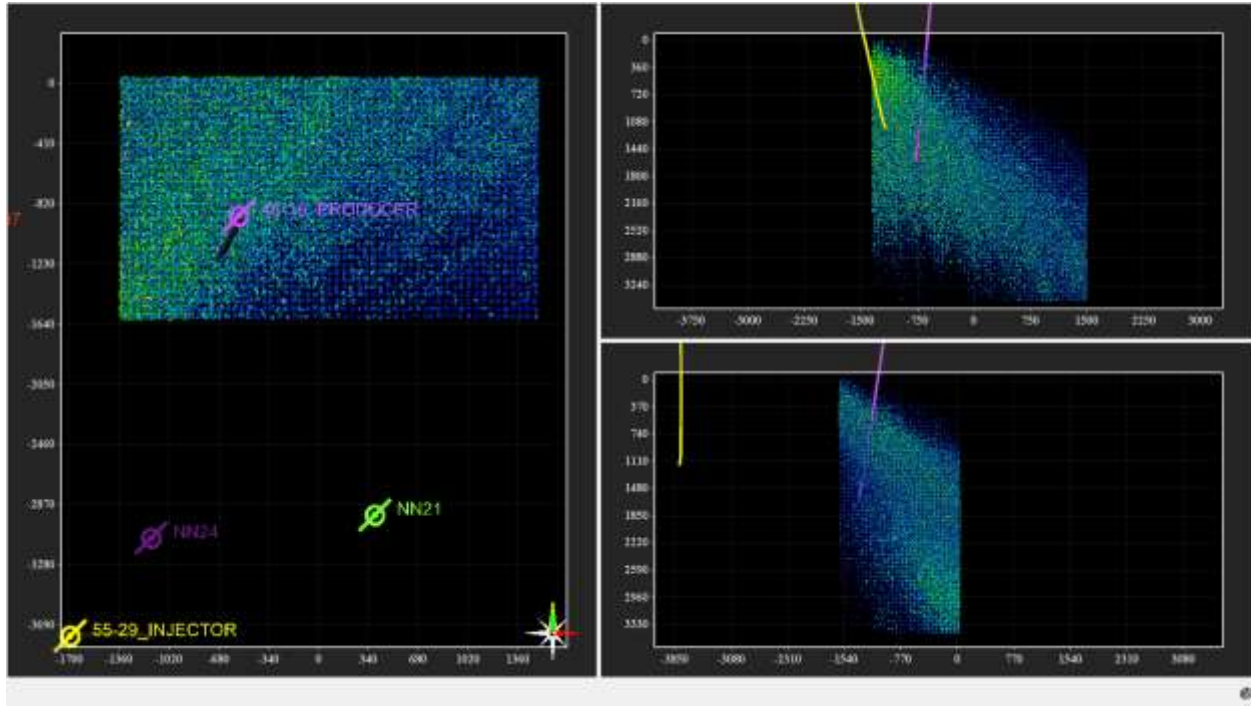


Figure 12 - 17:23

1745 Oscillating liquid and gas flow with gradually more gas.

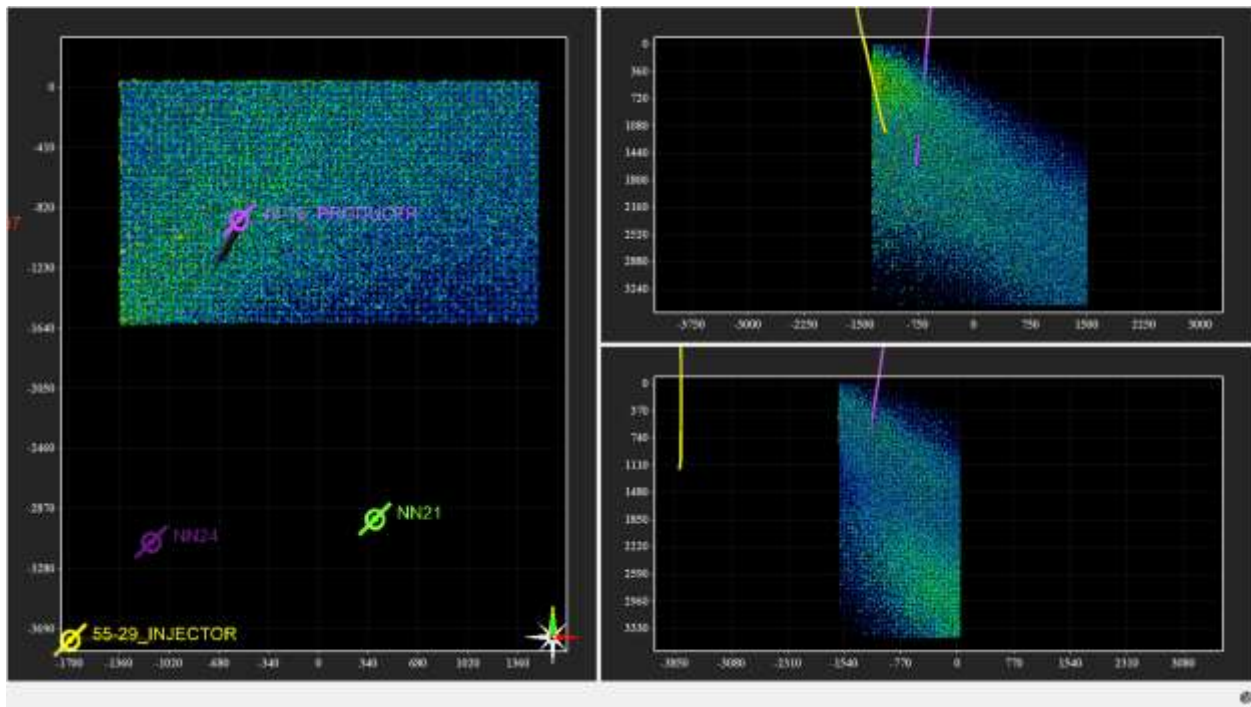


Figure 13 - 17:53

1812 Oscillating liquid and gas flow, dominated by gas.

DOCUMENT NO: S3-REP-01-5-ALTAROCK_REDUX	REVISION NO: 05 Appendix G: 150	REVISION DATE: 29/04/2014	Page 11 of 47	PM APPROVAL: SCOTT TAYLOR
--	---------------------------------------	------------------------------	---------------	------------------------------

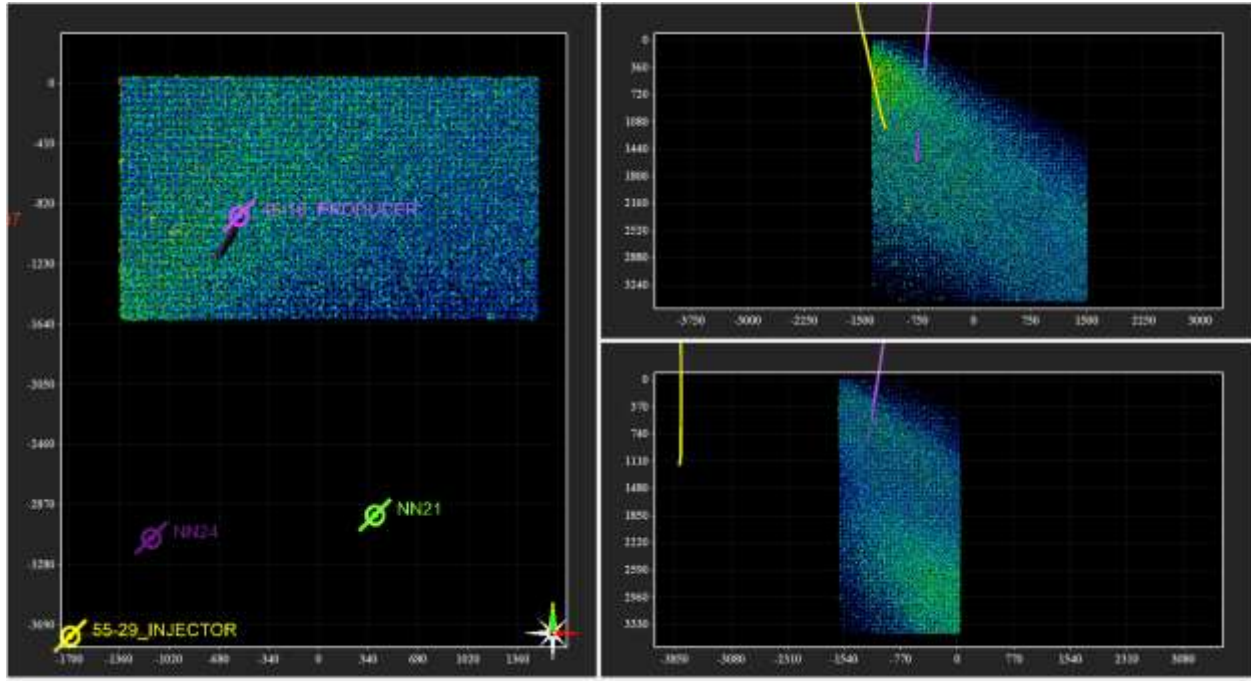


Figure 14 - 18:23

1835 Shut well in.

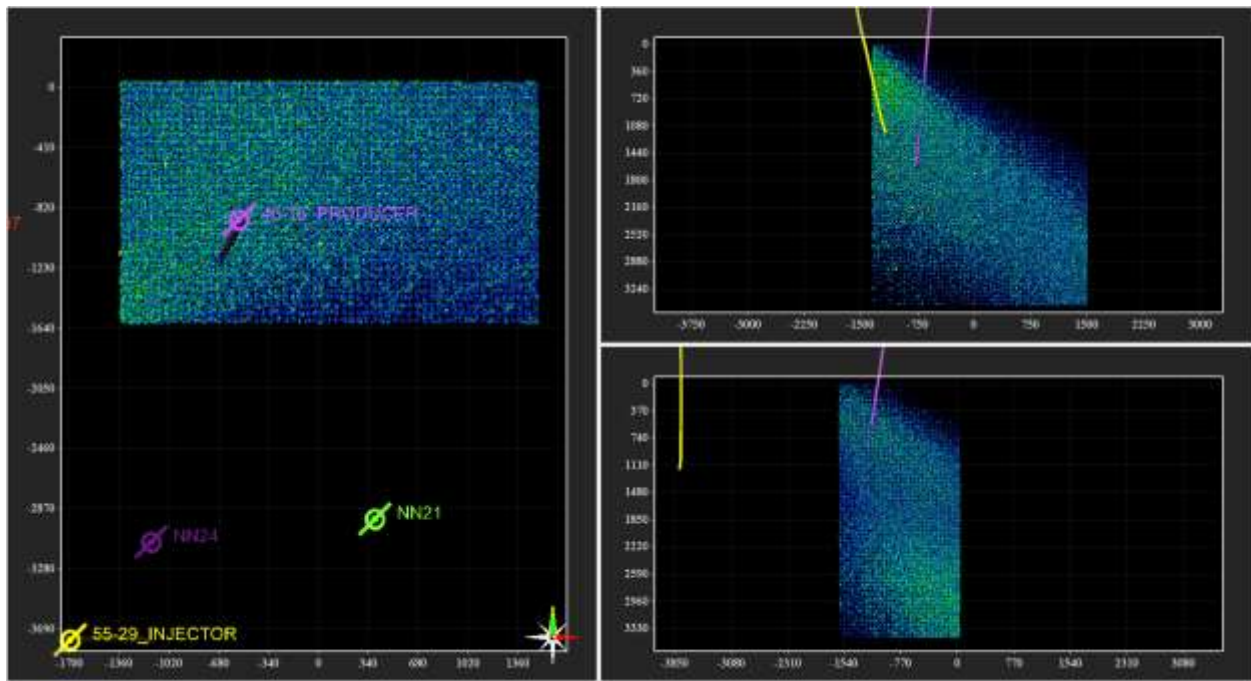


Figure 15 - 18:53

DOCUMENT NO: S3-REP-01-5-ALTAROCK_REDUX	REVISION NO: 05 Appendix G: 151	REVISION DATE: 29/04/2014	Page 12 of 47	PM APPROVAL: SCOTT TAYLOR
--	---------------------------------------	------------------------------	---------------	------------------------------

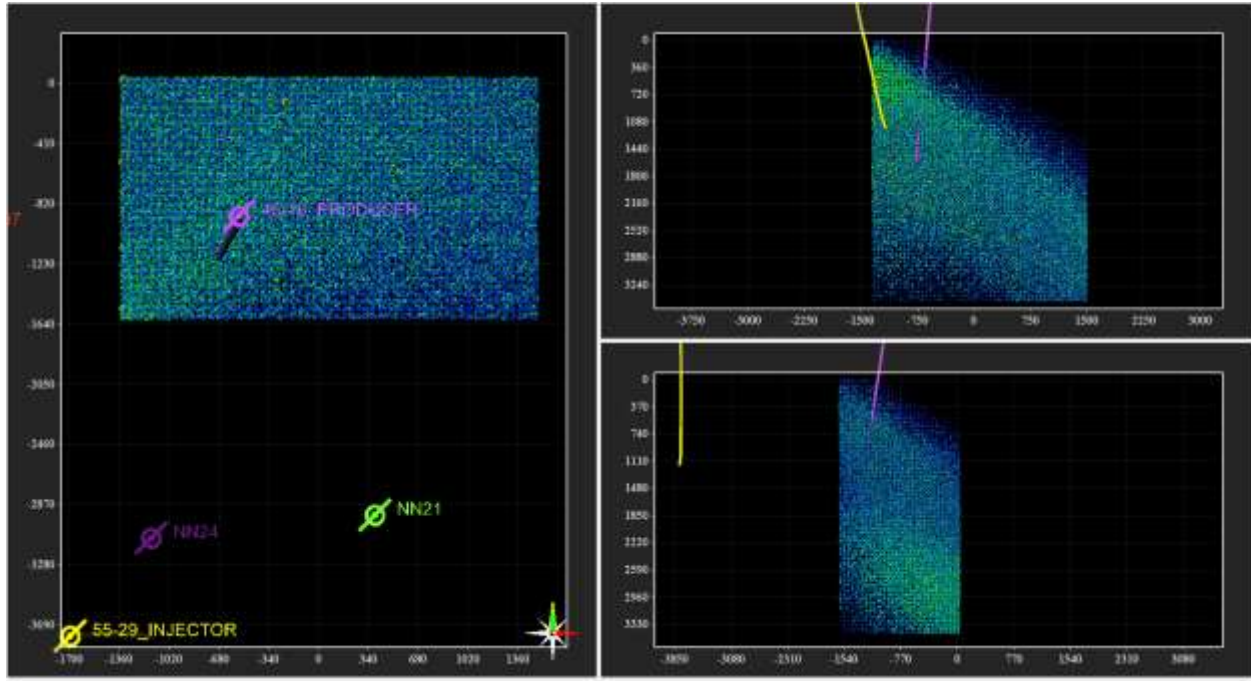


Figure 16 - 19:23

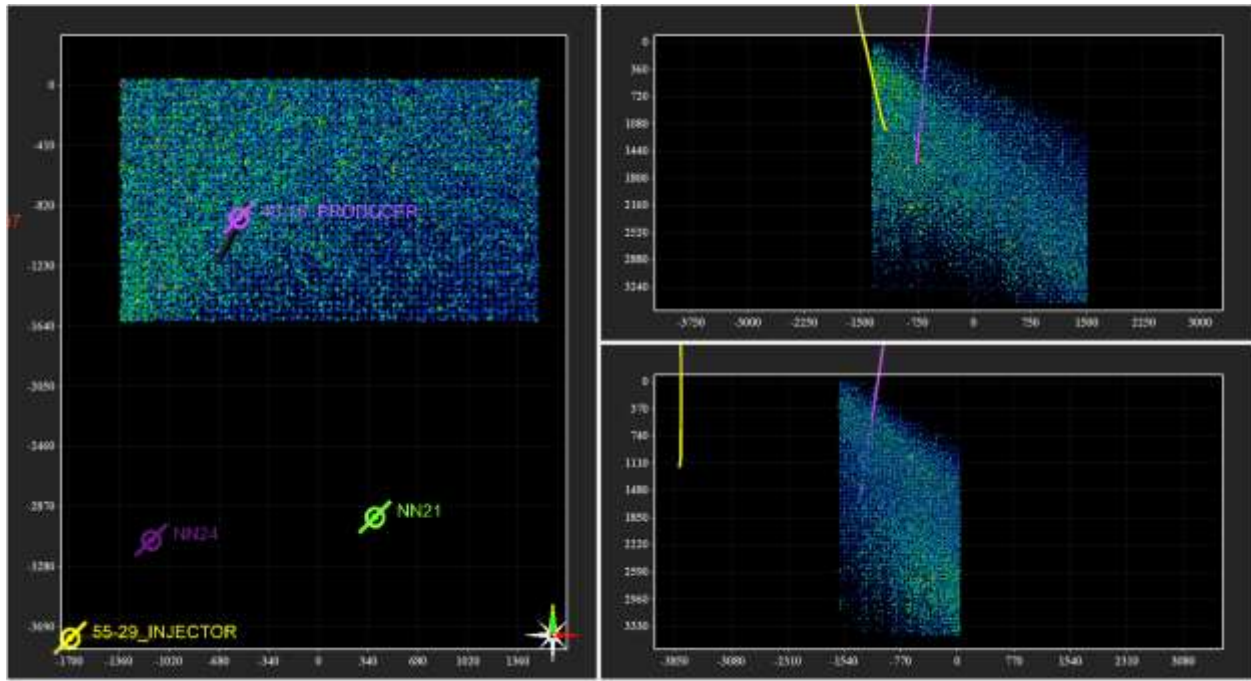


Figure 17 - 19:53

DOCUMENT NO: S3-REP-01-5-ALTAROCK_REDUX	REVISION NO: 05 Appendix G: 152	REVISION DATE: 29/04/2014	Page 13 of 47	PM APPROVAL:
				SCOTT TAYLOR

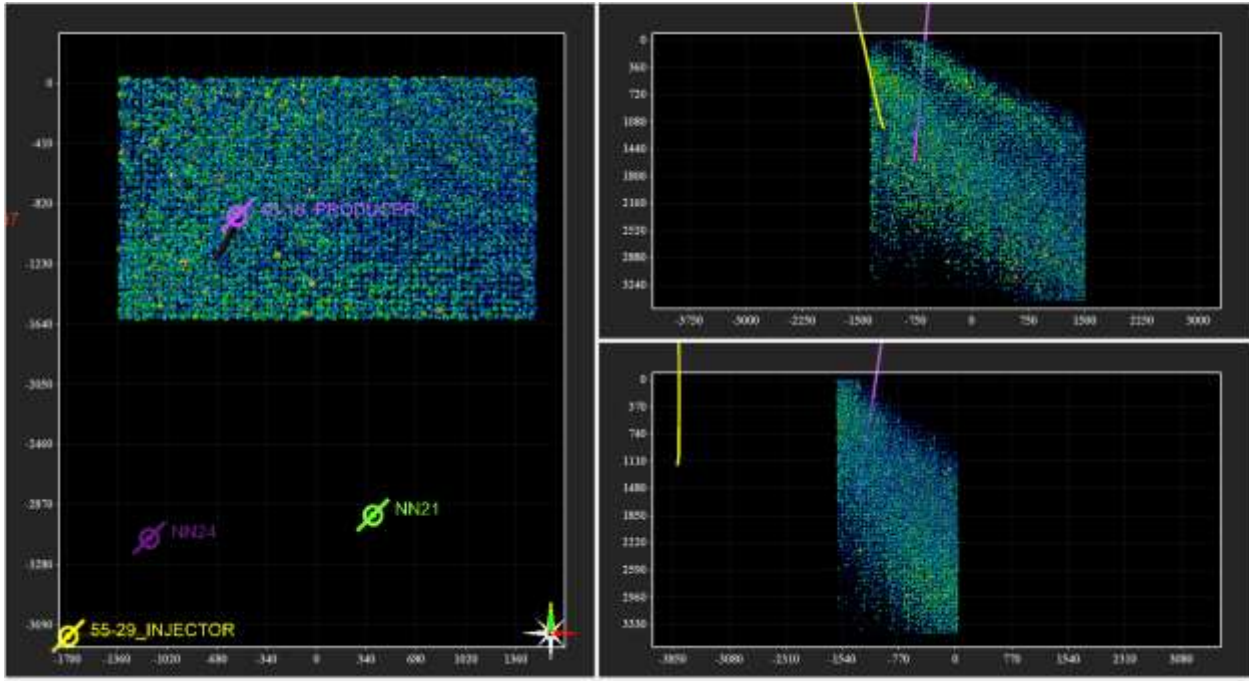


Figure 18 - 20:23

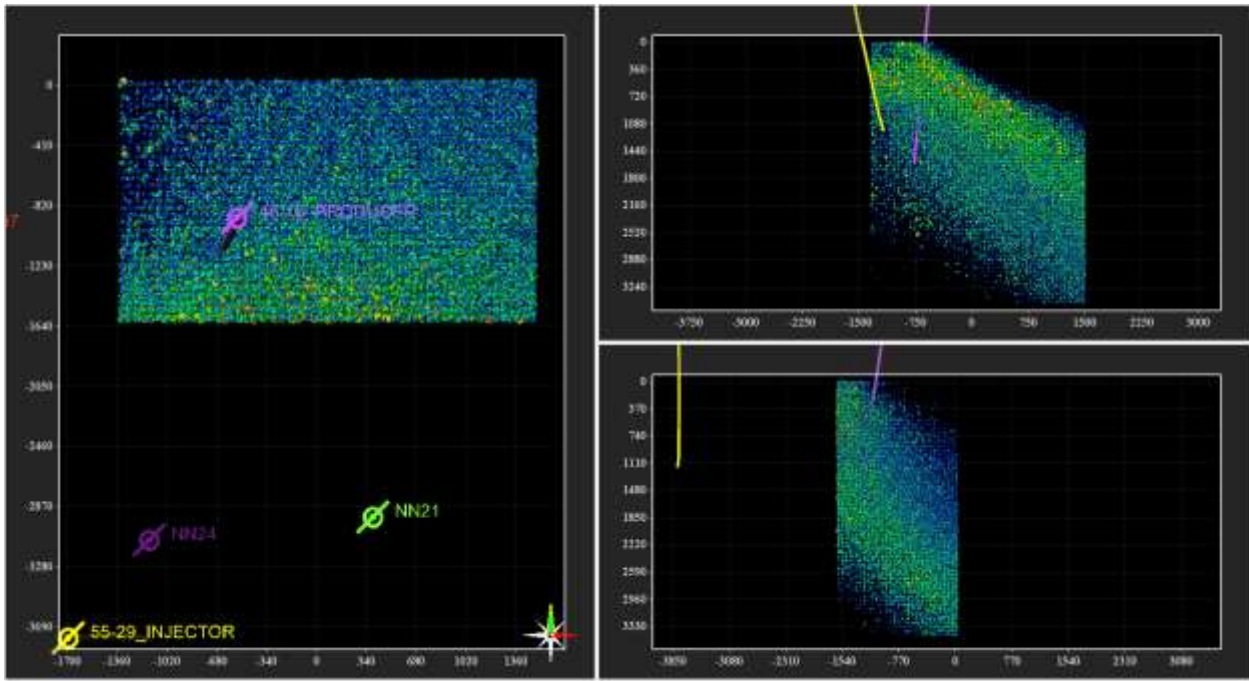


Figure 19 - 20:53

DOCUMENT NO: S3-REP-01-5-ALTAROCK_REDUX	REVISION NO: 05 Appendix G: 153	REVISION DATE: 29/04/2014	Page 14 of 47	PM APPROVAL: SCOTT TAYLOR
--	---------------------------------------	------------------------------	---------------	------------------------------

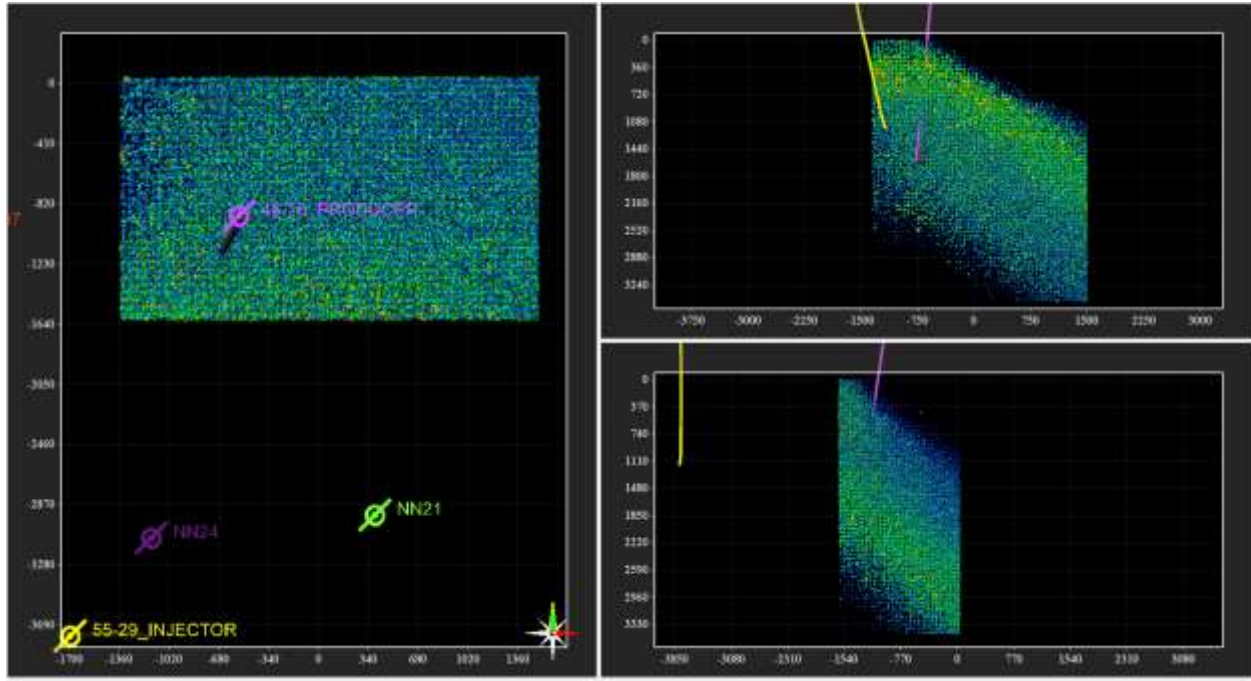


Figure 20 - 21:23

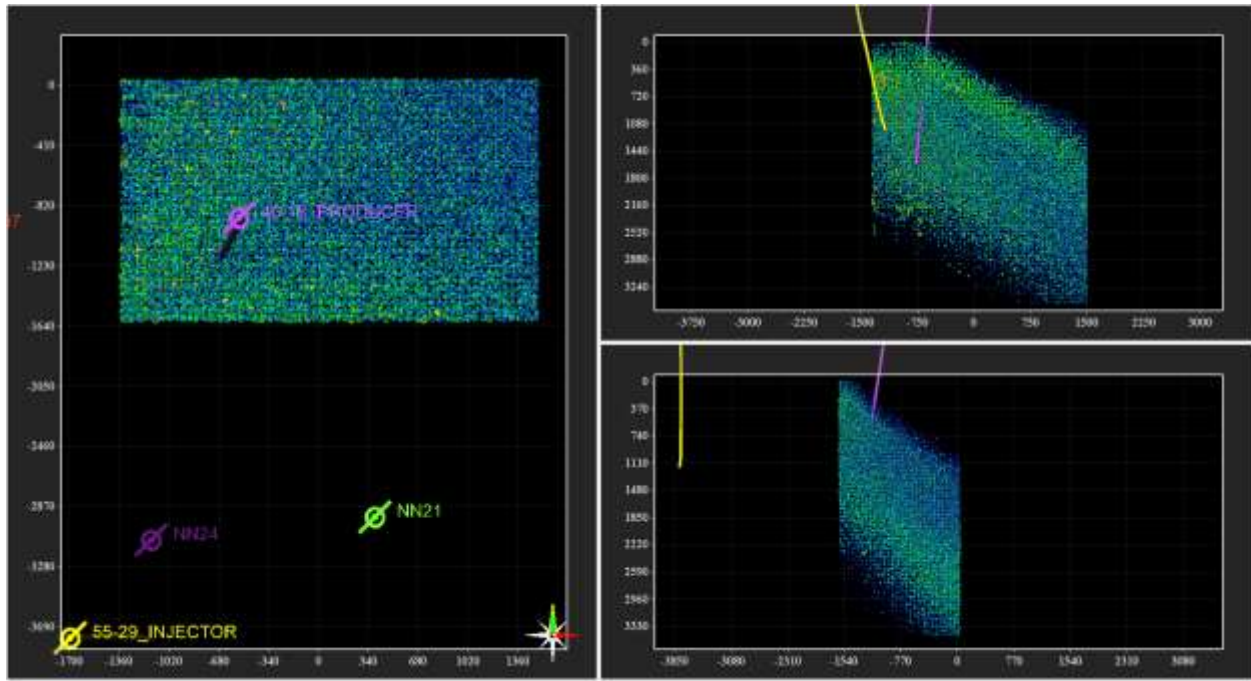


Figure 21 - 21:53

DOCUMENT NO: S3-REP-01-5-ALTAROCK_REDUX	REVISION NO: 05 Appendix G: 154	REVISION DATE: 29/04/2014	Page 15 of 47	PM APPROVAL:
				SCOTT TAYLOR

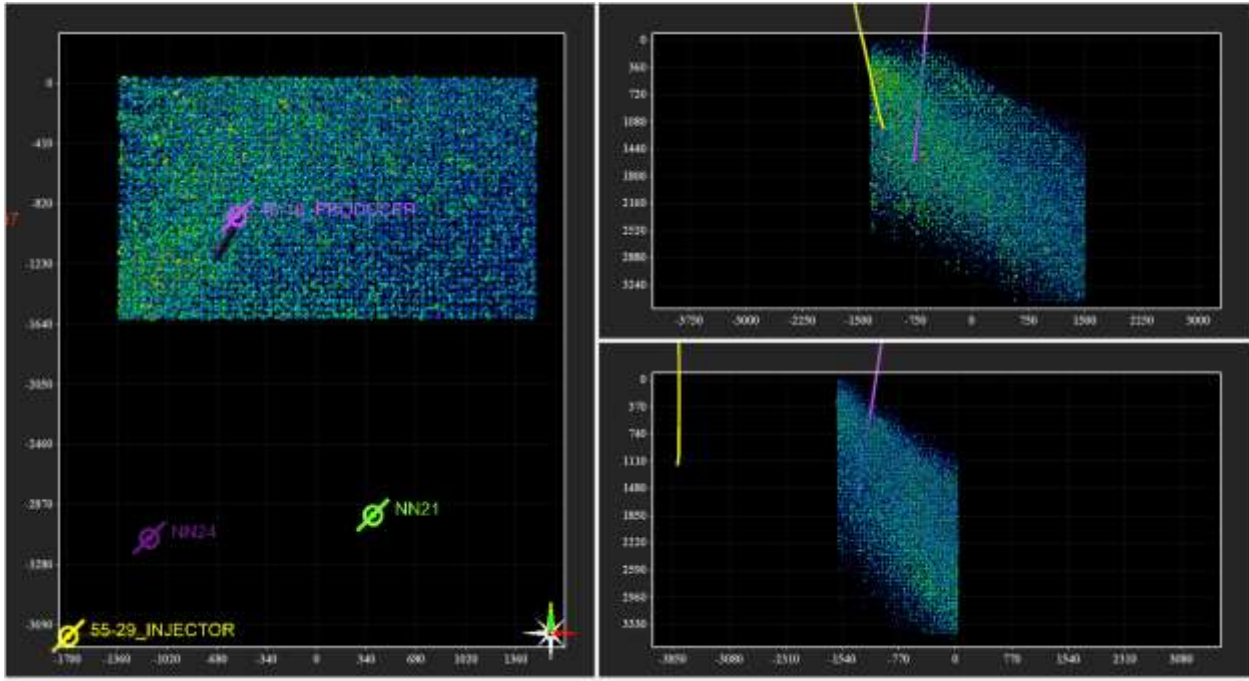


Figure 22 - 22:23

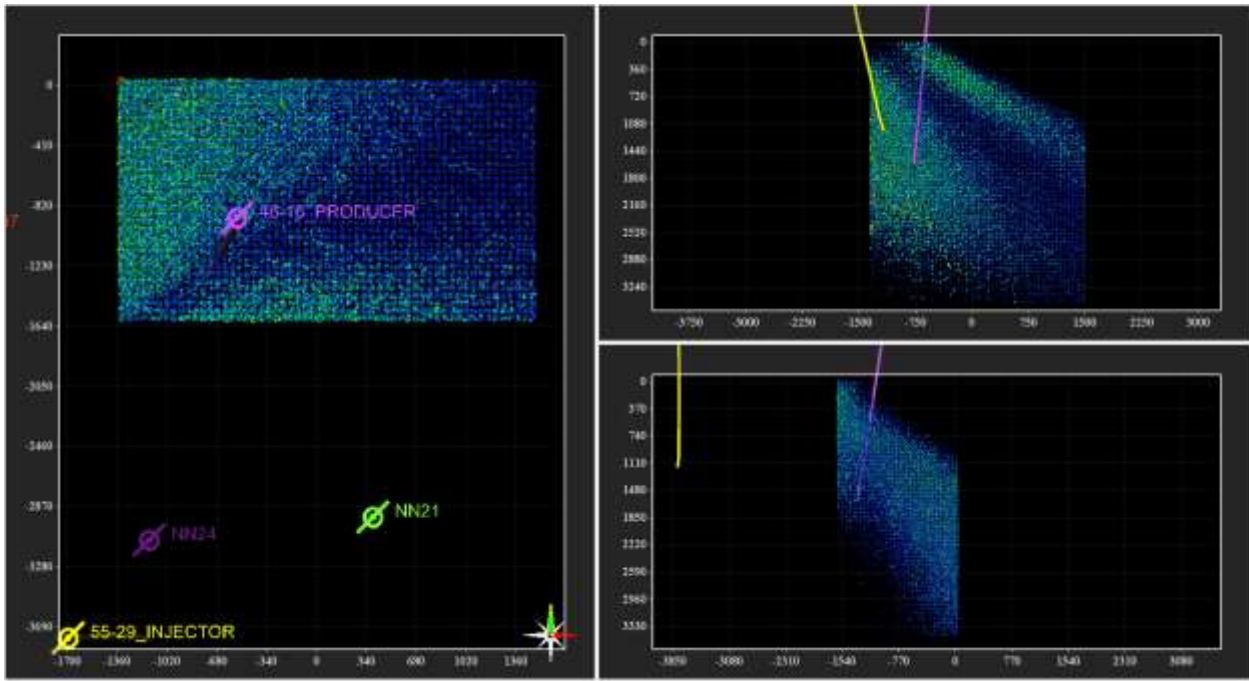


Figure 23 - 22:53

DOCUMENT NO: S3-REP-01-5-ALTAROCK_REDUX	REVISION NO: 05 Appendix G: 155	REVISION DATE: 29/04/2014	Page 16 of 47	PM APPROVAL:
				SCOTT TAYLOR

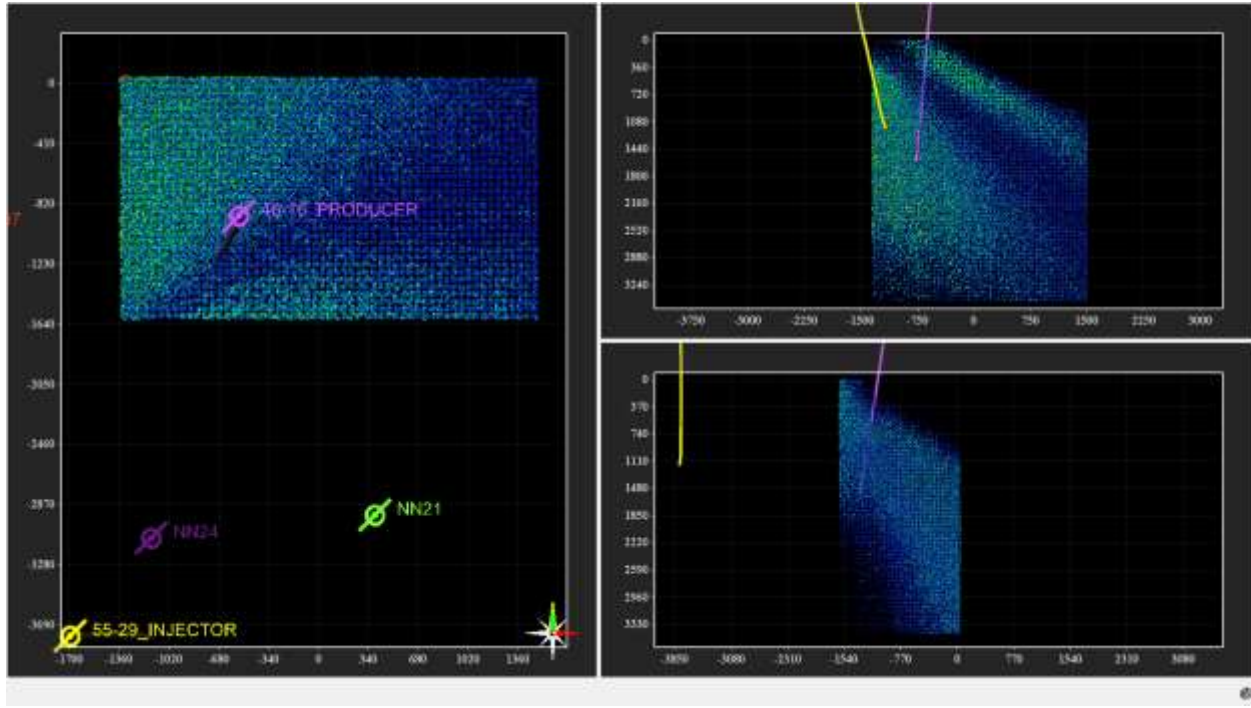


Figure 24 - 23:23

DOCUMENT NO: S3-REP-01-5-ALTAROCK_REDUX	REVISION NO: 05 Appendix G: 156	REVISION DATE: 29/04/2014	Page 17 of 47	PM APPROVAL: SCOTT TAYLOR
---	--	-------------------------------------	---------------	-------------------------------------

9 Sept. 2013

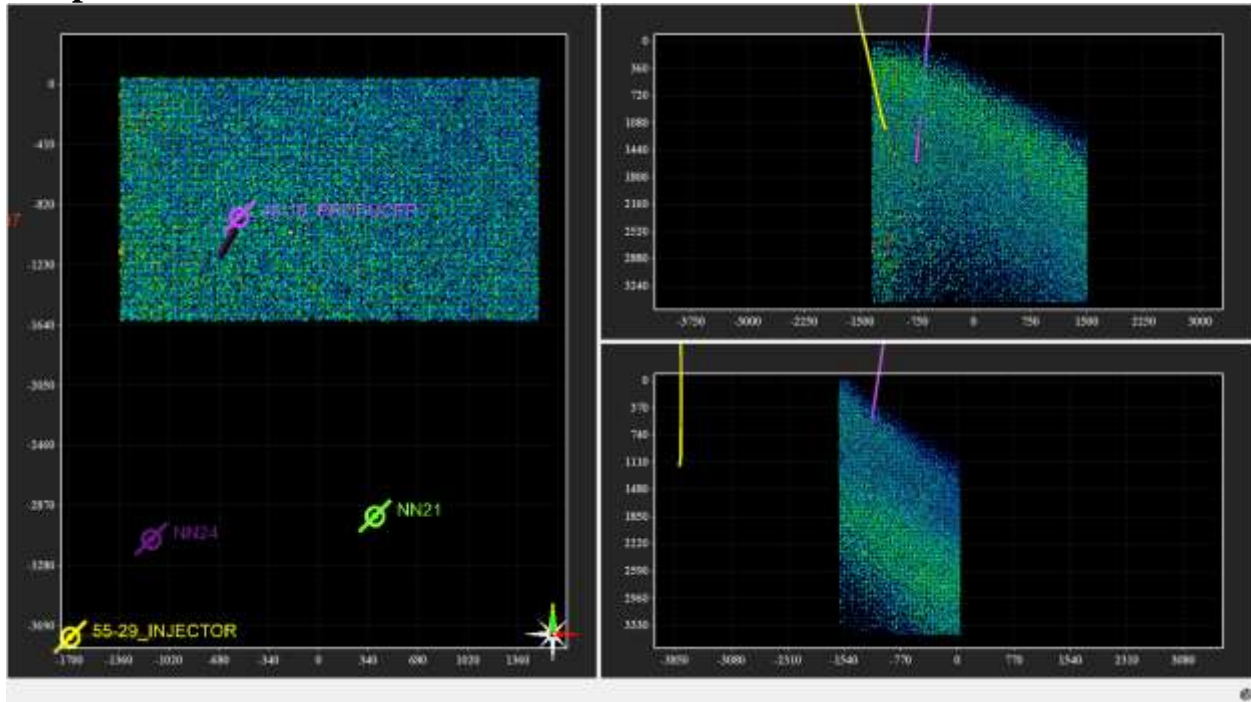


Figure 25 - 8:44

0845 Pressure gage reading 550 psi.

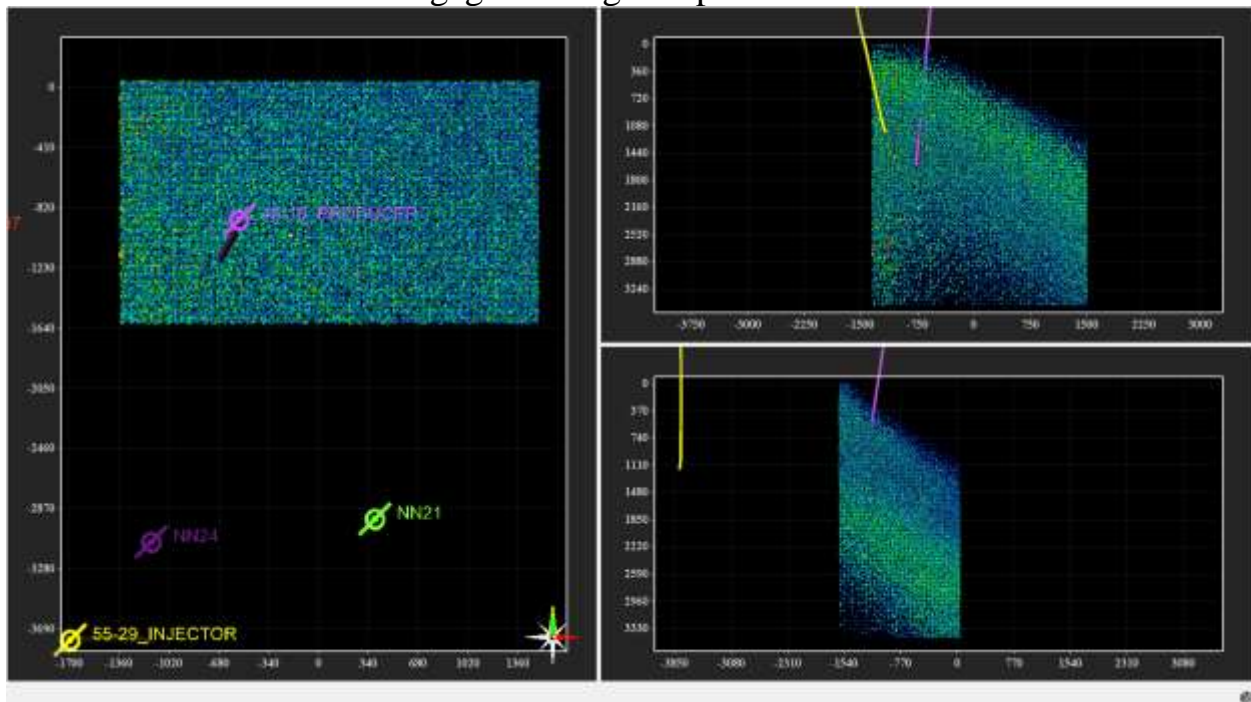


Figure 26 - 9:14

DOCUMENT NO: S3-REP-01-5-ALTAROCK_REDUX	REVISION NO: 05 Appendix G: 157	REVISION DATE: 29/04/2014	Page 18 of 47	PM APPROVAL: SCOTT TAYLOR
--	---------------------------------------	------------------------------	---------------	------------------------------

0940 Cleaning sample port tube in preparation for collecting gas sample.

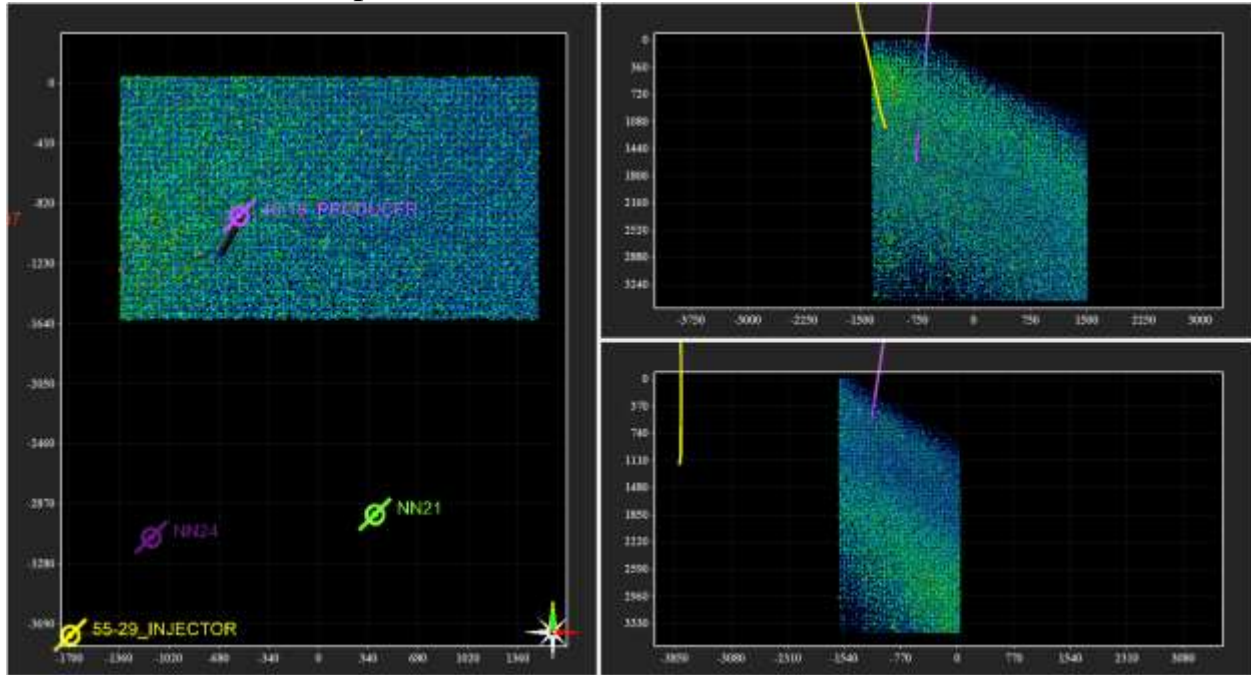


Figure 27 - 9:44

1010 Open well to moderate flow to purge line and sample bottle.

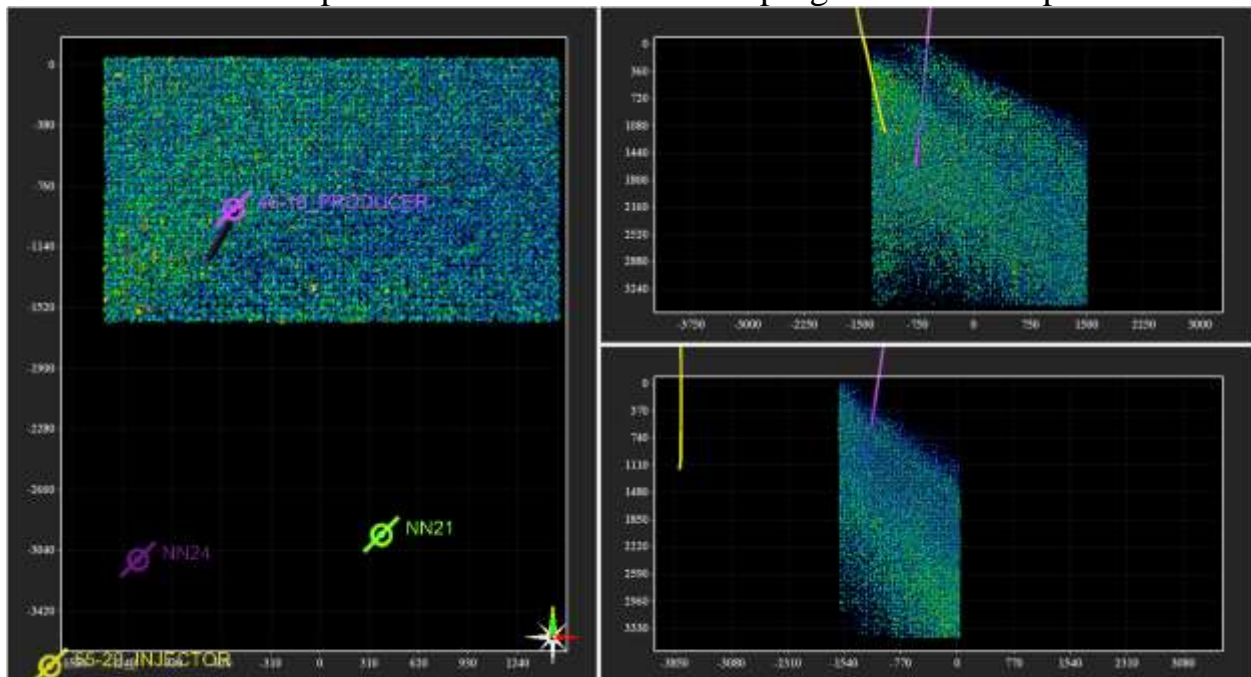


Figure 28 - 10:14

DOCUMENT NO: S3-REP-01-5-ALTAROCK_REDUX	REVISION NO: 05 Appendix G: 158	REVISION DATE: 29/04/2014	Page 19 of 47	PM APPROVAL: SCOTT TAYLOR
--	---------------------------------------	------------------------------	---------------	------------------------------

1017 Completed gas sampling and secured sample bottle, and opening well. Strong flow of non-condensable gas.

1027 Pressure gage reading 500 psi.

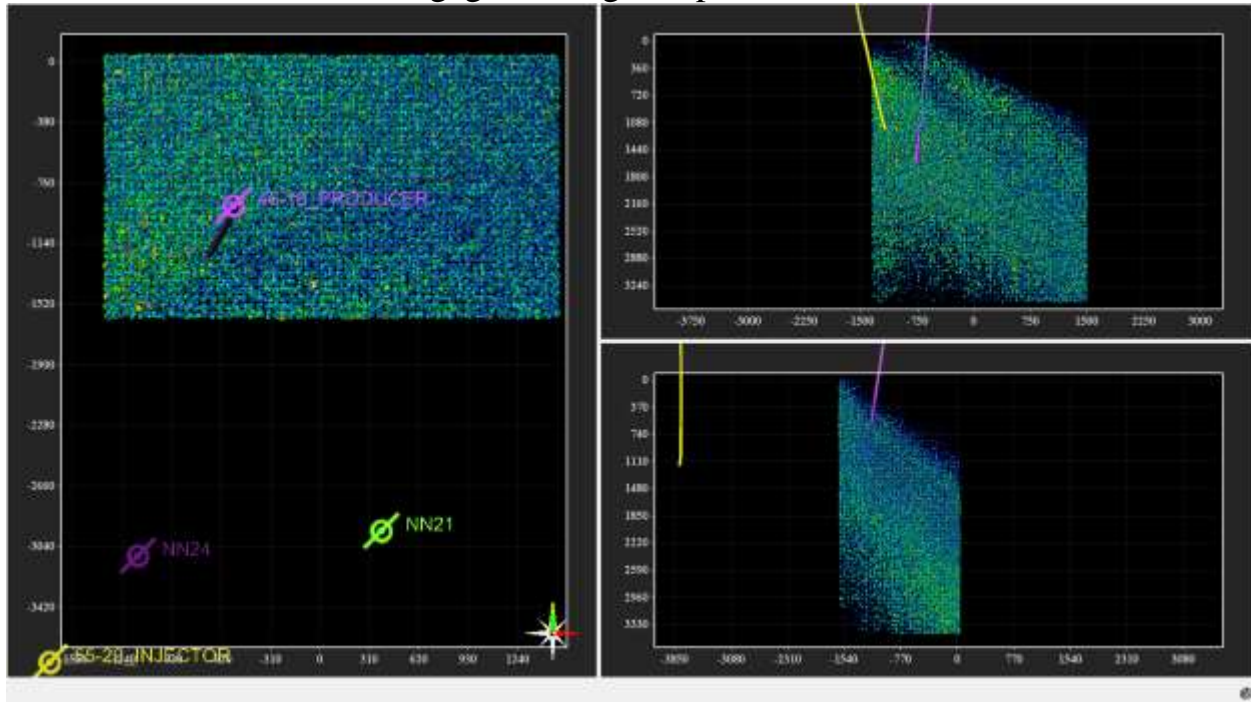


Figure 29 - 10:44

1047 Pressure gage reading 480 psi.

1050 Very small puffs of liquid occasionally occurring with the gas flow.

DOCUMENT NO: S3-REP-01-5-ALTAROCK_REDUX	REVISION NO: 05 Appendix G: 159	REVISION DATE: 29/04/2014	Page 20 of 47	PM APPROVAL: SCOTT TAYLOR
--	---------------------------------------	------------------------------	---------------	------------------------------

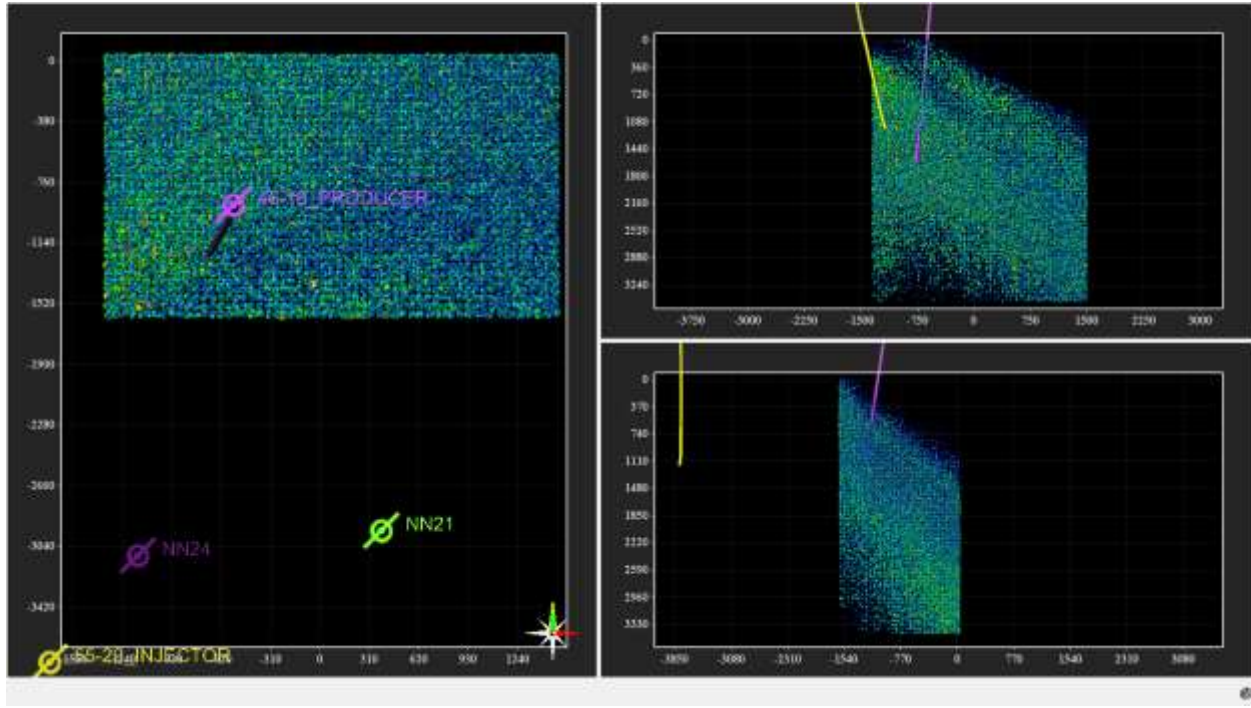


Figure 30 - 11:14

1115 Pressure gage reading 400 PSI.
 1122 Transition from gas to gas with occasional light water spray.

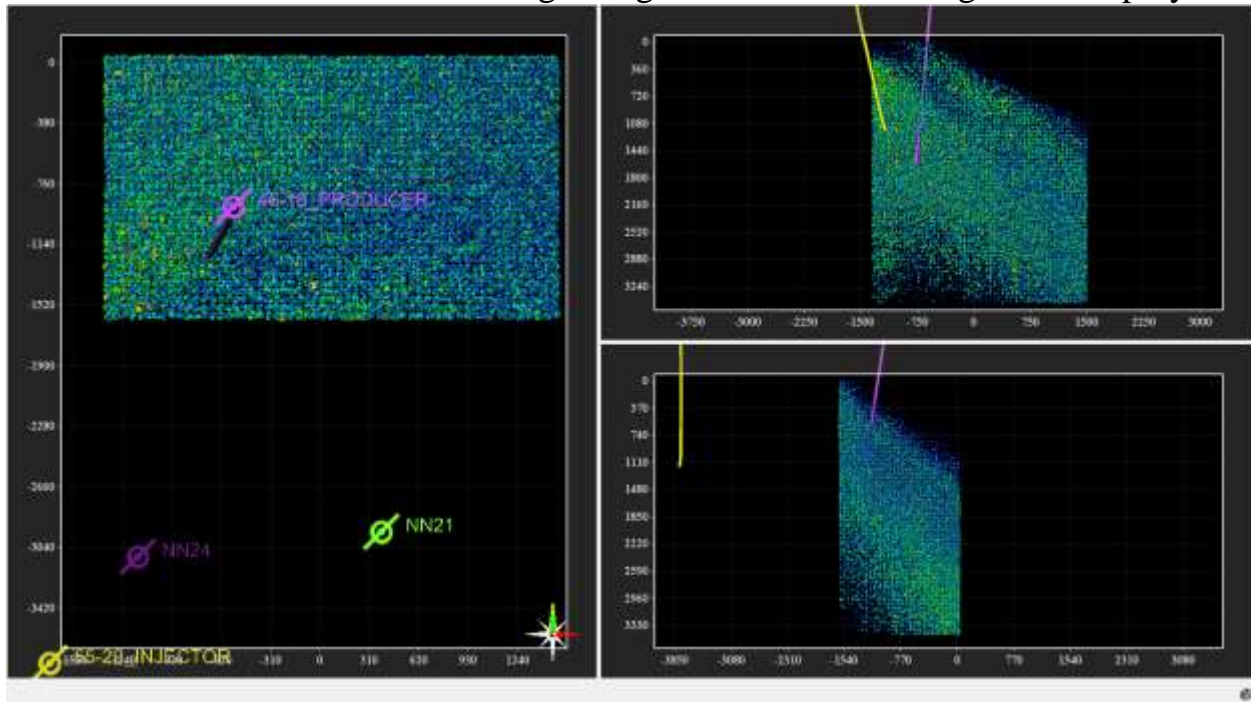


Figure 31 - 11:44

1144 Total liquid flow.

DOCUMENT NO: S3-REP-01-5-ALTAROCK_REDUX	REVISION NO: 05 Appendix G: 160	REVISION DATE: 29/04/2014	Page 21 of 47	PM APPROVAL: SCOTT TAYLOR
--	---------------------------------------	------------------------------	---------------	------------------------------

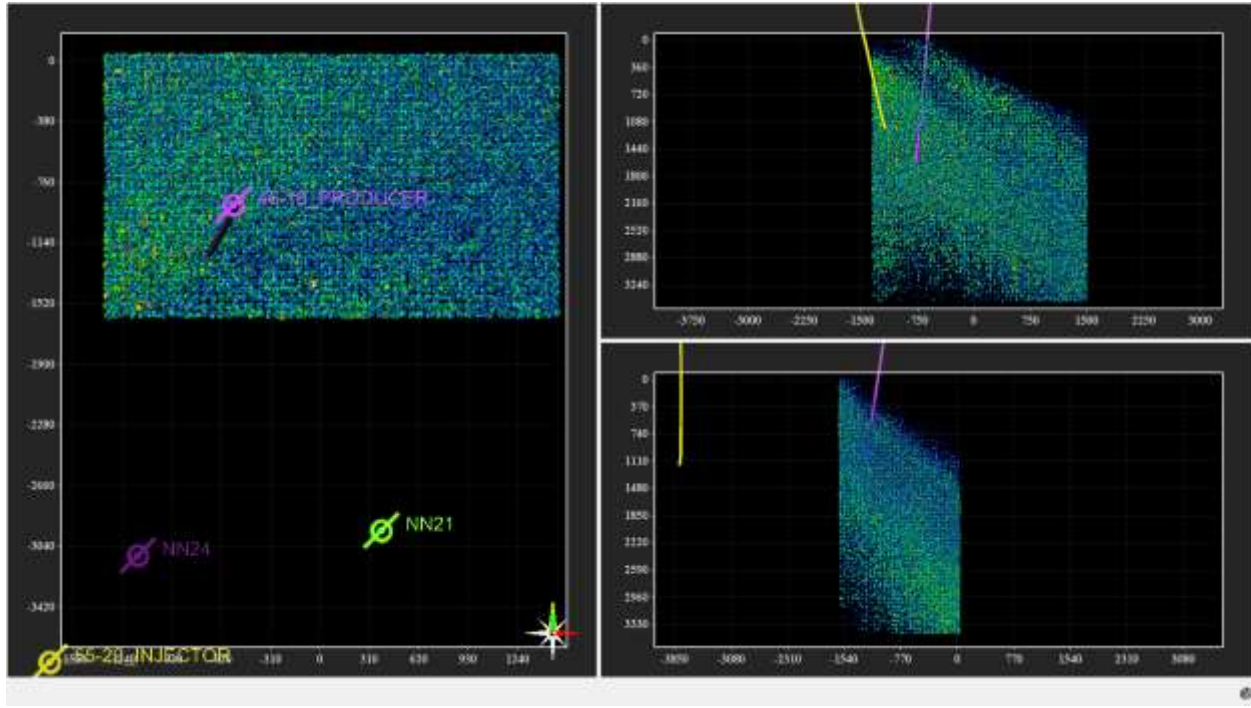


Figure 32 - 12:14

1230-1700

Oscillating gas and liquid flow, becoming mostly gas over time with short low-flow burps of very thick drilling fluid.

DOCUMENT NO: S3-REP-01-5-ALTAROCK_REDUX	REVISION NO: 05 Appendix G: 161	REVISION DATE: 29/04/2014	Page 22 of 47	PM APPROVAL: SCOTT TAYLOR
--	---------------------------------------	------------------------------	---------------	------------------------------

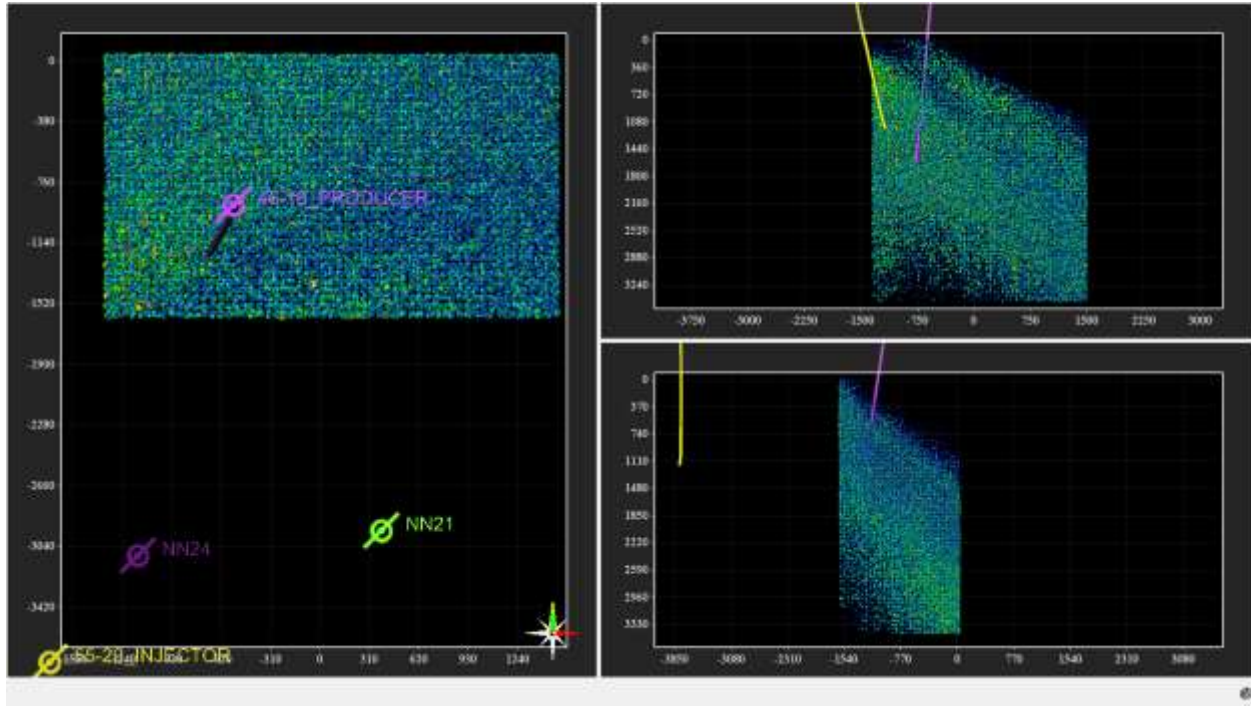


Figure 33 - 12:44

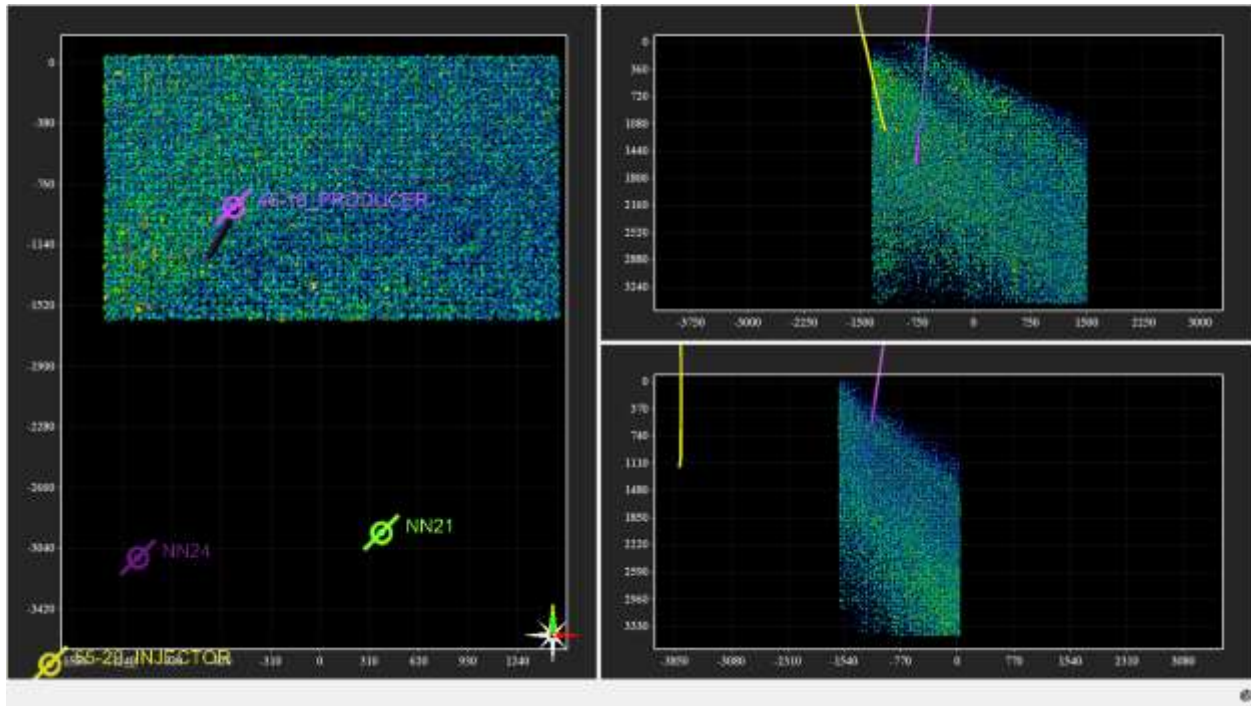


Figure 34 - 13:14

DOCUMENT NO: S3-REP-01-5-ALTAROCK_REDUX	REVISION NO: 05 Appendix G: 162	REVISION DATE: 29/04/2014	Page 23 of 47	PM APPROVAL:
				SCOTT TAYLOR

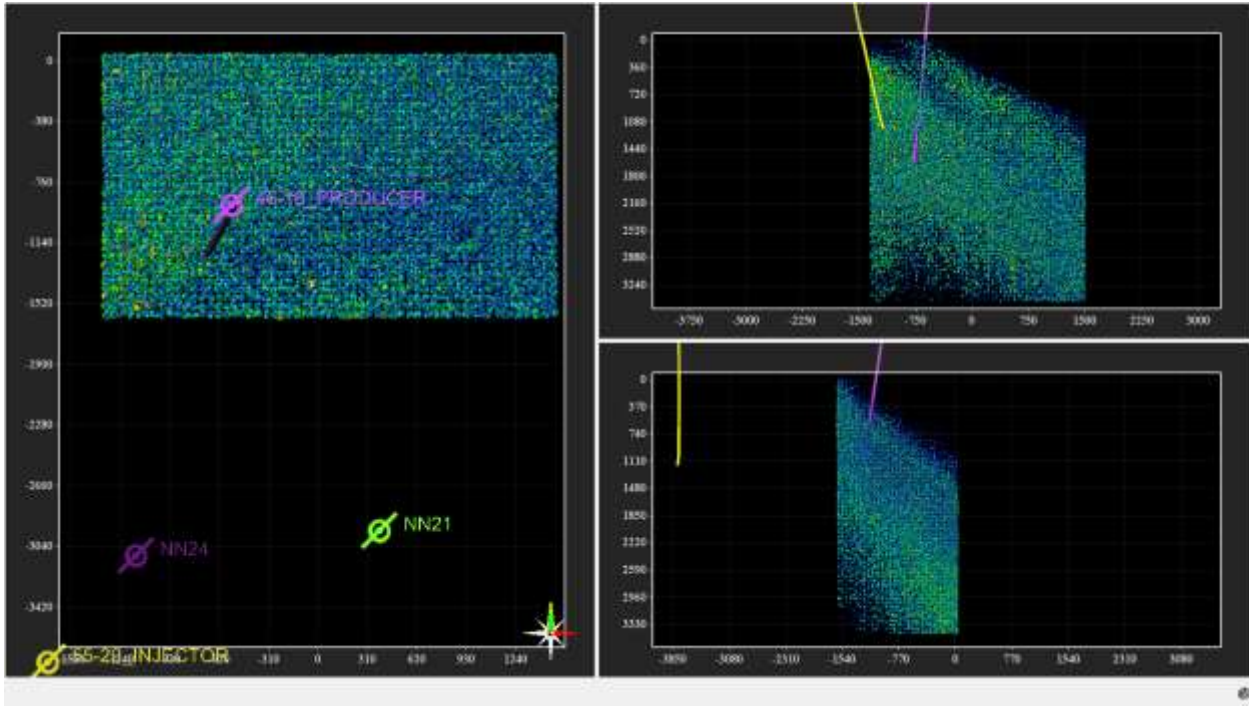


Figure 35 -13:44

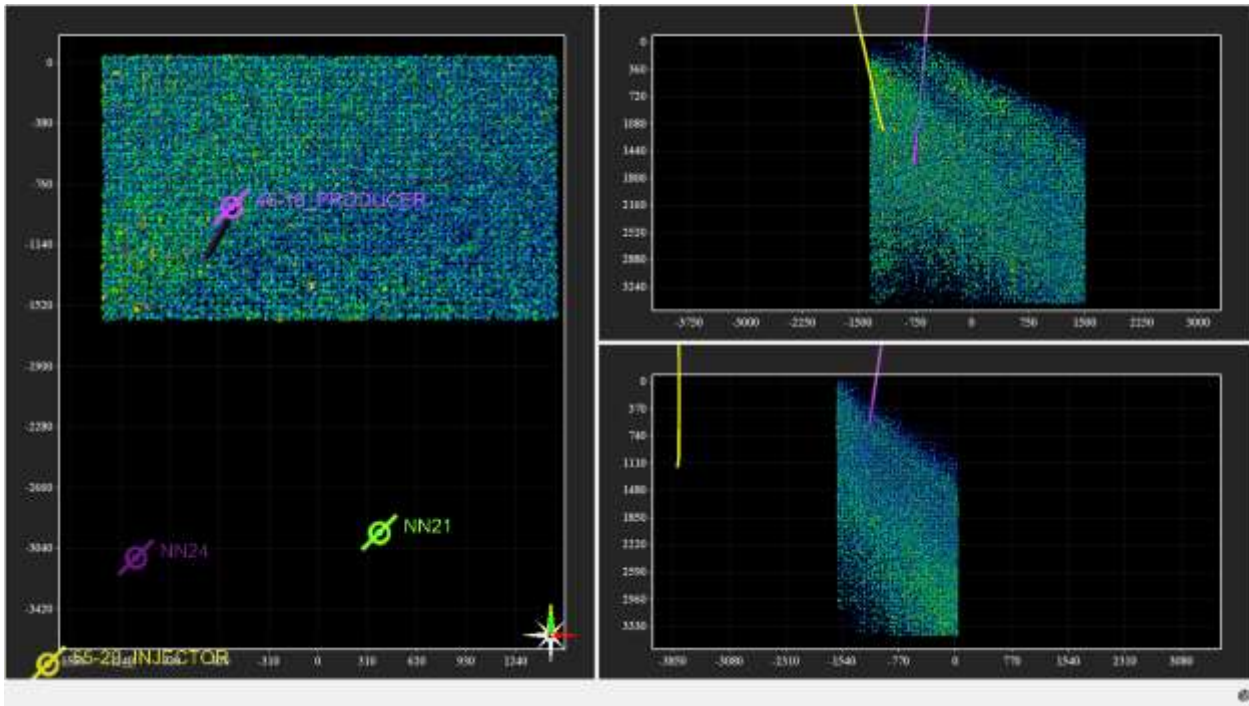


Figure 36 - 14:14

DOCUMENT NO: S3-REP-01-5-ALTAROCK_REDUX	REVISION NO: 05 Appendix G: 163	REVISION DATE: 29/04/2014	Page 24 of 47	PM APPROVAL:
				SCOTT TAYLOR

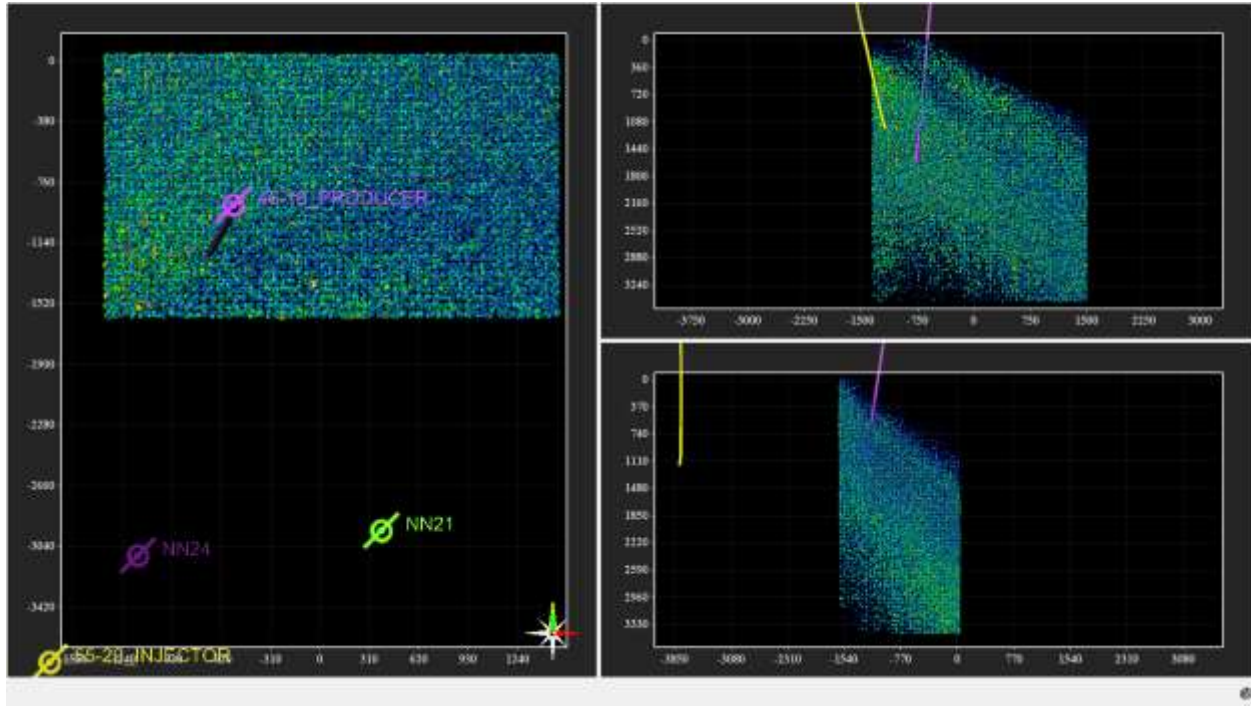


Figure 37 - 14:44

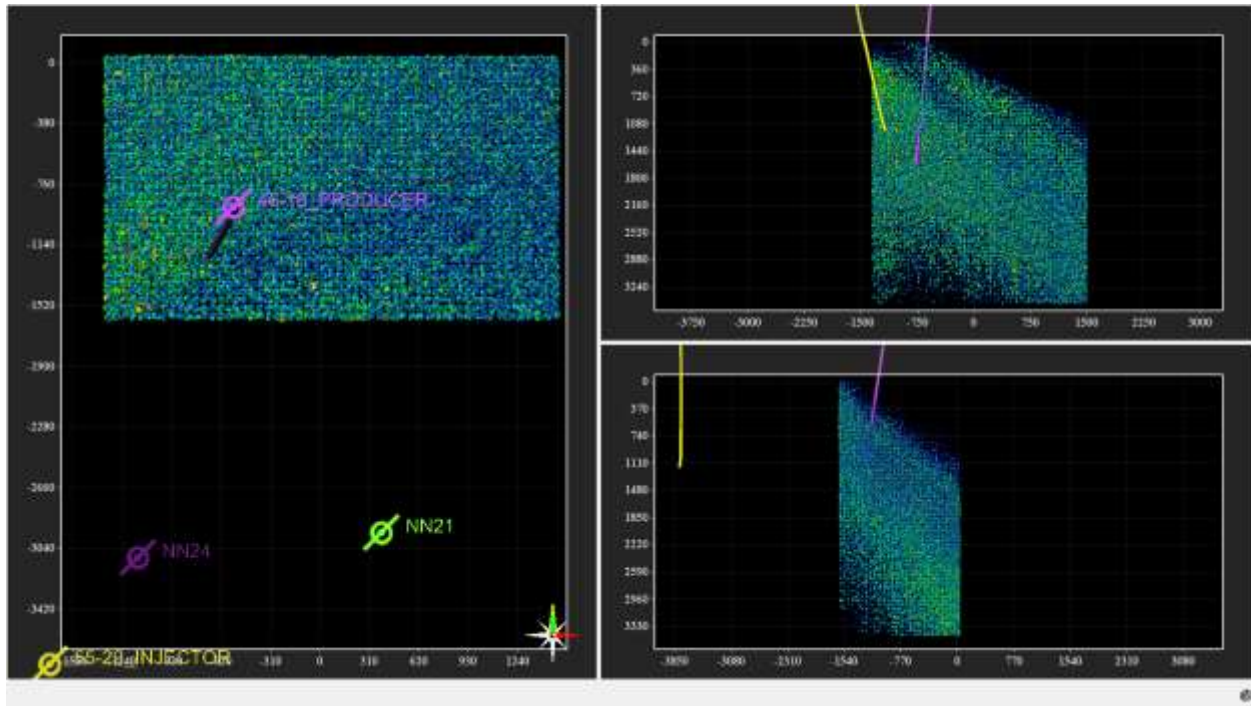


Figure 38 - 15:14

DOCUMENT NO: S3-REP-01-5-ALTAROCK_REDUX	REVISION NO: 05 Appendix G: 164	REVISION DATE: 29/04/2014	Page 25 of 47	PM APPROVAL:
				SCOTT TAYLOR

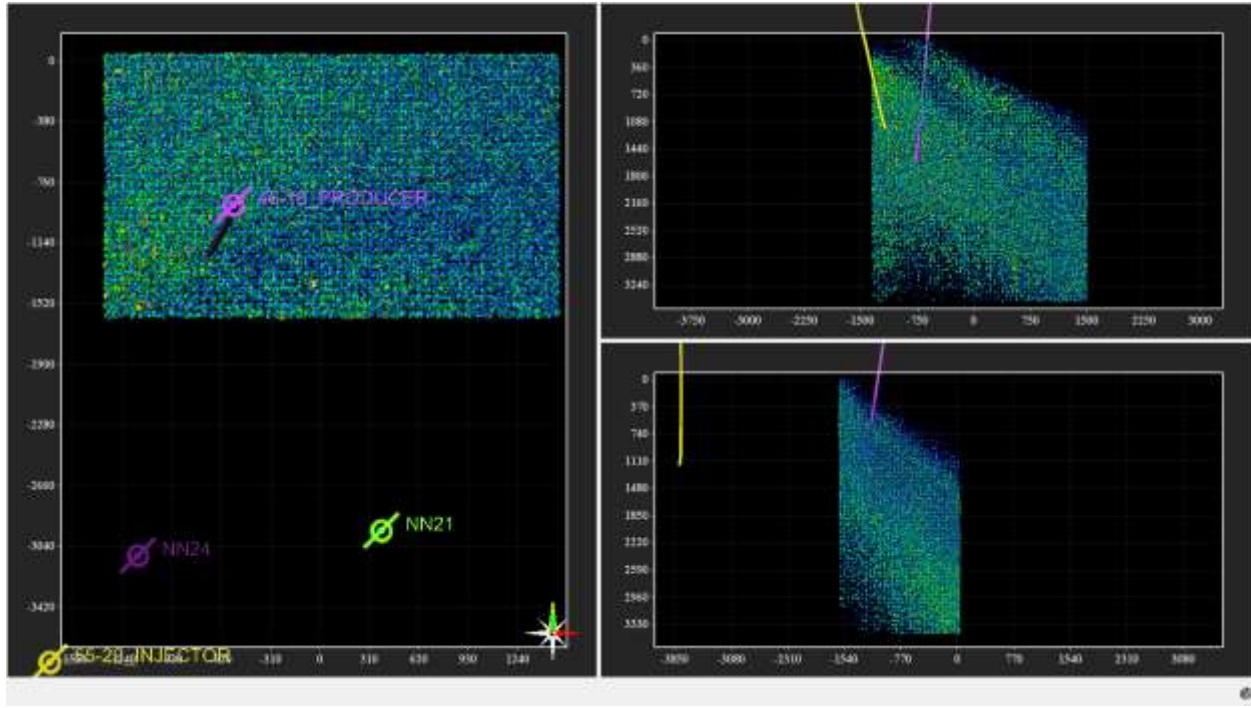


Figure 39 - 15:44

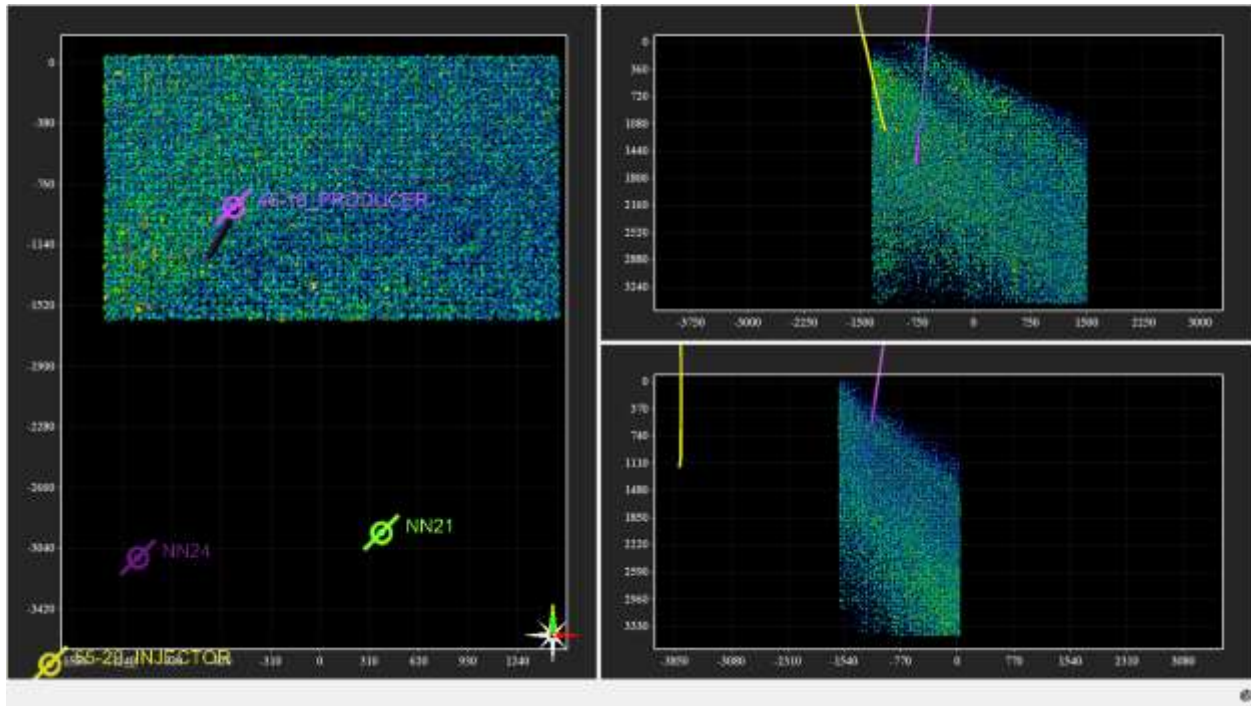


Figure 40 - 16:14

DOCUMENT NO: S3-REP-01-5-ALTAROCK_REDUX	REVISION NO: 05 Appendix G: 165	REVISION DATE: 29/04/2014	Page 26 of 47	PM APPROVAL:
				SCOTT TAYLOR

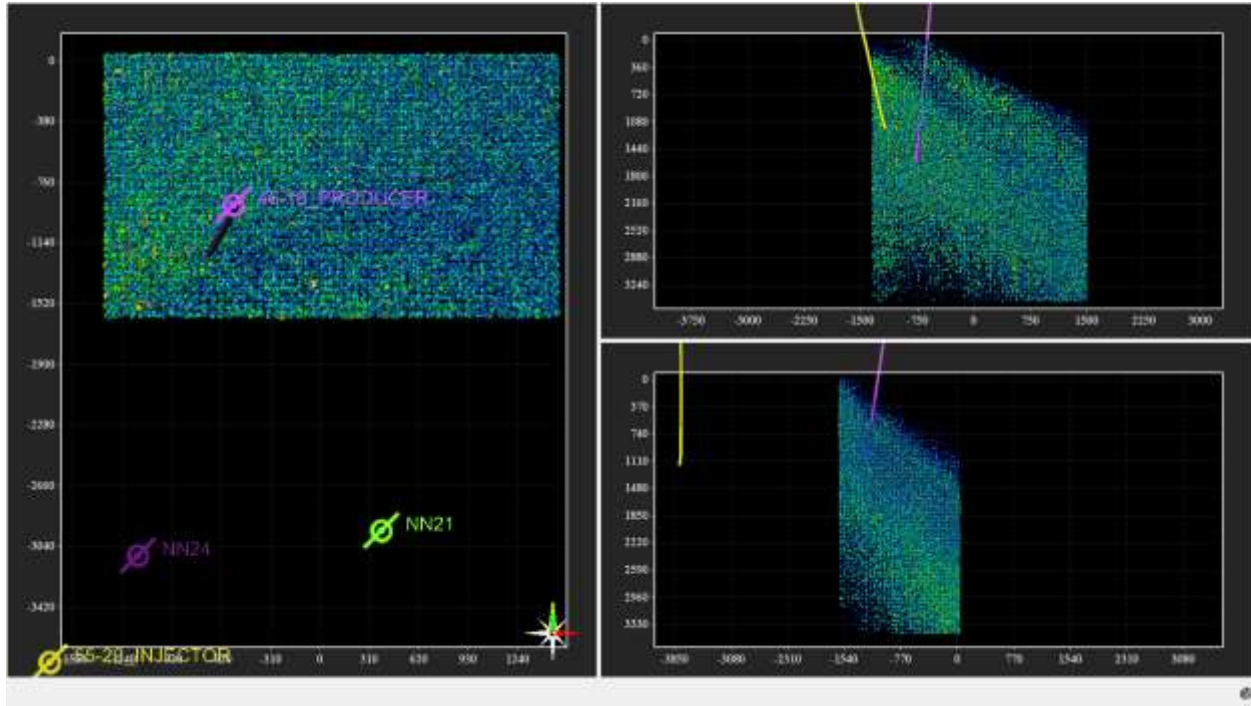


Figure 41 - 16:44

1700

Shut in well.

DOCUMENT NO: S3-REP-01-5-ALTAROCK_REDUX	REVISION NO: 05 Appendix G: 166	REVISION DATE: 29/04/2014	Page 27 of 47	PM APPROVAL: SCOTT TAYLOR
--	---------------------------------------	------------------------------	---------------	------------------------------

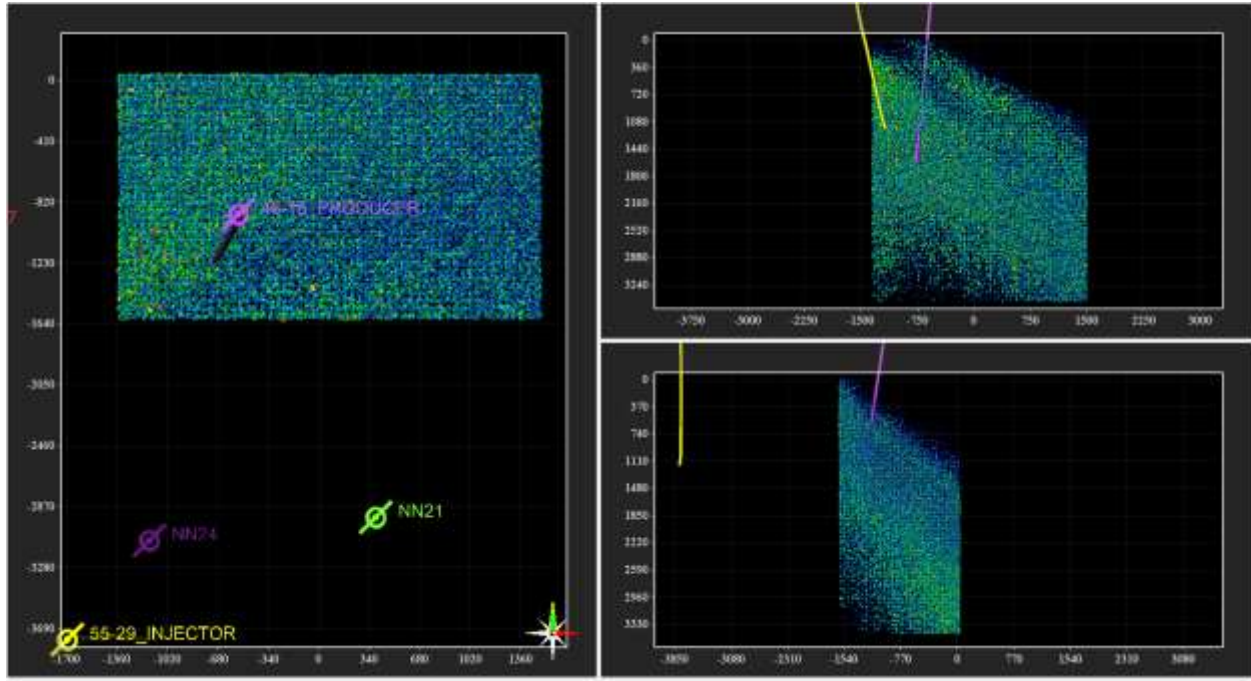


Figure 42 - 17:14

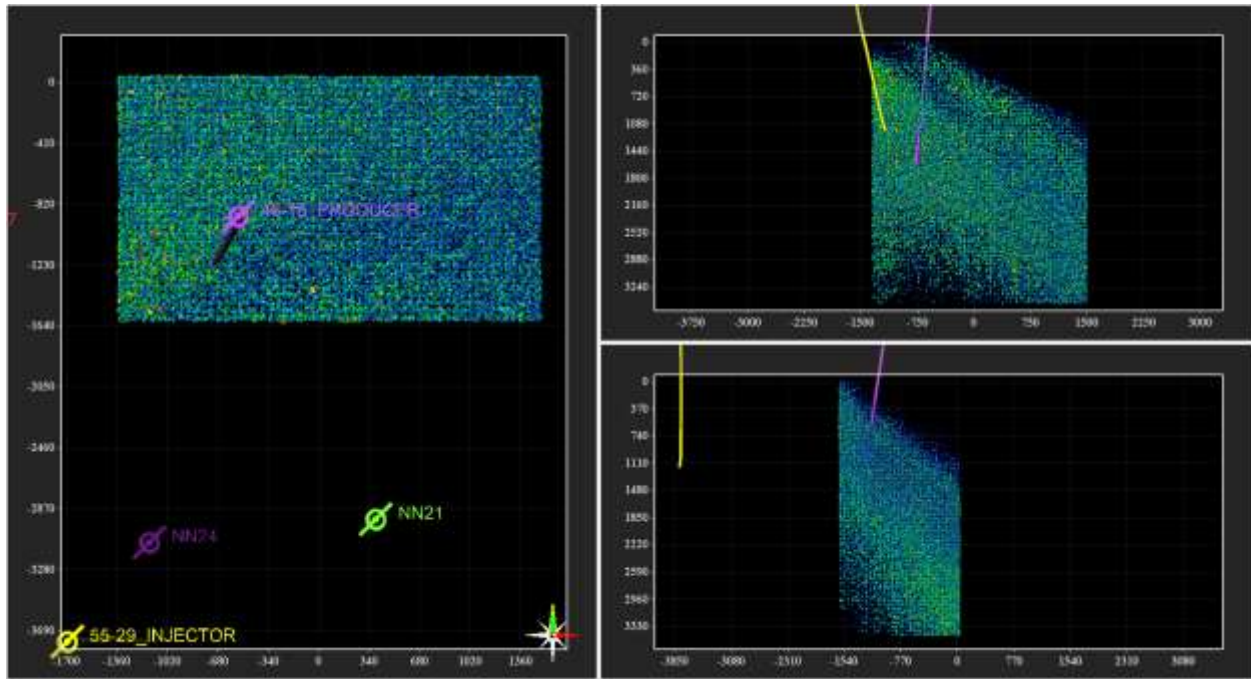


Figure 43 - 17:44

DOCUMENT NO: S3-REP-01-5-ALTAROCK_REDUX	REVISION NO: 05 Appendix G: 167	REVISION DATE: 29/04/2014	Page 28 of 47	PM APPROVAL:
				SCOTT TAYLOR

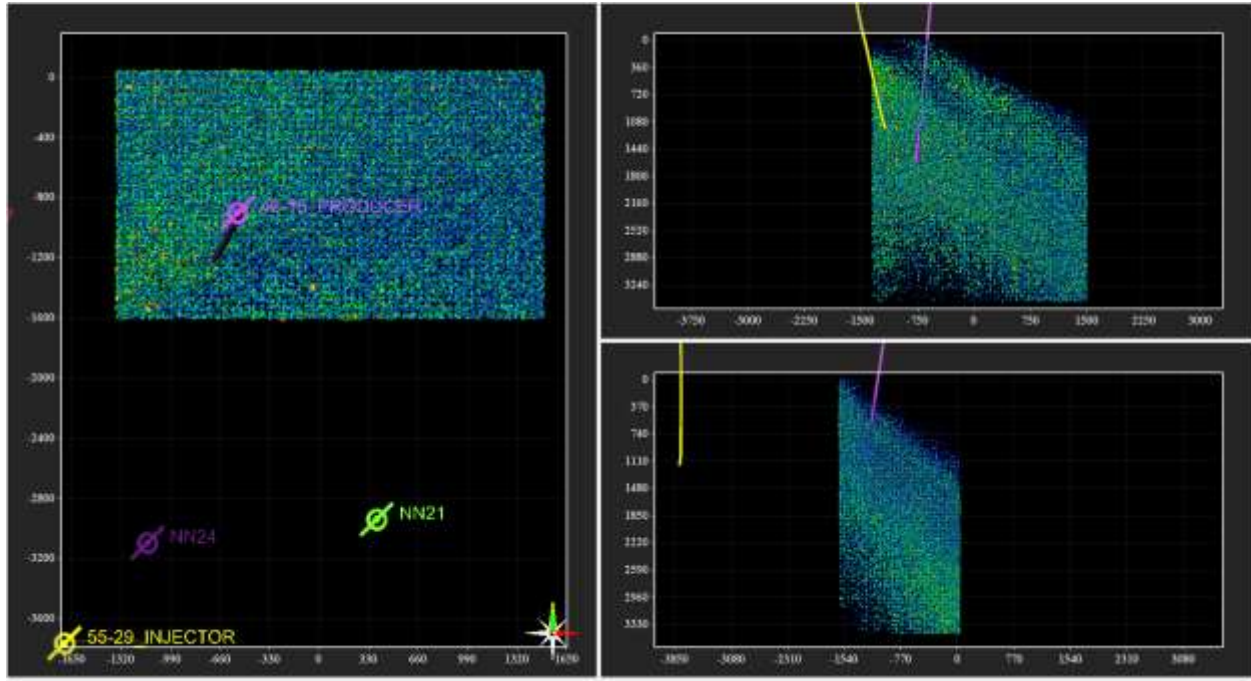


Figure 44 - 18:14

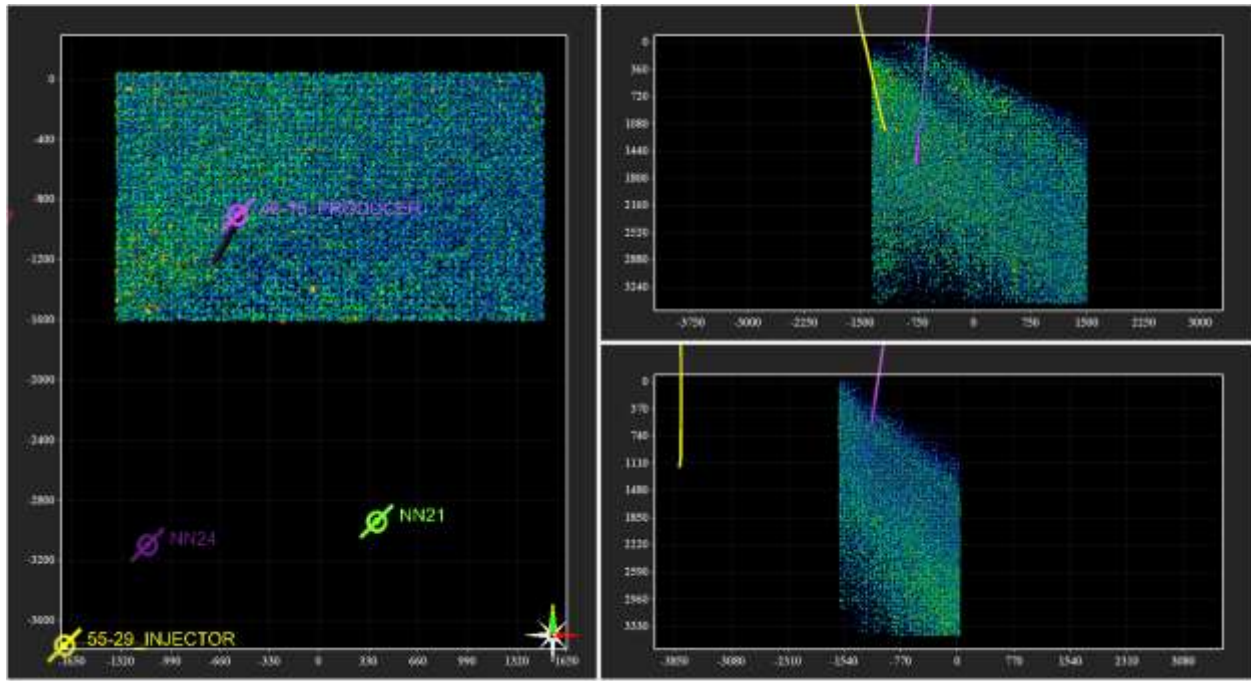


Figure 45 - 18:44

DOCUMENT NO: S3-REP-01-5-ALTAROCK_REDUX	REVISION NO: 05 Appendix G: 168	REVISION DATE: 29/04/2014	Page 29 of 47	PM APPROVAL:
				SCOTT TAYLOR

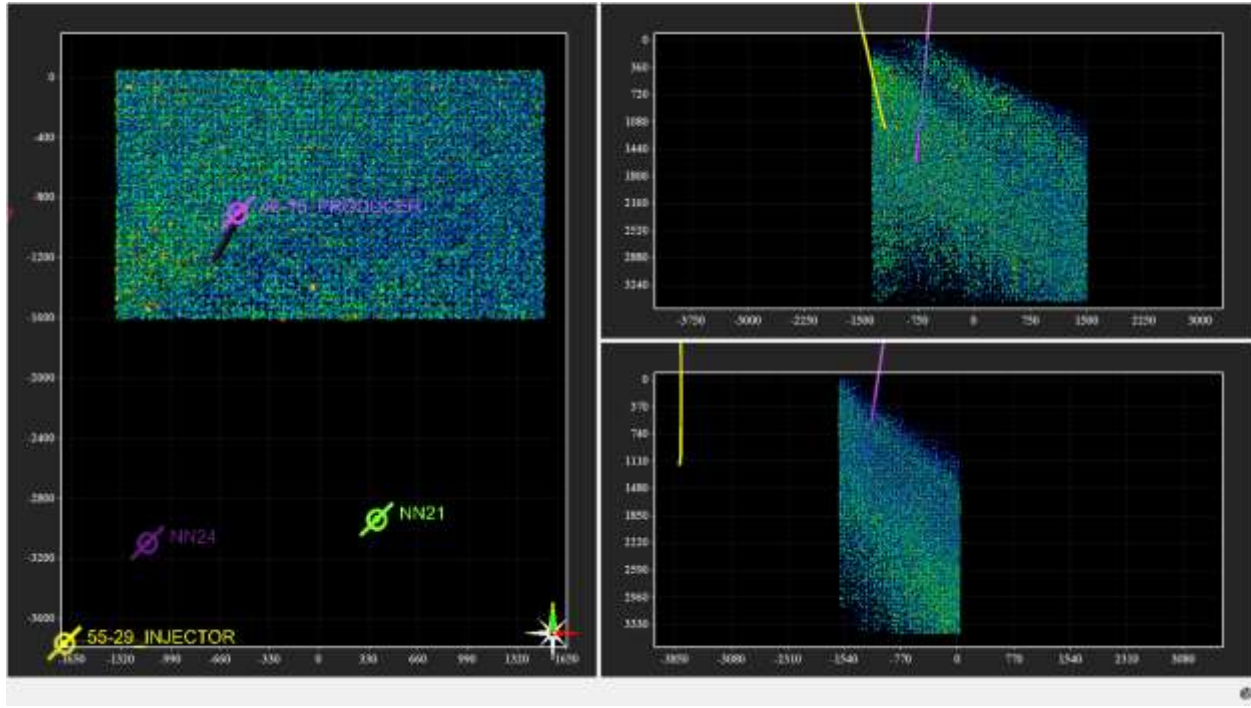


Figure 46 - 19:14

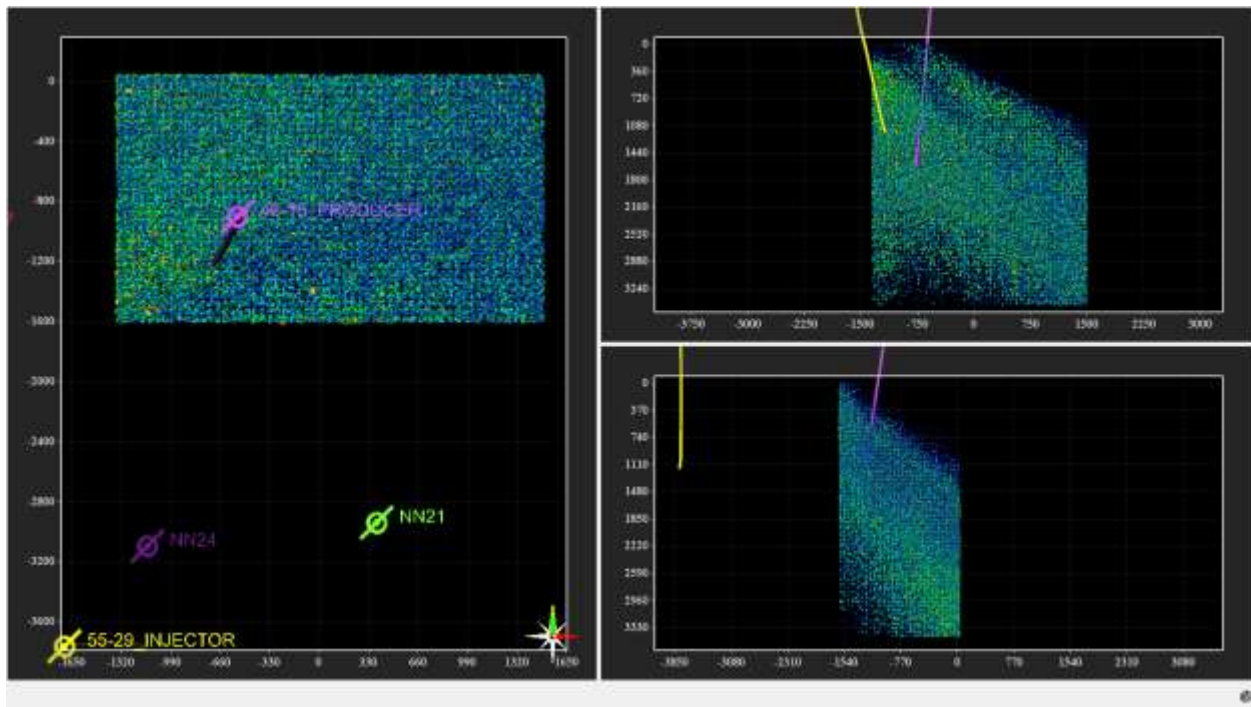


Figure 47 - 19:44

DOCUMENT NO: S3-REP-01-5-ALTAROCK_REDUX	REVISION NO: 05 Appendix G: 169	REVISION DATE: 29/04/2014	Page 30 of 47	PM APPROVAL:
				SCOTT TAYLOR

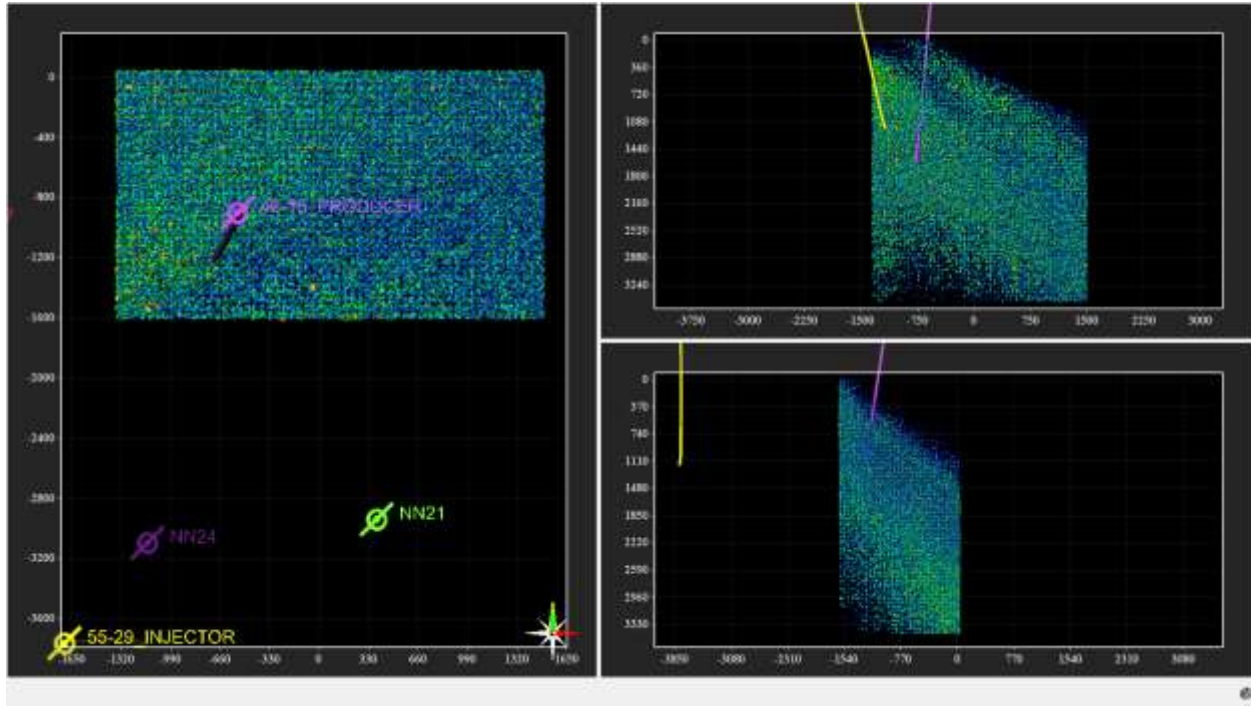


Figure 48 - 20:14

DOCUMENT NO: S3-REP-01-5-ALTAROCK_REDUX	REVISION NO: 05 Appendix G: 170	REVISION DATE: 29/04/2014	Page 31 of 47	PM APPROVAL:
				SCOTT TAYLOR

10 Sept. 2013

0850 Start injecting at 55-29.
0936 Pressure gage reading 425 psi.
Open well to flow.
0945 55-29 at full pressure and flow (400 psi, 160 gpm).
1005 Pressure gage reading 150 PSI.
1017 Transition from 100% gas to mixed gas and dilute drilling fluid.

DOCUMENT NO: S3-REP-01-5-ALTAROCK_REDUX	REVISION NO: 05 Appendix G: 171	REVISION DATE: 29/04/2014	Page 32 of 47	PM APPROVAL: SCOTT TAYLOR
---	--	-------------------------------------	---------------	-------------------------------------

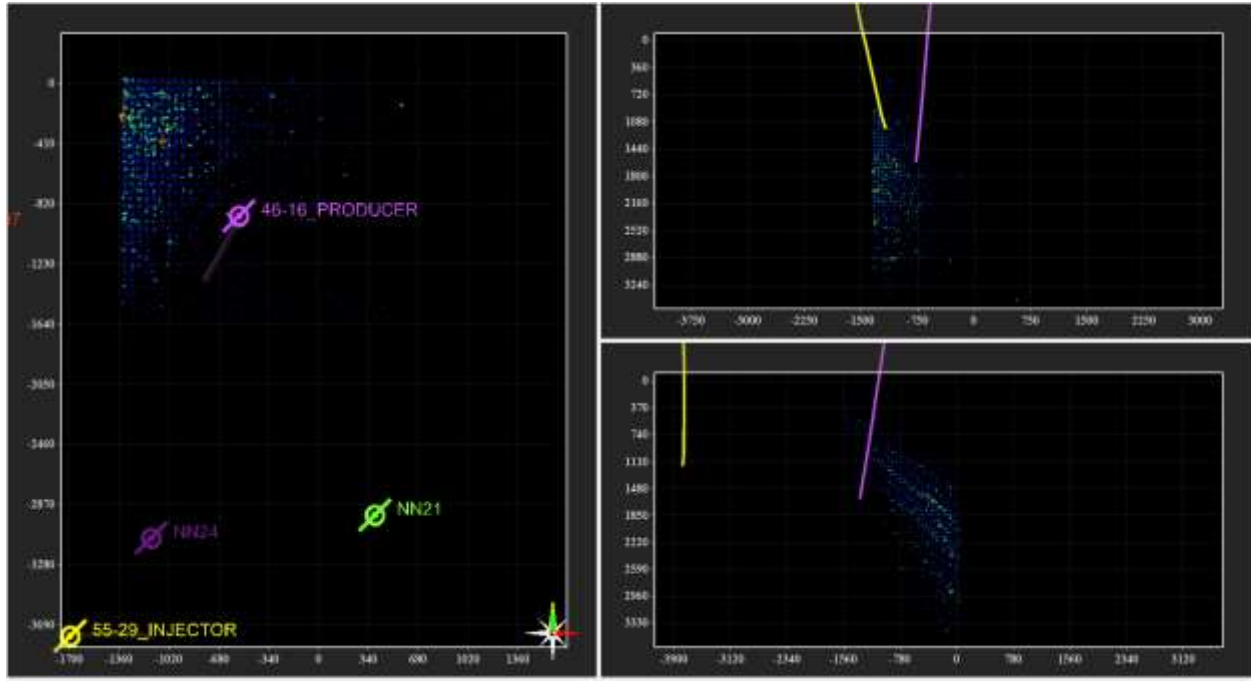


Figure 49 - Orthographic view north of LASEA volume at 10:30:00

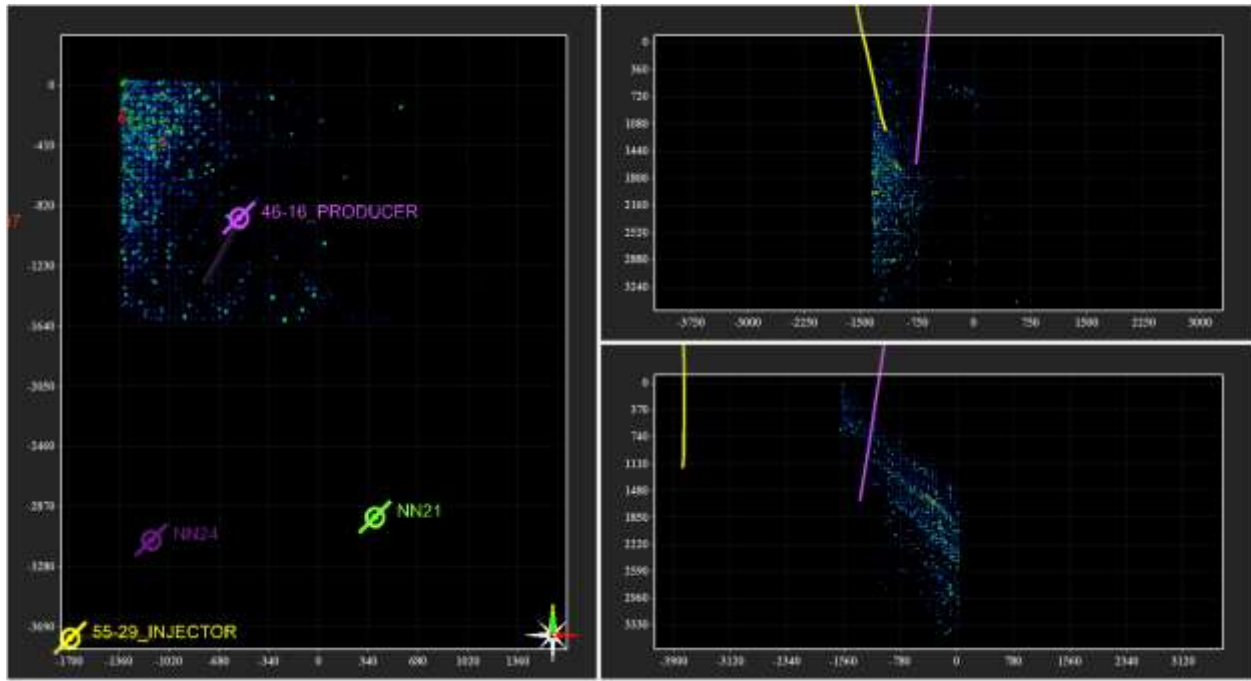


Figure 50 - Orthographic view north of LASEA volume at 11:00:00

1125 Strong liquid flow, increasingly more muddy.

DOCUMENT NO: S3-REP-01-5-ALTAROCK_REDUX	REVISION NO: 05 Appendix G: 172	REVISION DATE: 29/04/2014	Page 33 of 47	PM APPROVAL: SCOTT TAYLOR
--	---------------------------------------	------------------------------	---------------	------------------------------

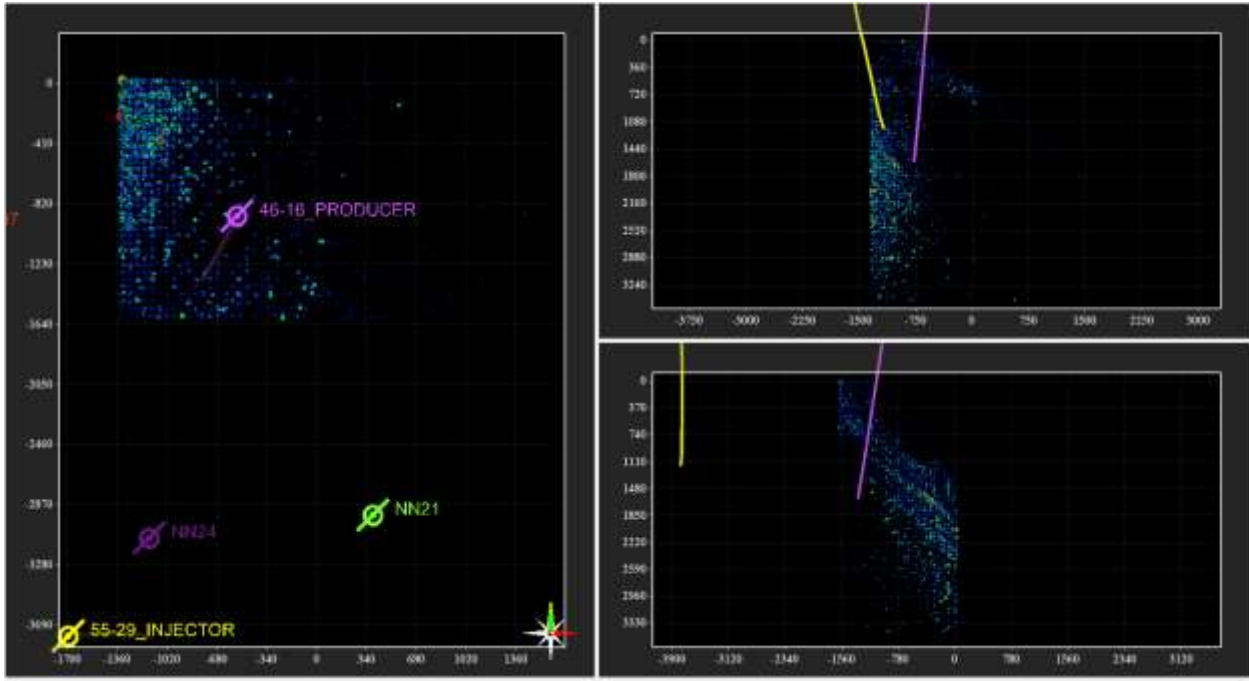


Figure 51 - Orthographic view north of LASEA volume at 11:30:00

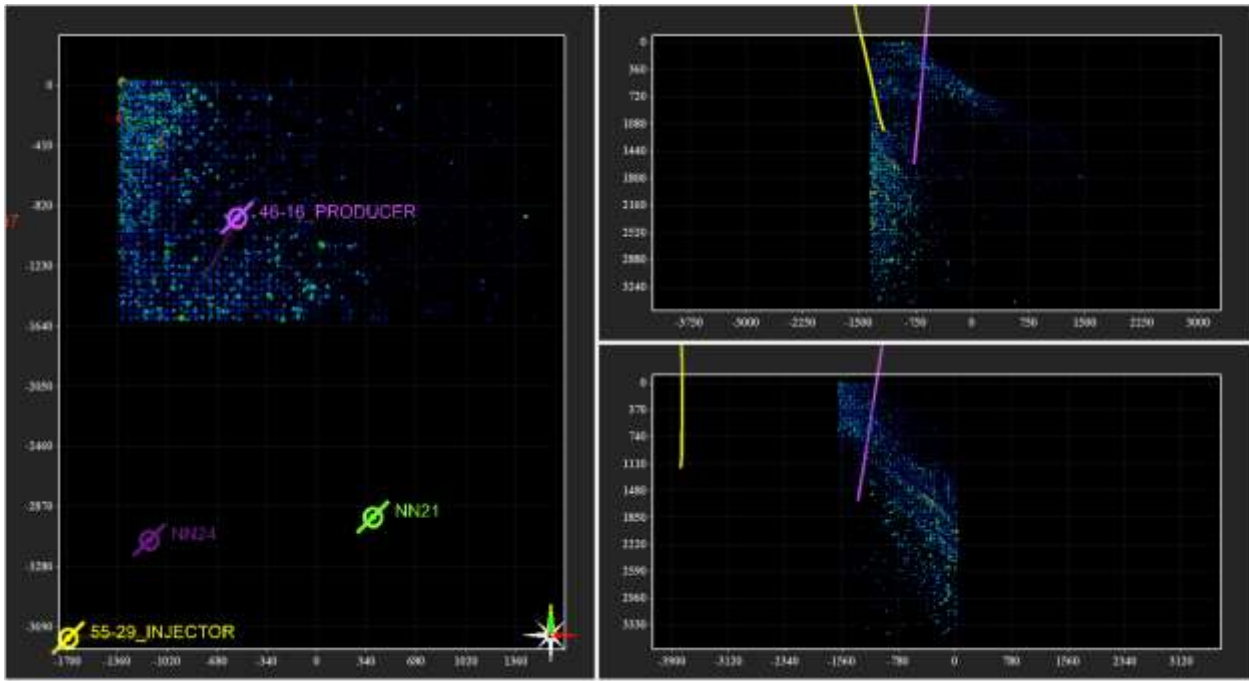


Figure 52 - Orthographic view north of LASEA volume at 12:00:00

1226

Transition from liquid to gas.

DOCUMENT NO: S3-REP-01-5-ALTAROCK_REDUX	REVISION NO: 05 Appendix G: 173	REVISION DATE: 29/04/2014	Page 34 of 47	PM APPROVAL: SCOTT TAYLOR
--	---------------------------------------	------------------------------	---------------	------------------------------

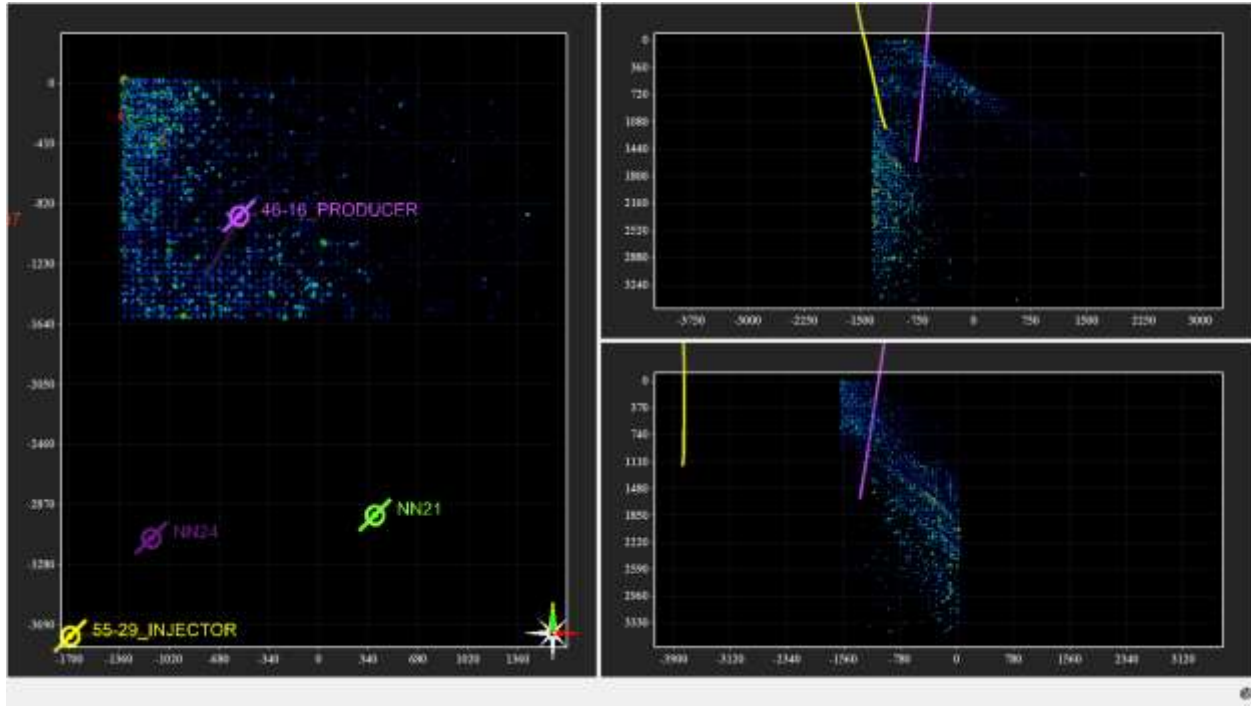


Figure 53 - 12:30

1246-1413

Gas flow with intermittent flows of thick mud.

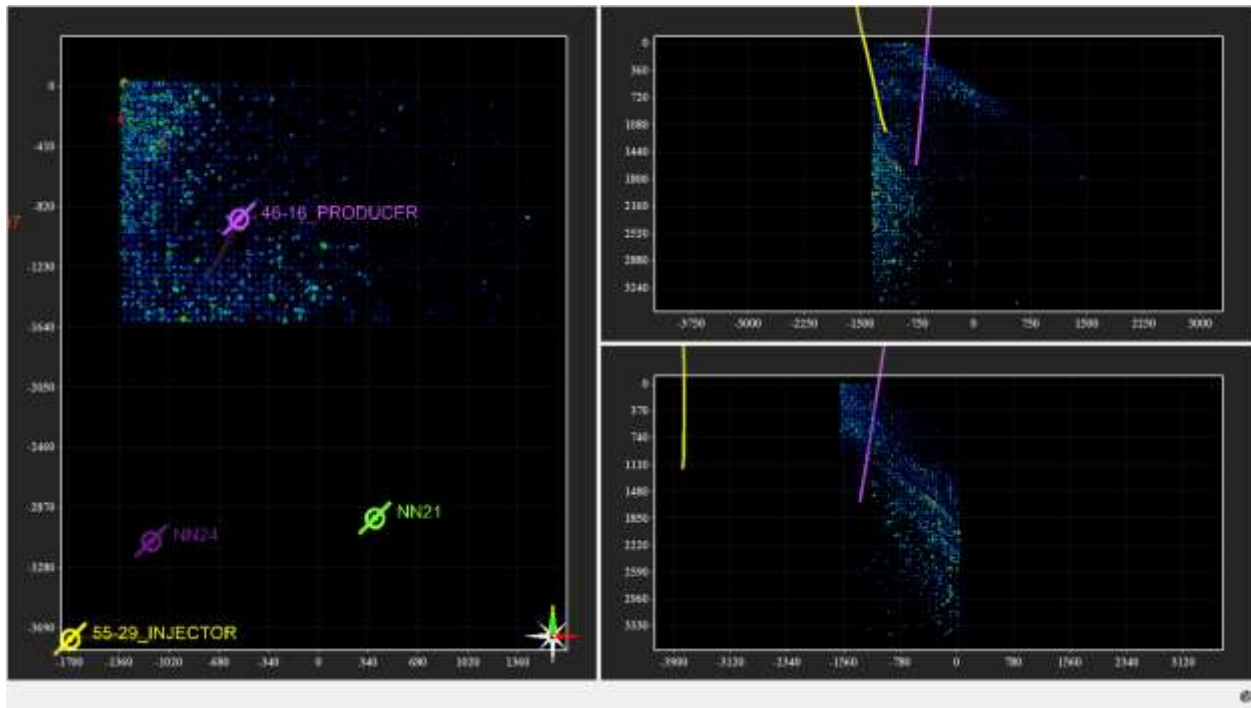


Figure 54 - 13:00

DOCUMENT NO: S3-REP-01-5-ALTAROCK_REDUX	REVISION NO: 05 Appendix G: 174	REVISION DATE: 29/04/2014	Page 35 of 47	PM APPROVAL: SCOTT TAYLOR
--	---------------------------------------	------------------------------	---------------	------------------------------

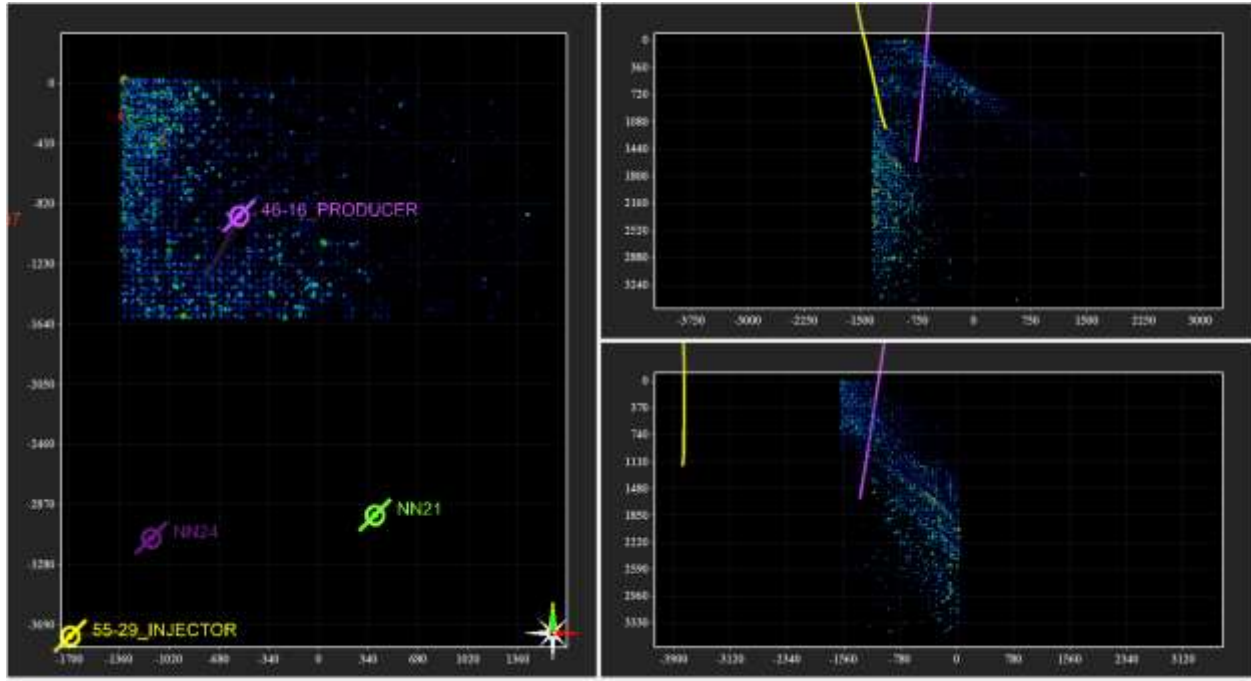


Figure 55 - 13:30

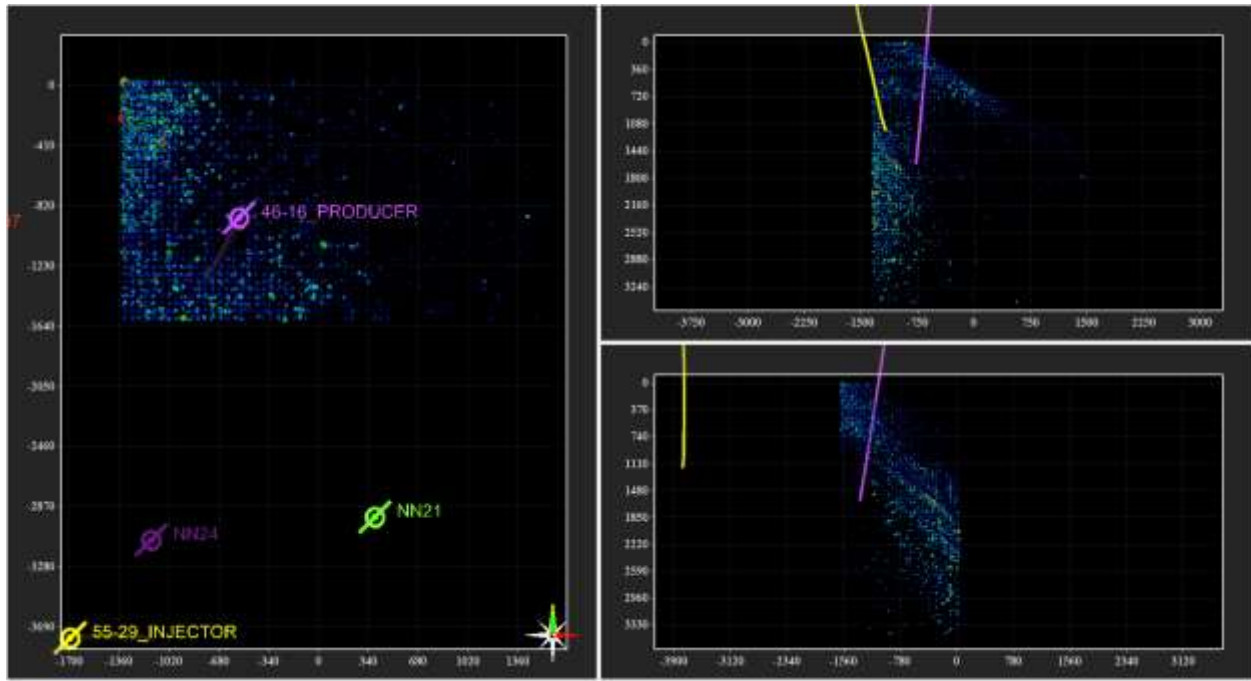


Figure 56 - 14:00

1413

Shut well in to attach gas sample bottle.

DOCUMENT NO: S3-REP-01-5-ALTAROCK_REDUX	REVISION NO: 05 Appendix G: 175	REVISION DATE: 29/04/2014	Page 36 of 47	PM APPROVAL: SCOTT TAYLOR
--	---------------------------------------	------------------------------	---------------	------------------------------

- 1416 Opened well to flush and fill gas sample bottle.
- 1420 Shut in well just as muddy water started to mix with gas flow.
- 1421 Opened well, flowing muddy water.
- 1428 Transition to gas flow.

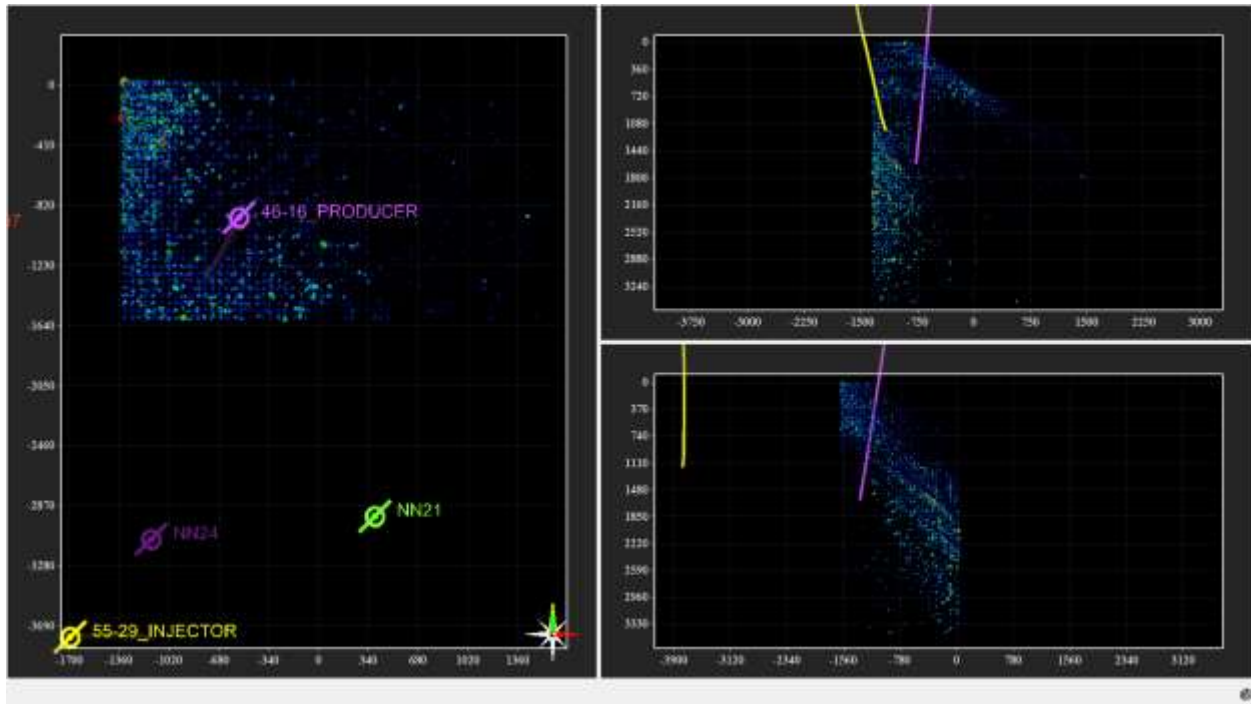


Figure 57 - 14:30

- 1441 Flow rate of gas dropping off to such a slow rate that ear plugs are not needed.

DOCUMENT NO: S3-REP-01-5-ALTAROCK_REDUX	REVISION NO: 05 Appendix G: 176	REVISION DATE: 29/04/2014	Page 37 of 47	PM APPROVAL: SCOTT TAYLOR
--	---------------------------------------	------------------------------	---------------	------------------------------

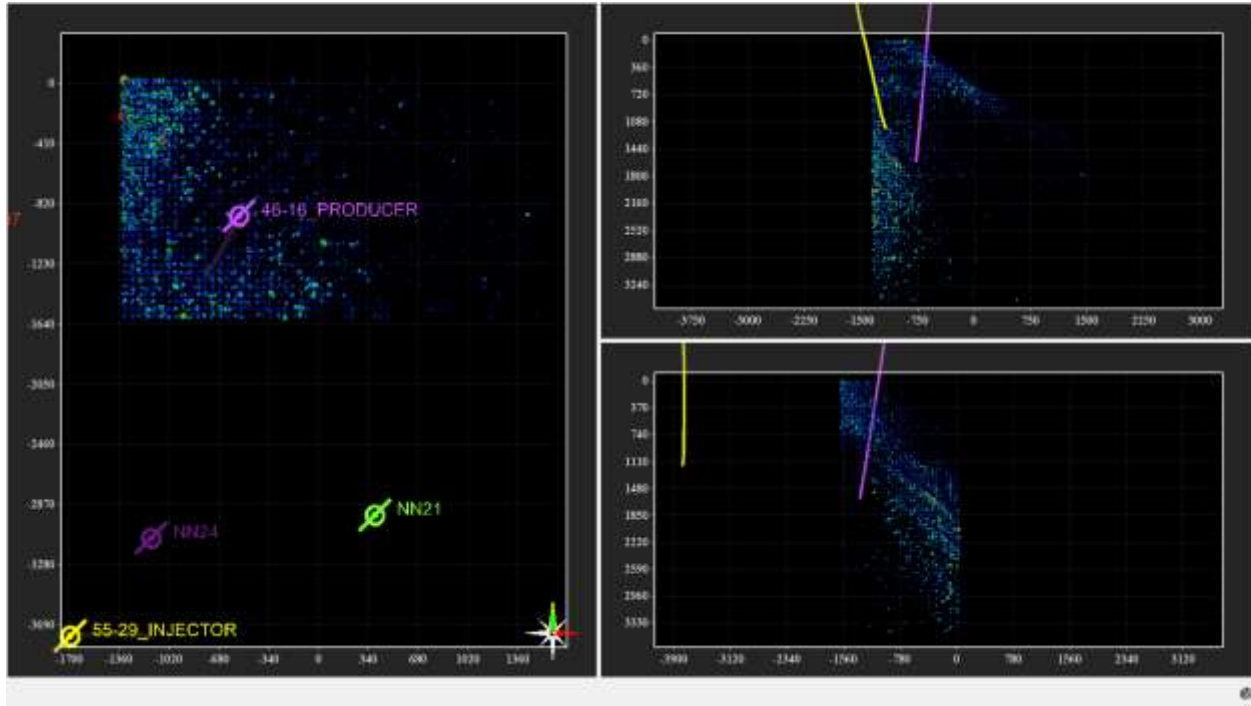


Figure 58 - 15:00

1451-1515 Very low gas flow rate with occasional burps of very thick mud.
 1515 Shut well in.

DOCUMENT NO: S3-REP-01-5-ALTAROCK_REDUX	REVISION NO: 05 Appendix G: 177	REVISION DATE: 29/04/2014	Page 38 of 47	PM APPROVAL:
				SCOTT TAYLOR

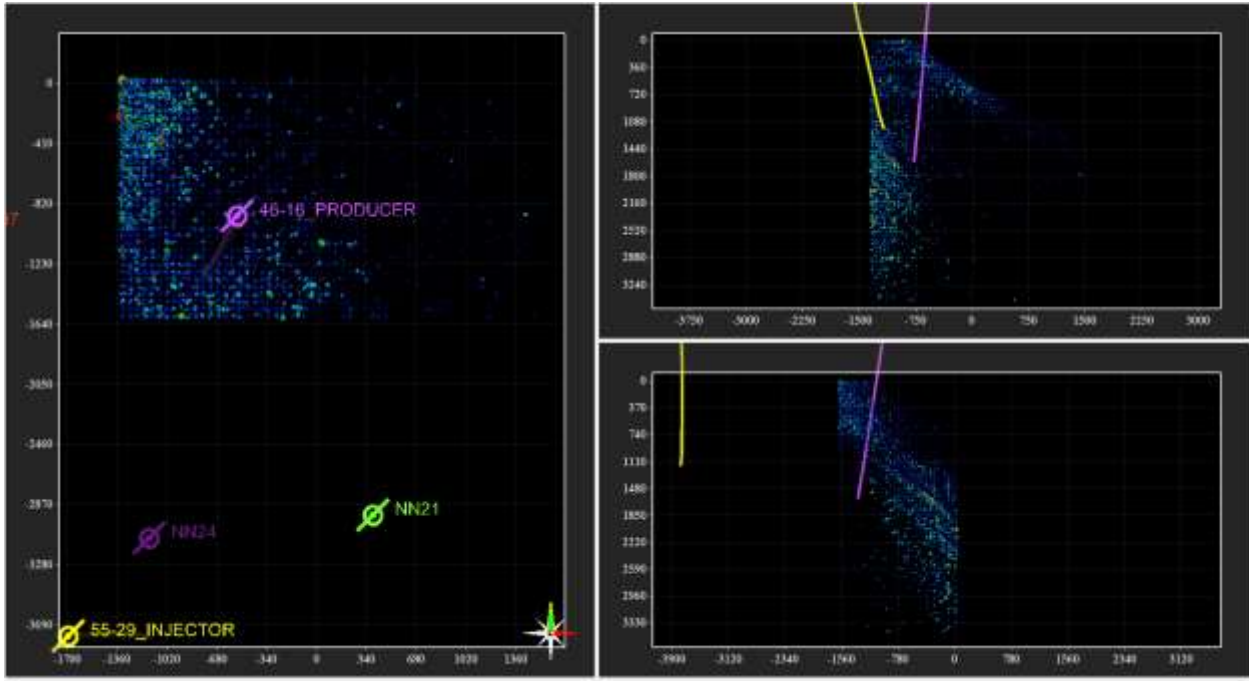


Figure 59 - 15:30

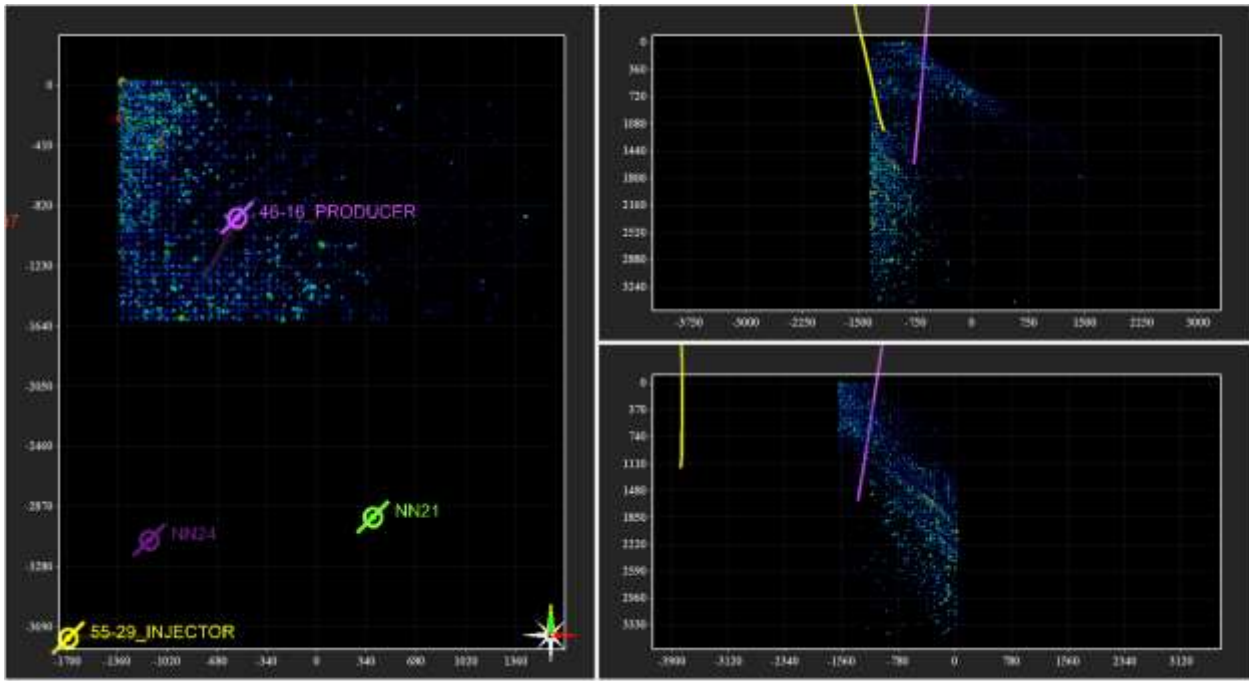


Figure 60 - 16:00

DOCUMENT NO: S3-REP-01-5-ALTAROCK_REDUX	REVISION NO: 05 Appendix G: 178	REVISION DATE: 29/04/2014	Page 39 of 47	PM APPROVAL: SCOTT TAYLOR
--	---------------------------------------	------------------------------	---------------	------------------------------

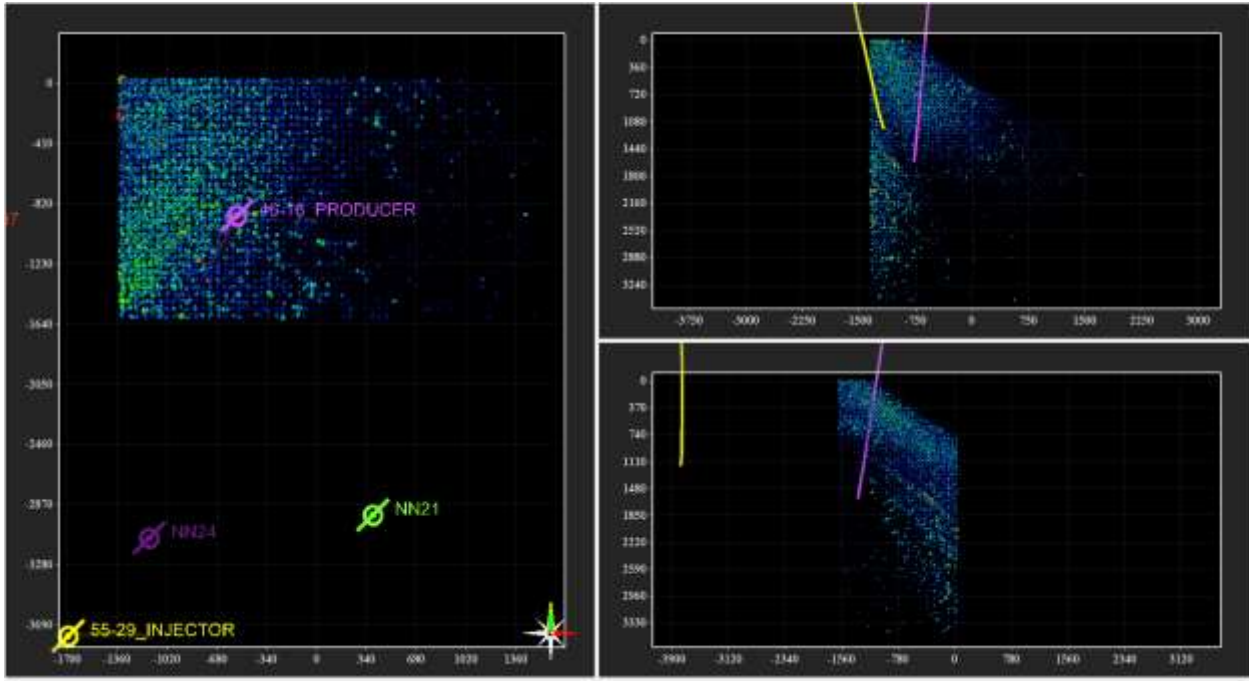


Figure 61 - 16:30

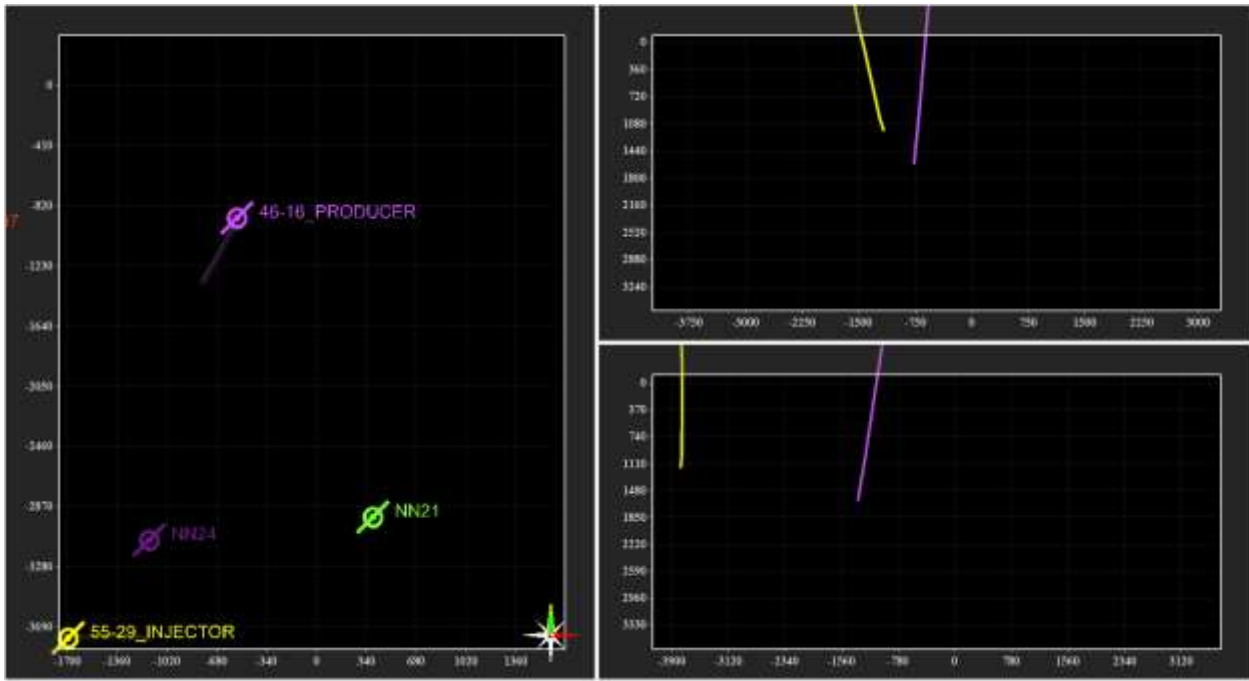


Figure 62 - 16:30

DOCUMENT NO: S3-REP-01-5-ALTAROCK_REDUX	REVISION NO: 05 Appendix G: 179	REVISION DATE: 29/04/2014	Page 40 of 47	PM APPROVAL: SCOTT TAYLOR
--	---------------------------------------	------------------------------	---------------	------------------------------

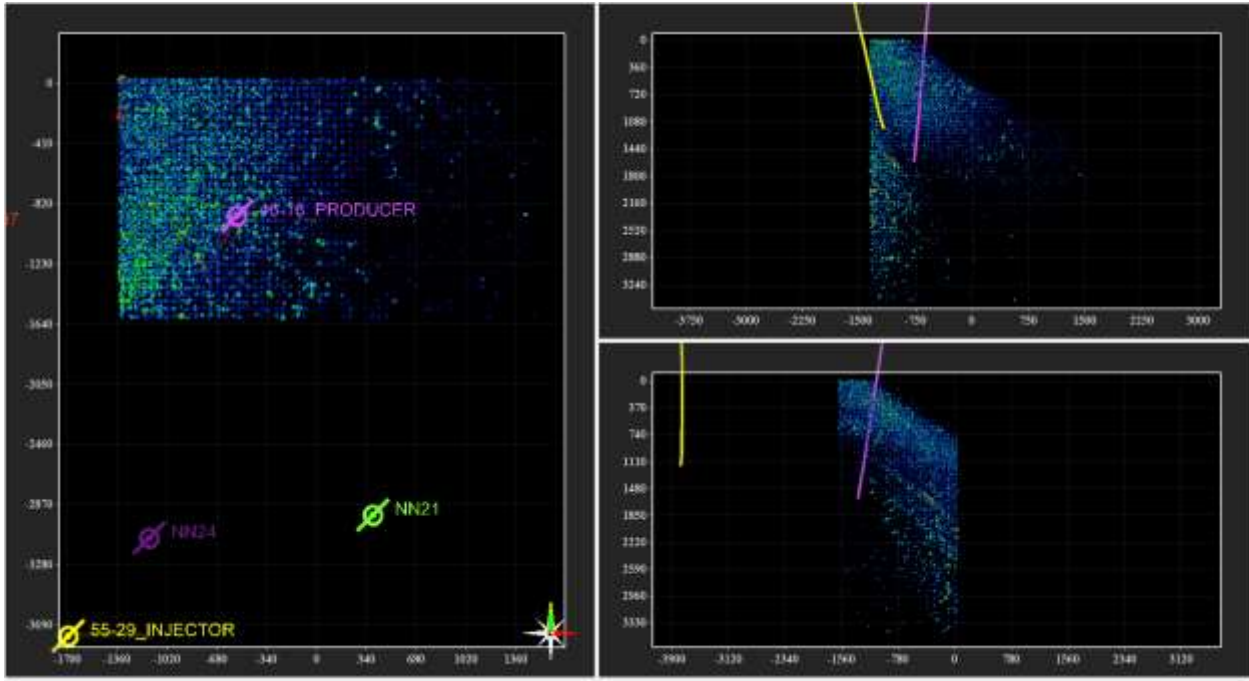


Figure 63 - 17:00

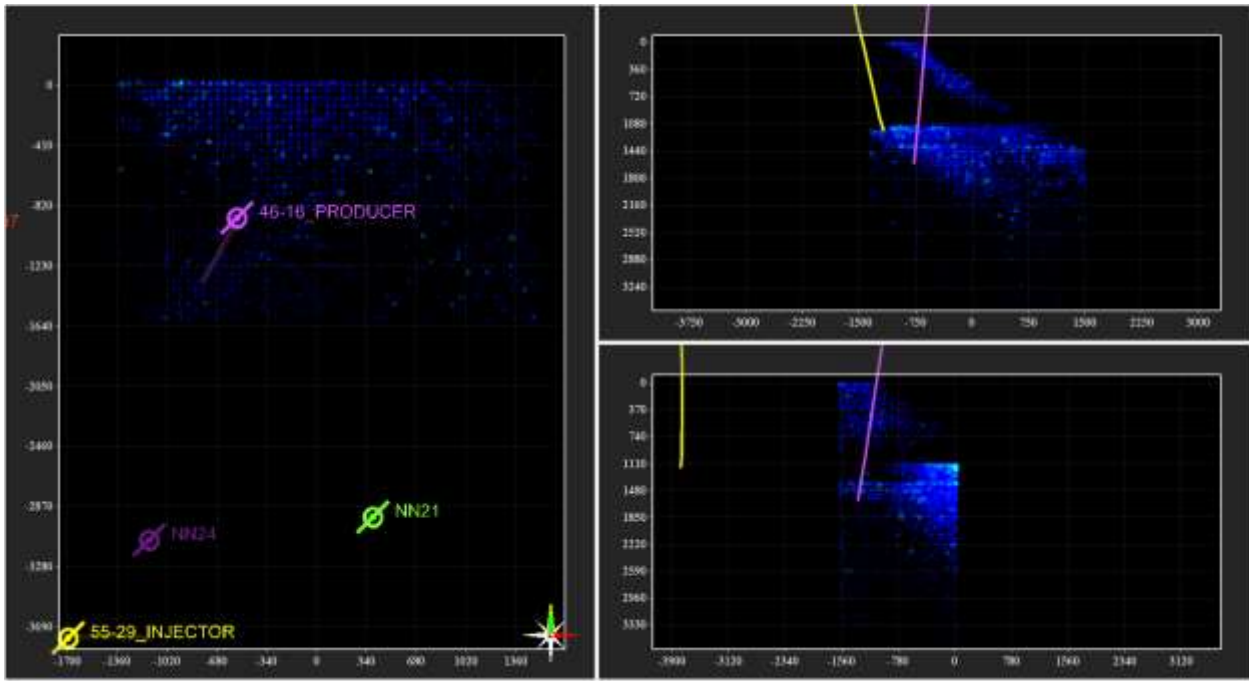


Figure 64 - 17:00

DOCUMENT NO: S3-REP-01-5-ALTAROCK_REDUX	REVISION NO: 05 Appendix G: 180	REVISION DATE: 29/04/2014	Page 41 of 47	PM APPROVAL:
				SCOTT TAYLOR

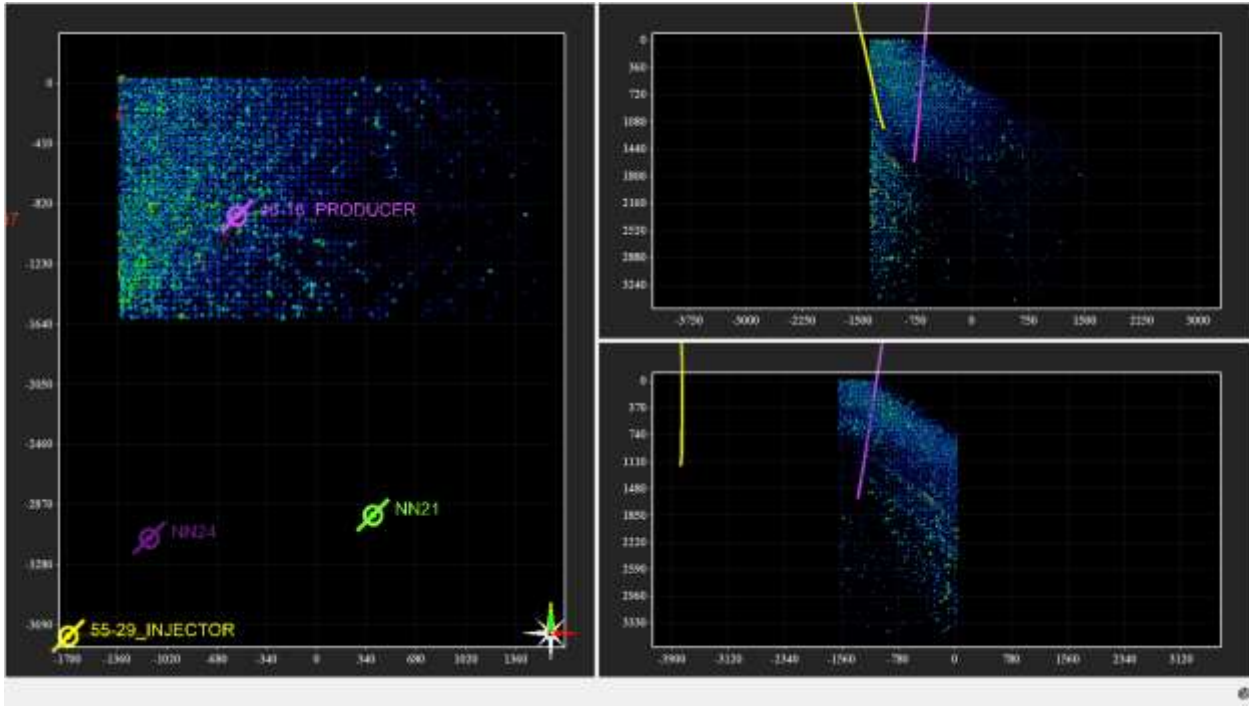


Figure 65 - 17:30

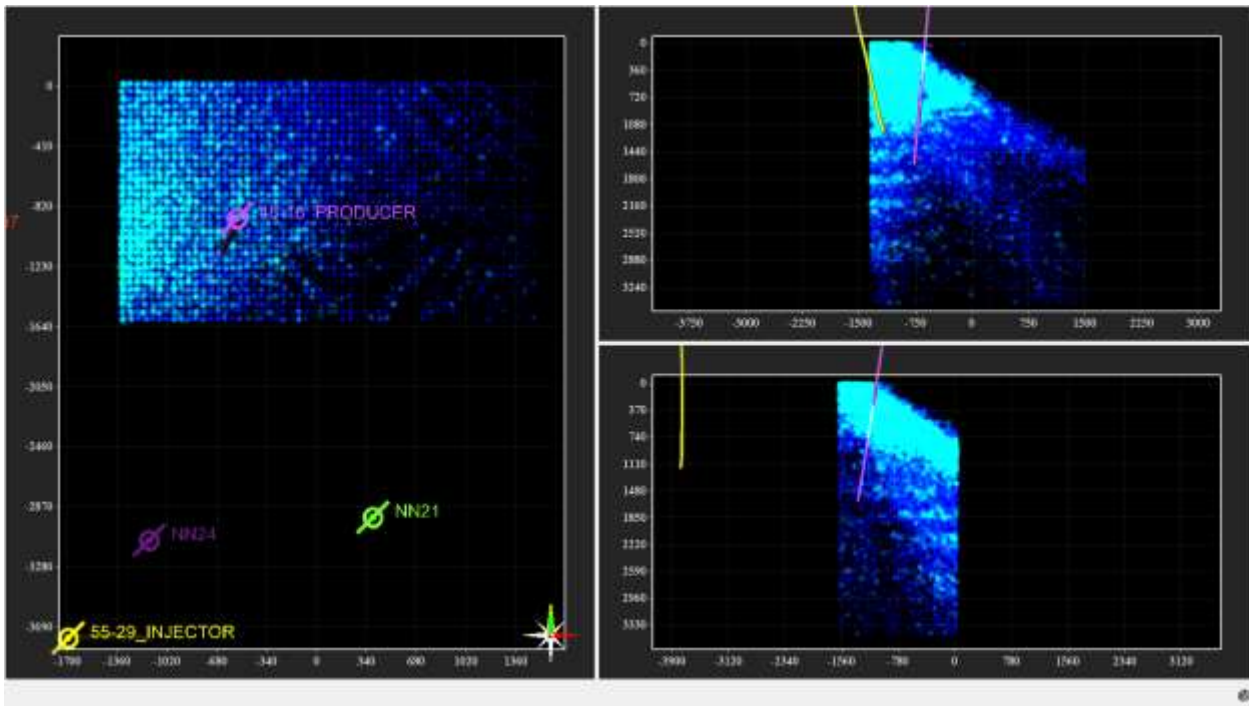


Figure 66 - 17:30

DOCUMENT NO: S3-REP-01-5-ALTAROCK_REDUX	REVISION NO: 05 Appendix G: 181	REVISION DATE: 29/04/2014	Page 42 of 47	PM APPROVAL: SCOTT TAYLOR
--	---------------------------------------	------------------------------	---------------	------------------------------

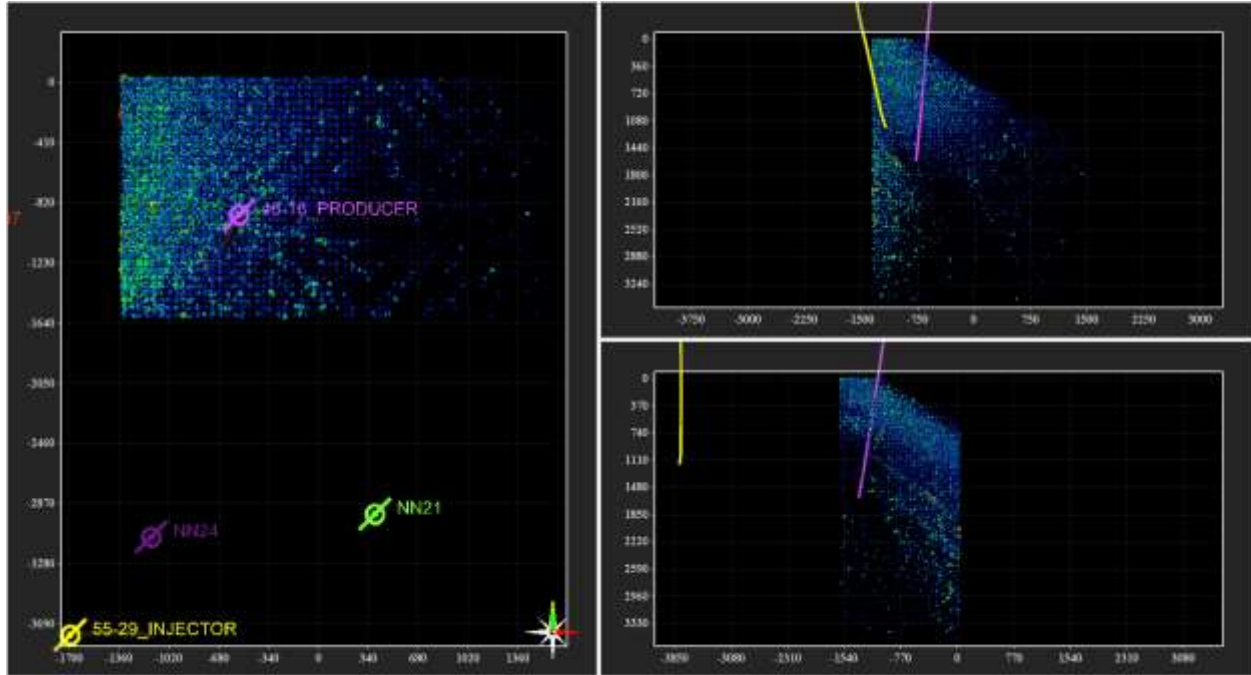


Figure 67 - 18:00

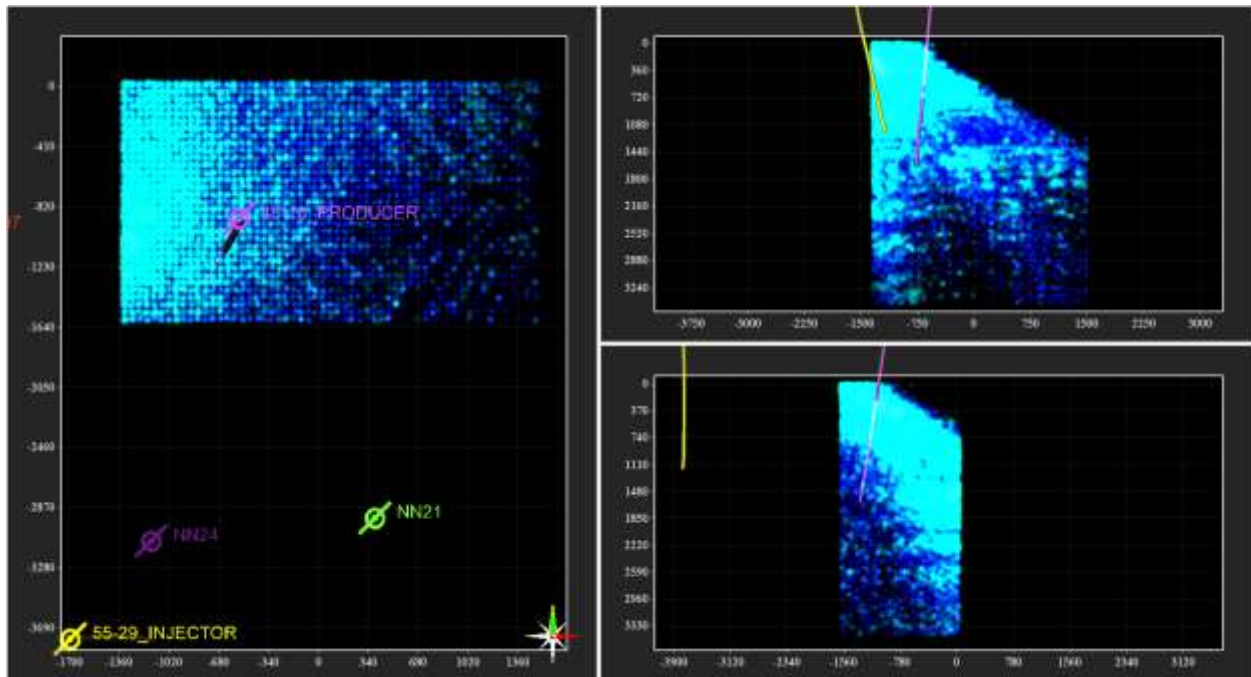


Figure 68 - 18:00

11 Sept. 2013

DOCUMENT NO: S3-REP-01-5-ALTAROCK_REDUX	REVISION NO: 05 Appendix G: 182	REVISION DATE: 29/04/2014	Page 43 of 47	PM APPROVAL: SCOTT TAYLOR
--	---------------------------------------	------------------------------	---------------	------------------------------

0700 Injection pumps at 55-29 shut down.

AW very rough calculations:

Estimate flow for Sunday and Monday, 3,000 gal. each day

Estimate flow for Tuesday, 4,000 gal.

13 3/8 " casing, 0.8818 cu. ft. per linear ft., a bit over 6.6 gal/linear ft.

Ergo – total displacement of well-bore could be about 1500 ft, or about 1/2 of the liquid volume between the top of the static water (2070' BGL) and the bridge (5,000 ft. BGL); total flow volume far less than the liquid volume above the bridge. Regardless of the accuracy of these estimates, it is clear that not enough fluid has been discharged to equal the volume of fluid above the bridge.

Any fluid flowed from the well from below the bridge would have to pass through the bridge and pass up through a substantial column of thermally equilibrated water/drilling mud (300°F at the bridge depth of 5000 ft., please see temperature chart below). The limited flow volumes for these three days would hardly be enough to heat up the well bore or produce hot discharge.

The liquid during each flow period ranged from dirty water to thick mud. At this time one could only speculate as to the dilute mud fraction. Is it a result of mud flocculation in between flow episodes or is there a component of hydrothermal water seeping through the bridge?

2.1 LASEA ANALYSIS

I have worked all weekend on the report. In Q1 Sigma Cubed focused efforts on imaging low amplitude seismic emissions from the 46-16 Pad. We created 2-hour LASEA time frames for all 7-days of the project. Additionally, we ran ultra high resolution 15-minute and 30-minute time frames for the three separate times that AltaRock opened up and flowed the 46-16 well. The six (6) volumes shall be referenced as

1. Open46-16_Sept08_30_min
2. Open46-16_Sept08_15_min
3. Open46-16_Sept9_30_min
4. Open46-16_Sept09_15_min
5. Open46-16_Sept10_15_min
6. Open46-16_Sept10_30_min

In addition we executed another set of jobs that will do the whole volume with a 250 m grid interval which took 6 weeks of substantial CPU load on our cluster but will give DOE / AltaRock everything for this project that can possibly be provided. We are finalizing the images and interpretation for the high-resolution part of the project around the 46-16, which again, is the primary target of this survey.

DOCUMENT NO: S3-REP-01-5-ALTAROCK_REDUX	REVISION NO: 05 Appendix G: 183	REVISION DATE: 29/04/2014	Page 44 of 47	PM APPROVAL: SCOTT TAYLOR
---	--	-------------------------------------	---------------	-------------------------------------

In addition Sigma Cubed filed a patent and implemented new visualization techniques to transform the LASEA data from a very pixelated display as in Figure 1 below, into a richer, more intuitive dynamic energy volume as shown in Figure 2 below.

DOCUMENT NO: S3-REP-01-5-ALTAROCK_REDUX	REVISION NO: 05 Appendix G: 184	REVISION DATE: 29/04/2014	Page 45 of 47	PM APPROVAL: SCOTT TAYLOR
---	--	-------------------------------------	---------------	-------------------------------------

3 PAD 55-29 INJECTION ANALYSIS

3.1 PAD 55-29 INJECTION SUMMARY

The following notes and information pertain to water injection at NWG 55-29 during the Sigma Cubed seismic noise study carried out in September, 2013.

September 10, 2013

0850 Start injection and water well pumps at Pad 55-29
 0920 Injecting at 230.0 gpm. Wellhead pressure built to 200 psi.
 0945 Injecting at 160.0 gpm. Wellhead pressure built to 400 psi.
 0945-23:59 Injection slowly decreased from 160.0 gpm down to 139.9 gpm; WHP slowly increased from 400 psi to 430 psi.

September 11, 2013

0000-1859 Injection continued slow decline from 139.9 gpm to 136.7 gpm and WHP was maintained at 430 psi.
 1859 PAS line opened to flow to sump, producing rusty water for ~10 minutes before clearing up. Water well flow at 148 gpm.
 1930 PAS line water sample collected (18.7° C, clear).
 1934 PAS line closed.
 1935-2359 Injection continued slow decline from 148.0 gpm to 137.2 gpm. WHP maintained at 430 psi.

September 12, 2013

0000-0700 Injection continued slow decline from 137.2 gpm to 136.0 gpm. WHP maintained at 430 psi until pumps were shut down.

Casing Evaluation

The week prior to the injection described above, AltaRock performed a casing evaluation which paired injection with pressure-temperature-spinner (PTS) logging, video camera, and multi-finger caliper log. It was determined that there were two, large casing leaks at measured depths of 1767 ft and 2240 ft. AltaRock estimates that 90% of the water injected to 55-29 exits equally from these two leaks, leaving just 10% to exit in the open hole. Geographic coordinates for the fluid exits are given in Table 1.

DOCUMENT NO: S3-REP-01-5-ALTAROCK_REDUX	REVISION NO: 05 Appendix G: 185	REVISION DATE: 29/04/2014	Page 46 of 47	PM APPROVAL: SCOTT TAYLOR
---	--	-------------------------------------	---------------	-------------------------------------



Figure 69 - Injection pump used at Pad 55-29

Table 1 - Locations of fluid loss zones in 55-29. UTM is NAD84, Zone 10. Lat/long is WGS84.

Measured Depth (ft)	Vertical Depth (ft)	Elevation (ft)	Vertical Depth (m)	Elevation (m)	Easting (m)	Northing (m)	Long.	Lat.
0	0	5815	0	1772.4	635642.1	4842836	-121.316	43.7261
1767.0	1765.7	4049.3	538.2	1234.2	635659.5	4842836.7	- 121.3157	43.7262
2240.0	2237.9	3577.1	682.1	1090.3	635667.6	4842837.0	- 121.3156	43.7261
9125.0	8975.7	-3160.7	2735.8	-963.4	636093.0	4842843.5	- 121.3103	43.7261

FINAL PROJECT REPORT



RELEASE RECORD				
REVISION	SECTION	COMPANY	RECIPIENT	DATE
4	ALL	ALTAROCK ENERGY, INC	TRENTON CLADOUHOS	4/27/14
5	ALL	ALTAROCK ENERGY, INC	TRENTON CLADOUHOS	8/24/14
6	ALL	Davenport Newberry Holdings	Albert Waibel	9/10/14

Albert Waibel
Corporate Geologist
Davenport Newberry Holdings
4010 Stone Way North, Suite 400
Seattle, WA 98103
awaibel@hevanet.com
(503) 260-7215

REVISION RECORD				
REVISION	SECTION	AUTHOR	SUMMARY OF CHANGE	DATE
A0	ALL	Scott Taylor	Template	7/31/13
1	ALL	Brian Fuller	First pass LASEA	11/20/13
2	ALL	Brian Fuller	Updated LASEA volume	12/30/13
3	ALL	Brian Fuller	Updated LASEA volume	1/10/14
4	ALL	Scott Taylor	Input fine resolution LASEA run	4/27/14
5	ALL	Scott Taylor	Crystal images	5/28/14
6	ALL	Scott Taylor	Reponses to feedback from Al Waibel July 2014	8/24/14

SIGMA³

Sigma Cubed, Inc.

4700 West Sam Houston Parkway North, Suite 150,

Houston, TX, 77041

Phone: +1.281.363.8500

**COPYRIGHT © 2014 Sigma Cubed Integrated Reservoir Solutions, Inc. (“Sigma³”)
ALL RIGHTS RESERVED**

This document contains trade secret and other proprietary information that is owned by Sigma³ and is protected by intellectual property rights under common law and applicable statute. This information, either through the use of this document or through other use of the technology contained herein, is strictly prohibited unless you have the express written permission of Sigma³.

Table of Contents

1	EXECUTIVE SUMMARY	4
1.1	Technical Objectives.....	4
1.2	Structure of final report.....	4
1.3	Project Deliverables	5
1.3.1	Raw data.....	5
1.3.2	ELECTRONIC Project Software & 3D VIEWER.....	5
1.3.3	Data Analysis	5
2	DESCRIPTION OF TECHNOLOGY	6
2.1	Description of LASEA.....	6
2.1.1	Background Information.....	6
2.1.2	Overview of Data Processing.....	7
2.1.3	Use of P-waves.....	7
2.1.4	Physical Justification For LASEA	7
2.1.5	LASEA Output.....	10
2.1.6	Pre-processing Workflow	11
2.1.7	LASEA Processing Specifics.....	11
2.2	Detailed Description of Hotspot Visualization Technology	13
3	PAD 46-16 ANALYSIS.....	14
3.1	Datum.....	15
3.2	Time Synchronization.....	15
3.3	46-16 Field notes for Well 46-16.....	15
3.4	Workflow	16
3.5	September 8 th 2013.....	17
3.6	September 9 th 2013.....	28
3.7	September 10 th 2013.....	38
4	Pad 55-29 INJECTION ANALYSIS	44
4.1	Analysis of Lower Amplitudes	56
4.2	Pad 55-29 Injection SUMMARY	57
5	ON THE UTILITY OF LASEA AS A COMMERCIAL EGS EXPLORATION TOOL	59
6	SUMMARY OF FIELD ACQUISITION	60

1 EXECUTIVE SUMMARY

The Sigma Cubed (“S3”) portion of the Davenport Energy 109 Grant by the US Department of Energy (“DOE”) was to determine if S3’s proprietary Low-Amplitude-Seismic-Emission Analysis (“LASEA”) technique had any utilitarian value for geothermal exploration.

The specific objective of this research grant is to attempt to evidence a repeatable seismic signature, or fingerprint associated with coherent signals from fluid- producing fractures associated with well 46-16 production. A secondary task was added, with additional funding, to evaluate LASEA for imaging EGS development efforts. This final S3 report addresses these two complementary goals as separate items in order to avoid confusion. The structure of this report is more fully described below in Section 1.2.

The critical test with controls was the well 46-16 intermittent flowing. The plan as laid out was to compare signals resulting from fluid flow within near well bore fractures prior to, during, and after each of the three well-flowing episodes. With each flow episode there was significant fluid discharge, both gas and liquid phases. S3 has been supplied with the timing and durations for each of the flow events.

1.1 TECHNICAL OBJECTIVES

Imaging injection activity on the 46-16 well is the primary goal of the project and imaging the activity on the 55-29 was a secondary goal. For each well the primary objective is to determine if areas of anomalously high levels of seismic energy can be detected and located. Secondary objectives are contingent upon detection and localization of anomalously high levels of coherent seismic energy. For valid localized coherent seismic energy S3 has attempted to define the characteristics of the anomaly such as:

- spatial extent,
- time variance of amplitude,
- and seismic frequency dependence

1.2 STRUCTURE OF FINAL REPORT

The report is structured in six (6) sections:

1. **Section 1** is a written executive summary covering the primary and secondary program objectives and checklist of deliverables
2. **Section 2** is a detailed explanation of the LASEA technology. This section is written as a general description of data processing methodologies, written for DOE staff and their National Lab consultants as the primary audience.
3. **Section 3** is a technical analysis outlining how LASEA was used to characterize the flow paths around 46-16 using the signal from venting gas from the well on three separate days. To help evidence the technical analysis this section contains several 2D images, both planar and vertical, of the LASEA results in the region around well 46-16. This includes results during at least two separate well flowing events and two interlude events, to show reproducibility (or lack thereof).

4. **Section 4** is a technical analysis outlining how LASEA was used to characterize the flow paths around 55-29 using the signal from injecting water into the well for 2+ days. To help evidence the technical analysis this section contains several 2D images, both planar and vertical, of the LASEA results in the region around well 46-16. This includes results during at least two separate well flowing events and two interlude events, to show reproducibility (or lack thereof).
5. **Section 5** provides an analysis specifically addressing the results of the S3 test using LASEA technology, as it applies to value as a geothermal exploration tool.
6. **Section 6** provides a summary of the acquisition operations and annotates key information.

1.3 PROJECT DELIVERABLES

The following is a list of project deliverables as specified in the Davenport Energy 109 Grant by the US Department of Energy (“DOE”).

1.3.1 RAW DATA

Raw field records covering the complete acquisition were sent to Dr. David Blackwell at Southern Methodist University.

1.3.2 ELECTRONIC PROJECT SOFTWARE & 3D VIEWER

Todd Broussard set has delivered a CRYSTAL project to AltaRock together with a 1 year CRYSTAL license.

1.3.3 DATA ANALYSIS

Sections 2 through 5 provide a comprehensive technical analysis. To help evidence the technical analysis this report contains many time-lapse 2D images, both planar and vertical, of the LASEA results in the region around wells 46-16, and 55-29.

2 DESCRIPTION OF TECHNOLOGY

Two key proprietary methods were utilized for this project. The first method is related to protected data processing intellectual property: WO/2011/156788 – RESERVOIR MAPPING WITH FRACTURE PULSE SIGNAL. 15.12.2011. G01V 1/48. PCT/US2011/040091. HIPOINT RESERVOIR IMAGING FULLER, Brian. For the purposes of this report, this technology shall be referred to as Low-Amplitude-Seismic-Emission Analysis (“LASEA”). LASEA will be more fully described in section 2.1.

The second method is a proprietary visualization technology previously developed to provide a more instructive manner of investigating data derived from LASEA. This technology shall be referred to as “hotspot”.

2.1 DESCRIPTION OF LASEA

LASEA is a method and system that includes acquiring a seismic dataset while injecting fluids into the subsurface while seismic data are recorded at multiple sensor locations. Seismic travel times are computed between all sensors and all nodes of a 3D grid of subsurface locations. A velocity model is required to compute the travel times. Travel times and travel time delays between pairs of sensors are then used as input to estimate the dominant seismic signal that arrives at the receivers from specific subsurface locations during a specific time period. The estimate of the dominant seismic signal is cross correlated with each seismic data trace in the time frame to estimate the total seismic energy that has arrived at the seismic sensors during the specific period of time. The premise this technology is that coherent seismic energy may be extracted from long periods of ‘focused-listening’ at each grid node. In other words, rather than listening for and using only identifiable low-amplitude earthquake-type events as the only form of seismic activity, the dominant signal is assumed to be persistent but low-amplitude seismic energy that might otherwise be considered noise. The seismic energy coefficient values are related to the acoustic response at each subsurface position and are compared to other grid node positions within a 3D volume. The comparison of energy coefficients in space and through time is primarily done via quantitative analysis of ‘energy hot spots’ and analyzed visually in a modern 3D seismic viewing software package. The goal of the visualization is to determine the position of seismic activity that is in response to fluid injection in the earth. For the purposes of the analysis in sections 3 and 4, on the 55-29 and 46-16 wells respectively, the grid search was in 50 meter voxels (3-dimensional segments of the project volume)

2.1.1 BACKGROUND INFORMATION

Hydraulic fracture stimulation is an economically important technology applied to oil and gas reservoirs to increase oil and gas production. Fracturing technology has dramatically increased the available hydrocarbon reserves of the United States over the past 10 years. During hydraulic fracture stimulation highly pressurized fluids are injected into reservoir rock. The pressurized fluids overcome the breaking strength of the rock and generate fractures that act as pathways by which oil and natural gas can migrate to the borehole and be brought to the surface. The injected fluids, which may reach volumes of 4,000 gallons per minute or more, flow through fractures created by the high-pressure fluids and through previously existing natural fractures in the rock.

Similarly the US DOE has placed a priority on renewable energy sources. One such promising technology is Enhanced Geothermal development. Much like hydraulic fracture stimulation, one must create or induce

conductivity between a water injection well and a producing well in order to extract the energy stored in the fluids.

2.1.2 OVERVIEW OF DATA PROCESSING

Before proceeding into the next section that describes the major findings of this study, we discuss the fundamental calculations that are the basis of LASEA or Low Amplitude Seismic Emission Analysis. The following eight slides discuss the LASEA method and method of displaying the result. Results from the Newberry Volcano project then follow.

2.1.3 USE OF P-WAVES

The data processing applied to the AltaRock dataset is specifically for P-waves (compressional waves). Shear waves, or S-waves, were not considered for three reasons. First, we do not have S-wave velocity information for this location and velocity information is a critical element in LASEA calculations. Second, we have observed that S-waves in the seismic frequency band that we consider do not propagate through the upper few hundred meters of the earth as well as they do at depth. While our observations are for sedimentary formations, we have no evidence at this location to contradict our observation, hence S-waves may not even be present in the recorded data. Finally, we have never done LASEA analysis with S-waves due in part to the complexity in the polarity of S-waves and S-wave splitting. P-waves are much more predictable than S-waves and therefore more reliable for LASEA computations.

2.1.4 PHYSICAL JUSTIFICATION FOR LASEA

Conventional microseismic methods focus on analysis of relatively high-amplitude short duration seismic events like the one shown in Figure 1 below. Events like this one originate when rocks break in response to injection of hydraulic stimulation fluids or changes in stress due to large temperature variations. They are generally very small earthquakes with magnitude on the order of -3 to -1.

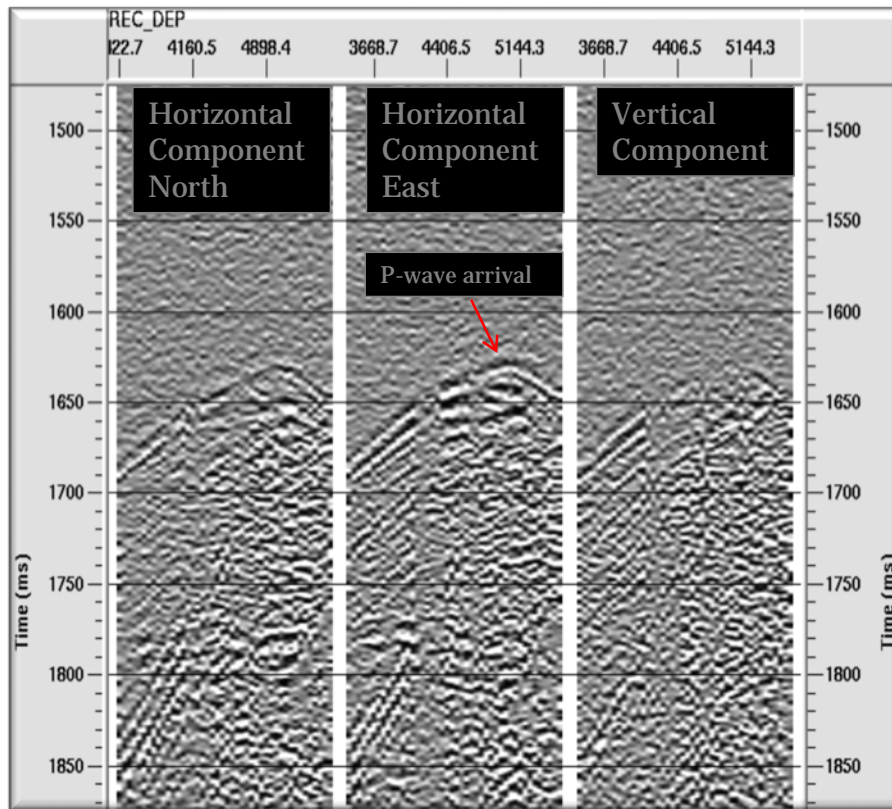


Figure 1 – The microseismic event shown above was recorded with very similar equipment to the equipment used in this project. This event has a short duration, on the order of 1/100th of a second and is in the earthquake magnitude range of -1 to -3. In contrast to the short-duration events like the one above, LASEA concentrates on long duration or persistent seismic signals that persist for from many minutes to hours.

SigmaCubed has developed a method that we call LASEA (Low Amplitude Seismic Emission Analysis) that provides a direct measure of seismic energy output from points in a volume of earth over time. Anomalously large amplitude values may correspond to locations in the earth where fluids are moving, where stresses change due to temperature fluctuations, or where subsurface points are in direct connection with a source of variable pressure.

When fluids in natural fractures are subjected to varying pressure from fluid sources or changing temperature, the fluids push on the adjacent rock walls generating low-amplitude vibrations that can be recorded by geophones. Rocks can also fracture in response to stress changes related to temperature variations. These vibrations can be persistent over long periods of time. Natural processes such as volcanic activity can continue for millennia. The LASEA method takes advantage of persistent seismic signals in spite of relatively small amplitudes of magnitude of -3 or smaller.

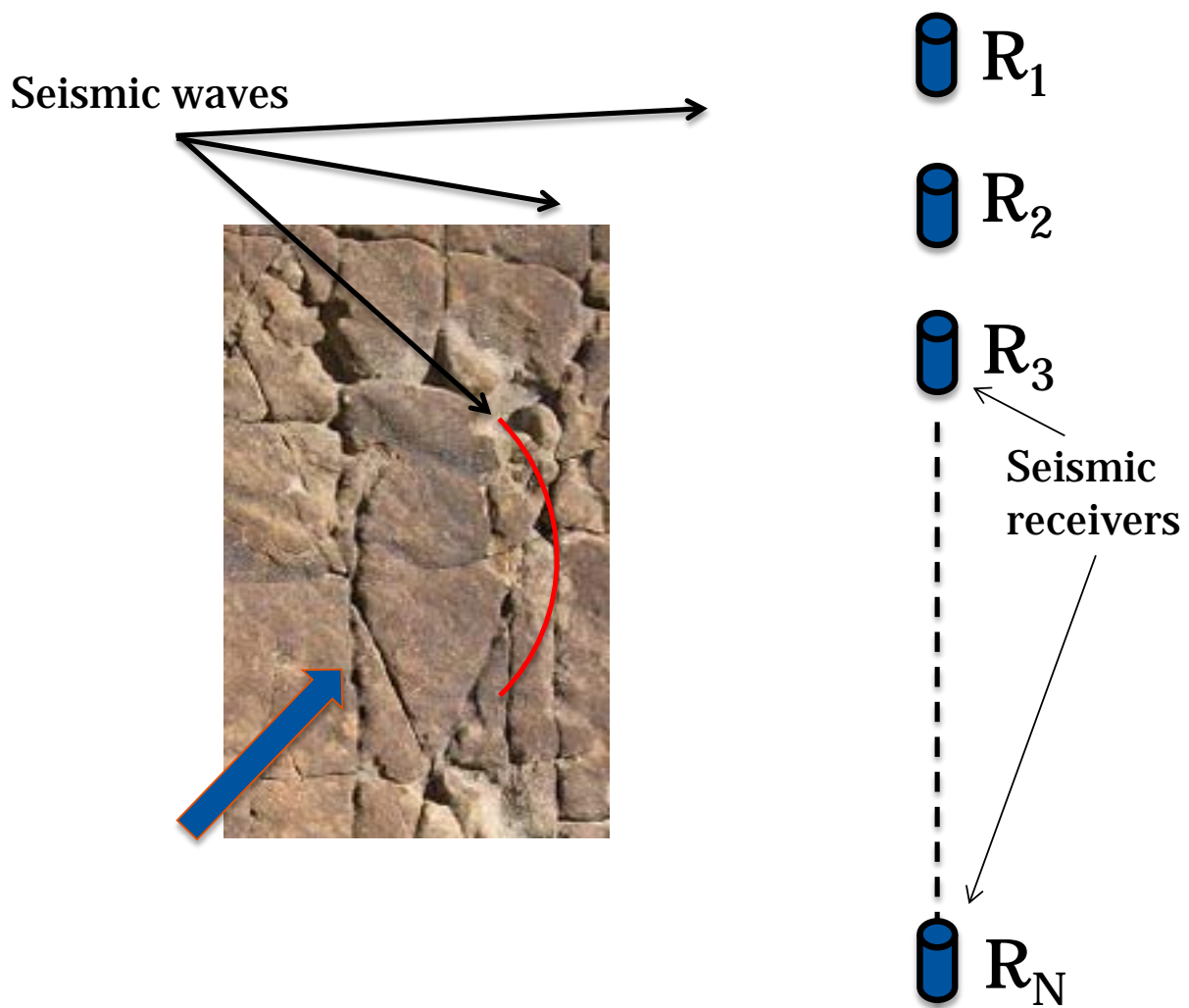


Figure 2 - Fluid within fractures transmits energy in the form of pressure to the adjacent rock walls to generate seismic waves. Energy transfer can also be in the form of conductive heat transfer that could cause stress and rock fractures.

The LASEA data processing algorithm (patent pending) extracts low-amplitude seismic signals emitted from discrete grid nodes within the earth. The method essentially uses focused seismic receiver arrays to measure energy flow from a point over long time periods (many minutes to many hours).

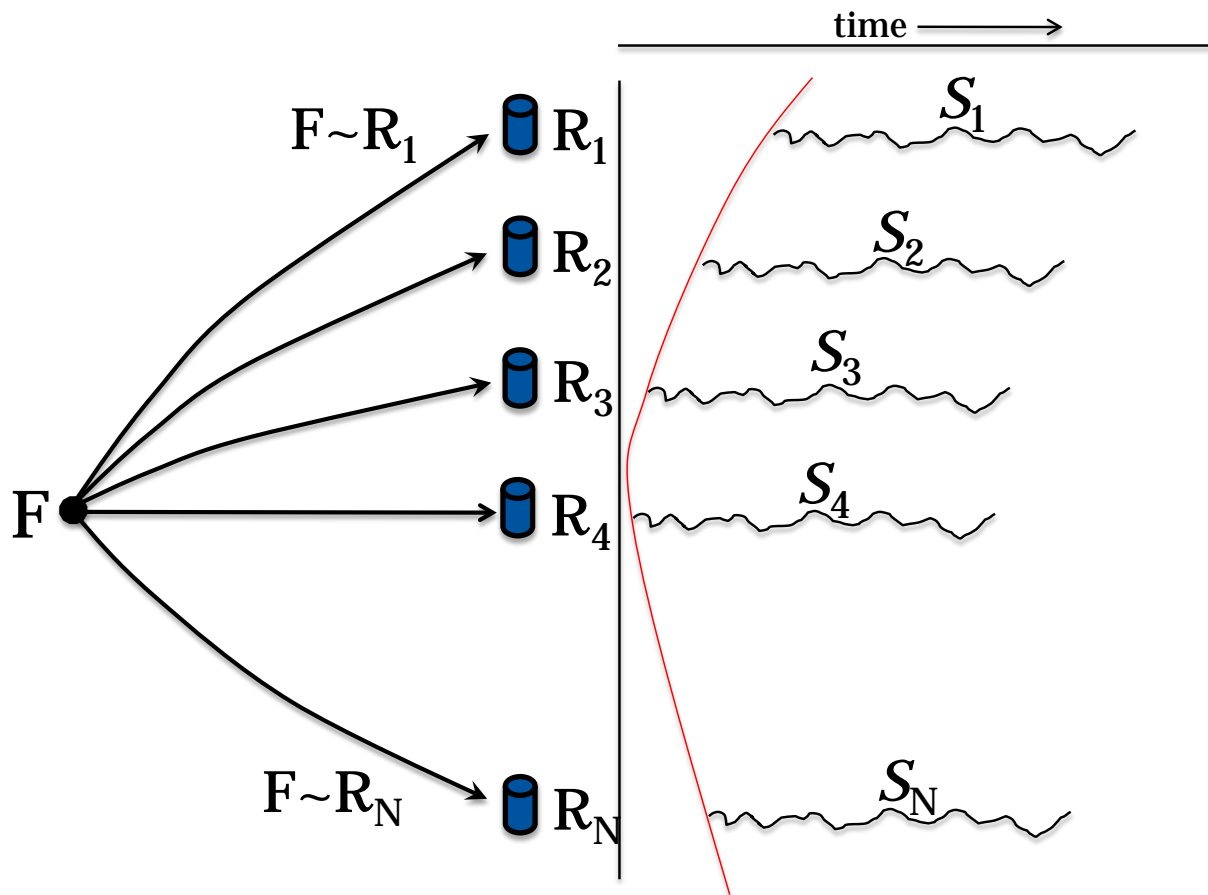


Figure 3 - The LASEA algorithm essentially uses an array of 3-component geophones as an antenna to measure seismic energy flux from each grid node in a 3D volume somewhere near the observation wells. The algorithm is much more focused and precise than a simple energy measurement as it employs elements of Kirchhoff Depth Migration, virtual source concepts, and other technologies. The algorithm is computationally intensive but computers with sufficient computational capacity can be employed to efficiently calculate results. The output from the algorithm is an estimate of energy output from each grid node in a volume defined by the user. Amplitudes of output sample values are comparable to one another but at this time the output is not computed or reported in standard energy or power output measures such as watts.

LASEA can be used to monitor production from producing fields to determine where fluids are being produced or for monitoring subsurface hydrothermal activity. Combined with reservoir simulators, this information could provide the most accurate means currently available to estimate reservoir capacity and accessible reserves in place.

2.1.5 LASEA OUTPUT

LASEA scans a full 3D volume of the earth at a user-specified grid interval and computes the amount of seismic energy detected from that location over some time period, normally on the order of a few minutes to hours. LASEA then outputs a number corresponding to the energy measurement for that grid node and time. The grid node energy measurements can then be viewed in a 3D viewer to observe trends in the energy. The energy measurement at each grid node through time can then be manipulated and displayed in a modern 3D/4D visualization software package as is depicted in Figure 6 below or many of the Figures that follow in the results sections.

2.1.6 PRE-PROCESSING WORKFLOW

The data processing steps applied to the Davenport Newberry data prior to being input to the LASEA process are shown below:

1. Load data from field disks to ProMAX data format (ProMAX is a leading industry seismic data processing software package)
2. Apply geometry assignment to all data (receiver X, Y, and elevation)
3. Determine horizontal geophone component orientation and apply rotation to Vertical, North, and East directions
4. Bandpass filter (Butterworth bandpass 12 Hz, 18 dB/Oct, 60 Hz, 45 dB/Oct - discussed below)

Step 4 was done to maximize signal quality with respect to “noise” where “noise” is defined as seismic energy that is not of interest to this project and that may interfere with the signal quality of the desired data. Examples of seismic energy not of interest to this project are high frequency background noise and culturally generated noise.

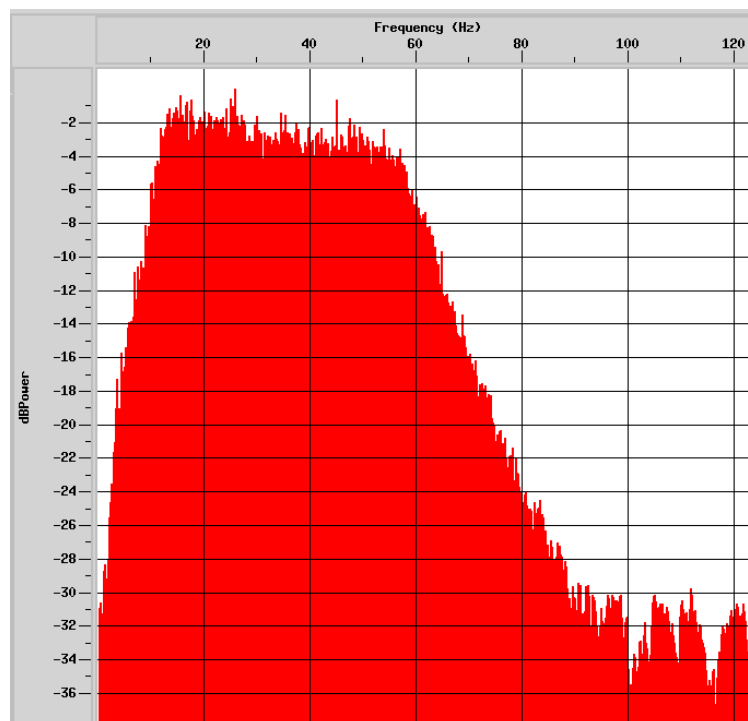
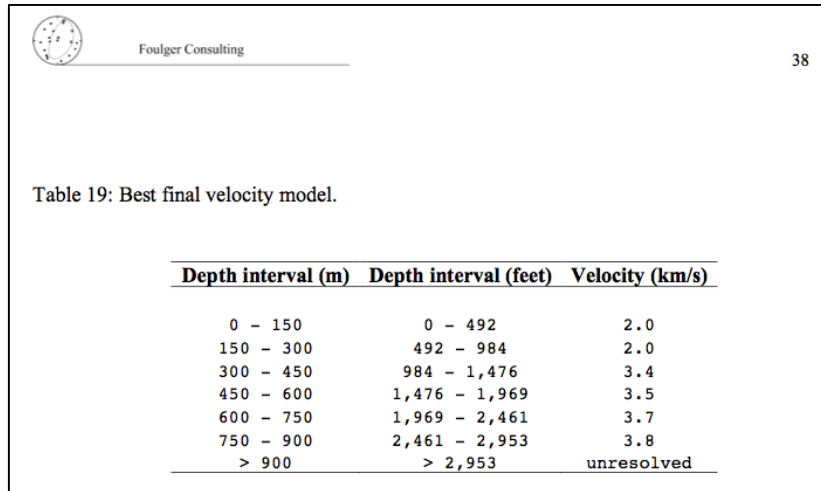


Figure 4 - The amplitude spectrum and filter panel displays of the data were analyzed and it was found that below 15 Hz there is a significant amount of coherent energy in the near-surface waveguide (more later on this subject) and a significant random noise component enters the data above 60 Hz. We therefore applied a Butterworth bandpass filter with the following parameters 12 Hz, 18 dB/Octave slope, 60 Hz, 45 dB/Octave slope. The spectrum of a typical record after the filter is shown above.

2.1.7 LASEA PROCESSING SPECIFICS

The grid node spacing for computations was 50 m. The velocity field was taken from previous work in Table 19 of an unpublished report titled “Report to AltaRock Energy Inc. Newberry Calibration Shot Project” by Gillian R. Foulger, of Foulger Consulting, dated October 09, 2010. The table directly from the report is shown below:

Table 1 - Report to AltaRock Energy Inc. Newberry Calibration Shot Project” by Gillian R. Foulger, of Foulger Consulting, dated October 09, 2010



<u>Depth interval (m)</u>	<u>Depth interval (feet)</u>	<u>Velocity (km/s)</u>
0 - 150	0 - 492	2.0
150 - 300	492 - 984	2.0
300 - 450	984 - 1,476	3.4
450 - 600	1,476 - 1,969	3.5
600 - 750	1,969 - 2,461	3.7
750 - 900	2,461 - 2,953	3.8
> 900	> 2,953	unresolved

Depths greater than 900 m were unresolved in the Foulger report and for the LASEA analysis were assumed to be 3.8 km/s via extension of the deepest velocity determined in Table 1.

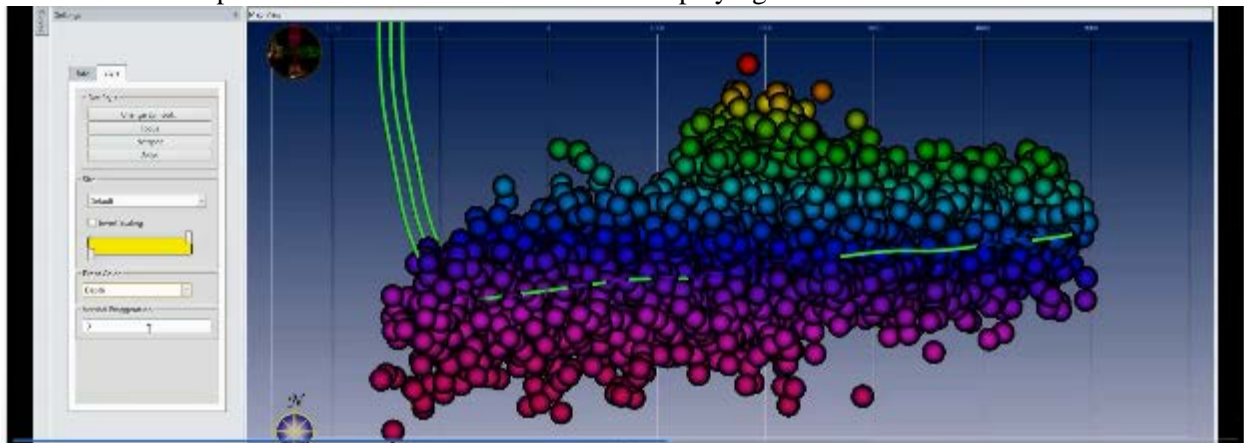
Further refinement of the velocity field may be possible with seismic sources that may be generated by upcoming fracture stimulation at the Newberry site.

The dots shown on the LASEA display are effectively the result of a series of cross correlations and sums that include input from thirty (30) minutes of continuously recorded data (over 3 gigabytes of data). An additional data smoother was also applied such that for any given grid node in the volume, the data sample that is displayed is an average of the LASEA value for that 30 min periods. The time smoothing provides way to diminish the effect of anomalous amplitudes, both large and small.

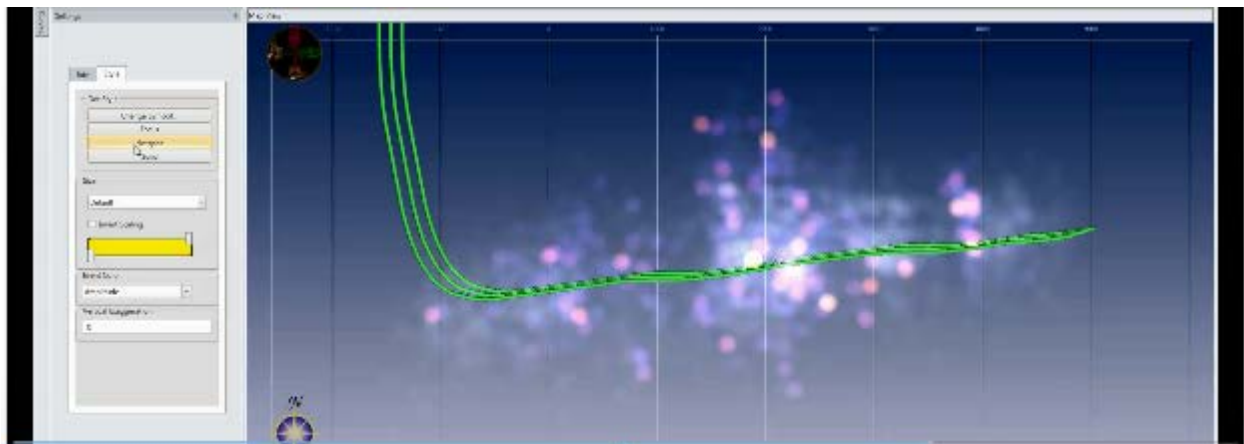
2.2 DETAILED DESCRIPTION OF HOTSPOT VISUALIZATION TECHNOLOGY

Without “Hotspot”, microseismic events that are roughly in the same position as each other will overlap and obscure their neighbors from view and making analysis more difficult. “Hotspot” is using an effect called “Additive Blending” which, instead of obscuring its overlapping neighbors, adds the overlapping microseismic events, or cumulative coherent LASEA amplitudes colors together so you can see a cumulative cloud of values. This view can allow a user to quickly spot high energy locations as opposed to simply being able to identify areas of high microseismic or LASEA event occurrence.

The first screen capture below is a standard method of displaying microseismic event data.



The second screen capture below demonstrates the transformation of the same data into Hotspot. As we are seeking to see a repeatable seismic energy fingerprint for this project, we decided to display results in hotspot.



3 PAD 46-16 ANALYSIS

This section provides a comprehensive LASEA output for the 46-16 well injection with the high resolution LASEA data presented in three segments for Sunday September 8th, Monday September 9th, & Tuesday September 10th respectively. We ran 30 minute and 15 minute stack-time intervals and output the following data:

- ❖ Open46-16_Sept08_30_min
- ❖ Open46-16_Sept08_15_min
- ❖ Open46-16_Sept09_30_min
- ❖ Open46-16_Sept09_15_min
- ❖ Open46-16_Sept10_15_min
- ❖ Open46-16_Sept10_30_min

The analysis will focus on the 30 minutes stack as the 3D viewer is currently incapable of handling the volume of data for the 15 minutes stack.

The provided annotations to each figure are logically integrated with the imagery. Each of these views are orthographic projections as follows:

- 1) Left pane is North up in map / plan view
- 2) Top Right pane is depth view looking west
- 3) Bottom right is depth view looking North

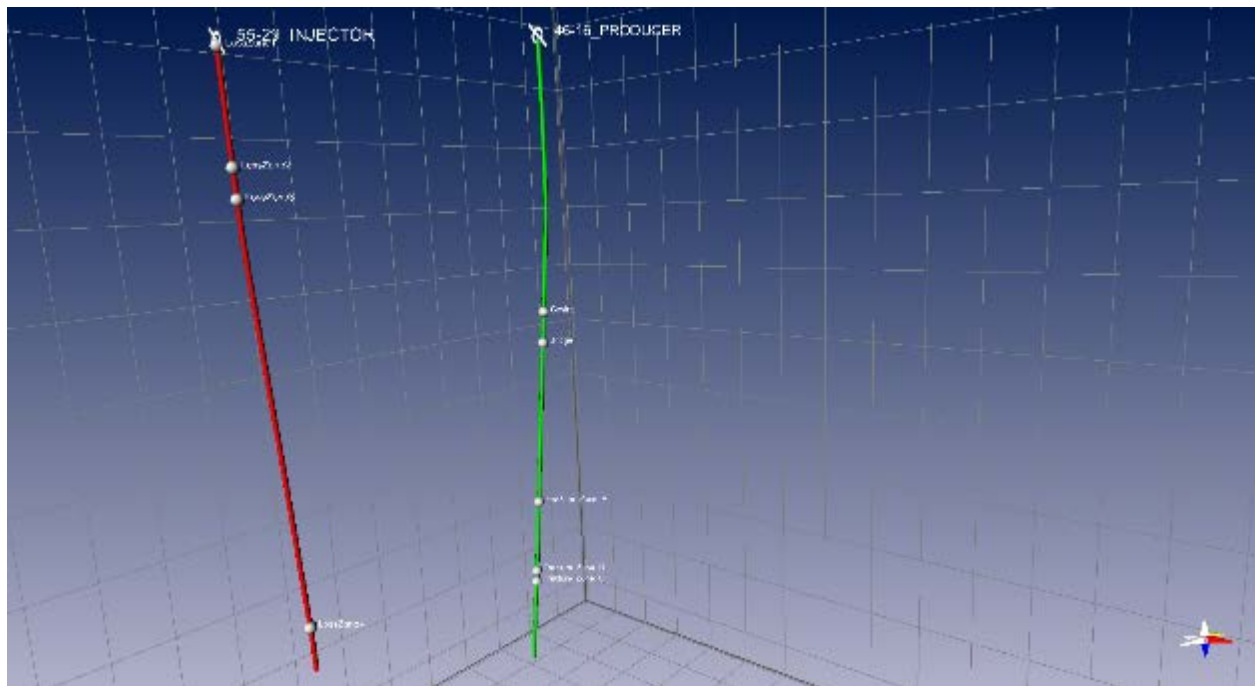


Figure 5 – 3D CRYSTAL viewer of the 46-16 well and annotated zones (depths) of interest identified by AltaRock. Depth view has been exaggerated by 200%

3.1 DATUM

- ❖ The project is in meters.
- ❖ The depth values are relative to TVDSS.
- ❖ The KB elevation for the 46-16 is 1875.12 m.

3.2 TIME SYNCHRONIZATION

For clarity and cohesion with the supplied AltaRock observer logs, all figures and references to time are in 24hours local Oregon time.

3.3 46-16 FIELD NOTES FOR WELL 46-16

The following text in italics in this section is from the technical field notes provided by AltaRock.

Estimated flow for Sunday September 8th, and Monday September 9th, 3,000 gal. each day. Estimate flow for & Tuesday September 10th is 4,000 gal. 46-16 has 13 3/8 " casing, 0.8818 cu. ft. per linear ft., a bit over 6.6 gal/linear ft. Estimated total displacement of well-bore could be about 1500 feet, or about 1/2 of the liquid volume between the top of the static water (2070' BGL) and the bridge (5,000 ft. BGL); total flow volume far less than the liquid volume above the bridge. Regardless of the accuracy of these estimates, it is clear that not enough fluid has been discharged to equal the volume of fluid above the bridge.

Any fluid flowed from the well from below the bridge would have to pass through the bridge and pass up through a substantial column of thermally equilibrated water/drilling mud (300°F at the bridge depth of 5000 ft., please see temperature chart below). The limited flow volumes for these three days would hardly be enough to heat up the well bore or produce hot discharge.

The liquid during each flow period ranged from dirty water to thick mud. At this time one could only speculate as to the dilute mud fraction. Geophysical logs showed possible fluid flow around 11,000 ft. The audience (Davenport Newberry team, DOE, etc.) is interested in what energy associated with fluid flow is associated with the specific points of interest identified below. Any other zones of energy along the wellbore shall be highlighted accordingly:

- ❖ *Well 46-16 was drilled to around 11,000 ft. (3352m)*
- ❖ *Casing was set at about 4800 ft. (1460m)*
- ❖ *A permeable bridge is in the well bore at around 5,000 ft. (1625m)*
- ❖ *Minor fractures were observed at around 7900 ft. (2568m).*
- ❖ *Evidence of major fractures was observed around 9200-9400 ft. (2990-3055m).*

3.4 WORKFLOW

The project workflow is segmented into seven (7) key steps that encompass field operations, data acquisition, data analysis, data processing and visualization of output information:

1. AltaRock Injected fluids into the subsurface;
2. S3 acquired continuous high fidelity seismic data from multiple vertical arrays of three-component sensors;
3. S3 computed travel times between a subsurface position and the multiple vertical arrays of three-component sensors;
4. S3 computed seismic travel time differences between the multiple vertical arrays of three-component sensors locations;
5. S3 cross correlated seismic data from the multiple vertical arrays of three-component sensors to determine coefficients associated with the subsurface position; and
6. S3 summated the coefficients associated with the subsurface position to obtain the value associated the subsurface position.
7. Visualize the data

3.5 SEPTEMBER 8TH

LASEA outputs will be presented in sequence to illustrate:

- 1) initial state prior to flow
- 2) state during flow
- 3) state after shut in

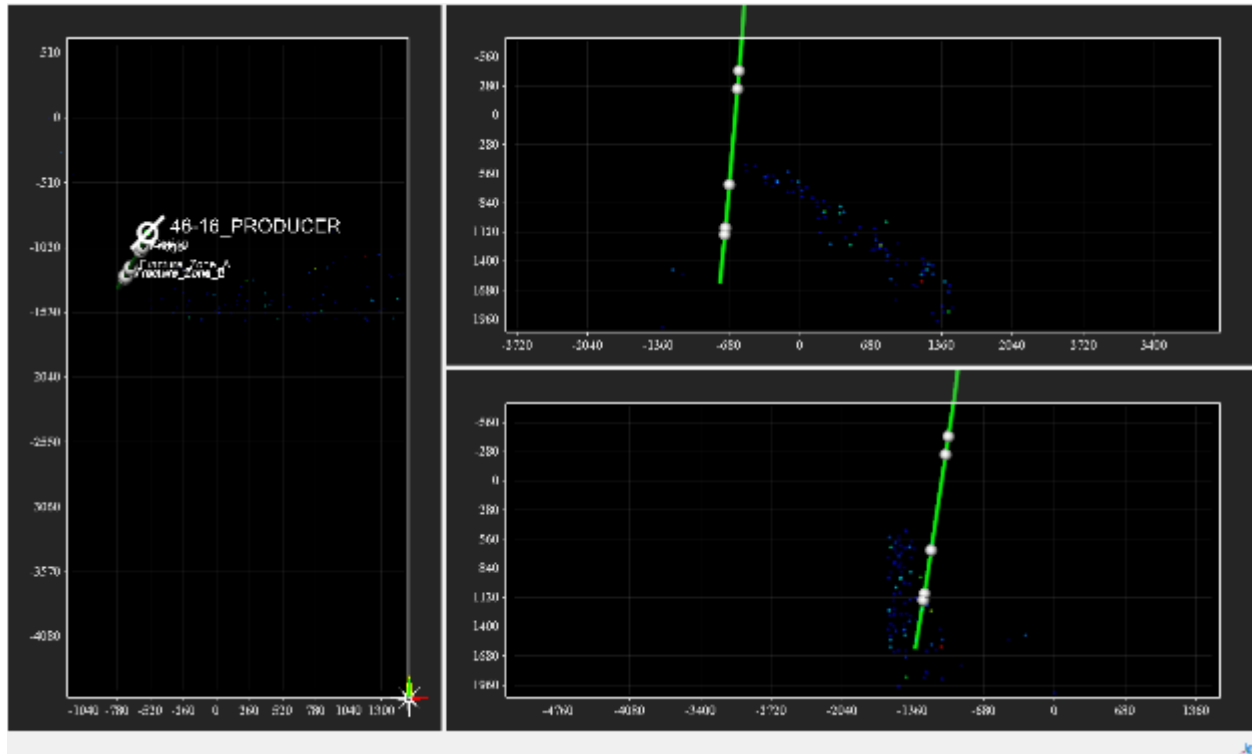


Figure 6 - 11:53 local time. Perspective is North Up. Visualized using Hotspot technology. This corresponds to time prior to opening of the valves. One notes from this perspective that there is a slightly dipping LASEA response corresponding to identified natural fracture systems at 2568m, indicated as Fracture Zone A

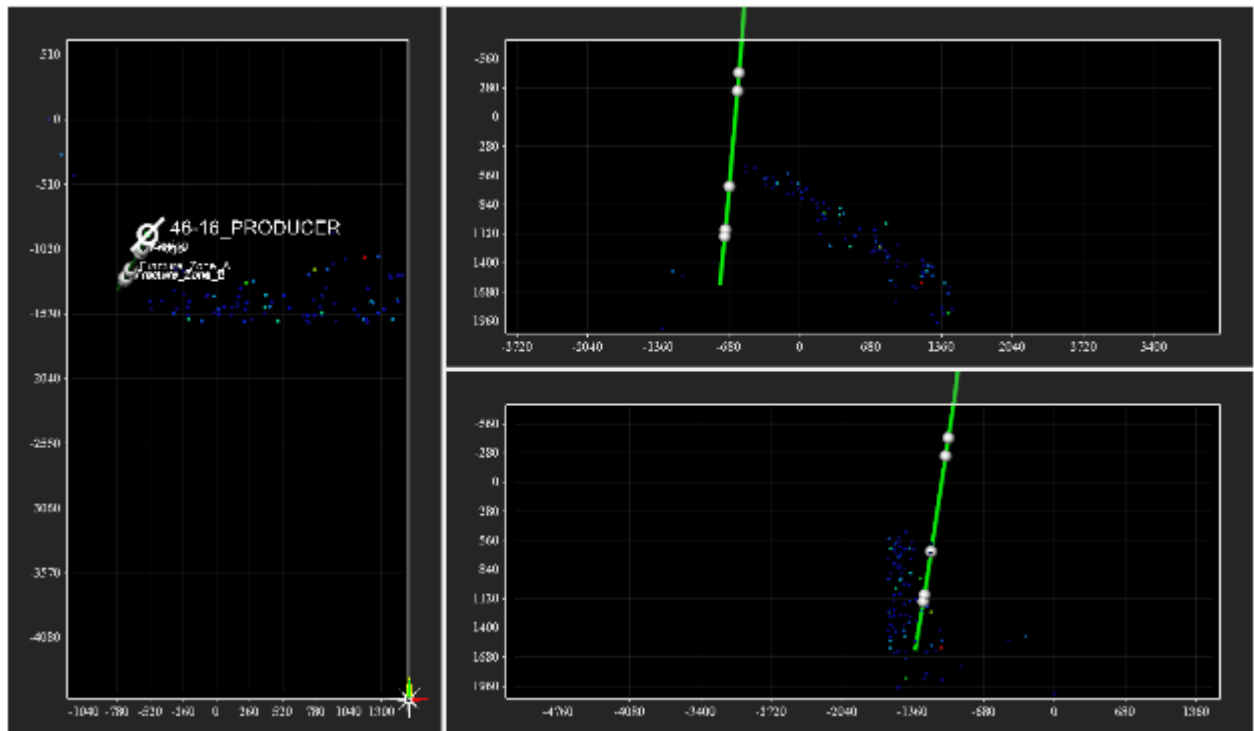


Figure 7 - Same time period and viewing perspective as FIG 7. Visualization technology changed to gridded amplitudes colored by relative intensity of coherent amplitudes.

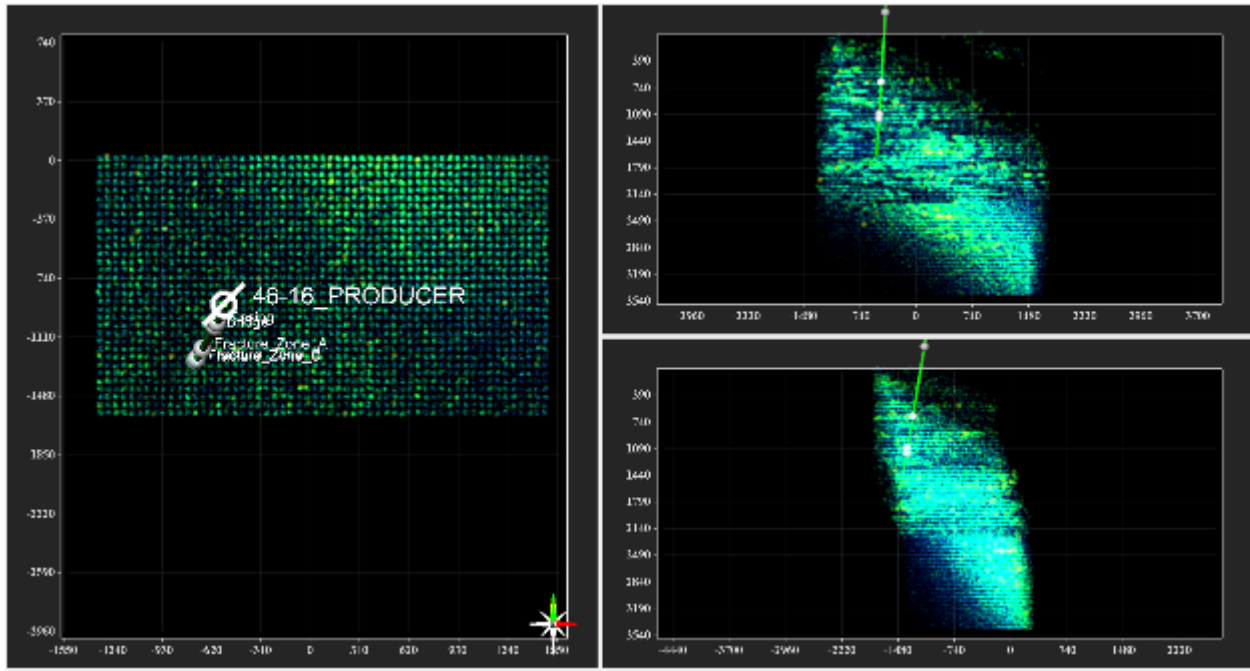


Figure 8 - 14:53 – local time. Perspective is North Up. Visualized using Hotspot technology. This corresponds to time 43 minutes after opening of the valves. One notes from this perspective that there is a significant rise in LASEA response. We see activity at Fracture Zones A, B & C.

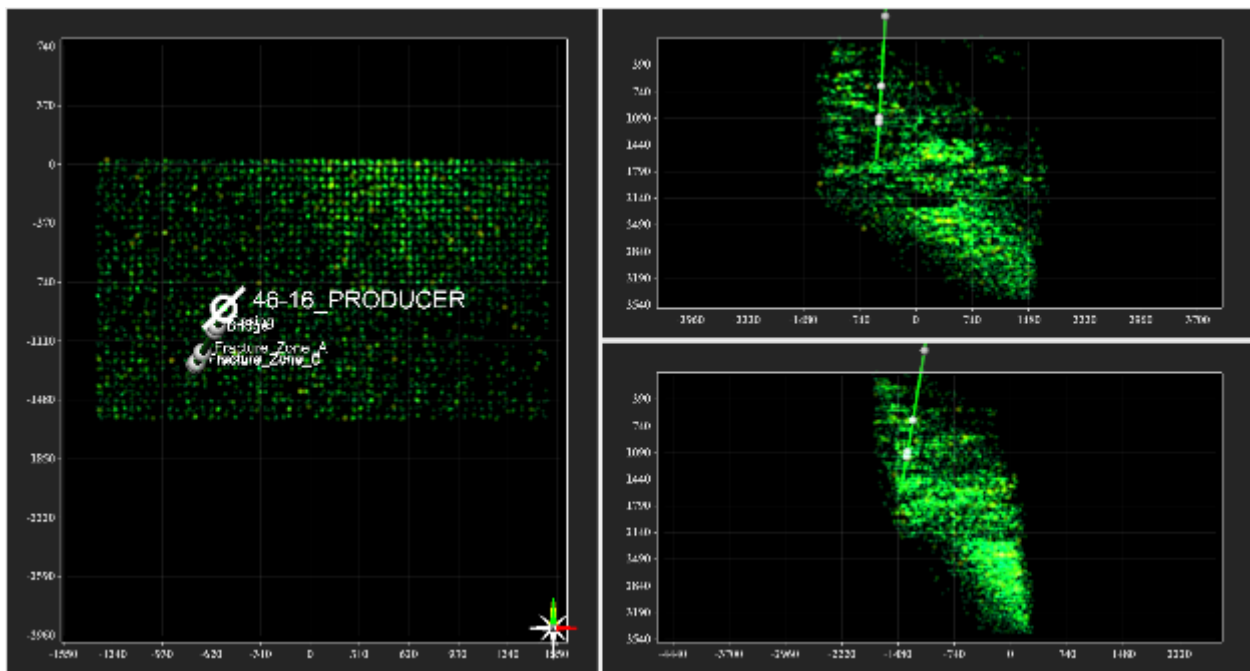


Figure 9 - 14:53 local time. Perspective is North Up. Same as Figure 13, however only the top 50% of energy is imaged. This corresponds to time 43 minutes after opening of the valves. One notes from this perspective that there is a consistent LASEA response. We see activity at Fracture Zones A, B & C.

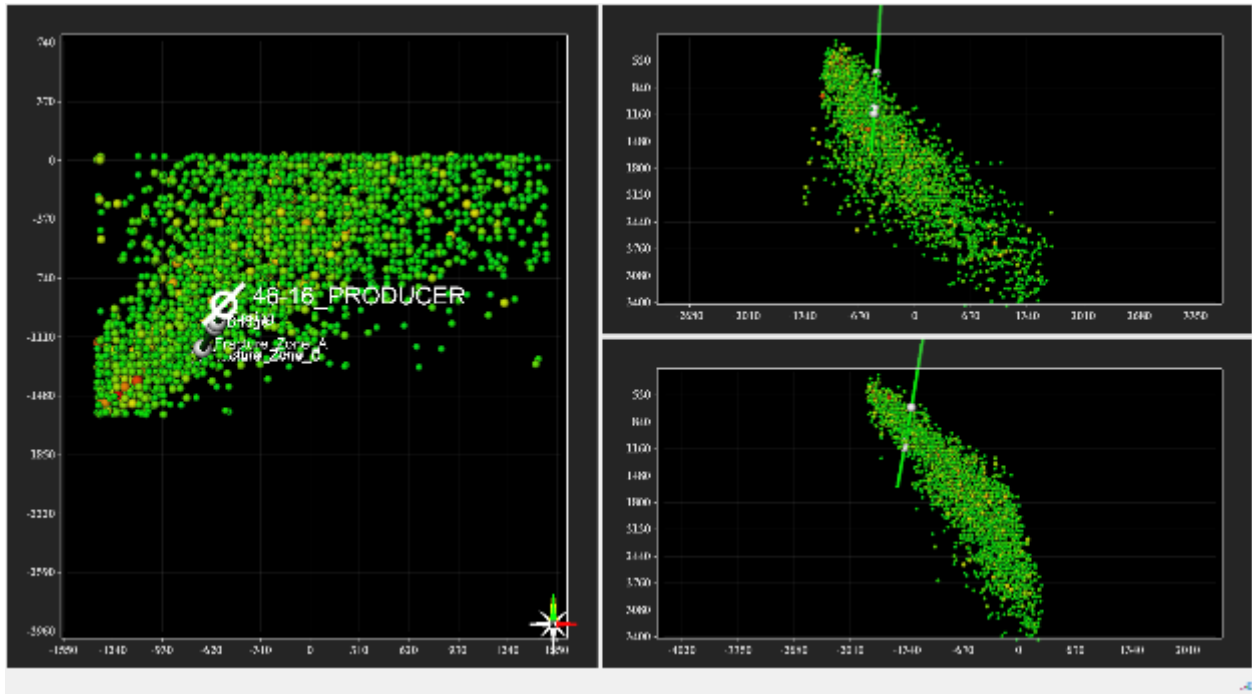


Figure 10 - 14:53 local time. Perspective is North Up. Same perspective as Figure 14, however visualized using conventional spheres with gridded amplitudes colored by relative intensity of coherent amplitudes. This corresponds to time 43 minutes after opening of the valves. One notes from this perspective that there is a consistent LASEA response. We see activity at Fracture Zones A, B & C.

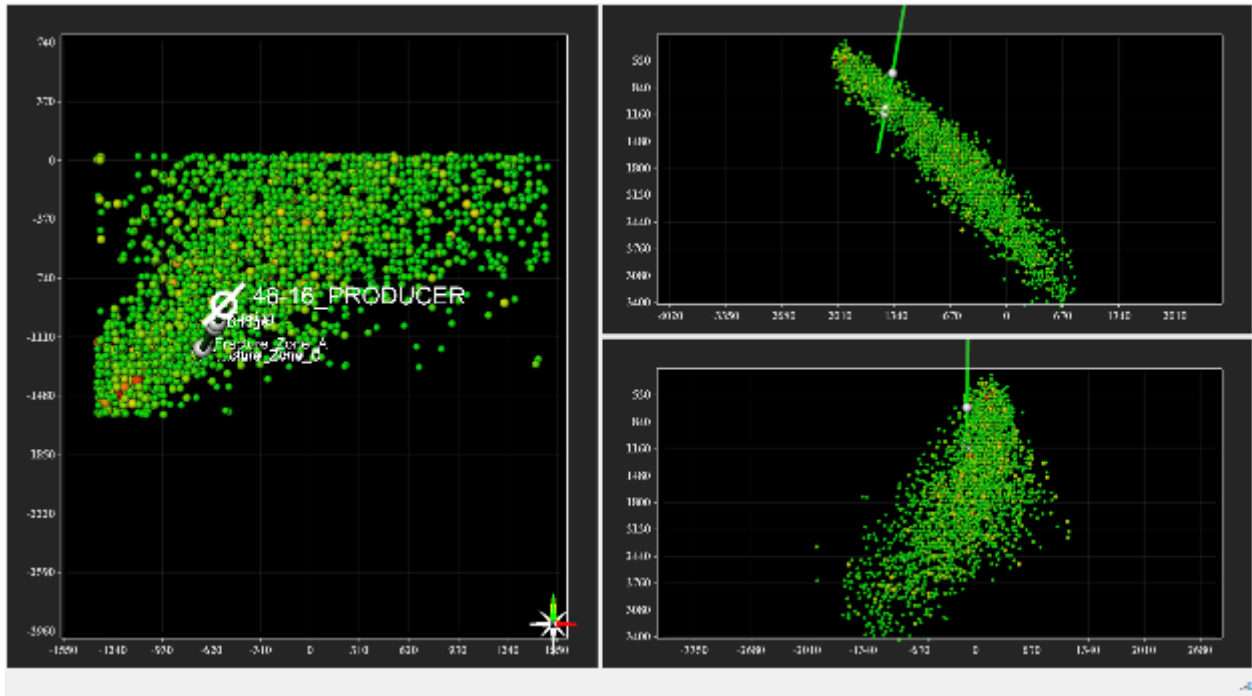


Figure 11 - 14:53 local time. Perspective rotated to maximize view of Fracture Zones A, B & C. Visualized using conventional spheres with gridded amplitudes colored by relative intensity of coherent amplitudes. This corresponds to time 43 minutes after opening of the valves. One notes from this perspective that there is a consistent LASEA response. We see activity at Fracture Zones A, B & C.

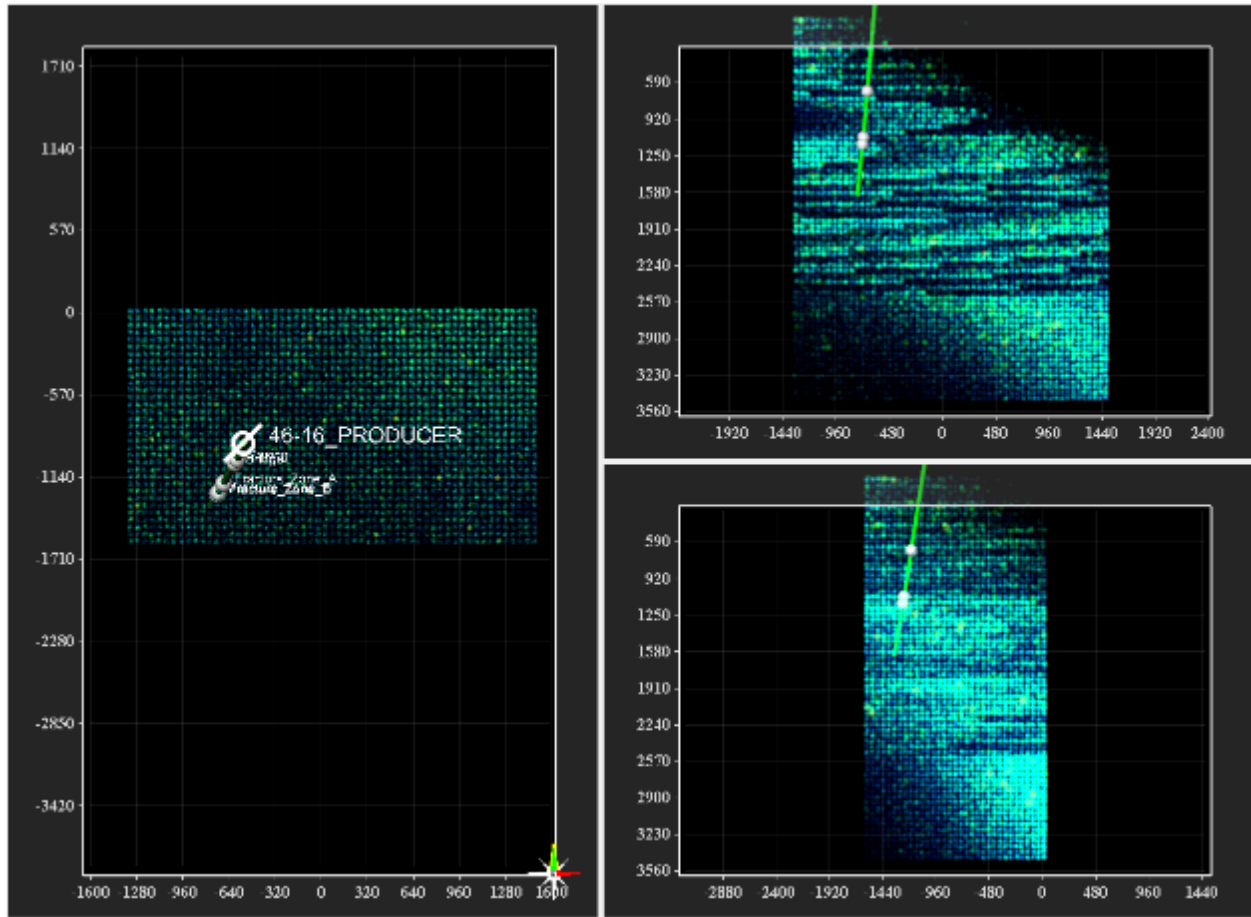


Figure 12 - 18:24 – local time. Perspective is North Up. Visualized using Hotspot technology. This corresponds to the LASEA response just at the time of shut-in (18:35) local. One clearly sees the highest intensity response at Fracture Zones B & C.

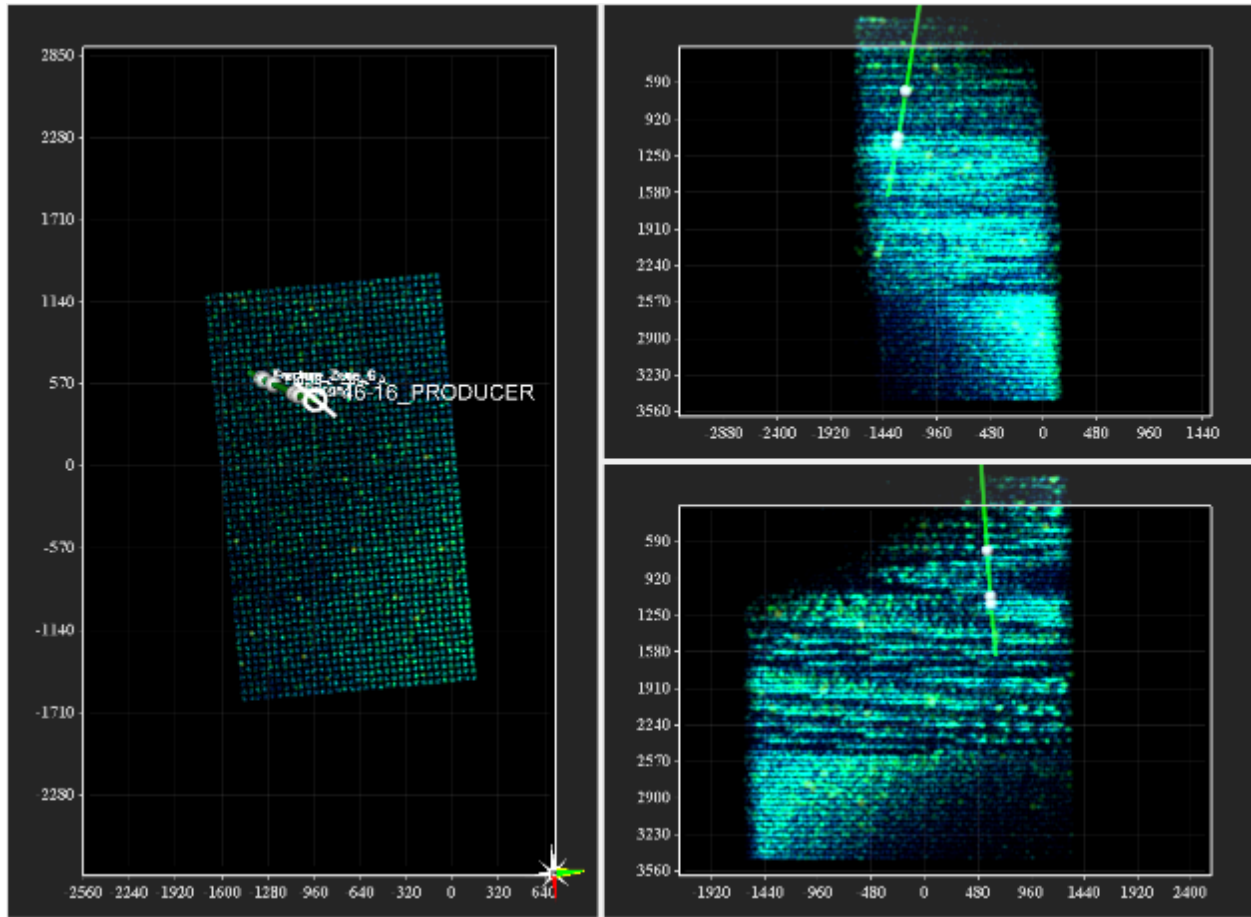


Figure 13 - 18:24 – local time. Perspective is West Up. Visualized using Hotspot technology. This corresponds to the LASEA response just at the time of shut-in (18:35) local. One clearly sees the highest intensity response at Fracture Zones B & C.

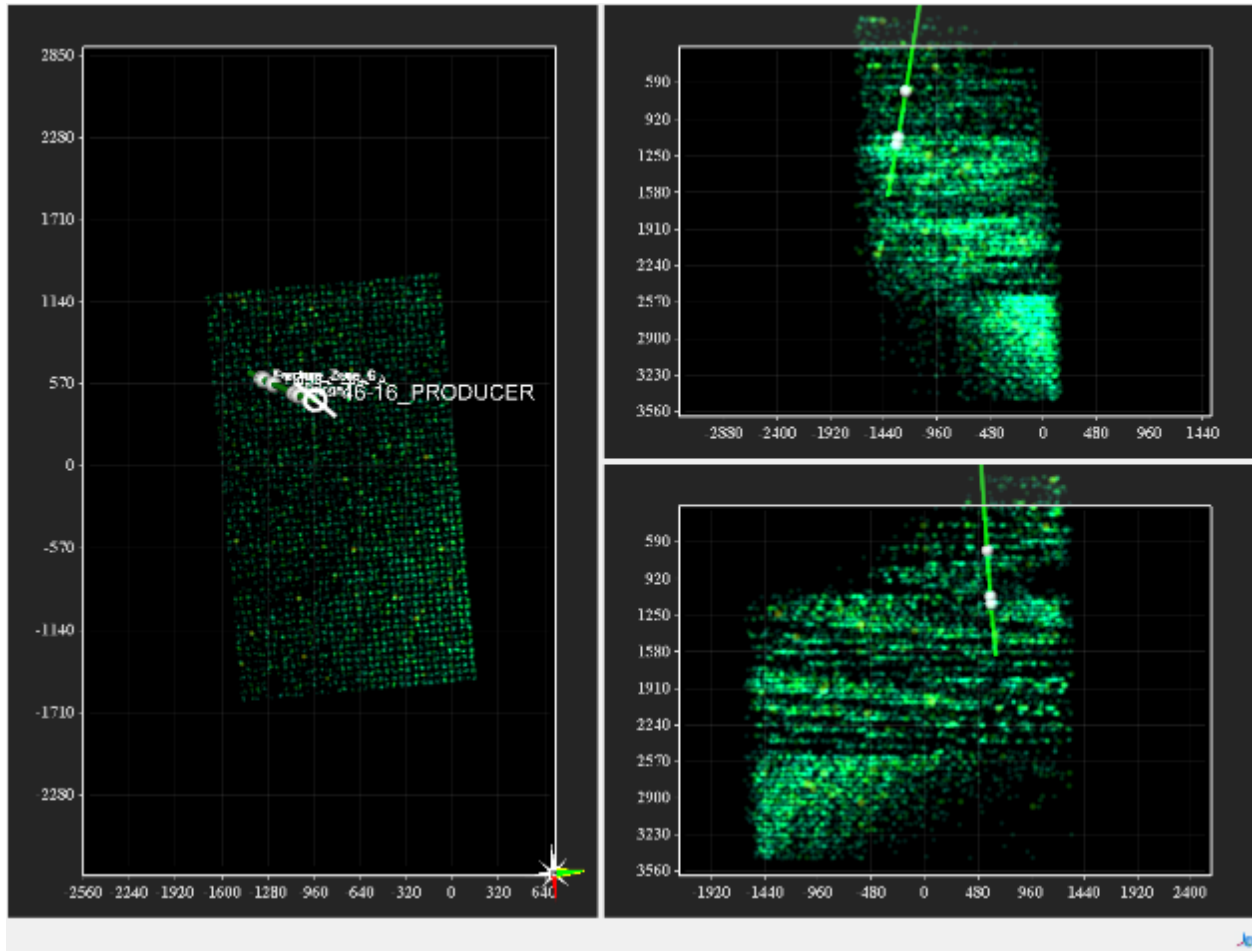


Figure 14 - 18:24 – local time. Perspective is West Up. Visualized using Hotspot technology with 50% top energy. This corresponds to the LASEA response just at the time of shut-in (18:35) local. One clearly sees the highest intensity response at Fracture Zones B & C.

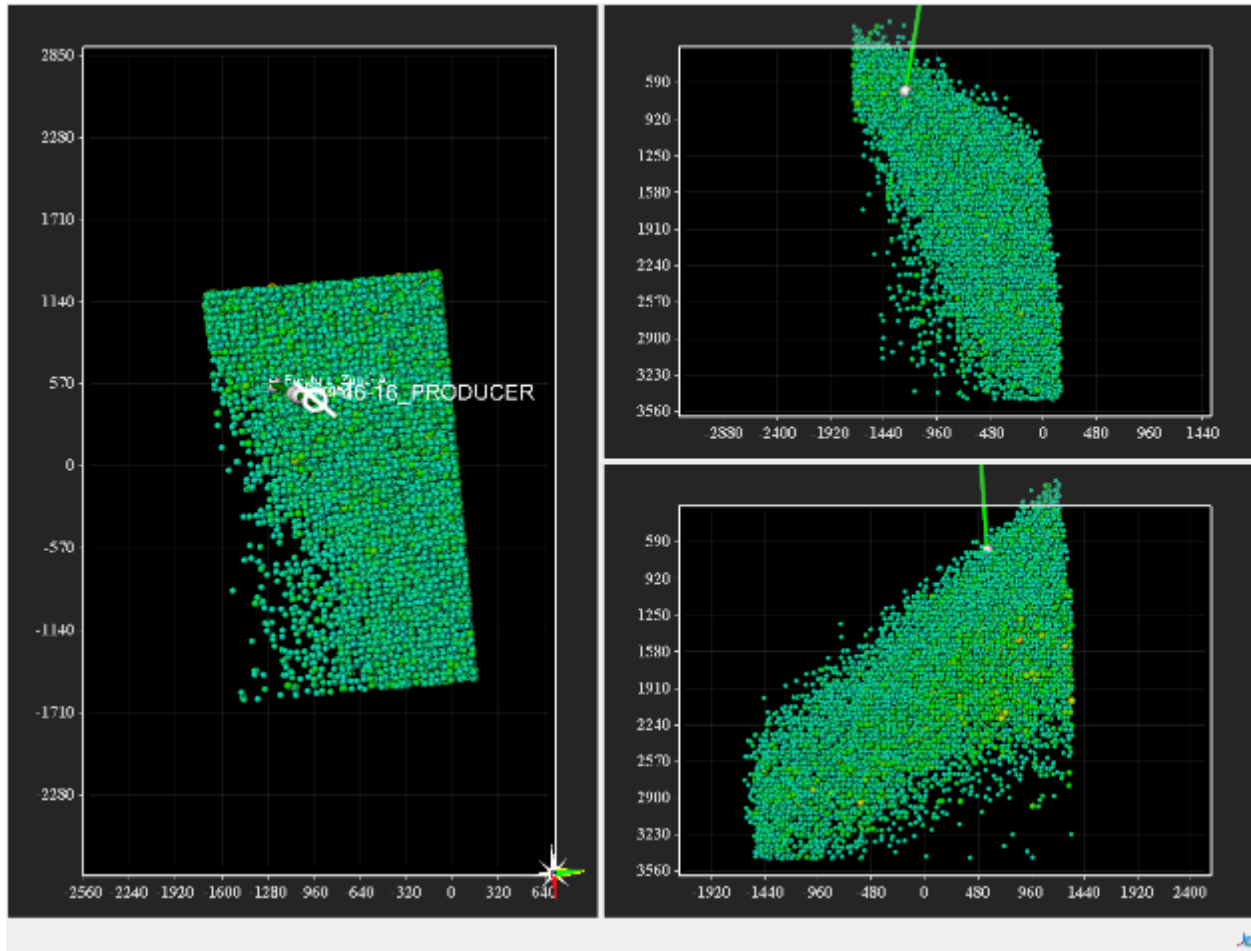


Figure 15 - 18:24 – local time. Perspective is West Up. Visualized using conventional technology. This corresponds to the LASEA response just at the time of shut-in (18:35) local. One clearly sees the highest intensity response at Fracture Zones B & C.

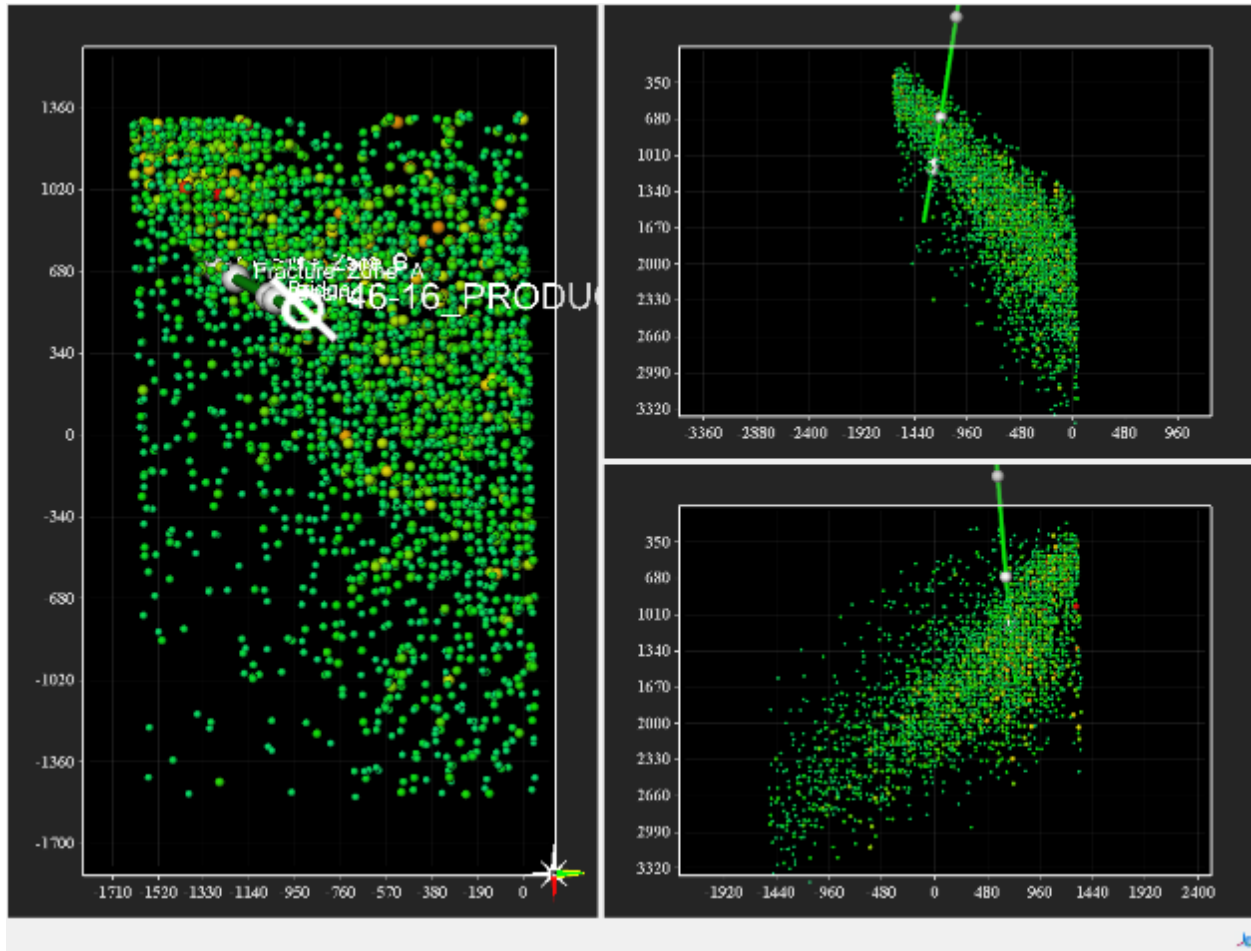


Figure 16 - 22:24 Local time. Perspective is West Up. Visualized using conventional technology. This corresponds to the LASEA response four (4) hours after of shut-in (18:35) local. One clearly sees the highest intensity response at Fracture Zones B & C, with some connectivity to Zone A.

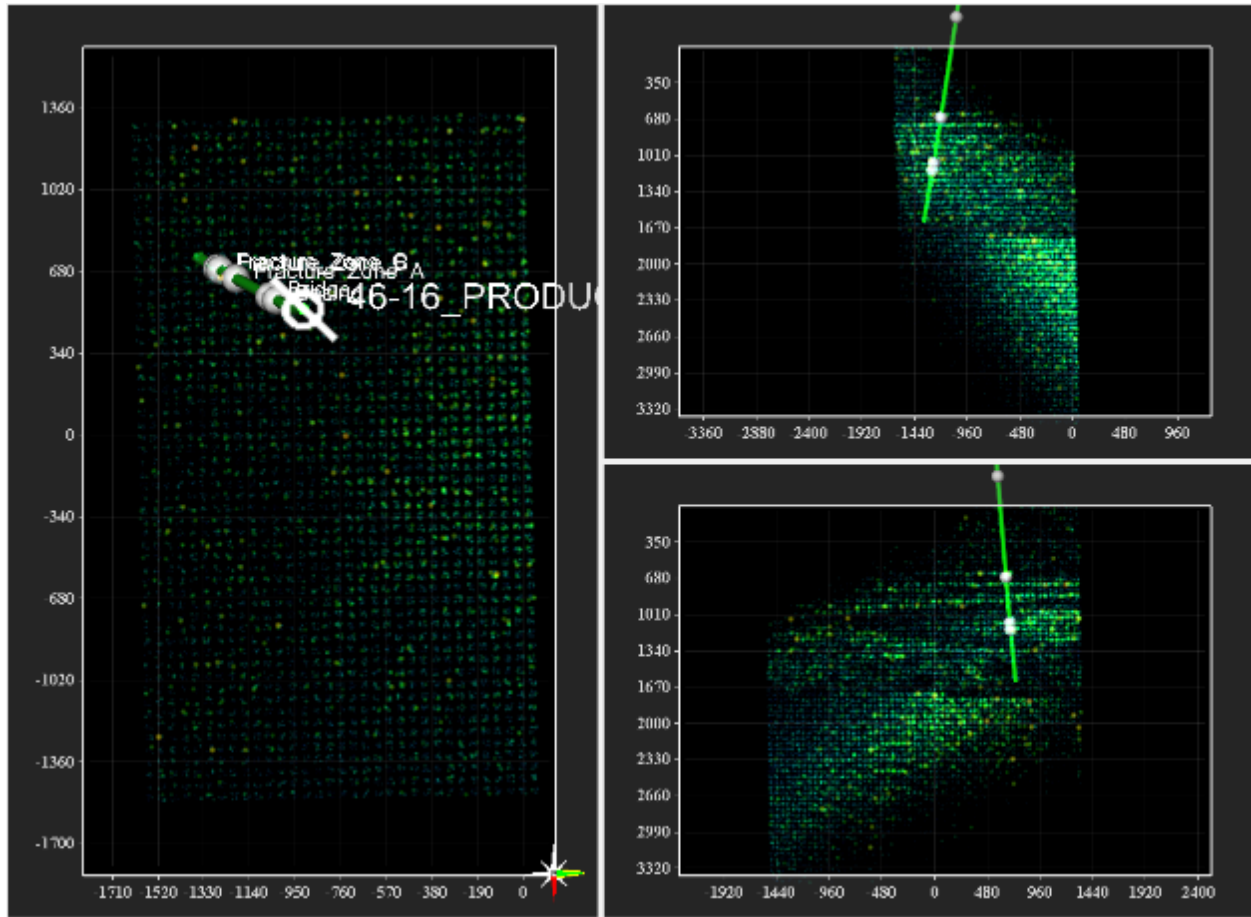


Figure 17 - 22:24 Local time. Perspective is West Up. Visualized using hotspot technology. This corresponds to the LASEA response four (4) hours after of shut-in (18:35) local. One clearly sees the highest intensity response at Fracture Zones B & C, with some connectivity to Zone A. Note that hotspot potentially hi-lights subtle geological features. In the absence of an integrated geological model this is speculation.

3.6 SEPTEMBER 9TH 2013

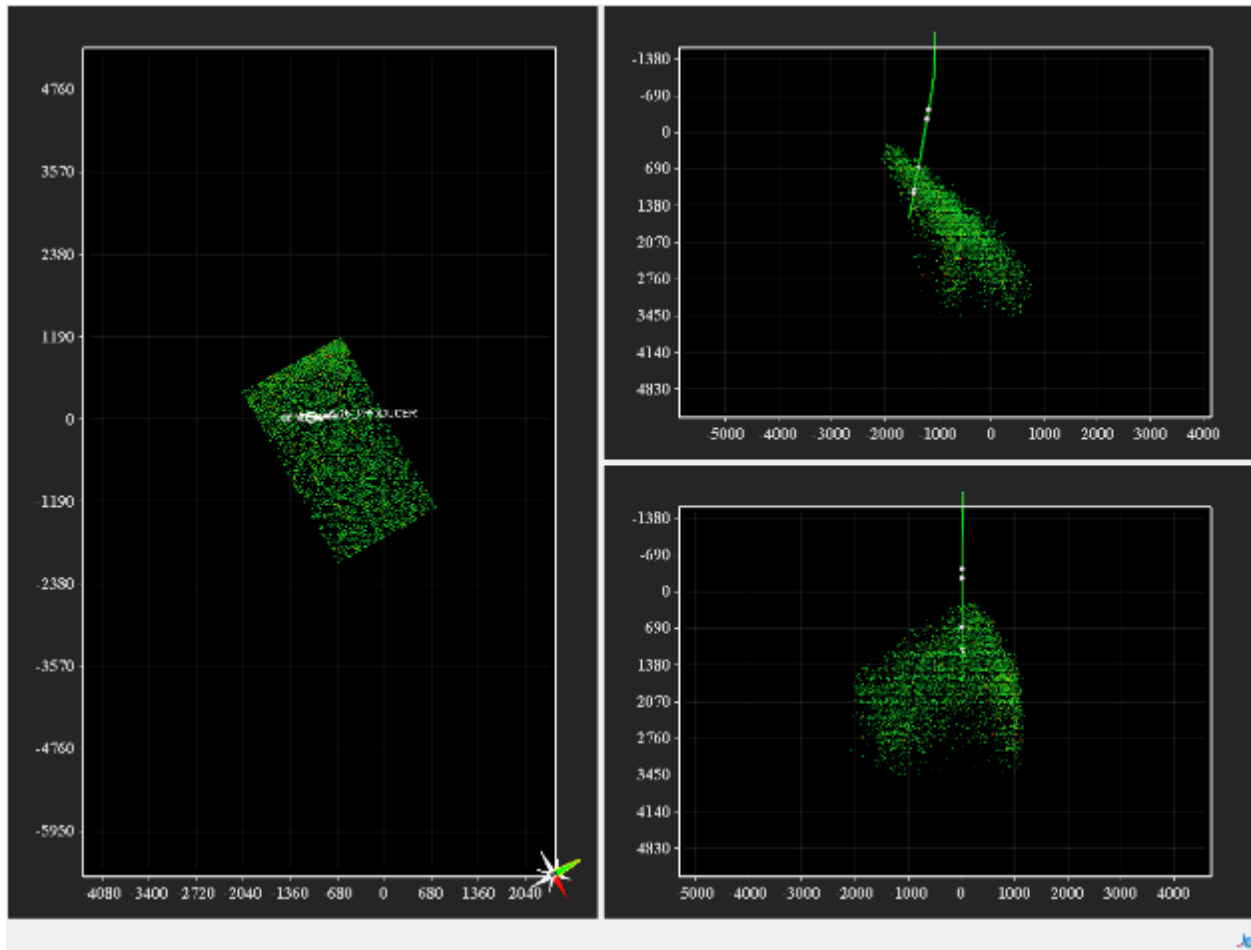


Figure 18 - 8:43 – Perspective NNW.

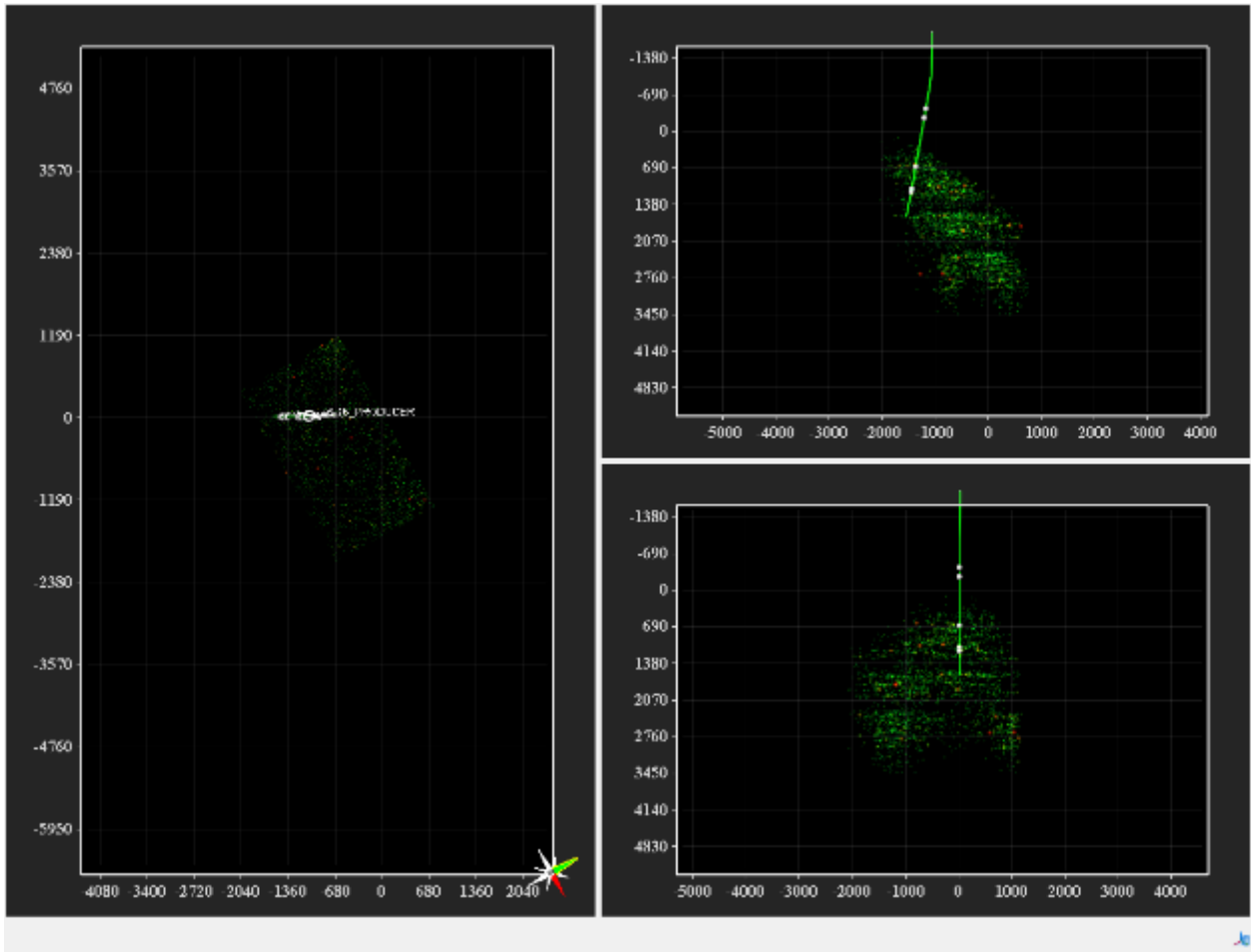
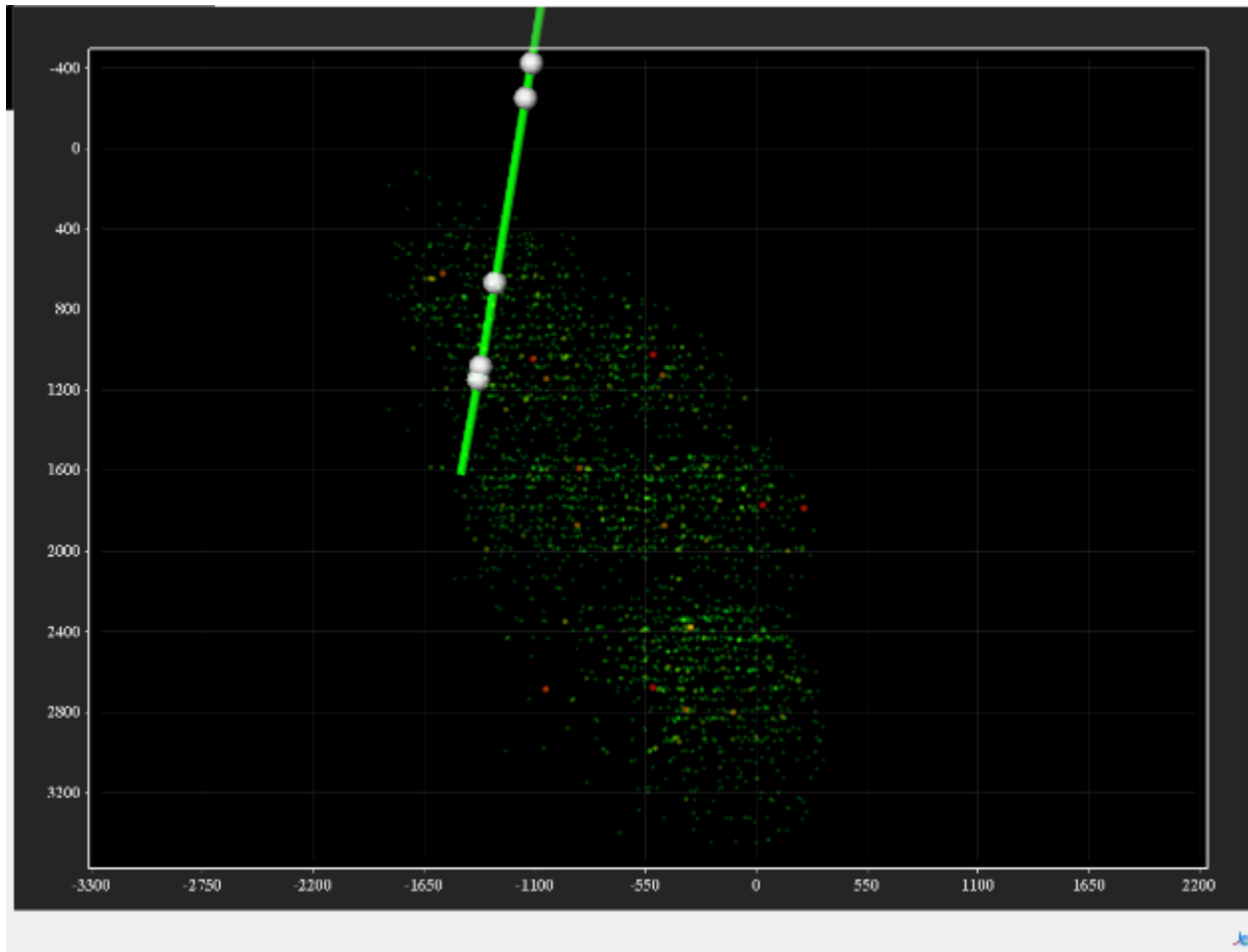
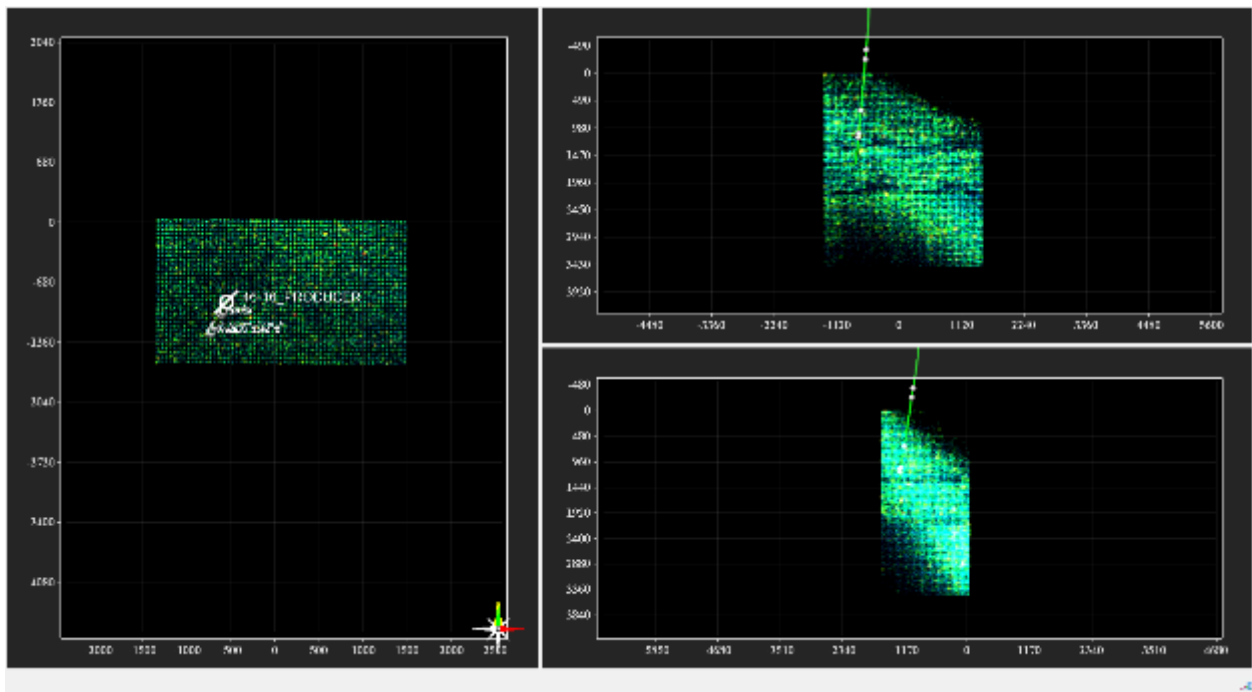


Figure 19 - Hotspot. NNW. prior to flow

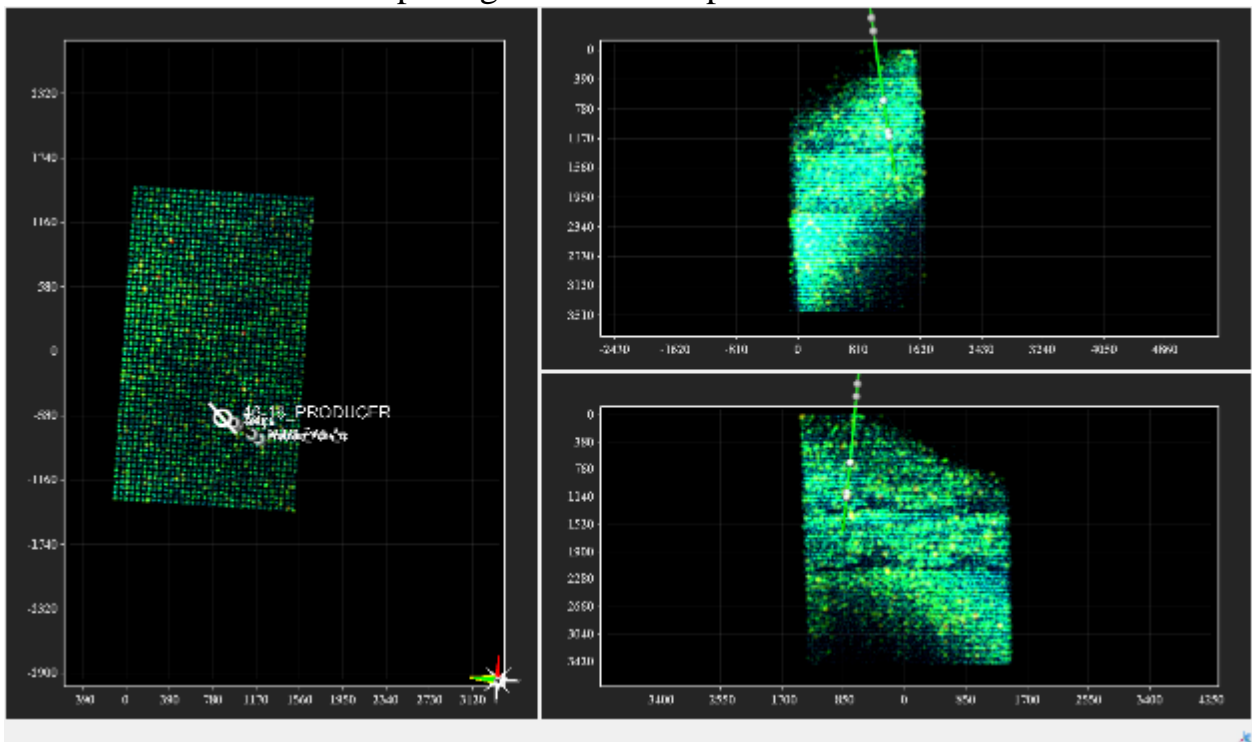


Zoomed view prior to opening flow.

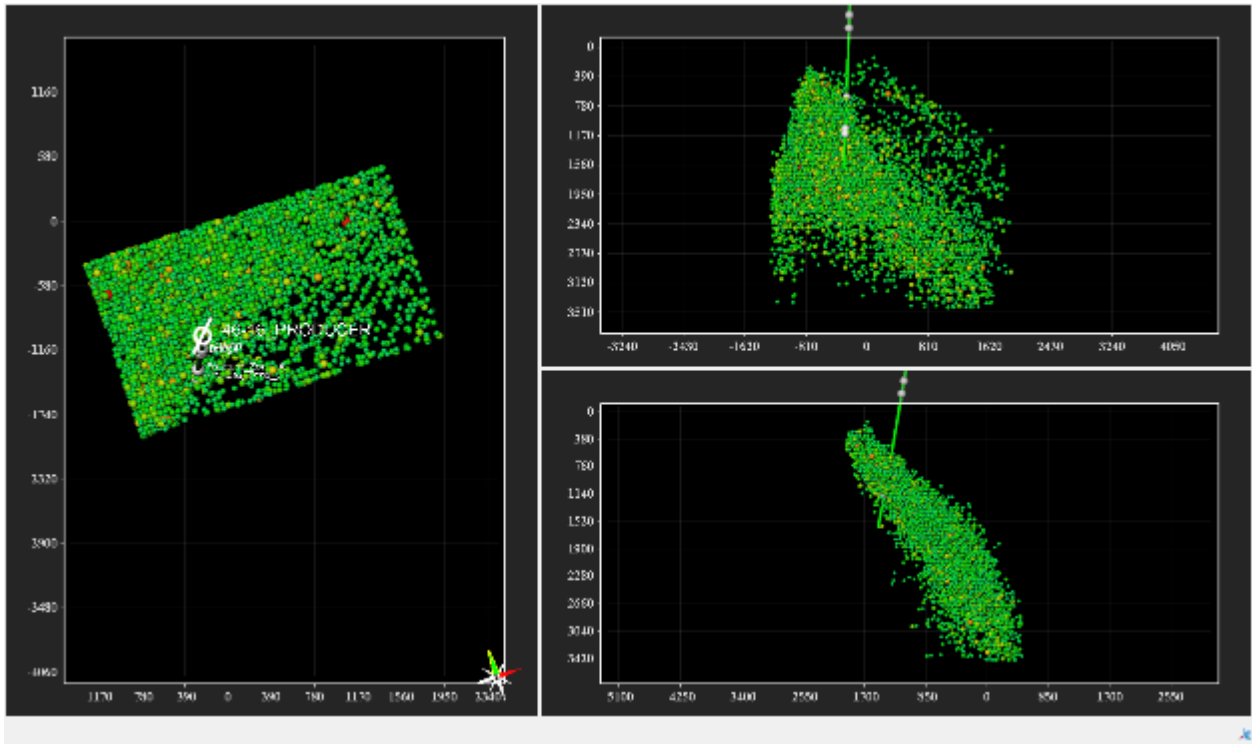
1010 Open well to moderate flow to purge line and sample bottle.



10:44 – 34 minutes after opening well. North up



10:44 – 34 minutes after opening well. E up



10:44 – 34 minutes after opening well. NNE – regular view

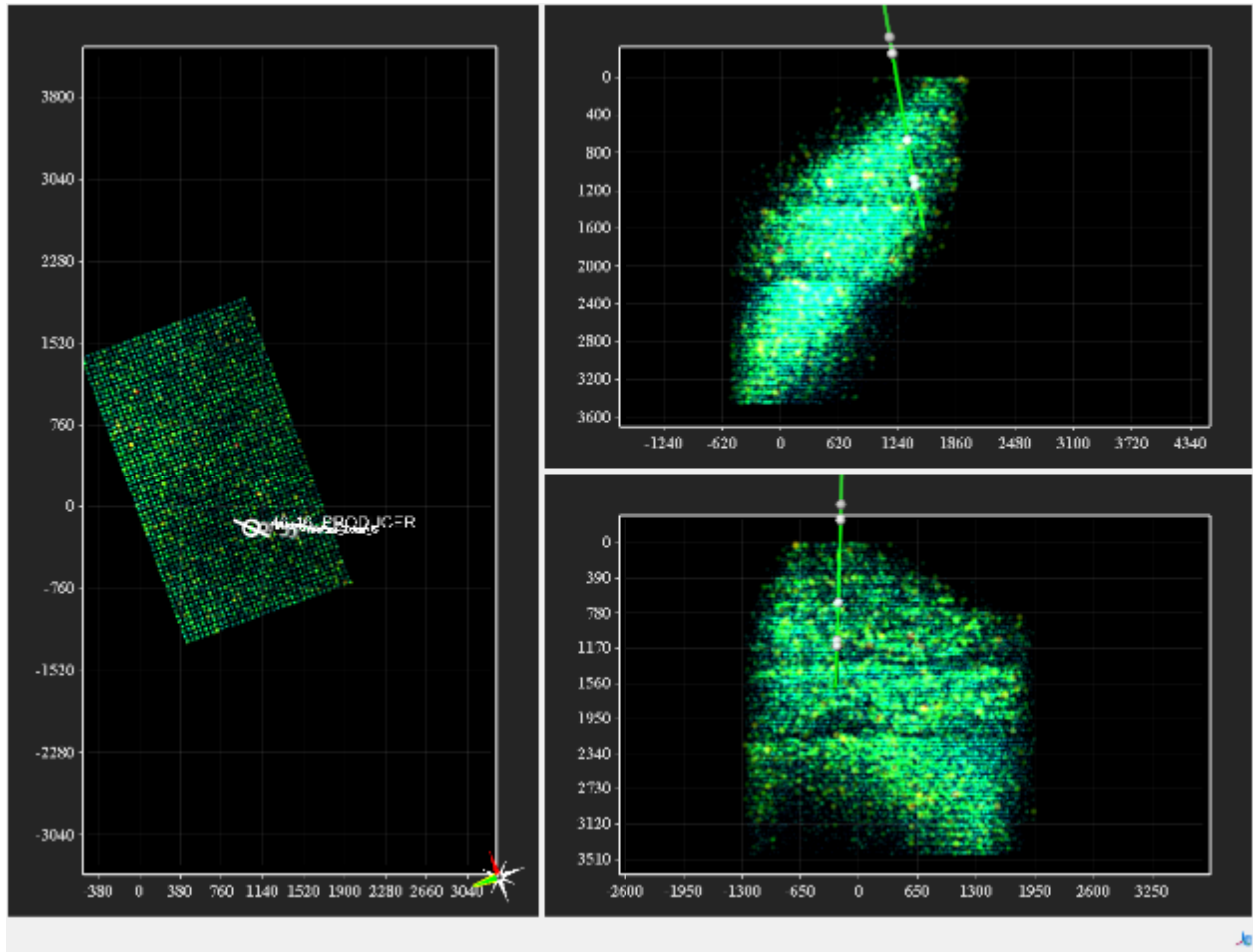
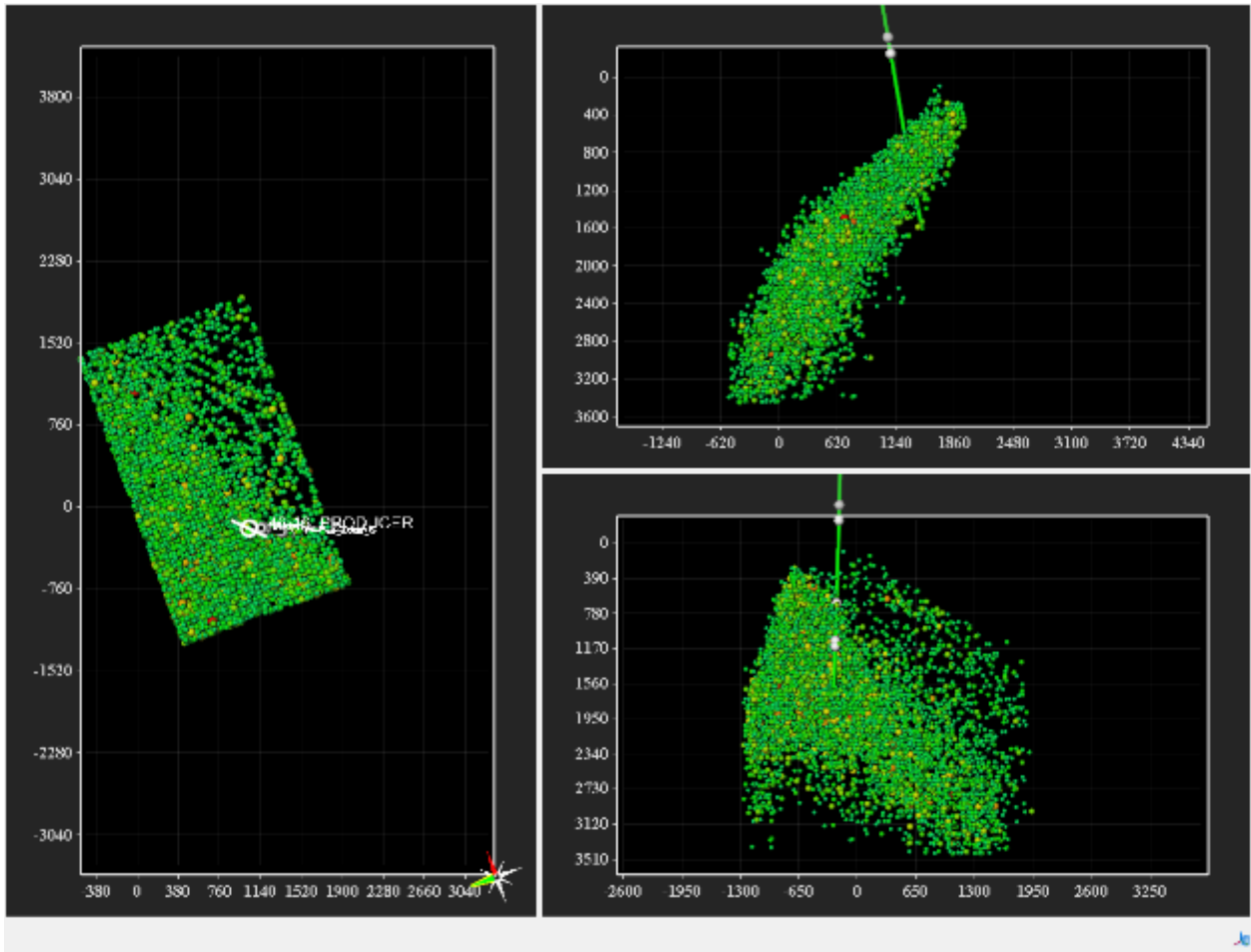
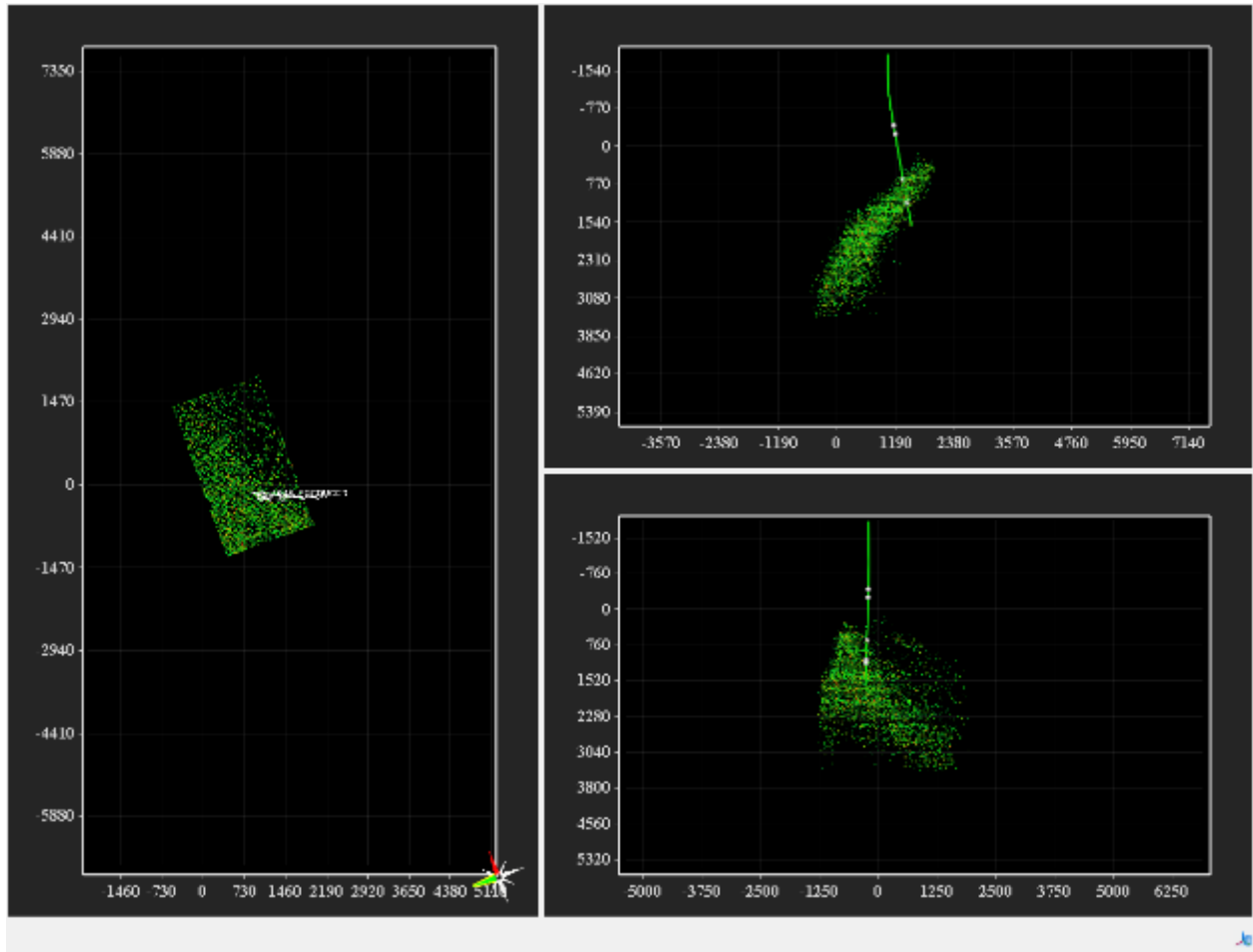


Figure 20 - 12:14. 30 minutes after total liquid flow at 11:44

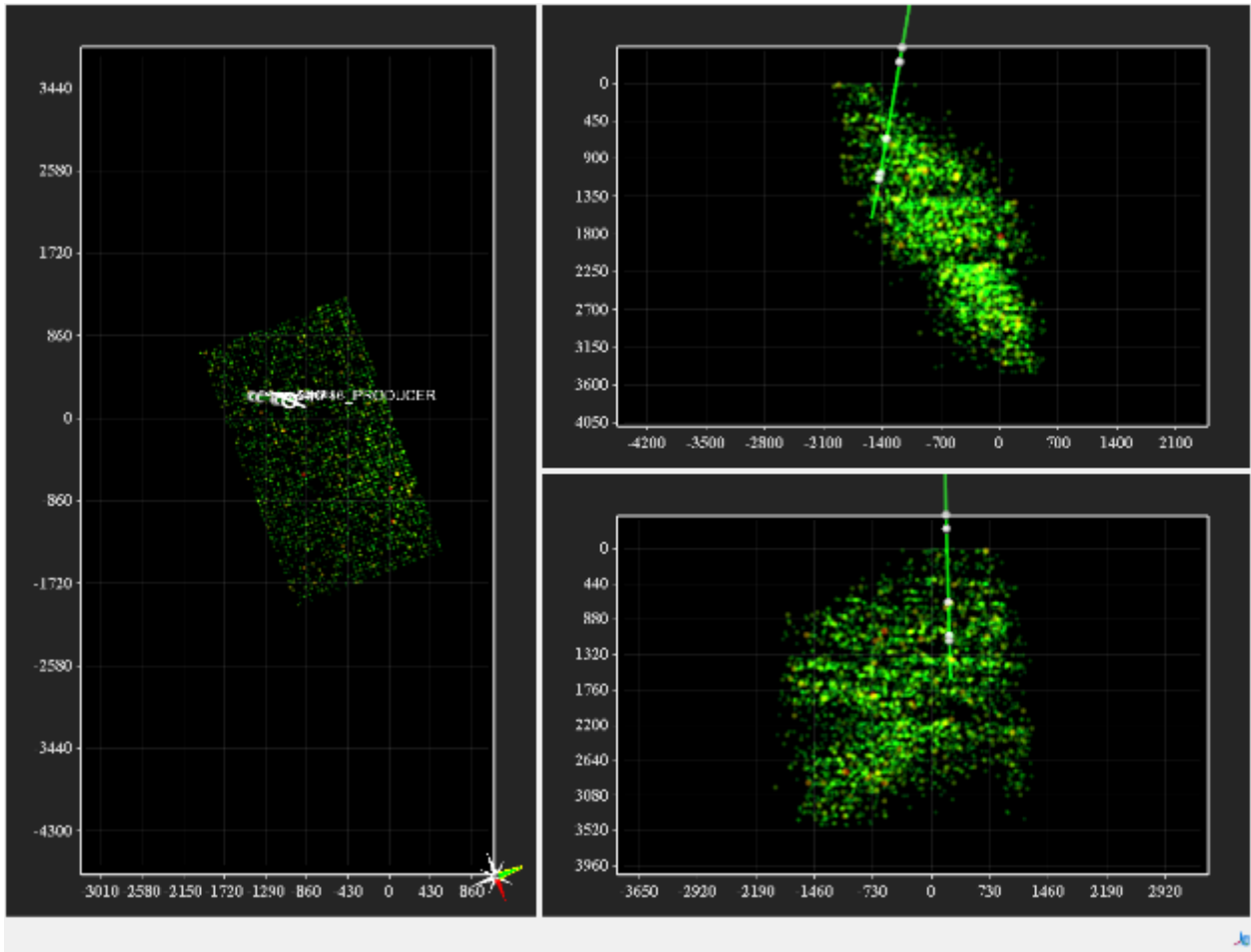


12:14. 30 minutes after total liquid flow at 11:44. Regular visualization. View slightly east of north

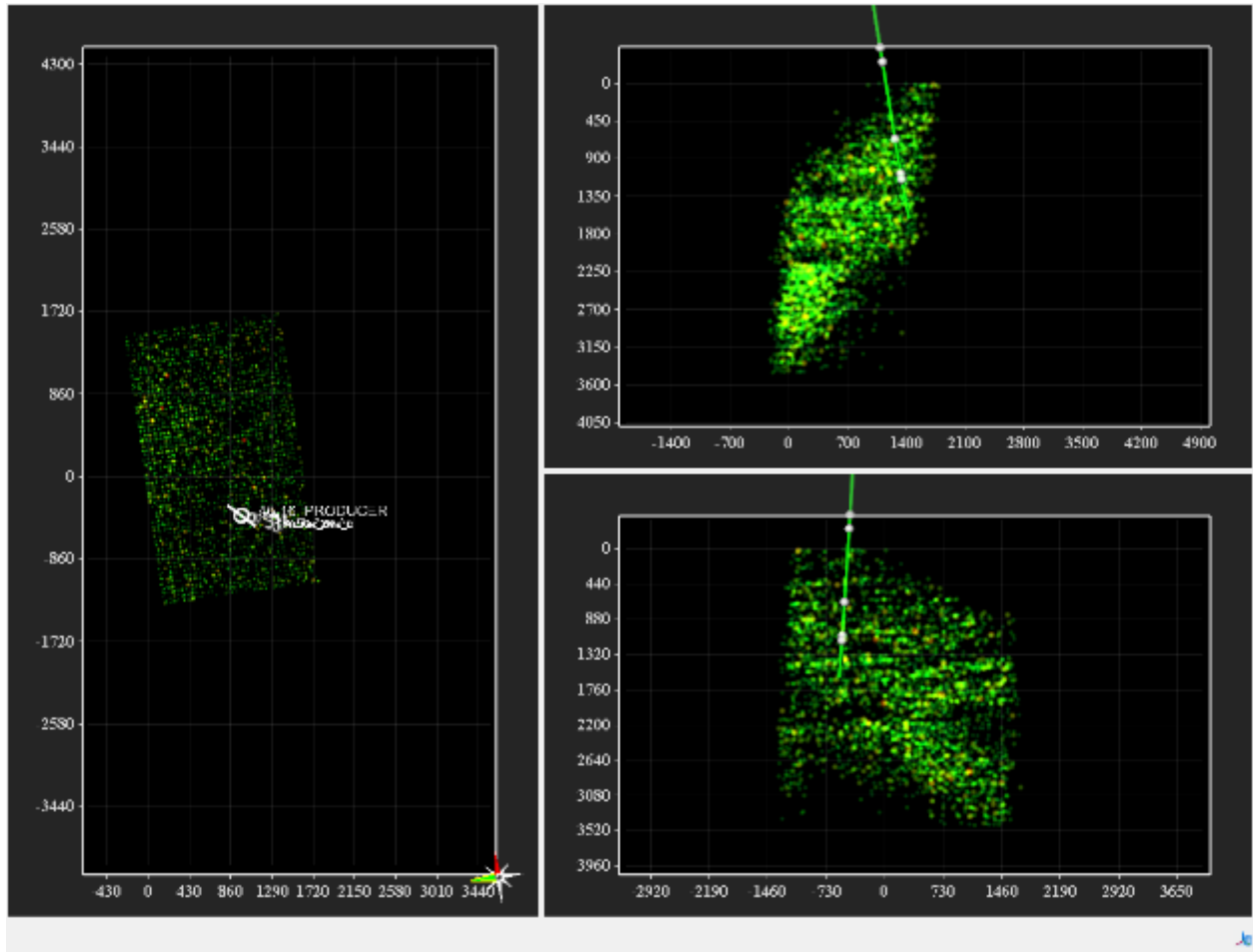
1700 Shut in well.



Slightly east of north. 3 hours and 15 minutes after shut in at 17:00. 20:14 local time.

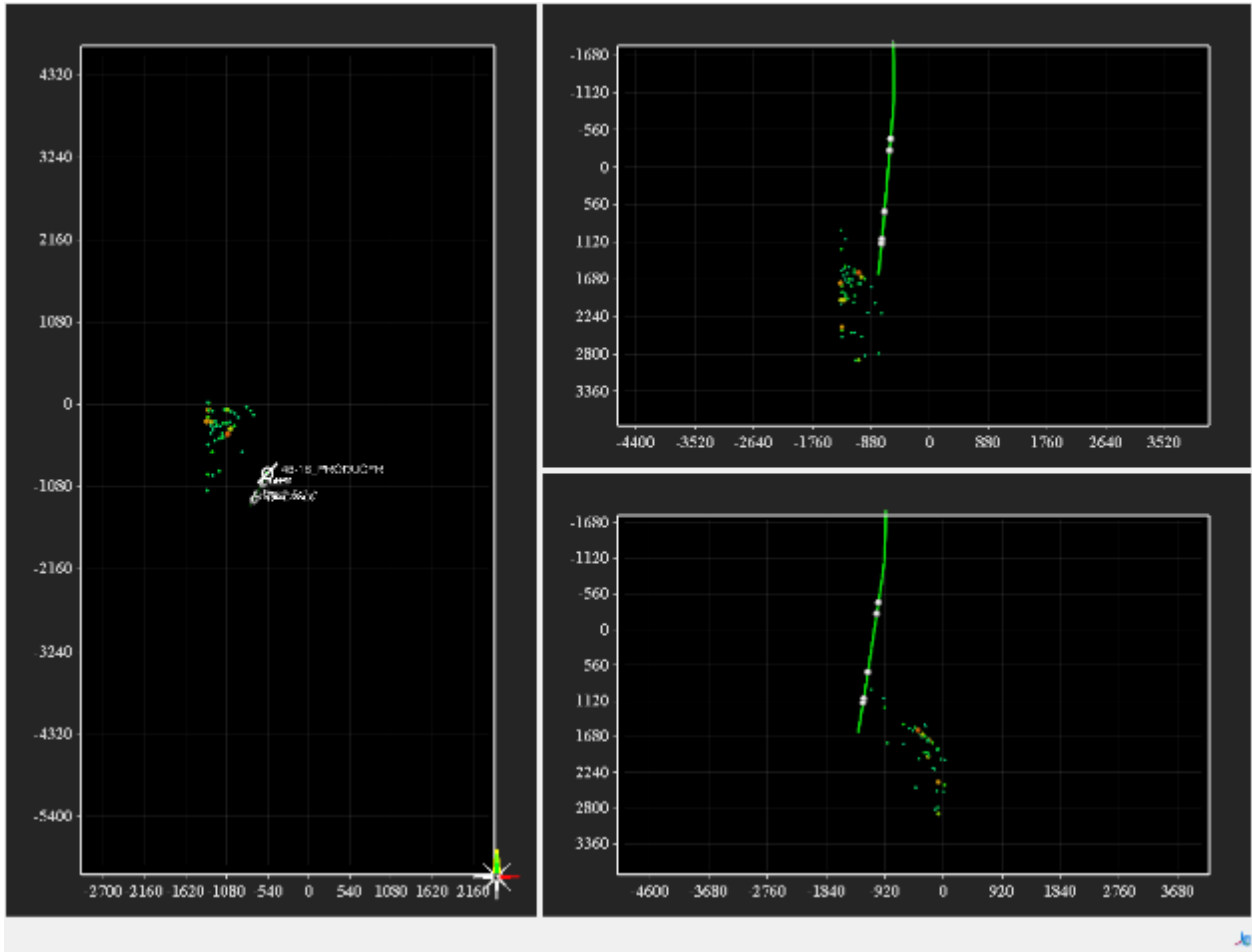


West up. 3 hours and 15 minutes after shut in at 17:00. 20:14 local time



East Up. 3 hours and 15 minutes after shut in at 17:00. 20:14 local time

3.7 SEPTEMBER 10TH 2013



North Up. Traditional view. 0800 local. Prior to injection,

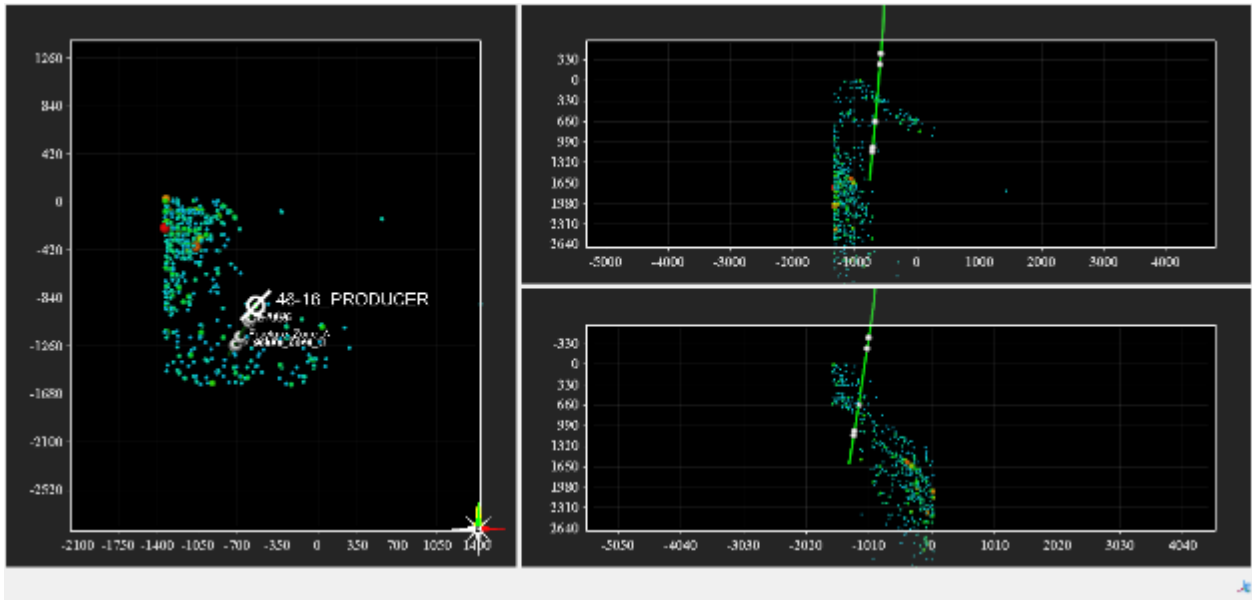


Figure 21 - 14:34. Shut well in at 14:14 to attach gas sample bottle. North Up. Top 50% energy.

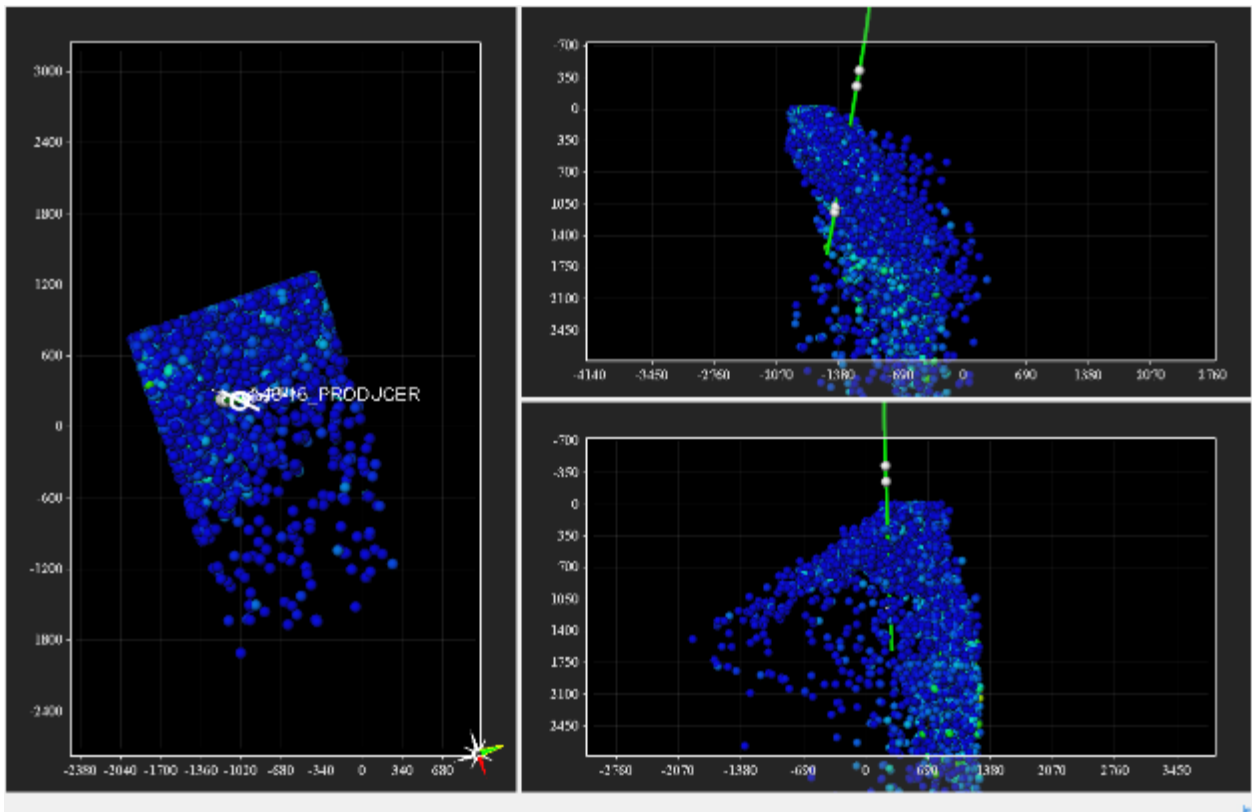
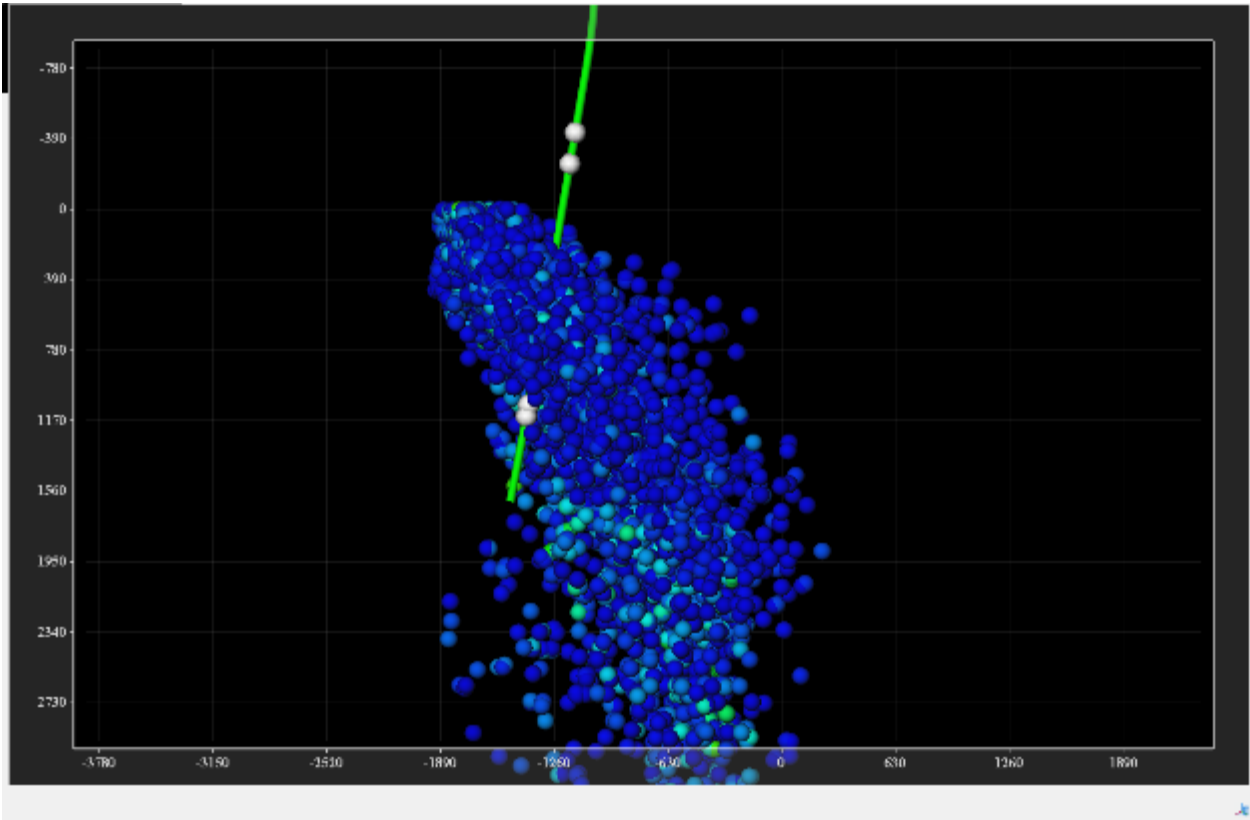
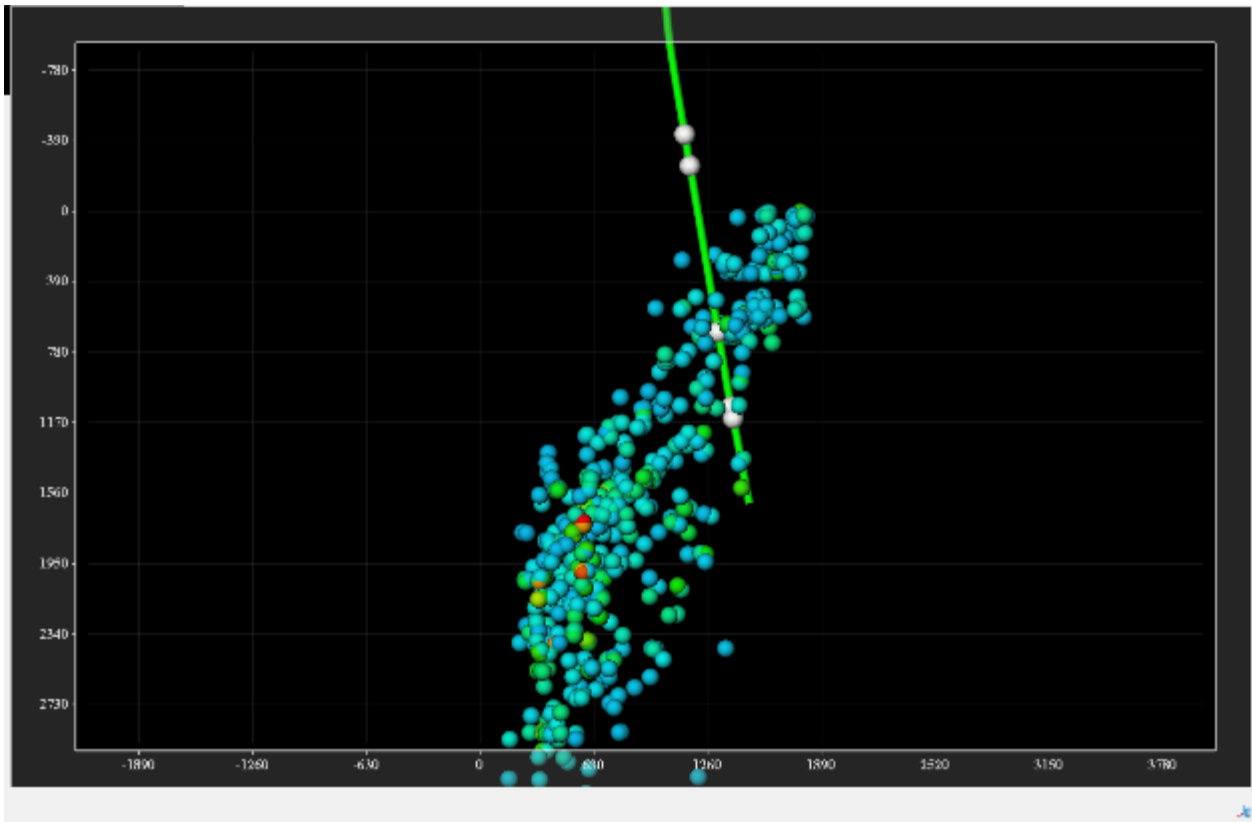


Figure 22 - 14:34. Shut well in at 14:14 to attach gas sample bottle. North Up. Top 90% energy.



Maximal response at Fracture Zones B and C.



Top 50% energy. Zoom into Fracture Zones B and C.

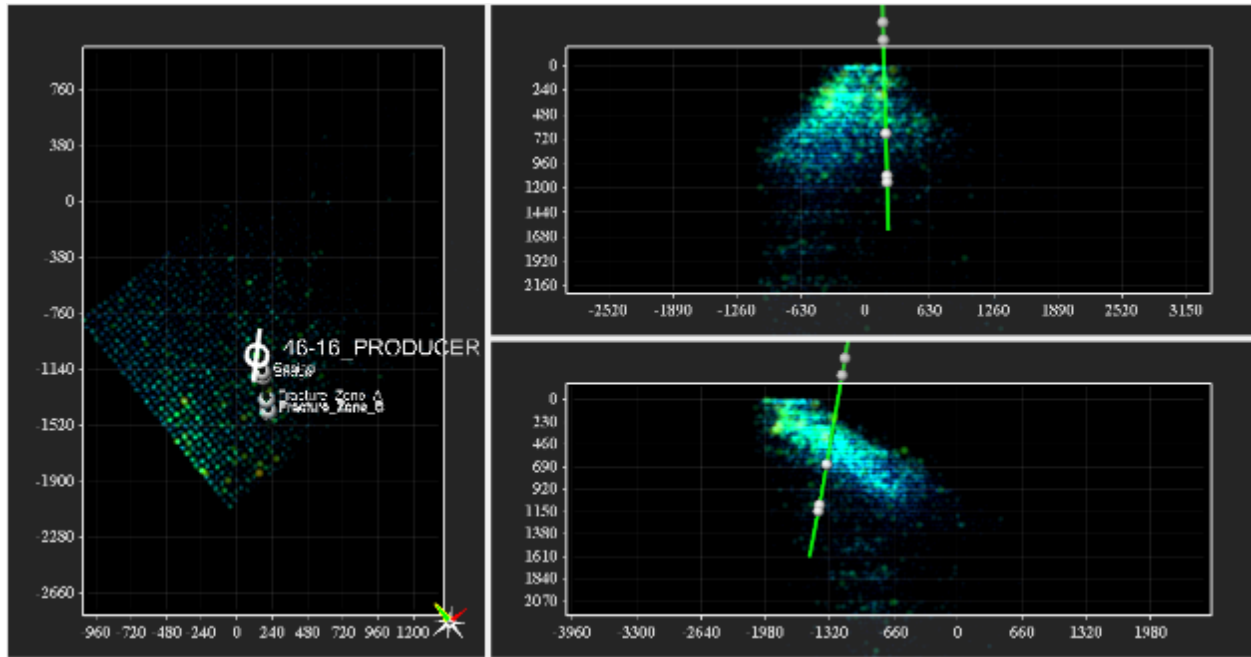


Figure 23 - 17:16. Slightly east of north. After shut in.

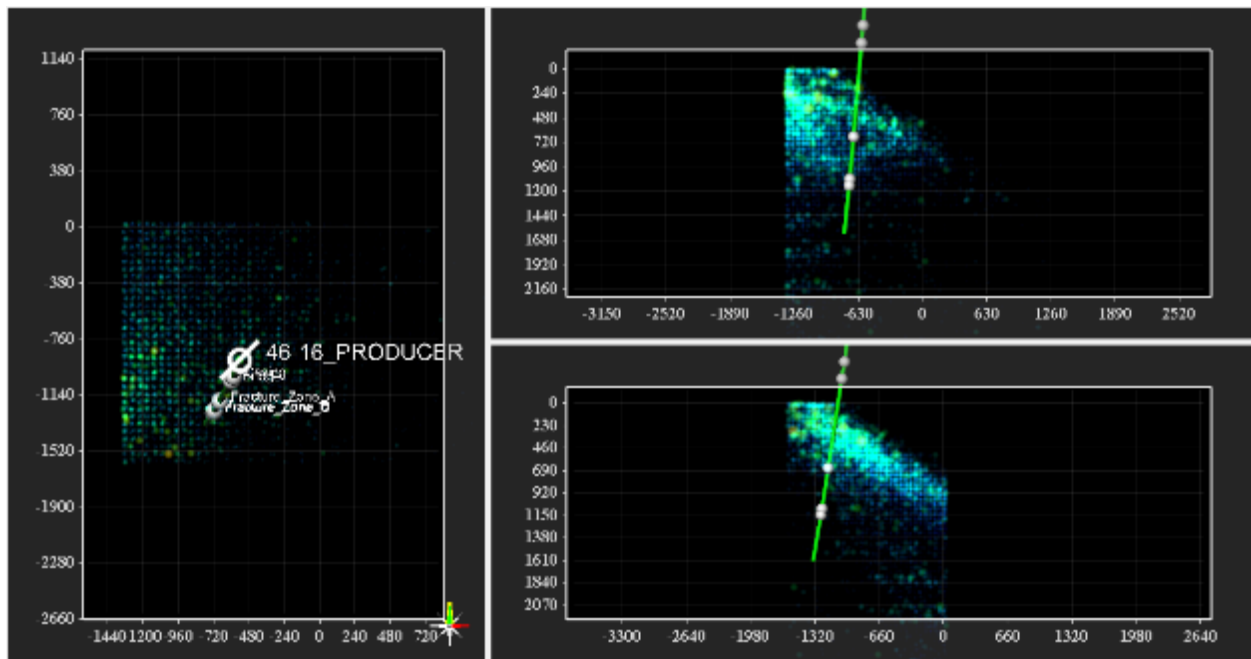


Figure 24 - 17:16. North up. After shut in.

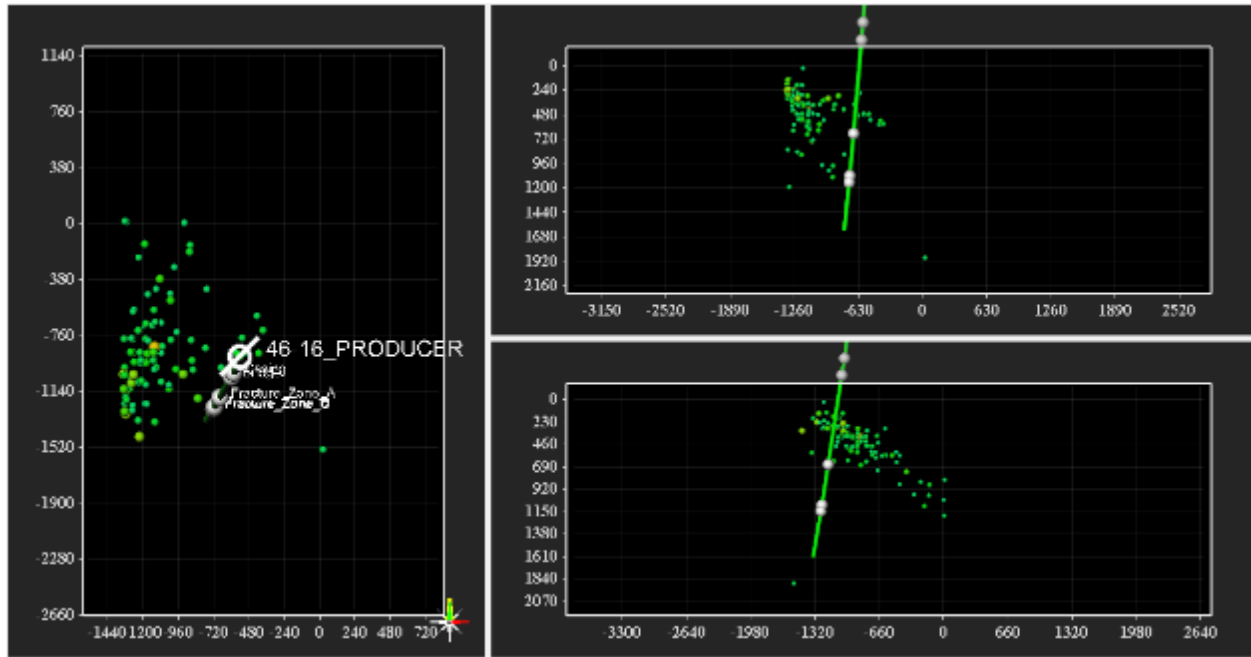


Figure 25 – 17:16 after shut in. Top 50%

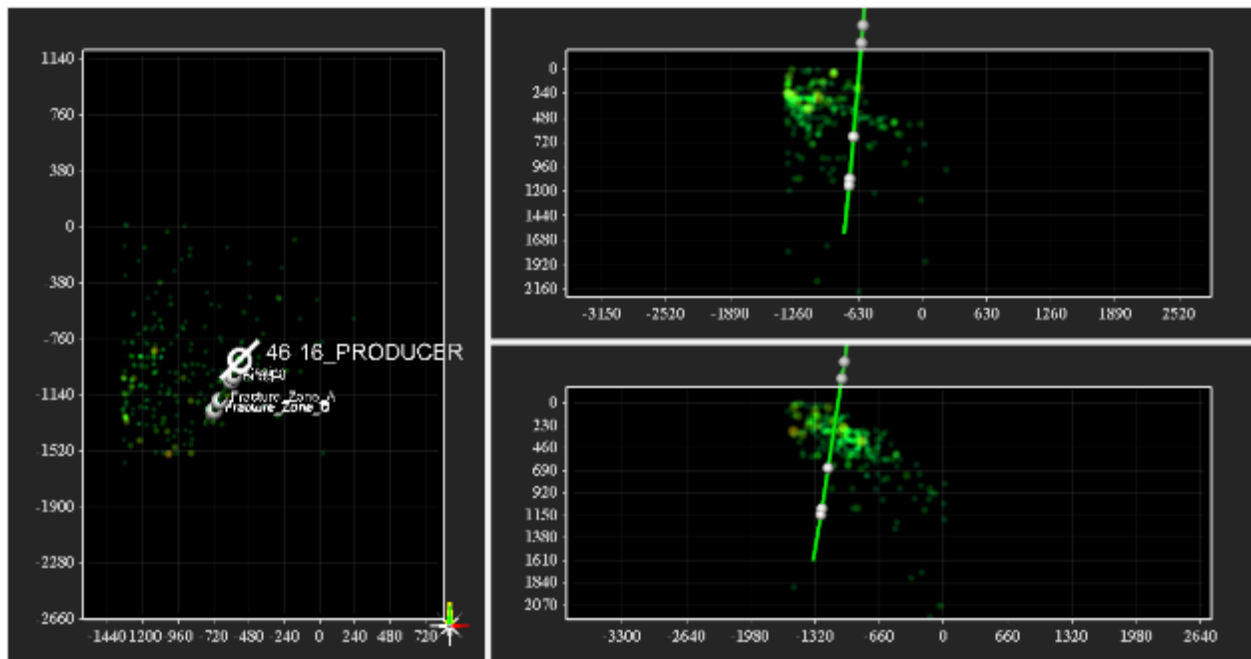


Figure 26 - 17:16 after shut in. Top 50%. Hotspot

4 PAD 55-29 INJECTION ANALYSIS

This section provides a detailed discussion of results for the 55-19 injection Newberry passive seismic project conducted for Altarock in September, 2013 by S3. Seismic energy computations were made for a single horizontal plane an elevation of -1250 m (-4101 feet) relative to mean sea level. This elevation equates to approximately 10,000 feet below the mean surface elevation in the area of interest.

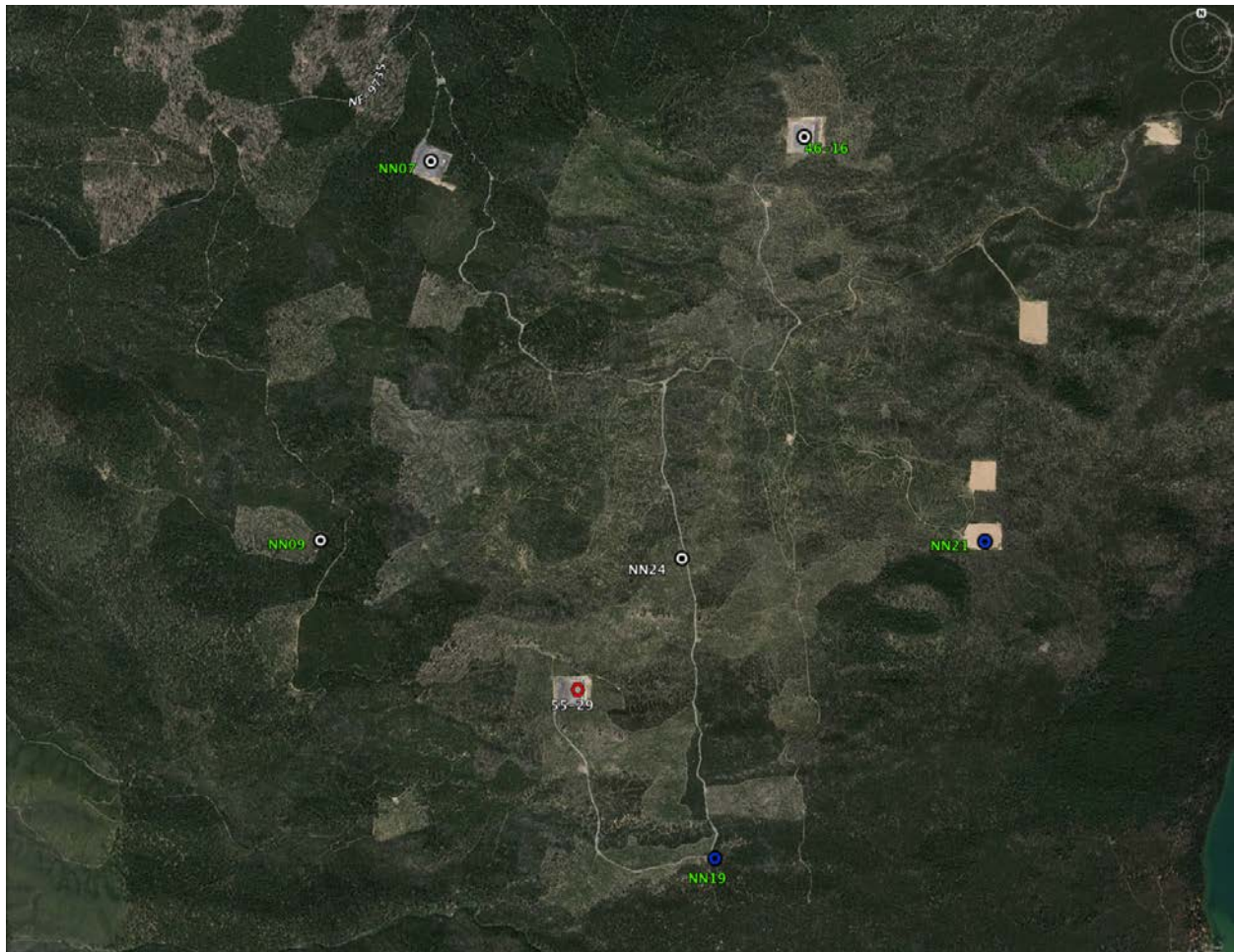


Figure 27 – Location of 55-29 injection well in relation to seismic monitoring stations and the 46-16 well

The following figure provides an example of processed data captured and analyzed during the 55-29 segment of the program. This event occurred September 11, 2013 at 54 minutes after midnight local time (09:53 GMT). Water injection had been underway for the previous 16 hours when this event occurred. The water injection rate was about 138 gpm and surface pressure 400 psi at the time of the event.

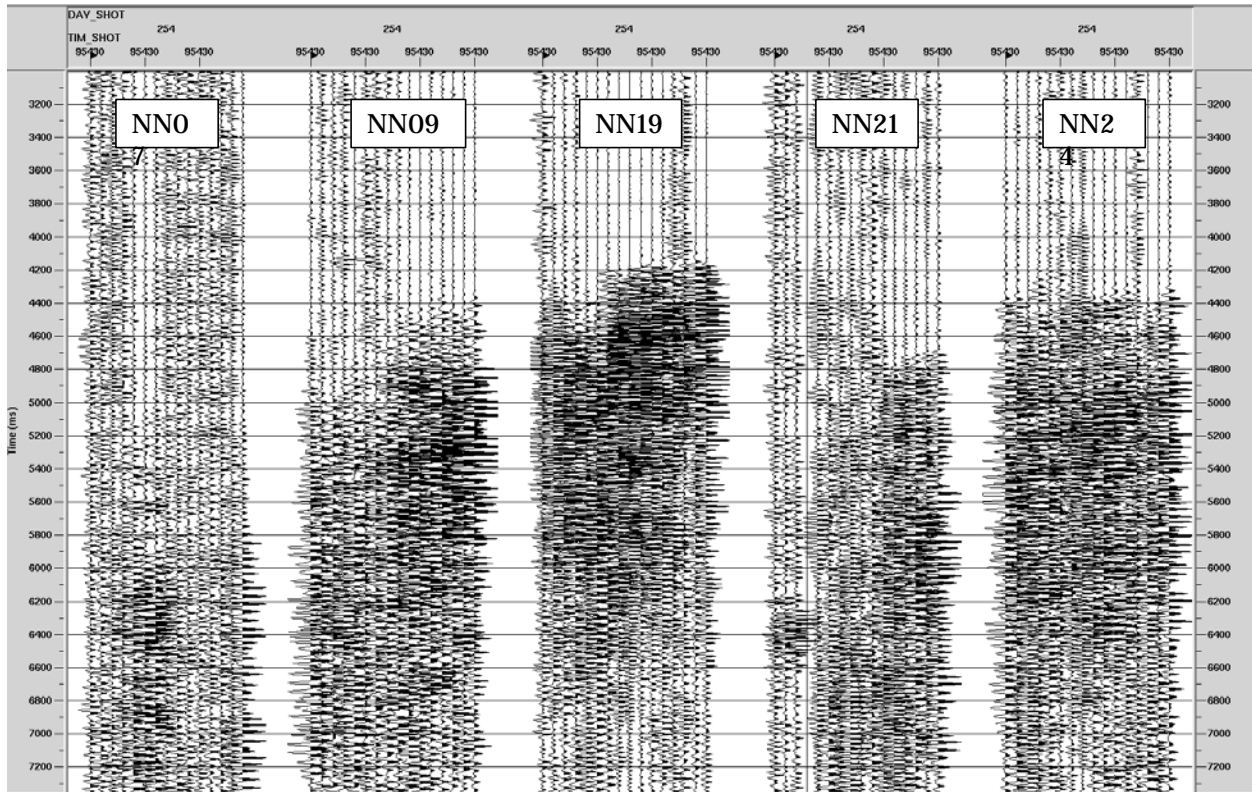


Figure 28 The data shown is the vertical component with an Ormsby bandpass filter applied with parameters 15-21-36-48 Hz. While the arrivals are indistinct relative to arrivals we see in oil and gas microseismic data, the travel times are precise enough to see that this event occurred nearest to well NN19. A first order estimate of the location is shown on the next slide. The differences in event arrival times indicates that this event occurred at less than 1,000 m depth.



Figure 29 Approximate location (X/Y) of discrete microseismic event

The following figures show seven (7) separate time periods in which the highest level of seismic activity occurred in the study area measured at an elevation of -1250 m (msl). The analysis was carried out on a 2D grid plane at elevation -1250 m with a 200 m grid spacing in both the North-South and East-West direction. The grid plane was 6 km by 6 km centered near the middle of the 5 observation wells. The highest seismic activity zones are mostly located near the 55-29 well though there are some variations.

The time periods of the 7 period of highest activity are shown on the time scale at the bottom of each display. The radius of spheres on the following displays are proportional to the energy measured within each time period shown. The values plotted range from 9,000-24,000 energy units that are internally consistent but the number range itself is arbitrary. In other words there is no meaning in comparing these numbers to any other power or energy measurement in seismology outside of this dataset.

When the spheres are large there was a larger amount of seismic energy detected at the grid node and when they are small there is a smaller amount of energy detected. The smallest amounts of energy detected on some grid nodes were zero so the grid nodes shown showed energy levels that were many-fold over the lowest amplitudes. The grid nodes change color in the following displays. The color of the grids is related to a discrete segment of time used in the LASEA analysis. For clarity these times are sequentially hi-lighted in the bottom of each figure.

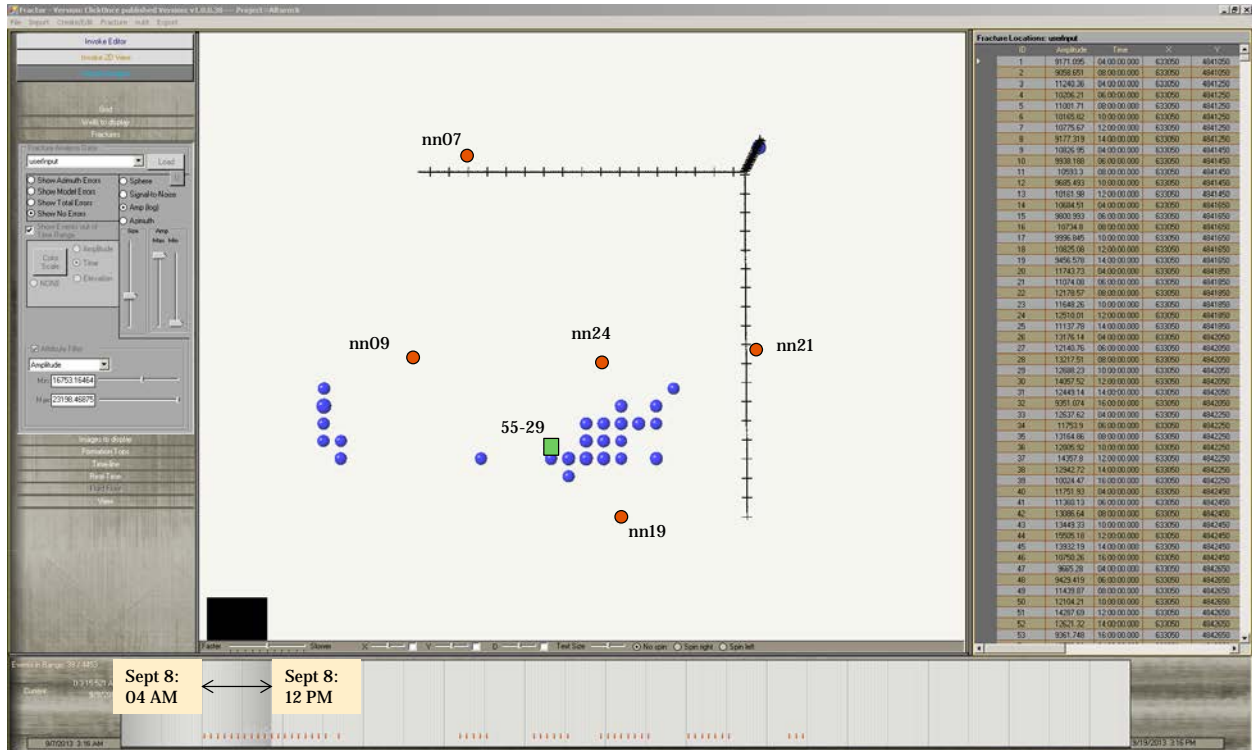


Figure 30 Activity time period 1

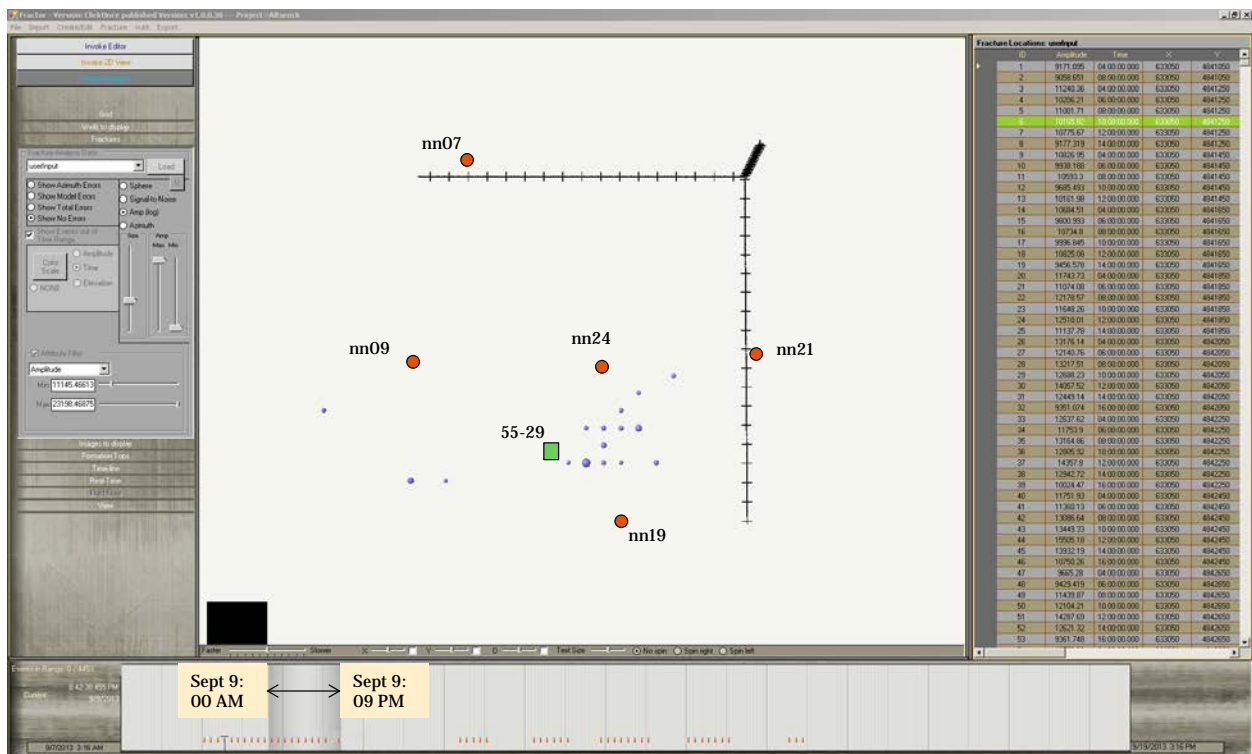


Figure 31 Active time period 2: similar to period 1 but with lower amplitude

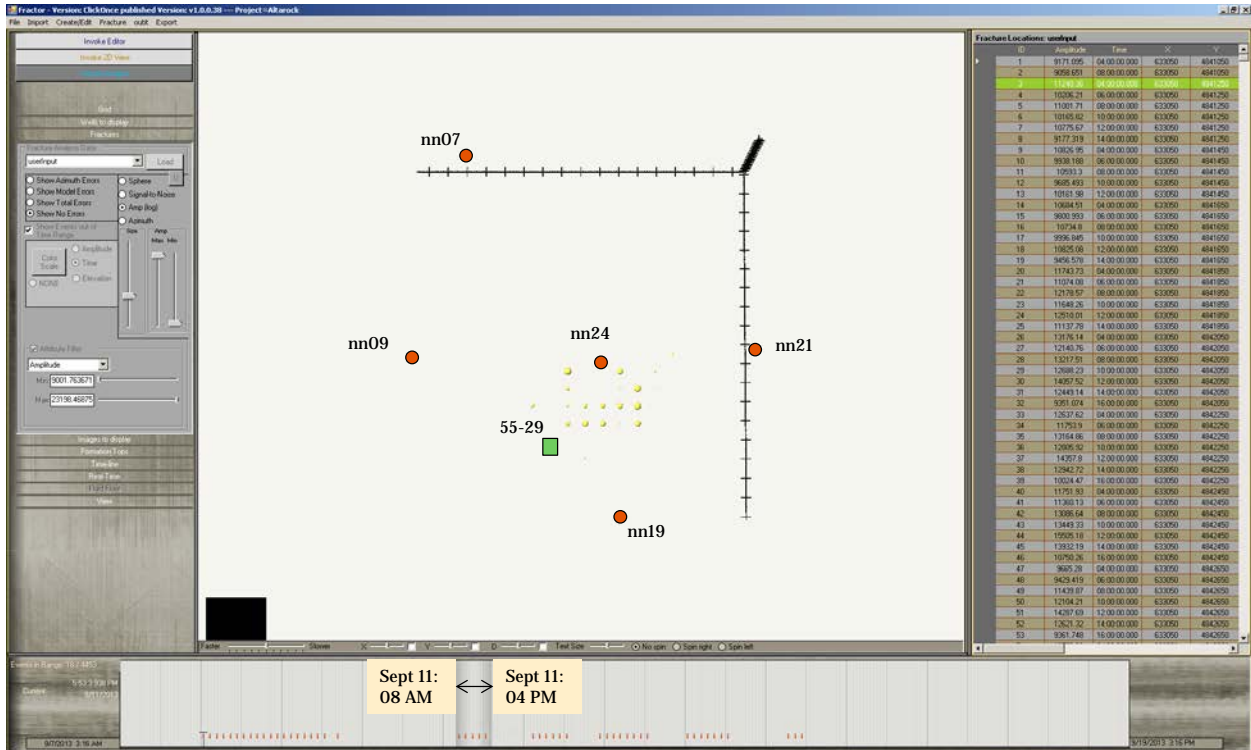


Figure 32 Active time period 3: Lower amplitudes continue but move to the NE

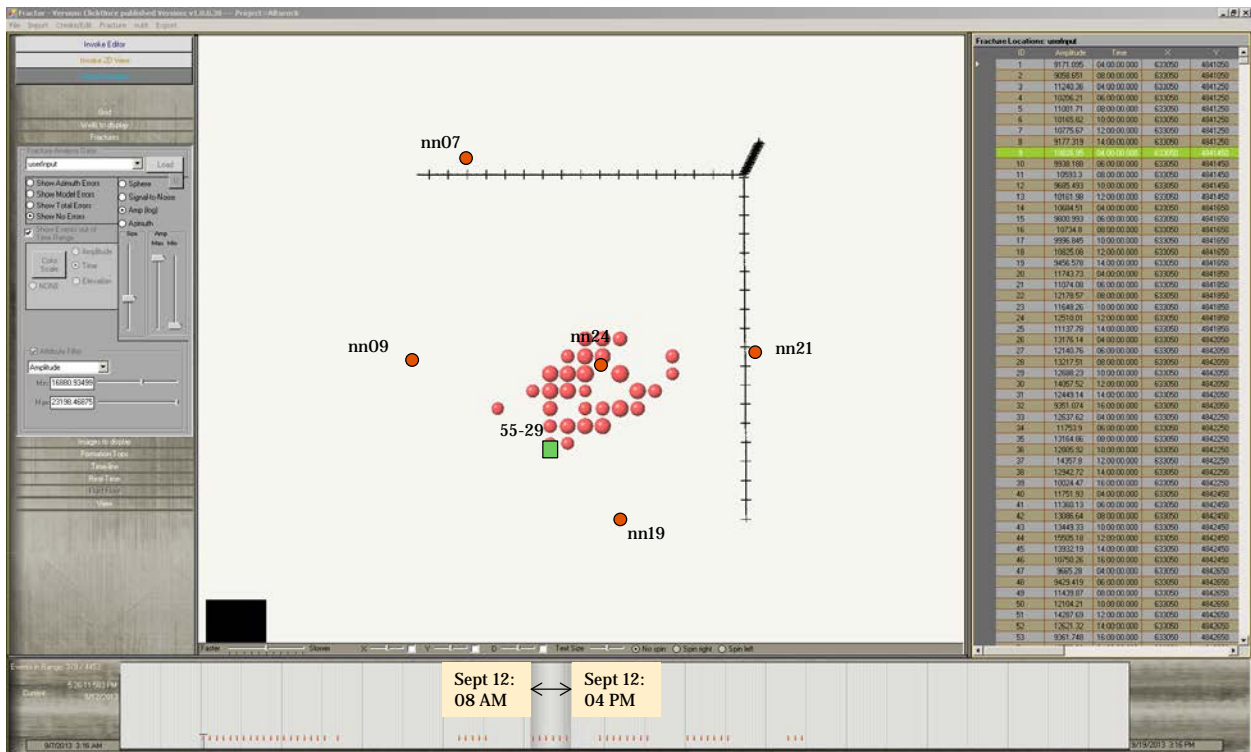


Figure 33 Active time period 4: Amplitudes increase and remain to NE of 55-29

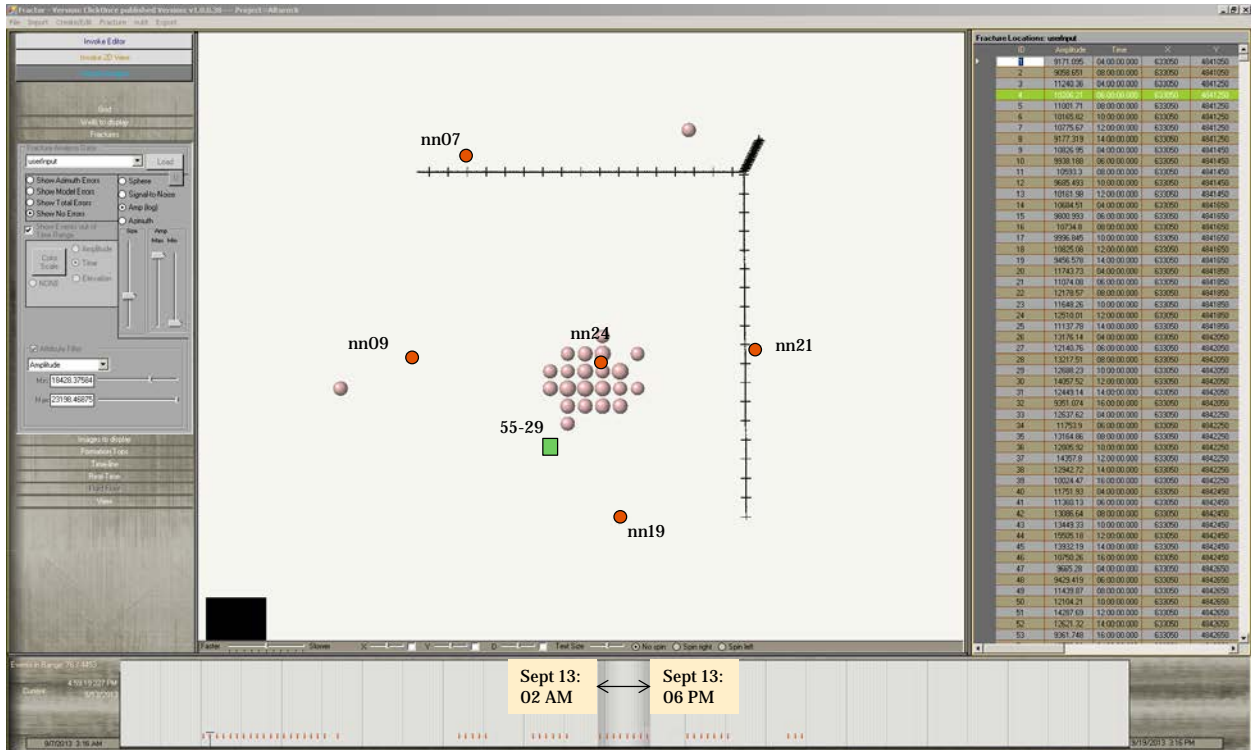


Figure 34 Active time period 5: Similar to period 4

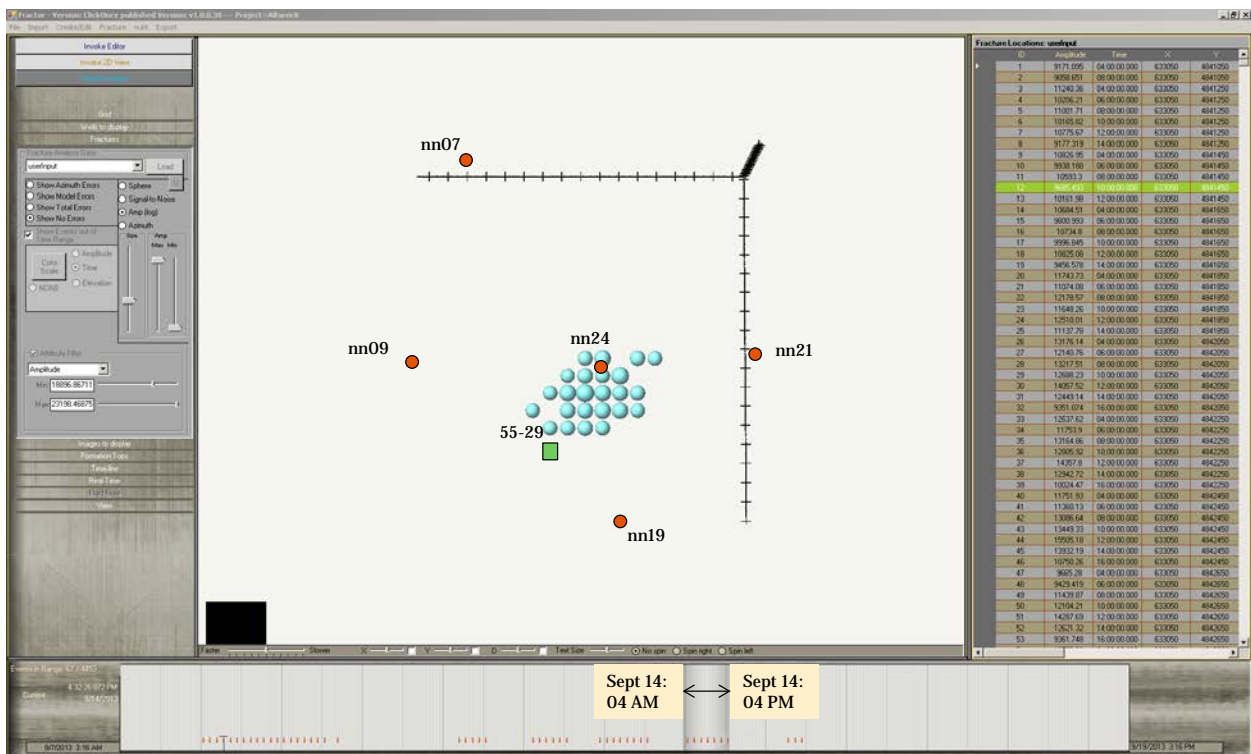


Figure 35 Active time period 6: continued energy NE of 55-29

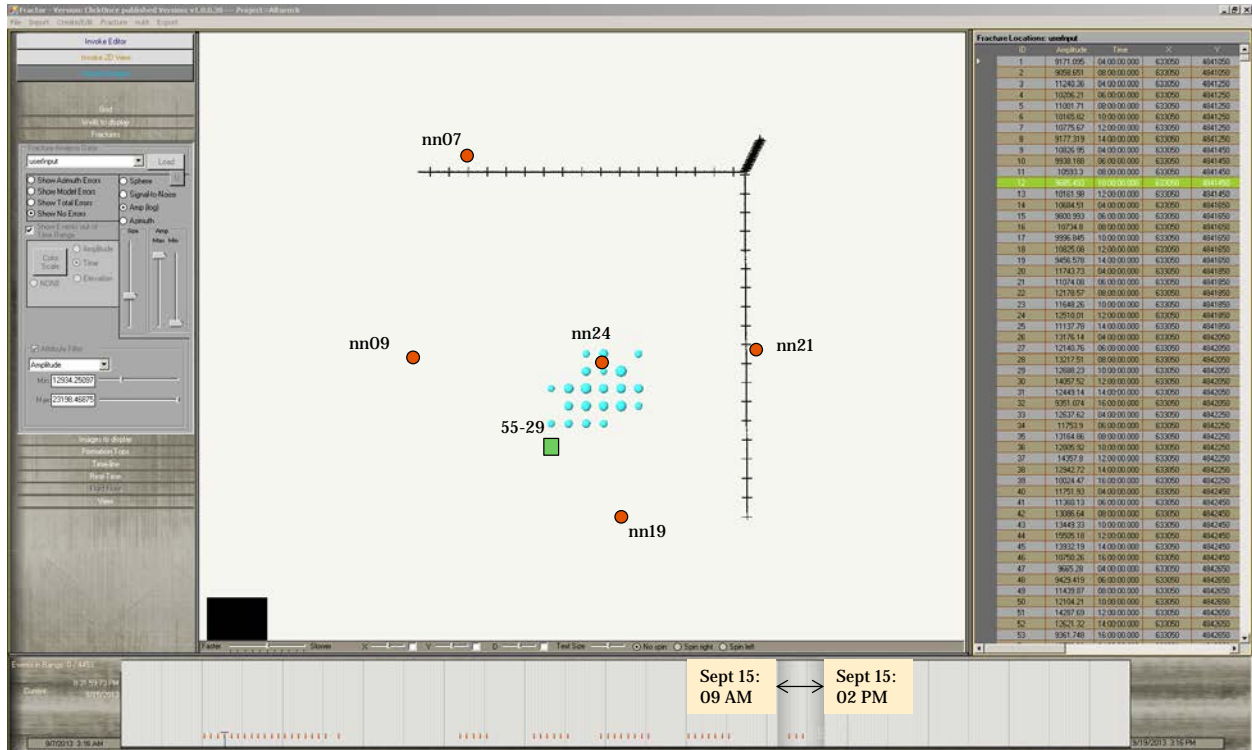


Figure 36 Active time period 7: continued energy NE of 55-29, end of survey

Although engineering activity had already been underway in the 55-29 well prior to this seismic survey, the measured seismic energy increased significantly around the 55-29 well on September 12 in response to active injection in the 55-29 well starting September 10. The seismic activity between September 8-11 moved decidedly to the Northeast of the 55-29. Seismic activity increased around noon on Sept 12.

One might speculate* that this result indicates the fracture energy from the injection moved primarily northeast from the 55-29 well and that uptake wells might most profitably be drilled northeast of the 55-29 well. These comments are speculation and will require more in-depth analysis by engineering experts familiar with the geology and engineering properties of the field location. The following slides show time periods in which the lowest level of seismic amplitude activity occurred in the study area and in particular the analysis is focused on the area around the 46-16 well. As in the slides above, these computations were done for a constant horizontal plane at an elevation of -1250 m (msl). The analysis was carried out on a 2D grid plane at elevation -1250 m with a 200 m grid spacing in both the North-South and East-West direction. The grid plane was 6 km by 6 km centered near the middle of the 5 observation wells.

The highest seismic activity zones were shown in the slides above and they dominated the amplitude spectrum but a primary question of this survey is whether this type of survey can detect the seismic response related to fluid flowing in fractures near the 46-16. Fluids were produced from the 46-16 Sept 08, 09, and 10 so we focus in the following analysis on amplitudes that are lower than the dominant amplitudes measured near the 55-29 well. Note that seismic energy might be due to the fluid motion itself or might be due to rocks breaking in response to stress changes as the fluid pressures change in the rock. We make no claim at this time that we can differentiate the direct cause of the seismic energy that is measured. The grid nodes change color in the following displays. At the current time the color of the grids has no meaning.

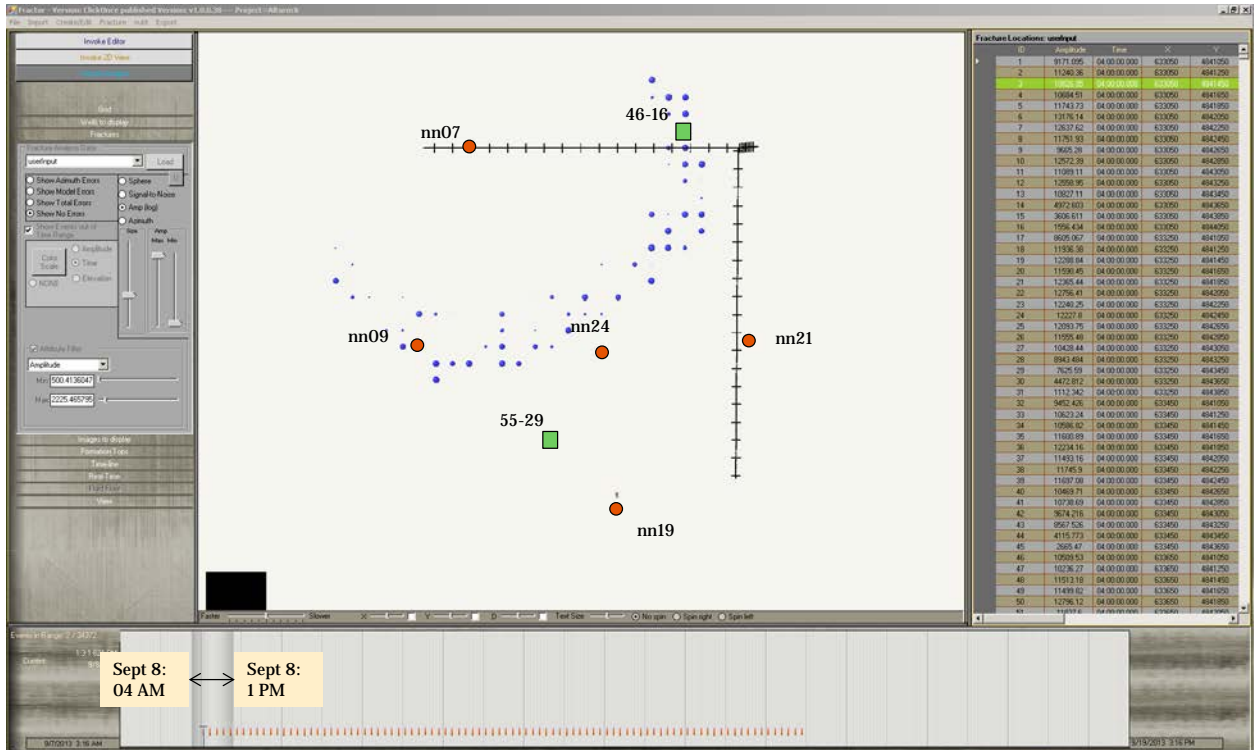


Figure 37 Lowest Amplitudes: September 08 – The well was opened at 14:10 local time. This plot shows the amplitudes prior to opening the flow.

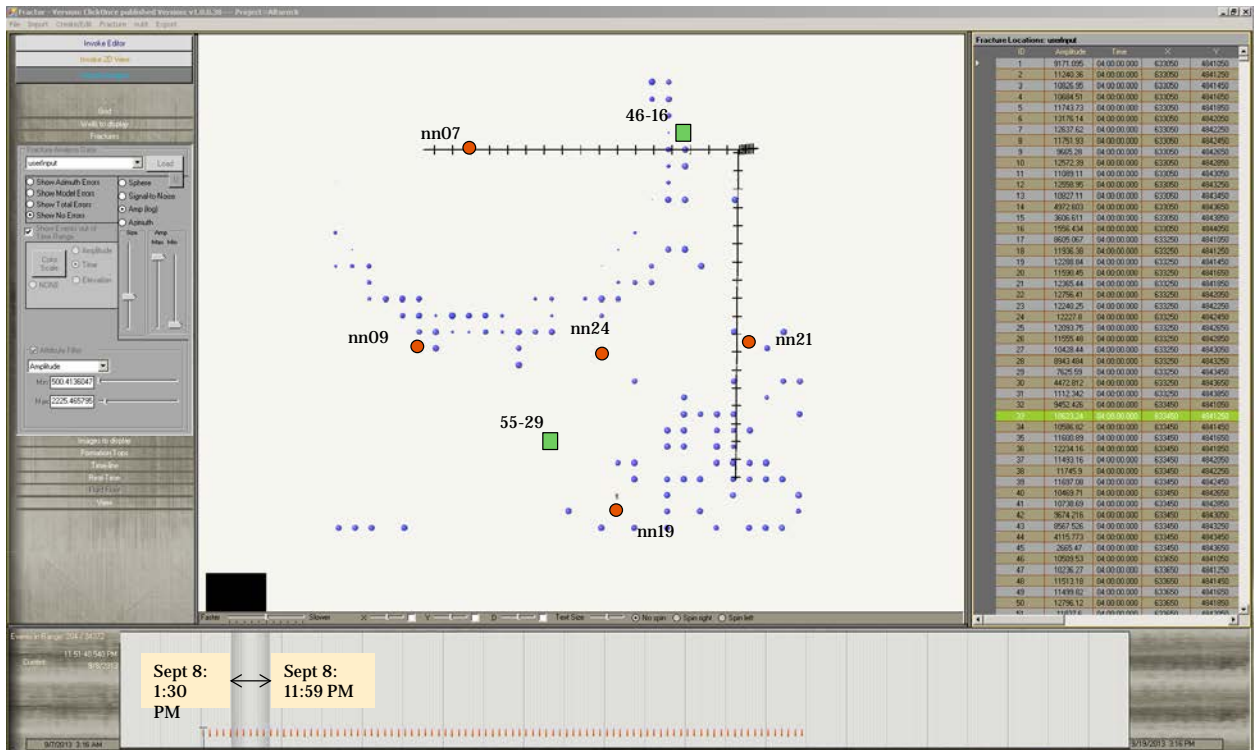


Figure 38 Lowest Amplitudes: September 08 – The well was opened at 14:10 local time. This plot shows the amplitudes

after opening the flow at 14:10 until midnight on Sept 08. Activity near the 46-16 does not change in an obvious way in response to the first day of flowing the well.

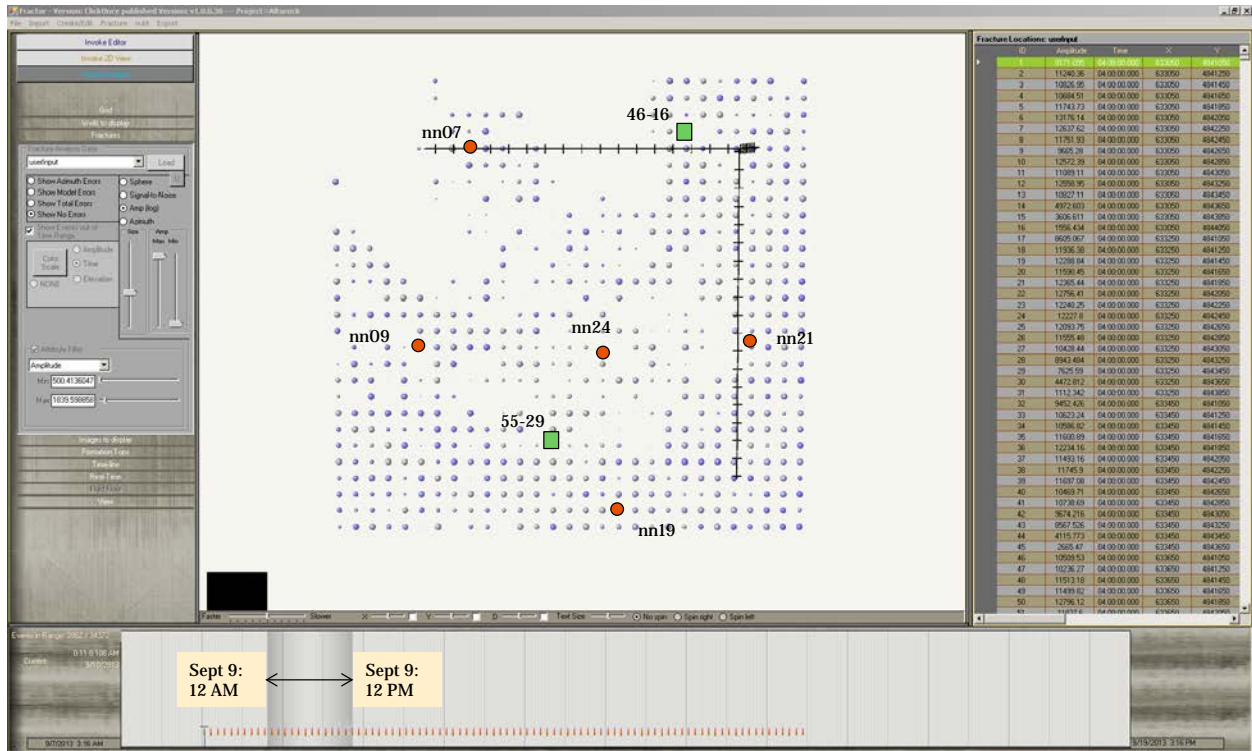


Figure 39 Lowest Amplitudes: September 09 – General activity increases throughout the area and in particular near observation well nn07 which had previously been a particularly quiet location.

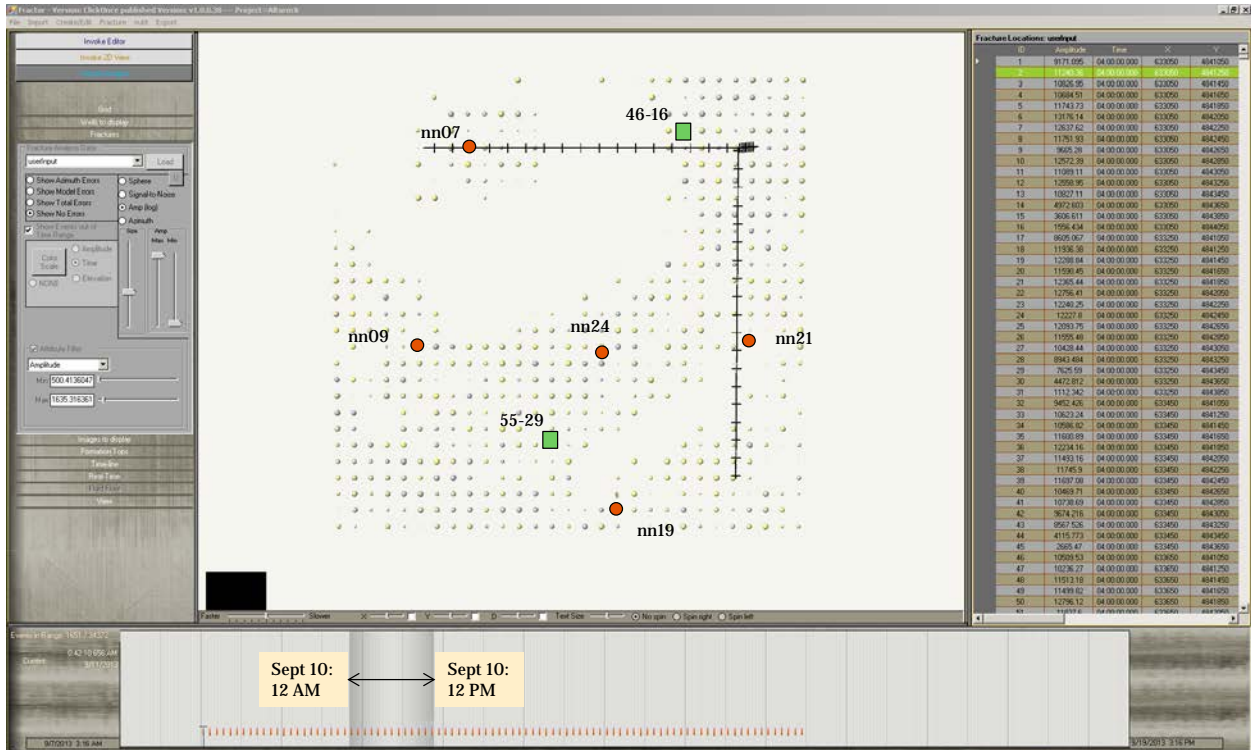


Figure 40 Lowest Amplitudes: September 10 – Flow continues in the 46-16 and general energy level remains near levels of the previous day. The well is shut in at 15:15 local time on this day.



Figure 41 Lowest Amplitudes: September 11 – Low amplitudes are diminished from the previous day. Injection begins on the 55-29.

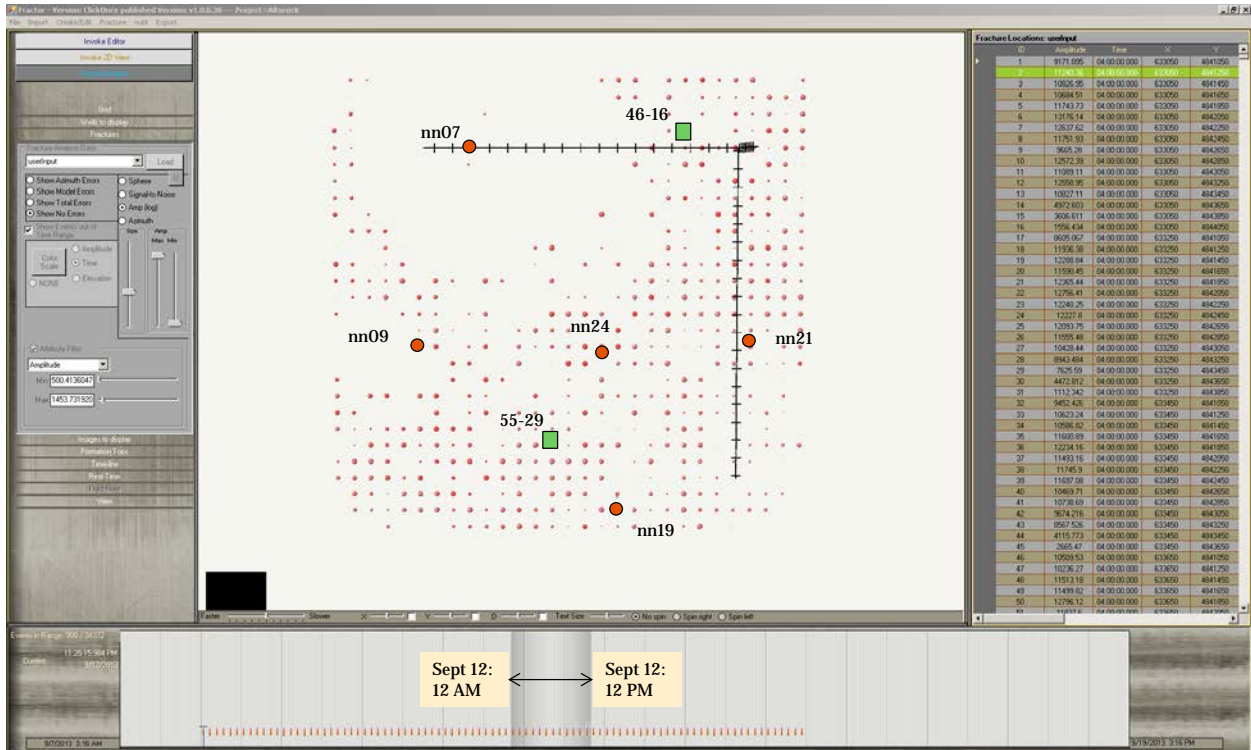


Figure 42 Lowest Amplitudes: September 12 – Low amplitudes return to levels nearer pre-injection in the 46-16, particularly near the nn07 observation well.

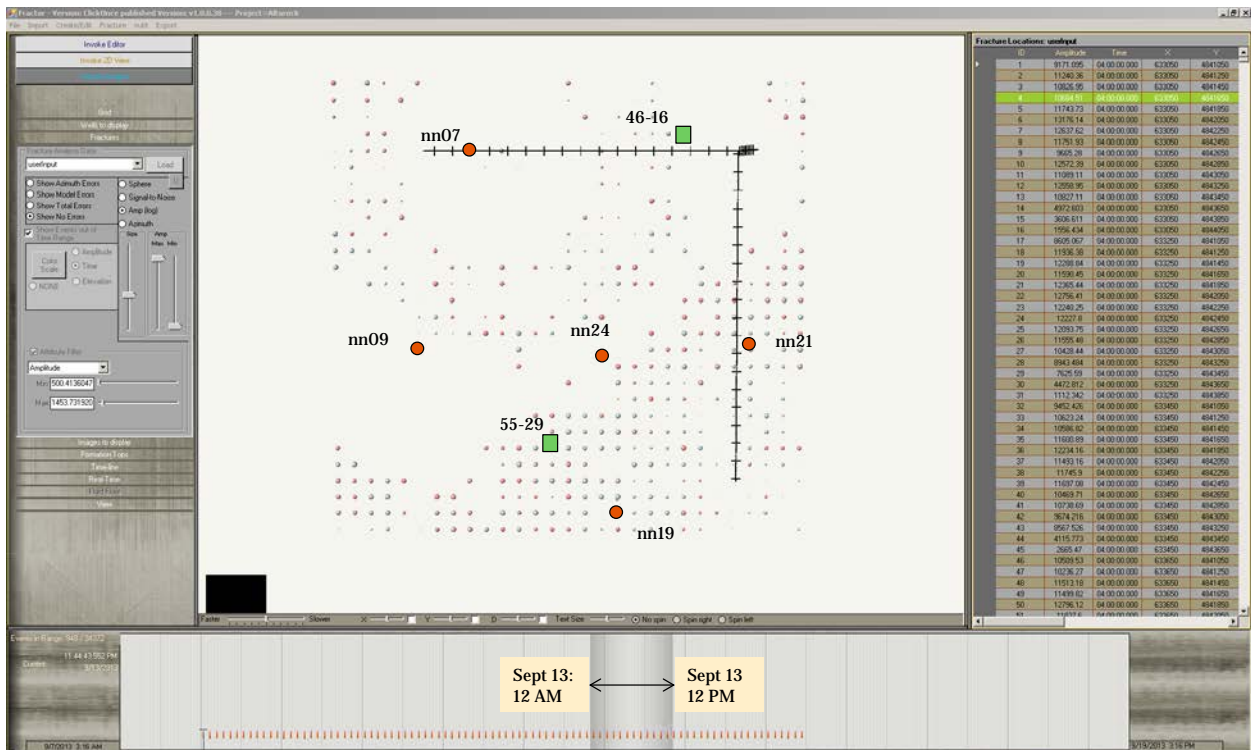


Figure 43 Lowest Amplitudes: September 13 – Low amplitudes return to levels near pre-injection in the 46-16, particularly near the nn07 observation well.

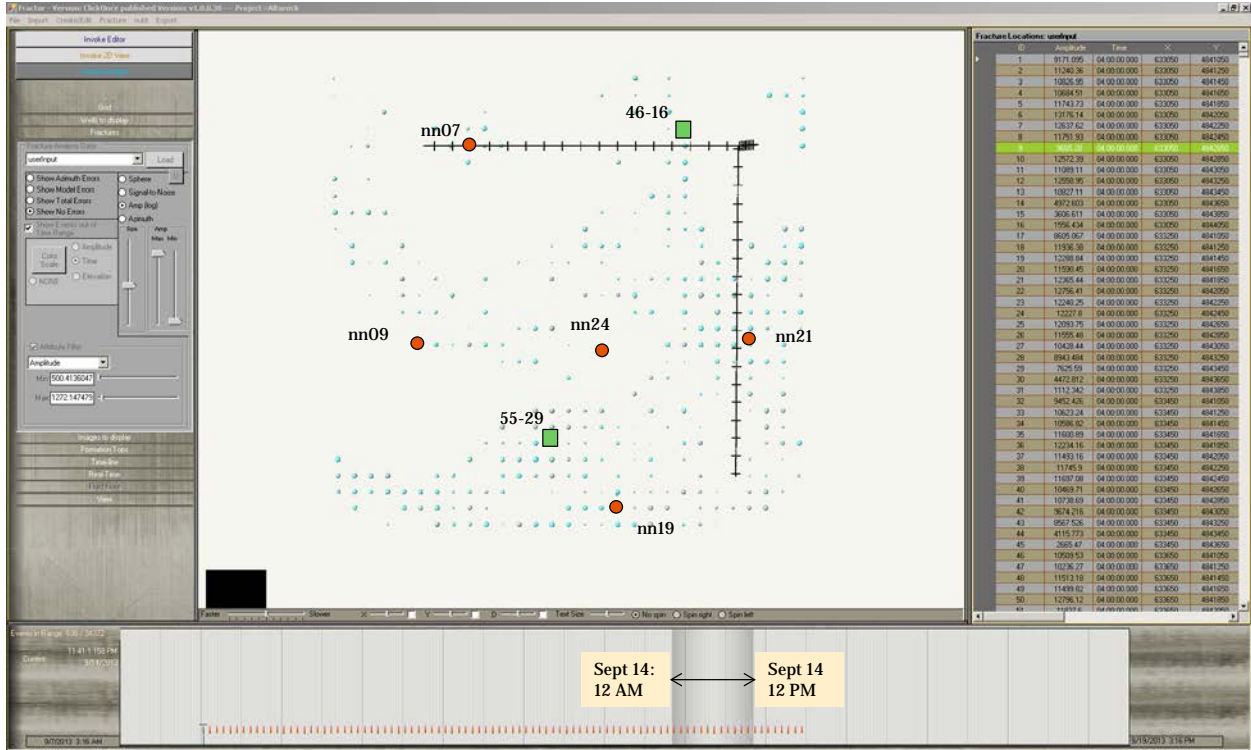


Figure 44 Lowest Amplitudes: September 14 – Some activity returns to near the nn07

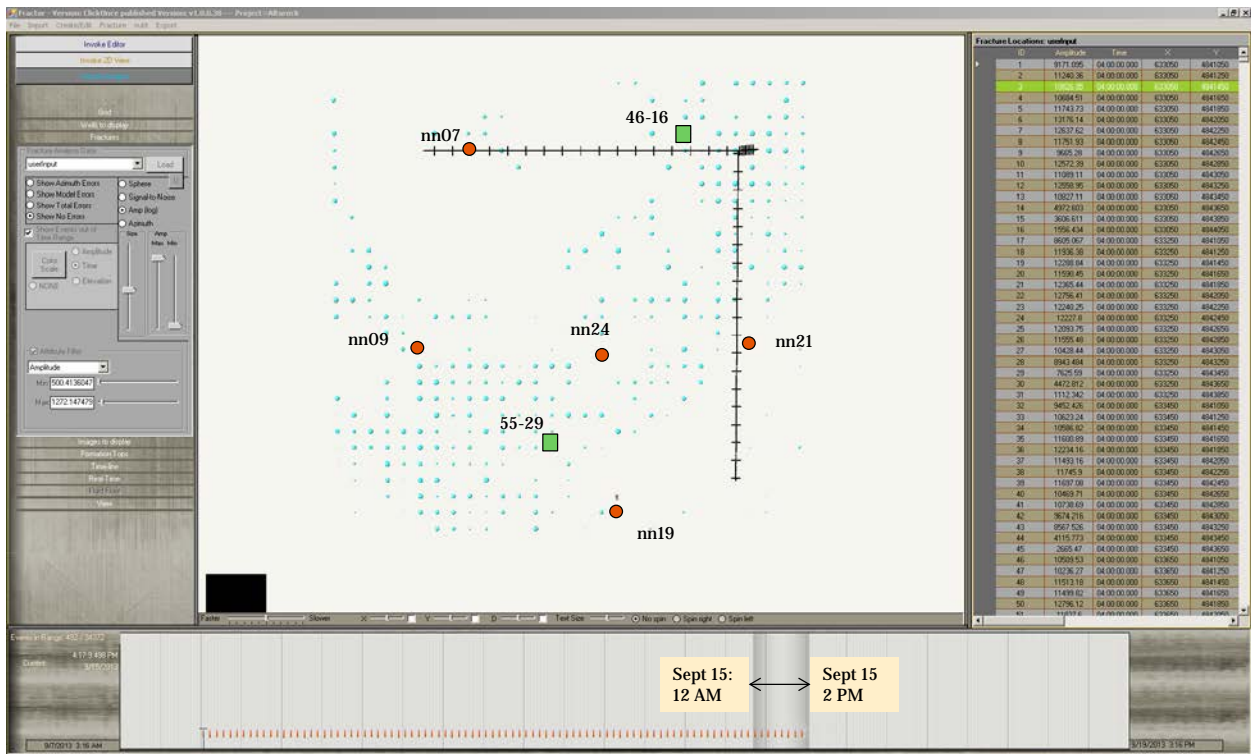


Figure 45 Lowest Amplitudes: September 15 – final day of recording

4.1 ANALYSIS OF LOWER AMPLITUDES

Opening the 46-16 well appears to have increased the energy measurement in the entire area but particularly near the nn07 which may have tantalizing implications. It is possible that a repetition of this analysis with different seismic frequency bands would yield more information about the question of detecting fluid flow in the subsurface. That analysis will take months of computer cluster time and further development that are outside the scope of this contract.

4.2 PAD 55-29 INJECTION SUMMARY

The following notes and information pertain to water injection at NWG 55-29 during the Sigma Cubed seismic noise study carried out in September, 2013.

September 10, 2013

0850 Start injection and water well pumps at Pad 55-29
0920 Injecting at 230.0 gpm. Wellhead pressure built to 200 psi.
0945 Injecting at 160.0 gpm. Wellhead pressure built to 400 psi.
0945-23:59 Injection slowly decreased from 160.0 gpm down to 139.9 gpm; WHP slowly increased from 400 psi to 430 psi.

September 11, 2013

0000-1859 Injection continued slow decline from 139.9 gpm to 136.7 gpm and WHP was maintained at 430 psi.
1859 PAS line opened to flow to sump, producing rusty water for ~10 minutes before clearing up. Water well flow at 148 gpm.
1930 PAS line water sample collected (18.7° C, clear).
1934 PAS line closed.
1935-2359 Injection continued slow decline from 148.0 gpm to 137.2 gpm. WHP maintained at 430 psi.

September 12, 2013

0000-0700 Injection continued slow decline from 137.2 gpm to 136.0 gpm. WHP maintained at 430 psi until pumps were shut down.

Casing Evaluation

The week prior to the injection described above, AltaRock performed a casing evaluation which paired injection with pressure-temperature-spinner (PTS) logging, video camera, and multi-finger caliper log. It was determined that there were two, large casing leaks at measured depths of 1767 feet and 2240 ft. AltaRock estimates that 90% of the water injected to 55-29 exits equally from these two leaks, leaving just 10% to exit in the open hole. Geographic coordinates for the fluid exits are given in Table 1.



Figure 46 - Injection pump used at Pad 55-29

Table 2 - Locations of fluid loss zones in 55-29. UTM is NAD84, Zone 10. Lat/long is WGS84.

Measured Depth (feet)	Vertical Depth (feet)	Elevation (feet)	Vertical Depth (m)	Elevation (m)	Easting (m)	Northing (m)	Long.	Lat.
0	0	5815	0	1772.4	635642.1	4842836	-121.316	43.7261
1767.0	1765.7	4049.3	538.2	1234.2	635659.5	4842836.7	- 121.3157	43.7262
2240.0	2237.9	3577.1	682.1	1090.3	635667.6	4842837.0	- 121.3156	43.7261
9125.0	8975.7	-3160.7	2735.8	-963.4	636093.0	4842843.5	- 121.3103	43.7261

5 ON THE UTILITY OF LASEA AS A COMMERCIAL EGS EXPLORATION TOOL

LASEA was able to identify coherent energy from the 46-16 well at identified known zones of natural fractures.

The pattern on Sunday September 8th, Monday September 9th and Tuesday September 10th all show a lower LASEA response prior to injection. It is noteworthy that prior to start up LASEA response, although weaker than latter stages, is consistently concentrated around one or more of the identified natural fracture zones.

The pattern on Sunday September 8th, Monday September 9th and Tuesday September 10th all show a stronger LASEA response during and up to the termination of injection. It is noteworthy that the LASEA response is consistently concentrated around one or more of the identified natural fracture zones.

The pattern on Sunday September 8th, Monday September 9th and Tuesday September 10th all show a diminished LASEA response after the termination of injection. It is noteworthy that the LASEA response is consistently concentrated around one or more of the identified natural fracture zones.

LASEA requires computational enhancements to reduce cycle times in order to be a viable commercial tool for EGS exploration. Further enhancements to CRYSTAL visualization tools will be required to efficiently display results.

In the absence of a robust reservoir model derived from multiple well logs and 3D reflection seismic, the results demonstrated herein are interesting but not conclusive.

6 SUMMARY OF FIELD ACQUISITION

1. Review Schedule of mobilization, rig-up, recording, rig-down, and demobilization:

Mobilization Date:	9/2/2013	Duration (Days):	3 Days
Rig In Date:	9/5/2013	Duration (Days):	2 Days
Monitoring Date:	9/7/2013	Duration (Days):	7 Day
De-installation:	9/14/2013	Duration (Days):	2 Day
Demobilization Date:	9/15/2013		

- Sigma³ may de-install as late as Sept. 25th due to crew allocation requirements at no charge.

2. Preliminary Field operation & Treatment schedule:

<input type="checkbox"/> Single Wells	<input checked="" type="checkbox"/> Multiple Wells		
Total # of Stages: Well#1	N/a	Hours per stage:	n/a
Stages per day:		# of Total Days:	

3. Site Information:

Country/County/Province, Parish:	Deschutes County / Oregon
Nearest Town:	Bend Oregon
Nearest Hospital:	St. Charles Medical Center 2500 NE Neff Road Bend, OR 97701 (541) 382-4321
Directions to Treatment Well:	START = 13571 Rose Rd Willis, TX 77378 Likely best route goes through Boise Idaho and then US 20 across Oregon to Bend. Turn east on McKay Butte Road also called Forest Service Road 9735. Turn is across from well-marked turn to La Pine State Park Turn is 22.6 miles south of Bend, Oregon

	<p>Or, 7.3 miles north of La Pine, Oregon</p> <p>Drive 7.5 miles to gate into geothermal lease. You will be met by Kyla Grasso or Trenton Cladouhos of AltaRock at the gate.</p> <p>.</p> <p>END NWG 55-29 = 43.726097°, -121.315601°</p>
Directions to Observation Well:	Five 700-900 foot deep observation wells are 1-3 km from Treatment Well. Trenton Cladouhos of AltaRock will lead field installation team to observation wells.

4. Acquisition Program Detail:

<input checked="" type="checkbox"/> Daylight Ops	<input type="checkbox"/> 24 Hour Ops
--	--------------------------------------

4.1. Observation Well(s):

Wellbore Diagram:	5" Steel Casing.
-------------------	------------------

History (Producer, Age, Other):	Drilled for monitoring in 2011 and 2012
---------------------------------	---

Map/ Surface Plat showing monitor locations in reference to Treatment well(s): See attached Google Earth KML and map below.



4.2. Observation Wells

# of Observation Well:	5	# of Levels in Observation Well:	15	
Location Particulars				
M-1-9-15 Location (SHL)	X/Long (NAD-27)	PENDING	Y/Lat (NAD-27)	PENDING
M-1-9-15 Location (BHL)				
Code	Long	Lat	Elevation (km)	Elevation (feet)
NN07	-121.325	43.7515	1.43	4690.4

NN19	-121.307	43.7183	1.56	5116.8
NN21	-121.29	43.7332	1.69	5543.2
NN17	-121.328	43.7208	1.48	4854.4
NN09	-121.333	43.7332	1.41	4624.8

4.3. Observation Wellhead Configuration(s):

Type of Connector needed for Wireline pack-off:		Waiting on specs from Sigma.	
Ancillary equipment required		Crane with 5-ton lifting capacity and 75-ft mast for rig-in/out	
Wellhead height above ground :	+/- 6 feet	Man lift needed to rig in/out?	yes
Tabulated (ASCII, Excel) Deviation Survey file:			
CCL Log:	NONE		
Other Logs:			
Temperature Profile:	NA		
Temperature at Plug:	< 60 F		